nutrients

Special Issue Reprint

Food Functional Factors and Nutritional Health

Edited by
Guowei Le and Bowen Li

mdpi.com/journal/nutrients

MDPI

Food Functional Factors and Nutritional Health

Food Functional Factors and Nutritional Health

Guest Editors

Guowei Le
Bowen Li

MDPI

Basel • Beijing • Wuhan • Barcelona • Belgrade • Novi Sad • Cluj • Manchester

Guest Editors
Guowei Le
School of Food Science and Technology
Jiangnan University
Wuxi
China

Bowen Li
College of Food Science
Southwest University
Chongqing
China

Editorial Office
MDPI AG
Grosspeteranlage 5
4052 Basel, Switzerland

This is a reprint of the Special Issue, published open access by the journal *Nutrients* (ISSN 2072-6643), freely accessible at: https://www.mdpi.com/journal/nutrients/special_issues/MQ0XD15A8I.

For citation purposes, cite each article independently as indicated on the article page online and as indicated below:

Lastname, A.A.; Lastname, B.B. Article Title. *Journal Name* **Year**, *Volume Number*, Page Range.

ISBN 978-3-7258-9163-4 (Hbk)
ISBN 978-3-7258-9164-1 (PDF)
https://doi.org/10.3390/books978-3-7258-9164-1

© 2026 by the authors. Articles in this reprint are Open Access and distributed under the Creative Commons Attribution (CC BY) license. The reprint as a whole is distributed by MDPI under the terms and conditions of the Creative Commons Attribution-NonCommercial-NoDerivs (CC BY-NC-ND) license (https://creativecommons.org/licenses/by-nc-nd/4.0/).

Contents

Bowen Li and Guowei Le
Food Functional Factors and Nutritional Health
Reprinted from: *Nutrients* **2026**, *18*, 2550, https://doi.org/10.3390/nu18152550 . . . . . **1**

Yipin Lyu, Jie Zhang, Chi Cheng, Xue Tang, Pantian Huang, Feitong Liu, et al.
Lactopontin in a Simulated Infant Formula Protein Matrix Promotes Bone Development via the Gut–Bone Axis in Growing Rats
Reprinted from: *Nutrients* **2026**, *18*, 1265, https://doi.org/10.3390/nu18081265 . . . . . **5**

Suxia Shen, Ning Xu, Zhaotian Yang, Zixuan Han, Lin Zeng, Ajibola Nihmot Ibrahim and Yan Zhang
Chlorophyll Supplementation Delays Aging in *Drosophila melanogaster* via Enhanced Stress Resistance and Detoxification Network Remodeling
Reprinted from: *Nutrients* **2026**, *18*, 1465, https://doi.org/10.3390/nu18091465 . . . . . **23**

Wenjuan Gong, Xintong Wang, Wen Zhang, Huihui Wang, Wei Xiong, Yixuan Li, et al.
Edible Bird's Nest as a Multi-Component Functional Food for Brain Aging: From Single-Bioactive Actions to Network- Regulatory Mechanisms
Reprinted from: *Nutrients* **2026**, *18*, 671, https://doi.org/10.3390/nu18040671 . . . . . **49**

Yunxuan Tang, Wenjing Liu, Jiayan Zhang, Bai Juan, Ying Zhu, Lin Zhu, et al.
Advances in Intestinal-Targeted Release of Phenolic Compounds
Reprinted from: *Nutrients* **2025**, *17*, 2598, https://doi.org/10.3390/nu17162598 . . . . . **76**

Qiushi Li, Chenxi Zhang, Guandong Fang, Shuang Qiu, Man Yuan, Nan Qian, et al.
Structural Characterization and Efficacy in Alleviating Lung Inflammation of Sialylated Glycopeptides from Edible Bird's Nest
Reprinted from: *Nutrients* **2025**, *17*, 1745, https://doi.org/10.3390/nu17101745 . . . . . **104**

Guozhen Wu, Xinming Wang, Hongjing Dong, Jinqian Yu, Tao Li and Xiao Wang
Coix Seed Oil Alleviates Hyperuricemia in Mice by Ameliorating Oxidative Stress and Intestinal Microbial Composition
Reprinted from: *Nutrients* **2025**, *17*, 1679, https://doi.org/10.3390/nu17101679 . . . . . **121**

Lan Cheng, Yue Chen, Jianyun He, Xinxin Cheng, Yuting Wang, Xiaoxia Lin, et al.
Effects of 12-Week Anti-Inflammatory Dietary Education on Depressive Symptoms Among Depressed Patients with Breast Cancer Undergoing Adjuvant Chemotherapy: A Randomized Controlled Trial
Reprinted from: *Nutrients* **2025**, *17*, 957, https://doi.org/10.3390/nu17060957 . . . . . **142**

Ning Kang, Zhexin Fan, Li Yang, Jie Shen, Yuechenfei Shen, Zhifeng Fang, Baokun Li, Bo Yang and Jiancheng Wang
Camel Milk Protein Ameliorates Ulcerative Colitis by Modulating Gut Microbiota and Amino Acid Metabolism
Reprinted from: *Nutrients* **2025**, *17*, 780, https://doi.org/10.3390/nu17050780 . . . . . **161**

Nan Qian, Chen-Xi Zhang, Guan-Dong Fang, Shuang Qiu, Yu Song, Man Yuan, et al.
Interventional Effects of Edible Bird's Nest and Free Sialic Acids on LPS-Induced Brain Inflammation in Mice
Reprinted from: *Nutrients* **2025**, *17*, 531, https://doi.org/10.3390/nu17030531 . . . . . **184**

nutrients

MDPI

Editorial

Food Functional Factors and Nutritional Health

Bowen Li [1,*] and Guowei Le [2]

[1] China-Hungary Belt and Road Joint Laboratory on Food Science, Chongqing Key Laboratory of Speciality Food Co-Built by Sichuan and Chongqing, College of Food Science, Southwest University, Chongqing 400715, China
[2] School of Food Science and Technology, Jiangnan University, Wuxi 214122, China
* Correspondence: lbw1965841356@gmail.com

Diet fundamentally affects our long-term health. Over the past decade, the scientific understanding of this relationship has moved beyond simply counting calories or balancing macronutrients. Therefore, we recognize dietary habits as a combination of physiological needs, environmental influences, and conscious choices [1]. This shift requires us to look closer and deeper at how specific food components, particularly food functional factors, such as bioactive peptides, polyphenols, specific dietary fibers, and functional lipids, affect our metabolism. Recent research highlights how these specific nutritional inputs help maintain metabolic balance and influence cellular aging. More studies that explore these mechanisms, from molecular pathways to public health, aiming to turn nutritional science into practical, long-term health benefits.

The reality of the current food environment, which is increasingly dominated by ultra-processed foods (UPFs), should be addressed first before we get benefits from functional foods [2]. Even as our knowledge of nutrition grows, the convenience and high appeal of these processed products often put people toward unhealthy choices that override our natural fullness signals. These foods are typically loaded with altered nutrients, such as oxidized lipids and advanced glycation end products. Emerging evidence links them directly to the rising rates of obesity, type 2 diabetes, and cardiovascular diseases. For instance, a large-scale prospective cohort study recently published in The Lancet Regional Health—Europe clearly demonstrated that higher UPF intake is significantly associated with an increased risk of type 2 diabetes [3]. This risk goes beyond just high sugar and fat content. The breakdown of the natural physical structure of the food (the food matrix) and the pro-inflammatory nature of UPFs are also key drivers of metabolic harm. Common additives like emulsifiers can disrupt the gut microbiota, trigger intestinal inflammation and promote obesity [4]. In contrast, simply replacing a portion of UPFs in the diet with an equal amount of unprocessed or minimally processed foods can significantly lower the incidence of metabolic diseases. To protect public health moving forward, we need clearer policies and industry-wide food reformulation. Research should not only assess the harm of UPFs but also explore how integrating specific food functional factors into daily diets might offset some of these pro-inflammatory and metabolic disruptions.

In contrast to the risks associated with UPFs, intentional dietary patterns rich in functional factors offer profound therapeutic benefits. Increasing evidence demonstrates that whole-grain diets, caloric restriction, and specific amino acid limitations can improve insulin sensitivity, balance lipid profiles, and potentially extend health span. For instance, dietary methionine restriction (MR) has been shown to fundamentally alter lipid metabolism in ways that may promote longevity and ameliorate ulcerative colitis [5,6]. In preclinical models, MR reduced fat accumulation, enhanced insulin sensitivity, and reversed obesity

by activating the FGF21 signaling pathway and downregulating hepatic lipogenic genes, such as Scd1. Interestingly, the transcription factor HNF4α has been identified as a key determinant of cellular sensitivity to MR, offering a promising target for precision nutrition to identify individuals who would benefit most from dietary MR intervention [7]. Of note, these targeted dietary approaches serve as powerful, non-pharmacological tools for preventing and managing chronic diseases. Moving forward, the field requires larger clinical trials to validate how various functional factors and targeted dietary approaches can serve as non-pharmacological tools for preventing and managing chronic diseases.

To fully understand how food functional factors lead to such broad health benefits, we should pay attention to the gut microbiota. Functional factors, such as prebiotics, dietary polyphenols, and complex carbohydrates, contribute to the development of the gut microbiome. These microbes metabolize functional factors to produce beneficial metabolites, which in turn regulate our energy metabolism, systemic inflammation, and gut barrier integrity. This makes the microbiome an excellent target for therapies utilizing probiotics, prebiotics, and emerging postbiotics to restore metabolic balance [8]. However, the field of microbiome-based nutrition needs to move past simply observing links and start proving cause and effect. We need to identify exactly which bacteria interact with specific functional factors to drive precise health outcomes, eventually bringing standardized, customized symbiotic treatments into regular clinical care [9].

Individuals metabolize food functional factors differently due to individual differences such as genetics and lifestyle. A one-size-fits-all approach to diet is no longer practical. While general, population-wide dietary guidelines provide a good baseline, they fail to meet the unique needs of groups like pregnant women, the elderly, athletes, or people managing conditions such as diabetes. This brings us to the necessity of personalized nutrition [10]. By analyzing an individual's genetic makeup, metabolic profile, and microbiome, we can offer highly tailored advice on which functional factors will yield the greatest health benefits. Future research should focus on combining data from genomics and metabolomics to build reliable, algorithm-driven tools for personalized recommendations. Importantly, we need to translate these advanced scientific concepts into affordable and accessible strategies for everyday healthcare providers and the public.

Aligning with these advancements, our current issue presents a comprehensive synthesis of how bioactive components within complex food matrices modulate physiological health through intricate regulatory networks. Highlighting the intersection of aging and nutritional intervention, studies demonstrate that dietary supplementation with spinach-derived chlorophyll can significantly extend Drosophila lifespan and enhance stress resistance by remodeling detoxification networks via the CncC (Nrf2) signaling pathway [Contribution 1]. The collection further establishes edible bird's nest (EBN) as a paradigm for multi-target regulation, where its unique protein-glycoprotein-sialic acid core and specific sialylated glycopeptides provide neuroprotection and alleviate inflammation across the gut–brain and gut-lung axes [Contributions 2–4]. Investigations into metabolic and organ health reveal that Coix seed oil effectively manages hyperuricemia by promoting uric acid homeostasis and intestinal integrity [Contribution 5], while camel milk proteins and lactopontin-fortified matrices are shown to mitigate colitis and support bone development through the modulation of the gut microbiota and the gut-bone axis [Contributions 6 and 7]. Additionally, the issue addresses technological and clinical translation, exploring advanced intestinal-targeted delivery systems for phenolic compounds to overcome bioavailability barriers [Contribution 8], as well as the efficacy of anti-inflammatory dietary education in improving the mental health and quality of life of breast cancer patients [Contribution 9]. These collective findings advance functional food research from a reductionist approach to

https://doi.org/10.3390/nu18152550

a systems-biology perspective, providing critical academic support for precision nutrition and the development of evidence-based health interventions.

In conclusion, the relationship between food functional factors and nutritional health is profoundly complex and multifaceted, encompassing severe modern risks driven by UPFs as well as therapeutic opportunities offered by specific dietary patterns and microbiome modulation. The future of nutritional science clearly lies in a highly personalized, mechanism-based approach that fully harnesses the biological power of food functional factors. We encourage the scientific and medical communities to continue relentlessly exploring the fundamental regulatory principles of dietary habits on metabolic health. By promoting evidence-based diets rich in functional factors and integrating multi-omics technologies, we can work towards a future where precise, individualized nutrition serves as the ultimate cornerstone of preventive medicine.

Funding: This research was funded by Chongqing Technology Innovation and Application Development Special Key Project (CSTB2024TIAD-KPX0014) and the Fundamental Research Funds for the Central Universities (SWU-KQ25008).

Conflicts of Interest: The authors declare no conflicts of interest.

List of Contributions:

1. Shen, S.; Xu, N.; Yang, Z.; Han, Z.; Zeng, L.; Ibrahim, A.N.; Zhang, Y. Chlorophyll Supplementation Delays Aging in Drosophila melanogaster via Enhanced Stress Resistance and Detoxification Network Remodeling. *Nutrients* **2026**, *18*, 1465. https://doi.org/10.3390/nu18091465.
2. Li, Q.; Zhang, C.; Fang, G.; Qiu, S.; Yuan, M.; Qian, N.; Wang, D.; Cheng, X. Structural Characterization and Efficacy in Alleviating Lung Inflammation of Sialylated Glycopeptides from Edible Bird's Nest. *Nutrients* **2025**, *17*, 1745. https://doi.org/10.3390/nu17101745.
3. Qian, N.; Zhang, C.-X.; Fang, G.-D.; Qiu, S.; Song, Y.; Yuan, M.; Wang, D.-L.; Cheng, X.-R. Interventional Effects of Edible Bird's Nest and Free Sialic Acids on LPS-Induced Brain Inflammation in Mice. *Nutrients* **2025**, *17*, 531. https://doi.org/10.3390/nu17030531.
4. Gong, W.; Wang, X.; Zhang, W.; Wang, H.; Xiong, W.; Li, Y.; Wen, P.; Sun, Y. Edible Bird's Nest as a Multi-Component Functional Food for Brain Aging: From Single-Bioactive Actions to Network-Regulatory Mechanisms. *Nutrients* **2026**, *18*, 671. https://doi.org/10.3390/nu18040671.
5. Wu, G.; Wang, X.; Dong, H.; Yu, J.; Li, T.; Wang, X. Coix Seed Oil Alleviates Hyperuricemia in Mice by Ameliorating Oxidative Stress and Intestinal Microbial Composition. *Nutrients* **2025**, *17*, 1679. https://doi.org/10.3390/nu17101679.
6. Kang, N.; Fan, Z.; Yang, L.; Shen, J.; Shen, Y.; Fang, Z.; Li, B.; Yang, B.; Wang, J. Camel Milk Protein Ameliorates Ulcerative Colitis by Modulating Gut Microbiota and Amino Acid Metabolism. *Nutrients* **2025**, *17*, 780. https://doi.org/10.3390/nu17050780.
7. Lyu, Y.; Zhang, J.; Cheng, C.; Tang, X.; Huang, P.; Liu, F.; Hu, R.; Huppertz, T.; Wang, X.; Zhou, P. Lactopontin in a Simulated Infant Formula Protein Matrix Promotes Bone Development via the Gut–Bone Axis in Growing Rats. *Nutrients* **2026**, *18*, 1265. https://doi.org/10.3390/nu18081265.
8. Tang, Y.; Liu, W.; Zhang, J.; Juan, B.; Zhu, Y.; Zhu, L.; Zhao, Y.; Daglia, M.; Xiao, X.; He, Y. Advances in Intestinal-Targeted Release of Phenolic Compounds. *Nutrients* **2025**, *17*, 2598. https://doi.org/10.3390/nu17162598.
9. Cheng, L.; Chen, Y.; He, J.; Cheng, X.; Wang, Y.; Lin, X.; Huang, Z.; Miao, X.; Xia, S. Effects of 12-Week Anti-Inflammatory Dietary Education on Depressive Symptoms Among Depressed Patients with Breast Cancer Undergoing Adjuvant Chemotherapy: A Randomized Controlled Trial. *Nutrients* **2025**, *17*, 957. https://doi.org/10.3390/nu17060957.

References

1. Zhang, F.; Zhou, G.; Schewe, M.; Kulling, S.E.; Ding, Y.; Mozaffarian, D.; Zuo, T. Dietary urbanization destabilizes host-gut microbiome homeostasis and informs precision nutrition for human health. *Cell Metab.* **2025**, *37*, 2128–2148. [CrossRef] [PubMed]
2. Monteiro, C.A.; Louzada, M.L.C.; Steele-Martinez, E.; Cannon, G.; Andrade, G.C.; Baker, P.; Bes-Rastrollo, M.; Bonaccio, M.; Gearhardt, A.N.; Khandpur, N.; et al. Ultra-processed foods and human health: The main thesis and the evidence. *Lancet* **2025**, *406*, 2667–2684. [CrossRef] [PubMed]
3. Dicken, S.J.; Dahm, C.C.; Ibsen, D.B.; Olsen, A.; Tjønneland, A.; Louati-Hajji, M.; Cadeau, C.; Marques, C.; Schulze, M.B.; Jannasch, F.; et al. Food consumption by degree of food processing and risk of type 2 diabetes mellitus: A prospective cohort analysis of the European Prospective Investigation into Cancer and Nutrition (EPIC). *Lancet Reg. Health-Eur.* **2024**, *46*, 101043. [CrossRef] [PubMed]
4. Korem, T.; Zeevi, D.; Zmora, N.; Weissbrod, O.; Bar, N.; Lotan-Pompan, M.; Avnit-Sagi, T.; Kosower, N.; Malka, G.; Rein, M.; et al. Bread Affects Clinical Parameters and Induces Gut Microbiome-Associated Personal Glycemic Responses. *Cell Metab.* **2017**, *25*, 1243–1253.e1245. [CrossRef] [PubMed]
5. Sanderson, S.M.; Gao, X.; Dai, Z.; Locasale, J.W. Methionine metabolism in health and cancer: A nexus of diet and precision medicine. *Nat. Rev. Cancer* **2019**, *19*, 625–637. [CrossRef] [PubMed]
6. Yang, H.; Yang, Y.; Qian, J.; Hu, W.; Liu, J.; Mwabulili, F.; Li, P.; Xie, Y. Dietary methionine restriction ameliorates ulcerative colitis in mice: A role for the H_2S and short-chain fatty acids balance via gut microbiota remodeling. *Food Res. Int.* **2026**, *233*, 119038. [CrossRef] [PubMed]
7. Xu, Q.; Li, Y.; Gao, X.; Kang, K.; Williams, J.G.; Tong, L.; Liu, J.; Ji, M.; Deterding, L.J.; Tong, X.; et al. HNF4α regulates sulfur amino acid metabolism and confers sensitivity to methionine restriction in liver cancer. *Nat. Commun.* **2020**, *11*, 3978. [CrossRef] [PubMed]
8. Song, J.; Ding, M.; Joyce, P.W.S.; Pi, X.; Zhang, B.; Li, B. Decoding the HMO-microbiome axis: Bridging maternal milk to infant health outcomes. *Gut Microbes* **2026**, *18*, 2649456. [CrossRef] [PubMed]
9. Shapiro, H.; Jickeli, B.; Niv, I.; Ernan, B.; Elinav, E. The interplay between the microbiome and immune cells in metabolic homeostasis and disease. *Cell Metab.* **2026**, *38*, 1–21. [CrossRef] [PubMed]
10. Zhang, S.; Sun, Y.; Jiang, J.; Nie, S. Human-Centered Innovation: Precision Nutrition and the Future of Food. *Adv. Sci.* **2026**, e23337. [CrossRef] [PubMed]

Disclaimer/Publisher's Note: The statements, opinions and data contained in all publications are solely those of the individual author(s) and contributor(s) and not of MDPI and/or the editor(s). MDPI and/or the editor(s) disclaim responsibility for any injury to people or property resulting from any ideas, methods, instructions or products referred to in the content.

nutrients

MDPI

Article

Lactopontin in a Simulated Infant Formula Protein Matrix Promotes Bone Development via the Gut–Bone Axis in Growing Rats

Yipin Lyu [1], Jie Zhang [1,2,*], Chi Cheng [2], Xue Tang [1], Pantian Huang [3,4], Feitong Liu [4], Ruibiao Hu [3,4], Thom Huppertz [5,6], Xinyan Wang [1] and Peng Zhou [1,5]

[1] School of Food Science and Technology, Jiangnan University, Wuxi 214122, China
[2] School of Chemical Engineering and Materials, Changzhou Institute of Technology, Changzhou 213000, China
[3] Biostime (Changsha) Nutrition Foods Limited, Changsha 410219, China
[4] Health and Happiness (H&H) China Limited, Guangzhou 510700, China
[5] International Joint Research Laboratory for Dairy Science and Technology, Jiangnan University, Wuxi 214122, China
[6] School of Food and Nutritional Sciences, University College Cork, T12 YN60 Cork, Ireland
* Correspondence: jiezhang11@jiangnan.edu.cn

Abstract

Background: Lactopontin (L-OPN) is a pivotal bioactive protein present in breast milk that supports bone development, but its efficacy in a formula matrix is unknown. This study aimed to evaluate the effects of L-OPN-fortified formula on bone growth in a growing rat model and to explore the underlying mechanisms. Methods: Weanling rats (n = 8/group) received daily gavage for four weeks: (1) CON—deionized water; (2) PRO—750 mg/kg·BW mixed protein; or (3) L-OPN—750 mg/kg·BW of the PRO formula fortified with L-OPN. Results: The results showed that the formula fortified with L-OPN could significantly increase bone volume and trabecular bone number ($p < 0.05$). Furthermore, both femur length and thickness, as well as overall body length, were significantly increased ($p < 0.001$). In addition, the L-OPN-fortified formula specifically increased the relative abundance of *Bacteroides* and *Parabacteroides* in rat feces ($p < 0.05$). Metabolomic analysis revealed that L-OPN supplementation significantly altered bile acid metabolism, notably increasing serum levels of 12-ketolithocholic acid (12-KLCA), which correlated strongly with bone metrics. Conclusions: These preclinical findings provide a basis for future research in infant formula.

Keywords: lactopontin; bone health; *Parabacteroides*; bile acid

1. Introduction

Human milk is the gold standard for infant nutrition, providing not only essential macronutrients but also a suite of bioactive components critical for optimal growth and development [1]. Among these, lactopontin (L-OPN), a highly phosphorylated glycoprotein, is particularly abundant in human milk yet markedly deficient in conventional infant formulas [2]. Accumulating evidence underscores L-OPN's pivotal role in early-life bone health, with studies demonstrating its ability to directly stimulate osteoblast activity and promote skeletal mineralization [3,4]. This positions L-OPN as a key candidate for fortifying next-generation infant formulas aimed at better mimicking the bone-supportive benefits of breastfeeding.

However, the efficacy of L-OPN must be evaluated within its natural context of protein–protein interactions. In bovine and human milk, L-OPN does not act in isolation; it forms stable complexes with other bioactive proteins, most notably lactoferrin (LF), through electrostatic interactions [5]. The binding of L-OPN and LF has been extensively studied. It has been demonstrated that bovine-source L-OPN and LF form a stable complex at a ratio of 1:3 (dissociation constant, Kd = 10^{-6} M) [6]. The well-characterized L-OPN–LF complex exhibits distinct functional properties compared to its individual constituents: it demonstrates greater resistance to gastrointestinal digestion [7,8] and enhanced binding and uptake by intestinal cells, which in turn promotes intestinal cell proliferation and strengthens immune responses [9–11]. Critically, this complexation fundamentally alters the protein's digestibility and bioactivity profile. Therefore, a significant research gap exists regarding whether L-OPN can retain or even leverage its osteogenic potential when incorporated into a simulated infant formula protein matrix, where its interaction landscape differs from that of native milk. Demonstrating its efficacy in such a complex system is essential for its practical application.

Addressing this gap necessitates moving beyond simple phenotypic observation to investigate the underlying mechanisms. The gut–bone axis has emerged as a central pathway through which dietary factors regulate skeletal metabolism. Gut microbiota are master regulators of host physiology, capable of transforming primary bile acids into a diverse array of secondary metabolites that act as signaling molecules [12]. Recent research has established direct links between specific bile acid profiles and the regulation of both bone formation and resorption [13]. Given that L-OPN can interact with the gut lumen and modulate microbial communities, as evidenced by our previous work showing L-OPN-induced enrichment of Parabacteroides [3,4], a known producer of secondary bile acids [14], a plausible and testable mechanism emerges: dietary L-OPN, even within a complex formula matrix, may promote bone development by remodeling the gut microbiota, thereby altering the bile acid metabolic profile towards a more osteogenic state.

Thus, the present study was designed to address these interconnected questions using a well-established growing rat model. We aimed to (1) determine whether supplementation with L-OPN in a simulated infant formula protein matrix can promote bone development, and (2) investigate the role of the gut microbiota–bile acid–bone axis as a key mechanistic pathway underlying this effect. We hypothesized that L-OPN-fortified protein powder would enhance bone growth via microbiota-driven modulation of bile acid metabolism. This study presents a preliminary exploration of the potential application of bovine L-OPN in infant formula.

2. Materials and Methods

2.1. Materials

L-OPN (Lacprodan OPN-10, protein content 90%, purity > 95%) was provided by Arla Food Ingredients Group (Beijing, China). Milk protein concentrate (MPC) and whey protein isolate (WPI) were purchased from Agropur Dairy (Edmonton, AB, Canada). Paraformaldehyde was purchased from Servicebio Co., Ltd. (Wuhan, China). The rat bone alkaline phosphatase (BALP) and Type I collagen cross-linked carboxyl-terminal peptide (CTX-I) Enzyme-linked immunosorbent assay (ELISA) kit was purchased from Elabscience Biotechnology Co., Ltd. (Wuhan, China). Animal RNA extraction kit, All-in-one RT SuperMix for qPCR and SYBR Mix were purchased from Vazyme Biotechnology Co., Ltd. (Nanjing, China). The PCR primers (specific sequence shown in Table S1) were purchased from Sangon Biotech Co., Ltd. (Shanghai, China); chromatographically pure methanol, acetonitrile and formic acid were purchased from Thermo Scientific (Waltham, MA, USA).

https://doi.org/10.3390/nu18081265

2.2. Animal Experimental Design

All animal experiment protocols were reviewed and approved by the Laboratory Animal Management and Animal Welfare Ethics Committee of Jiangnan University, with the ethics approval number JN.NO 20250515S0560720[268]. Based on the experimental results of similar studies, through the calculation of the G*Power 3.1 software: set $\alpha = 0.05$, $\beta = 0.8$, effect size d = 1.6, it was concluded that at least 8 animals are needed in each group. Twenty-four 3-week-old male SPF-grade Sprague-Dawley (SD) rats were purchased from Charles River Laboratory Animal Technology Co., Ltd. (SCXK (Zhejiang) 2021-0006) (Jiaxing, China). All the rats had free access to the same standard diet and drinking water throughout the experimental period. The ambient temperature was between 20 and 26 °C, and the relative humidity was between 40 and 70%. After adapting to the environment, the rats were randomly divided into three groups (n = 8 per group): (1) the control group (CON) was administered deionized water by gavage; (2) the protein matrix group (PRO) was administered 750 mg/kg·BW of a mixed-protein solution by gavage daily; (3) the L-OPN-fortified group (L-OPN) was administered 750 mg/kg·BW of the same protein matrix, fortified with L-OPN, by gavage daily.

The mixed-protein solution for both the PRO and L-OPN groups was formulated to simulate the whey protein-to-casein ratio (~60:40) found in mature human milk, a key compositional feature often referenced in infant formula design [15]. This matrix was prepared by mixing milk protein concentrate (MPC) and whey protein isolate (WPI) in an equal mass ratio. It is important to note that this experimental matrix was designed specifically to model the protein fraction of human milk/infant formula and does not replicate the full nutritional profile of a commercial infant formula, including its energy density, carbohydrate and fat content, vitamin/mineral fortification, or specific processing conditions. All the animals had ad libitum access to a standard, nutritionally complete rodent diet (e.g., AIN-93G) to meet their basal nutritional requirements. The L-OPN group received the identical PRO matrix supplemented with purified L-OPN to achieve a final dose of 15 mg/kg·BW.

The body weight of the rats was recorded weekly. The experiment was ended after continuous intragastric administration for 4 weeks. Feces were collected. Blood was drawn from the abdominal aorta under isoflurane anesthesia and the rats were sacrificed. The tissues of the femur, liver, kidney, spleen and intestine were dissected and collected.

2.3. Determination of Serum Bone Metabolism Markers

The measurement of BALP and CTX-I in rat serum was performed using ELISA kits (see Section 2.1) and was performed in accordance with the instructions provided by the manufacturer.

2.4. Micro-CT

Micro-CT testing on femurs was performed according to the method previously described [15], with slight modifications. The isolated femurs were fixed in 4% paraformaldehyde solution for 24–48 h and subsequently rinsed three times with PBS solution. The specimens were then stored in 75% alcohol solution at 4 °C until future use. The processed femurs were scanned using the Bruker SkyScan 1276 small animal scanning imaging system (Kontich, Belgium) at a resolution of 18 μm, voltage of 65 kV, current of 385 μA, and a 1 mm Al filter. The scanning mode was high-resolution mode and the scanning time was 4 min. Three-dimensional reconstruction was carried out using scanning data, and the microstructure parameters of the bone tissue in the target area were analyzed by system analysis software.

https://doi.org/10.3390/nu18081265

2.5. Determination of Apparent Indicators of the Femur

Fresh femurs separated were weighed using an analytical balance, and the length, width and thickness of the femurs were measured with a vernier caliper. After the femurs were dried at 105 °C to a constant weight, the backbone weight of the femurs was determined.

2.6. Determination of Mechanical Properties of the Femur

The TA.XT plus texture analyzer (Stable Micro Systems, Godalming, UK) was used for the three-point bending of femurs according to the method previously described [16]. Briefly, a 12 mm span (HDP/3PB fixture) and a cross-head speed of 0.6 mm/min were used, with the load applied consistently to the mid-diaphysis. Load–deflection curves were analyzed to obtain the elastic limit load, peak load (N), and the deflection at peak load (mm).

2.7. RNA Extraction from Bone Tissue and qPCR

The total RNA of the bone tissue was extracted using the FastPure Plant Total RNA Isolation Kit, with the operation carried out in accordance with the manufacturer's instructions. The purity and concentration of the extracted RNA were determined using Nanodrop. Complementary DNA was synthesized from qualified samples using HiScript III All-in-one RT SuperMix (Vazyme Biotech, Nanjing, China). DNA was obtained after 20 μL of the reaction system was subjected to a reaction procedure at 50 °C for 15 min and 85 °C for 5 s. A RT-qPCR analysis was performed using SYBR Mix (Vazyme Biotech, Nanjing, China). Pre-denaturation was carried out at 95 °C for 5 min, denaturation for 15 s, and annealing for 30 s at 60 °C. The number of cycles was 40. Taking β-actin as the internal reference gene, relative quantification was performed using the $2^{-\Delta\Delta Ct}$ method [17]. The primers used in the experiments of this chapter are shown in Table S1.

2.8. Amplification of 16S rRNA V3-V4 Gene, Library Construction and Sequencing Analysis

The experimental procedure was conducted according to the method of previous studies [18,19]. Fecal DNA from the rats was extracted using a commercial kit and assessed for purity and concentration via agarose gel electrophoresis. An aliquot of each DNA sample was diluted with sterile water to 1 ng/μL. A polymerase chain reaction (PCR) was performed using the diluted genomic DNA as template; barcode-indexed specific primers; a High-Fidelity PCR Master Mix with GC Buffer; and a high-efficiency, high-fidelity enzyme. The resulting PCR products were electrophoresed on a 2% agarose gel, and those that passed quality control were purified using magnetic beads. The purified products were quantified enzymatically, and the samples were pooled in equal amounts based on their respective PCR product concentrations. The pooled mixture was re-analyzed by 2% agarose gel electrophoresis, and target bands were excised and recovered using a Qiagen gel extraction kit (Hilden, Germany).

A sequencing library was constructed with the TruSeq® DNA PCR-Free Sample Preparation Kit (San Diego, CA, USA). The final libraries were quantified using Qubit and quantitative PCR (Q-PCR). Upon passing quality inspection, the libraries were sequenced on the NovaSeq6000 platform. Offline sequencing data were demultiplexed according to the barcode and primer sequences, followed by removal of these adapter sequences. A sequence analysis was performed by the Uparse software (Uparse v7.0.1001, http://drive5.com/uparse/, accessed on 15 August 2025). Sequences with ≥97% similarity were assigned to the same OTUs. Representative sequence for each OTU was screened for further annotation. Amplicon sequence variants (ASVs) were analyzed by Deblur (1.1.0), which uses error profiles to obtain putative error-free sequences from the Illumina sequencing

platform. For each representative sequence, the Silva Database (http://www.arb-silva.de/) was used based on the Mothur algorithm to annotate taxonomic information. In order to study the phylogenetic relationship of different OTUs, and the difference in the dominant species in different samples (groups), multiple sequence alignments were conducted using the MAFFT (v7.490, https://mafft.cbrc.jp/alignment/software/, accessed on 15 August 2025). OTU abundance information was normalized using a standard of sequence number corresponding to the sample with the fewest sequences. Subsequent analyses of alpha diversity and beta diversity were all performed based on this output-normalized data. A sample diversity analysis was conducted with the phyloseq (v1.40.0) and vegan (v2.6.2) packages in R (v4.2.0). LEfSe (v1.1.2) was used for linear discriminant analysis effect size (LEfSe) analysis, with the LDA score threshold set to 2. Intergroup differences in species abundance were assessed using *t*-tests in R, and corresponding plots were generated.

2.9. Determination of Metabolomics in Serum

Metabolomics analysis in serum was conducted according to the method described in previous studies [20,21]. After thawing on ice, the serum samples were vortexed for 10 s to ensure homogeneity. A 50 μL aliquot was transferred into a labeled centrifuge tube, followed by the addition of 300 μL of 20% acetonitrile in a methanol solution containing internal standards. The mixture was vortexed for 3 min. Both the fecal and serum samples were then centrifuged at 12,000× *g* for 10 min at 4 °C. A 300 μL portion of the supernatant was transferred to a new labeled tube and recentrifuged under the same conditions for 3 min. Finally, 200 μL of supernatant was collected into a corresponding vial insert for LC-MS analysis.

All the samples were analyzed using two complementary LC-MS methods. Chromatographic separation was performed on a Waters ACQUITY Premier HSS T3 column (1.8 μm, 2.1 × 100 mm) with mobile phase A (0.1% formic acid in water) and B (0.1% formic acid in acetonitrile). The MS section alternated between full-scan MS and data-dependent MS^n scans using dynamic exclusion. Analysis was conducted on a Q Exactive HF-X mass spectrometer equipped with electrospray ionization in both positive and negative modes. Full scan spectra were acquired from m/z 75–1000 at a resolution of 35,000.

Raw data were converted to the mzXML format using ProteoWizard. Peak detection, alignment, and retention time correction were performed with XCMS. Peaks with a missing rate > 50% within any sample group were filtered out. Missing values were imputed using a KNN algorithm for values with ≤50% missingness, or replaced with 1/5 of the minimum value for those exceeding 50%. Peak areas were normalized by support vector regression (SVR).

An unsupervised PCA (principal component analysis) was performed by the statistics function prcomp within R (www.r-project.org). The data was unit variance-scaled before the unsupervised PCA. For two-group analysis, differential metabolites were determined by VIP (VIP > 1) and *p*-value (*p*-value < 0.05, Student's *t* test). VIP values were extracted from the OPLS-DA result, which also contains score plots and permutation plots, and was generated using the R package MetaboAnalystR. The data was log-transformed (log2) and mean-centered before OPLS-DA. In order to avoid overfitting, a permutation test (200 permutations) was performed. Identified metabolites were annotated using the KEGG Compound database (http://www.kegg.jp/kegg/compound/, accessed on 15 August 2025), and annotated metabolites were then mapped to the KEGG Pathway database (http://www.kegg.jp/kegg/pathway.html, accessed on 15 August 2025). Significantly enriched pathways were identified with a hypergeometric test's *p*-value for a given list of metabolites.

2.10. Molecular Docking

The molecular structures of the FXR (PDB ID: 3DCT) and TGR5 (PDB ID: 7DW0) were downloaded from the RCSB protein database (https://www.rcsb.org/). Before docking, water molecules and irrelevant atoms were removed. 12-KLCA structures were downloaded from https://hmdb.ca/metabolites, accessed on 25 December 2025. Virtual screening was performed using AutoDock Vina 1.2 [22]. For each protein–ligand complex, the search algorithm generated nine distinct binding poses. The docking grid box was centered on the active site. All the generated poses were ranked by their predicted binding affinity (expressed in kcal/mol). The pose with the most negative docking score was selected as the representative conformation for further analysis, including visualization of binding modes and characterization of non-covalent interactions.

2.11. Statistical Analysis

Data are expressed in the form of mean ± standard deviation (Mean ± SD). Normality was assessed using the Shapiro–Wilk test, and homogeneity of variances was evaluated by Levene's test. Since the data met the assumptions of normality and equal variance, the differences among more than two groups were calculated using one-way ANOVA followed by Duncan's multiple range test (the figures in Sections 3.1–3.4). An unpaired two-tailed Student's *t*-test was used to compare the means between the two groups (the figures in Sections 3.5 and 3.6). A *p*-value < 0.05 was considered statistically significant (* $p < 0.05$, ** $p < 0.01$, *** $p < 0.001$). All the statistical analyses were performed using GraphPad Prism version 8.0. Data points that were extreme outliers, defined as those deviating from the intra-group mean by more than ±3 standard deviations, were excluded.

3. Results and Discussion

3.1. The Effect of L-OPN-Fortified Formula on the Growth Performance of Rats

As shown in Figure 1a, the body weight gain trends of the CON, PRO and L-OPN groups were similar throughout the experimental period. The final body weight of the L-OPN group increased by 7.1% and 5.3% compared to the CON and PRO groups, respectively (Figure 1b). However, these differences were not statistically significant ($p > 0.05$). In contrast to body weight, body length for the L-OPN group increased significantly ($p < 0.001$) by 8.8% and 5.6% compared with the CON and PRO groups, respectively (Figure 1c). This selective stimulation of longitudinal growth by L-OPN suggests a targeted anabolic effect on the growth plate rather than a general nutritional boost. Notably, the magnitude of body length increase exceeds what would be expected from protein intake alone, implying that L-OPN may modulate endochondral ossification pathways. This aligns with emerging evidence that L-OPN can directly interact with chondrocytes to enhance proliferation and matrix mineralization during skeletal development [3]. Importantly, the absence of hepatorenal toxicity or immune organ hypertrophy further supports the safety profile of L-OPN fortification in infant formula. The organ index results are presented in Figure 1d–g. No significant differences ($p > 0.05$) were observed among the three groups in terms of the weight ratios of liver, kidney, spleen, or muscle, suggesting that systemic metabolic balance was not affected.

https://doi.org/10.3390/nu18081265

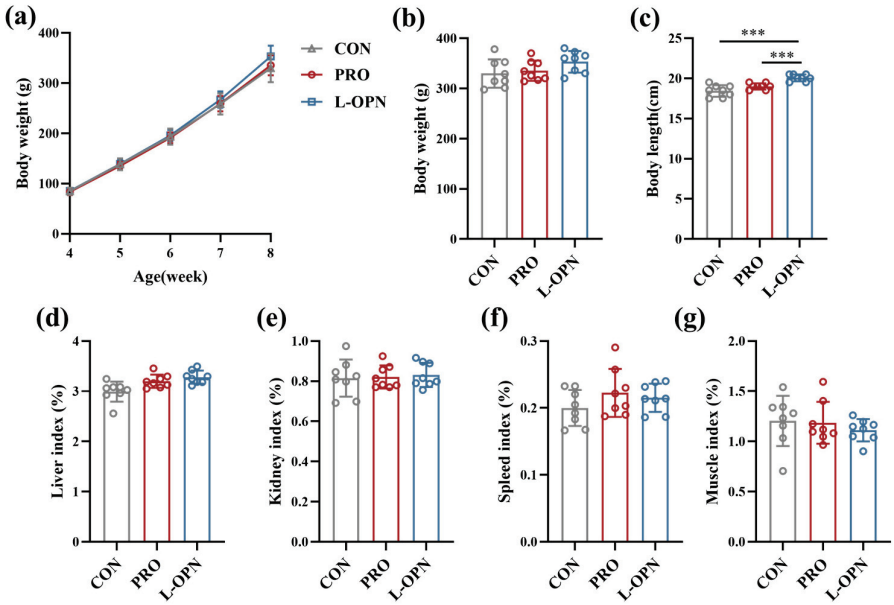


Figure 1. Growth performance of rats in the CON, PRO and L-OPN groups: (**a**) changes in rat body weight; (**b**) he final body weight of rats; (**c**) the body length of rats; (**d**) liver index; (**e**) kidney index; (**f**) Spleen index; (**g**) muscle index; *** $p < 0.001$.

3.2. The Effect of L-OPN-Fortified Formula on Serum Bone Metabolism Indicators

Given that body length growth mainly reflects the efficiency of longitudinal bone development, this study evaluated serum bone metabolism markers to further elucidate the underlying mechanism. As shown in Figure 2, serum BALP content in the L-OPN group was significantly ($p < 0.05$) increased by 23.1% compared with the PRO group. In addition, the bone resorption marker CTX-I was also significantly increased, by 11.5% ($p < 0.05$). These results indicate that the L-OPN-fortified formula simultaneously enhances both osteoblastic and osteoclastic activities, thereby comprehensively promoting bone turnover. This pattern aligns with the high-turnover metabolic state characteristic of growing bone and suggests that accelerated bone remodeling provides sustained matrix support for longitudinal bone growth [23].

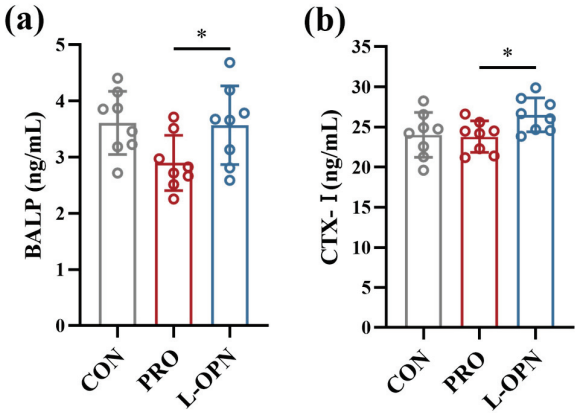


Figure 2. Serum bone metabolism indicators of rats in the CON, PRO and L-OPN groups. The content of (**a**) BALP; (**b**) content of CTX-I; * $p < 0.05$.

3.3. The Effect of L-OPN-Fortified Formula on Bone Characteristics

Femoral phenotypic analysis further revealed the unique regulatory mechanism of L-OPN in the mixed protein system. As shown in Figure 3, compared with the CON group, the L-OPN group had significantly ($p < 0.05$) higher femoral mass. Moreover, relative to the PRO group, femoral length, thickness and wet weight in the L-OPN group were

significantly higher ($p < 0.05$), by 3.9%, 4.4% and 15.8%, respectively, whereas femoral width and dry weight showed slight, non-significant increases ($p > 0.05$). Of note, L-OPN intervention alone selectively promotes longitudinal growth, increasing length by 5.8% without altering width [4], whereas in the mixed-protein system, both longitudinal and transverse bone development were enhanced simultaneously (Figure 3c,d). This difference suggests that within a breast milk-simulating protein matrix, L-OPN and other milk proteins may release novel bioactive peptides through co-digestion, thereby potentially activating periosteal osteogenesis and contributing to lateral bone mass accumulation.

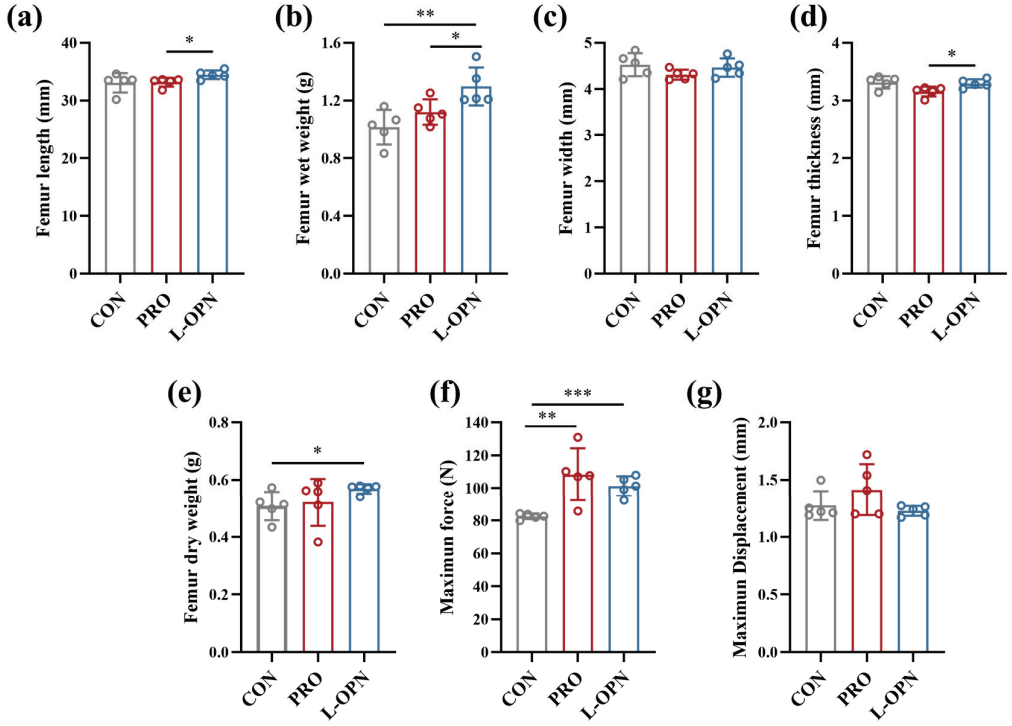


Figure 3. Bone characteristics of rats in the CON, PRO and L-OPN groups. (**a**) Femoral length; (**b**) Femoral wet weight; (**c**) Femoral dry weight; (**d**) Femoral width; (**e**) Femoral thickness; (**f**) Maximum force; (**g**) Maximum displacement; * $p < 0.05$, ** $p < 0.01$, *** $p < 0.001$.

The biomechanical properties of the femur are critical for motor function and the stability of the skeletal system [24]. As shown in Figure 3f,g, compared with the CON group, the maximum load increased significantly in both the PRO and L-OPN groups ($p < 0.05$). No significant differences were observed in maximum load or maximum deflection between the L-OPN and PRO groups ($p > 0.05$). These results indicate that supplementation with dairy protein enhances bone strength. Moreover, within the protein matrix, L-OPN promoted both longitudinal growth (Figure 3a) and transverse development (Figure 3d) of the femur while maintaining its intrinsic strength (Figure 3f) and toughness (Figure 3g). We hypothesize that the hydrolysis of caseins and/or whey proteins in the presence of L-OPN activates osteoprogenitor cells, thereby stimulating bone growth. This mirrors the bioefficacy of human milk components. The preserved biomechanical properties (Figure 3f,g) confirm that accelerated growth does not compromise structural integrity.

3.4. The Effect of L-OPN-Fortified Formula on Bone Microstructure

Three-dimensional reconstruction and quantitative analysis showed that compared with the CON group, the PRO intervention did not significantly alter femoral microstructure (Figure 4). In contrast, the L-OPN group markedly improved femoral microarchitecture: bone volume fraction increased by 31.0% relative to the PRO group ($p < 0.01$), the thickness

and quantity of trabecular bone increased by 8.7% and 15.2% ($p < 0.05$) respectively, and the trabecular separation decreased by 20.5% ($p < 0.05$). Moreover, compared with the CON group, L-OPN significantly increased bone volume ($p < 0.001$) and trabecular bone quantity ($p < 0.01$).

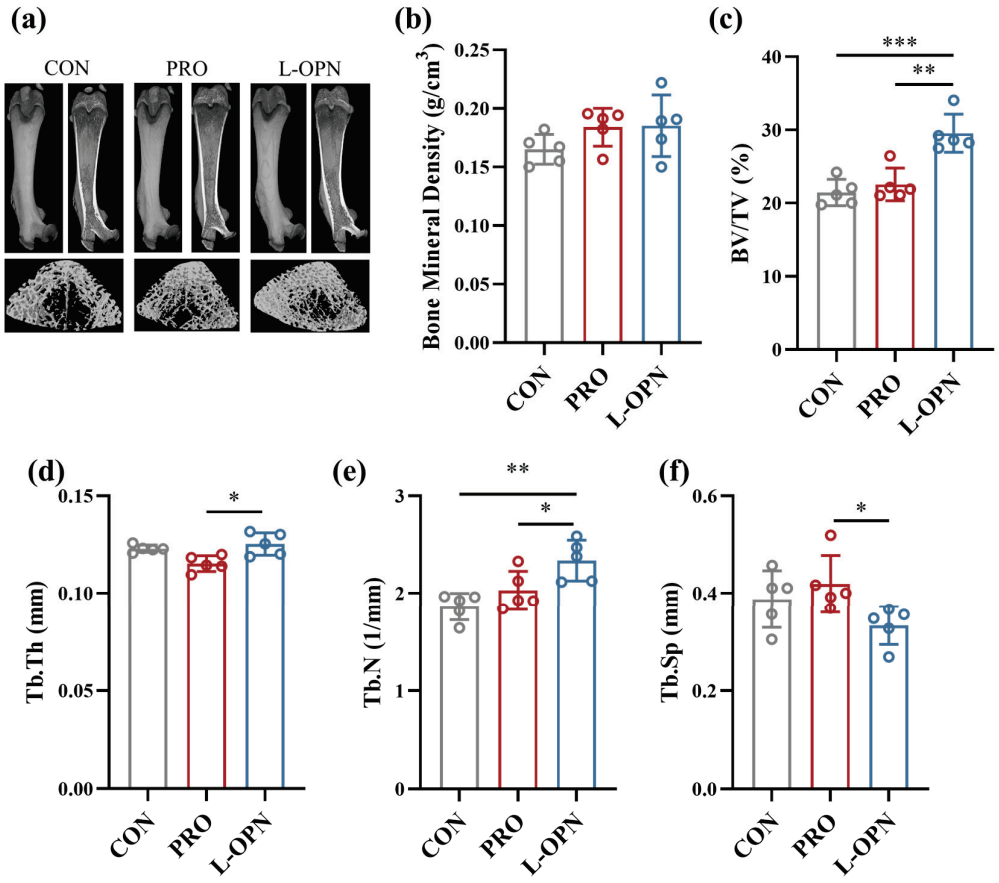


Figure 4. Femoral microstructure of rats in the CON, PRO and L-OPN groups: (**a**) three-dimensional reconstruction image of the femur; (**b**) bone mineral density of rat femur; (**c**) bone volume; (**d**) trabecular bone thickness; (**e**) the number of trabeculae; (**f**) trabecular bone separation degree; * $p < 0.05$, ** $p < 0.01$, *** $p < 0.001$.

Three-dimensional reconstruction further indicated a pronounced reduction in medullary cavity volume. This pattern exhibits dual regulatory characteristics: similar to L-OPN intervention alone, it stimulates bone volume accumulation by promoting trabecular bone formation; unlike L-OPN alone, it simultaneously enhances the thickness of existing trabeculae. These findings align with previous reports on bovine colostrum protein, containing L-OPN, in mitigating bone loss in ovariectomized models [25]. The observed decrease in medullary cavity volume indicates the occurrence of endocortical apposition, a process that has been demonstrated to enhance the cross-sectional area and bending resistance of the structure [15]. Collectively, these microarchitectural enhancements provide a structural foundation for the observed increases in femoral mass and biomechanical competence, thereby emphasizing L-OPN potential not only in promoting growth but also in preventing age- or disease-related trabecular deterioration.

3.5. The Effect of L-OPN-Fortified Formula on Gut Microbiota

L-OPN may promote bone growth and development by modulating the intestinal microbiota composition [3]. In this study, we also assessed changes in the gut microbiota of rats following intervention with the L-OPN-fortified formula. The diversity of the composi-

tion of intestinal flora in rat feces was analyzed, as shown in Figure 5a–c. α-Diversity is an indicator that describes the richness, uniformity and distribution of species in microbial communities [26], whereas β-diversity quantifies the differences in species diversity among different samples [27]. The L-OPN-fortified formula had no significant effect on the α-diversity indices, i.e., the Chao1, Shannon, and Simpson indices ($p > 0.05$). This was similar to the result that there was no significant change in the α-diversity of the intestinal microbiota in obese pregnant mice after L-OPN intervention [28]. However, L-OPN fortification significantly increased β-diversity (Figure 5d, $p < 0.05$), confirming the overall reconstruction of the microbiota structure. To clarify the specific changes in the intestinal microbiota, the composition at the phylum level was analyzed, with results shown in Figure 5e–h. *Firmicutes* and *Bacteroides* are the two dominant phyla. The abundance ratio (B/F) of these two phyla is often used to assess the balance of the intestinal microbiota. Intervention with the L-OPN-fortified formula significantly increased the abundance of *Bacteroidetes* (by 25.2%, $p < 0.01$), while significantly reducing the abundance of *Firmicutes* (by 12.8%, $p < 0.05$), resulting in a significant increase of 43.6% in the B/F ratio ($p < 0.01$). This indicates that in the complex protein system simulating breast milk, L-OPN-fortified intervention significantly regulates the diversity and composition of the intestinal flora in growing rats.

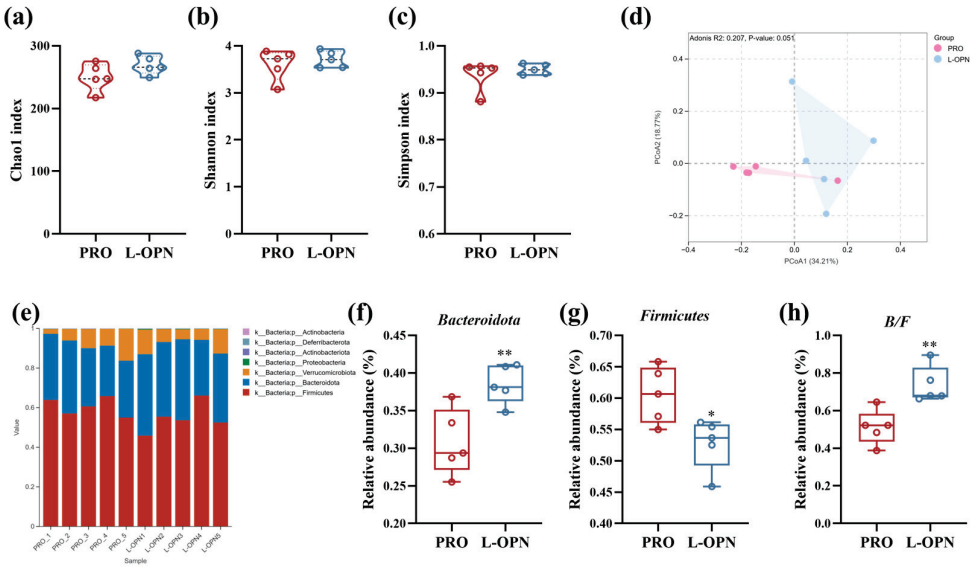


Figure 5. Intestinal flora composition of rats in the CON, PRO and L-OPN groups: (**a**) Chao1 index; (**b**) Shannon index; (**c**) Simpson index; (**d**) β diversity; (**e**) accumulation diagram of microbiota composition; (**f**) relative abundance of *Bacteroidota*; (**g**) relative abundance of *Firmicutes*; (**h**) *Bacteroidota/Firmicutes*; * $p < 0.05$, ** $p < 0.01$.

The LEfSe analysis further identified the key responding microbiota (Figure 6). In the L-OPN group, the genera that contributed the most to the difference (LDA > 3) were *Bacteroides* and *Parabacteroides*, respectively. The most contributing bacterial species (LDA > 3) were *Bacteroides uniformis*, *Parabacteroides distasonis* and *Parabacteroides sp CT06*. As shown in Figure 6b–f, compared with the control group, the relative abundances of the above-mentioned genera/species in the L-OPN group were significantly increased ($p < 0.05$). Among them, the abundance of *Parabacteroides*, *Parabacteroides_distasonis* and *Parabacteroides_sp_CT06* increased significantly, increasing by 83%, 119% and 123% respectively. This result is consistent with the findings in a previous study that L-OPN intervention promotes an increase in *Parabacteroides* abundance [3], indicating that in the complex protein system, L-OPN can still exert regulatory effects on specific intestinal microbiota.

https://doi.org/10.3390/nu18081265

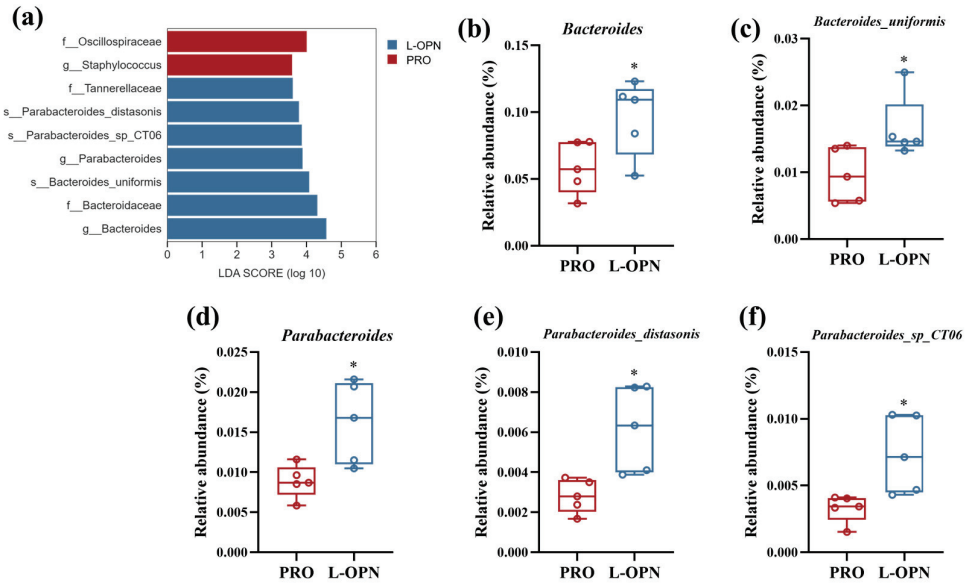


Figure 6. The relative abundance of different bacterial genera/species: (**a**) LEfSe diagram of the microbiota; relative abundance of (**b**) *Bacteroides*; (**c**) *Bacteroides_uniformis*; (**d**) *Parabacteroides*; (**e**) *Parabacteroides_distasonis* relative abundance; (**f**) *Parabacteroides_sp_CT06*. * $p < 0.05$.

A correlation analysis was conducted on the important differentially expressed intestinal microbiota and skeletal indicators screened out above. The heat map (Figure 7) showed that, except for serum bone metabolism indicators (BALP, CTX-I) and trabecular bone separation, all the other apparent indicators were significantly positively correlated with the abundance changes in representative intestinal flora genera/species. Among them, *Parabacteroides* showed a very strong positive correlation with bone development indicators: body length (r = 0.72, $p < 0.05$), femoral thickness (r = 0.89, $p < 0.01$), bone volume (r = 0.77, $p < 0.05$), and trabecular bone thickness (r = 0.95, $p < 0.001$). These correlations suggest an association between the genus Parabacteroides (especially *Parabacteroides distasonis*) and bone development. The specific enrichment of Parabacteroides, particularly *Parabacteroides distasonis*, as a known producer of secondary bile acids, is consistent with a potential role between L-OPN, microbial metabolism, and bone anabolism. *Parabacteroides distasonis* has been demonstrated to enhance intestinal barrier function and suppress systemic inflammation [14], both of which are conducive to osteoblast activity [29]. Furthermore, its capacity to deconjugate and transform primary bile acids into bioactive secondary forms [30] may directly influence the bile acid–bone signaling axis identified in our metabolomics data. Our data reveal an associative interaction (L-OPN–*Parabacteroides*–bile acid–bone), which demonstrates the capacity of dietary proteins to manifest systemic effects that are associated with gut microbes.

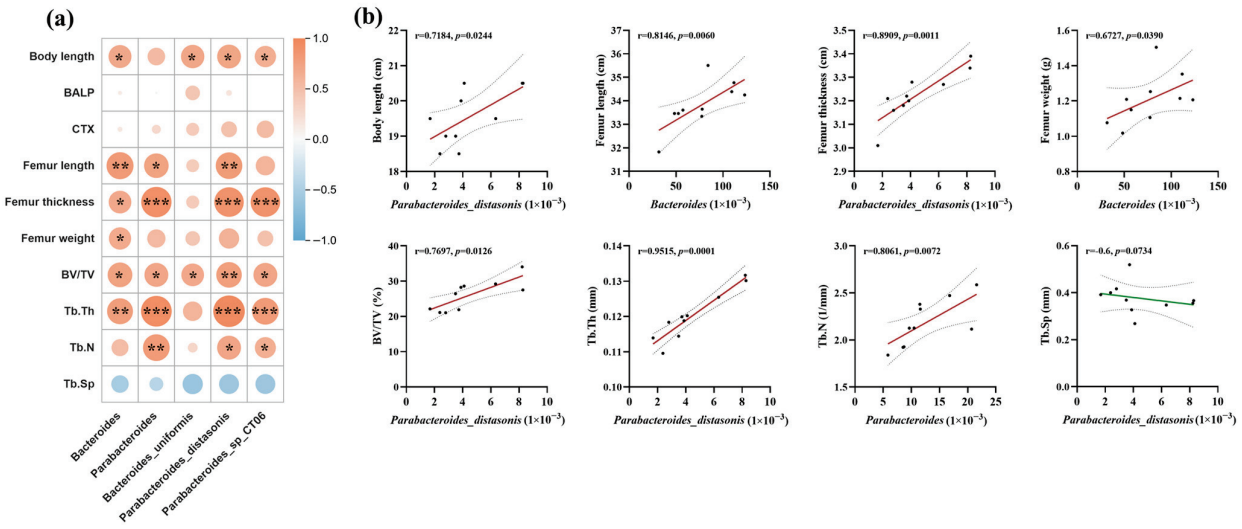


Figure 7. Correlation analysis of differential bacterial genera/species and skeletal indicators: (**a**) Correlation analysis heat map: The color of the graph within the grid reflects the degree of correlation. Red indicates a positive correlation, while blue indicates a negative correlation. The darker the color (the larger the circle), the greater the absolute value of the correlation. Asterisks indicate a significant correlation, with * $p < 0.05$, ** $p < 0.01$, and *** $p < 0.001$. (**b**) Correlation scatter plot, including correlation coefficients and significance, with solid lines representing linear fitting curves and dashed lines representing 95% confidence intervals, every dot represents a sample of a rat.

3.6. The Effect of L-OPN-Fortified Formula on Serum Metabolites

To explore whether the changes in the composition of the intestinal microbiota after L-OPN intervention would regulate bone metabolism by regulating serum metabolites, non-target metabolomics analysis was conducted on serum samples. The two-dimensional score graph of the orthogonal partial least squares discriminant analysis (OPLS-DA) model shows (Figure 8a) that there are significant differences in the metabolic profiles between the L-OPN-fortified group and the control group. Metabolic set enrichment analysis (MSEA) revealed that the top three metabolic sets in terms of significance were primary bile acid biosynthesis, steroid biosynthesis, and retinol metabolism (Figure 8b). Based on the difference multiple and significance (Fold Change > 2, $p < 0.05$), 32 significantly upregulated metabolites and 12 significantly downregulated metabolites were identified in the L-OPN enhancement group (Figure 8c). Based on the KEGG database annotations, significantly altered metabolites were categorized into functional pathways. As illustrated in Figure 8d, 84.6% of these metabolites are associated with metabolic pathways. The Sankey plot (Figure 8e) also presented the same result, and the significant differences in metabolites were found in the glycerophospholipid metabolic pathway. It was found that only the L-OPN intervention led to an increase in the abundance of *Parabacteroides*, promoting the metabolism of bile acids and resulting in a significant enrichment of serum differential metabolites in the pathways related to fat digestion and absorption (Figure 8c). Therefore, this study further focused on the changes in bile acid metabolism to explore its potential regulatory mechanism on bone metabolism under L-OPN intervention.

As shown in Figure 9a, a total of 31 bile acids were identified. Among them, Lithocholic acid (LCA) and 12-Ketolithocholic acid (12-KLCA), Sulfoglycolithocholate (SLCG-SO_3), 7-Ketolithocholic acid (7-KLCA) and Cholic acid (CA) exhibited the highest peak areas, indicating their relatively abundant accumulation or strong ionization response under the analytical conditions. Compared with the CON group, the total bile acid content in the serum of rats in the L-OPN group (23.06 ± 1.85 μmol/L) was significantly increased by 18.7% ($p < 0.001$). The level of CA increased extremely significantly by 94.9% ($p < 0.01$), and the level of 12-KLCA was also significantly upregulated, by 91.1% ($p < 0.05$). CA has physi-

ological activities such as maintaining bile acid homeostasis, improving inflammation, and protecting nerves. Clinically, CA is used to treat cholestatic diseases, which can improve lipid metabolism and prevent liver damage [31]. CA also suppresses osteoclast differentiation by inhibiting the AMPK signaling pathway [32]. 12-KLCA is an anti-inflammatory secondary bile acid derived from the microbiota that targets and regulates group 3 innate lymphoid cells (ILC3s), and it is a potential intervention molecule for ulcerative colitis [33] and metabolic diseases [34]. The gut microbiota are involved in the metabolism of bile acids. The results of the correlation analysis also showed (Figure 9c,d) that the level of bile acids was significantly correlated with the relative abundance of *Bacteroides* (r = 0.82, $p < 0.01$), and was also significantly positively correlated with the abundance of *Parabacteroides distasonis* (r = 0.83).

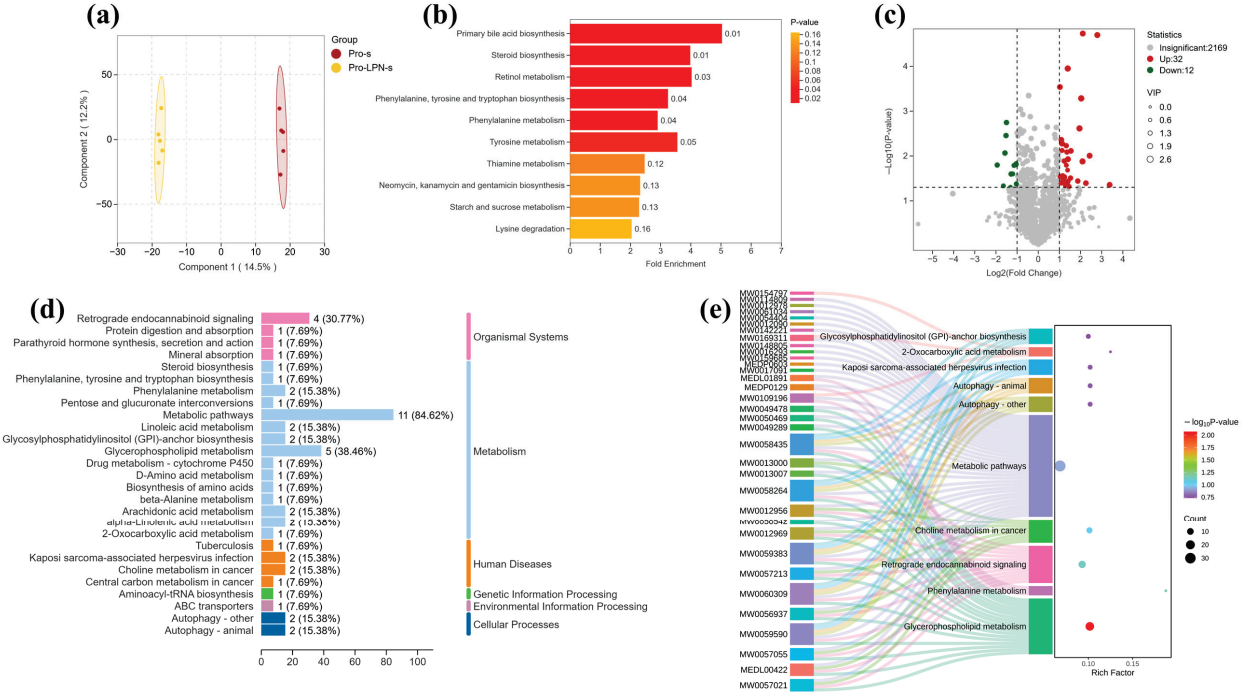


Figure 8. Serum metabolite composition of rats in the PRO and L-OPN groups. Serum metabolite (**a**) OPLS-DA graph; (**b**) MSEA enrichment analysis chart; (**c**) volcano map; classification of serum differential metabolites (**d**) metabolite pathways; (**e**) KEGG Sankey bubble chart.

Certain specific bile acids have also been confirmed to have the function of regulating bone metabolism. For instance, chenodeoxycholic acid can activate the differentiation of bone marrow stem cells into osteoblasts mediated by *Runx2* while inhibiting the generation of adipocyte-like phenotypes [35]. Intervention with 200 mg/kg taurodeoxycholic acid for four weeks can significantly increase the femoral bone volume and bone mineral density of mice [36]. Therefore, a correlation analysis was conducted between bile acid levels and bone indicators (Figure 10). The results indicated that body length, bone volume, and trabecular bone separation were significantly correlated with bile acid levels. Among them, the level of 12-KLCA was positively correlated with body length (r = 0.78, $p < 0.01$) and bone volume (r = 0.77, $p < 0.05$), and significantly negatively correlated with trabecular bone separation degree (r = 0.77, $p < 0.01$). This suggests that the observed changes in bile acids, particularly 12-KLCA, may be associated with the metabolic conditions of bone.

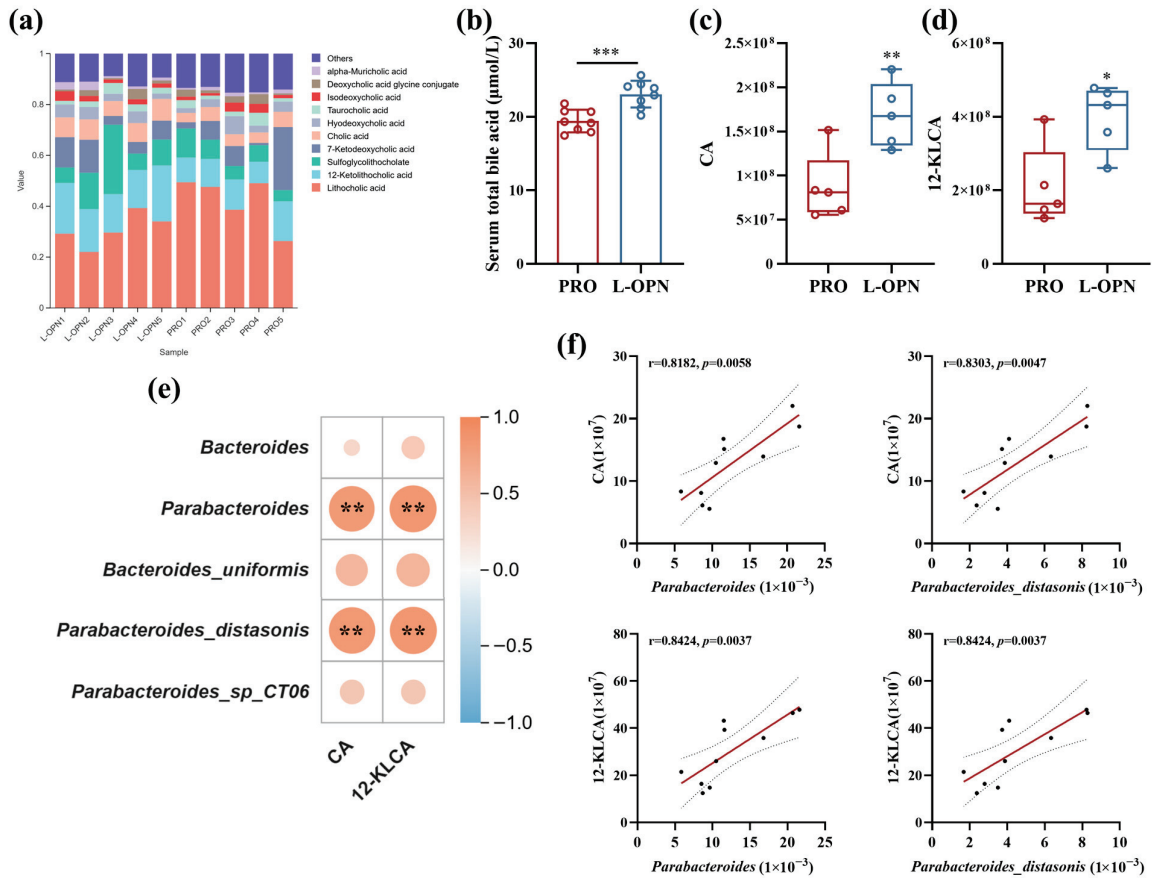


Figure 9. Analysis of the composition of serum bile acids and their correlation with intestinal flora: (**a**) serum bile acid profile; (**b**) serum total bile acid content; (**c**) serum bile acid response value; (**d**) serum 12-ketocholic acid response value; correlation between serum differential bile acids and differential intestinal flora (**e**) heat map and (**f**) scatter plot. The color of the graph within the grid reflects the degree of correlation. Red indicates a positive correlation, while blue indicates a negative correlation. The darker the color, the greater the absolute value of the correlation. Solid lines represent linear fitting curves, and dashed lines represent 95% confidence intervals, every dot represents a sample of a rat. * $p < 0.05$, ** $p < 0.01$, *** $p < 0.001$.

The metabolic status of the bile acids was determined, and it was found that the bile acid transport receptors at the terminal ileum also changed (Figure S1). Among them, the gene expressions of *Asbt* and *Ostα* were upregulated by 1.42 times and 0.98 times respectively compared with the control group ($p < 0.001$), indicating that L-OPN promoted the reabsorption of the bile acids and the enterohepatic circulation, and optimized the metabolism of the bile acids. Bone cell membrane receptor *Tgr5* and nuclear receptor *Fxr* are important targets for bile acid regulation of bone metabolism [32].

The results of the molecular docking (Figure S1a,b) showed that 12-KLCA could interact with human TGR5 [37] and FXR [38], with binding energies of −6.1 kcal/mol and −7.8 kcal/mol, respectively. L-OPN enhancement significantly upregulated the expression of bile acid receptor *Fxr* (increased by 1.47 times, $p < 0.05$) and *Tgr5* (increased by 3.59 times, $p < 0.001$) in the femur. It also activated the expression of the downstream transcription factor *Runx2* (increasing by 2.57 times, $p < 0.001$). Ileal bile acid transporters (ASBT and OSTα) and bone FXR/TGR5 receptors create a coordinated signaling loop. 12-KLCA is a microbiota-derived secondary bile acid enriched in our study that correlates strongly with bone metrics and demonstrates favorable binding to TGR5 and FXR. TGR5 activates osteoblast differentiation via cAMP/PKA, while FXR suppresses osteoclastogenesis. Together, these findings position bile acids not merely as metabolic intermediates but as

potential endocrine mediators, thereby providing a plausible framework through which gut microbial activity could be translated into skeletal anabolism.

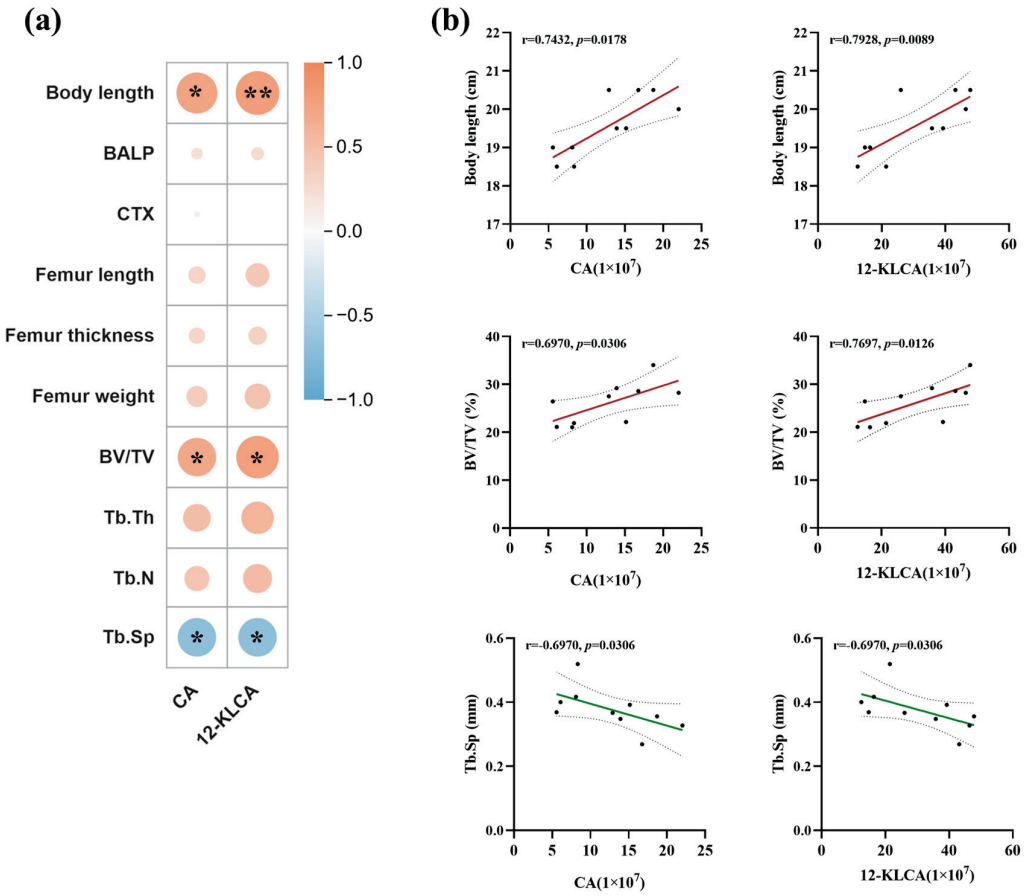


Figure 10. Correlation analysis of differential bile acids and bone indicators. Correlation between serum differential bile acids and femoral indicators (**a**) heat map and (**b**) scatter plot. The color of the graph within the grid reflects the degree of correlation. Red indicates a positive correlation, while blue indicates a negative correlation. The darker the color, the greater the absolute value of the correlation. Solid lines represent linear fitting curves, and dashed lines represent 95% confidence intervals, every dot represents a sample of a rat. * $p < 0.05$, ** $p < 0.01$.

In addition to the gut–bone axis pathway, which was identified in our previous studies [3,4], L-OPN may also be involved in bone regulation by promoting calcium absorption and generating osteogenic peptides. Consequently, we further validate the latter two mechanisms. As shown in Figure S2a–c, the L-OPN-fortified formula significantly upregulated ($p < 0.05$) the expression of genes related to calcium transmembrane transport (*Trpv6*, *Cacnald*, *Atp2b1*) and key protein genes of the cell bypass pathway (*Cldn15*, *Occludin*) in the jejunum of rats. However, no significant change was observed in the blood calcium level ($p > 0.05$), and although the bone mineral content slightly increased, the difference was not significant ($p > 0.05$). The above results indicate that promoting calcium absorption is not the main way for L-OPN to exert its bone-promoting effect. In addition, there was no significant difference in the content of L-OPN derived polypeptide WS7 in the serum of the two groups of rats ($p > 0.05$), and there was no significant correlation between the WS7 level and the body length, femoral length, and bone volume of the rats ($p > 0.05$), indicating that the bone growth promoting effect of the L-OPN-fortified formula was not related to WS7. Despite this, it cannot be ruled out that L-OPN may generate other polypeptides with osteogenic activity in the protein matrix. This hypothesis requires further experimental verification.

https://doi.org/10.3390/nu18081265

4. Conclusions

In conclusion, this study provides preliminary evidence that L-OPN-fortified formula is associated with the concurrent modulation of the gut microbiome, bile acid metabolism (notably 12-KLCA), and bone tissue, supporting healthy skeletal development in a juvenile rodent model. However, this study has several limitations that warrant consideration. First, the experiments were conducted in a rodent model; although growing rats are a well-established surrogate for infant skeletal development, translatability to human infants requires validation in clinical studies. Second, while we identified 12-KLCA as a potential mediator, causal evidence linking this bile acid metabolite to osteogenesis was not established; future studies using metabolite supplementation or receptor knockout models are needed. Finally, the protein matrix used herein simulates only key aspects of infant formula and does not fully recapitulate its complex composition (e.g., lipids, carbohydrates, and micronutrients), which may modulate L-OPN bioactivity in real-world formulations. Therefore, while L-OPN presents as a promising multifunctional nutritional component, its functional significance and true potential for infant health remain uncertain and warrant further investigation under more physiologically and clinically relevant conditions.

Supplementary Materials: The following supporting information can be downloaded at https://www.mdpi.com/article/10.3390/nu18081265/s1: Table S1: Primer sequence; Figure S1: Changes in bile acid metabolism. Molecular docking results of 12-KLCA with (a) TGR5 and (b) FXR; (c) Expression levels of genes related to ileal bile acid transport; (d) Expression levels of femoral bile acid receptors and downstream genes; * $p < 0.05$, *** $p < 0.001$; Figure S2: Changes in calcium and WS7 metabolism in rats. (a) Serum calcium content; (b) Bone mineral content; (c) Expression level of jejunal calcium transporter genes; (d) Serum WS7 content; (d–g) Correlation between the content of WS7 in rat serum and body length, femoral length and bone volume; * $p < 0.05$, ** $p < 0.01$, *** $p < 0.001$.

Author Contributions: Y.L.: conceptualization, writing—original draft, methodology, and investigation. J.Z.: writing—reviewing and editing, funding acquisition, and project administration. C.C.: investigation. X.T.: writing—reviewing and editing. P.H.: writing—reviewing and editing. F.L.: writing—reviewing and editing. R.H.: writing—reviewing and editing. T.H.: writing—reviewing and editing. X.W.: investigation. P.Z.: writing—reviewing and editing, funding acquisition, and project administration. All authors have read and agreed to the published version of the manuscript.

Funding: This work was supported by the National Key R&D Program of China (2022YFD2101504), the Basic Research Program of Jiangsu Province (BK20251621) and the Fundamental Research Funds for the Central Universities (JUSRP202416004).

Institutional Review Board Statement: The animal study protocol was approved by the Ethics Committee of Jiangnan University (protocol code: JN.NO 20250515S0560720[268] and date of approval: 23 May 2025).

Informed Consent Statement: Not applicable.

Data Availability Statement: The data presented in this study are available on request from the corresponding author due to being a part of an ongoing study.

Conflicts of Interest: P.H. and R.H. were employed by Biostime (Changsha) Nutrition Foods Limited. P.H., F.L. and R.H. were employed by Health and Happiness (H&H) China Limited. The remaining authors declare that the research was conducted in the absence of any commercial or financial relationships that could be construed as a potential conflict of interest.

References

1. Lind, M.V.; Larnkjær, A.; Mølgaard, C.; Michaelsen, K.F. Breastfeeding, Breast Milk Composition, and Growth Outcomes. In *Recent Research in Nutrition and Growth*; S. Karger AG: Basel, Switzerland, 2018; pp. 63–77. [CrossRef]
2. Schack, L.; Lange, A.; Kelsen, J.; Agnholt, J.; Christensen, B.; Petersen, T.E.; Sorensen, E.S. Considerable variation in the concentration of osteopontin in human milk, bovine milk, and infant formulas. *J. Dairy Sci.* **2009**, *92*, 5378–5385. [CrossRef]

3. Lyu, Y.; Hu, J.; Wang, X.; Zhang, J.; Li, X.; Cui, M.; Liu, D.; Tang, X.; Zhou, P. Bovine lactopontin promotes bone development in growing rats by altering the composition of intestinal flora and bile acid metabolism. *Food Funct.* **2025**, *16*, 928–942. [CrossRef]
4. Lyu, Y.; Hu, J.; Wang, X.; Zhang, J.; Li, X.; Cui, M.; Tang, X.; Zhou, P. Lactopontin regulates gut microbiota and calcium absorption to promote bone growth in growing rats. *Int. J. Biol. Macromol.* **2025**, *302*, 140557. [CrossRef] [PubMed]
5. Azuma, N.; Maeta, A.; Fukuchi, K.; Kanno, C. A rapid method for purifying osteopontin from bovine milk and interaction between osteopontin and other milk proteins. *Int. Dairy J.* **2006**, *16*, 370–378. [CrossRef]
6. Yamniuk, A.P.; Burling, H.; Vogel, H.J. Thermodynamic characterization of the interactions between the immunoregulatory proteins osteopontin and lactoferrin. *Mol. Immunol.* **2009**, *46*, 2395–2402. [CrossRef] [PubMed]
7. Liu, L.; Jiang, R.; Lonnerdal, B. Assessment of bioactivities of the human milk lactoferrin-osteopontin complex in vitro. *J. Nutr. Biochem.* **2019**, *69*, 10–18. [CrossRef]
8. Liu, L.; Jiang, R.; Liu, J.; Lonnerdal, B. The bovine Lactoferrin-Osteopontin complex increases proliferation of human intestinal epithelial cells by activating the PI3K/Akt signaling pathway. *Food Chem.* **2020**, *310*, 125919. [CrossRef]
9. Jiang, R.; Liu, L.; Du, X.; Lonnerdal, B. Evaluation of Bioactivities of the Bovine Milk Lactoferrin-Osteopontin Complex in Infant Formulas. *J. Agric. Food Chem.* **2020**, *68*, 6104–6111. [CrossRef]
10. Ceroni, C.; Dayon, L.; Van den Abbeele, P.; Roch, A.; Dervaux, J.; Ernest, M.; Sirugue, P.; Baudot, A.; Kraus, M.R.C.; Brandenberg, N.; et al. Lactoferrin-osteopontin complexes: Insights into intestinal organoid bioavailability and gut microbiota modulation. *Commun. Biol.* **2025**, *8*, 1017. [CrossRef]
11. Levy, E.; Marcil, V.; Tagharist Ep Baumel, S.; Dahan, N.; Delvin, E.; Spahis, S. Lactoferrin, Osteopontin and Lactoferrin-Osteopontin Complex: A Critical Look on Their Role in Perinatal Period and Cardiometabolic Disorders. *Nutrients* **2023**, *15*, 1394. [CrossRef]
12. Cai, J.; Sun, L.; Gonzalez, F.J. Gut microbiota-derived bile acids in intestinal immunity, inflammation, and tumorigenesis. *Cell Host Microbe* **2022**, *30*, 289–300. [CrossRef] [PubMed]
13. Xiang, T.; Deng, Z.; Yang, C.; Tan, J.; Dou, C.; Luo, F.; Chen, Y. Bile acid metabolism regulatory network orchestrates bone homeostasis. *Pharmacol. Res.* **2023**, *196*, 106943. [CrossRef]
14. Wang, K.; Liao, M.; Zhou, N.; Bao, L.; Ma, K.; Zheng, Z.; Wang, Y.; Liu, C.; Wang, W.; Wang, J.; et al. *Parabacteroides distasonis* Alleviates Obesity and Metabolic Dysfunctions via Production of Succinate and Secondary Bile Acids. *Cell Rep.* **2019**, *26*, 222–235. [CrossRef] [PubMed]
15. Bouxsein, M.L.; Boyd, S.K.; Christiansen, B.A.; Guldberg, R.E.; Jepsen, K.J.; Müller, R. Guidelines for assessment of bone microstructure in rodents using micro-computed tomography. *J. Bone Miner. Res.* **2010**, *25*, 1468–1486. [CrossRef] [PubMed]
16. Tang, X.; Li, S.; Sun, Y.; Zhang, Y.; Zhou, K.; Yu, Q. Evaluating the Activity of Sodium Butyrate to Prevent Osteoporosis in Rats by Promoting Osteal GSK-3 beta/Nrf2 Signaling and Mitochondrial Function. *J. Agric. Food Chem.* **2020**, *68*, 6588–6603. [CrossRef]
17. Bustin, S.A.; Benes, V.; Garson, J.A.; Hellemans, J.; Huggett, J.; Kubista, M.; Mueller, R.; Nolan, T.; Pfaffl, M.W.; Shipley, G.L.; et al. The MIQE Guidelines: Minimum Information for Publication of Quantitative Real-Time PCR Experiments. *Clin. Chem.* **2009**, *55*, 611–622. [CrossRef]
18. Avershina, E.; Frisli, T.; Rudi, K. De Novo Semi-alignment of 16S rRNA Gene Sequences for Deep Phylogenetic Characterization of Next Generation Sequencing Data. *Microbes Environ.* **2013**, *28*, 211–216. [CrossRef]
19. Callahan, B.J.; McMurdie, P.J.; Rosen, M.J.; Han, A.W.; Johnson, A.J.A.; Holmes, S.P. DADA2: High-resolution sample inference from Illumina amplicon data. *Nat. Methods* **2016**, *13*, 581–583. [CrossRef]
20. Thévenot, E.A.; Roux, A.; Xu, Y.; Ezan, E.; Junot, C. Analysis of the Human Adult Urinary Metabolome Variations with Age, Body Mass Index, and Gender by Implementing a Comprehensive Workflow for Univariate and OPLS Statistical Analyses. *J. Proteome Res.* **2015**, *14*, 3322–3335. [CrossRef]
21. Chen, Y.; Zhang, R.; Song, Y.; He, J.; Sun, J.; Bai, J.; An, Z.; Dong, L.; Zhan, Q.; Abliz, Z. RRLC-MS/MS-based metabonomics combined with in-depth analysis of metabolic correlation network: Finding potential biomarkers for breast cancer. *Analyst* **2009**, *134*, 2003–2011. [CrossRef]
22. Trott, O.; Olson, A.J. AutoDock Vina: Improving the speed and accuracy of docking with a new scoring function, efficient optimization, and multithreading. *J. Comput. Chem.* **2010**, *31*, 455–461. [CrossRef] [PubMed]
23. Stagi, S.; Cavalli, L.; Iurato, C.; Seminara, S.; Brandi, M.L.; De, M.M. Bone metabolism in children and adolescents: Main characteristics of the determinants of peak bone mass. *Clin. Cases Miner. Bone Metab.* **2013**, *10*, 172–179. [PubMed]
24. Tan, J.; Ng, C.-A.; Hart, N.H.; Rantalainen, T.; Sim, M.; Scott, D.; Zhu, K.; Hands, B.; Chivers, P. Reduced Peak Bone Mass in Young Adults with Low Motor Competence. *J. Bone Miner. Res.* **2023**, *5*, 665–677. [CrossRef] [PubMed]
25. Du, M.; Xu, W.; Yi, H.; Han, X.; Wang, C.; Zhang, L. Protective effects of bovine colostrum acid proteins on bone loss of ovariectomized rats and the ingredients identification. *Mol. Nutr. Food Res.* **2011**, *55*, 220–228. [CrossRef]
26. Klimenko, E.S.; Belkova, N.L.; Rychkova, L.V.; Darenskaya, M.A.; Tugarinova, O.A.; Semenova, N.V.; Savinova, Y.S.; Bugun, O.V.; Balzhirova, D.B.; Kolesnikova, L.I. Alpha Diversity Indices as Indicators of the Variability of Gut Microbiota in Obese Adolescents of Different Ethnicities. *Bull. Exp. Biol. Med.* **2024**, *176*, 176. [CrossRef]

27. Song, W.; Bai, Y.Y.; Hu, J.H.; Li, L.L.; He, W.W.; Liu, C.C.; Li, L.; Ning, X.; Zhu, L.N.; Cui, X.L.; et al. *Lactobacillus coryniformis* subsp. torquens inhibits bone loss in obese mice via modification of the gut microbiota. *Food Funct.* **2023**, *14*, 4522–4538. [CrossRef]
28. Han, L.; Li, Q.; Du, M.; Mao, X. Bovine milk osteopontin improved intestinal health of pregnant rats fed a high-fat diet through improving bile acid metabolism. *J. Dairy Sci.* **2024**, *107*, 24–39. [CrossRef]
29. Greenbaum, J.; Lin, X.; Su, K.-J.; Gong, R.; Shen, H.; Shen, J.; Xiao, H.-M.; Deng, H.-W. Integration of the Human Gut Microbiome and Serum Metabolome Reveals Novel Biological Factors Involved in the Regulation of Bone Mineral Density. *Front. Cell. Infect. Microbiol.* **2022**, *12*, 853499. [CrossRef]
30. Ezeji, J.C.; Sarikonda, D.K.; Hopperton, A.; Erkkila, H.L.; Cohen, D.E.; Martinez, S.P.; Cominelli, F.; Kuwahara, T.; Dichosa, A.E.K.; Good, C.E.; et al. *Parabacteroides distasonis*: Intriguing aerotolerant gut anaerobe with emerging antimicrobial resistance and pathogenic and probiotic roles in human health. *Gut Microbes* **2021**, *13*, 1922241. [CrossRef]
31. Polak, Y.; Van Dussen, L.; Kemper, E.M.; Vaz, F.M.; Klouwer, F.C.C.; Engelen, M.; Hollak, C.E.M. The clinical and biochemical effectiveness and safety of cholic acid treatment for bile acid synthesis defects: A systematic review. *Orphanet J. Rare Dis.* **2024**, *19*, 466. [CrossRef]
32. Li, Z.; Huang, J.; Wang, F.; Li, W.; Wu, X.; Zhao, C.; Zhao, J.; Wei, H.; Wu, Z.; Qian, M.; et al. Dual Targeting of Bile Acid Receptor-1 (TGR5) and Farnesoid X Receptor (FXR) Prevents Estrogen-Dependent Bone Loss in Mice. *J. Bone Miner. Res.* **2018**, *34*, 765–776. [CrossRef]
33. Li, N.; Ma, P.; Li, Y.; Shang, X.; Nan, X.; Shi, L.; Han, X.; Liu, J.; Hong, Y.; Li, Q.; et al. Gut microbiota-derived 12-ketolithocholic acid suppresses the IL-17A secretion from colonic group 3 innate lymphoid cells to prevent the acute exacerbation of ulcerative colitis. *Gut Microbes* **2023**, *15*, 2290315. [CrossRef]
34. Shang, X.; Fu, Y.; Wang, Y.; Yan, S. Ramulus Mori (Sangzhi) alkaloids ameliorate high-fat diet induced obesity in rats by modulating gut microbiota and bile acid metabolism. *Front. Endocrinol.* **2024**, *15*, 1506430. [CrossRef]
35. Id Boufker, H.; Lagneaux, L.; Fayyad-Kazan, H.; Badran, B.; Najar, M.; Wiedig, M.; Ghanem, G.; Laurent, G.; Body, J.J.; Journe, F. Role of farnesoid X receptor (FXR) in the process of differentiation of bone marrow stromal cells into osteoblasts. *Bone* **2011**, *49*, 1219–1231. [CrossRef]
36. Ahn, T.K.; Kim, K.T.; Joshi, H.P.; Park, K.H.; Kyung, J.W.; Choi, U.Y.; Sohn, S.; Sheen, S.H.; Shin, D.E.; Lee, S.H.; et al. Therapeutic Potential of Tauroursodeoxycholic Acid for the Treatment of Osteoporosis. *Int. J. Mol. Sci.* **2020**, *21*, 4274. [CrossRef]
37. Chen, G.; Wang, X.; Ge, Y.; Ma, L.; Chen, Q.; Liu, H.; Du, Y.; Ye, R.D.; Hu, H.; Ren, R. Cryo-EM structure of activated bile acids receptor TGR5 in complex with stimulatory G protein. *Signal Transduct. Target. Ther.* **2020**, *5*, 142. [CrossRef]
38. Akwabi-Ameyaw, A.; Bass, J.Y.; Caldwell, R.D.; Caravella, J.A.; Chen, L.; Creech, K.L.; Deaton, D.N.; Jones, S.A.; Kaldor, I.; Liu, Y.; et al. Conformationally constrained farnesoid X receptor (FXR) agonists: Naphthoic acid-based analogs of GW 4064. *Bioorganic Med. Chem. Lett.* **2008**, *18*, 4339–4343. [CrossRef]

Disclaimer/Publisher's Note: The statements, opinions and data contained in all publications are solely those of the individual author(s) and contributor(s) and not of MDPI and/or the editor(s). MDPI and/or the editor(s) disclaim responsibility for any injury to people or property resulting from any ideas, methods, instructions or products referred to in the content.

nutrients

MDPI

Article

Chlorophyll Supplementation Delays Aging in *Drosophila melanogaster* via Enhanced Stress Resistance and Detoxification Network Remodeling

Suxia Shen [1,2,3,4], Ning Xu [1,2,3,4], Zhaotian Yang [1,2,3,4], Zixuan Han [1,2,3,4], Lin Zeng [1,2,3,4], Ajibola Nihmot Ibrahim [1,2,3,4] and Yan Zhang [1,2,3,4,*]

[1] College of Food Science and Nutritional Engineering, China Agricultural University, Beijing 100083, China; shen_sx573776028@163.com (S.S.); siriussalazar@163.com (N.X.); yangzhaotian1997@163.com (Z.Y.); better2802@163.com (Z.H.); zenglin6016@163.com (L.Z.); aomawunmi@gmail.com (A.N.I.)
[2] Sanya Institute of China Agricultural University, Sanya 572025, China
[3] Key Laboratory of Fruits and Vegetables Processing, Ministry of Agriculture and Rural Affairs, Beijing 100083, China
[4] Frontier Technology Research Institute of China Agricultural University in Shenzhen, Shenzhen 518000, China
* Correspondence: zhangyan348@163.com; Tel./Fax: +86-10-62737434-23

Abstract

Background: Chlorophyll (Chl), widespread in fruits and vegetables, has been shown to have numerous nutritional functions, including beneficial effects on obesity. However, whether Chl has an anti-aging effect remains unclear. Methods: Here, we studied the beneficial effects and mechanism of Chl on delaying aging using a *Drosophila* model. Results: The results showed that dietary supplementation of Chl in an appropriate dose (3.925 mg/L) significantly extended the lifespan (7.66–13.94%), improved climbing ability, increased CAT activity, reduced MDA content, enhanced stress resistance to starvation, heat stress, and cold shock in *Drosophila*. Notably, lifespan extension was not associated with dietary restriction, reproductive sacrifice, or circadian rhythm regulation. RNA-Seq analysis showed that Chl supplementation led to differential expression of 723 genes in female flies and 435 genes in male flies. KEGG analysis revealed that these differentially expressed genes were significantly enriched in the xenobiotic metabolism (XM) pathway. Within this pathway, phase II detoxifying enzyme genes associated with the CncC (Nrf2) signaling pathway (*GstD10*, *GstE7*, *Ugt37A3*, and *AOX2*) were significantly downregulated in both sexes. In contrast, protective target genes from the same pathway (*cat*, *Mrp4*, *Hsp68*) were significantly upregulated, as confirmed by qPCR. Conclusions: Taken together, our data indicate that Chl supplementation delays aging in *Drosophila melanogaster* via enhanced stress resistance and remodeling of the detoxification network.

Keywords: chlorophyll; anti-aging; antioxidant; stress resistance; Nrf2; *Drosophila melanogaster*

1. Introduction

Aging in humans is a complex biological process characterized by a time-dependent progressive decline in physiological integrity, resulting in functional impairment and heightened susceptibility to mortality [1]. This degenerative process is associated with several hallmarks of biological alterations, including reduced food intake, decreased mobility, diminished reproductive capacity, impaired antioxidant defenses, and an imbalance in gut homeostasis [2]. These degenerative processes represent the foremost risk factor for major human pathologies, including cancer [3,4]. Therefore, promoting "healthy aging"—the

maintenance of functional capacity in later life by mitigating the progression of age-related pathologies—has become a critical imperative for us [5,6].

Aging is not only a change in appearance but also involves the comprehensive effects of genes, cellular functions, metabolic disorders, and environmental factors [7,8]. The genetics of aging research has revealed a complex network of interacting intracellular signaling pathways and higher-order processes. Many of the pathways and processes, such as dietary restriction, that have been identified are known to be critical in homeostatic responses to environmental change [9]. Studies have established that numerous genes are implicated in their regulation. For example, activation of the single *forkhead box o* (FoxO), which is inhibited by phosphorylation via the InR/IRS/Akt axis, results in a robust lifespan extension in *Drosophila* [10]. These results offer novel insights into the genetic regulation of aging processes.

While altering the progression of aging at the organismal level remains highly challenging, achieving relative rejuvenation at the cellular or tissue level is feasible. This can be accomplished through the application of bioactive plant-derived compounds or advanced technological interventions [11,12]. Studies have found that certain phytochemicals, such as polyphenols, lycopene, aspirin, and berberine, can decelerate the aging process, extend lifespan, or mitigate aging-related diseases [13–15]. Some phytochemicals may induce hormesis, a biphasic dose–response phenomenon where low doses elicit stimulatory benefits while high doses exert inhibitory effects [16]. For instance, 200 μM Epigallocatechin-3-gallate (EGCG) significantly extended the lifespan of *C. elegans*, while 1000 μM EGCG reduced worm longevity [17]; similarly, Proshkina et al. [18] reported that short-term and intermittent quercetin exposure was more effective in lifespan extension than long-term continuous exposure in *D. melanogaster*. Such effects, usually driven by appropriate low doses, enhance brain resilience, improve organismal stress tolerance, and slow aging by activating host defense pathways (e.g., Nrf2 antioxidant signaling) and stress-tolerance genes (e.g., *GST*, *Hsp70*) [19–21]. Chlorophyll (Chl), the most abundant plant secondary metabolite in nature, with an annual production exceeding 1.2 billion tons [14,22], plays pivotal roles across multiple domains. Its applications span from food coloring and functional food additives to biomedical materials and renewable energy systems [23,24]. Additionally, emerging evidence from recent research reveals Chl's bioactive potential in areas of obesity suppression, gut microbiota modulation, and lipid metabolism regulation [25–27]. However, there is almost no research on Chl's anti-aging properties and the underlying mechanisms.

Drosophila melanogaster has a rich history in biological research, contributing to many key discoveries in genetics, development, and neurobiology. Thegenome contains~63% that have human orthologs [28]~75% of known human pathogenic genes are homologous to fruit flies [29,30]. The model organism is characterized by its small size, short lifespan, and rapid reproductive cycle, making it an ideal system for investigating the anti-aging mechanisms of natural extracts [11]. This study employs the *Drosophila* model system to investigate the anti-aging mechanisms underlying Chl's age-delaying effects.

2. Materials and Methods

2.1. Chl Extraction and Purification

Chl extraction was performed using the method of Li et al. [31] Briefly, fresh spinach leaves of *Spinacia oleracea* 'Super King' (Japanese cultivar) harvested in May from Linyi City, Shandong Province, China, were homogenized using a T25 digital ULTRA-TURRAX® homogenizer (IKA Works GmbH & Co. KG, Staufen, Germany) with a mixture of anhydrous ethanol and petroleum ether. The homogenate was centrifuged (CR21GII, Hitachi Group, Tokyo, Japan), and the supernatant was subjected to phase separation in a separatory funnel. The petroleum ether phase (containing Chl) was washed, dried, and then

https://doi.org/10.3390/nu18091465

concentrated via rotary evaporation (RE-5210A, Shanghai Yarong Biochemical Instrument Factory, Shanghai, China) at 36 °C under reduced pressure. The purification was performed by column chromatography on neutral alumina (200–300 mesh) with stepwise elution, mainly removing carotenoids and lutein. Finally, the organic solvent in the purified Chl was removed using a multifunctional nitrogen blower, and Chl (Chl a:Chl b ≈ 3:1) [32] with a purity of 86.6% was obtained [33] and stored at −80 °C in the dark. The remaining minor components (13.4%) mainly consisted of homologous lipophilic pigments, Chl degradation products, and lipids.

2.2. Media Preparation, Drosophila Stocks, and Husbandry

Media preparation was performed according to the methodology of Dr. Juan Du's laboratory (China Agricultural University, Beijing, China). The media used for larval development and longevity assays are shown in Table 1. For the yeast medium, combine water, $CaCl_2$, sucrose, and dextrose and mix well. Increase heat and add cornmeal and yeast; boil for 10 min; add agar, and keep boiling for 5 min. Allow food to cool to 60 °C; add ethyl paraben and propionic acid; and dispense. The yeast was bought from Angel Yeast Co., Ltd. (low-sugar, high-activity dry yeast powder, Yichang City, Hubei Province, China). Chl groups were to add Chl to the yeast medium to a final concentration of 15.7 mg/L, 7.85 mg/L, and 3.925 mg/L, respectively, before it was dispensed. As Chl is easily degraded by light, the media prepared were stored in the refrigerator at 4 °C and protected from light, and were freshly prepared every six days. The Chl content in the culture medium was determined based on a literature review, with comprehensive consideration of daily vegetable intake, equivalent dose conversion, typical dosage ranges of plant extracts, and the solubility properties of chlorophyll, and was further confirmed through preliminary experiments.

Table 1. Formula of culture medium.

Yeast Medium		Grape Juice Medium		Medium for Hunger Experiment	
Ingredient	**Per Liter Food**	**Ingredient**	**Per Liter Food**	**Ingredient**	**Per Liter Food**
Water (mL)	1000	Water (mL)	800	Water (mL)	965
$CaCl_2$ (g)	0.726	Sucrose (g)	15	Agar (g)	15
Sucrose (g)	31.62	Agar (g)	37.5	Ethyl Paraben (mL; 10% *w*/*v*)	30
Dextrose (g)	63.2	Grape juice (mL)	200	Propionic Acid (mL)	5
Cornmeal (g)	77.7	Ethyl Paraben (mL; 10% *w*/*v*)	15		
Yeast (g)	32.2				
Agar (g)	8				
Ethyl Paraben (mL; 10% *w*/*v*)	15				
Propionic Acid (mL)	5				

Grape juice medium was used to collect *Drosophila* eggs. The preparation method is to boil pure water, sucrose, and agar in a pot. Add grape juice, stir over low heat, cool to 60 °C, add nipagin, evenly dispense, and store in the refrigerator at 4 °C, protected from light after cooling and solidification. When using it, apply a small amount of yeast paste (3 g of yeast and 10 g of water) on the surface of the medium.

The wild-type *Drosophila melanogaster* Canton-S and W^{1118} (NO.5905) stocks were obtained from Dr. Juan Du's laboratory (China Agricultural University, Beijing, China). Fly stocks were maintained on standard food in an incubator at 25 °C, 60% humidity, with

a 12 h light/12 h dark cycle unless otherwise stated. Flies for aging were collected and transferred to fresh food every 3 days.

Prior to all experiments, fly cultures were maintained at constant density for at least 2 generations. Embryo collections were synchronized to ensure developmental uniformity [34].

2.3. Survival Analysis

The lifespan assay was conducted as described by Libert et al. [34] and Castillo-Quan et al. [35] Adult flies were collected over 24 h and promptly transferred to yeast food. Following collection, flies were allowed to mature and mate for 48 h, after which males and females were separated under light CO_2 anesthesia and placed in vials with appropriate food (Canton-S, n = 160 to 200 per group; W^{1118}, n = 200 to 260 per group, 15 to 20 per vial). In subsequent experiments, unless otherwise specified, collection and processing were according to this procedure. Vials were stored on their side, which allowed the flies to wander away from the food even at an advanced age. Vials were changed every 3 days, at which time dead flies were removed and counted. Survival curves were tracked until all flies had died, and the mean, median, and maximum lifespans of the flies were determined.

There were five groups for each fly stock and each sex. One standard food group was maintained in an incubator with a 12 h light/12 h dark cycle as a daily reference group. The blank control group and three Chl experimental groups, as shown in Section 2.2 were maintained in an incubator under continuous 24 h dark conditions.

For starvation resistance, flies were collected as described and placed on yeast food to age for 10 days. Flies were then placed in fresh vials containing 1.5% agar with 3% ethyl paraben (10% w/v) and 0.5% propionic acid (n = 100 per group, 10 per vial). Vials were changed daily, and the number of dead flies was recorded every 12 h until all flies died, and survival curves were constructed.

2.4. Climbing Index Measurement

After collection and mating, as in the longevity assays, 15-day-old adult flies were placed in a vertical empty tube and adapted for 5 min (n = 80 to 100 per group, 10 per vial). After gently shaking the flies to the bottom of the tube, the flies habitually climbed upwards. The number of flies that reached the top of the tube within 10 s was recorded (A). Each group of flies was tested at least 5 times, with a minimum interval of 5 min between each test, and shaken with a similar force each time. The climbing index was calculated as CI = A/total.

2.5. Feeding and Body Weight Assays

Food intake detection was determined according to the method of Libert et al. [34]. After collection and mating as outlined for the longevity assays, 15-day-old adult flies were weighed and then fed standard food supplemented with 0.5% (w/v) FD&C Blue #1 (Shanghai Dye Research Institute Co., Ltd., Shanghai, China). FD&C Blue #1 (Synonyms: Acid Blue 9, Erioglaucine; Brilliant Blue FCF, $C_{37}H_{34}N_2O_9S_3Na_2$) was shown to be harmless to flies and is routinely used to color human food, drugs, and household chemicals. The dye does not decompose at low pH and is thermo-stable. Flies were exposed to dyed food for 20 min, after which groups of 5 female/male flies (8–10 groups per sample) were homogenized in 200 µL of PBS and cleared by centrifugation at 8000× g for 10 min. After centrifugation, the absorbance of the supernatant was measured at 625 nm.

2.6. Reproduction Assays

Flies were collected as virgins within 6 h of eclosion. Following collection, the virgins were placed on yeast medium and aged for 24 h. Then, males and females were separated

https://doi.org/10.3390/nu18091465

and randomly assigned to groups. After 10 days of feeding with appropriate medium, ten replicate vials of 10 females and 15 males were established containing the grape juice medium (covered with yeast paste: 3 g yeast and 10 g water) for 24 h to stimulate egg production (10 vials per group). The flies were then removed, and egg counts were performed on day 5.

2.7. Circadian Rhythm Measurement

Circadian rhythm of individual male flies was measured using the *Drosophila* Activity Monitoring (DAM) System (DAM2, Trikinetics, Waltham, MA, USA) [36]. Male flies (aged 15 days) were loaded individually into glass tubes with a length of 65 mm and an inner diameter of 5 mm. The flies (n = 16) were entrained to a 12 h light/12 h dark cycle for 3 days and then released to constant darkness for at least six days to measure their rhythmicity. Chi-squared periodogram analysis determined whether a fly was significantly rhythmic ($\alpha = 0.05$). Data analysis was done on a Macintosh computer running the FaasX (Fly activity analysis suite, 1.22 (32-bits)) software (obtained from https://trikinetics.com, NeuroPSI, France). Individual flies with power ($\geq$10) and "width" values of 1.5 or more were considered rhythmic [37]. Activity data were collected using MATLAB (R2022a, MathWorks, Natick, MA, USA) for each fly, and were binned every 30 min for the circadian rhythm analyses.

2.8. Hydrogen Peroxide (H_2O_2) Challenge Test

For the acute oxidative stress test, this study employed a modified hydrogen peroxide (H_2O_2) challenge assay, based on the method of Wongchum et al. [38] Hydrogen peroxide was diluted with 6% glucose solution to a final concentration of 30%, and 200 μL of the diluent was added onto a filter paper. Flies were then transferred to measuring tubes lined with the H_2O_2 filter paper, with 10 flies per tube and 10 replicate tubes per group. The number of fly deaths was counted every 3 h until all were dead, and a survival curve was drawn.

2.9. Antioxidant Enzyme Activities and MDA Content

A sample (more than 100 flies per sample) of males or females of 15-day-old adult flies that were fed base and test diets was collected, respectively. Fruit flies were anesthetized with CO_2, and a tissue homogenate was prepared by adding physiological saline (5 flies with 100 μL). The homogenate was centrifuged in a low-temperature centrifuge for 15 min (4 °C, 8000 r/min). Malondialdehyde (MDA) levels, superoxide dismutase (SOD) activity, and catalase (CAT) were measured separately by using MDA kit (cat. BC0025), SOD kit (cat. BC0175), and CAT kit (cat. BC0205) produced by Beijing Solarbio Science & Technology Co., Ltd. (Beijing, China).

2.10. Environmental Stress Test

Fifteen-day-old adult flies (more than 100 flies per sample, 10 flies per vial, 10 vials per sample) were prepared for testing. In the cold shock recovery experiment, we exposed all flies to a 4 °C environment until their complete activity ceased. Afterward, the fruit flies were transferred to room temperature, and the time required for recovery from cold shock was recorded. For the heat stress resistance experiment, the flies were kept in a constant temperature incubator at 39 °C, and their survival status was recorded every hour until they all died. Survival curves were drawn at the end.

2.11. Triglyceride and Glucose Assays

After collection and mating as outlined for the longevity assays, 15-day-old adult flies (10 females or males) were transferred into a 1.5 mL centrifuge tube and quick-frozen in

liquid nitrogen (10 tubes per group). After homogenization in 200 μL of 0.05% PBS/Triton-X buffer, the triglyceride content of each group was determined according to the TAG kit method (# A110-2-1, Nanjing Jiancheng Bioengineering Research Institute Co., Ltd., Nanjing, China). For the glucose assay, the flies were starved for 1 h, centrifuged, and the supernatant was taken. The glucose was then determined using the glucose content detection kit method (Beijing Solarbio Science & Technology Co., Ltd., Beijing, China) according to the instruction manual.

2.12. RNA Sequencing

RNA sequencing was performed as described by Zhu et al. [2]. Briefly, the female or male flies (Canton-S) were cultured in the standard medium and in medium supplemented with 3.925 mg/mL Chl for 15 days. Total RNA was extracted from different groups, and the integrity was determined by the Bioanalyzer 2100 system (Agilent Technologies, Santa Clara, CA, USA). The total amount of RNA samples was detected by the ND-2000 (Thermo Fisher Scientific, Waltham, MA, USA). Then, mRNA was enriched from total RNA and randomly fragmented. After library construction and quality inspection, transcriptome sequencing was performed on the Illumina platform (Illumina, San Diego, CA, USA). To identify DEGs (differentially expressed genes), the expression level of each transcript was calculated according to the transcripts per million reads (TPM) method. Subsequently, DESeq2 (v1.49.4, Bioconductor, USA & Germany) was used for differential expression analysis, and the ClusterProfiler R package (v4.0.2, YuLab-SMU, Southern Medical University, Guangzhou, China) was used for GO and KEGG pathway enrichment analysis. RNA-seq was performed at Majorbio Bio-pharm Biotechnology Co., Ltd. (Shanghai, China). Finally, based on the differentially expressed transcription factor (TF) genes shared between males and females annotated from RNA-seq data, upstream regulators of these differentially expressed TF genes were predicted, and their motif analyses were performed using RStudio (version 2026.01.2-418, Posit PBC, Boston, MA, USA) combined with the AnimalTFDB and JASPAR databases (1000 bp–0 bp, Cor > 0.5).

2.13. Quantitative RT–PCR (qRT-PCR)

Total RNA was extracted from approximately 10 flies using an extraction reagent kit (R1200, Beijing Solarbio Science & Technology Co., Ltd., Beijing, China). The cDNAs were synthesized by reverse transcription using HiScript III RT SuperMix for qPCR (+gDNA wiper) (R323, Nanjing Vazyme Biotech Co., Ltd., Nanjing, China). The cDNA preparation was then subjected to real-time quantitative PCR (SYBR Green I Chimeric Fluorescence Method) according to the protocol of Taq Pro Universal SYBR qPCR Master Mix (Q712, Nanjing Vazyme Biotech Co., Ltd., Nanjing, China). $2^{-\Delta\Delta CT}$ method was used to calculate the relative expression of mRNA of each gene. All the primers used are listed in Table 2.

Table 2. List of primers used in gene expression study.

Gene Name	Primer Sequences (5′ to 3′)	Gene Name	Primer Sequences (5′ to 3′)
AOX2	F:TTCGGTGGAAACCTCTGTCG R:GCTCGAAGGAGTCCTCGATG	*GstE7*	F:ATTATTGAGGTCTATGACTTCCT R:GTCCACCTTTACGAAGACCT
GstD10	F:TGTGGAGTTCGATAAGAAGAC R:ATTGGCATACCGCTTGAAAT	*cat*	F:TGACTACAAAAACTCCCAAACG R:TTGATTCCAATGGGTGCTC
sod1	F:GGAAAACGCGCATAAACATT R:GGATTTCTGGATGTGGTGCT	*sod2*	F:AATTTCGCAAACTGCAAGC R:TGATGCAGCTCCATGATCTC
Mrp4	F:AAGAACGTGGACGGTCAAAC R:GCAAATTGTCGAACTCAGCA	*Hsp68*	F:TTAAGGATGGTGAGGCCAAG R:CACGGAATTGTTGGTGTTTG
rp49	F:GCACCAAGCACTTCATCC R:CGATCTCGCCGCAGTAAA		

https://doi.org/10.3390/nu18091465

2.14. Statistical Analysis

Each experiment was performed at least in triplicate. The results obtained were analyzed and the graphs were drawn using Prism 9 (Version No.6, GraphPad, San Diego, CA, USA). Data are presented as the mean ± standard deviation (S.D). Comparisons of survival rates between groups were conducted using the log-rank test for significance. Apart from survival rates, one-way analysis of variance (ANOVA), *t*-test, and chi-square test were used to determine statistical significance. The differences between groups were considered statistically significant at $p < 0.05$ for all tests, and significance was denoted as * $p < 0.05$, ** $p < 0.01$, *** $p < 0.001$, and **** $p < 0.0001$.

3. Results and Discussion

3.1. Effects of Chl Supplementation on the Lifespan and Athletic Ability in Drosophila

As age increases, the body's resistance to harsh external environments decreases, causing some aging-related diseases and affecting life expectancy [39]. Studies have shown that lifespan is the most direct reflection of aging [40], and motor ability is negatively correlated with aging. Therefore, we detected the effect of Chl supplementation on the healthspan of fruit flies through lifespan and climbing ability.

Female and male *Drosophila* were reared on media containing different concentrations of Chl for the lifespan test. Compared with the control group, Chl supplementation at a certain concentration significantly increased the survival rate, mean lifespan, median lifespan, and maximum lifespan in flies (Figure 1A and Table 3). For the Canton-S (female and male) and W^{1118} (male), 3.925 mg/L was the optimal concentration for addition; while, for W^{1118} (female), the optimal concentration was 15.7 mg/L. Among them, the mean lifespan increased by 12.01% (from 46.71 to 52.32 days, $p < 0.001$), 13.93% (from 30.79 to 35.08 days, $p < 0.0001$), 8.01% (from 56.33 to 60.84 days, $p < 0.001$), and 7.66% (from 50.42 to 54.28 days, $p < 0.0001$), respectively. This suggested that there is an optimal dose of Chl for lifespan extension, and Chl has a greater impact on the lifespan of Canton-S than W^{1118}. It is worth noting that the Chl concentration producing the optimal anti-aging effect was not the highest, but a relatively moderate dose among the experimental groups. This is consistent with hormesis to some extent, whereby nutrients or natural supplements exert anti-aging effects at relatively low doses [16]. These findings are also in line with several recent studies [41,42]. The results indicate that Chl supplementation can delay aging in *Drosophila*, but there are differences in the effects across varieties and genders.

A prior study, which focused on the oxidative stress tolerance of *Caenorhabditis elegans* (*C. elegans*) fed with Chl, demonstrated that Chl extends the lifespan of *C. elegans* by up to 25% [43]. This finding aligns with the results of our current research. Interestingly, increasing evidence shows that many food-derived small molecules, also called phytochemicals, can extend lifespan in various animal species, such as plant polyphenolics from strawberry, spinach, blueberry, and tea [13,44]. These studies also indirectly confirm that Chl prolongs the lifespan of fruit flies. In addition, many studies have found differences in experimental results among fruit fly varieties and gender [28,45]. Hodge et al. found that under unrestricted diet conditions, the lifespan of W^{1118} (white eye) is significantly prolonged, while the lifespan of Canton-S (red eye) remains unchanged in continuous darkness. The core reason for this difference may be that the white gene defect in W^{1118} leads to a lack of red pigment protection in its eyes, making it more sensitive to light damage. Therefore, the dark environment has a more significant effect on extending its lifespan [46].

Table 3. Life-span data for *Drosophila*.

Genetic Background	Groups Chl Level (mg/L)	Flies (*n*)		Median Survival (d)		Mean Longevity (d ± SE)		Maximum Longevity (d ± SE)		Mean Increase (%)	
		Female	Male	Female	Male	Female	Male	Female	Male	Female	Male
Canton-S											
	LT (0)	159	185	48	30	45.74 ± 1.16	28.20 ± 0.70	70.20 ± 0.73	52.20 ± 2.04	−2.07	−8.41
	C (0)	163	163	51	30	46.71 ± 1.28	30.79 ± 0.78	70.20 ± 1.53	52.80 ± 1.53	—	—
	L (3.925)	197	198	57	36	52.32 ± 1.14	35.08 ± 0.60	74.40 ± 0.60	54.00 ± 1.34	12.01 ***	13.93 ****
	M (7.85)	196	167	57	33	50.57 ± 1.20	34.20 ± 0.73	73.80 ± 0.73	55.80 ± 1.53	8.26 *	11.07 **
	H (15.7)	197	198	54	33	48.78 ± 1.16	32.17 ± 0.68	71.40 ± 0.60	55.20 ± 0.73	4.43	4.48
W^{1118}											
	LT (0)	226	252	57	51	52.70 ± 1.05	48.96 ± 0.77	82.80 ± 1.53	75.00 ± 1.20	−6.44 **	−2.90
	C (0)	249	229	60	54	56.33 ± 1.09	50.42 ± 0.85	84.60 ± 1.12	76.20 ± 1.53	—	—
	L (3.925)	198	238	63	57	56.52 ± 1.33	54.28 ± 0.94	86.40 ± 1.12	82.80 ± 0.73	0.33	7.66 ****
	M (7.85)	206	244	63	54	57.15 ± 1.34	51.30 ± 0.80	85.20 ± 0.73	81.00 ± 2.12	1.46	1.75
	H (15.7)	196	241	66	54	60.84 ± 1.31	50.63 ± 0.81	87.60 ± 1.12	76.20 ± 1.53	8.01 ***	0.42

* $p < 0.05$, ** $p < 0.001$, *** $p < 0.001$, **** $p < 0.001$ vs. control.

https://doi.org/10.3390/nu18091465

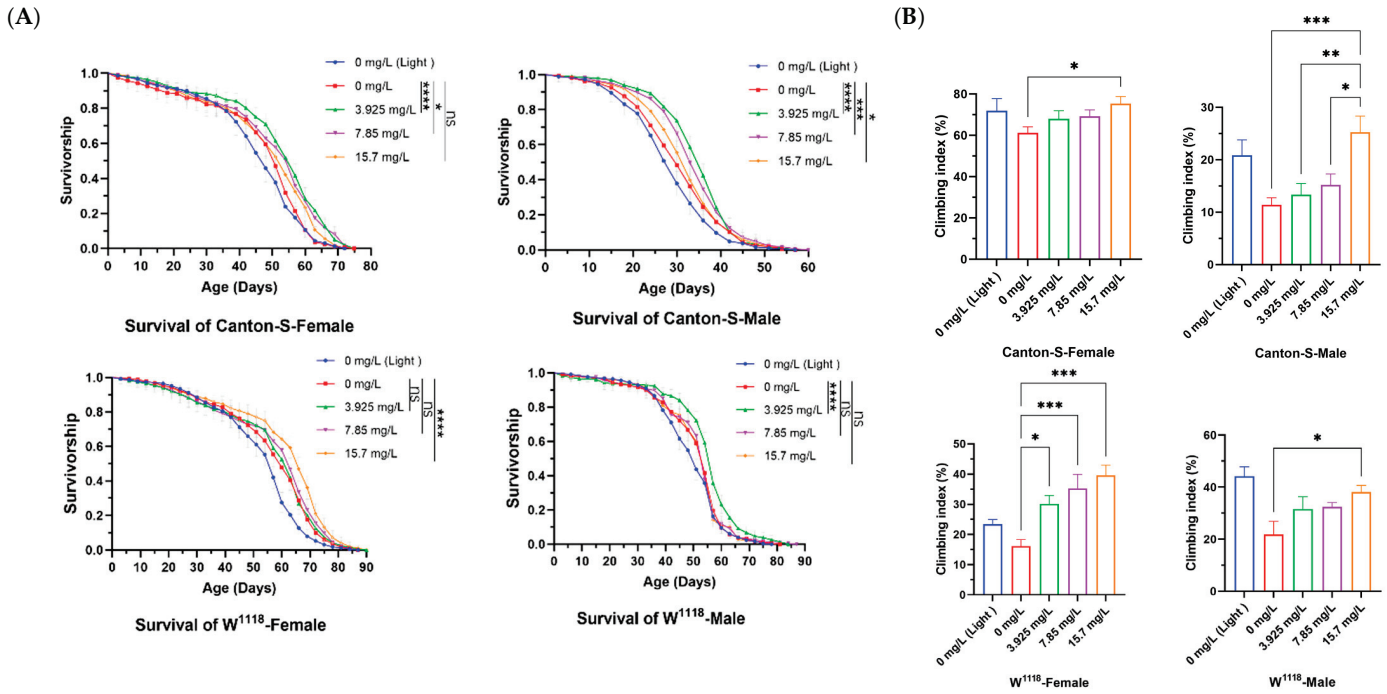


Figure 1. Effects of Chl on the lifespan and athletic ability of *Drosophila*. (**A**) Survivorship curves; (**B**) Climbing ability. Data are presented as the mean ± SD. In panel (**A**), the *p*-values were determined by log-rank test. In panel (**B**), the *p*-values were determined by one-way ANOVA with Dunnett's multiple comparisons test. * $p < 0.05$; ** $p < 0.01$; *** $p < 0.001$; **** $p < 0.0001$ vs. the control group. ns, no significant difference between the two groups.

As the body ages, physiological functions and self-regulation abilities gradually decline, and the crawling ability of fruit flies is an excellent indicator of the degree of aging and health status of the body. The better the ability to crawl vertically upwards against gravity, the younger the body state of the fruit flies [47]. The locomotor abilities of flies fed with or without Chl for 15 days were detected. Compared with control flies, the climbing ability of all flies fed with Chl improved, especially with 15.7 mg/L (Figure 1B). The results show that Chl supplementation could improve the motor behavior of flies and contribute to their health span.

3.2. Effects of Chl Supplementation on the Food Intake and Fecundity of Drosophila

Caloric restriction (CR) and dietary restriction (DR) have been shown to prolong the lifespan of multiple species [48]. Pharmacological intervention may extend lifespan via compensatory effects from the sacrificed reproductive capacity and reduced food intake that induces dietary restriction [34]. To eliminate interference from these factors, we tested whether Chl-fed flies exhibit altered feeding behavior or reproductive investment, which might explain their longevity effect.

The results show that the food consumption of flies with Chl at three concentrations (3.925, 7.85, and 15.7 mg/L) was not significantly different from that of the control group (Figure 2A), suggesting that Chl did not alter the food intake behavior of flies. To confirm that Chl supplementation would not affect the food intake of flies, we analyzed the body weight of flies at 15 days after Chl addition. The results showed no obvious change in body weight of Chl-supplemented flies compared with the control group (Figure 2B), demonstrating that the extension of flies' lifespan was not driven by additional calorie restriction.

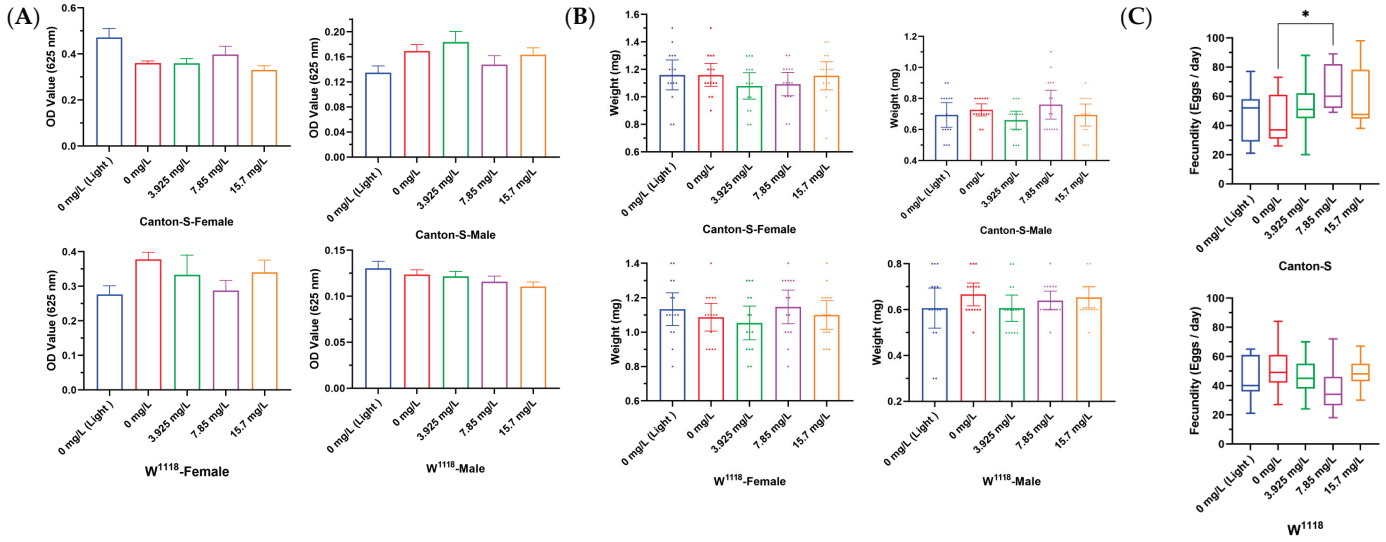


Figure 2. Effects of Chl on the (**A**) food intake (relative food consumption), (**B**) weight and (**C**) fecundity of *Drosophila*. All data are presented as the mean ± SD. The *p*-values were determined by one-way ANOVA with Dunnett's multiple comparisons test. * $p < 0.05$ vs. the control group.

In our experiments, the fecundity of treated flies was also not affected by Chl (Figure 2C). Interestingly, the reproductive rate of Canton-S fed with 7.85 mg/L Chl actually increased (from 43.27 to 66.67 eggs/day, $p < 0.05$). This may suggest that the regulation of chlorophyll in fruit flies is a "positive synergy" rather than a "trade-off" (most longevity interventions often accompany a decrease in reproductive capacity). In summary, the results indicate that Chl prolongs the lifespan of fruit flies without restricting dietary intake or sacrificing their reproductive capacity.

3.3. Regulatory Effect of Chl on the Circadian Rhythm in Drosophila

The circadian rhythm of fruit flies is primarily regulated by light signals, and prolonged darkness can gradually uncover and potentially alter their endogenous rhythms [49]. Research has indicated that there is a mutual interaction between circadian rhythm and aging [50]. To explore whether chlorophyll extends fruit fly lifespan by interfering with their circadian rhythm changes under dark conditions, we measured the circadian rhythm of 15-day-old male flies.

It was found that the percentage of rhythmic flies of Canton-S was significantly improved from 40% to 58.33% when fed with 15.7 mg/L Chl ($p < 0.05$), indicating that Chl may interfere with the circadian rhythm of fruit flies. However, the W^{1118} strain showed opposite results under Chl treatment (Figure 3 and Table 4). We speculate that the regulatory effect on rhythm may be related to the concentration of Chl, and the Chl concentration administered to W^{1118} was not optimal. However, the circadian rhythm of fruit flies in the group of 3.925 mg/L Chl was improved to 100%, albeit not significantly. In addition, it was discovered that the circadian rhythm of W^{1118} was significantly stronger than that of the Canton-S group. The reason for this difference may be that Canton-S maintains its rhythm by receiving light signals through red eye pigments, and under dark conditions, its own rhythmicity is poor [46]. Therefore, Chl exerts a regulatory effect on the circadian rhythm of fruit flies, but this effect is relatively weak and lacks consistency with the lifespan experiment results. Therefore, intervening in fruit fly lifespan via rhythm regulation is not the primary pathway of chlorophyll.

https://doi.org/10.3390/nu18091465

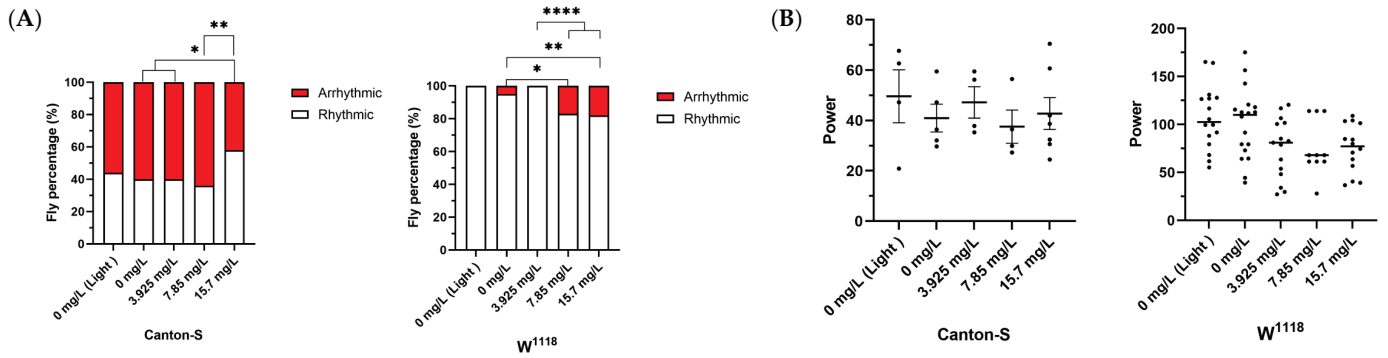


Figure 3. Regulatory effect of Chl on the circadian rhythm of *Drosophila*. (**A**) Percentage of rhythmic and arrhythmic flies; (**B**) Circadian power value of flies with rhythm. Data are presented as the mean ± SD. The *p*-values were determined by one-way ANOVA with Dunnett's multiple comparisons test. * $p < 0.05$; ** $p < 0.01$; **** $p < 0.0001$.

Table 4. Circadian rhythm data for *Drosophila*.

Genetic Background	Groups Chl Level (mg/L)	Num	% Rhythmic	Tau	Power
Canton-S					
	0 (Light)	9	44.44	15.13 ± 3.13	49.63 ± 10.52
	0	10	40	16.9 ± 3.00	40.98 ± 5.52
	3.925	10	40	17.88 ± 3.39	47.2 ± 6.21
	7.85	11	36.36	23.63 ± 0.13	37.55 ± 6.61
	15.7	12	58.33 *	20.43 ± 2.18	42.77 ± 6.36
W^{1118}					
	0 (Light)	16	100	23.84 ± 0.06	106.76 ± 8.23
	0	19	94.74	23.78 ± 0.06	100.58 ± 8.70
	3.925	15	100	23.87 ± 0.06	75.44 ± 8.08
	7.85	12	83.33 *	25.05 ± 0.65	75.85 ± 9.11
	15.7	17	82.35 **	23.79 ± 0.07	74.97 ± 6.69

* $p < 0.05$, ** $p < 0.001$ vs. control.

3.4. Effect of Chl on the Oxidative Stress Resistance

The free-radical theory of aging postulates that oxidative damage underlies the aging process. Notably, a common feature of many lifespan-extending compounds is their potent antioxidant capacity [51]. H_2O_2 was employed to generate hydroxyl radicals (OH), which elevated reactive oxygen species (ROS) levels and accelerated aging in fruit flies upon induction [52]. This model was used to examine whether Chl extends lifespan by enhancing antioxidant capacity [2]. The results showed that supplementation with a specific concentration of Chl significantly improved the survival rate of flies under H_2O_2-induced oxidative stress (Figure 4A). In Canton-S flies, antioxidant capacity was significantly enhanced in both females and males treated with 3.925 mg/L Chl, the mean survival time of flies was extended by 17.6% (from 15.38 to 18.08 h, $p < 0.05$) and 11.1% (from 12.90 to 14.33 h, $p < 0.05$). In W^{1118} flies, males exhibited antioxidant capacity in the 3.925 mg/L Chl group, with mean survival time increased from 23.43 to 24.84 h (6%, $p < 0.01$); while females showed elevated antioxidant capacity in the 7.85 mg/L and 15.7 mg/L Chl groups, with stronger stress resistance observed in females at 15.7 mg/L Chl (mean survival time increased by 9.6%, $p < 0.01$). Interestingly, the antioxidant capacity across different groups followed a trend consistent with the earlier lifespan assay, and the antioxidant activity of the female group was greater than that of the male group. Together, these findings indicate that Chl can enhance the antioxidant defense system in fruit flies.

https://doi.org/10.3390/nu18091465

Furthermore, to investigate whether Chl extends the lifespan of *Drosophila* by enhancing antioxidant enzyme activity, the levels of superoxide dismutase (SOD) and catalase (CAT) and the antioxidant/detoxification-related genes (*cat*, *sod1*, *sod2*, and *Mrp4*) in Chl-treated fruit flies were investigated. As shown in Figure 4B,C, CAT activity was significantly increased in both Canton-S and W^{1118} strains in a dose-dependent manner following Chl supplementation. In the 15.7 mg/L Chl group, the CAT activity was increased by 54.8% (Canton-S, female, $p < 0.05$), 73% (Canton-S, male, $p < 0.05$), 55.7% (W^{1118}, female, $p < 0.01$), and 62.9% (W^{1118}, male, $p < 0.05$), respectively. While SOD activity was markedly elevated only in W^{1118} flies. Also in the 15.7 mg/L Chl group, the SOD activity was increased by 33.1% (W^{1118}, female, $p < 0.05$) and 30.5% (W^{1118}, male, $p < 0.05$). It can be seen that the effect of Chl on CAT activity in flies is greater than that on SOD. Malondialdehyde (MDA), a marker of lipid peroxidation, reflects the extent of oxidative damage in vivo. As illustrated in Figure 4D, MDA levels were significantly reduced upon Chl treatment in all groups except female W^{1118} flies. MDA levels were reduced by 26.5% (Canton-S, female, $p < 0.05$), 28% (Canton-S, male, $p < 0.01$) and 37.3% (W^{1118}, male, $p < 0.0001$), respectively. The qPCR results were consistent with these findings (Figure 4E). In the Chl-treated groups at appropriate concentrations (3.925 mg/mL or 1.9625 mg/mL), the expression levels of *cat* and *Mrp4* genes were higher than those in the control group in both male and female *Drosophila*. However, the expression levels of *sod1* and *sod2* genes in Chl groups showed no significant changes compared with the control groups. Together, the change in the antioxidant capacity of fruit flies may be caused by Chl's enhancement of the activities of antioxidant enzymes (mainly CAT) and its inhibition of the production of MDA.

These results suggest that Chl enhances the antioxidant capacity in *Drosophila* (in vivo), which is consistent with previous findings that reported that Chl significantly reduced the damage from juglone-induced acute oxidative stress, especially at low concentrations [43]. A similar finding has been reported for other phytochemicals, like resveratrol and quercetin, which could improve the ability to resist oxidative stress and prolong life by scavenging ROS [12,15,53]. Another study has suggested that the genetic pathways underpinning lifespan extension and stress resistance are likely interconnected [54]. The Nrf2 signaling pathway (the CncC analog) [55] is one such critical pathway. Furthermore, functional nutrients maintain cellular redox homeostasis by activating the core transcription factor Nrf2 (CncC), as well as its downstream stress-resistance genes (e.g., heat shock protein 68 and 70, *Hsp68* and *Hsp70*), antioxidant enzymes including superoxide dismutase (SOD), catalase (CAT), and glutathione S-transferase (GST), and related proteins such as the transporter Mrp4. This mitigates aging-associated oxidative stress and metabolic dysfunction, thereby delaying senescence and age-related disorders [56–58]. Given that Chl is a nutrient likely to exert hormetic effects, and Chl supplementation modulates the expression of *cat* and *Mrp4*, genes associated with the CncC (Nrf2) pathway, elevates catalase (CAT) activity in a dose-dependent manner, and reduces malondialdehyde (MDA) levels. These findings therefore indicate that Chl enhances antioxidant responses in *Drosophila* by regulating the CncC (Nrf2) signaling pathway, thereby exerting protective effects and extending lifespan. However, Chl does not activate the CncC (Nrf2) pathway canonically, as the mRNA expression levels of *sod1* and *sod2* showed no significant differences between the control and treatment groups, and SOD activity was also largely unchanged in the Canton-S strain.

Some studies have shown that antioxidant activity alone cannot fully explain longevity [59,60]. Therefore, the life-extending effect of Chl is likely not based solely on mitigating oxidative stress.

https://doi.org/10.3390/nu18091465

3.5. Effects of Chl on the Resistance to Starvation Stress, Heat Shock, and Cold Shock

Interventions that extend lifespan are often associated with enhanced stress resistance across multiple model organisms, and the CncC (Nrf2) pathway is also involved in regulating stress resistance in *Drosophila*. To determine if Chl delays aging by enhancing stress resilience in *Drosophila*, multiple physiological markers in 15-day-old flies were assessed. In addition to measuring the antioxidant capacity, their resistance to starvation, heat stress, and cold shock were evaluated.

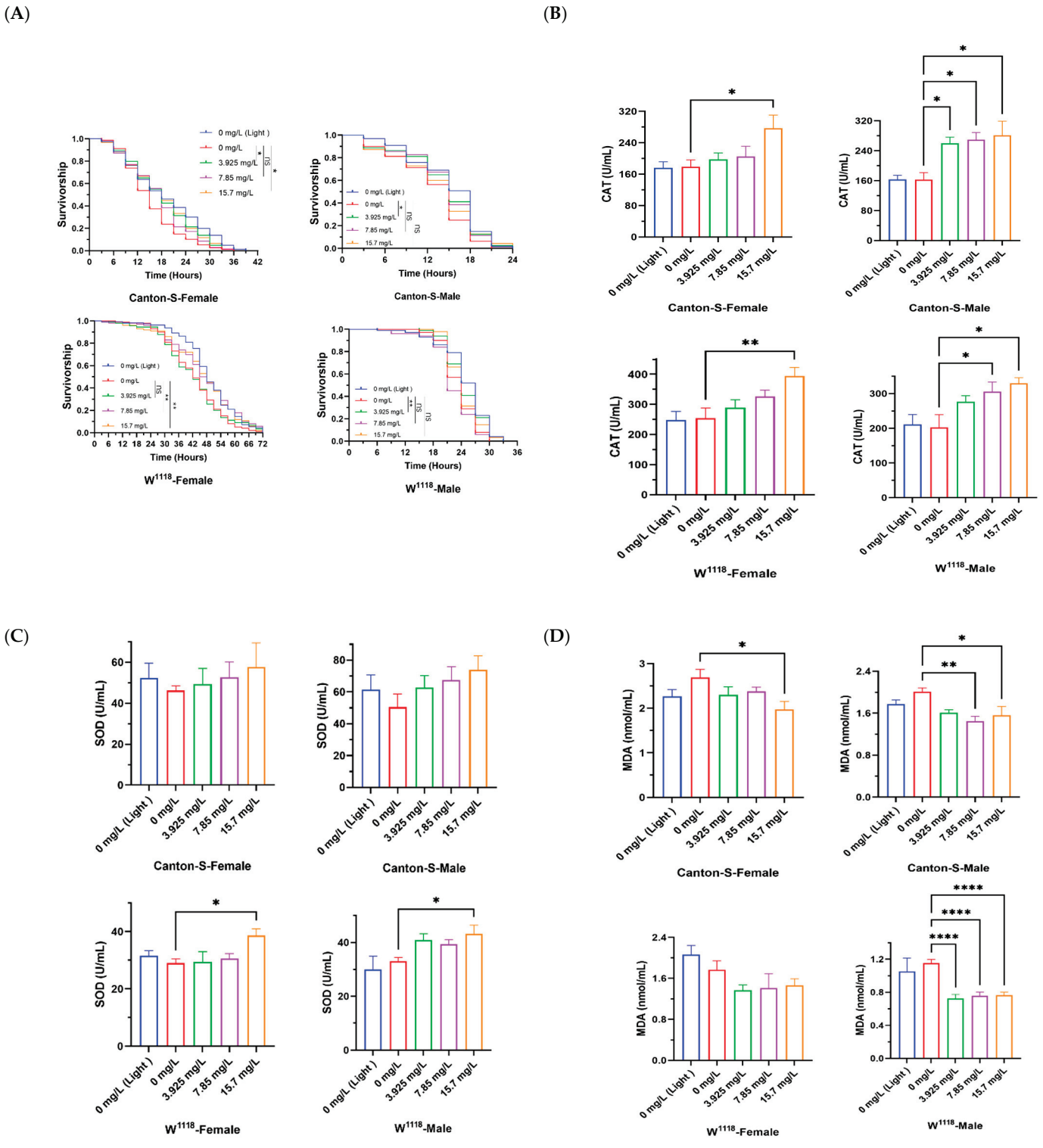


Figure 4. *Cont.*

(**E**)

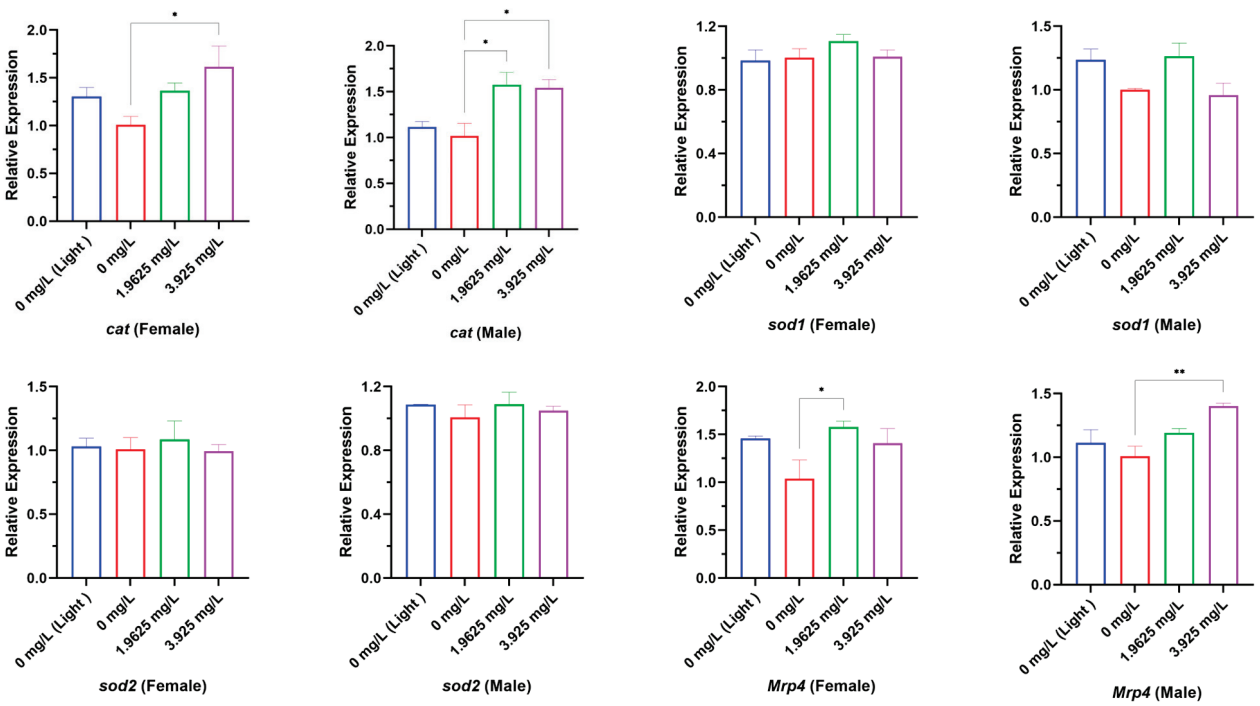


Figure 4. Effects of Chl supplementation on the antioxidant capacity in *Drosophila*. (**A**) Survivorship curves of flies induced by H_2O_2; (**B**,**C**) Activities of CAT and SOD; (**D**) The content of MDA; (**E**) qPCR analysis of antioxidant and detoxification-related genes. Data are presented as the mean ± SD. In panel (**A**), the *p*-values were determined by log-rank test. In panels (**B**–**D**), the *p*-values were determined by one-way ANOVA with Dunnett's multiple comparisons test. * $p < 0.05$; ** $p < 0.01$ and **** $p < 0.0001$ vs. the control group. ns, no significant difference between the two groups.

Under starvation, fruit flies enter a state of stress and greatly shorten their lifespan [61]. We put *Drosophila* on an agar-only medium to provide water without nutrients, and monitored and recorded their deaths. As shown in Figure 5A, compared with the control group, 3.925 mg/L Chl extract extended the mean lifespan of Canton-S flies by 15.2% (from 111.6 to 128.6 h, female, $p < 0.01$) and 21.8% (62.16 to 75.72 h, male, $p < 0.01$), respectively. For W^{1118} flies, all Chl groups extended the mean lifespan of female flies (increased by 39.8% on average, $p < 0.0001$), and 7.85 mg/L Chl extended the mean lifespan of male flies (12.8%, from 114.7 to 129.4 h, $p < 0.05$). Simultaneously, it was observed that triglyceride (in W^{1118}) and, more notably, glucose levels (in both Canton-S and W^{1118}) were significantly reduced following chlorophyll intervention compared to the control (Figure 5B,C). These results suggest that Chl may contribute to the extension of *Drosophila* lifespan by affecting energy storage, and this may be related to its ability to inhibit α-amylase and α-glucosidase activities [27].

At 4 °C, *Drosophila* falls into a transient dormant state, and its body performance is greatly impaired [61]. The cold shock test was to judge whether the Chl has a slowing effect on the flies when they deal with the low-temperature, uncomfortable environment (Figure 5D). Compared with the control group, the flies in the 3.925 mg/L and 15.7 mg/L Chl groups woke up quickly and significantly ($p < 0.0001$). Resuscitation times were 93 s and 82 s (female, Canton-S), 113 s and 101 s (male, Canton-S), 115 s and 99 s (female, W^{1118}), 109 s and 105 s (male, W^{1118}), respectively. At the same time, the ability of Chl to protect *Drosophila* lifespan under high-temperature conditions was explored. As shown in Figure 5E, Chl can significantly prolong the lifespan of flies under heat stress ($p < 0.0001$), except in female Canton-S flies. After feeding with Chl, the mean lifespan of male and female W^{1118} flies was extended by 21.3% and 15.3%, respectively, and the mean lifespan of female

Canton-S flies was extended by 16.4%, compared with the control group. Meanwhile, our results revealed that the expression level of *Hsp68* was also significantly upregulated, showing a positive correlation with the improved stress resistance in *Drosophila*. As a canonical direct downstream target gene of the CncC (Nrf2) pathway, *Hsp68* further supports that chlorophyll may enhance stress resistance and extend lifespan by modulating the CncC (Nrf2) signaling pathway. To sum up, flies fed with Chl show resistance to starvation stress, heat shock, cold shock, and upregulate the expression of *Hsp68*, suggesting that Chl may modulate the CncC (Nrf2) signaling pathway and enhance the overall health status and survival resilience of organisms.

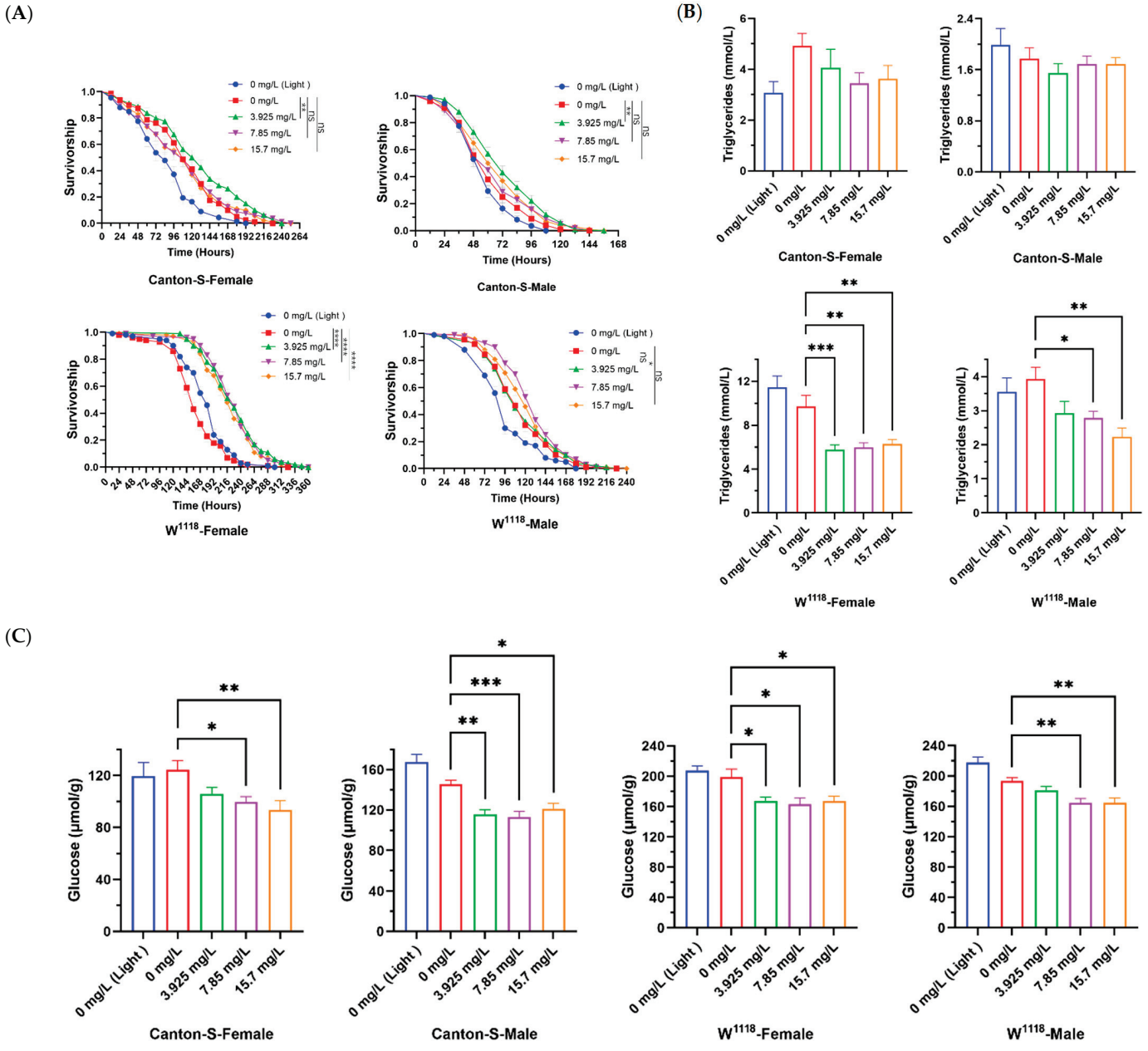


Figure 5. *Cont.*

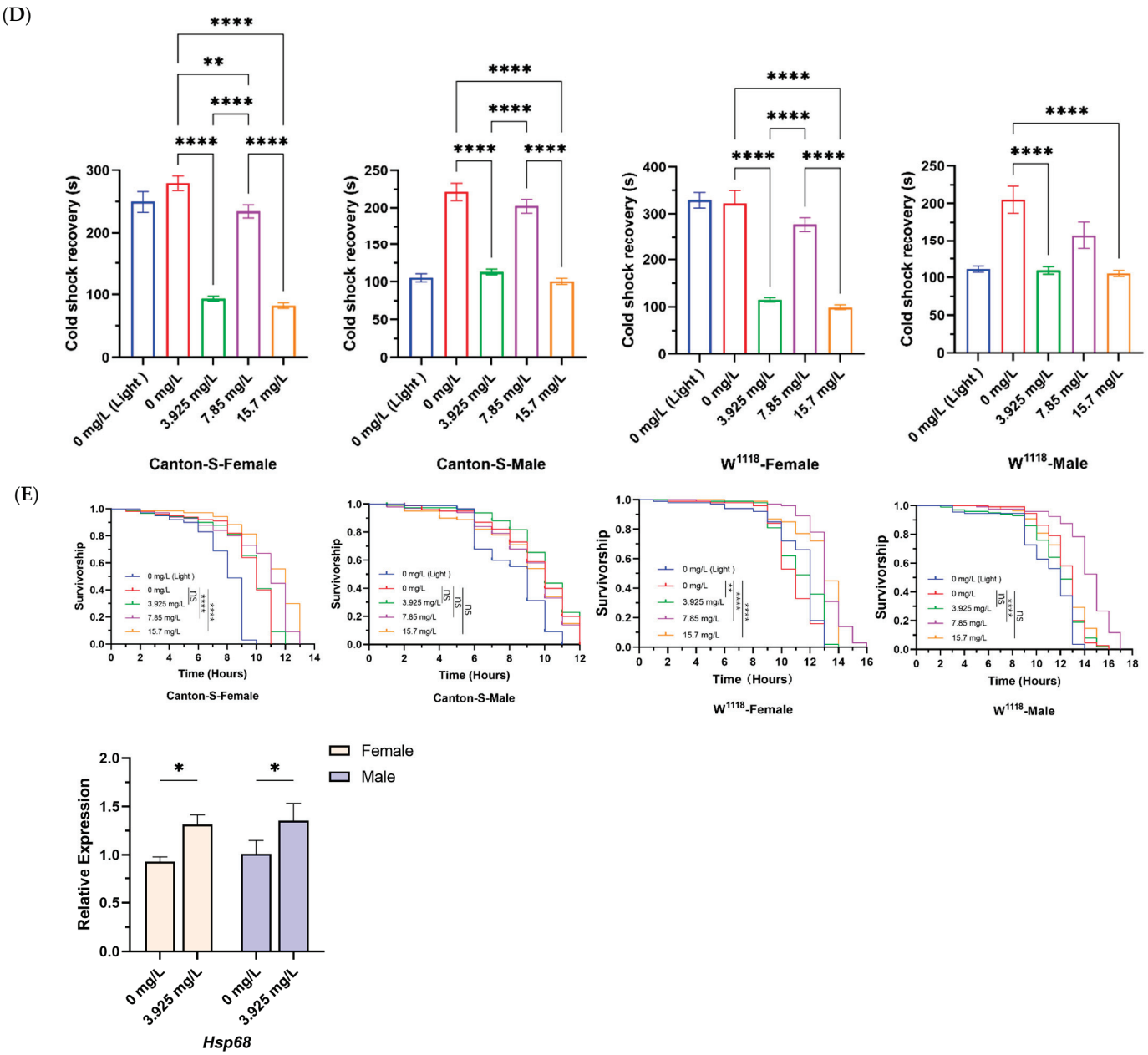


Figure 5. Effect of Chl on stress resistance in *Drosophila*. (**A**) Resistance to starvation; (**B**) The relative level of triglyceride; (**C**) The relative level of glucose; (**D**) Resistance to cold shock; (**E**) Resistance to heat stress and qPCR analysis of stress resistance-related gene. Data are presented as the mean ± SD. In panel (**A**,**E**), the *p* values were determined by log-rank test. In panels (**B**–**D**), the *p* values were determined by one-way ANOVA with Dunnett's multiple comparisons test. * $p < 0.05$; ** $p < 0.01$; *** $p < 0.001$ and **** $p < 0.0001$. ns, no significant difference between the two groups.

3.6. Effect of Chl Supplementation on Gene Expression in Drosophila

To comprehensively investigate the anti-aging mechanisms of Chl, RNA-sequencing was performed on the 15-day-old Canton-S fruit flies treated with or without Chl (control). The Canton-S strain was selected because both males and females exhibited stable and consistent responses to Chl at a concentration of 3.925 mg/L in lifespan, oxidative stress, and stress-resistance experiments. Therefore, this concentration was applied to the Chl treatment group. The expression profiles of approximately 20,000 genes were obtained from the sequencing database. Principal component analysis (PCA) revealed clear separation between sample groups and good reproducibility within groups (Figure 6A). Moreover, differential expression analysis was performed using the DESeq2 software (v1.49.4, Bio-

conductor, USA & Germany), and the screening conditions were set at p-adjust < 0.05 and $|FC| \geq 1.5$. Compared to the control groups, long-term Chl treatment significantly altered the transcript levels of 723 genes in females and 435 genes in males. Specifically, in females, 158 genes were upregulated, and 565 were downregulated, while in males, 132 genes were upregulated, and 303 were downregulated (Figure 6B). The bioinformatic analysis revealed 118 same genes were regulated in both female and male groups (Figure 6C).

Gene ontology (GO) enrichment analysis demonstrated that the same genes affected by Chl were mainly involved in biological processes (BP), such as chaperone-mediated protein folding, protein refolding, response to heat, protein folding, and response to temperature stimulus. In terms of molecular function (MF), the most abundant GO functions were unfolded protein binding (Figure 6D). Owing to this, the genes affected by Chl are primarily involved in protein synthesis and modification, as well as in responses to environmental stimuli. Kyoto Encyclopedia of Genes and Genomes (KEGG) pathway enrichment analysis of differentially expressed same genes revealed that the following three signaling pathways were involved in the aging process. These pathways include drug metabolism-other enzymes, drug metabolism-cytochrome P450, and metabolism of xenobiotics by cytochrome P450 (Figure 6E). The result showed that the xenobiotics metabolism (XM) pathway exhibited a strong association with aging. Therefore, real-time PCR was used to verify gene expression levels in the XM pathway. The results also showed that, compared with the group without Chl treatment, the expression levels of these genes, including *GstD10*, *GstE7*, and *AOX2*, were significantly decreased after Chl supplementation in *Drosophila* (Figure 6H). The results suggest that the XM pathway indeed plays a crucial role in delaying aging by Chl in fruit flies.

The *GstD10* and *GstE7* are glutathione *S*-transferases (GSTs), a phase II antioxidant enzyme, that represent a major group of detoxification enzymes [62], catalyzing the nucleophilic attack of glutathione (GSH) on toxic electrophilic substrates and producing a less dangerous compound [63,64]. The GST genes are upregulated in response to oxidative stress and are inexplicably overexpressed in many tumors, leading to problems during cancer chemotherapy [64,65]. However, we found that although Chl supplementation significantly decreased MDA, a marker of oxidative damage, and increased CAT activities, it unexpectedly decreased the enzymatic activities of *GstD10 and GstE7*. This is similar to studies on some phytochemicals, such as quercetin, which have anti-aging activity [12,13], but also inhibits GST [66]. The responses of GST genes may protect the steady-state response of the organism [67]. In a study on *Hyphantria cunea* and their response to the oxidative stress caused by the infection of *Hyphantria cunea* nucleopolyhedrovirus (HcNPV), the expression levels of most GSTs were downregulated at low concentrations of HcNPV, and the reason may be that ROS levels were under the threshold of the body system [68]. Similarly, Chl and its metabolites possess potent direct antioxidant and electrophilic substance scavenging capacities [26], accompanied by a significant decrease in malondialdehyde (MDA) levels. Thus, our findings indicate that Chl also reduces the demand for GST-dependent detoxification pathways in *Drosophila*, thereby downregulating their activities through feedback to conserve resources and energy, and maintain organismal homeostasis.

https://doi.org/10.3390/nu18091465

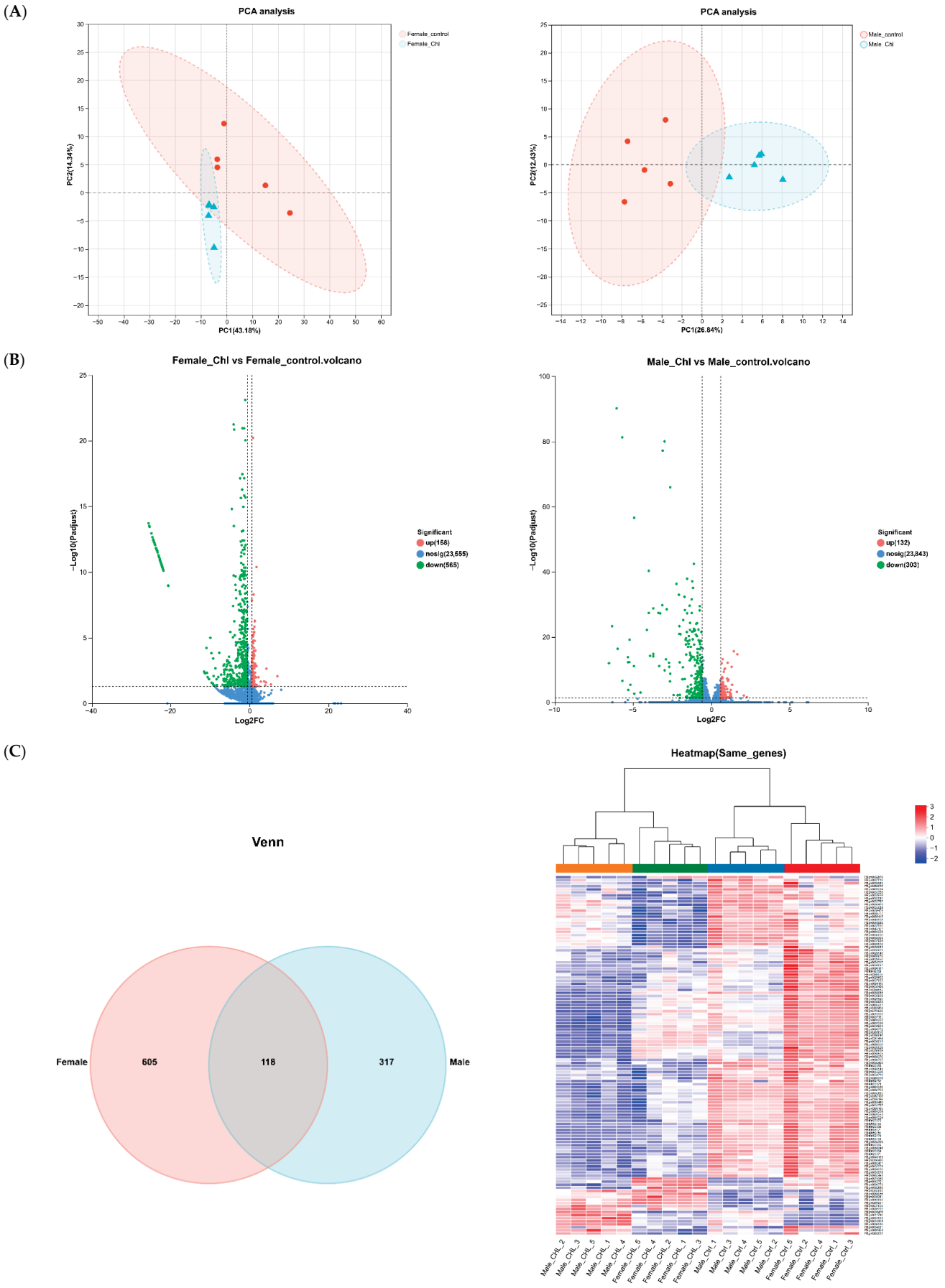


Figure 6. *Cont.*

https://doi.org/10.3390/nu18091465

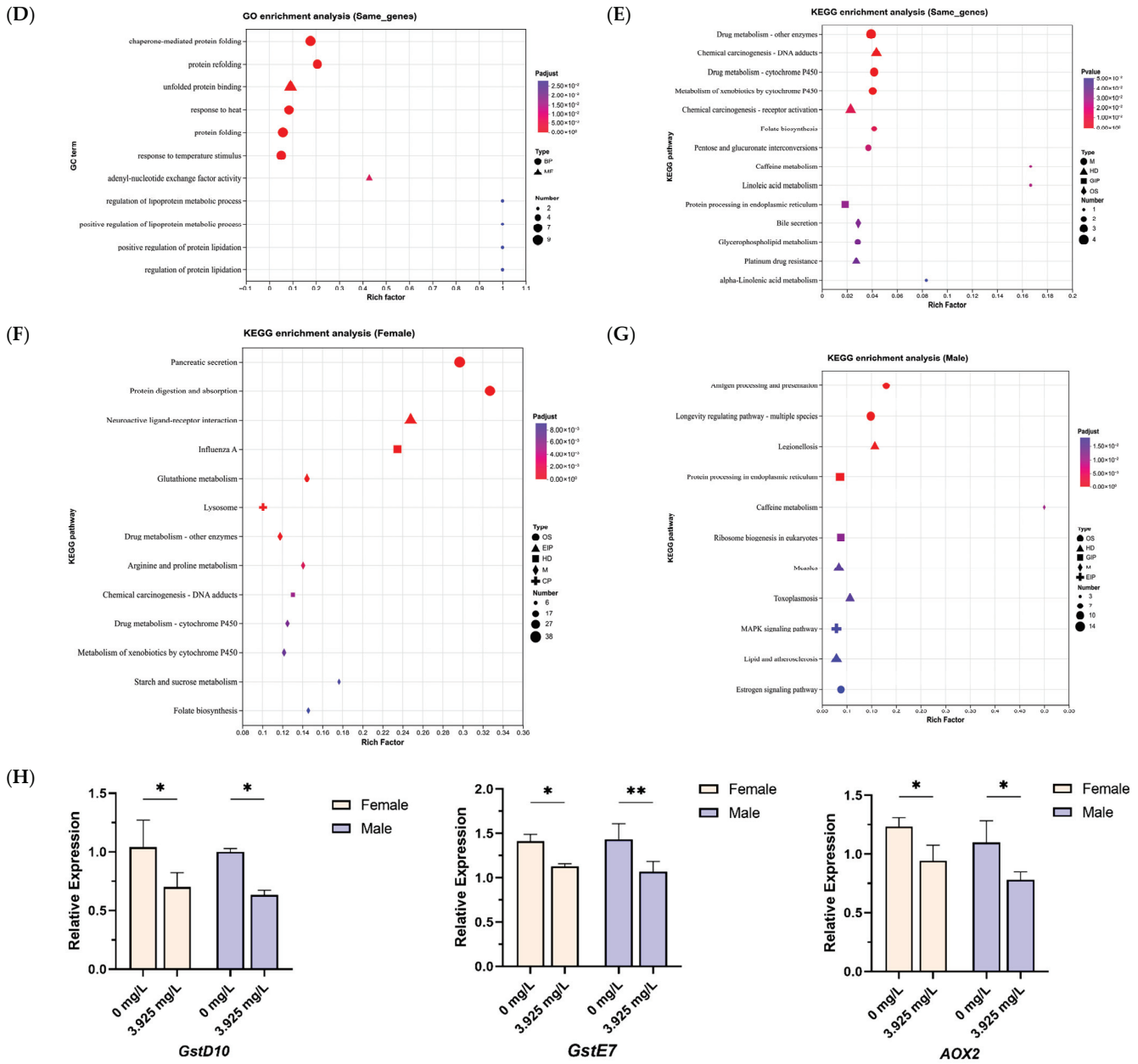


Figure 6. Effects of Chl supplementation on gene expression in *Drosophila*. (**A**) PCA analysis showing the similarity between samples; (**B**) Volcano plots showing the number of differentially expressed genes in flies fed with or without Chl (*p*-adjust < 0.05, FC ≥ 1.5); (**C**) Venn diagram and heatmap (same genes) showing the same differentially expressed genes between female and male group; (**D**) Gene ontology (GO) and (**E**) KEGG pathway analysis of the same differentially expressed genes between female and male group; (**F**,**G**) KEGG pathway analysis of the differentially expressed genes in female or male flies. (**H**) mRNA expression levels of the cofactors biosynthesis pathway-related genes. The type of GO analysis: BP, biological process; MF, molecular function. The type of KEGG analysis: M, metabolism; HD, human diseases; GIP, genetic information processing; OS, organismal systems; EIP, environmental information processing; CP, cellular processes. In panel (**E**), data are presented as the mean ± SD. The *p* values were determined by *t*-test. * $p < 0.05$ and ** $p < 0.01$ vs. the control group.

Combined with the previous studies on *Drosophila* stress resistance (Sections 3.4 and 3.5), the significantly differentially expressed genes can be roughly divided into two categories: one consists of canonical targets of CncC (Nrf2), which are associated with basic antioxidant defense, protein homeostasis, and toxin efflux, and belong to protective genes (*cat*,

Mrp4, *Hsp68*; upregulated); the other is highly sensitive to intracellular ROS/electrophile levels and classified as stress-inducible (*GstD10*, *GstE7*, *AOX2*, *Ugt37A3*; downregulated). Therefore, the results of this study indicate that Chl does not activate the CncC (Nrf2) pathway canonically, but rather activates it moderately and selectively, upregulating protective target genes (*cat*, *Mrp4*, *Hsp68*). Meanwhile, the effective scavenging of ROS by Chl leads to the feedback downregulation of classic phase II detoxifying enzymes such as *GST*, *AOX*, and *UGT*, thereby conserving metabolic resources. Chl selectively activates the CncC (Nrf2) signaling pathway, remodels the redox state and detoxification network of *Drosophila*, thereby extending the lifespan of *Drosophila*. Research has concluded that there is no generalized age-related trend in activities of various antioxidant enzymes in *Drosophila* [69]. Nevertheless, the administration of dietary antioxidants should theoretically combat aging and/or age-related diseases and therefore extend lifespan [70]. However, KEGG analysis did not reveal enrichment of the CncC (Nrf2) pathway. This may be because there is no independent CncC pathway in KEGG, only a homologous mapping of the mammalian Nrf2 pathway, resulting in incomplete annotation.

The above experiments show that there are differences in varieties and gender between the results. Therefore, separate KEGG pathway enrichment analyses were conducted on differentially expressed genes in females and males. The results indicated that, besides the XM pathway, the lysosomal pathway was strongly associated with aging in females (Figure 6F). However, this pathway was inhibited, and we speculated that the reason for the downregulation of detoxification pathway may be the same as in the previous XM pathway, while the lifespan regulation pathway showed a significant association with aging in males (Figure 6G), with *InR's* (insulin receptor homolog in flies) downregulation. This result may be related to the classical theory that dietary restriction can prolong life [48]. Caloric restriction is likely related to reduced GH/insulin/insulin-like growth factor-1 (IGF-1) levels, and InR (Insulin-like receptor), which is one of the IGF-1 signaling molecules [71].

Interestingly, results also show that the nutrient metabolism pathways of flies were affected after feeding Chl, such as pancreatic secretion pathway, protein digestion and absorption pathway, and starch and sucrose metabolism pathway in female flies, and lipid and atherosclerosis pathway. This is consistent with our previous experimental result (Section 3.5) that feeding Chl affects the nutrient metabolism and energy storage in flies. Thus, the effect of Chl on environmental stress and prolonging life may be related to these pathways.

3.7. Transcription Factor Motif Analysis

Based on 118 differentially expressed transcription factor (TF) genes shared by both sexes annotated from RNA-seq, upstream regulatory factors were predicted for these TFs using RStudio (version 2026.01.2-418) combined with the Animal TFDB and JASPAR databases. The screening region was set from 1000 bp upstream of the transcription start site (TSS) to the TSS itself (0 bp), with a binding strength threshold of correlation (Cor) > 0.5. A transcription factor regulatory network was subsequently constructed (Figure 7A). As illustrated in the figure, three differentially expressed genes, namely *Aox2*, *Ugt37A3*, and *GstE7*, were selected as target genes to predict their upstream transcription factors. The results indicate that *Vsx2*, *Pdp1*, and *croc* regulated these three genes, respectively. Further analysis identified transcription factor binding motifs at the following positions: "GTTAATTAG" at 538–546 bp upstream of the *Aox2* TSS, "GCTTATGCAATT" at 226–237 bp upstream of the *Ugt37A3* TSS, and "AACGTCAACA" at 589–598 bp upstream of the *GstE7* TSS (Figure 7B–D). However, one GST gene (*GstD10*) was excluded from promoter analysis because its upstream 1000 bp sequence could not be reliably retrieved from the

current genome annotation, possibly due to an incomplete gene model or its location near a scaffold boundary.

Subsequently, KEGG enrichment analysis was performed on these three transcription factors (*Vsx2*, *Pdp1*, and *croc*). The results (Figure 7E) show that they were enriched in signaling pathways, including FoxO, apoptosis, and longevity-regulating pathways. Although these pathways were not identical to those directly enriched by the differentially expressed genes in the transcriptome, they were functionally related, and both were closely associated with aging regulation [72,73]. In summary, the motif analysis supports the reliability of the transcriptomic results from a transcriptional regulatory perspective and provides initial insights into the potential upstream regulatory mechanisms through which chlorophyll may exert its effects.

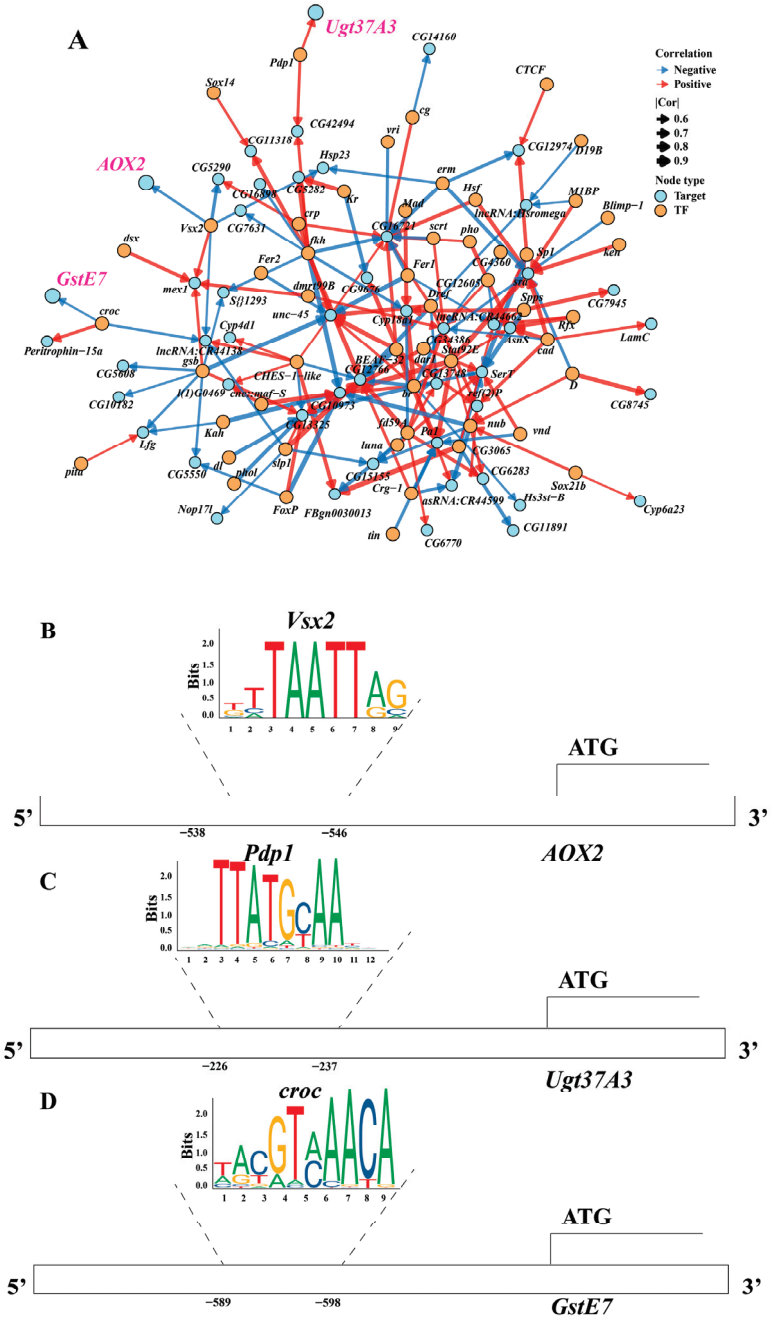


Figure 7. *Cont.*

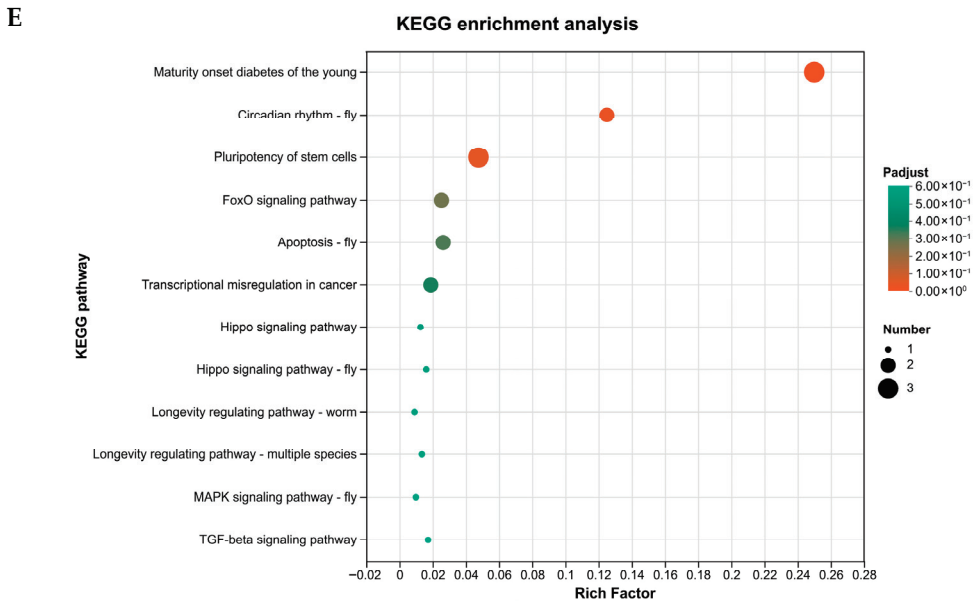


Figure 7. Transcription factor motif analysis of differentially expressed genes upon chlorophyll treatment. (**A**) Transcription factor regulatory map (screening within 1000 bp upstream of TSS, Cor > 0.5); (**B**–**D**) Transcription binding site maps (*Vsx2*, *Pdp1*, and *croc*); (**E**) TF (transcription factor) enrichment analysis.

4. Conclusions

This study demonstrates that Chl supplementation extends the mean lifespan of *Drosophila melanogaster*. Chl given at a certain dose (3.925 mg/L) prolonged longevity, increased athletic ability, and resistance to heat shock, cold shock, starvation stress, and oxidative stress in the flies. The prolongation of the flies' lifespan is not related to restriction of dietary intake, sacrifice of reproductive capacity, or rhythm regulation. The change in the stress resistance of *Drosophila* may be caused by Chl's effect on energy metabolism (glucose and triglyceride levels). This includes Chl's enhancement of the activities of antioxidant enzymes (mainly CAT) and its inhibition of the production of MDA. Gene expression and qPCR studies display upregulated expression of *cat*, *Mrp4*, *Hsp68*, and downregulated expression of *GstD10* and *GstE7*, *Ugt37A3*, and *AOX2* in the XM pathway. The motif analysis supports the reliability of the transcriptomic results.

In summary, our findings demonstrate that Chl acts as a hormetic nutrient. Dietary supplementation with Chl optimizes energy substrates in *Drosophila* (reduces glucose and lipid levels and modulates nutrient metabolism pathways). In addition, it moderately and selectively activates the CncC (Nrf2) signaling pathway with upregulation of protective target genes (*cat*, *Mrp4*, *Hsp68*), decreases MDA content, increases CAT activity, and downregulates classic phase II detoxifying enzyme genes including *GstD10*, *GstE7*, *AOX2*, and *Ugt37A3*. Ultimately, Chl supplementation reshapes the detoxification network and converts this protective advantage at the cellular level into an observable survival advantage at the biological level, that is, significantly improves the resistance to oxidative stress, starvation, high temperature, low temperature, and other environmental stresses, extending the lifespan and motor activity of *Drosophila.* The benefits brought by Chl may be far more than changes in several indicators at the molecular level, but translated into the overall improvement of the organism's "health resilience" and "viability".

Nevertheless, the present study has several limitations that warrant further investigation. First, the optimal anti-aging dose of Chl remains to be determined, as the dose is a critical factor determining whether a compound exerts protective or toxic effects. Given that Chl shows a hormetic response in enhancing antioxidant capacity in *Drosophila*, addi-

tional dose–response studies are needed to identify the most effective concentration. In addition, the chlorophyll concentration used in this study was preliminarily determined through experiments in *Drosophila* as an in vivo model. Given interspecific differences in metabolism [74], the chlorophyll dosage requires further optimization, and its biological effects need to be verified in subsequent aging-related studies using mice and humans. Second, aging is a highly complex process, and the metabolism of dietary nutrients may differ across species. Since this study was performed only in the *Drosophila* model, the generalizability of our findings to other organisms, including mammals, remains to be validated. Finally, other potential mechanisms underlying the anti-aging effects of Chl remain unexplored. For example, whether the gut-brain-aging axis is involved in Chl-mediated longevity benefits requires further examination. Addressing these questions will be crucial for understanding the precise molecular mechanisms underlying Chl's anti-aging effects and may uncover novel therapeutic targets for age-related diseases.

Author Contributions: S.S.: conceptualization, formal analysis, investigation, writing—original draft. N.X.: methodology, software, writing—review and editing. Z.Y.: methodology, software, writing—review and editing. Z.H.: writing—review and editing. L.Z.: writing—review and editing. A.N.I.: writing—review and editing. Y.Z.: resources, funding acquisition, project administration, supervision, validation, writing—review and editing. All authors have read and agreed to the published version of the manuscript.

Funding: This work was supported by the "Tianchi Talent" Introduction Plan: Distinguished Expert Program, National Natural Science Foundation of China (No. 32472494), Hainan Provincial Natural Science Foundation of China (No. 323CXTD381), Shenzhen Science and Technology Innovation Commission under the Major Science and Technology Special Project (Grant No. KCXFZ20240903094006009).

Data Availability Statement: The raw data supporting the conclusions of this article will be made available by the authors on request.

Conflicts of Interest: The authors declare no conflicts of interest.

References

1. Leidal, A.M.; Levine, B.; Debnath, J. Autophagy and the Cell Biology of Age-Related Disease. *Nat. Cell Biol.* **2018**, *20*, 1338–1348. [CrossRef] [PubMed]
2. Zhu, K.; Du, D.; Shi, Y.; Hu, F.; Zhang, W.; Ni, H.; Hafeez, E.; Chen, D. Poria Cocos Polysaccharide Delays Aging by Enhancing the Antioxidant Ability and Suppressing the Expression of the Branched-Chain Amino Acid Transferase-Encoding Gene in *Drosophila melanogaster*. *J. Agric. Food Chem.* **2025**, *73*, 9033–9046. [CrossRef]
3. Kennedy, B.K.; Berger, S.L.; Brunet, A.; Campisi, J.; Cuervo, A.M.; Epel, E.S.; Franceschi, C.; Lithgow, G.J.; Morimoto, R.I.; Pessin, J.E.; et al. Geroscience: Linking Aging to Chronic Disease. *Cell* **2014**, *159*, 709–713. [CrossRef]
4. Scott, A.J.; Ellison, M.; Sinclair, D.A. The Economic Value of Targeting Aging. *Nat. Aging* **2021**, *1*, 616–623. [CrossRef] [PubMed]
5. López-Otín, C.; Kroemer, G. Hallmarks of Health. *Cell* **2021**, *184*, 33–63. [CrossRef] [PubMed]
6. Partridge, L.; Deelen, J.; Slagboom, P.E. Facing up to the Global Challenges of Ageing. *Nature* **2018**, *561*, 45–56. [CrossRef]
7. Park, K.; Jeon, M.C.; Lee, D.; Kim, J.-I.; Im, S.-W. Genetic and Epigenetic Alterations in Aging and Rejuvenation of Human. *Mol. Cells* **2024**, *47*, 100137. [CrossRef]
8. Bong, D.; Kwon, H.C.; Lee, S.-J.V. Multilayered Regulation of Longevity in *Caenorhabditis elegans*. *Mol. Cells* **2026**, *49*, 100308. [CrossRef]
9. Campisi, J.; Kapahi, P.; Lithgow, G.J.; Melov, S.; Newman, J.C.; Verdin, E. From Discoveries in Ageing Research to Therapeutics for Healthy Ageing. *Nature* **2019**, *571*, 183–192. [CrossRef]
10. Martins, R.; Lithgow, G.J.; Link, W. Long Live FOXO: Unraveling the Role of FOXO Proteins in Aging and Longevity. *Aging Cell* **2016**, *15*, 196–207. [CrossRef]
11. Chen, J.-C.; Wang, R.; Wei, C.-C. Anti-Aging Effects of Dietary Phytochemicals: From *Caenorhabditis elegans*, *Drosophila melanogaster*, Rodents to Clinical Studies. *Crit. Rev. Food Sci. Nutr.* **2024**, *64*, 5958–5983. [CrossRef]
12. Xue, F.; Li, X.; Qin, L.; Liu, X.; Li, C.; Adhikari, B. Anti-Aging Properties of Phytoconstituents and Phyto-Nanoemulsions and Their Application in Managing Aging-Related Diseases. *Adv. Drug Deliv. Rev.* **2021**, *176*, 113886. [CrossRef] [PubMed]

13. Okoro, N.O.; Odiba, A.S.; Osadebe, P.O.; Omeje, E.O.; Liao, G.; Fang, W.; Jin, C.; Wang, B. Bioactive Phytochemicals with Anti-Aging and Lifespan Extending Potentials in *Caenorhabditis elegans*. *Molecules* **2021**, *26*, 7323. [CrossRef]
14. Shen, J.; Shan, J.; Zhong, L.; Liang, B.; Zhang, D.; Li, M.; Tang, H. Dietary Phytochemicals That Can Extend Longevity by Regulation of Metabolism. *Plant Foods Hum. Nutr.* **2022**, *77*, 12–19. [CrossRef] [PubMed]
15. Si, H.; Liu, D. Dietary Antiaging Phytochemicals and Mechanisms Associated with Prolonged Survival. *J. Nutr. Biochem.* **2014**, *25*, 581–591. [CrossRef]
16. Mattson, M.P. Hormesis Defined. *Ageing Res. Rev.* **2008**, *7*, 1–7. [CrossRef]
17. Xiong, L.-G.; Chen, Y.-J.; Tong, J.-W.; Gong, Y.-S.; Huang, J.-A.; Liu, Z.-H. Epigallocatechin-3-Gallate Promotes Healthy Lifespan through Mitohormesis during Early-to-Mid Adulthood in *Caenorhabditis elegans*. *Redox Biol.* **2018**, *14*, 305–315. [CrossRef]
18. Proshkina, E.; Lashmanova, E.; Dobrovolskaya, E.; Zemskaya, N.; Kudryavtseva, A.; Shaposhnikov, M.; Moskalev, A. Geroprotective and Radioprotective Activity of Quercetin, (-)-Epicatechin, and Ibuprofen in *Drosophila melanogaster*. *Front. Pharmacol.* **2016**, *7*, 505. [CrossRef]
19. Scuto, M.; Majzúnová, M.; Torcitto, G.; Antonuzzo, S.; Rampulla, F.; Di Fatta, E.; Trovato Salinaro, A. Functional Food Nutrients, Redox Resilience Signaling and Neurosteroids for Brain Health. *Int. J. Mol. Sci.* **2024**, *25*, 12155. [CrossRef]
20. Scuto, M.C.; Lombardo, C.; Musso, N.; Bonacci, P.G.; Lupo, G.; Anfuso, C.D.; Salinaro, A.T. Micro- and Nanoplastics and Human Health: Role of Food Nutrients Targeting Nfe2l2 Gene in Diabetes. *Nutrients* **2026**, *18*, 600. [CrossRef] [PubMed]
21. Scuto, M.C.; Anfuso, C.D.; Lombardo, C.; Di Fatta, E.; Ferri, R.; Musso, N.; Zerbo, G.; Terrana, M.; Majzúnová, M.; Lupo, G.; et al. Neuronutrition and Nrf2 Brain Resilience Signaling: Epigenomics and Metabolomics for Personalized Medicine in Nervous System Disorders from Bench to Clinic. *Int. J. Mol. Sci.* **2025**, *26*, 9391. [CrossRef]
22. Lee, J.; Kwak, M.; Chang, Y.K.; Kim, D. Green Solvent-Based Extraction of Chlorophyll a from *Nannochloropsis* sp. Using 2,3-Butanediol. *Sep. Purif. Technol.* **2021**, *276*, 119248. [CrossRef]
23. Liu, J.; Kong, T.; Xiong, H.-M. Mulberry-Leaves-Derived Red-Emissive Carbon Dots for Feeding Silkworms to Produce Brightly Fluorescent Silk. *Adv. Mater.* **2022**, *34*, 2200152. [CrossRef] [PubMed]
24. Miyatake, T.; Tamiaki, H. Self-Aggregates of Natural Chlorophylls and Their Synthetic Analogues in Aqueous Media for Making Light-Harvesting Systems. *Coord. Chem. Rev.* **2010**, *254*, 2593–2602. [CrossRef]
25. Li, Y.; Cui, Y.; Hu, X.; Liao, X.; Zhang, Y. Chlorophyll Supplementation in Early Life Prevents Diet-Induced Obesity and Modulates Gut Microbiota in Mice. *Mol. Nutr. Food Res.* **2019**, *63*, 1801219. [CrossRef] [PubMed]
26. Li, Y.; Lu, F.; Wang, X.; Hu, X.; Liao, X.; Zhang, Y. Biological Transformation of Chlorophyll-Rich Spinach (*Spinacia oleracea* L.) Extracts under In Vitro Gastrointestinal Digestion and Colonic Fermentation. *Food Res. Int.* **2021**, *139*, 109941. [CrossRef]
27. Wang, X.; Yang, Z.; Shen, S.; Ji, X.; Chen, F.; Liao, X.; Zhang, H.; Zhang, Y. Inhibitory Effects of Chlorophylls and Its Derivative on Starch Digestion In Vitro. *Food Chem.* **2023**, *413*, 135377. [CrossRef]
28. Qiu, S.; Xiao, C.; Meldrum Robertson, R. Different Age-Dependent Performance in *Drosophila* Wild-Type Canton-S and the White Mutant W^{1118} Flies. *Comp. Biochem. Physiol. Part A Mol. Integr. Physiol.* **2017**, *206*, 17–23. [CrossRef]
29. Abdul Halim, M.; Tan, F.H.P.; Azlan, A.; Rasyid, I.I.; Rosli, N.; Shamsuddin, S.; Azzam, G. Ageing, *Drosophila melanogaster* and Epigenetics. *Malays J. Med. Sci.* **2020**, *27*, 7–19. [CrossRef]
30. Yamaguchi, M.; Yoshida, H. *Drosophila* as a Model Organism. In *Drosophila Models for Human Diseases*; Yamaguchi, M., Ed.; Springer: Singapore, 2018; pp. 1–10, ISBN 978-981-13-0529-0.
31. Li, F.; Zhou, L.; Cao, J.; Wang, Z.; Liao, X.; Zhang, Y. Aggregation Induced by the Synergy of Sodium Chloride and High-Pressure Improves Chlorophyll Stability. *Food Chem.* **2022**, *366*, 130577. [CrossRef]
32. Sánchez, C.; Baranda, A.B.; Martínez de Marañón, I. The Effect of High Pressure and High Temperature Processing on Carotenoids and Chlorophylls Content in Some Vegetables. *Food Chem.* **2014**, *163*, 37–45. [CrossRef] [PubMed]
33. Cao, J.; Li, F.; Li, Y.; Chen, H.; Liao, X.; Zhang, Y. Hydrophobic Interaction Driving the Binding of Soybean Protein Isolate and Chlorophyll: Improvements to the Thermal Stability of Chlorophyll. *Food Hydrocoll.* **2021**, *113*, 106465. [CrossRef]
34. Libert, S.; Zwiener, J.; Chu, X.; VanVoorhies, W.; Roman, G.; Pletcher, S.D. Regulation of *Drosophila* Life Span by Olfaction and Food-Derived Odors. *Science* **2007**, *315*, 1133–1137. [CrossRef]
35. Castillo-Quan, J.I.; Tain, L.S.; Kinghorn, K.J.; Li, L.; Grönke, S.; Hinze, Y.; Blackwell, T.K.; Bjedov, I.; Partridge, L. A Triple Drug Combination Targeting Components of the Nutrient-Sensing Network Maximizes Longevity. *Proc. Natl. Acad. Sci. USA* **2019**, *116*, 20817–20819. [CrossRef] [PubMed]
36. Lv, P.; Yang, X.; Du, J. LKRSDH-Dependent Histone Modifications of Insulin-like Peptide Sites Contribute to Age-Related Circadian Rhythm Changes. *Nat. Commun.* **2024**, *15*, 3336. [CrossRef]
37. Klarsfeld, A.; Leloup, J.-C.; Rouyer, F. Circadian Rhythms of Locomotor Activity in *Drosophila*. *Behav. Process.* **2003**, *64*, 161–175. [CrossRef]
38. Wongchum, N.; Dechakhamphu, A. Xanthohumol Prolongs Lifespan and Decreases Stress-Induced Mortality in *Drosophila melanogaster*. *Comp. Biochem. Physiol. Part C Toxicol. Pharmacol.* **2021**, *244*, 108994. [CrossRef] [PubMed]

39. Jo, A.R.; Imm, J.-Y. Effects of Aronia Extract on Lifespan and Age-Related Oxidative Stress in *Drosophila melanogaster*. *Food Sci. Biotechnol.* **2017**, *26*, 1399–1406. [CrossRef]
40. Zou, Y.-X.; Ruan, M.-H.; Luan, J.; Feng, X.; Chen, S.; Chu, Z.-Y. Anti-Aging Effect of Riboflavin via Endogenous Antioxidant in Fruit Fly *Drosophila melanogaster*. *J. Nutr. Health Aging* **2017**, *21*, 314–319. [CrossRef]
41. Scuto, M.; Rampulla, F.; Reali, G.M.; Spanò, S.M.; Trovato Salinaro, A.; Calabrese, V. Hormetic Nutrition and Redox Regulation in Gut-Brain Axis Disorders. *Antioxidants* **2024**, *13*, 484. [CrossRef]
42. Park, S.; Kim, B.-K.; Park, S.-K. Supplementation with Phosphatidylethanolamine Confers Anti-Oxidant and Anti-Aging Effects via Hormesis and Reduced Insulin/IGF-1-like Signaling in *C. elegans*. *Mech. Ageing Dev.* **2021**, *197*, 111498. [CrossRef] [PubMed]
43. Wang, E.; Wink, M. Chlorophyll Enhances Oxidative Stress Tolerance in *Caenorhabditis elegans* and Extends Its Lifespan. *PeerJ* **2016**, *4*, e1879. [CrossRef] [PubMed]
44. Youdim, K.A.; Joseph, J.A. A Possible Emerging Role of Phytochemicals in Improving Age-Related Neurological Dysfunctions: A Multiplicity of Effects. *Free Radic. Biol. Med.* **2001**, *30*, 583–594. [CrossRef]
45. Moskalev, A.A.; Zaĭnullin, V.G. Life-Span in Generations of Chronic Irradiated *Drosophila* Wild Type Isogenic and Geterogenic Strains. *Radiatsionnaia Biol. Radioecol.* **2006**, *46*, 436–440.
46. Hodge, B.A.; Meyerhof, G.T.; Katewa, S.D.; Lian, T.; Lau, C.; Bar, S.; Leung, N.Y.; Li, M.; Li-Kroeger, D.; Melov, S.; et al. Dietary Restriction and the Transcription Factor Clock Delay Eye Aging to Extend Lifespan in *Drosophila melanogaster*. *Nat. Commun.* **2022**, *13*, 3156. [CrossRef] [PubMed]
47. He, J.; Li, X.; Yang, S.; Li, Y.; Lin, X.; Xiu, M.; Li, X.; Liu, Y. Gastrodin Extends the Lifespan and Protects against Neurodegeneration in the *Drosophila* PINK1 Model of Parkinson's Disease. *Food Funct.* **2021**, *12*, 7816–7824. [CrossRef]
48. Di Francesco, A.; Deighan, A.G.; Litichevskiy, L.; Chen, Z.; Luciano, A.; Robinson, L.; Garland, G.; Donato, H.; Vincent, M.; Schott, W.; et al. Dietary Restriction Impacts Health and Lifespan of Genetically Diverse Mice. *Nature* **2024**, *634*, 684–692. [CrossRef]
49. Allemand, R. Influence of Light Condition Modification on the Circadian Rhythm of Vitellogenesis and Ovulation in *Drosophila melanogaster*. *J. Insect Physiol.* **1976**, *22*, 1075–1080. [CrossRef]
50. Nagayach, A.; Bhaskar, R.; Ghosh, S.; Abomughaid, M.M.; Han, S.S.; Singh, K.K.; Almutary, A.G.; Chaudhary, K.; Atteri, S.; Chauhan, A.S.; et al. Interplay between Circadian Rhythm, Ageing and Neurodegenerative Disorder. *Open Biol.* **2025**, *15*, 240161. [CrossRef]
51. Cheng, S.-C.; Li, W.-H.; Shi, Y.-C.; Yen, P.-L.; Lin, H.-Y.; Liao, V.H.-C.; Chang, S.-T. Antioxidant Activity and Delayed Aging Effects of Hot Water Extract from *Chamaecyparis obtusa* var. *formosana* Leaves. *J. Agric. Food Chem.* **2014**, *62*, 4159–4165. [CrossRef]
52. Grasemann, H.; Holguin, F. Oxidative Stress and Obesity-Related Asthma. *Paediatr. Respir. Rev.* **2021**, *37*, 18–21. [CrossRef] [PubMed]
53. Minich, D.M.; Brown, B.I.; Minich, D.M.; Brown, B.I. A Review of Dietary (Phyto)Nutrients for Glutathione Support. *Nutrients* **2019**, *11*, 2073. [CrossRef]
54. Baumeister, R.; Schaffitzel, E.; Hertweck, M. Endocrine Signaling in *Caenorhabditis elegans* Controls Stress Response and Longevity. *J. Endocrinol.* **2006**, *190*, 191–202. [CrossRef]
55. Spiers, J.G.; Breda, C.; Robinson, S.; Giorgini, F.; Steinert, J.R. *Drosophila* Nrf2/Keap1 Mediated Redox Signaling Supports Synaptic Function and Longevity and Impacts on Circadian Activity. *Front. Mol. Neurosci.* **2019**, *12*, 86. [CrossRef] [PubMed]
56. Calabrese, E.J.; Nascarella, M.; Pressman, P.; Hayes, A.W.; Dhawan, G.; Kapoor, R.; Calabrese, V.; Agathokleous, E. Hormesis Determines Lifespan. *Ageing Res. Rev.* **2024**, *94*, 102181. [CrossRef] [PubMed]
57. Govindan, S.; Amirthalingam, M.; Duraisamy, K.; Govindhan, T.; Sundararaj, N.; Palanisamy, S. Phytochemicals-Induced Hormesis Protects *Caenorhabditis elegans* against α-Synuclein Protein Aggregation and Stress through Modulating HSF-1 and SKN-1/Nrf2 Signaling Pathways. *Biomed. Pharmacother.* **2018**, *102*, 812–822. [CrossRef]
58. Castillo-Quan, J.I.; Li, L.; Kinghorn, K.J.; Ivanov, D.K.; Tain, L.S.; Slack, C.; Kerr, F.; Nespital, T.; Thornton, J.; Hardy, J.; et al. Lithium Promotes Longevity through GSK_3/NRF_2-Dependent Hormesis. *Cell Rep.* **2016**, *15*, 638–650. [CrossRef]
59. Halliwell, B. Free Radicals and Antioxidants: Updating a Personal View. *Nutr. Rev.* **2012**, *70*, 257–265. [CrossRef]
60. Sadowska-Bartosz, I.; Bartosz, G. Effect of Antioxidants Supplementation on Aging and Longevity. *Biomed. Res. Int.* **2014**, *2014*, 404680. [CrossRef]
61. Kharat, P.; Sarkar, P.; Mouliganesh, S.; Tiwary, V.; Priya, V.B.R.; Sree, N.Y.; Annapoorna, H.V.; Saikia, D.K.; Mahanta, K.; Thirumurugan, K. Ellagic Acid Prolongs the Lifespan of *Drosophila melanogaster*. *GeroScience* **2020**, *42*, 271–285. [CrossRef]
62. Hayes, J.D.; Pulford, D.J. The Glut Athione S-Transferase Supergene Family: Regulation of GST and the Contribution of the Lsoenzymes to Cancer Chemoprotection and Drug Resistance Part I. *Crit. Rev. Biochem. Mol. Biol.* **1995**, *30*, 445–520. [CrossRef] [PubMed]
63. Gonzalez, D.; Fraichard, S.; Grassein, P.; Delarue, P.; Senet, P.; Nicolaï, A.; Chavanne, E.; Mucher, E.; Artur, Y.; Ferveur, J.-F.; et al. Characterization of a *Drosophila* Glutathione Transferase Involved in Isothiocyanate Detoxification. *Insect Biochem. Mol. Biol.* **2018**, *95*, 33–43. [CrossRef]
64. Nebert, D.W.; Vasiliou, V. Analysis of the Glutathione S-Transferase (GST) Gene Family. *Hum. Genom.* **2004**, *1*, 460. [CrossRef]

65. Santhi Priya, S.; Kumar Ebenezar, K. Susceptibility of Polymorphic GST as a Risk Factor in Oxidative Stress-Induced Cancer Development. In *Handbook of Oxidative Stress in Cancer: Therapeutic Aspects*; Springer: Singapore, 2022; pp. 3757–3772, ISBN 978-981-16-5422-0.
66. Li, X.; Schuler, M.A.; Berenbaum, M.R. Molecular Mechanisms of Metabolic Resistance to Synthetic and Natural Xenobiotics. *Annu. Rev. Entomol.* **2007**, *52*, 231–253. [CrossRef] [PubMed]
67. Sun, L.; Yin, J.; Du, H.; Liu, P.; Cao, C. Characterisation of GST Genes from the *Hyphantria cunea* and Their Response to the Oxidative Stress Caused by the Infection of *Hyphantria cunea* Nucleopolyhedrovirus (HcNPV). *Pestic. Biochem. Physiol.* **2020**, *163*, 254–262. [CrossRef]
68. Chen, X.; Li, H.; Zhang, J.; Ding, Y.; You, J. Does Cadmium Affect the Toxicokinetics of Permethrin in *Chironomus dilutus* at Sublethal Level? Evidence of Enzymatic Activity and Gene Expression. *Environ. Pollut.* **2016**, *218*, 1005–1013. [CrossRef]
69. Orr, W.C.; Radyuk, S.N.; Sohal, R.S. Involvement of Redox State in the Aging of *Drosophila melanogaster*. *Antioxid. Redox Signal* **2013**, *19*, 788–803. [CrossRef] [PubMed]
70. Lennicke, C.; Cochemé, H.M. Redox Signalling and Ageing: Insights from *Drosophila*. *Biochem. Soc. Trans.* **2020**, *48*, 367–377. [CrossRef]
71. Anisimov, V.N.; Bartke, A. The Key Role of Growth Hormone–Insulin–IGF-1 Signaling in Aging and Cancer. *Crit. Rev. Oncol. Hematol.* **2013**, *87*, 201–223. [CrossRef]
72. Birnbaum, A.; Wu, X.; Tatar, M.; Liu, N.; Bai, H. Age-Dependent Changes in Transcription Factor FOXO Targeting in Female *Drosophila*. *Front. Genet.* **2019**, *10*, 312. [CrossRef]
73. Lu, T.-C.; Brbić, M.; Park, Y.-J.; Jackson, T.; Chen, J.; Kolluru, S.S.; Qi, Y.; Katheder, N.S.; Cai, X.T.; Lee, S.; et al. Aging Fly Cell Atlas Identifies Exhaustive Aging Features at Cellular Resolution. *Science* **2023**, *380*, eadg0934. [CrossRef] [PubMed]
74. Pandey, U.B.; Nichols, C.D. Human Disease Models in *Drosophila melanogaster* and the Role of the Fly in Therapeutic Drug Discovery. *Pharmacol. Rev.* **2011**, *63*, 411–436. [CrossRef] [PubMed]

Disclaimer/Publisher's Note: The statements, opinions and data contained in all publications are solely those of the individual author(s) and contributor(s) and not of MDPI and/or the editor(s). MDPI and/or the editor(s) disclaim responsibility for any injury to people or property resulting from any ideas, methods, instructions or products referred to in the content.

nutrients

MDPI

Review

Edible Bird's Nest as a Multi-Component Functional Food for Brain Aging: From Single-Bioactive Actions to Network-Regulatory Mechanisms

Wenjuan Gong [1,2,†], Xintong Wang [1,†], Wen Zhang [1], Huihui Wang [1], Wei Xiong [3], Yixuan Li [1], Pengcheng Wen [2,*] and Yanan Sun [1,*]

[1] Key Laboratory of Precision Nutrition and Food Quality, Department of Nutrition and Health, China Agricultural University, Beijing 100083, China; gongwj2023@163.com (W.G.); xtwang@cau.edu.cn (X.W.); zhangwen02919@126.com (W.Z.); whhlyh1227@163.com (H.W.); liyixuan@cau.edu.cn (Y.L.)
[2] College of Food Science and Engineering, Gansu Agricultural University, Lanzhou 730070, China
[3] Food Laboratory of Zhongyuan, Luohe 462000, China; xiongwei@zyfoodlab.cn
* Correspondence: wenpch@126.com (P.W.); 15153515695@163.com (Y.S.)
† These authors contributed equally to this work.

Abstract

Functional food research has long emphasized isolated bioactive compounds, yet such single-target strategies often show limited efficacy against complex, multifactorial processes such as brain aging. In this review, we examine edible bird's nest (EBN) as a representative multi-component functional food and discuss how its complex food matrix may exert coordinated neuroprotective effects. We summarize the major bioactive constituents of EBN, including sialic acid, functional glycoproteins, and bioactive peptides, and organize their actions into functional modules related to oxidative stress, neuroinflammation, apoptosis, synaptic maintenance, and neurotrophic support. Emerging evidence on the prebiotic potential of EBN and its modulation of the gut–brain axis is also integrated, highlighting interactions between peripheral metabolic regulation and central nervous system function. By comparing EBN with conventional functional ingredients such as vitamins C and E, coenzyme Q10, curcumin, and omega-3 fatty acids, we propose that EBN represents a distinctive "network-regulatory" food system in which nutritional support and pathway modulation are intrinsically linked. Overall, this review provides a conceptual framework for understanding how complex food matrices can be rationally applied to support brain health and reduce age-related neurodegenerative risk.

Keywords: functional foods; edible bird's nest; brain aging; multi-target effects; food-derived sources

1. Introduction

Complex dietary foods composed of multiple interacting bioactive constituents have attracted increasing attention in functional food research due to their potential to provide coordinated, multi-target physiological regulation beyond isolated compounds. Representative substances such as ginseng, goji berry, and ganoderma epitomize this preventive wisdom [1,2]. Modern science increasingly recognizes certain dietary foods as promising reservoirs of complex bioactive compounds, whose multi-component nature provides a unique basis for addressing multifaceted health challenges. Among these foods, edible bird's nest (EBN) occupies a distinctive position as an uncommon but established dietary

component in several Asian regions [3]. Composed primarily of the salivary secretions of swiftlets, EBN has been consumed for centuries as a nutrient-dense food and is often regarded as a premium functional ingredient [4]. These findings suggest that EBN represents a complex functional food matrix rather than a single bioactive source, providing a scientific basis for exploring its multi-target regulatory potential in health maintenance. The critical distinction lies in the fundamental difference between EBN's matrix structure and that of botanical supplements rich in phytochemicals, such as ginseng and goji berries. Most plant-derived functional foods consist primarily of small-molecule secondary metabolites [5], whereas EBN's biological activity stems from its unique protein–glycoprotein–sialic acid core structure [6]. This compositional characteristic indicates a distinct mechanism of action. Therefore, this review proposes a "network regulation" framework that integrates systems biology thinking with food matrix theory. The innovation of this framework lies not in introducing novel biological mechanisms, but in elucidating how naturally complex foods such as EBN achieve coordinated multi-target regulation in the context of brain aging.

The urgency of this research direction stems from the macro-context of global demographic shifts and the specific challenges in brain health. In recent years, the global aging process has accelerated, with projections indicating that by 2050, individuals aged 65 and above will comprise 16% of the global population [7]. This trend is accompanied by a significant increase in the prevalence of age-related neurodegenerative diseases, such as Alzheimer's disease (AD) and Parkinson's disease (PD), which pose formidable challenges to global public health systems [8]. Brain aging is a complex pathological process involving multidimensional mechanisms, including oxidative stress, neuroinflammation, mitochondrial dysfunction, protein homeostasis imbalance, and dysregulation of the gut–brain axis [9]. Owing to its high metabolic rate, lipid-rich composition, and relatively limited antioxidant capacity, the brain is especially vulnerable to redox imbalance and oxidative injury during aging [10,11]. Consequently, oxidative stress serves as a central initiator, triggering inflammatory cycles that form a vicious circle with gut microbiota dysbiosis, collectively accelerating neuronal damage and cognitive decline [12]. This intricate interplay of multiple mechanisms often renders traditional single-target intervention strategies limited in efficacy.

In light of this context, the adage "prevention is better than cure" has garnered increasing significance, prompting research efforts aimed at identifying multi-targeted, safe intervention strategies derived from natural dietary resources [13]. It is imperative to note that the compelling preclinical rationale for EBN currently far outpaces the clinical evidence in humans. High-quality randomized controlled trials (RCTs) investigating its effects on cognitive outcomes are notably absent. Therefore, this review reframes EBN as a complex food-derived system, whose long history of dietary consumption has prompted modern investigations into its multi-component, network-regulatory functions relevant to brain aging. By organizing EBN bioactive components into functional modules and integrating direct neuroprotective actions with emerging evidence on gut–brain axis modulation, this review seeks to clarify how complex dietary matrices can exert coordinated effects on brain aging. Through comparison with conventional functional ingredients, we further highlight the distinctive advantages of such complex food systems and provide a conceptual framework for their rational application in brain health maintenance and neurodegenerative disease prevention.

2. Nutritional Components and Bioactive Substances in EBN

EBN is a nest constructed by swiftlets using their saliva or a mixture of saliva and down feathers. It is primarily produced in Southeast Asian countries such as Indonesia, Malaysia, Thailand, and Vietnam (Figure 1) [4].

https://doi.org/10.3390/nu18040671

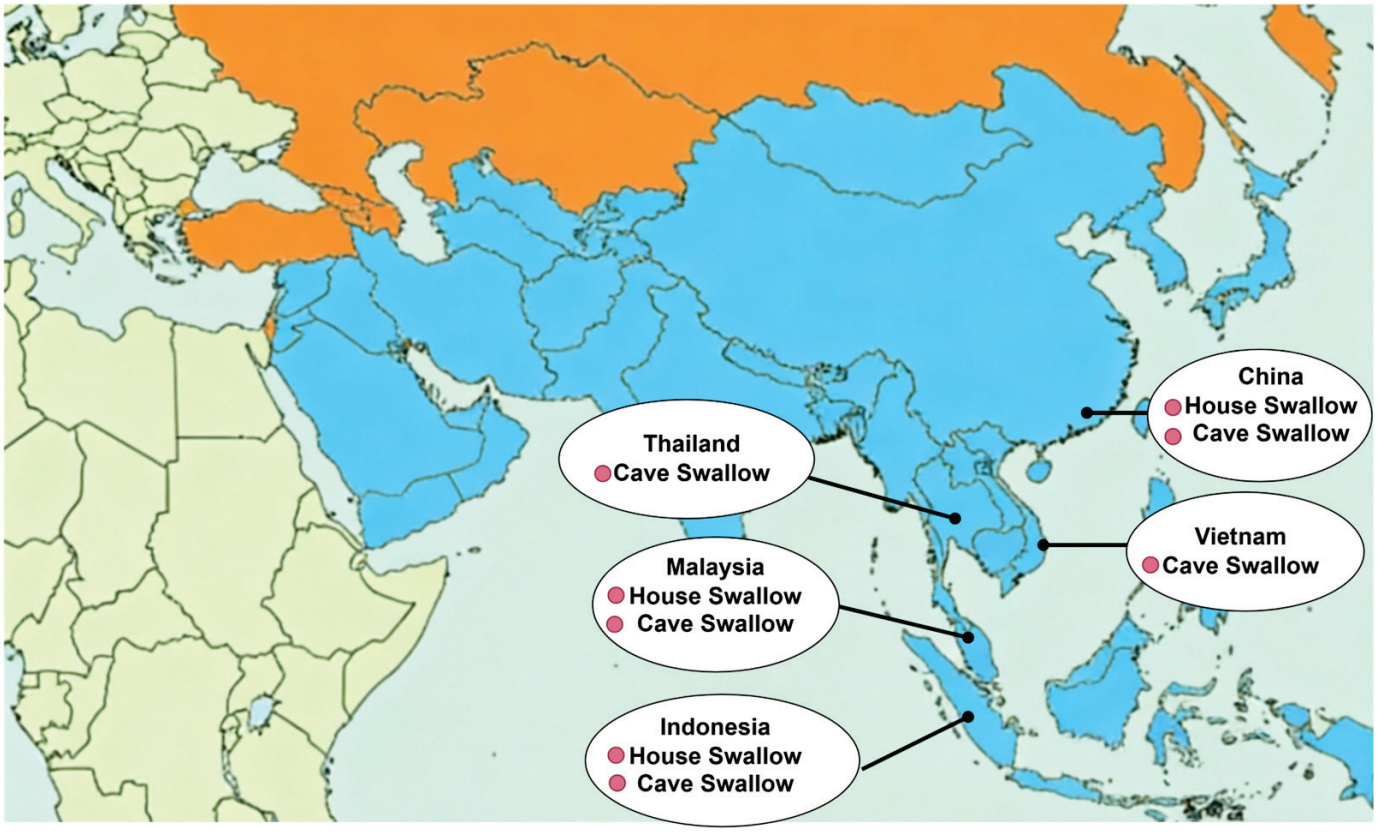


Figure 1. Primary production areas and types of edible bird's nest (EBN). Blue-shaded regions indicate the major EBN-producing countries in Southeast Asia. Red dots denote representative production types, including house swallow nests and cave swallow nests. The map was created using Figdraw (Version 2.0, www.figdraw.com).

Numerous researchers have investigated the active constituents of EBN (Figure 2), identifying that its nutritional composition predominantly consists of proteins, carbohydrates, amino acids, minor lipids, and trace elements, including calcium (Ca), iron (Fe), and selenium (Se) [14]. The composition of EBN is subject to variation due to factors such as the species of swiftlet, available food resources, nesting season, and processing methods [15]. For example, Quek et al. conducted an analysis of the nutritional composition, physicochemical properties, and antioxidant characteristics of EBN sourced from domesticated swiftlets, brown swiftlets, and the Malay Peninsula. This study considered three dimensions: production methods, swiftlet species, and geographical origin. The total amino acid content in nests of the brown swiftlet (*Aerodramus fuciphagus*) was found to be 64.57 g/100 g, surpassing that of the giant swiftlet (*Aerodramus maximus*) nests by 23%. EBN obtained from farmed brown swiftlets and the Malay Peninsula demonstrated the highest antioxidant activity, ranging from 2.33 to 3.49 mg ascorbic acid equivalent per gram (mg AAE/g), and the highest sialic acid content, measured at 13.57 g/100 g. In contrast, EBN derived from cave-dwelling giant swiftlets and regions in East Malaysia was notably rich in minerals such as calcium and magnesium. The radical scavenging activity of 1,1-diphenyl-2-picrylhydrazyl (DPPH) and the ferrous reduction antioxidant capacity (FRAP) of EBN derived from domesticated brown swiftlets in the Malay Peninsula region are approximately twice as elevated as those from other geographic regions [16].

https://doi.org/10.3390/nu18040671

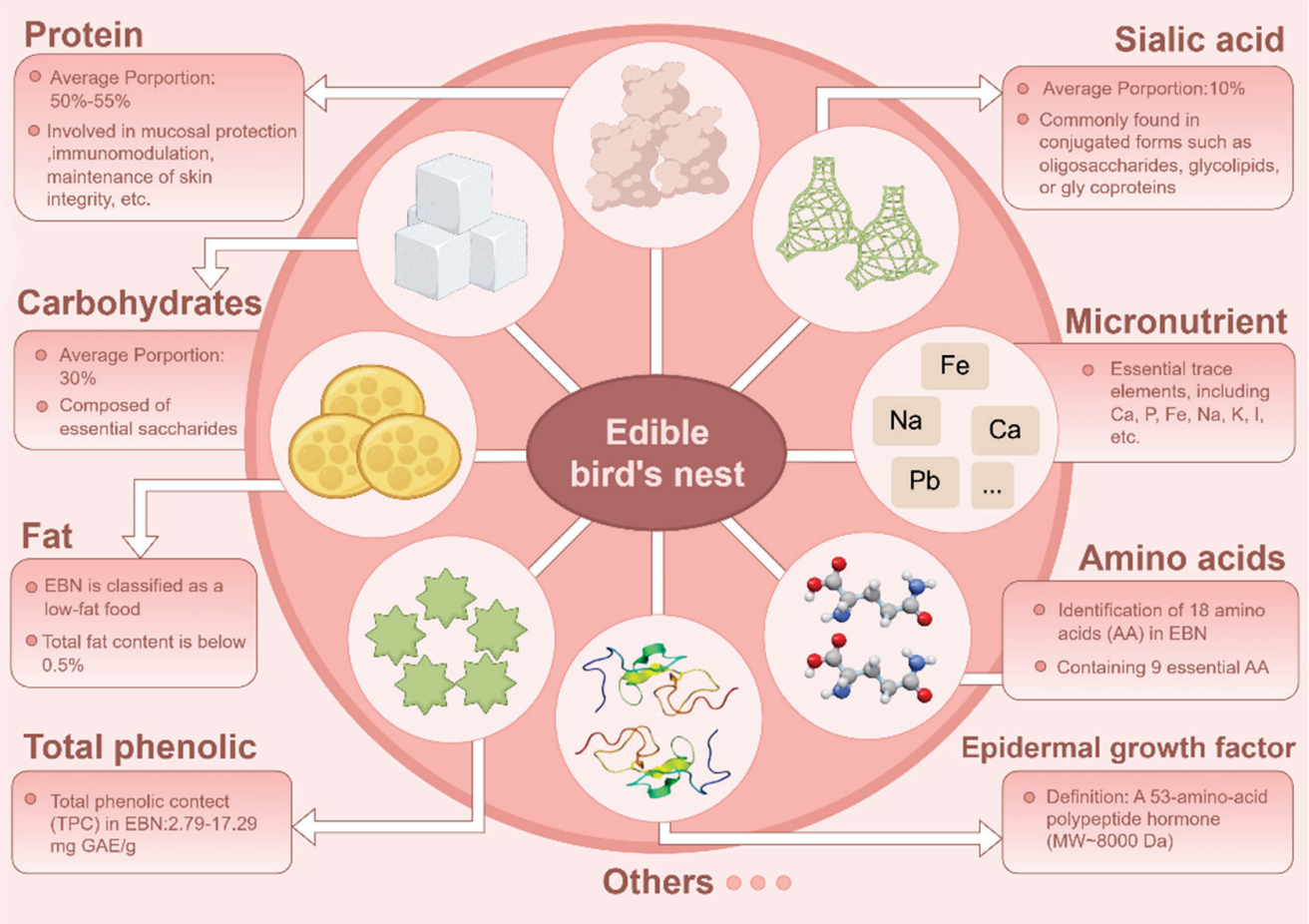


Figure 2. Bioactive nutritional composition of edible bird's nest (EBN). The primary nutritional constituents of EBN are protein, carbohydrates, sialic acid, amino acids, fats, trace elements, epidermal growth factor (EGF), and total phenols. This figure was created using Figdraw (Version 2.0, www.figdraw.com).

2.1. Proteins

Proteins represent the predominant component of EBN, with an average content ranging from 50% to 55% [17]. Zukefli utilized ultrasonication-assisted methods, detergent-assisted techniques (specifically Triton X-100 and SDS), and Tris-HCl buffer dissolution to analyze and compare the protein profiles of EBN sourced from two distinct Malaysian locations. The results indicated a significantly higher concentration of water-soluble proteins in EBN [18]. Through the application of various separation and analytical techniques, including gel permeation chromatography (GPC) and reverse-phase high-performance liquid chromatography (RP-HPLC), numerous researchers have identified 58 unique protein molecules within EBN. Notable among these are acidic mammalian chitinase (AM Case), lysyl oxidase homologue 3 (LOXL3), mucin-5AC (MUC5AC), ovoinhibitor, Nucleobindin-2 (NUCB2), calcium-binding protein and glucose regulator protein. These proteins are implicated in a range of biological functions, including immunoregulation, mucosal protection, maintenance of skin integrity, and regulation of enzymatic activity [19]. Wang et al. conducted an analysis of the protein composition of four EBN strains sourced from three major production regions using label-free quantitative proteomics, identifying a total of 37 functional proteins. Among these, six core proteins were identified, specifically mucin 5B (MUC5B), lysyl oxidase-like protein 2 (LOXL2), chitinase (CHIA), ovomucoid-like protein (OIH), and calcium-binding protein 45 (CAB45). Gene Ontology (GO) functional annotation revealed that the majority of EBN proteins are classified within the secreted

protein category and exhibit various enzymatic activities [20]. Notably, EBN also contains a 66 kDa protein that functions as an IgE-mediated allergen, which has the potential to induce anaphylactic shock in children [21]. Additionally, Yew et al. identified 29 proteins in EBN extract through de novo peptide sequencing utilizing tandem mass spectrometry. These proteins are implicated in various biological mechanisms, including immunoregulation, extracellular matrix formation, neurodevelopment, cell survival and apoptosis, cell proliferation and migration, antioxidant activity, and other fundamental cellular processes. For example, the study demonstrated that EBN contains a variety of proteins that play significant roles in cell proliferation and migration. These include members of the repulsive guidance molecule domain family B, which facilitate neurite extension and axonal growth, as well as proteins such as lin-9 and the hyaluronan-mediated motility receptor, which are also implicated in cell proliferation and migration [22]. Furthermore, bioactive peptides produced through the enzymatic hydrolysis of EBN exhibit a wide range of biological and nutritional properties. Antioxidant peptides derived from this process possess advantageous pharmacokinetic and pharmacodynamic attributes, including high bioavailability in humans, strong antioxidant activity, and minimal adverse effects [14]. For instance, Zhang et al. conducted an extraction of EBN samples using hot water at 100 °C, followed by enzymatic digestion with pepsin (10,000 units), trypsin (36 mg), and bile extract (112.5 mg). The study employed pH variations to mimic the intestinal environment, ranging from 8.9 to 2 and returning to 8.9, in conjunction with a 10 kDa dialysis membrane to simulate gastrointestinal digestion and absorption processes. The results indicated that undigested aqueous extracts of EBN displayed minimal antioxidant activity, whereas digested samples showed a significant enhancement in antioxidant activity at comparable concentrations [23]. In a separate investigation, researchers employed pepsin–trypsin hydrolysis on EBN and identified two novel antioxidant pentapeptides in the resulting hydrolysate: Pro-Phe-His-Pro-Tyr and Leu-Leu-Gly-Asp-Pro. These peptides demonstrated resistance to gastrointestinal proteases and exhibited no cytotoxic effects in vitro on human lung MRC-5 cells, while also providing protection to human hepatocellular carcinoma HepG2 cells against hydroxyl radical-induced damage [24]. Additionally, Lee et al. utilized alkaline enzyme hydrolysis on EBN protein, followed by isolation, purification, and identification of antioxidant and anti-inflammatory peptides using ultrafiltration, gel chromatography, and mass spectrometry. Molecular docking analysis revealed that peptide segment 1 (LFWSPSVYLK) and peptide segment 2 (GWPHLEDNYLDW) possess hydrophobic and antioxidant amino acids, which effectively inhibit the formation of the Keap1-Nrf2 complex through competitive interactions. In contrast, peptide 3 (NPPADLHK) and peptide 4 (GDLAYLDQGHR) demonstrated significant regulatory effects on the IKK-β binding site, facilitated by interactions between their anti-inflammatory amino acids and C-terminal arginine/lysine residues [25].

2.2. Carbohydrates

Carbohydrates represent the second most abundant class of substances after proteins, comprising approximately 30% of the total composition. They predominantly consist of seven of the eight essential sugars necessary for human biological activity, including 7.2% N-acetylgalactosamine, 5.3% N-acetylglucosamine, 16.9% galactose, 0.7% fucose, and N-acetylneuraminic acid (sialic acid) [6,26]. The carbohydrates in EBN combine with proteins to form glycoproteins, a complex structure that endows bird's nest with unique biological activity [27].

2.3. Sialic Acids

EBN is a rich dietary source of sialic acid (SA), accounting for approximately 10% of the total, and is typically found in bound forms such as oligosaccharides, glycolipids, or glyco-

proteins. SA are classified into four distinct types based on the substituent group attached to the carbon 5 position: N-acetylneuraminic acid (Neu5Ac or NANA), N-glycolylneuraminic acid (Neu5Gc), diamino neuraminic acid (KDN), and neuraminic acid (Neu) [28]. In the context of EBN, SA specifically refers to Neu5Ac. This compound is a critical component of EBN, essential for infant brain development as it significantly contributes to synaptic connectivity, neuronal growth, memory formation, and immune system enhancement [29]. Empirical evidence suggests a strong correlation between mammalian cognitive capabilities and variations in brain SA concentrations. Exogenously administered SA is localized within synaptic regions, where it affects the dynamics of positive neurotransmitter movement, neurotransmitter release, and modifications to existing synaptic structures [30]. Furthermore, research indicates that a reduction in both endogenous and exogenous brain SA concentrations can lead to irreversible cognitive decline, although SA supplementation has been shown to enhance learning processes [31].

2.4. Amino Acids

Eighteen amino acids have been identified in EBN, including the nine essential amino acids necessary for human growth and repair [32]. Studies suggest that the total essential amino acid content in EBN is 17.8 g/100 g, which is substantially higher than that found in common high protein foods, such as eggs (4.7–7.0 g/100 g) and milk (1.1 g/100 g) [16]. Notably, lysine and tryptophan, which are typically absent in most plant proteins, are present in EBN, rendering it a complete amino acid source for vegetarians. Arginine and serine are the predominant essential and non-essential amino acids, comprising 4.0–4.7% and 4.0–5.5% of the total amino acid content, respectively [33]. Additionally, EBN is enriched with antioxidant amino acids, including proline, histidine, phenylalanine, and tryptophan, indicating its potential utility as a high-quality essential amino acid supplement in dietary nutritional interventions [34].

2.5. Fats

EBN is classified as a low-fat food product, characterized by a total fat content of less than 0.5%. The triglyceride profile of EBN demonstrates unique functional properties: polyunsaturated fatty acids represent the largest fraction at 48.43%, with linoleic acid, an essential fatty acid, comprising 47.15% of this category. Saturated fatty acids make up 25.35% of the total, with palmitic acid being the most prevalent at 21.33%. Monounsaturated fatty acids account for 24.74%, primarily consisting of oleic acid at 21.97% [35].

2.6. Microelements

EBN is also a source of essential trace elements, including Ca, phosphorus (P), Fe, sodium (Na), potassium (K), and iodine (I). The concentrations of these minerals and metal ions may originate from the swiftlets, the birds responsible for constructing EBN, or from environmental seepage. Due to the diverse geographic origins and types of samples, there is significant variability in their concentration ranges [36]. Studies have reported relatively high Na content (6017 mg/kg), along with notable levels of magnesium (Mg) (344 mg/kg), K (138 mg/kg), and Ca (68 mg/kg). Other minerals such as P, Fe, chromium (Cr), and selenium (Se) are present at concentrations of 0.037, 4.52, 0.30, and 0.14 mg/kg, respectively [15]. However, EBN also contains toxic elements, including lead (Pb), cadmium (Cd), arsenic (As), and mercury (Hg), which necessitates rigorous monitoring of the processing procedures [36].

2.7. Epidermal Growth Factor

Epidermal Growth Factor (EGF) is a low molecular weight polypeptide hormone consisting of 53 amino acids, with an approximate molecular weight of 8000 Da. It is

https://doi.org/10.3390/nu18040671

integral to cellular and tissue growth, proliferation, differentiation, and development [37, 38]. Additionally, EGF significantly influences physiological processes such as cellular damage repair, wound healing, tissue regeneration, and inflammatory responses [34]. In vivo, EGF modulates the proliferation, migration, and neurogenesis of neural stem cells (NSCs). Consequently, it is postulated that EBN extract may exhibit EGF-like activity, producing similar effects on NSCs [22].

2.8. Total Phenols

The total phenolic content (TPC) in EBN ranges from 2.79 to 17.29 mg GAE/g, which is higher than that found in honey and vegetables such as broccoli, carrot, and ginger, which have TPC ranges of 1.1–2.0 mg GAE/g and 0.3–4.0 mg GAE/g, respectively [16]. It is important to note that these phenolic compounds, likely derived from the swiftlet's insectivorous diet or as metabolic byproducts, represent a heterogeneous and minimally characterized fraction within EBN. While contributing to its overall antioxidant capacity, they are not considered the principal bioactive drivers of EBN's neuroprotective effects, which are more closely linked to its unique proteinaceous and sialylated components (e.g., glycoproteins, SA). Their role may be ancillary, potentially engaging in synergistic interactions within EBN's complex food matrix.

3. The Mechanisms of Brain Aging

Cognitive aging is a multifaceted process characterized by changes in various molecular and cellular pathways, which ultimately contribute to the onset of mild cognitive impairment (MCI), AD, and other dementias [39]. Current widely recognized mechanisms include oxidative stress [40], neuroinflammation [41], mitochondrial dysfunction [42], protein homeostasis imbalance [43], and dysregulation of the gut–brain axis (Figure 3) [44].

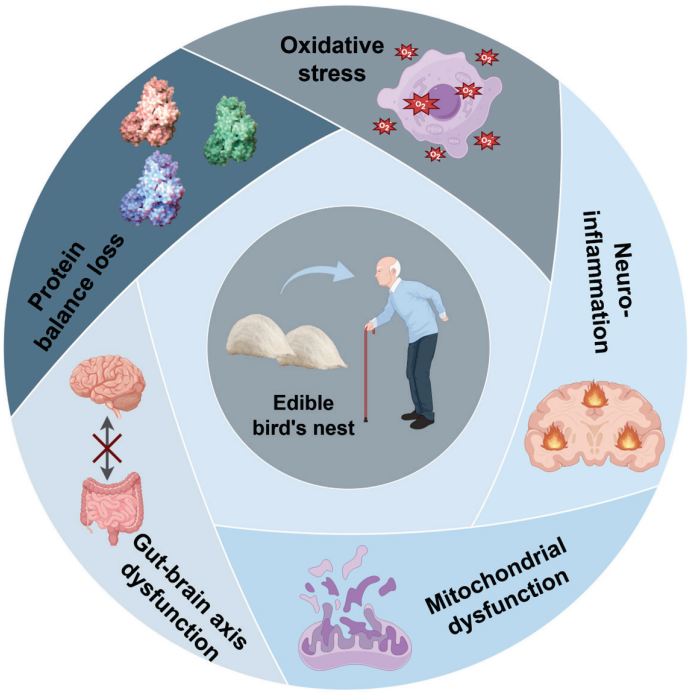


Figure 3. Schematic illustration of the multi-target regulatory mechanisms of edible bird's nest (EBN) in counteracting brain aging. EBN is positioned at the center, surrounded by five key pathological processes associated with brain aging: oxidative stress, neuroinflammation, mitochondrial dysfunction, protein balance loss, and gut-brain axis dysfunction. The colored circular icons represent each distinct pathological mechanism. This figure was created using Figdraw (Version 2.0, www.figdraw.com).

3.1. Oxidative Stress

Oxidative stress is defined as an imbalance between oxidants and antioxidants in the body, resulting in the excessive production of reactive oxygen species (ROS). These ROS can inflict damage on biomolecules such as DNA, proteins, and lipids [45]. Within neurons, types of ROS include superoxide anions generated by the respiratory chain and various oxidases, hydroxyl radicals formed through the reaction of hydrogen peroxide with copper or ferrous iron, and nitric oxide (NO) produced in response to elevated intracellular Ca^{2+} levels [46]. As individuals age, there is a notable increase in ROS production within neurons, coupled with the accumulation of oxidative damage, which significantly correlates with the severity of neurodegenerative diseases [47]. Morales-Martínez et al. demonstrated, using α-synuclein transgenic rats, a positive correlation between the levels of various oxidative stress biomarkers and neurodegeneration across multiple brain regions [30]. Moreover, ROS generated through oxidative stress and the subsequent cellular damage, such as compromised proteins and lipids, function as 'danger signals' that activate microglia and astrocytes, thereby triggering neuroinflammatory responses [48].

3.2. Neuroinflammation

Neuroinflammation is characterized by the activation of immune responses by microglia and astrocytes within the central nervous system [49]. Under normal physiological conditions, astrocytes and microglia are essential for maintaining neuronal homeostasis and facilitating waste clearance in the brain [50]. However, when these cells become overactivated, they release substantial quantities of pro-inflammatory cytokines, including IL-1β, IL-6, and TNF-α, as well as chemokines and additional reactive ROS. Moreover, activated microglia express inducible nitric oxide synthase (iNOS), resulting in the production of substantial amounts of NO, which can induce oxidative damage to neurons, culminating in apoptosis and the loss of neuronal function [42]. Studies suggest that with advancing age, microglial migration and phagocytic activity decline, while the population of inflammatory microglia increases by two-to four fold in the brains of aged mice [41]. Additionally, during neuroinflammation, astrocytes upregulate the expression of interleukin-17 (IL-17) and the TrkB transmembrane receptor. IL-17, upon binding to its receptor, may recruit NF-κB activator 1, thereby promoting the production of pro-inflammatory cytokines. During neuroinflammatory conditions, astrocytes may also compromise blood–brain barrier integrity, potentially facilitating the entry of undesirable immune cells and neurotoxic substances into the brain parenchyma [51]. Evidence indicates that the activation of microglia and astrocytes contributes to the aggregation of β-amyloid (Aβ) and the hyperphosphorylation of the microtubule-associated protein Tau within the brain, processes that subsequently precipitate neuronal degeneration and ultimately lead to the onset of AD [52].

Neuroinflammation and oxidative stress exhibit a reciprocal and interconnected relationship, wherein the inflammatory response precipitates oxidative stress, and oxidative stress subsequently activates multiple signaling pathways, including NF-κB, to enhance pro-inflammatory gene expression, thereby intensifying neuroinflammation [53].

3.3. Mitochondrial Dysfunction

Mitochondria, essential intracellular organelles, predominantly generate ROS at respiratory chain complexes I and III. These ROS can inflict oxidative damage on mitochondrial DNA (mt DNA), resulting in mt DNA mutations that lead to defective respiratory chain components. This defect, in turn, generates additional ROS, establishing a self-perpetuating cycle of ROS production and mt DNA mutation accumulation [54]. Neurons, due to their intricate morphology and substantial metabolic demands, are particularly reliant on mitochondria and are thus especially vulnerable to mitochondrial dysfunction. As age pro-

gresses, mitochondrial capacity to produce and sustain the high energy levels requisite for neuronal function diminishes. When mitochondrial dysfunction surpasses a critical threshold, the brain's resilience to damage deteriorates, initiating various neurodegenerative processes [55]. Research has identified a detrimental cycle characterized by excessive production of ROS, inflammatory responses, and mitochondrial dysfunction. Mitochondrial damage leads to the activation of glial cells, and the inflammatory mediators produced as a result further impair mitochondrial function, thereby exacerbating neurodegeneration [56]. For example, mitochondrial dysfunction and disrupted mitochondrial autophagy may contribute to amyloid pathology and neurodegeneration in AD [57]. Similarly, mitochondrial dysfunction is a critical hallmark of PD progression, with various risk factors associated with Parkinson's pathogenesis exerting their effects by inducing mitochondrial dysfunction. In mouse models of PD induced by rotenone, a significant reduction in the activity of mitochondrial complex I has been observed within the striatum [58].

3.4. Proteostasis Imbalance

Proteostasis refers to the homeostatic regulation of cellular processes involved in protein synthesis, folding, repair, degradation, and renewal [59]. As organisms age, proteostasis gradually declines, resulting in the accumulation of proteins that are misfolded, oxidized, glycated, or ubiquitinated. This deterioration leads to the formation of toxic protein aggregates [60]. The accumulation of misfolded and aggregated proteins particularly impacts post-mitotic cell types, such as neurons [61]. Additionally, pathological protein aggregation is a prominent hallmark of neurodegenerative diseases. In various neurodegenerative disorders, misfolded proteins abnormally accumulate both intracellularly and extracellularly, forming characteristic aggregates. For example, Aβ and tau protein aggregates are found in AD, alpha-synuclein aggregates in PD, and TAR DNA-binding protein-43 (TDP-43) and Superoxide dismutase 1 (SOD1) aggregates in amyotrophic lateral sclerosis. These protein aggregates exhibit propagating properties, enabling them to spread between neurons [62]. Moreover, protein degradation plays a critical role in memory processes during both normal aging and pathological conditions. Recent studies suggest that hippocampal autophagy is essential for enhancing learning and memory by facilitating activity dependent structural and functional synaptic plasticity. Activation of hippocampal autophagy has been shown to ameliorate age-related memory impairments in murine models. In models of AD in mice, enhancing autophagy has been demonstrated to decrease Aβ accumulation in the brain, thereby restoring synaptic integrity and memory function [63].

3.5. Dysfunction of the Gut–Brain Axis

A bidirectional communication system, known as the microbiota–gut–brain axis (MGBA), exists between the central nervous system, gut microbiota, and the gastrointestinal tract [64]. Gut microbiota are pivotal in the processes of aging and the pathogenesis of neurodegenerative diseases, although the intricate signaling pathways involved are not yet fully understood. Currently identified pathways include metabolic, immune, neural, and endocrine signaling mechanisms [65]. In comparison to younger individuals, the gut microbiota of elderly populations undergoes significant alterations. Studies comparing the microbiomes of young and aged rats reveal a notable reduction in microbial diversity in the gut microbiota of older rats, along with distinct compositional differences. For example, in aged rats, there is a decrease in the relative abundance of Bacteroides in the intestines, whereas the abundance of Firmicutes is significantly higher compared to young rats [66]. Simultaneously, the integrity and function of the intestinal barrier decline with age, negatively impacting blood–brain barrier (BBB) permeability and exacerbating

https://doi.org/10.3390/nu18040671

neuroinflammation and functional deterioration within the central nervous system [67]. Supporting evidence from further research indicates that during aging, increased intestinal permeability, mediated by the gut microbiota, facilitates the translocation of harmful intestinal metabolites, such as N6-carboxymethyllysine, across the intestinal barrier into the systemic circulation. The accumulation of these metabolites in the brain can lead to microglial damage [68]. Conversely, microbial metabolites, including short-chain fatty acids (SCFAs), tryptophan, cytokines, and neuroactive substances are released into the bloodstream. Once in circulation, the microbiome and its metabolites can modulate peripheral immune cells, interact with the BBB to alter its integrity, and cross the BBB to influence cerebral function [69].

4. The Role of EBN Intervention in Brain Aging

Current research provides systematic evidence from both animal models and cellular studies, suggesting that EBN exerts a multi-target protective effect in the context of aging and neurodegenerative diseases (Table 1). In animal studies, EBN has been shown to alleviate neurofunctional impairments induced by various etiological factors through multiple mechanisms. Specifically, in a model of menopause-associated cognitive decline, dietary supplementation with EBN significantly mitigates memory and cognitive deterioration by upregulating the expression of Sirtuin-1 (SIRT1) protein in the hippocampus, downregulating genes associated with neurodegeneration and apoptosis, and modulating redox balance [70,71]. Furthermore, in lipopolysaccharide (LPS)-induced neuroinflammatory models involving Wistar rats and C57BL/6J mice, administration of EBN water extract or EBN itself effectively suppresses abnormal elevations of pro-inflammatory cytokines (such as TNF-α and IL-6) and oxidative stress markers (including MDA), demonstrating anti-inflammatory effects by inhibiting TICAM1 expression within the NF-κB signaling pathway [72,73]. In a mouse model of PD, treatment with specific EBN extracts (pancreatic enzyme-digested extract and aqueous extract) not only enhanced the activity of endogenous antioxidant enzymes, including Superoxide dismutase (SOD) and glutathione peroxidase (GPx), but also inhibited the abnormal activation of microglia, excessive NO production, and lipid peroxidation reactions. These actions collectively contributed to the protection of dopaminergic neurons in the substantia nigra [74]. In models of AD induced by chronic cerebral hypoperfusion, EBN intervention was associated with reduced neuronal loss in the hippocampus and cortex and reduced levels of the oxidative stress marker F2-isoprostane [75]. Additionally, EBN water extract powder demonstrates preventive potential against vascular dementia by inhibiting acetylcholinesterase (AChE) activity, thereby reducing Aβ accumulation [17]. At the cellular level, the aqueous extract of EBN and its functional protein components, lactoferrin and ovotransferrin, exhibited significant antioxidant and anti-apoptotic properties in models of SH-SY5Y cell damage induced by 6-hydroxydopamine (6-OHDA) and hydrogen peroxide [74,76,77]. Comparative studies using different EBN extracts (e.g., pancreatic enzyme-digested vs. aqueous) at maximum non-toxic dose (MNTD) further elucidated their respective efficacies in enhancing cell viability and mitigating oxidative stress and apoptosis [76]. Notably, the specific EBN extracts (crude extract S1 and aqueous extract S2) promoted proliferation, migration, and neuronal differentiation in embryonic mouse neural stem cells (NE-4C), indicating neurotrophic activity [22]. Further investigations reveal that the SA component present in EBN substantially enhances mitochondrial function in SH-SY5Y cells [78]. Importantly, the primary active component, SA, when administered in purified form, exhibits significant independent neuroprotective properties. In double transgenic AD (2 $\times$ Tg-AD) mice, SA administration not only enhanced spatial learning and memory abilities but also reduced

https://doi.org/10.3390/nu18040671

Aβ plaque deposition and inhibited tau protein hyperphosphorylation, thereby alleviating neuronal synaptic damage [79].

Table 1. Animal and cell studies on the effects of EBN and SA intervention in brain aging.

Model	Species	Tested Material and Dosage	Duration	Experimental Results	Ref.
Menopause-related cognitive decline (Ovariectomy)	SD rat	EBN mixed with diet at concentrations of 6%, 3%, and 1.5% (*w*/*w*)	12 weeks	• Reduced escape latency time • Increased expression of SIRT1 in the hippocampus • Reduced levels of caspase-3 and malondialdehyde in the hippocampal region and frontal cortex • Reduced PSEN1, PSEN2 and APP gene expression • Increased levels of SOD1, SOD2, SOD3, and CAT	[70,71]
Neuroinflammation (LPS)	Wister rat	EBN water extract of 125, 250 and 500 mg/kg	7 days	• Reduced escape latency time • Reduced levels of TNF-α, IL-1β, IL-6, ROS and TBARS	[72]
Neuroinflammation (LPS)	C57BL/6J mice	EBN of 200 mg/kg/d	7 weeks	• Reduced escape latency time • Increased neuronal count • Inhibition of glial cell activation • Reduced levels of TNF-α, IL-1β, and IL-6 • Inhibited expression of TICAM1	[73]
PD (6-OHDA)	C57BL/6J mice	Pancreatic enzyme-digested extract and aqueous extract of EBN at 20 mg/kg and 100 mg/kg, respectively.	28 days	• Improved locomotor distance and balance • Reduced loss of TH-positive neurons in the substantia nigra • Decreased expression of the microglial marker CD11b • Increased expression of the antioxidant marker GPX1	[74]
AD (2VO)	SD rat	EBN of 60 and 120 mg/kg	8 weeks	• Increased neuronal count in the hippocampal CA1 region • Reduced hippocampal F2-prostaglandin levels	[75]
Vascular dementia (MCAO)	Wister rat	EBN water extract powder of 10, 50 and 100 mg/kg	2 weeks before and 3 weeks after surgery	• Reduced escape latency time • Decreased Aβ42 deposition in the hippocampus • Inhibited AChE activity	[17]
PD (6-OHDA)	SH-SY5Y cells	Pancreatic enzyme-digested extract and aqueous extract of EBN at 1/2 MNTD and MNTD, respectively	-	• NO production and reduced lipid peroxidation	[74]
PD (6-OHDA)	SH-SY5Y cells	Pancreatic enzyme digestion of crude extracts (75 μg/mL) and aqueous extracts (150 μg/mL)	-	• Pancreatic enzyme extract demonstrates superior efficacy in enhancing cellular viability • The aqueous extract exhibits greater effectiveness in mitigating ROS accumulation, alleviating early apoptotic membrane phosphatidylserine efflux, and inhibiting caspase-3 cleavage	[76]
Oxidative stress (H_2O_2)	SH-SY5Y cells	EBN (1000 μg/mL) and its constituents lactoferrin (LF, 5 μg/mL) and ovoferritin (OVF, 10 μg/mL)	-	• Enhances free radical scavenging activity and reduces ROS • Upregulates the expression of SOD1, SOD2 and PARP1 genes	[77]
Neural stem cell model	NE-4C	Pancreatic enzyme-digested crude extract (S1; MNTD = 130 μg/mL) and the aqueous extract (S2; MNTD = 290 μg/mL)	-	• Promoting cell proliferation, migration and neuronal differentiation	[22]

Table 1. *Cont.*

Model	Species	Tested Material and Dosage	Duration	Experimental Results	Ref.
AD	2 × Tg-AD mice	SA of 17, 84 and 420 mg/kg	9 months	• Reduced escape latency time • Decreased Aβ and neurofibrillary tangles • Increased number of Nissl bodies	[79]
Mitochondrial dysfunction	SH-SY5Y cells	SA extracts at concentrations of 20, 40, 60, 80 and 100 μg/mL in EBN	-	• Cell viability peaked at 60 μg/mL • The number of active mitochondria increased significantly by 195%	[78]

To better conceptualize the multi-level effects of EBN, we summarize the major molecular targets and functional outcomes in an integrative schematic (Figure 4). The figure illustrates how EBN modulates antioxidant, anti-inflammatory, apoptotic, mitochondrial, and proteostatic pathways, which together influence core mechanisms of brain aging and contribute to neuronal protection and cognitive support.

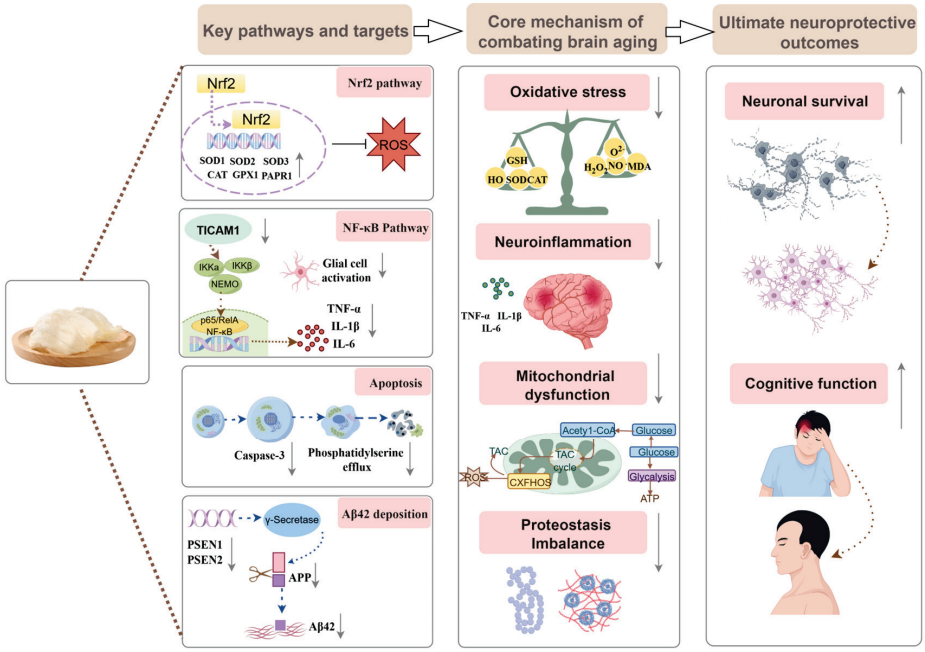


Figure 4. Integrative network-regulatory model of edible bird's nest (EBN) against brain aging. This diagram is divided into two main sections. Key molecular pathways and targets regulated by EBN include: the Nrf2 antioxidant pathway (downstream targets SOD1-3, CAT, GPX1, PARP1), the TICAM1/NF-κB neuroinflammatory pathway (triggering glial cell activation and pro-inflammatory cytokines TNF-α, IL-1β, IL-6), apoptosis markers (Caspase-3, oxidative stress markers), and amyloid-related genes associated with Aβ42 deposition (PSEN1, PSEN2, APP). The core pathological mechanisms of brain aging counteracted by EBN encompass oxidative stress, neuroinflammation, mitochondrial dysfunction, and the interplay among these processes. Colored boxes represent distinct pathway categories or pathological mechanisms. Arrows indicate activation or inhibition, while lines with horizontal bars denote inhibitory effects. All abbreviations are defined in the text. This figure was created using Figdraw (Version 2.0, www.figdraw.com).

To date, there is a near-complete absence of high-quality RCTs evaluating EBN's impact on cognitive function or progression to neurodegenerative diseases in human populations. The current preclinical literature collectively indicates that EBN exerts neuroprotective effects at multiple biological levels in both cellular and animal models. Nevertheless, the strength and translational significance of this evidence should be interpreted with appropriate caution. In several animal studies, the observed behavioral improvements

appear not only statistically significant but also biologically meaningful. For instance, in the ovariectomized mouse model, high-dose EBN reversed memory deficits and, in some tasks, achieved effects comparable to those of estrogen replacement therapy. This suggests that the reported outcomes are not merely marginal changes but may reflect functionally relevant recovery. At the same time, most studies rely on group-wise comparisons without standardized reporting of effect sizes, which limits quantitative comparison across experiments. Another issue concerns the heterogeneity of experimental materials. EBN preparations differ substantially among studies in terms of species origin, geographic source, processing, and extraction methods. Although commonly used disease models, such as LPS induced neuroinflammation and 6-OHDA induced dopaminergic injury, are well established, variability in EBN preparation complicates the interpretation of whether differences in efficacy arise from biological mechanisms or methodological factors. Most current studies also employ relatively small sample sizes and acute or accelerated pathological paradigms. These models are valuable for mechanistic exploration, but they do not fully recapitulate the slow and progressive nature of human brain aging. Consequently, the reported effects should be viewed primarily as evidence of mechanistic plausibility rather than direct indicators of clinical benefit. Taken together, the existing preclinical data provide a solid biological rationale for EBN's neuroprotective potential, but they mainly serve as a foundation for carefully designed human studies rather than definitive proof of efficacy.

Although direct experimental evidence is currently insufficient to demonstrate that EBN directly delays brain aging via the MGBA, its unique composition and observed physiological effects suggest considerable potential for exerting neuroprotective effects through modulation of this axis. Research findings suggest that EBN ameliorates gut microbiota dysbiosis by inhibiting the growth of pathogenic bacteria, promoting the proliferation of beneficial bacteria, and stimulating the production of SCFAs. In comparison to monosaccharide SA, EBN demonstrates superior prebiotic activity [80]. Further studies have shown that prolonged consumption of EBN enhances the abundance of beneficial gut bacteria such as *Bacteroides* and *Akkermansia*, while concurrently reducing the prevalence of Firmicutes. This suggests that EBN consumption may regulate gut function by promoting beneficial microbial communities. Moreover, EBN-derived gut metabolites can directly stimulate the proliferation of intestinal epithelial cells, thereby reinforcing the physical barrier of the intestinal wall [81]. In conclusion, current research tentatively supports the notion that EBN exhibits prebiotic-like properties by modulating the gut microbiota. The specific mechanisms involved include the promotion of beneficial bacteria, the inhibition of pathogenic bacterial growth, and the optimization of microbial community structure. Simultaneously, EBN enhances intestinal barrier function by stimulating the production of SCFAs and directly promoting the proliferation of intestinal epithelial cells. These effects provide essential theoretical support for the neuroprotective effects of EBN via the MGBA. While direct evidence concerning its role in mitigating brain aging requires further exploration, EBN shows considerable research potential and promising application prospects.

5. Comparison of EBN with Other Anti-Cognitive Decline Substances

The fundamental pathological mechanisms underlying brain aging encompass a multitude of pathways, with oxidative stress receiving considerable attention as a pivotal link among various mechanistic hypotheses. This section undertakes a comparative analysis of EBN with antioxidants and other dietary substances that counteract brain aging, aiming to elucidate its distinctive properties and identify existing research gaps. This analysis serves as a reference for the development of future intervention strategies.

https://doi.org/10.3390/nu18040671

5.1. EBN and Traditional Antioxidants

Antioxidants are classified into endogenous and exogenous types. Endogenous antioxidants, synthesized within the body, are further divided into enzymatic and non-enzymatic categories. In contrast, exogenous antioxidants are acquired through dietary sources [82], including vitamin E, vitamin C (ascorbic acid), and coenzyme Q10.

5.1.1. Vitamin E

Vitamin E (VE) encompasses a group of fat-soluble compounds characterized by significant antioxidant properties. Structurally, VE is composed of tocopherols and tocotrienols, each of which exists in four isomeric forms: α, β, γ, and δ [83]. Notably, approximately 90% of VE present in plasma and brain tissue samples is in the form of α-tocopherol [84]. Research suggests that VE plays a crucial role in maintaining cellular redox homeostasis by neutralizing reactive ROS and mitigating lipid peroxidation. Supplementation with α-tocopherol has been shown to enhance cognitive function in patients with dementia, reduce the risk of cognitive decline, and stabilize cognitive performance [85]. Nevertheless, some studies report no significant benefits in certain subpopulations with specific dietary backgrounds, and excessive or high-dose supplementation may disrupt the equilibrium of endogenous antioxidant enzyme systems [83,86]. Unlike EBN, VE is capable of integrating into lipid structures within the central nervous system, where it acts synergistically with other intracellular antioxidants to inhibit lipid peroxidation induced by oxygen radicals [87].

5.1.2. Vitamin C

Vitamin C (VC), also referred to as ascorbic acid, is a water-soluble antioxidant that mitigates oxidative damage by neutralizing oxygen-free radicals [88]. A deficiency in VC can lead to increased production of ROS and heightened oxidative stress through mitochondrial respiration, thereby contributing to the pathogenesis of AD [89]. In addition to its inherent antioxidant capabilities, VC alleviates oxidative stress by regenerating oxidized VE and enhancing the reductive capacity of NADH and NADPH [90]. Empirical studies have shown that individuals who supplement with VC experience a 16% reduction in the risk of developing AD compared to control groups [91]. Nevertheless, under certain redox conditions, VC may exhibit pro-oxidant effects, which are dependent on the individual's redox status, dosage, and the route of administration [92]. Conversely, EBN has shown no significant toxicity in animal studies, although its long-term safety in humans necessitates further investigation.

5.1.3. Coenzyme Q10

Coenzyme Q10 (CoQ-10) is an endogenous, lipophilic antioxidant that is highly concentrated in mitochondria, where it plays a pivotal role in cellular energy metabolism and antioxidant defense mechanisms. It exists in two primary forms: the oxidized coenzyme Q10 (ubiquinone) and its reduced counterpart (ubiquinol) [93]. Within the mitochondria, CoQ-10 functions as a critical electron carrier in the mitochondrial electron transport chain during oxidative phosphorylation, facilitating electron transfer from Complexes I and II to Complex III. Additionally, it is involved in the metabolism of pyrimidines and fatty acids, and acts as a cofactor for dihydroorate dehydrogenase in mitochondrial uncoupling proteins, as well as in the regulation of the mitochondrial permeability transition pore [94]. Beyond its mitochondrial functions, CoQ-10 is also localized in other subcellular organelles, including lysosomes, peroxisomes, the Golgi apparatus, and the endoplasmic reticulum. It is ubiquitously distributed throughout the brain, present in both neurons and glial cells [95]. Research has demonstrated that dietary supplementation with CoQ-10 ameliorates the

https://doi.org/10.3390/nu18040671

pathological phenotype of the brain and enhances cognitive function in transgenic mouse models of AD. Mechanistically, CoQ-10 administration significantly reduced oxidative stress levels in the brain, evidenced by decreased carbonyl density and decreased Aβ deposition [96]. Similarly, in rat models of AD, intracerebroventricular injection of Aβ resulted in pronounced oxidative stress, indicated by increased serum malondialdehyde (MDA, a terminal product of lipid peroxidation) and elevated total oxidant levels. Further investigations have shown that CoQ-10 supplementation not only effectively mitigated this oxidative damage but also significantly enhanced the organism's overall antioxidant capacity [97].

In conclusion, while traditional antioxidants primarily function as scavengers, brain aging is a multifaceted process involving various pathways, including oxidative stress, inflammation, and apoptosis. EBN, through the synergistic action of its multiple components, exhibits broader potential in combating brain aging by modulating the body's antioxidant defenses, controlling inflammation, and supporting neurotrophic systems.

5.2. EBN and Other Food-Derived Sources with Anti-Brain-Aging Properties

With the progression of nutritional neuroscience, the identification of substances with neuroprotective properties in everyday diets has emerged as a central focus in research aimed at combating brain aging. These compounds exert their influence on brain health through various bioactive mechanisms, including antioxidant effects, anti-inflammatory properties, and neurotransmitter regulation. To further contextualize EBN's potential, we compare it with other dietary strategies that have attracted substantial research interest in brain health. The following discussion contrasts EBN's multi-component, food-matrix approach with interventions centered on isolated, high-potency phytochemicals (e.g., curcumin, quercetin) or essential nutrients (e.g., omega-3 fatty acids). Specifically, curcumin and quercetin are included as representative plant-derived polyphenols with potent anti-inflammatory and antioxidant properties [98,99], omega-3 fatty acids as essential nutrients crucial for neuronal membrane integrity and synaptic function [100], and lutein as a major carotenoid with antioxidant and neuroprotective effects [101]. In addition to single-entity compounds, we further include medicinal mushrooms (e.g., *Hericium erinaceus* and *Ganoderma lucidum*) and ginseng (*Panax ginseng*) as representative traditional multi-component functional foods. These categories are characterized by complex phytochemical or fungal metabolite matrices that act through coordinated modulation of neurotrophic, anti-inflammatory, and antioxidant pathways rather than a single dominant molecule [102,103].

This structured comparison aims to contrast EBN's multi-component, food-matrix approach with the paradigm of high-potency, single-entity compounds and essential nutrients. This comparison is intended to illustrate different paradigms of nutritional intervention rather than direct equivalence in composition.

5.2.1. Representative Polyphenol: Curcumin

Curcumin, chemically known as 1,7-bis (4-hydroxy-3-methoxyphenyl)-1,6-heptadiene-3,5-dione, is the principal polyphenolic component of turmeric and is characterized by its high lipophilicity [104]. The neuroprotective effects of curcumin on the aging brain are mediated through multiple signaling pathways, including the reduction in oxidative stress, inhibition of Aβ formation, and attenuation of neuroinflammation. Inhibition of NF-κB reduces inflammatory responses, while activation of nuclear factor erythroid 2-related factor 2 (Nrf2) promotes the expression of antioxidant response elements. Additionally, curcumin enhances autophagy and the expression of neurotrophic factors, thereby facilitating the clearance of deleterious protein aggregates [105]. In aged female Wistar rats, intraperitoneal administration of curcumin at 30 mg/kg (5 days weekly for 8 weeks) suggests potential

https://doi.org/10.3390/nu18040671

in delaying brain aging by reducing oxidative stress, inhibiting apoptosis, and enhancing SOD activity, which in turn increases vascular endothelial growth factor (VEGF) and brain-derived neurotrophic factor (BDNF) expression [106]. Curcumin also appears to improve cognitive function by decreasing GSK-3β activity through the PI3K/Akt pathway [107]. In cellular models, it mitigates oxidative damage in aged PC12 cells, reduces reactive oxygen species production, prevents mitochondrial membrane potential loss, and promotes Nrf2 nuclear translocation to maintain mitochondrial function [108]. Preliminary clinical studies suggest curcumin supplementation may aid memory consolidation, enhance cognitive function, and reduce age-related memory decline [109]. Meta-analyses reveal that curcumin supplementation, particularly at 0.8 g/day for at least 24 weeks, effectively enhances cognitive function, with more significant benefits observed in elderly and Asian populations compared to younger and Western groups [110]. Curcumin is characterized by limited intestinal absorption and rapid hepatic metabolism, leading to extremely low bioavailability, which necessitates enhancement through nanocarriers [111]. Feng et al. demonstrated that the intranasal administration of curcumin molecules, which self-assemble into carrier-free curcumin nanoparticles, can inhibit the TLR4/NF-κB pathway that mediates the polarization of glial cells from the M1 to the M2 phenotype. This process reduces the Aβ burden in AD transgenic mice and exhibits stronger inhibitory effects on Aβ aggregation compared to free curcumin with monovalent effects [112].

5.2.2. Representative Lipid: Deep-Sea Fish Oil (Omega-3 Fatty Acids)

Omega-3 fatty acids, particularly docosahexaenoic acid (DHA) and eicosapentaenoic acid (EPA), are critical components of fish oil. They play an essential role in maintaining neuronal membrane stability, synaptic plasticity, and anti-inflammatory signaling pathways, thereby supporting brain health and delaying cognitive decline [113]. Brain tissue contains a high concentration of DHA, accounting for 40% of synaptic membrane lipids. In contrast, EPA levels in the brain are 10 to 20 times lower, yet EPA remains crucial for microglial function [114]. Research has demonstrated a correlation between the intake of EPA and DHA and enhanced cognitive health in later life, as well as a reduced risk of dementia over a lifetime [115]. Several mechanisms have been proposed to explain these effects, including the enhancement of neurogenesis and the modulation of inflammation and neuroinflammation through the production of bioactive lipid mediators. A recent prospective study involving older adults examined the relationship between fish oil supplementation, which is rich in EPA and DHA, and the risk of developing dementia. The study found that over an average follow-up period of 7.92 years, 2054 participants were diagnosed with dementia. After adjusting for major risk factors, the intake of fish oil supplements was significantly associated with a reduced risk of dementia in adults aged 60–73 years (Odds Ratio = 0.87, 95% Confidence Interval: 0.79–0.96, $p = 0.004$) [116]. However, results from clinical trials have been inconsistent and varied, likely due to significant heterogeneity in trial designs [117]. Additionally, DHA has been shown to promote synapse formation by increasing the expression of drebrin, a dendritic spine marker protein, and PSD-95, a postsynaptic density protein [118]. DHA and EPA facilitate the dissociation of Nrf2 from its inhibitor Keap1, and promote the translocation of Nrf2 to the cell nucleus, where it interacts with the antioxidant response element [119]. Additionally, research indicates that EPA competes with arachidonic acid (ARA) for binding to cyclooxygenase (COX) and 5-lipoxygenase (5-LOX) enzymes, thereby attenuating ARA metabolism and decreasing the production of ARA-derived inflammatory mediators. DHA also competes with ARA for incorporation into cell membranes, thereby reducing neuroinflammation [120]. In contrast to EBN, DHA and EPA serve as essential 'building blocks' for the nervous system, whereas

https://doi.org/10.3390/nu18040671

EBN primarily functions as a 'regulatory modulator' without providing foundational structural components.

5.2.3. Representative Carotenoid: Lutein

Carotenoids, naturally occurring pigments prevalent in fruits and vegetables, are categorized into lipophilic carotenes, such as lycopene, α-carotene, and β-carotene, and more polar xanthophylls, including lutein, zeaxanthin, astaxanthin and β-cryptoxanthin. Lutein is notably the predominant carotenoid in the brain [121]. Its neuroprotective properties are attributed to its antioxidant activity, its ability to prevent neuroinflammation, and its role in enhancing levels of GAP-43, neural cell adhesion molecule (NCAM), and BDNF, which collectively promote neurogenesis and improve neural plasticity [122]. As an effective free radical scavenger, lutein demonstrates a particularly high capacity for quenching singlet oxygen, a capability directly linked to its extensive conjugated double bond structure [121]. Research conducted by Leila Nazari et al. has shown that lutein significantly alleviates cognitive impairment in a rat model of AD induced by Aβ [123]. Various behavioral assessments, including the Morris water maze and novel object recognition tests, have confirmed that lutein intervention effectively reduces deficits in spatial memory and recognition in these model animals. At the mechanistic level, lutein significantly ameliorated abnormal oxidative stress levels in the serum of AD rats. This was evidenced by a reduction in MDA content and total oxidation status, coupled with an increase in total antioxidant capacity. Similarly, another study demonstrated that intraperitoneal administration of lutein enhanced mitochondrial function by activating the Nrf2 pathway, thereby attenuating inflammation in C57BL/6J mice subjected to traumatic brain injury [124]. In a H_2O_2 induced oxidative stress model of BV-2 microglia, lutein treatment significantly upregulated the synthesis of SOD2, suggesting that lutein mitigates oxidative damage by augmenting endogenous antioxidant defenses [125]. Moreover, lutein has been shown to upregulate SIRT1 expression by inhibiting miR-135b-5p, which in turn suppresses M1 glial cell polarization and inflammation, thereby ameliorating PD [126]. However, the bioavailability of lutein is limited due to its intrinsic physicochemical properties. Its pronounced hydrophobicity hinders dissolution and transport within the aqueous environment of the gastrointestinal tract, thereby obstructing efficient delivery to absorption sites in the small intestine. Additionally, the conjugated double bond system within its molecular structure makes it prone to oxidative degradation during processing and storage, thereby compromising its stability and efficacy [127]. Similar to curcumin, lutein requires the use of nano-carriers to enhance its therapeutic efficacy.

5.2.4. Representative Flavonoid: Quercetin

Flavonoids, a class of polyphenolic compounds prevalent in plant-based foods such as fruits, vegetables, tea leaves, and wine, exhibit significant neuroprotective potential across various subclasses. Notably, flavanols such as quercetin demonstrate substantial efficacy in inhibiting Aβ aggregation and mitigating AD-associated pathology [128]. Quercetin (3,3′,4′,5,7-dihydroxyflavone) is abundantly found in plants, including apples, onions, broccoli, wine, green tea, and *Ginkgo biloba* [129]. In addition to directly targeting Aβ, quercetin reduces oxidative stress, inhibits neuroinflammation, enhances mitochondrial function, and promotes neuronal survival [128]. Research suggests that quercetin can traverse the BBB and exert neuroprotective effects by modulating multiple signaling pathways, including the Nrf2/ARE pathway, which serves as a fundamental defense mechanism for cells against oxidative damage [130]. Research has demonstrated that quercetin intervention at a dosage of 60 mg/kg/day effectively reverses cognitive impairment in AD model mice and significantly suppresses the expression of pro-inflammatory cytokines, including TNF-α,

https://doi.org/10.3390/nu18040671

IL-6, and IL-1β, within the brain. The study further elucidated that the neuroprotective effects of quercetin are closely linked to its activation of the Nrf2/HO-1 signaling pathway and its facilitation of M2 anti-inflammatory phenotype polarization in microglia [131]. Moreover, evidence suggests that quercetin modulates multiple downstream pathways, such as PI3K/Akt signaling activation, CREB phosphorylation, and NF-κB inhibition, by upregulating the expression of key neurotrophic factors like BDNF and nerve growth factor (NGF). These synergistic effects collectively enhance neuronal resilience, thereby promoting improvements in memory and learning functions [132]. However, it is important to note that due to its poor water solubility and low BBB permeability, quercetin exhibits an oral bioavailability of approximately 2% [133]. To address this challenge, numerous researchers have utilized nano-delivery systems and liposomal surface modifications to improve the efficiency of BBB penetration. A multifunctional nanoparticle platform, designated as Anti-VCAM1-GM1@Q, has been developed. This platform targets vascular cell adhesion molecule 1 on brain vascular endothelial cells, inhibiting its signaling pathway, while concurrently employing monosialoglycerolipid to enhance the ability of quercetin to traverse the BBB. This dual mechanism exerts synergistic anti-inflammatory effects, significantly mitigating neuroinflammation and cognitive impairment [134]. Furthermore, the menthol-modified quercetin liposomes (Men-Qu-Lips) developed by Liu et al. exhibited exceptional encapsulation efficiency and stability. These liposomes effectively crossed the BBB, reducing oxidative stress and neuroinflammation in the brains of aging mice, thereby protecting neurons and enhancing their learning and memory capabilities [133].

5.2.5. Representative Functional Products: Medicinal Mushrooms

Medicinal mushrooms, including *Hericium erinaceus* (lion's mane) and *Ganoderma lucidum* (reishi), represent a class of food-derived complex natural products with growing evidence for neuroprotective and anti-Alzheimer's potential. Lion's mane mushroom has been widely studied for its rich profile of bioactive compounds such as erinacines and hericenones, which have been shown to stimulate the synthesis of NGF and support neurite outgrowth, thereby contributing to neuronal maintenance and cognitive function in vitro and in vivo models of neural injury and neurodegenerative pathology (e.g., NGF promotion and neurite enhancement) [135]. Beyond its neurotrophic effects, Lion's mane mushroom extract exhibits antioxidant and anti-inflammatory properties. It helps mitigate oxidative stress and inflammation by regulating cellular defense pathways and cytokine production [102]. Preclinical studies have also demonstrated that lion's mane polysaccharide-enriched extracts reduce ROS accumulation, prevent mitochondrial depolarization, and preserve cholinergic system function in AD models, further highlighting their multi-mechanistic neuroprotective capacities [136]. Moreover, emerging review evidence supports the idea that *H. erinaceus* bioactive constituents act synergistically to regulate neurotrophic, antioxidative, and anti-cytotoxic processes, positioning this mushroom as a functional dietary candidate for cognitive support and age-related neuronal health [137].

Reishi mushroom (*G. lucidum*) and other medicinal fungi exhibit complementary neuroprotective potential through distinct classes of bioactive metabolites, including triterpenoids and polysaccharides, which have been shown to modulate neuroinflammation via pathways such as TLR4/NF-κB and attenuate microglial overactivation associated with neurodegenerative progression [103]. Systematic analyses suggest that multiple medicinal mushroom species (e.g., *Hericium*, *Ganoderma*, *Cordyceps*) may alleviate cognitive impairment in animal models, indicating that mushroom supplementation could contribute to neuronal resilience through diverse mechanisms, including antioxidation, immunomodulation, and regulation of neurotrophic signaling [138]. While clinical evidence remains limited, the cumulative preclinical data provide a strong rationale for further investigation

https://doi.org/10.3390/nu18040671

of medicinal mushroom-derived compounds as functional food strategies for supporting cognitive function and mitigating neurodegenerative risk.

5.2.6. Representative Traditional Multi-Component: Ginseng

Ginseng has been widely studied for its neuroprotective potential in the context of AD, with multiple major components, including ginsenosides and gintonin, demonstrating modulation of key pathological processes such as Aβ metabolism, neuroinflammation, oxidative stress, and mitochondrial dysfunction [139]. Ginsenosides, the principal bioactive saponins in *Panax ginseng*, have been reported to target multiple mechanisms in AD models, including attenuation of Aβ formation, inhibition of tau hyperphosphorylation, and enhancement of neurotrophic signaling [139]. In preclinical studies, isolated ginsenosides (e.g., Rg1) have been shown to improve cognitive performance and reduce amyloid plaque burden in animal models by activating antioxidant and anti-inflammatory pathways, as well as supporting cholinergic system function [140,141]. Mechanistically, ginsenosides exhibit anti-neuroinflammatory effects through inhibition of pro-inflammatory cytokine production and modulation of NF-κB related signaling, which are implicated in AD pathology [140]. Furthermore, several clinical and observational studies suggest that long-term ginseng consumption is associated with cognitive benefits in the elderly, pointing to its potential utility as a preventive dietary strategy for age-related cognitive decline, although findings are still preliminary and warrant further large-scale trials [142].

Through a systematic comparison of various food-derived anti-brain aging compounds, it becomes apparent that each compound offers distinct benefits and limitations in addressing cognitive decline, attributable to their unique chemical properties and mechanisms of action. Curcumin and quercetin feature broad signaling interactions but are constrained by bioavailability; omega-3 fatty acids serve as structural components; lutein targets oxidative stress and synaptic pathways; medicinal mushrooms and ginseng provide multi-component bioactivity but from different biochemical matrices. In comparison, EBN's value lies in its multi-target network-regulatory capacity, engaging antioxidant, anti-inflammatory, apoptotic, and neurotrophic pathways within a single food matrix. This integrated regulatory pattern potentially bridges the gap between traditional antioxidant supplementation and structurally oriented nutrient interventions, supporting cognitive resilience in aging (Figure 5).

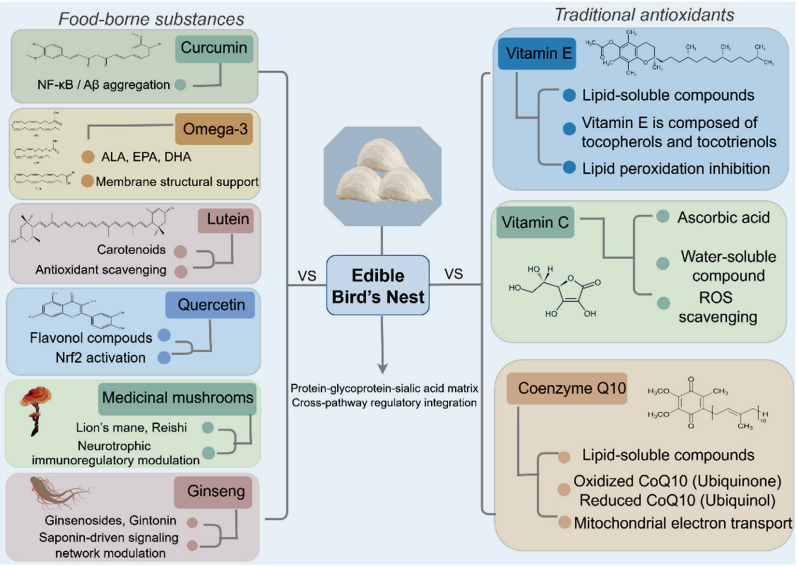


Figure 5. Comparison of edible bird's nest with food-borne substances and traditional antioxidants. This diagram is divided into three major categories: food-derived substances (curcumin, omega-3

fatty acids, lutein, quercetin) and their key molecular targets and mechanisms of action; traditional antioxidants (vitamin E, vitamin C, coenzyme Q10) and their primary functions; and EBN, positioned as a multi-component protein-glycoprotein-sialic acid matrix with cross-pathway regulatory integration capabilities. Abbreviations: ALA, α-linolenic acid; EPA, eicosapentaenoic acid; DHA, docosahexaenoic acid; ROS, reactive oxygen species; Nrf2, nuclear factor erythroid 2-related factor 2; NF-κB, nuclear factor kappa-light-chain-enhancer of activated B cells. This figure was created using Figdraw (Version 2.0, www.figdraw.com).

6. Safety, Quality Control, and Regulatory Considerations of EBN

In addition to efficacy, the translational development of EBN as a functional food or nutraceutical necessitates rigorous attention to safety, quality control, and regulatory compliance. IgE-mediated allergenicity has been reported in sensitive individuals, particularly in children, indicating that EBN proteins can act as food allergens and should be clearly labeled for consumer safety [21]. Furthermore, the composition of EBN varies considerably depending on swiftlet species, geographic origin, nesting environment, and post-harvest processing methods, leading to substantial batch-to-batch variability in bioactive profiles [16,143]. Such heterogeneity presents challenges for dose standardization and reproducibility of biological effects. Contamination issues also warrant attention. Several studies have reported the presence of heavy metals such as Pb, Hg, and Cd in EBN samples, likely derived from environmental exposure and processing conditions [36]. These findings highlight the necessity of rigorous quality control systems, including raw material screening, standardized processing, and contaminant monitoring. From a regulatory perspective, EBN is generally classified as a traditional food in many Asian countries, whereas in Western contexts it may fall under the category of nutraceuticals or novel foods. This distinction has important implications for safety evaluation, labeling, and health-claim substantiation. Future translational research should therefore integrate toxicological assessment, dose optimization, and regulatory alignment to ensure the safe and effective use of EBN in brain health applications.

7. Future Research Directions

In mechanistic studies, it is essential to establish humanized in vitro models of the BBB, such as co-culture systems comprising hCMEC/D3 cells and astrocytes, to assess the penetration efficiency and transport mechanisms of active components in EBN. This approach will facilitate the validation of EBN's impact on BBB permeability. In clinical research, there remains a pronounced lack of RCTs and long-term follow-up data in middle-aged and elderly populations at risk for neurodegenerative disorders. Future studies should therefore prioritize rigorously designed RCTs. Importantly, the sample size for definitive trials should not be arbitrarily defined but determined through a priori power calculations based on effect sizes and variance estimates obtained from well-designed pilot studies. Trial design should include clearly defined and clinically relevant primary cognitive endpoints, such as changes in composite scores derived from validated batteries (e.g., ADAS-Cog or MoCA), together with secondary outcomes reflecting daily functioning and neuropsychiatric status. In addition, stratification or adjustment for key confounders, including sex, baseline dietary habits (including prior exposure to EBN), and genetic or metabolic risk factors, will be essential to ensure interpretability and generalizability of findings. For industrial applications, the development of co-encapsulated EBN-probiotic microcapsules is recommended to achieve sustained intestinal release and synergistic enhancement of the microbiota.

https://doi.org/10.3390/nu18040671

8. Conclusions and Outlook

In conclusion, EBN exhibits promising potential for application in mitigating brain aging. Its antioxidant, anti-inflammatory, and neuroprotective properties may contribute positively to decelerating the brain aging process. Active constituents such as SA, glycoproteins, and EGF are postulated to exert advantageous effects on nervous system function. Nonetheless, rigorous basic experimental and clinical research is imperative to scientifically substantiate its neuroprotective mechanisms and effects. Future investigations should focus on elucidating the molecular and cellular mechanisms of EBN, thereby providing a theoretical basis for the development of anti-brain-aging therapeutics. Additionally, its potential utility in the prevention and treatment of neurodegenerative diseases warrants evaluation to improve the quality of life for the elderly population.

Author Contributions: W.G. and X.W.: Conceptualization, Resources, Investigation, Visualization, Writing—original draft; W.Z.: Investigation, Methodology, Formal analysis; H.W. and W.X.: Investigation, Methodology; Y.L.: Methodology, Formal analysis, Validation; P.W.: Conceptualization, Project administration, Resources; Y.S.: Conceptualization, Project administration, Resources. All authors have read and agreed to the published version of the manuscript.

Funding: This work was financially supported by the National Key Research and Development Program of China (2022YFF0710402).

Data Availability Statement: No new data were created or analyzed in this study. Data sharing is not applicable to this article.

Conflicts of Interest: The authors declare no conflicts of interest.

Abbreviations

EBN: Edible bird's nest; AD: Alzheimer's disease; PD: Parkinson's disease; Ca: Calcium; Fe: Iron; GPC: Chromatography; RP-HPLC: Reverse-phase high-performance liquid chromatography; AM Case: Acidic mammalian chitinase; LOXL3: Lysyl oxidase homologue 3; MUC5AC: Mucin-5AC; NUCB2: Nucleobindin-2; MUC5B: Mucin 5B; LOXL2: Lysyl oxidase-like protein 2; CHIA: Chitinase; OIH: Ovomucoid-like protein; CAB45: Calcium-binding protein 45; GO: Gene Ontology; SA: sialic acid; Neu5Ac or NANA: Acetylneuraminic acid; Neu5Gc: N-glycolylneuraminic acid; KDN: Diamino neuraminic acid; Neu: Neuraminic acid; P: Phosphorus; Na: Sodium; K: Potassium; I: Iodine; Mg: Magnesium; Cr: Chromium; Se: Selenium; Pb: Lead; Cd: Cadmium; As: Arsenic; Hg: Mercury; EGF: Epidermal growth factor; NSCs: Neural stem cells; TPC: Total phenolic content; MCI: Mild cognitive impairment; ROS: Reactive oxygen species; NO: Nitric oxide; iNOS: Nitric oxide synthase; IL-17: Leukin-17; Aβ: β-amyloid; mt DNA: Mitochondrial DNA; TDP-43: Tar DNA-binding protein-43; SOD1: Superoxide dismutase 1; MGBA: Microbioa–gut–brain axis; BBB: Blood–brain barrier; SCFAs: Short-chain fatty acids; SIRT1: Sirtuin-1; LPS: Lipopolysaccharide; SOD: Superoxide dismutase; GPx: Glutathione peroxidase; AchE: Acetylcholinesterase; ACh: Acetylcholine; 6-OHDA: 6-hydroxydopamine; MNTD: maximum non-toxic dose; VE: Vitamin E; VC: Vitamin C; CoQ-10: Coenzyme Q10; VEGF: Vascular endothelial growth factor; BDNF: Brain-derived neurotrophic factor; DHA: Docosahexaenoic acid; EPA: Eicosapentaenoic acid; NCAM: Neural cell adhesion molecule; NGF: Nerve growth factor

References

1. Ekiz, E.; Oz, E.; Abd El-Aty, A.M.; Proestos, C.; Brennan, C.; Zeng, M.; Tomasevic, I.; Elobeid, T.; Cadirci, K.; Bayrak, M.; et al. Exploring the Potential Medicinal Benefits of Ganoderma lucidum: From Metabolic Disorders to Coronavirus Infections. *Foods* **2023**, *12*, 1512. [CrossRef]
2. Karunarathna, S.C.; Patabendige, N.M.; Hapuarachchi, K.K.; Promputtha, I. Exploring the health benefits of Ganoderma: Antimicrobial properties and mechanisms of action. *Front. Cell. Infect. Microbiol.* **2025**, *15*, 1535246. [CrossRef] [PubMed]

3. Zulkefle, N.N.; Ibrahim, M.A.; Azuan, N.F.; Ch'ng, S.E.; Ismail, N.; Abu Bakar, M.Z.; Chan, K.W.; Zhang, C. A Review on the Edible Bird's Nest Quality and Manufacturing Standards of the Three Largest Exporting Countries in the World. *J. Food Qual.* **2024**, *2024*, 5608357. [CrossRef]
4. Chua, K.H.; Mohamed, I.N.; Mohd Yunus, M.H.; Shafinaz Md Nor, N.; Kamil, K.; Ugusman, A.; Kumar, J. The Anti-Viral and Anti-Inflammatory Properties of Edible Bird's Nest in Influenza and Coronavirus Infections: From Pre-Clinical to Potential Clinical Application. *Front. Pharmacol.* **2021**, *12*, 633292. [CrossRef] [PubMed]
5. de Araujo, F.F.; de Paulo Farias, D.; Neri-Numa, I.A.; Pastore, G.M. Polyphenols and their applications: An approach in food chemistry and innovation potential. *Food Chem.* **2021**, *338*, 127535. [CrossRef]
6. Unal, K.I.; Chang, L.S.; Wan Mustapha, W.A.; Mohd Razali, N.S.; Babji, A.S.; Lim, S.J. Extraction, structural analysis and biological activities of edible bird's nest sialylated mucin (SiaMuc) glycoproteins: A review. *Food Biosci.* **2024**, *61*, 104791. [CrossRef]
7. Xiao, Y.; Duan, C.; Gong, P.; Zhao, Q.; Wang, X.h.; Geng, F.; Zeng, J.; Luo, T.; Xu, Y.; Zhao, J. Kinsenoside from Anoectochilus roxburghii (Wall.) Lindl. suppressed oxidative stress to attenuate aging-related learning and memory impairment via ERK/Nrf2 pathway. *J. Ethnopharmacol.* **2024**, *319*, 117152. [CrossRef]
8. Jiang, Q.; Liu, J.; Huang, S.; Wang, X.Y.; Chen, X.; Liu, G.H.; Ye, K.; Song, W.; Masters, C.L.; Wang, J.; et al. Antiageing strategy for neurodegenerative diseases: From mechanisms to clinical advances. *Signal Transduct. Target. Ther.* **2025**, *10*, 76. [CrossRef]
9. Qiao, J.; Wang, C.; Chen, Y.; Yu, S.; Liu, Y.; Yu, S.; Jiang, L.; Jin, C.; Wang, X.; Zhang, P.; et al. Herbal/Natural Compounds Resist Hallmarks of Brain Aging: From Molecular Mechanisms to Therapeutic Strategies. *Antioxidants* **2023**, *12*, 920. [CrossRef]
10. Tian, R.; Abarientos, A.; Hong, J.; Hashemi, S.H.; Yan, R.; Drager, N.; Leng, K.; Nalls, M.A.; Singleton, A.B.; Xu, K.; et al. Genome-wide CRISPRi/a screens in human neurons link lysosomal failure to ferroptosis. *Nat. Neurosci.* **2021**, *24*, 1020–1034. [CrossRef]
11. Zhang, Q.; Su, G.; Zhao, T.; Wang, S.; Sun, B.; Zheng, L.; Zhao, M. The memory improving effects of round scad (Decapterus maruadsi) hydrolysates on sleep deprivation-induced memory deficits in rats via antioxidant and neurotrophic pathways. *Food Funct.* **2019**, *10*, 7733–7744. [CrossRef]
12. Wang, J.; Li, L.; Wang, Z.; Cui, Y.; Tan, X.; Yuan, T.; Liu, Q.; Liu, Z.; Liu, X. Supplementation of lycopene attenuates lipopolysaccharide-induced amyloidogenesis and cognitive impairments via mediating neuroinflammation and oxidative stress. *J. Nutr. Biochem.* **2018**, *56*, 16–25. [CrossRef]
13. Grant, W.B.; Blake, S.M. Diet's Role in Modifying Risk of Alzheimer's Disease: History and Present Understanding. *J. Alzheimer's Dis.* **2023**, *96*, 1353–1382. [CrossRef] [PubMed]
14. Jie, C.; Ning, X.; Yu, Z.; Yuwei, D.; Yuye, W.; Lingyu, L.; Lin, J. Using RSM for Optimum of Optimum Production of Peptides from Edible Bird's Nest By-Product and Characterization of Its Antioxidant's Properties. *Foods* **2022**, *11*, 859. [CrossRef]
15. Chok, K.C.; Ng, M.G.; Ng, K.Y.; Koh, R.Y.; Tiong, Y.L.; Chye, S.M. Edible Bird's Nest: Recent Updates and Industry Insights Based On Laboratory Findings. *Front. Pharmacol.* **2021**, *12*, 746656. [CrossRef] [PubMed]
16. Quek, M.C.; Chin, N.L.; Yusof, Y.A.; Law, C.L.; Tan, S.W. Characterization of edible bird's nest of different production, species and geographical origins using nutritional composition, physicochemical properties and antioxidant activities. *Food Res. Int.* **2018**, *109*, 35–43. [CrossRef]
17. Sirinupong, N.; Chansuwan, W.; Kaewkaen, P.; Manna, P. Effect of Edible Bird's Nest on Protecting against Cognitive Deficit and Ameliorating Beta-Amyloid in Hippocampal Rats' Model of Cerebral Ischemia. *J. Food Biochem.* **2024**, *2024*, 7367894. [CrossRef]
18. Zukefli, S.N.; Chua, L.S.; Rahmat, Z. Protein Extraction and Identification by Gel Electrophoresis and Mass Spectrometry from Edible bird's Nest Samples. *Food Anal. Methods* **2016**, *10*, 387–398. [CrossRef]
19. Yuan, M.; Lin, X.; Wang, D.; Dai, J. Proteins: Neglected active ingredients in edible bird's nest. *Chin. Herb. Med.* **2023**, *15*, 383–390. [CrossRef]
20. Wang, X.; Hu, D.; Liao, F.; Chen, S.; Meng, Y.; Dai, J.; Dong, T.T.X.; Lao, Z.; Yu, L.; Liang, Y.; et al. Comparative proteomic analysis of edible bird's nest from different origins. *Sci. Rep.* **2023**, *13*, 15859. [CrossRef]
21. Goh, D.L.; Chua, K.Y.; Chew, F.T.; Liang, R.C.; Seow, T.K.; Ou, K.L.; Yi, F.C.; Lee, B.W. Immunochemical characterization of edible bird's nest allergens. *J. Allergy Clin. Immunol.* **2001**, *107*, 1082–1087. [CrossRef] [PubMed]
22. Yew, M.Y.; Koh, R.Y.; Chye, S.M.; Zainal Abidin, S.A.; Othman, I.; Ng, K.Y. Neurotrophic properties and the de novo peptide sequencing of edible bird's nest extracts. *Food Biosci.* **2019**, *32*, 100466. [CrossRef]
23. Yida, Z.; Imam, M.U.; Ismail, M. In vitro bioaccessibility and antioxidant properties of edible bird's nest following simulated human gastro-intestinal digestion. *BMC Complement. Altern. Med.* **2014**, *14*, 468. [CrossRef] [PubMed]
24. Ghassem, M.; Arihara, K.; Mohammadi, S.; Sani, N.A.; Babji, A.S. Identification of two novel antioxidant peptides from edible bird's nest (Aerodramus fuciphagus) protein hydrolysates. *Food Funct.* **2017**, *8*, 2046–2052. [CrossRef]
25. Lee, C.H.; Hamdan, N.; Nyakuma, B.B.; Wong, S.L.; Wong, K.Y.; Tan, H.; Jamaluddin, H.; Lee, T.H. Purification, identification and molecular docking studies of antioxidant and anti-inflammatory peptides from Edible Bird's Nest. *Food Chem.* **2024**, *454*, 139797. [CrossRef]
26. Hao, L.Q.; Rahman, O.A. Swiftlets and Edible Bird's Nest Industry in Asia. *Pertanika J. Sch. Res. Rev.* **2016**, *2*, 32–48.

27. Ali, A.; Bukhsh, K.K.; Muzaffar, H.; Hussain, S.A. An advanced approach towards maximizing the potential of edible bird's nest: Overcoming digestibility challenges through thermal processing (A mini-review). *Food Humanit.* **2025**, *5*, 100850. [CrossRef]
28. Dai, Y.; Cao, J.; Wang, Y.; Chen, Y.; Jiang, L. A comprehensive review of edible bird's nest. *Food Res. Int.* **2021**, *140*, 109875. [CrossRef]
29. Chu, W.; Phan, C.W.; Lim, S.J.; Babji, A.S. Insights on the molecular mechanism of neuroprotection exerted by edible bird's nest and its bioactive constituents. *Food Sci. Hum. Wellness* **2023**, *12*, 1008–1019. [CrossRef]
30. Morales-Martínez, A.; Martínez-Gómez, P.A.; Martinez-Fong, D.; Villegas-Rojas, M.M.; Pérez-Severiano, F.; Del Toro-Colín, M.A.; Delgado-Minjares, K.M.; Blanco-Alvarez, V.M.; Leon-Chavez, B.A.; Aparicio-Trejo, O.E.; et al. Oxidative Stress and Mitochondrial Complex I Dysfunction Correlate with Neurodegeneration in an α-Synucleinopathy Animal Model. *Int. J. Mol. Sci.* **2022**, *23*, 11394. [CrossRef]
31. Rawal, P.; Zhao, L. Sialometabolism in Brain Health and Alzheimer's Disease. *Front. Neurosci.* **2021**, *15*, 648617. [CrossRef] [PubMed]
32. Azmi, N.A.; Lee, T.H.; Lee, C.H.; Hamdan, N.; Cheng, K.K. Differentiation Unclean and Cleaned Edible Bird's Nest using Multivariate Analysis of Amino Acid Composition Data. *Pertanika J. Sci. Technol.* **2021**, *29*, 677–691. [CrossRef]
33. Ng, S.R.; Mohd Noor, H.S.; Ramachandran, R.; Tan, H.Y.; Ch'ng, S.-E.; Chang, L.S.; Babji, A.S.; Lim, S.J. Recovery of glycopeptides by enzymatic hydrolysis of edible bird's nest: The physicochemical characteristics and protein profile. *J. Food Meas. Charact.* **2020**, *14*, 2635–2645. [CrossRef]
34. Hui Yan, T.; Babji, A.S.; Lim, S.J.; Sarbini, S.R. A Systematic Review of Edible Swiftlet's Nest (ESN): Nutritional bioactive compounds, health benefits as functional food, and recent development as bioactive ESN glycopeptide hydrolysate. *Trends Food Sci. Technol.* **2021**, *115*, 117–132. [CrossRef]
35. Hun Lee, T.; Hau Lee, C.; Alia Azmi, N.; Kavita, S.; Wong, S.; Znati, M.; Ben Jannet, H. Characterization of Polar and Non-Polar Compounds of House Edible Bird's Nest (EBN) from Johor, Malaysia. *Chem. Biodivers.* **2020**, *17*, e1900419. [CrossRef]
36. Lee, T.H.; Wani, W.A.; Lee, C.H.; Cheng, K.K.; Shreaz, S.; Wong, S.; Hamdan, N.; Azmi, N.A. Edible Bird's Nest: The Functional Values of the Prized Animal-Based Bioproduct From Southeast Asia-A Review. *Front. Pharmacol.* **2021**, *12*, 626233. [CrossRef]
37. Chua, L.S.; Zukefli, S.N. A comprehensive review on edible bird nests and swiftlet farming. *J. Integr. Med.* **2016**, *14*, 415–428. [CrossRef]
38. Chan, G.K.L. Searching for Active Ingredients in Edible Bird's Nest. *J. Complement. Med. Altern. Healthc.* **2018**, *6*, 555683. [CrossRef]
39. Xiong, W.; Fang, B.; Wang, X.; Zhang, M.; Du, M.; Sun, J.; Chen, J.; Li, Y.; Sun, C.; Lei, X.; et al. Dietary Lipid Intervention in the Prevention of Brain Aging. *Engineering* **2024**, *37*, 128–137. [CrossRef]
40. Ionescu-Tucker, A.; Cotman, C.W. Emerging roles of oxidative stress in brain aging and Alzheimer's disease. *Neurobiol. Aging* **2021**, *107*, 86–95. [CrossRef]
41. Zhang, W.; Sun, H.S.; Wang, X.; Dumont, A.S.; Liu, Q. Cellular senescence, DNA damage, and neuroinflammation in the aging brain. *Trends Neurosci.* **2024**, *47*, 461–474. [CrossRef]
42. Mattson, M.P.; Arumugam, T.V. Hallmarks of Brain Aging: Adaptive and Pathological Modification by Metabolic States. *Cell Metab.* **2018**, *27*, 1176–1199. [CrossRef]
43. Lopez-Otin, C.; Blasco, M.A.; Partridge, L.; Serrano, M.; Kroemer, G. The hallmarks of aging. *Cell* **2013**, *153*, 1194–1217. [CrossRef] [PubMed]
44. Yadav, H.; Jaldhi; Bhardwaj, R.; Anamika; Bakshi, A.; Gupta, S.; Maurya, S.K. Unveiling the role of gut-brain axis in regulating neurodegenerative diseases: A comprehensive review. *Life Sci.* **2023**, *330*, 122022. [CrossRef] [PubMed]
45. Calcinotto, A.; Kohli, J.; Zagato, E.; Pellegrini, L.; Demaria, M.; Alimonti, A. Cellular Senescence: Aging, Cancer, and Injury. *Physiol. Rev.* **2019**, *99*, 1047–1078. [CrossRef] [PubMed]
46. Zia, A.; Pourbagher-Shahri, A.M.; Farkhondeh, T.; Samarghandian, S. Molecular and cellular pathways contributing to brain aging. *Behav. Brain Funct.* **2021**, *17*, 6. [CrossRef]
47. Niedzielska, E.; Smaga, I.; Gawlik, M.; Moniczewski, A.; Stankowicz, P.; Pera, J.; Filip, M. Oxidative Stress in Neurodegenerative Diseases. *Mol. Neurobiol.* **2016**, *53*, 4094–4125. [CrossRef]
48. Houldsworth, A. Role of oxidative stress in neurodegenerative disorders: A review of reactive oxygen species and prevention by antioxidants. *Brain Commun.* **2024**, *6*, fcad356. [CrossRef]
49. Shi, F.D.; Yong, V.W. Neuroinflammation across neurological diseases. *Science* **2025**, *388*, eadx0043. [CrossRef]
50. Gaikwad, S.; Senapati, S.; Haque, M.A.; Kayed, R. Senescence, brain inflammation, and oligomeric tau drive cognitive decline in Alzheimer's disease: Evidence from clinical and preclinical studies. *Alzheimer's Dement.* **2024**, *20*, 709–727. [CrossRef]
51. Adamu, A.; Li, S.; Gao, F.; Xue, G. The role of neuroinflammation in neurodegenerative diseases: Current understanding and future therapeutic targets. *Front. Aging Neurosci.* **2024**, *16*, 1347987. [CrossRef]
52. Kinney, J.W.; Bemiller, S.M.; Murtishaw, A.S.; Leisgang, A.M.; Salazar, A.M.; Lamb, B.T. Inflammation as a central mechanism in Alzheimer's disease. *Alzheimer's Dement.* **2018**, *4*, 575–590. [CrossRef] [PubMed]

53. Wang, S.; Sun-Waterhouse, D.; Neil Waterhouse, G.I.; Zheng, L.; Su, G.; Zhao, M. Effects of food-derived bioactive peptides on cognitive deficits and memory decline in neurodegenerative diseases: A review. *Trends Food Sci. Technol.* **2021**, *116*, 712–732. [CrossRef]
54. Aging Biomarker, C.; Bao, H.; Cao, J.; Chen, M.; Chen, M.; Chen, W.; Chen, X.; Chen, Y.; Chen, Y.; et al. Biomarkers of aging. *Sci. China Life Sci.* **2023**, *66*, 893–1066. [CrossRef] [PubMed]
55. Ashleigh, T.; Swerdlow, R.H.; Beal, M.F. The role of mitochondrial dysfunction in Alzheimer's disease pathogenesis. *Alzheimer's Dement.* **2023**, *19*, 333–342. [CrossRef]
56. Yan, X.; Wang, B.; Hu, Y.; Wang, S.; Zhang, X. Abnormal Mitochondrial Quality Control in Neurodegenerative Diseases. *Front. Cell Neurosci.* **2020**, *14*, 138. [CrossRef]
57. Caballol, N.S.; Saleki, S.; Palomares, D.; Ibrahim, T.; Kienlen-Campard, P. Dysfunctional mitochondria during accelerated senescence and their impact on Alzheimer's disease neuropathology. *Alzheimer's Dement.* **2023**, *19*, e076710. [CrossRef]
58. Moradi Vastegani, S.; Nasrolahi, A.; Ghaderi, S.; Belali, R.; Rashno, M.; Farzaneh, M.; Khoshnam, S.E. Mitochondrial Dysfunction and Parkinson's Disease: Pathogenesis and Therapeutic Strategies. *Neurochem. Res.* **2023**, *48*, 2285–2308. [CrossRef]
59. Wilson, M.R.; Satapathy, S.; Vendruscolo, M. Extracellular protein homeostasis in neurodegenerative diseases. *Nat. Rev. Neurol.* **2023**, *19*, 235–245. [CrossRef]
60. Lopez-Otin, C.; Blasco, M.A.; Partridge, L.; Serrano, M.; Kroemer, G. Hallmarks of aging: An expanding universe. *Cell* **2023**, *186*, 243–278. [CrossRef]
61. Hipp, M.S.; Kasturi, P.; Hartl, F.U. The proteostasis network and its decline in ageing. *Nat. Rev. Mol. Cell Biol.* **2019**, *20*, 421–435. [CrossRef] [PubMed]
62. Wilson, D.M., III; Cookson, M.R.; Van Den Bosch, L.; Zetterberg, H.; Holtzman, D.M.; Dewachter, I. Hallmarks of neurodegenerative diseases. *Cell* **2023**, *186*, 693–714. [CrossRef] [PubMed]
63. Cozachenco, D.; Ribeiro, F.C.; Ferreira, S.T. Defective proteostasis in Alzheimer's disease. *Ageing Res. Rev.* **2023**, *85*, 101862. [CrossRef] [PubMed]
64. Sorboni, S.G.; Moghaddam, H.S.; Jafarzadeh-Esfehani, R.; Soleimanpour, S. A Comprehensive Review on the Role of the Gut Microbiome in Human Neurological Disorders. *Clin. Microbiol. Rev.* **2022**, *35*, e0033820. [CrossRef]
65. Zhu, X.; Li, B.; Lou, P.; Dai, T.; Chen, Y.; Zhuge, A.; Yuan, Y.; Li, L. The Relationship Between the Gut Microbiome and Neurodegenerative Diseases. *Neurosci. Bull.* **2021**, *37*, 1510–1522. [CrossRef]
66. Li, Y.; Ning, L.; Yin, Y.; Wang, R.; Zhang, Z.; Hao, L.; Wang, B.; Zhao, X.; Yang, X.; Yin, L.; et al. Age-related shifts in gut microbiota contribute to cognitive decline in aged rats. *Aging* **2020**, *12*, 7801–7817. [CrossRef]
67. Sarubbo, F.; Moranta, D.; Tejada, S.; Jiménez, M.; Esteban, S. Impact of Gut Microbiota in Brain Ageing: Polyphenols as Beneficial Modulators. *Antioxidants* **2023**, *12*, 812. [CrossRef]
68. Mossad, O.; Batut, B.; Yilmaz, B.; Dokalis, N.; Mezo, C.; Nent, E.; Nabavi, L.S.; Mayer, M.; Maron, F.J.M.; Buescher, J.M.; et al. Gut microbiota drives age-related oxidative stress and mitochondrial damage in microglia via the metabolite N(6)-carboxymethyllysine. *Nat. Neurosci.* **2022**, *25*, 295–305. [CrossRef]
69. Ge, T.; Yao, X.; Zhao, H.; Yang, W.; Zou, X.; Peng, F.; Li, B.; Cui, R. Gut microbiota and neuropsychiatric disorders: Implications for neuroendocrine-immune regulation. *Pharmacol. Res.* **2021**, *173*, 105909. [CrossRef]
70. Hou, Z.; He, P.; Imam, M.U.; Qi, J.; Tang, S.; Song, C.; Ismail, M. Edible Bird's Nest Prevents Menopause-Related Memory and Cognitive Decline in Rats via Increased Hippocampal Sirtuin-1 Expression. *Oxidative Med. Cell. Longev.* **2017**, *2017*, 7205082. [CrossRef]
71. Zhiping, H.; Imam, M.U.; Ismail, M.; Ismail, N.; Yida, Z.; Ideris, A.; Sarega, N.; Mahmud, R. Effects of edible bird's nest on hippocampal and cortical neurodegeneration in ovariectomized rats. *Food Funct.* **2015**, *6*, 1701–1711. [CrossRef]
72. Careena, S.; Sani, D.; Tan, S.N.; Lim, C.W.; Hassan, S.; Norhafizah, M.; Kirby, B.P.; Ideris, A.; Stanslas, J.; Bin Basri, H.; et al. Effect of Edible Bird's Nest Extract on Lipopolysaccharide-Induced Impairment of Learning and Memory in Wistar Rats. *Evid.-Based Complement. Altern. Med.* **2018**, *2018*, 9318789. [CrossRef]
73. Nan, Q.; Chen-Xi, Z.; Guan-Dong, F.; Shuang, Q.; Yu, S.; Man, Y.; Dong-Liang, W.; Xiang-Rong, C. Interventional Effects of Edible Bird's Nest and Free Sialic Acids on LPS-Induced Brain Inflammation in Mice. *Nutrients* **2025**, *17*, 531. [CrossRef]
74. Yew, M.Y.; Koh, R.Y.; Chye, S.M.; Othman, I.; Soga, T.; Parhar, I.; Ng, K.Y. Edible bird's nest improves motor behavior and protects dopaminergic neuron against oxidative and nitrosative stress in Parkinson's disease mouse model. *J. Funct. Foods* **2018**, *48*, 576–585. [CrossRef]
75. Ismaeil, R.A.; Hui, C.K.; Affandi, K.A.; Alallam, B.; Mohamed, W.; Mohd Noor, M.F. Neuroprotective effect of edible bird's nest in chronic cerebral hypoperfusion induced neurodegeneration in rats. *Neuroimmunol. Neuroinflamm.* **2021**, *8*, 297. [CrossRef]
76. Yew, M.Y.; Koh, R.Y.; Chye, S.M.; Othman, I.; Ng, K.Y. Edible bird's nest ameliorates oxidative stress-induced apoptosis in SH-SY5Y human neuroblastoma cells. *BMC Complement. Altern. Med.* **2014**, *14*, 391. [CrossRef]

77. Hou, Z.; Imam, M.U.; Ismail, M.; Azmi, N.H.; Ismail, N.; Ideris, A.; Mahmud, R. Lactoferrin and ovotransferrin contribute toward antioxidative effects of Edible Bird's Nest against hydrogen peroxide-induced oxidative stress in human SH-SY5Y cells. *Biosci. Biotechnol. Biochem.* **2015**, *79*, 1570–1578. [CrossRef]
78. Rashed, A.A.; Ahmad, H.; Abdul Khalid, S.K.; Rathi, D.G. The Potential Use of Sialic Acid From Edible Bird's Nest to Attenuate Mitochondrial Dysfunction by In Vitro Study. *Front. Pharmacol.* **2021**, *12*, 633303. [CrossRef] [PubMed]
79. Xiao, M.; Yao, C.; Liu, F.; Xiang, W.; Zuo, Y.; Feng, K.; Lu, S.; Xiang, L.; Li, M.; Li, X.; et al. Sialic Acid Ameliorates Cognitive Deficits by Reducing Amyloid Deposition, Nerve Fiber Production, and Neuronal Apoptosis in a Mice Model of Alzheimer's Disease. *NeuroSci* **2022**, *3*, 28–40. [CrossRef]
80. Wu, J.; Lu, P.; Zhang, H.; Fan, Q.; Liu, X. Comparison of prebiotic activity of dietary sialoglycoprotein and N-acetylneuraminic acid: Sialylation is a key factor. *Food Biosci.* **2023**, *56*, 103397. [CrossRef]
81. Li, C.; Xu, X.; Lin, X.; Yuan, M.; Wang, D.; Zhang, X. Edible bird's nest plays an immune regulation by influencing intestinal flora changes in mice. *J. Funct. Foods* **2024**, *118*, 106254. [CrossRef]
82. Guo, J.; Zhu, Y.; Zhi, J.; Lou, Q.; Bai, R.; He, Y. Antioxidants in anti-Alzheimer's disease drug discovery. *Ageing Res. Rev.* **2025**, *107*, 102707. [CrossRef] [PubMed]
83. Razali, R.A.; Ngah, W.Z.W.; Makpol, S.; Yanagisawa, D.; Kato, T.; Tooyama, I. Shifting Perspectives on the Role of Tocotrienol vs. Tocopherol in Brain Health: A Scoping Review. *Int. J. Mol. Sci.* **2025**, *26*, 6339. [CrossRef] [PubMed]
84. de Leeuw, F.A.; Honer, W.G.; Schneider, J.A.; Morris, M.C. Brain gamma-Tocopherol Levels Are Associated with Presynaptic Protein Levels in Elderly Human Midfrontal Cortex. *J. Alzheimer's Dis.* **2020**, *77*, 619–627. [CrossRef]
85. Remington, R.; Lortie, J.J.; Hoffmann, H.; Page, R.; Morrell, C.; Shea, T.B. A Nutritional Formulation for Cognitive Performance in Mild Cognitive Impairment: A Placebo-Controlled Trial with an Open-Label Extension. *J. Alzheimer's Dis.* **2015**, *48*, 591–595. [CrossRef]
86. Kaye, A.D.; Thomassen, A.S.; Mashaw, S.A.; MacDonald, E.M.; Waguespack, A.; Hickey, L.; Singh, A.; Gungor, D.; Kallurkar, A.; Kaye, A.M.; et al. Vitamin E (alpha-Tocopherol): Emerging Clinical Role and Adverse Risks of Supplementation in Adults. *Cureus* **2025**, *17*, e78679. [CrossRef]
87. Sindhu, R.K.; Kaur, P.; Kaur, P.; Singh, H.; Batiha, G.E.; Verma, I. Exploring multifunctional antioxidants as potential agents for management of neurological disorders. *Environ. Sci. Pollut. Res. Int.* **2022**, *29*, 24458–24477. [CrossRef]
88. Bej, E.; Cesare, P.; d'Angelo, M.; Volpe, A.R.; Castelli, V. Neuronal Cell Rearrangement During Aging: Antioxidant Compounds as a Potential Therapeutic Approach. *Cells* **2024**, *13*, 1945. [CrossRef]
89. Sharma, V.; Aran, K.R. Unraveling the molecular mechanisms of vitamin deficiency in Alzheimer's disease pathophysiology. *Aging Health Res.* **2025**, *5*, 100226. [CrossRef]
90. Mock, J.T.; Chaudhari, K.; Sidhu, A.; Sumien, N. The influence of vitamins E and C and exercise on brain aging. *Exp. Gerontol.* **2017**, *94*, 69–72. [CrossRef]
91. Yu, J.-T.; Xu, W.; Tan, C.-C.; Andrieu, S.; Suckling, J.; Evangelou, E.; Pan, A.; Zhang, C.; Jia, J.; Feng, L.; et al. Evidence- based prevention of Alzheimer's disease: Systematic review and meta- analysis of 243 observational prospective studies and 153 randomised controlled trials. *J. Neurol. Neurosurg. Psychiatry* **2020**, *91*, 1201–1209. [CrossRef] [PubMed]
92. Figueroa-Mendez, R.; Rivas-Arancibia, S. Vitamin C in Health and Disease: Its Role in the Metabolism of Cells and Redox State in the Brain. *Front. Physiol.* **2015**, *6*, 397. [CrossRef] [PubMed]
93. Nankivell, M.C.; Rosenfeldt, F.; Pipingas, A.; Pase, M.P.; Reddan, J.M.; Stough, C. Coenzyme Q10 and Cognition: A Review. *Nutrients* **2025**, *17*, 2896. [CrossRef] [PubMed]
94. Mantle, D.; Hargreaves, I. Coenzyme Q10 and the Blood-Brain Barrier: An Overview. *J. Clin. Med.* **2025**, *14*, 2748. [CrossRef]
95. Mantle, D.; Heaton, R.A.; Hargreaves, I.P. Coenzyme Q10, Ageing and the Nervous System: An Overview. *Antioxidants* **2021**, *11*, 2. [CrossRef]
96. Dumont, M.; Kipiani, K.; Yu, F.; Wille, E.; Katz, M.; Calingasan, N.Y.; Gouras, G.K.; Lin, M.T.; Beal, M.F. Coenzyme Q10 decreases amyloid pathology and improves behavior in a transgenic mouse model of Alzheimer's disease. *J. Alzheimer's Dis.* **2011**, *27*, 211–223. [CrossRef]
97. Komaki, H.; Faraji, N.; Komaki, A.; Shahidi, S.; Etaee, F.; Raoufi, S.; Mirzaei, F. Investigation of protective effects of coenzyme Q10 on impaired synaptic plasticity in a male rat model of Alzheimer's disease. *Brain Res. Bull.* **2019**, *147*, 14–21. [CrossRef]
98. Hewlings, S.J.; Kalman, D.S. Curcumin: A Review of Its Effects on Human Health. *Foods* **2017**, *6*, 92. [CrossRef]
99. Boots, A.W.; Haenen, G.R.; Bast, A. Health effects of quercetin: From antioxidant to nutraceutical. *Eur. J. Pharmacol.* **2008**, *585*, 325–337. [CrossRef]
100. Dyall, S.C. Long-chain omega-3 fatty acids and the brain: A review of the independent and shared effects of EPA, DPA and DHA. *Front. Aging Neurosci.* **2015**, *7*, 52. [CrossRef]
101. Johnson, E.J. Role of lutein and zeaxanthin in visual and cognitive function throughout the lifespan. *Nutr. Rev.* **2014**, *72*, 605–612. [CrossRef]

102. Szućko-Kociuba, I.S.; Trzeciak-Ryczek, A.; Kupnicka, P.; Chlubek, D. Neurotrophic and Neuroprotective Effects of *Hericium erinaceus*. *Int. J. Mol. Sci.* **2023**, *24*, 15960. [CrossRef]
103. Kushairi, N.; Tarmizi, N.A.K.A.; Phan, C.W.; Macreadie, I.; Sabaratnam, V.; Naidu, M.; David, P. Modulation of neuroinflammatory pathways by medicinal mushrooms, with particular relevance to Alzheimer's disease. *Trends Food Sci. Technol.* **2020**, *104*, 153–162. [CrossRef]
104. Zielinska, A.; Alves, H.; Marques, V.; Durazzo, A.; Lucarini, M.; Alves, T.F.; Morsink, M.; Willemen, N.; Eder, P.; Chaud, M.V.; et al. Properties, Extraction Methods, and Delivery Systems for Curcumin as a Natural Source of Beneficial Health Effects. *Medicina* **2020**, *56*, 336. [CrossRef] [PubMed]
105. Islam, M.R.; Rauf, A.; Akter, S.; Akter, H.; Al-Imran, M.I.K.; Fakir, M.N.H.; Thufa, G.K.; Islam, M.T.; Hemeg, H.A.; Abdulmonem, W.A.; et al. Neuroprotective Potential of Curcumin in Neurodegenerative Diseases: Clinical Insights Into Cellular and Molecular Signaling Pathways. *J. Biochem. Mol. Toxicol.* **2025**, *39*, e70369. [CrossRef] [PubMed]
106. Cheriki, M.; Habibian, M.; Moosavi, S.J. Curcumin attenuates brain aging by reducing apoptosis and oxidative stress. *Metab. Brain Dis.* **2024**, *39*, 833–840. [CrossRef]
107. Rekha, A.; Afzal, M.; Babu, M.A.; Menon, S.V.; Nathiya, D.; Supriya, S.; Mishra, S.B.; Gupta, S.; Goyal, K.; Rana, M.; et al. GSK-3β dysregulation in aging: Implications for tau pathology and Alzheimer's disease progression. *Mol. Cell. Neurosci.* **2025**, *133*, 104005. [CrossRef]
108. Liao, L.; Shi, J.; Jiang, C.; Zhang, L.; Feng, L.; Liu, J.; Zhang, J. Activation of anti-oxidant of curcumin pyrazole derivatives through preservation of mitochondria function and Nrf2 signaling pathway. *Neurochem. Int.* **2019**, *125*, 82–90. [CrossRef]
109. Baghcheghi, Y.; Razazpour, F.; Mirzaee, F.; Dalfardi, M.; Pourfridoni, M.; Hedayati-Moghadam, M. Exploring the molecular mechanisms of curcumin in modulating memory impairment in neurodegenerative disorders. *Mol. Biol. Rep.* **2024**, *52*, 45. [CrossRef]
110. Wang, W.; Zhao, R.; Liu, B.; Li, K. The effect of curcumin supplementation on cognitive function: An updated systematic review and meta-analysis. *Front. Nutr.* **2025**, *12*, 1549509. [CrossRef]
111. Tabanelli, R.; Brogi, S.; Calderone, V. Improving Curcumin Bioavailability: Current Strategies and Future Perspectives. *Pharmaceutics* **2021**, *13*, 1715. [CrossRef] [PubMed]
112. Feng, Q.; Zhang, X.; Zhao, X.; Liu, J.; Wang, Q.; Yao, Y.; Xiao, H.; Zhu, Y.; Zhang, W.; Wang, L. Intranasal Delivery of Pure Nanodrug Loaded Liposomes for Alzheimer's Disease Treatment by Efficiently Regulating Microglial Polarization. *Small* **2024**, *20*, e2405781. [CrossRef] [PubMed]
113. Aktary, N.; Jeong, Y.; Oh, S.; Shin, Y.; Sung, Y.; Rahman, M.; Ramos Santiago, L.; Choi, J.; Song, H.G.; Nurkolis, F.; et al. Unveiling the therapeutic potential of natural products in Alzheimer's disease: Insights from in vitro, in vivo, and clinical studies. *Front. Pharmacol.* **2025**, *16*, 1601712. [CrossRef] [PubMed]
114. Bazinet, R.P.; Metherel, A.H.; Chen, C.T.; Shaikh, S.R.; Nadjar, A.; Joffre, C.; Laye, S. Brain eicosapentaenoic acid metabolism as a lead for novel therapeutics in major depression. *Brain Behav. Immun.* **2020**, *85*, 21–28. [CrossRef]
115. Saleh, R.N.M.; Minihane, A.M. Fish, n-3 fatty acids, cognition and dementia risk: Not just a fishy tale. *Proc. Nutr. Soc.* **2022**, *81*, 27–40. [CrossRef]
116. Liu, X.; Zhuang, P.; Li, Y.; Wu, F.; Wan, X.; Zhang, Y.; Jiao, J. Association of fish oil supplementation with risk of incident dementia: A prospective study of 215,083 older adults. *Clin. Nutr.* **2022**, *41*, 589–598. [CrossRef]
117. Dyall, S.C.; Plourde, M. Omega-3 polyunsaturated fatty acids in neurodegenerative disorders: Mixed designs = mixed results. *Prog. Lipid Res.* **2025**, *100*, 101356. [CrossRef]
118. Wen, M.; Zhao, Y.; Shi, H.; Wang, C.; Zhang, T.; Wang, Y.; Xue, C. Short-term supplementation of DHA as phospholipids rather than triglycerides improve cognitive deficits induced by maternal omega-3 PUFA deficiency during the late postnatal stage. *Food Funct.* **2021**, *12*, 564–572. [CrossRef]
119. Niazi, N.U.K.; Jiang, J.; Ou, H.; Chen, R.; Yang, Z. Sleep Deprivation and Alzheimer's Disease: A Review of the Bidirectional Interactions and Therapeutic Potential of Omega-3. *Brain Sci.* **2025**, *15*, 641. [CrossRef]
120. Wen, J.; Satyanarayanan, S.K.; Li, A.; Yan, L.; Zhao, Z.; Yuan, Q.; Su, K.P.; Su, H. Unraveling the impact of Omega-3 polyunsaturated fatty acids on blood-brain barrier (BBB) integrity and glymphatic function. *Brain Behav. Immun.* **2024**, *115*, 335–355. [CrossRef]
121. Flieger, J.; Forma, A.; Flieger, W.; Flieger, M.; Gawlik, P.J.; Dzierżyński, E.; Maciejewski, R.; Teresiński, G.; Baj, J. Carotenoid Supplementation for Alleviating the Symptoms of Alzheimer's Disease. *Int. J. Mol. Sci.* **2024**, *25*, 8982. [CrossRef]
122. Jayakanthan, M.; Manochkumar, J.; Efferth, T.; Ramamoorthy, S. Lutein, a versatile carotenoid: Insight on neuroprotective potential and recent advances. *Phytomedicine* **2024**, *135*, 156185. [CrossRef] [PubMed]
123. Nazari, L.; Komaki, S.; Salehi, I.; Raoufi, S.; Golipoor, Z.; Kourosh-Arami, M.; Komaki, A. Investigation of the protective effects of lutein on memory and learning using behavioral methods in a male rat model of Alzheimer's disease. *J. Funct. Foods* **2022**, *99*, 105319. [CrossRef]

124. Gunal, M.Y.; Sakul, A.A.; Caglayan, A.B.; Erten, F.; Kursun, O.E.D.; Kilic, E.; Sahin, K. Protective Effect of Lutein/Zeaxanthin Isomers in Traumatic Brain Injury in Mice. *Neurotox. Res.* **2021**, *39*, 1543–1550. [CrossRef] [PubMed]
125. Pap, R.; Pandur, E.; Jánosa, G.; Sipos, K.; Agócs, A.; Deli, J. Lutein Exerts Antioxidant and Anti-Inflammatory Effects and Influences Iron Utilization of BV-2 Microglia. *Antioxidants* **2021**, *10*, 363. [CrossRef]
126. Huang, H.; Duan, J.; Duan, W.; Pu, X.; Ma, C.; Xu, Z. Lutein ameliorates Parkinson's disease by regulating miR-135b-5p/SIRT1 to inhibit microglial M1 polarization and inflammation. *Brain Res. Bull.* **2025**, *230*, 111487. [CrossRef]
127. Zhang, Y.; Kong, L.; Tan, L. Effectiveness of nanoscale delivery systems on improving the bioavailability of lutein in rodent models: A systematic review. *Crit. Rev. Food Sci. Nutr.* **2022**, *62*, 2375–2390. [CrossRef]
128. Zamanian, M.Y.; Khachatryan, L.G.; Heidari, M.; Darabi, R.; Golmohammadi, M.; Al-Aouadi, R.F.A.; Akkol, E.K. The Therapeutic Potential of Flavonols in Alzheimer's Disease: Inhibiting Amyloid-beta, Oxidative Stress, and Neuroinflammation. *Biofactors* **2025**, *51*, e70047. [CrossRef]
129. Yang, Y.; Zhang, Y.; Chen, L.; Li, Z.; Zhao, Q. Therapeutic potential of quercetin in depressive symptoms: A systematic review and meta-analysis of preclinical studies. *Front. Pharmacol.* **2025**, *16*, 1598053. [CrossRef]
130. Srivastava, A.; Kumari, A.; Jagdale, P.; Ayanur, A.; Pant, A.B.; Khanna, V.K. Potential of Quercetin to Protect Cadmium Induced Cognitive Deficits in Rats by Modulating NMDA-R Mediated Downstream Signaling and PI3K/AKT-Nrf2/ARE Signaling Pathways in Hippocampus. *Neuromol. Med.* **2023**, *25*, 426–440. [CrossRef]
131. Feng, Y.; Yu, X.; Han, J. Quercetin Regulates the Polarization of Microglia through the NRF2/HO1 Pathway and Mitigates Alzheimer's Disease. *Actas Esp. Psiquiatr.* **2024**, *52*, 786–799. [CrossRef] [PubMed]
132. Fiore, M.; Terracina, S.; Ferraguti, G. Brain Neurotrophins and Plant Polyphenols: A Powerful Connection. *Molecules* **2025**, *30*, 2657. [CrossRef] [PubMed]
133. Liu, W.Y.; Yu, Y.; Zang, J.; Liu, Y.; Li, F.R.; Zhang, L.; Guo, R.B.; Kong, L.; Ma, L.Y.; Li, X.T. Menthol-Modified Quercetin Liposomes with Brain-Targeting Function for the Treatment of Senescent Alzheimer's Disease. *ACS Chem. Neurosci.* **2024**, *15*, 2283–2295. [CrossRef] [PubMed]
134. Zhu, S.; Zhang, Y.; Li, C.; Deng, Z.; Yin, Y.; Dong, Z.; Kuang, L.; Li, C.; Hu, X.; Yin, T.; et al. Multiple synergistic anti-aging effects of vascular cell adhesion molecule 1 functionalized nanoplatform to improve age-related neurodegenerative diseases. *J. Control. Release* **2025**, *379*, 363–376. [CrossRef]
135. Lai, P.-L.; Naidu, M.; Sabaratnam, V.; Wong, K.-H.; David, R.P.; Kuppusamy, U.R.; Abdullah, N.; Malek, S.N.A. Neurotrophic Properties of the Lion's Mane Medicinal Mushroom, *Hericium erinaceus* (Higher Basidiomycetes) from Malaysia. *Int. J. Med. Mushrooms* **2013**, *15*, 539–554. [CrossRef]
136. Zhang, J.; An, S.; Hu, W.; Teng, M.; Wang, X.; Qu, Y.; Liu, Y.; Yuan, Y.; Wang, D. The Neuroprotective Properties of *Hericium erinaceus* in Glutamate-Damaged Differentiated PC12 Cells and an Alzheimer's Disease Mouse Model. *Int. J. Mol. Sci.* **2016**, *17*, 1810. [CrossRef]
137. Contato, A.G.; Conte-Junior, C.A. Lion's Mane Mushroom (*Hericium erinaceus*): A Neuroprotective Fungus with Antioxidant, Anti-Inflammatory, and Antimicrobial Potential—A Narrative Review. *Nutrients* **2025**, *17*, 1307. [CrossRef]
138. Phan, C.W.; David, P.; Naidu, M.; Wong, K.H.; Sabaratnam, V. Therapeutic potential of culinary-medicinal mushrooms for the management of neurodegenerative diseases: Diversity, metabolite, and mechanism. *Crit. Rev. Biotechnol.* **2015**, *35*, 355–368. [CrossRef]
139. Li, J.; Huang, Q.; Chen, J.; Qi, H.; Liu, J.; Chen, Z.; Zhao, D.; Wang, Z.; Li, X. Neuroprotective Potentials of Panax Ginseng Against Alzheimer's Disease: A Review of Preclinical and Clinical Evidences. *Front. Pharmacol.* **2021**, *12*, 688490. [CrossRef]
140. Shi, Z.; Chen, H.; Zhou, X.; Yang, W.; Lin, Y. Pharmacological effects of natural medicine ginsenosides against Alzheimer's disease. *Front. Pharmacol.* **2022**, *13*, 952332. [CrossRef]
141. Wu, J.; Zhang, L.; Liu, D.; Xia, J.; Yang, Y.; Tang, F.; Chen, L.; Ao, H.; Peng, C. Ginsenoside Rg1, lights up the way for the potential prevention of Alzheimer's disease due to its therapeutic effects on the drug-controllable risk factors of Alzheimer's disease. *J. Ethnopharmacol.* **2024**, *318*, 116955. [CrossRef]
142. Lho, S.K.; Kim, T.H.; Kwak, K.P.; Kim, K.; Kim, B.J.; Kim, S.G.; Kim, J.L.; Kim, T.H.; Moon, S.W.; Park, J.Y.; et al. Effects of lifetime cumulative ginseng intake on cognitive function in late life. *Alzheimer's Res. Ther.* **2018**, *10*, 50. [CrossRef]
143. Ma, F.; Liu, D. Sketch of the edible bird's nest and its important bioactivities. *Food Res. Int.* **2012**, *48*, 559–567. [CrossRef]

Disclaimer/Publisher's Note: The statements, opinions and data contained in all publications are solely those of the individual author(s) and contributor(s) and not of MDPI and/or the editor(s). MDPI and/or the editor(s) disclaim responsibility for any injury to people or property resulting from any ideas, methods, instructions or products referred to in the content.

nutrients

MDPI

Review

Advances in Intestinal-Targeted Release of Phenolic Compounds

Yunxuan Tang [1], Wenjing Liu [1], Jiayan Zhang [1], Bai Juan [1], Ying Zhu [1], Lin Zhu [1], Yansheng Zhao [1], Maria Daglia [2,3], Xiang Xiao [1] and Yufeng He [1,*]

[1] School of Food and Biological Engineering, Jiangsu University, Zhenjiang 212013, China; tang1834178338@163.com (Y.T.); 18660310376@163.com (W.L.); jiayanzhang1988@163.com (J.Z.); 1000005134@ujs.edu.cn (B.J.); ying307@126.com (Y.Z.); zhu-lin19820402@ujs.edu.cn (L.Z.); zhaoys@ujs.edu.cn (Y.Z.); xiaoxiang1@aliyun.com (X.X.)
[2] International Research Center for Food Nutrition and Safety, Jiangsu University, Zhenjiang 212013, China; maria.daglia@unina.it
[3] Department of Pharmacy, University of Naples "Federico II", Via D. Montesano 49, 80131 Naples, Italy
* Correspondence: hyf_fbs@foxmail.com

Abstract: Phenols are natural compounds with considerable bioactivities. However, the low bioavailability and chemical instability of phenols limit their biological functions. This review summarizes recent progress in phenol delivery systems that account for the specific physiological conditions of the gastrointestinal tract. It focuses on the delivery materials for intestinal targeting and the synergistic benefits of co-encapsulating phenols with other functional ingredients. To achieve targeted release of phenols in the digestive tract, factors such as pH, digestive enzymes, and gut microbiota should be fully considered in delivery system designing. Materials like chitosan, sodium alginate, pectin, and guar gum offer effective protection and targeted delivery of phenols due to their pH sensitivity and enzyme-degradable properties. Co-delivery systems that combine phenols with carotenoids or probiotics improve the functional properties of phenols, such as antioxidant activity, anti-inflammatory effect, and regulation of gut microbiota. Probiotics can enhance phenolic compound absorption and probiotic survival in a phenolic–probiotic co-encapsulation system through debonding, bioconversion, and synergistic effects.

Keywords: phenolic compound; intestinal-targeted delivery; co-encapsulation; wall material; bioavailability

1. Introduction

As modern lifestyles have changed, the global prevalence of chronic diseases such as obesity, hypertension, and hyperlipidemia has increased significantly [1,2]. For individuals with these conditions, these diseases diminish the living quality and increase the additional burden of medical care. For example, obesity is associated with an increased risk of type 2 diabetes, cardiovascular diseases, stroke, and certain cancers (such as breast, colorectal, endometrial, and pancreatic cancers) [3,4]. Recent studies have highlighted the value of food bioactive compounds to prevent and mitigate the impact of these chronic diseases [5].

Phenols are abundantly present in plants [6]. Research indicates that phenols offer a wide range of health benefits, including antioxidant, anti-inflammatory, lipid-lowering, and gut microbiota-modulating effects [7]. These properties make them effective in preventing various metabolic disorders, such as cardiovascular disease, diabetes, and obesity [7–9]. Additionally, phenols can modulate the gut microbiota by promoting beneficial bacteria (such as *Lactobacillus* and *Bifidobacterium*) while inhibiting harmful bacteria (e.g., *Escherichia coli* and *Salmonella*), thus maintaining gut health [10–12]. Despite their benefits, phenols face

several challenges during the digestion process. For example, phenols can bind to salivary proteases in oral cavity, which causes unpleasant astringent tastes, thereby limiting their palatability in food products [13]. In addition, phenols are chemically unstable and can be degraded under various conditions, resulting in the loss of their bioactive properties. This instability complicates their processing, storage, and transportation [14]. Table 1 provides a comprehensive overview of the bioactive properties and technological challenges associated with commonly consumed phenols, detailing their therapeutic potential and limitations in industrial applications. For instance, tea polyphenols can be degraded when they are exposed to light, high temperatures, or transition metals, undergoing irreversible chemical changes [15]. Furthermore, phenols are prone to instability in the acidic conditions of the stomach, preventing them from reaching the gut in their bioactive form [16]. These challenges not only hinder the bioaccessibility of phenols in the intestine but also restrict their application as plant-based nutritional supplements.

Various technological strategies are applied by researchers to overcome the challenges of phenols such as low bioavailability, instability, and limited effectiveness in the intestine. One promising approach is the intestinal-targeted release technology. This method involves designing specific carrier systems that enable the precise release of phenols within the intestinal tract. It not only addresses the issue of the astringent taste of phenolic compounds but also protects them from degradation by gastric acid and digestive enzymes, thereby prolonging their residence time in the intestinal tract [17]. Due to the complex physiological environments of the digestive system, developing effective phenol delivery systems requires consideration of the distinct conditions in different regions. For instance, the acidic pH and the presence of pepsin in the stomach necessitate that the delivery system materials be resistant to both acid and enzymatic breakdown [18]. The physiological environment of the small intestine must also be considered. The neutral pH and high digestive enzyme activity in the small intestine can challenge the stability of these systems. Therefore, colon-targeted delivery systems are often engineered with additional protective layers, such as stable polysaccharides combined with proteins, providing extra protection against degradation [19]. Additionally, the pH difference between the small intestine and colon can be exploited to develop pH-responsive shells for targeted phenol * delivery to the colon [20]. In recent years, there has been growing interests in co-delivery systems, which combine phenols with other bioactive compounds, such as carotenoids and probiotics. These systems can effectively deliver both phenols and other bioactives. Co-delivery systems are designed by selecting compatible bioactives based on their physicochemical properties (e.g., polarity, hydrophilicity, antioxidant properties) and functional activities (e.g., anti-inflammatory activity, anticancer activity and anti-obesity activity), thus enhancing the stability of the system and generating synergistic effects [21–23].

Table 1. Comprehensive characteristics of common phenolic compounds. Figures source: Retrieved from PubChem database (https://pubchem.ncbi.nlm.nih.gov) (accessed on 10 May 2025).

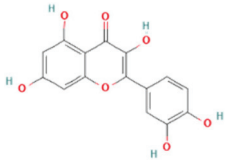
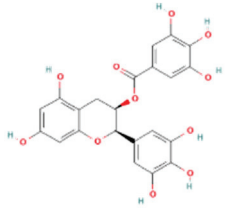
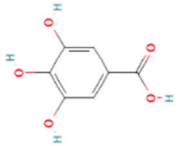
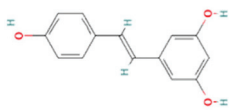
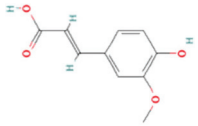
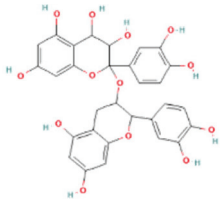
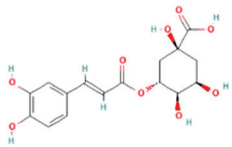
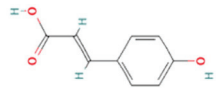
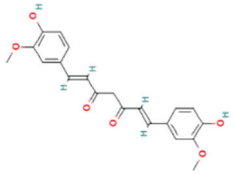
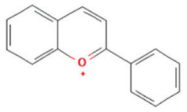
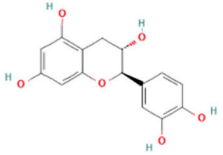
Bioactive Compound	Chemical Structure	Sources	Solubility (mg/mL)	Pharmacological Properties	Limitations	References
Quercetin		Apples, onions, buckwheat, green tea	0.002	Antioxidant, anti-inflammatory, anticancer, antiviral, antiproliferative, and anti-diabetic in clinical trials	Poor stability under light, heat, and alkaline conditions, poor gastrointestinal stability, and low bioaccessibility (<2%)	[24,25]
Epigallocatechin gallate (EGCG)		Green tea, black tea, white tea	10	Antioxidant, anti-inflammatory, and anti-colon cancer; efficacy confirmed in vivo in mouse liver injury models	Bitter taste, sensitive to high temperature, oxygen, and pH changes	[26]
Gallic acid		Tea leaves, grapes, berries, gallnuts, mangoes	50	Antioxidant, anti-inflammatory, analgesic, neuroprotective, anticancer, and anti-diabetic in vivo	Astringent taste, large particle size, poor absorption, low bioavailability, and rapid excretion. Unstable at high temperatures	[27,28]
Resveratrol		Grape skins, peanuts, polygonum cuspidatum	0.03	Antioxidant, anti-inflammatory, anti-obesity, and anti-colon cancer in vivo	Low water solubility, low oral bioavailability, sensitive to high temperature, oxygen, and light, prone to rapid degradation and inactivation during intestinal metabolism	[29,30]
Ferulic acid		Whole grains, angelica, oats, tomatoes	1	Antioxidant, anti-inflammatory, anti-tumor, and antihyperglycemic activities in vivo	Unstable to oxygen and prone to degradation, poor gastrointestinal stability	[31–34]

Table 1. *Cont.*

Bioactive Compound	Chemical Structure	Sources	Solubility (mg/mL)	Pharmacological Properties	Limitations	References
Procyanidin		Grape seeds, cocoa beans, apples, berries	0.01–0.05	Anti-obesity, antioxidant, and anti-type 2 diabetes in vivo	Unstable under pH changes, heat, humidity, gastrointestinal environment	[35,36]
Chlorogenic acid		Coffee beans, peaches, plums, apples, eggplants	5–10	Antimicrobial, anti-inflammatory, antioxidant, regulates glucose, lipid metabolism, and antitumor activities in vivo.	Unstable under heat, light, and alkaline conditions	[37,38]
Coumaric acid		Grapes, olives, coffee beans, tomatoes, carrots, cereals	0.6	Anti-inflammatory, antioxidant, and anti-colon cancer; improve cholesterol metabolism and enhance antioxidant capacity in vivo	Sensitive to pH, temperature, oxygen, light, and enzymes	[39,40]
Curcumin		Turmeric, curcuma zedoaria, curcuma aerugionosa	<0.0004	Prevents cancer, cardiovascular diseases, and diabetes, neuroprotective in vivo	Hydrophobic compounds, low bioavailability and high chemical transformation rate, sensitive in alkaline pH (>7), high temperature, and light	[41–43]
Anthocyanins		Blueberries, red cabbage, purple, potatoes	10	Antioxidant, anti-inflammatory, anticancer, and anti-diabetic, alleviates chronic intestinal diseases in vivo	Hydrophobic compounds, not resistant to gastric acid, and have low bioavailability	[44,45]
Catechin		Green tea, black tea, apples, grapes,	10	Antioxidant, antidiabetic, anti-inflammatory anticancer, and antibacterial, inhibit the pathogenesis of colorectal cancers in vivo	Sensitive to pH, temperature, oxygen, and light; instability in the gastrointestinal tract and limited membrane permeability across the intestine	[46,47]

Although existing reviews summarize advances in the preparation of phenol microcapsules, they predominantly concentrate on preparation methods and the design of delivery systems. There is, however, a clear need to investigate the intestinal-targeted release of phenol microcapsules, considering the unique environment of different digestive sites. Furthermore, the co-encapsulation of phenols with other bioactive compounds is gaining attention. This review examines the physiological conditions of the digestive tract and their influence on phenol delivery systems. It also presents wall materials like chitosan, sodium alginate, and pectin, which are ideal for developing phenol-based intestinal-targeted release systems. In addition, this paper also discusses the suitable delivery systems for different water-soluble phenolics as well as advances in the study of phenolics co-encapsulation with probiotics and their interaction.

2. Methods

A literature search was performed using the Web of Science, PubMed, and ScienceDirect databases to identify relevant studies published from January 2015 to December 2025. The search was limited to articles published in English in peer-reviewed journals. The following keywords and combinations were used for the search: "phenolic compounds," "intestinal targeted delivery," "polyphenol microencapsulation," "co-encapsulation of polyphenols with probiotics," and "intestinal-targeted release of polyphenols." Conference abstracts, non-English articles, duplicate records, and studies not directly related to the intestinal delivery of phenolic compounds were excluded.

The inclusion criteria encompassed original research articles (including in vitro, in vivo, and clinical studies) as well as review articles addressing advances in the targeted delivery of polyphenols and their interaction with gut microbiota or encapsulation techniques. Articles meeting the inclusion criteria were reviewed in full, and relevant references cited within these articles were also screened to ensure comprehensive coverage of the topic. A narrative synthesis of the selected literature was then conducted to summarize the current knowledge and identify gaps for future research.

3. Physiologic Environments of Digestive Tract and Their Effects on Phenol Delivery Systems

When preparing gastrointestinal targeted-release systems, selecting wall materials is extremely important. The characteristics of the gastrointestinal physiological environment are a major consideration. The gastrointestinal physiological environment and strategies for selecting wall materials are summarized in Figure 1.

3.1. Stomach

The intricate physiological environment of the stomach poses specific challenges to the design and use of intestinal-targeted release microcapsules. The acidic nature of gastric juice (pH 1.5–3.5), the presence of pepsin, and the protective function of gastric mucus together establish a unique microenvironment [48]. These factors significantly affect the stability and release properties of microcapsules, guiding the selection and design of their wall materials.

Hydrochloric acid is a major component of the stomach's environment, and its acidic properties pose a significant challenge to the stability of microencapsulated wall materials. Many natural and synthetic polymers, when used as wall materials, are vulnerable to degradation or solubilization under acidic conditions. This leads to the premature release and degradation of phenols in gastric acid and prevents phenols from reaching the intestines and fully exerting their functional effects. Pepsin, the dominant digestive enzyme in gastric juice, activates and cleaves peptide bonds in proteins, facilitating their breakdown

in an acidic environment. The presence of pepsin can degrade certain protein-based wall materials (e.g., gelatin), causing premature release of the core material and inhibiting the active ingredient from reaching the intestines to perform its intended activity [49,50]. To prevent this, acid-resistant and enzyme-resistant materials, such as pectin, chitosan, sodium alginate, and gum arabic, are often chosen to protect the microcapsules from premature degradation in the gastric environment.

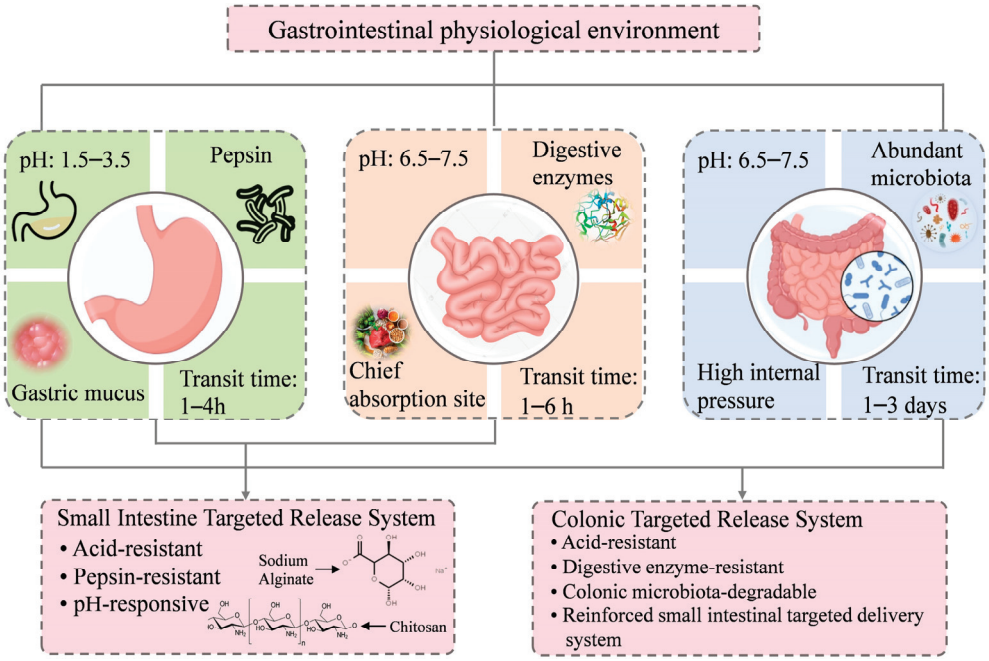


Figure 1. Schematic of the gastrointestinal physiological environment and wall material selection strategies.

3.2. Small Intestine

The small intestine, which plays a central role in nutrient absorption, features a dense network of villi and microvilli that dramatically expand its absorptive surface area. Targeted release of phenols and other bioactive compounds in this region increases their bioavailability, ensuring efficient uptake into systemic circulation and enhancing their physiological efficacy [51]. As the longest part of the digestive system, the small intestine facilitates the enzymatic breakdown of macromolecules, enabling efficient nutrient assimilation. The small intestine's near-neutral pH (6.5–7.5) provides optimal conditions for digestive enzymes, ensuring the efficient hydrolysis of nutrients [52]. Enzymes such as amylase, protease, and lipase secreted by the small intestine catalyze the breakdown of dietary macromolecules, with nutrient absorption occurring through mechanisms including passive diffusion, active transport, and endocytosis [53]. Thus, pH-responsive encapsulation systems are employed to protect phenols from gastric acidity while facilitating their release in the small intestine. In addition, acid-resistant and enzyme-resistant wall materials further improve the precision of intestinal-targeted delivery.

3.3. Colon

The colon, as the final segment of the gastrointestinal tract, is mainly responsible for water and electrolyte absorption, vitamin recovery, and the compaction and expulsion of undigested residues. New insights into the colon's role in host–microbiota crosstalk have identified it as a critical target for therapeutic interventions involving prebiotics, probiotics, and bioactive compounds to promote systemic health [54]. Colon-targeted phenol delivery has been shown to alleviate colitis, modulate gut microbiota, and strengthen the intestinal

barrier, offering both therapeutic and preventive benefits [55]. The design of phenol carriers, by taking into consideration the colon's physiological characteristics, ensures targeted delivery while minimizing unintended effects. The colonic lumen has a mildly alkaline pH (6.5–7.5) [56], which supports both enzymatic and microbial activities. The colon harbors a dense microbial community (10^{11}–10^{13} CFU), which greatly exceeds the microbial load in the stomach (10^3 CFU) and small intestine (10^4–10^8CFU) [57]. Obligate anaerobes, including *Bifidobacterium*, *Lactobacillus*, and *Bacteroides* species, predominate in this ecosystem, and their metabolic processes are enhanced by the alkaline pH of the colon. These microorganisms are vital for maintaining gut health, immune function, and metabolic homeostasis [58,59]. Thus, materials that resist degradation in the gastric and small intestinal environments but can be metabolized by colonic microbes are suitable for achieving colon-targeted release. Moreover, the higher pressures in the colon, resulting from peristalsis, may serve as an effective trigger for drug release [60].

Colon-targeted delivery systems require enhanced stability and prolonged intestinal retention compared to those targeting the small intestine. To achieve this, formulations often incorporate a combination of polysaccharides and proteins to strengthen the system's resistance to the harsh gastric and small intestinal environments. This ensures that the delivery system reaches the colon intact, enabling precise and site-specific release. Such an approach improves both the physiological resilience and release performance of the system in the colonic environment [19].

In summary, the gastrointestinal tract presents compartment-specific physiological environments: an acidic gastric lumen, a near-neutral small intestine, and a microbiota-rich colon. These environments impose distinct design requirements for microencapsulation. In the stomach, low pH (1.5–3.5), pepsin activity, and the mucus barrier can degrade polymer walls and prematurely release phenols. The small intestine (pH 6.5–7.5) necessitates acid-resistant yet pH-sensitive carriers that remain stable in gastric conditions but release contents site-specifically. In the colon, where the pH remains mildly alkaline and microbial density is high, delivery systems must exhibit microbial and enzymatic responsiveness, mechanical robustness, and extended retention. Thus, the selection of wall materials must account for the entire gastrointestinal landscape to ensure successful transit and precise release in the colon, enabling the bioactive payload to perform its intended function.

4. Wall Materials for Intestinal-Targeted Release

In the development of intestine-targeted delivery systems, the selected materials must possess sufficient mechanical strength to resist the oral and gastric environments while ensuring controlled release in the small intestine and colon. Therefore, the choice of wall material is of great significance. It is necessary to take into account the physicochemical properties of phenols, such as their hydrophilic/hydrophobic characteristics and charge attributes. In addition, to achieve targeted release in the small intestine or colon, both the mechanical strength and gastrointestinal stability of the wall material must be carefully considered. The following is an introduction to the commonly used wall materials in these two types of systems.

4.1. Small Intestine Targeted Release

Optimal wall materials for small intestine-targeted microcapsules must demonstrate high biocompatibility, chemical stability, and resistance to gastric acid. To overcome gastric conditions (pH 1.5–3.5, proteolytic enzymes, bile salts), pH-sensitive polymers—such as alginate, chitosan, and resistant oligosaccharides—are commonly employed to ensure site-specific payload release in the small intestine. Given its central role in nutrient absorption, the small intestine requires well-designed delivery systems to improve the bioavailability

and chemical stability of phenols. The physicochemical properties of encapsulating materials critically influence release kinetics across the gastrointestinal tract (oral cavity, stomach, small intestine), ultimately determining therapeutic outcomes. High-performance carriers must withstand degradation in the oral and gastric environments, while enabling pH- and enzyme-responsive release in the small intestine, with minimal leakage into the colon. The subsequent sections discuss commonly used wall materials for phenols encapsulation targeted to the small intestine.

4.1.1. Chitosan

Chitosan, a cationic polysaccharide obtained through chitin deacetylation, demonstrates excellent mechanical strength and resistance to gastrointestinal shear stress [61,62]. Its functional groups (-NH_2, -OH, -$COCH_3$) facilitate non-covalent interactions, including hydrogen bonding and electrostatic attraction with phenols, thereby enhancing payload stability [63]. Under gastric conditions (pH 1.5–3.5), protonation of the amine groups promotes electrostatic crosslinking, while the polymer's hydrophobic nature further prevents premature drug release [16]. At intestinal pH (7.0–7.5), chitosan undergoes deprotonation, which enables solubilization, while enzymatic degradation by proteases and carbohydrases facilitates site-specific release [54]. The cationic surface charge also promotes mucoadhesion through electrostatic interactions with negatively charged intestinal mucins, extending residence time and increasing local concentrations of phenols, thus improving absorption [16]. Its biocompatibility and low immunogenicity further support chitosan's potential for clinical application [64]. The dual pH responsiveness—resistance in the stomach and solubility in the intestine—makes chitosan ideal for spatiotemporal delivery systems. Accordingly, chitosan is considered a leading candidate for small intestinal drug delivery. In one example, Hassan et al. [65] developed microencapsulated systems by coating alginate–caffeic acid hydrogel beads with chitosan using ionic gelation. The chitosan layer minimized drug leakage in Simulated Gastric Fluid (SGF) (<20%) via surface erosion and Fickian diffusion, while in Simulated Intestinal Fluid (SIF), over 90% release was achieved within 180 min [65].

4.1.2. Sodium Alginate

Sodium alginate, a natural polysaccharide derived from brown algae such as kelp and Sargassum, is the sodium salt of alginic acid [66]. This biocompatible and non-toxic polymer is extensively applied in food and pharmaceutical delivery systems [67]. Structurally, it consists of β-D-mannuronic acid and α-L-guluronic acid residues linked via (1→4) glycosidic bonds [66]. As a polyanionic polymer, sodium alginate exhibits pH-responsive solubility: in acidic conditions (pH 1.5–3.5), protonation of carboxyl groups reduces hydrophilicity and contracts the polymer chains, contributing to gastric stability. In contrast, in the small intestine (pH 6.0–7.5), deprotonation increases solubility, facilitating pH-dependent release of encapsulated compounds [68]. Its excellent film-forming properties allow the construction of microcapsules with sufficient mechanical strength to withstand oral mastication and gastric peristalsis, thereby protecting sensitive phenols [69]. When crosslinked with divalent cations such as Ca^{2+}, sodium alginate forms ionotropic hydrogels that remain intact under gastric pH. These hydrogels disintegrate in the intestinal environment through a combination of cation exchange (Na^+ replacing Ca^{2+}) and pH-induced dissolution, enabling targeted intestinal release [68].

Zhao et al. [70] developed alginate-based enteric capsules to enhance the oral bioavailability of proteins. These capsules maintained structural integrity in SGF (pH 1.2) but disintegrated rapidly in SIF (pH 6.8), demonstrating their effectiveness for site-specific protein delivery [70]. Similarly, Cao et al. [71] reported that sodium alginate-composite

microcapsules significantly improved microbial viability under simulated gastrointestinal conditions. *Lactobacillus plantarum* showed a 71.49% survival rate in SGF and was released at 2.51×10^9 CFU in SIF, underscoring the formulation's resilience during digestion [71]. González et al. [72] optimized low-concentration alginate matrices for sustained intestinal release of olive secoiridoids. The system's sensitivity to alkaline pH and extended intestinal retention provided gastric protection while enabling controlled release, resulting in 88% bioaccessibility and improved systemic bioavailability [72].

4.1.3. Other Wall Materials

Protein-based encapsulation presents a promising strategy for targeted phenol delivery to the small intestine. Wang et al. [73] developed microcapsules using soy protein isolate (SPI) and whey protein isolate (WPI) as wall materials. These formulations effectively protected curcumin from gastric degradation and facilitated its release in the small intestine through pH and enzyme-responsive mechanisms. Among the two microcapsules, WPI-based microcapsules exhibited higher encapsulation efficiency (97.6%) and payload capacity (9.6%), whereas SPI-based microcapsules demonstrated greater proteolytic sensitivity and a cumulative curcumin release exceeding 85% during intestinal digestion [73].

In conclusion, pH-responsive polymers (e.g., chitosan, sodium alginate) and protein composites (e.g., SPI, WPI) are rationally selected as wall materials to enhance microcapsule stability and achieve site-specific release. These materials synergistically resist gastric acidity and promote controlled intestinal release, thereby improving phenol bioaccessibility and systemic uptake.

4.2. Colonic Targeted Release

Phenols have shown therapeutic potential in alleviating colitis and modulating gut microbiota through colon-specific mechanisms [74,75]. These effects are mediated by colonic microbiota, which transform phenols into bioactive metabolites via enzymatic cleavage of complex molecular structures [76]. However, unencapsulated phenols are susceptible to extensive degradation in the upper gastrointestinal tract (GIT), leading to reduced colonic bioavailability and compromised anti-inflammatory and microbiota-regulating efficacy [77,78]. Conventional microencapsulation techniques often fail to withstand gastric and intestinal environments due to inadequate mechanical strength, resulting in premature release of the payload in the upper GIT. This underscores the need for advanced colon-targeted delivery systems with improved gastrointestinal stability.

In designing such systems, physicochemical properties of wall materials need to be considered to guarantee the phenol stability at different GIT environments. Effective colon-targeted carriers must endure sequential physiological stresses—including gastric acidity (pH 1.5–3.5), digestive enzymes (e.g., pepsin, trypsin), and microbial fermentation in the colon. An ideal system should resist degradation throughout the oral cavity, stomach, and small intestine, and enable precise release in the colon to ensure sufficient local concentration for therapeutic activity. To meet these criteria, composite wall materials are commonly employed. Multilayered matrices can enhance structural stability and enable site-specific release in the colon.

4.2.1. Wall Materials for Microbial Degradation

The degradation of encapsulation materials in the colon is largely mediated by resident anaerobic bacteria, including *Bifidobacterium*, *Lactobacillus*, and *Bacteroides*. These microbes can specifically degrade certain polysaccharides, such as pectin and guar gum. Thus, polysaccharides are considered as effective wall materials for colon-targeted delivery. Their microbial metabolism promotes the controlled release of phenols in the lower gastrointestinal tract.

Pectin is a plant-derived heteropolysaccharide, which can form stable phenol encapsulation complexes through hydrogen bonding and electrostatic interactions. Its hydrophobic domains facilitate the selective encapsulation of curcumin, achieving up to 85.3% binding efficiencies [79]. Pectin degradation in the colon requires the synergistic action of microbial enzymes, including hydrolases, lyases, and esterases, produced by colonic microbiota such as *Bacteroides* and *Bifidobacterium* [80]. Pectin is resistant to degradation by endogenous enzymes in the stomach and small intestine. However, enzymes from intestinal microbes (primarily species from *Mycobacterium*, *Bifidobacterium*, and *Clostridium*) can break it down in the colon. This makes pectin a suitable material for colon-targeted phenol delivery [81]. However, pectin's hydrophilicity and pH-dependent swelling can limit its standalone use. To address these limitations, composite systems like pectin–chitosan polyelectrolytes are used. These systems can reduce aqueous solubility to less than 15% in SGF [82], while enhance stability and enable the controlled release of phenols in the colon [16]. For example, Andishmand et al. [82] developed a chitosan–pectin polyelectrolyte complexes. The complexes retained over 80% resveratrol during simulated upper gastrointestinal transit, and achieved 49% colon-targeted release of resveratrol [82].

Guar gum is a natural polysaccharide primarily extracted from guar beans (*Cyamopsis tetragonolobus*). It consists of mannose and galactose units, and is characterized by high water solubility and biodegradability [83,84]. The hydrophilic matrix of guar gum formed in cold water allows for the encapsulation of phenols with varying solubility profiles [85]. Guar gum exhibits pH-dependent swelling behavior in the gastrointestinal tract: it swells minimally in acidic conditions and undergoes maximal expansion in alkaline environments [86]. Furthermore, guar gum is resistant to digestion in the stomach and small intestine, but can be efficiently degraded by microbes in the colon. Gut microbes that can degrade guar gum include *Bacteroides*, *Ruminococcus*, and *Bifidobacterium* [87,88]. These characteristics make guar gum an effective wall material for colon-targeted phenol delivery. Kumar et al. [89] developed solid tablets using guar gum-encapsulated curcumin. In a simulated gastrointestinal environment over 24 h, these solid tablets released 42–86% of curcumin in the colon, while only 10% of the curcumin was released by the unencapsulated form. In an in vitro cytotoxicity study, the curcumin-encapsulated tablets exhibited stronger anticancer activity against HCT-15 cells than free curcumin, without any cytotoxic effects from the blank matrix. The underlying mechanisms of this enhanced activity warrant further investigation [89].

4.2.2. Reinforcement of Wall Materials to Withstand Small Intestine Digestion

Colon-targeted phenol delivery systems require greater mechanical and chemical robustness than those intended for small intestinal release. By selecting more robust wall materials, the colon-targeted phenol delivery system can effectively withstand small intestine digestion. To facilitate the release of core materials in the colon, Sun et al. [90] engineered polysaccharide-reinforced matrices that improved systemic stability, resulting in 92% colonic payload delivery in murine colitis models. Additionally, colon-targeted phenol release can be achieved by optimizing the concentration and preparation method of the wall materials. González et al. [72] showed that microcapsules of olive bitter glycosides, prepared with a higher concentration of sodium alginate and by spray-drying, overcame the sensitivity of alginate to the alkaline environment of the small intestine and the extended transit time to the colon. This approach prevented premature release of olive bittersweet in the small intestine, ensuring its intact release in the colon (90%) [72].

Through design modifications, wall materials intended for small intestinal-targeted release can be used for colon-targeted delivery. For instance, alginate can provide gastric protection and chitosan can provide small intestinal enzyme resistance. The composite

matrices of alginate and chitosan enable precise colonic delivery [16]. Wen et al. demonstrated the pH and enzyme-responsive release of quercetin using alginate–chitosan carriers, achieving 85% colonic bioavailability in pharmacokinetic studies [91].

In summary, for small-intestinal targeted delivery of phenols, a common system involves coating phenols with a large-molecular-weight polysaccharide (e.g., chitosan, sodium alginate) wall material. If the phenols are hydrophobic, a protein or a hydrophobicity-inducing polysaccharide is used as an inner layer. This ensures the system has enough mechanical strength to survive the gastric environment and releases phenols stably in the small intestine. Colonic drug delivery demands greater system strength and stability. To enhance mechanical stability, an additional protective layer can be applied to the small intestine-targeted delivery system. Alternatively, select wall materials degradable by colonic microbes for the inner layer and pair them with other large-molecular-weight polysaccharides as the outer layer. This shields phenolic compounds from degradation in the stomach and small intestine. Sometimes, proteins are added to enhance the solubility and embeddability of hydrophobic phenols.

5. Intestinal Release of Phenolic Compounds

Recent research has made significant progress in developing delivery systems for phenolic compounds. These studies aim to enhance the bioavailability and functionality of phenolic compounds, thereby maximizing their health benefits in the gut. Phenolic compounds such as gallic acid, anthocyanins, quercetin, resveratrol, and curcumin possess unique bioactivities and health benefits. However, these compounds face challenges in intestinal delivery, including low solubility, instability, and poor bioavailability (Table 1). Delivery systems must be carefully selected based on the distinct physicochemical properties of each phenolic compound. Amongst these physicochemical properties, water solubility needs special focus in designing targeted delivery systems of phenolic compounds (Figure 2).

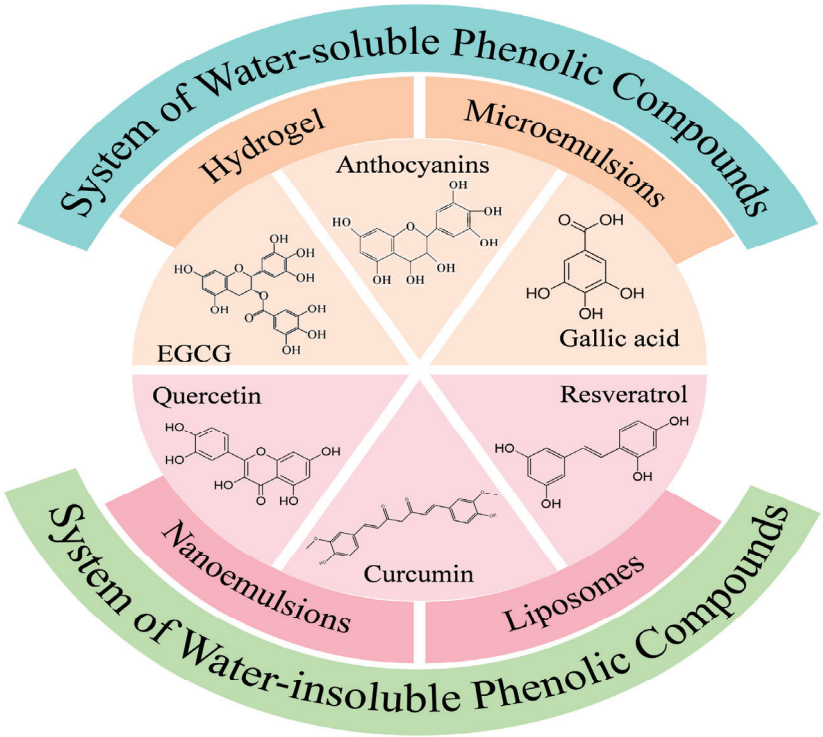


Figure 2. Schematic of delivery systems for water-soluble and non-water-soluble phenolic compounds.

5.1. Intestinal Targeted Delivery of Water-Soluble Phenolic Compounds

For water-soluble phenolic compounds such as gallic acid, anthocyanins, and epigallocatechin gallate (EGCG) [92,93], their favorable water solubility facilitates smooth transport through the gastrointestinal tract and rapid dispersion for absorption by the intestinal mucosa. However, these compounds remain susceptible to degradation from gastric acid and digestive enzymes. To overcome this challenge, researchers have developed targeted release systems based on hydrogels and microemulsions.

Hydrogel systems, with their hydrophilic network structure, can effectively load water-soluble phenolic compounds. By adjusting the cross-linking density and pore size of the hydrogel, the release rate of the compounds can be controlled to achieve intestinal targeted delivery [94]. Winda et al. prepared a hydrogel loaded with gallic acid using alginate gel and lactoferrin. The hydrogen bonds formed between the phenolic groups of gallic acid and lactoferrin effectively prevented the loss of gallic acid from the gel, thereby enhancing its stability [95]. Meanwhile, Zhao et al. [96] developed a nano-hydrogel system for water-soluble anthocyanins using alginate and hyaluronic acid as wall materials. This system can target the release of anthocyanins at sites of intestinal inflammation. Utilizing a colon-specific alginate gel shell and hyaluronic acid for inflammation-specific targeting, the nano-composites aggregate on the inflamed colon mucosa. This design protects anthocyanins from degradation in external and gastrointestinal environments and significantly improves local bioavailability by prolonging colon retention time [96,97].

Microemulsions significantly enhance the dispersion of water-soluble phenolic compounds within the gastrointestinal tract, thereby enhancing their bioavailability. Gao et al. [98] utilized a reverse microemulsion process to develop a modified corn starch microgel system. This innovative system achieved an impressive encapsulation efficiency of 63.89% for EGCG. Notably, the DPPH free radical scavenging activity of EGCG was elevated to 85.37%, reflecting the system's efficacy. Furthermore, the system demonstrated a markedly higher release of EGCG in SIF (60%) compared to SGF (<20%), clearly indicating its intestinal targeted delivery characteristic [98].

5.2. Intestinal Targeted Delivery of Water-Insoluble Phenolic Compounds

Quercetin, resveratrol, curcumin, and other phenolic compounds with poor water solubility present significant challenges in terms of gastrointestinal absorption and utilization [99–101]. The low solubility of these compounds in the gastrointestinal tract impedes the formation of a uniform solution, thereby limiting their contact with the intestinal mucosa and leading to reduced bioavailability [102,103]. To overcome these challenges, research has been directed toward the development of advanced drug delivery systems designed to enhance the solubility and stability of these compounds. Among the various approaches, nanoemulsions and liposomes have emerged as two of the most commonly utilized targeted release systems for water-insoluble phenolic compounds.

Nanoemulsions significantly enhance compound solubility via their nano-sized oil droplets. The surfactants in nanoemulsions prevent droplet aggregation, thereby ensuring stability within the gastrointestinal tract [104]. Chen et al. developed a whey protein isolate–inulin complex emulsion for quercetin encapsulation, achieving an encapsulation efficiency of 83.62% and remarkably enhancing water solubility by 389 times [105]. This delivery system demonstrated superior antioxidant capacity. Moreover, it maintained stability under gastric conditions, enabling targeted quercetin release in the small intestine and thereby improving bioavailability. Additionally, Wang et al. [106] formulated a dextran-based water-in-oil emulsion loaded with curcumin. This system protected curcumin from degradation and significantly enhanced its gastrointestinal absorption, leading to a 4.8-fold

increase in bioavailability. It effectively addressed the challenges of curcumin's poor water solubility and low oral bioavailability [101,106,107].

Liposomes, with their distinctive bilayer membrane structure, encapsulate water-insoluble phenolic compounds within the lipid bilayer, shielding them from adverse gastrointestinal conditions and facilitating absorption through interaction with intestinal mucosal cells [108,109]. Shruthi et al. [110] developed a resveratrol-encapsulated liposome using maltodextrin, lactose, and branched starch as wall materials. This liposome demonstrated stability in SGF and achieved a targeted release of 78.2% of resveratrol in SIF, thereby enhancing its bioavailability and water solubility [110,111].

In summary, the selection of delivery systems for phenolic compounds with varying water solubilities is a direct reflection of their differing physicochemical properties. Water-soluble phenolic compounds are more effectively delivered through hydrophilic systems such as hydrogels and microemulsions, whereas water-insoluble phenolic compounds are better suited to systems like nanoemulsions and liposomes, which are designed to improve solubility and stability. This classification based on water solubility provides a robust theoretical foundation and practical guidance for the development of precise intestinal targeted delivery systems tailored to the specific characteristics of different phenolic compounds.

6. Intestinal Delivery of Phenol-Containing Mixtures

In recent years, research on delivery systems for phenols has evolved from focusing solely on the encapsulation of individual compounds to exploring multi-component co-delivery systems. This transition is driven by the potential of co-delivery systems to simultaneously encapsulate multiple bioactive compounds, enabling synergistic interactions that enhance therapeutic outcomes. Consequently, there has been a growing interest in co-embedding phenols with other bioactive agents for targeted delivery to the gut, particularly when the co-embedded compounds are functionally compatible and capable of producing complementary biological effects [21,22]. Table 2 provides a comprehensive overview of recent studies on the co-encapsulation of polyphenols with other bioactive components, detailing their targeted encapsulation characteristics and the resulting biological activities.

6.1. Intestinal Co-Delivery of Multiple Phenols

Studies have demonstrated that combining phenols can enhance their overall bioactivity [112]. EGCG, a principal component of green tea phenols, possesses abundant phenolic hydroxyl groups and exhibits potent antioxidant, anti-inflammatory, and colon cancer-preventive properties. When co-administered with curcumin, EGCG has been shown to synergistically enhance its anticancer efficacy [26,104,113]. Moreover, selecting phenols with complementary physicochemical properties for co-embedding can significantly improve the stability and intestinal targeting of delivery systems. For instance, strongly hydrophobic curcumin can be incorporated into the hydrophobic core of zein–lysozyme nanoparticles via an anti-solvent method, while moderately hydrophobic EGCG can be adsorbed in the interfacial region between the zein core and caseinate shell. Yan et al. [23] leveraged these interactions to develop a novel plant protein-based nanoparticle system for co-encapsulating curcumin and EGCG with differing polarities. This system was achieved through EGCG-mediated covalent bonding with proteins or polysaccharide [23]. Enhanced encapsulation efficiency for curcumin, improved stability and bioavailability, and an increase in the composite's overall antioxidant capacity was further observed. These findings indicate that co-embedding phenols with distinct polarities can both stabilize protein-based delivery systems and induce synergistic therapeutic effects.

Curcumin and resveratrol exhibit a range of biological activities, including antioxidant, anti-inflammatory, and anticancer effects [114]. As hydrophobic phenols, both of them can interact with hydrophobic domains of proteins. By forming a hydrophobic nanoparticle core via protein–phenol coupling, high-efficiency co-encapsulation of curcumin and resveratrol can be achieved. Based on Yan et al.'s preliminary work [79], Liu et al. [115] designed a colloidal delivery system capable of co-delivering both compounds, which enhanced their water dispersibility, chemical stability, and bioaccessibility. The system achieved encapsulation rates of about 71% for curcumin and 85% for resveratrol. In vitro digestion experiments revealed that the formulation resisted degradation in the gastric environment and released its contents in the small intestine. This behavior was largely attributed to the formation of mixed micelles by lipid digestion products, facilitating solubilization of microcapsules in intestinal fluids and increasing the bioaccessibility of curcumin and resveratrol to 61.1% and 90.1%, respectively [115]. Interestingly, the co-loaded nanoparticles were smaller in size compared to those loaded with individual phenols. This is likely due to the close hydrophobic interactions between curcumin and resveratrol, which reduce internal molecular free space and promote a more compact nanoparticle structure.

6.2. Intestinal Co-Delivery of Phenols and Carotenoids

Carotenoids are widely distributed in green vegetables and yellow to orange fruits, with a range of biological activities [116]. Structurally, they can be divided into two main types: hydrocarbon carotenoids (such as α-carotene, β-carotene, γ-carotene, and lycopene) and oxygen-containing carotenoids, which are also known as xanthophylls (such as lutein, zeaxanthin, and astaxanthin) [117]. These compounds are recognized for their antioxidant, immunoregulatory, anticancer, and anti-aging effects [118]. Nevertheless, the extensive unsaturation in their hydrocarbon chains compromises their water solubility and bioavailability [119], and renders them susceptible to degradation. To address these limitations, co-pigmentation with active compounds such as phenols and flavonoids has been employed. These molecules can interact with carotenoids via hydrogen bonds, electrostatic interactions, and van der Waals forces, thereby enhancing their stability and antioxidant capacity [120]. Co-embedding carotenoids with phenols is thus a promising strategy for overcoming bioavailability challenges and amplifying functional benefits.

β-carotene is a natural hydrophobic carotenoid and a vitamin A precursor. β-carotene exhibits strong antioxidant properties, including scavenging free radicals and reactive oxygen and nitrogen species. It plays a crucial role in metabolic and cellular developmental processes [121]. However, its poor solubility in water and susceptibility to oxidation limit its use in dietary supplements [32]. Anthocyanins possess anticancer properties. When combined with β-carotene, the resulting formulation can enhance bioefficacy while reducing chemotherapy-related toxicity and resistance. Shi et al. [122] developed a gut-targeted antioxidant delivery system by co-encapsulating liposoluble β-carotene and water-soluble, positively charged anthocyanins using chitosan and oxidized konjac glucomannan as wall materials. The hydrophobic β-carotene was encapsulated within oxidized konjac glucomannan to form a double emulsion, while the positively charged anthocyanins and chitosan were adsorbed onto its surface. This system exhibited pH-responsive release in the intestine, because chitosan resists gastric acid and deprotonates in the neutral environment of the small intestine, facilitating the release of β-carotene and anthocyanin. This delivery system exhibited synergistic antioxidant activity, increased thermal stability, and successfully delivered both antioxidant compounds to the small intestine [122].

As a type of carotenoid, lutein is mainly obtained from marigold petals [123]. It serves as a key component of the human macular pigment, contributing to improved vision and retinal health [124]. Despite these benefits, lutein exhibits low water solubility and high

susceptibility to oxidative, thermal, and photolytic degradation [125]. To address this limitation, Yan et al. [126] developed a lutein-enriched emulsion with enhanced stability. A covalently bonded phenol–protein–polysaccharide complex (bovine serum albumin, chlorogenic acid, and dextran) was used as a novel emulsifier, along with vitamin E as a fat-soluble antioxidant. This formulation significantly improved the bioaccessibility of lutein (62.3%), resisted degradation by gastric acid and pepsin, and allowed for targeted release in the small intestine [126]. The presence of chlorogenic acid contributes to the improved physicochemical stability of the system.

6.3. Intestinal Co-Delivery of Phenols and Probiotics

Pathogens and harmful substances that are generated during digestion can disturb the microbial balance, and thereby lead to disease. Probiotics have been shown to maintain host health by regulating gut microbiota, modulating immune responses, and enhancing gut barrier integrity [127,128]. Among these probiotics, *Lactobacillus* and *Bifidobacterium* are the most frequently investigated general [129]. Although various single-strain probiotic delivery systems are available [130], Muhammad et al. [131] developed carboxymethylcellulose hydrogels incorporating *Lactobacillus plantarum* along with inulin and soy protein isolate, which significantly improved the storage stability and gastrointestinal viability of the probiotics [131]. However, growing evidence supports the superior efficacy of co-delivery systems that incorporate prebiotics or bioactive compounds, such as phenols [132,133]. These formulations leverage mutualistic interactions: probiotics enzymatically convert phenols into more bioavailable forms, while phenols protect probiotics from hostile environments in the upper gastrointestinal tract [17], enhancing their viability and fostering a beneficial microbiome. The interaction between phenolic compounds and probiotics in co-encapsulation systems are summarized in Figure 3. This synergistic relationship makes co-encapsulation systems a promising approach for colon-targeted delivery, particularly in the alleviation of gut dysbiosis and intestinal inflammation.

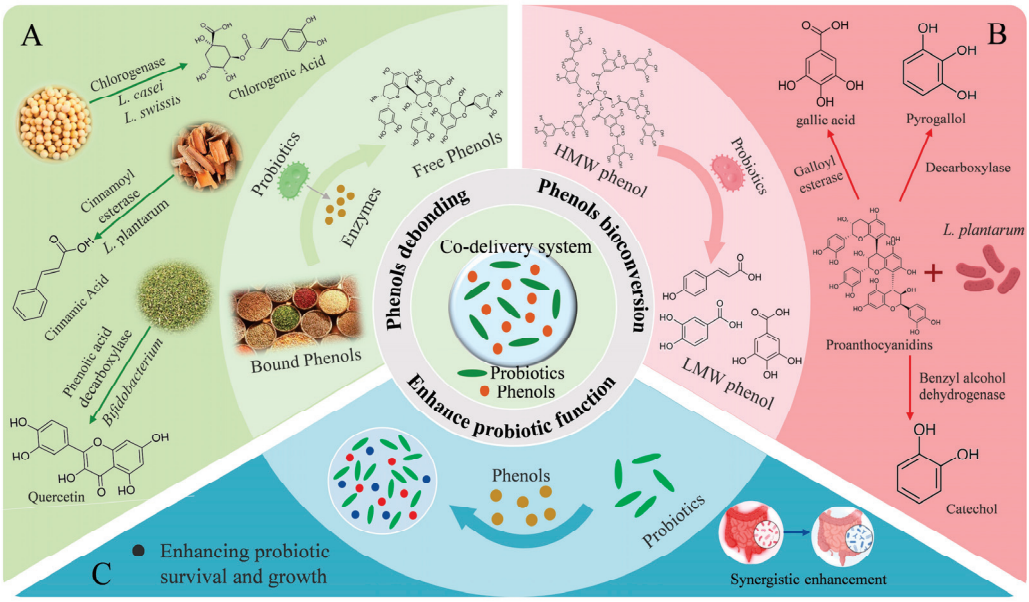


Figure 3. Schematic of the interaction between phenolic compounds and probiotics in co-encapsulation systems. (**A**) Probiotics promote the dissociation of bound phenolics to produce free phenolics. (**B**) Probiotics enhance the biotransformation of phenolic compounds. (**C**) Phenolic compounds promote probiotic growth and have a synergistic effect. *L. casei*: *Lactobacillus casei*; *L. swissis*: *Lactobacillus swissis*; *L. plantarum*: *Lactobacillus plantarum*; HMW phenol: high-molecular-weight phenol; LMW phenol: low-molecular-weight phenol.

6.3.1. Probiotics Promote Phenols Debonding to Enhance Bioactivity

Probiotics can enhance the functional potential of dietary phenols by mediating their enzymatic release from conjugated forms. The rutinose-bound glycosides of flavonols and flavanones are poorly absorbed in the intestine. Notably, *Bifidobacterium* can enzymatically hydrolyze rutin through phenolic acid decarboxylase to release the active aglycone to produce quercetin [134]. In addition, *Lactobacillus acidophilus* and *L. plantarum* produce β-glucosidases that break down flavonoid conjugates, leading to the formation of free phenols. This enzymatic release increases the bioavailability and enhances the health benefits of natural phenols [135,136].

Proanthocyanidins must be released from their food matrix to exert biological effects, a step facilitated by microbial metabolism. Holkema et al. co-encapsulated *Bifidobacterium animalis* with cinnamon extract rich in proanthocyanidins using microencapsulation technology [137]. This approach significantly improved the microbial survival in acidic environments and preserved the antioxidant potential of the phenols. These benefits may result from enzymatic activity of *B. animalis*, which enhances the release and bioavailability of proanthocyanidins in the gut.

Some probiotics can release phenolic compounds from plant cell walls during fermentation. They achieve this by producing specific hydrolytic enzymes such as β-glucosidase, cinnamoyl esterase, phenolic acid decarboxylase, and chlorogenase [138]. As a result, the levels of free phenolic compounds increase. Nelson et al. [38] conducted an experiment using *Lactobacillus casei* and *Lactobacillus swissis* to ferment soybeans. The experiment reached to two outcomes. First, it significantly increased the yield of chlorogenic acid. Second, it enhanced the biological activity of chlorogenic acid. These improvements may be attributed to the enzymatic activity of the probiotics, which promotes the release and bioavailability of phenolic compounds during fermentation [38].

6.3.2. Probiotics Promote Phenols Bioconversion to Enhance Bioactivity

The high molecular weights of phenols limit their gastrointestinal absorption, resulting in poor bioavailability. Probiotics can degrade larger compounds into smaller phenolic acids through specific enzymes, enhancing their absorption and physiological effects. For example, *L. plantarum* exhibits galloyl esterase, decarboxylase, and benzyl alcohol dehydrogenase activities, enabling the stepwise metabolism of grape seed phenols (e.g., proanthocyanidins) into gallic acid, pyrogallol, and catechol [139]. Similarly, *Streptococcus thermophilus* and *L. casei* can convert procyanidins into novel derivatives, including procyanidin isomers, m-coumaric acid, and p-coumaric acid, thereby increasing total antioxidant capacity [35]. Moreover, in a dynamic gastrointestinal simulation, *L. plantarum* facilitated the metabolism of grape phenols, significantly increasing the levels of benzoic acid, gallic acid, syringic acid, and vanillic acid in the transverse and descending colon.

Pereira et al. demonstrated that orange juice enriched with microencapsulated *Bifidobacterium longum* R0175 increased fecal phenolic acids, indicating probiotic-induced transformation of flavanones into bioavailable metabolites (phenolic acids) [140]. Using spray drying, Sharma et al. co-encapsulated *L. casei* with berry phenols, resulting in 72.6% encapsulation efficiency and 63.6% bioaccessibility, driven by probiotic-mediated bioconversion [141].

Zhang et al. [142] constructed a microgel-based delivery platform incorporating a natural phenol–metal framework derived from *Mesona chinensis*. The platform was used to simultaneously deliver phenols and *Akkermansia muciniphila* [142]. The *M. chinensis* polysaccharides stimulated SCFA production, jointly ameliorating acute liver injury via the gut–liver axis. In addition, *A. muciniphila* catalyzed the bioconversion of phenols into bioactive phenolic acids, enhancing antioxidant and anti-inflammatory effects. Notably,

the phenols acted as selective nutrients for *A. muciniphila*, promoting its proliferation. This dual-function microgel achieved targeted delivery of live *A. muciniphila* to the gut and facilitated hepatic accumulation of phenols, restoring intestinal balance and mitigating oxidative hepatic damage.

6.3.3. Phenols Enhance Probiotic Function

Phenols play a critical role in stabilizing probiotics, improving their survival in the gastrointestinal tract, and promoting growth and metabolic function. *L. case* is noted for its antihypertensive, antihyperglycemic effects, and its capacity to improve human lipid metabolism [143]. However, its oral delivery is challenged by susceptibility to gastric acid and bile, limiting intestinal colonization. To solve this problem, phenols are selected for co-encapsulation based on their hydrophobic or hydrophilic properties. Ma et al. reported that co-encapsulating hydrophobic phenols with hydrophilic *L. casei* improved the gastrointestinal tolerance and storage stability of strain, and enables its successful release in the intestine [144]. Gaudreau et al. [145] co-encapsulated *L. paracasei* ssp. paracasei with green tea extract phenols in calcium alginate microspheres, resulting in enhanced probiotic survival, improved encapsulation efficiency, and increased free radical scavenging capacity. A pectin–whey protein complex further augmented the bioactivity of the encapsulated compounds under simulated gastrointestinal conditions [145]. Cruz et al. [146] used spray drying to co-encapsulate blackberry anthocyanins with *L. acidophilus* in gum arabic and sodium alginate. The probiotic survival in gastrointestinal simulations was significantly improved [146]. In another study, tannic acid and engineered *Escherichia coli* Nissle 1917 (EcN) were co-encapsulated using self-polymerizable aromatic disulfides and sodium alginate. Tannic acid improved EcN's resistance to oxidative and inflammatory stress, and the colon-targeted delivery system alleviated DSS-induced colitis in mice by reducing inflammation, repairing the gut barrier, and modulating microbiota composition [147].

In addition to co-encapsulating individual probiotics with phenols for therapy, researchers have explored combining probiotic cross-feeding with phenol co-encapsulation to combat colon cancer. Cross-feeding involves the exchange of metabolic products among microbes to facilitate mutual growth and metabolism. For instance, *Lactobacillus gasseri* converts complex carbohydrates into lactic acid, which *Bifidobacterium bifidum* uses to support its growth. Benito et al. [148] designed a chitosan–alginate microcapsule encapsulating *B. bifidum*, *L. gasseri*, and quercetin. In colon cancer-bearing mice, co-encapsulated *B. bifidum* and *L. gasseri* reduced abnormal crypt foci and adenomas by 45% and 60%, respectively. Adding quercetin further enhanced reductions to 57% and 80%. This demonstrates quercetin's role in significantly boosting the anticancer efficacy of probiotics [148,149].

Table 2. Single and co-encapsulated targeted delivery systems for phenolic compounds.

	Phenols Name	Wall Material	Preparation Method	Intestinal Targeting Performance	Biological Activity	References
Single-encapsulation	Quercetin	Chitosan nanoparticles	Coaxial electro-spinning technique	Colon-targeted release	Significant improvement in bioavailability, enhanced anticancer activity (induction of cell apoptosis and oxidative stress).	[91]
		Whey protein isolate, inulin	High-pressure homogeniza-tion method	Small intestine-targeted release	Enhanced of the water solubility (389 times), increased of the digestibility (8.59%), enhancing both the stability and bioavailability of quercetin.	[94]
	Resveratrol	Shellac resin ammonium salts	Spray drying technology	Small intestine-targeted release	pH-sensitive, controlled and sustained release of resveratrol in simulated intestinal release experiment, excellent stability, enhanced antioxidant activity (higher radical scavenging activity of DPPH and ABTS compared to pure resveratrol).	[150]
		Pectin, chitosan, polyethylene glycol	Layer-by-layer self-assembly technique	Colon-targeted release	Colon-targeted release 49%, improved bioaccessibility.	[74]
	Anthocyanin	Cyclodextrin	Complexation technology	Small intestine-targeted release	Stable in stomach, released in intestine, promoting growth of beneficial bacteria.	[45]
		Sodium alginate, hyaluronic acid, foodborne nanoparticles	Electrostatic self-assembly method	Colon-targeted release	Colon-targeted release 35.9%, pH-responsive, enhanced bioavailability, gut microbiota modulation, anti-inflammatory properties and bioavailability.	[96]

Table 2. *Cont.*

	Phenols Name	Wall Material	Preparation Method	Intestinal Targeting Performance	Biological Activity	References
	Curcumin	Alginate, whey protein isolate, gum arabic	Layer-by-layer self-assembly technique	Small intestine-targeted release	Small intestine-targeted release 84%, improved bioavailability.	[104]
	Epigallocatechin gallate (EGCG)	Chitosan, zein	Antisolvent precipitation method	Colon-targeted release	Higher release efficiency in simulated intestinal fatty environment, the antioxidant activity of EGCG was significantly improved, and the microcapsules with zein had an antioxidant activity four times higher than those without zein.	[151]
	Caffeic acid	Chitosan, sodium alginate	Lonic gelation method	Small intestine-targeted release	Resistant to gastric environment, sustained release in small intestine (up to 180 min).	[56]
	Ferulic acid	Potato protein, pectin	PH-driven self-assembly	Colon-targeted release	Resistant to gastric environment, sustained release in intestine, antioxidant activity.	[150]
Co-encapsulation	Curcumin and EGCG	Zein, caseinate	Antisolvent method	Small intestine-targeted release	EGCG enhanced the dispersibility, encapsulation properties, and antioxidant activity of curcumin, enhanced the stability and bioaccessibility (87.3 ± 2.8%).	[23]
	Phenols (quercetin/rutin/curcumin/tea polyphenols) and *Lactobacillus casei*	Zein, chitosan	Complex coacervation	Colon-targeted release	Resistant to gastric environment, sustained release in intestine, antioxidant activity, improved bioavailability, and quercetin group probiotic activity significantly increased (1.03×10^{10} CFU).	[144]
	Gallic acid and *Lactobacillus*	Pectin, sodium alginate, fu brick tea polysaccharide	Layer-by-layer complex coacervation	Colon-targeted release	Alleviating colitis, improved probiotic survival rate (1×10^{9} CFU).	[90]

Table 2. *Cont.*

Phenols Name	Wall Material	Preparation Method	Intestinal Targeting Performance	Biological Activity	References
Anthocyanins and β-carotene	Chitosan, oxidized konjac glucomannan	Electrostatic adsorption method	Small intestine-targeted release	Improved synergistic antioxidant activity (enhanced thermal stability); reduced various cancers, infectious diseases, obesity, cardiovascular diseases.	[122]
Proanthocyanidins and *Bifidobacterium animalis*	Chitosan, alginate	Complex coacervation	Colon-targeted release	Enhanced anticancer activity (reduced aberrant crypt foci in mice by 57%).	[137,152]
Chlorogenic acid and lutein	Bovine serum albumin, dextran	Complex coacervation-freeze-drying technology	Small intestine-targeted release	Resisted gastric acid and pepsin, lutein bioaccessibility significantly improved (62.3%).	[126]
Coumaric acid and arbutin	Gelatin, polyglyceryl polyricinoleate, sodium chloride	Drop-wise dispersion	Colon-targeted release	Controlled release of arbutin and coumaric acid, improved bioaccessibility.	[153]
Chlorogenic acid and anthocyanins	Maltodextrin or maltodextrin, carboxymethyl cellulose, gum arabic or xanthan gum	Spray drying technology	Colon-targeted release	Higher retention of anthocyanins in encapsulated wild cherry powder (75%). Encapsulation reduced molecular transformation of anthocyanins and chlorogenic acid during in vitro digestion.	[154]

7. Conclusions and Future Perspectives

This review evaluates the influence of gastrointestinal physiological conditions on phenol delivery and introduces suitable wall materials for site-specific release. To achieve targeted release of phenols in the digestive tract, factors such as pH, digestive enzymes, and gut microbiota should be fully considered in delivery system designing. Materials such as chitosan, sodium alginate, and pectin have demonstrated potential in optimizing delivery performance under these varying conditions. Simultaneously, the choice of wall material also should be based on the water solubility of phenolic compounds. Phenolic compounds with good water solubility are suitable for hydrogels and microemulsions, while water-insoluble ones are more appropriate for nanoemulsions and liposomes. Co-encapsulation of phenols with carotenoids or probiotics improves their stability, bioactivity, and synergistic effects. These multi-component delivery platforms not only protect labile compounds from degradation but also improve bioaccessibility through complementary physicochemical properties and probiotic-mediated biotransformations. The integration of probiotics promotes phenol debonding and bioconversion, enhancing phenolic bioavailability, while phenols support probiotic survival and functionality in the harsh gastrointestinal environment. Such reciprocal interactions highlight the potential of co-delivery systems for targeted treatment of intestinal inflammation, oxidative stress, and related chronic diseases.

Moving forward, the development of advanced in vitro and simulated gastrointestinal models that more accurately mimic human physiological and microbial conditions remains essential. Moreover, optimizing the core-to-wall material ratio and clarifying its effect on the release behavior and sustained delivery of phenolic compounds require further systematic investigation. Notably, there is a significant lack of clinical trials addressing the release profiles and therapeutic efficacy of these microencapsulation systems in humans, especially considering inter-individual differences in digestion and metabolism. Future research should focus on designing multifunctional delivery platforms that integrate targeted release, protective encapsulation, and bioresponsive properties to bridge the gap between in vitro and in vivo results. In terms of applications, these delivery systems hold promise as plant-based dietary supplements in tablet or beverage forms aimed at alleviating conditions such as colitis and hepatitis. Such advancements are critical to fully realizing the preventive and therapeutic potential of phenolic compounds in managing chronic diseases.

Author Contributions: Y.T.: writing—original draft, writing—review and editing, conceptualization; W.L.: visualization, review and editing; J.Z.: conceptualization; B.J.: editing, supervision; Y.Z. (Ying Zhu): software, visualization; L.Z.: supervision; Y.Z. (Yansheng Zhao): supervision, visualization; M.D.: writing—review and editing; X.X.: writing—review and editing, conceptualization, supervision, funding acquisition; Y.H.: writing—review and editing, conceptualization, supervision, funding acquisition. All authors have read and agreed to the published version of the manuscript.

Funding: This work is supported by the National Natural Science Foundation of China (32302047), National Natural Science Foundation of China (32072200), the China Postdoctoral Science Foundation (2023M731378), Key Research & Development Plan of Jiangsu Province (BE2022353), Zhenjiang Science and Technology Plan Project Application (GJ2024011), Zhenjiang Science and Technology Plan Project Application (GJ2024011), Zhenjiang Innovation Capacity Construction Plan-Construction of Discipline Key Laboratories (SS2024005), and the Priority Academic Program Development of Jiangsu Higher Education Institutions (PAPD).

Conflicts of Interest: The authors declare no conflicts of interest.

References

1. Ali, Z.; Ma, H.; Rashid, M.T.; Ayim, I.; Wali, A. Reduction of Body Weight, Body Fat Mass, and Serum Leptin Levels by Addition of New Beverage in Normal Diet of Obese Subjects. *J. Food Biochem.* **2018**, *42*, e12554. [CrossRef]
2. Guo, L.; Guo, Y.; Ping, W.; Feng, L.; Zhu, J.; Ma, H.; Chen, Y.; Zhang, T. Camellia Oil Lowering Blood Pressure in Spontaneously Hypertension Rats. *J. Funct. Foods* **2020**, *70*, 103915. [CrossRef]
3. Wang, M.; Chen, M.; Guo, R.; Ding, Y.; Zhang, H.; He, Y. The Improvement of Sulforaphane in Type 2 Diabetes Mellitus (T2DM) and Related Complications: A Review. *Trends Food Sci. Technol.* **2022**, *129*, 397–407. [CrossRef]
4. Gao, R.; Qi, Z.; Lin, J.; Wang, G.; Chen, G.; Yuan, L.; Sun, Q. Chondroitin Sulfate Alleviated Obesity by Modulating Gut Microbiota and Liver Metabolome in High-Fat-Diet-Induced Obese Mice. *J. Agric. Food Chem.* **2023**, *71*, 9419–9428. [CrossRef]
5. Zhang, J.; Wen, C.; Zhang, H.; Duan, Y.; Ma, H. Recent Advances in the Extraction of Bioactive Compounds with Subcritical Water: A Review. *Trends Food Sci. Technol.* **2020**, *95*, 183–195. [CrossRef]
6. Cianciosi, D.; Forbes-Hernández, T.Y.; Regolo, L.; Alvarez-Suarez, J.M.; Navarro-Hortal, M.D.; Xiao, J.; Quiles, J.L.; Battino, M.; Giampieri, F. The Reciprocal Interaction between Polyphenols and Other Dietary Compounds: Impact on Bioavailability, Antioxidant Capacity and Other Physico-Chemical and Nutritional Parameters. *Food Chem.* **2022**, *375*, 131904. [CrossRef]
7. Wang, D.; Wang, T.; Zhang, Z.; Li, Z.; Guo, Y.; Zhao, G.; Wu, L. Recent Advances in the Effects of Dietary Polyphenols on Inflammation in Vivo: Potential Molecular Mechanisms, Receptor Targets, Safety Issues, and Uses of Nanodelivery System and Polyphenol Polymers. *Curr. Opin. Food Sci.* **2022**, *48*, 100921. [CrossRef]
8. Lyu, X.; Wang, X.; Wang, Q.; Ma, X.; Chen, S.; Xiao, J. Encapsulation of Sea Buckthorn (*Hippophae rhamnoides* L.) Leaf Extract via an Electrohydrodynamic Method. *Food Chem.* **2021**, *365*, 130481. [CrossRef]
9. Wang, T.; Xu, H.; Dong, R.; Wu, S.; Guo, Y.; Wang, D. Effectiveness of Targeting the NLRP3 Inflammasome by Using Natural Polyphenols: A Systematic Review of Implications on Health Effects. *Food Res. Int.* **2023**, *165*, 112567. [CrossRef]
10. Xie, F.; Yang, W.; Xing, M.; Zhang, H.; Ai, L. Natural Polyphenols-Gut Microbiota Interactions and Effects on Glycolipid Metabolism via Polyphenols-Gut-Brain Axis: A State-of-the-Art Review. *Trends Food Sci. Technol.* **2023**, *140*, 104171. [CrossRef]
11. Jiang, Q.; Charoensiddhi, S.; Xue, X.; Sun, B.; Liu, Y.; El-Seedi Hesham, R.; Wang, K. A Review on the Gastrointestinal Protective Effects of Tropical Fruit Polyphenols. *Crit. Rev. Food Sci. Nutr.* **2023**, *63*, 7197–7223. [CrossRef]
12. Suo, H.; Shishir, M.R.I.; Xiao, J.; Wang, M.; Chen, F.; Cheng, K.-W. Red Wine High-Molecular-Weight Polyphenolic Complex: An Emerging Modulator of Human Metabolic Disease Risk and Gut Microbiota. *J. Agric. Food Chem.* **2021**, *69*, 10907–10919. [CrossRef]
13. Lei, L.; Tang, Y.; Zheng, J.; Ma, G.; Zhou, Z. Influence of Two Polyphenols on the Structure and Lubrication of Salivary Pellicle: An in Vitro Study on Astringency Mechanism. *Friction* **2022**, *10*, 167–178. [CrossRef]
14. Sahraeian, S.; Rashidinejad, A.; Golmakani, M.-T. Recent Advances in the Conjugation Approaches for Enhancing the Bioavailability of Polyphenols. *Food Hydrocoll.* **2024**, *146*, 109221. [CrossRef]
15. Wang, J.; Li, H.; Chen, Z.; Liu, W.; Chen, H. Characterization and Storage Properties of a New Microencapsulation of Tea Polyphenols. *Ind. Crops Prod.* **2016**, *89*, 152–156. [CrossRef]
16. Tang, H.-Y.; Fang, Z.; Ng, K. Dietary Fiber-Based Colon-Targeted Delivery Systems for Polyphenols. *Trends Food Sci. Technol.* **2020**, *100*, 333–348. [CrossRef]
17. Misra, S.; Pandey, P.; Mishra, H.N. Novel Approaches for Co-Encapsulation of Probiotic Bacteria with Bioactive Compounds, Their Health Benefits and Functional Food Product Development: A Review. *Trends Food Sci. Technol.* **2021**, *109*, 340–351. [CrossRef]
18. Yang, X.; Yang, Y.; Yu, H.; Zhou, Y. Self-Assembled Polymers for Gastrointestinal Tract Targeted Delivery through the Oral Route: An Update. *Polymers* **2023**, *15*, 3538. [CrossRef]
19. Dehkordi, S.S.; Alemzadeh, I.; Vaziri, A.S.; Vossoughi, A. Optimization of Alginate-Whey Protein Isolate Microcapsules for Survivability and Release Behavior of Probiotic Bacteria. *Appl. Biochem. Biotechnol.* **2020**, *190*, 182–196. [CrossRef]
20. Chu, J.N.; Traverso, G. Foundations of Gastrointestinal-Based Drug Delivery and Future Developments. *Nat. Rev. Gastroenterol. Hepatol.* **2022**, *19*, 219–238. [CrossRef]
21. Chen, S.; Han, Y.; Huang, J.; Dai, L.; Du, J.; McClements, D.J.; Mao, L.; Liu, J.; Gao, Y. Fabrication and Characterization of Layer-by-Layer Composite Nanoparticles Based on Zein and Hyaluronic Acid for Codelivery of Curcumin and Quercetagetin. *ACS Appl. Mater. Interfaces* **2019**, *11*, 16922–16933. [CrossRef]
22. Chen, S.; McClements, D.J.; Jian, L.; Han, Y.; Dai, L.; Mao, L.; Gao, Y. Core–Shell Biopolymer Nanoparticles for Co-Delivery of Curcumin and Piperine: Sequential Electrostatic Deposition of Hyaluronic Acid and Chitosan Shells on the Zein Core. *ACS Appl. Mater. Interfaces* **2019**, *11*, 38103–38115. [CrossRef]
23. Yan, X.; Zhang, X.; McClements, D.J.; Zou, L.; Liu, X.; Liu, F. Co-Encapsulation of Epigallocatechin Gallate (EGCG) and Curcumin by Two Proteins-Based Nanoparticles: Role of EGCG. *J. Agric. Food Chem.* **2019**, *67*, 13228–13236. [CrossRef] [PubMed]
24. Zare, R.; Nadjarzadeh, A.; Zarshenas, M.M.; Shams, M.; Heydari, M. Efficacy of Cinnamon in Patients with Type II Diabetes Mellitus: A Randomized Controlled Clinical Trial. *Clin. Nutr.* **2019**, *38*, 549–556. [CrossRef] [PubMed]

25. Zhu, S.; Shao, F.; Obadi, M.; Li, H.; Qi, Y.; Xu, B. Enhancing in Vitro Starch Digestion of Tartary Buckwheat: Unveiling the Vital Role of Endogenous Polyphenols in Starch Fine Structure. *J. Cereal Sci.* **2024**, *116*, 103870. [CrossRef]
26. Wang, D.; Gao, Q.; Wang, T.; Kan, Z.; Li, X.; Hu, L.; Peng, C.-Y.; Qian, F.; Wang, Y.; Granato, D. Green Tea Polyphenols and Epigallocatechin-3-Gallate Protect against Perfluorodecanoic Acid Induced Liver Damage and Inflammation in Mice by Inhibiting NLRP3 Inflammasome Activation. *Food Res. Int.* **2020**, *127*, 108628. [CrossRef]
27. Patil, P.; Killedar, S. Chitosan and Glyceryl Monooleate Nanostructures Containing Gallic Acid Isolated from Amla Fruit: Targeted Delivery System. *Heliyon* **2021**, *7*, e06526. [CrossRef]
28. Keyvani-Ghamsari, S.; Rahimi, M.; Khorsandi, K. An Update on the Potential Mechanism of Gallic Acid as an Antibacterial and Anticancer Agent. *Food Sci. Nutr.* **2023**, *11*, 5856–5872. [CrossRef]
29. Ren, X.; Hou, T.; Liang, Q.; Zhang, X.; Hu, D.; Xu, B.; Chen, X.; Chalamaiah, M.; Ma, H. Effects of Frequency Ultrasound on the Properties of Zein-Chitosan Complex Coacervation for Resveratrol Encapsulation. *Food Chem.* **2019**, *279*, 223–230. [CrossRef]
30. Gu, T.; Wang, N.; Wu, T.; Ge, Q.; Chen, L. Antioxidative Stress Mechanisms behind Resveratrol: A Multidimensional Analysis. *J. Food Qual.* **2021**, *2021*, 5571733. [CrossRef]
31. Zduńska, K.; Dana, A.; Kolodziejczak, A.; Rotsztejn, H. Antioxidant Properties of Ferulic Acid and Its Possible Application. *Skin Pharmacol. Physiol.* **2018**, *31*, 332–336. [CrossRef]
32. Yu, Y.-B.; Cai, W.-D.; Wang, Z.-W.; Yan, J.-K. Emulsifying Properties of a Ferulic Acid-Grafted Curdlan Conjugate and Its Contribution to the Chemical Stability of β-Carotene. *Food Chem.* **2021**, *339*, 128053. [CrossRef]
33. Wang, C.; Cai, W.-D.; Yao, J.; Wu, L.-X.; Li, L.; Zhu, J.; Yan, J.-K. Conjugation of Ferulic Acid onto Pectin Affected the Physico-chemical, Functional and Antioxidant Properties. *J. Sci. Food Agric.* **2020**, *100*, 5352–5362. [CrossRef] [PubMed]
34. Daryagasht, M.; Moosavi, M.; Khorsandi, L.; Azadnasab, R.; Khodayar, M.J. Hepatoprotective and Anti-Hyperglycemic Effects of Ferulic Acid in Arsenic-Exposed Mice. *Food Chem. Toxicol.* **2023**, *178*, 113924. [CrossRef] [PubMed]
35. Li, S.; Chen, L.; Yang, T.; Wu, Q.; Lv, Z.; Xie, B.; Sun, Z. Increasing Antioxidant Activity of Procyanidin Extracts from the Pericarp of Litchi Chinensis Processing Waste by Two Probiotic Bacteria Bioconversions. *J. Agric. Food Chem.* **2013**, *61*, 2506–2512. [CrossRef] [PubMed]
36. Cong, J.; Cui, J.; Zhang, H.; Dzah, C.S.; He, Y.; Duan, Y. Binding Affinity, Antioxidative Capacity and in Vitro Digestion of Complexes of Grape Seed Procyanidins and Pork, Chicken and Fish Protein. *Food Res. Int.* **2020**, *136*, 109530. [CrossRef]
37. Aree, T. Atomic-Level Understanding on Conformational Flexibility of Neochlorogenic and Chlorogenic Acids and Their Inclusion Complexation with β-Cyclodextrin. *Food Hydrocoll.* **2023**, *141*, 108742. [CrossRef]
38. Akpabli-Tsigbe, N.D.K.; Osabutey, J.; Mintah, B.K.; Tano-Debrah, K.; Ma, Y. Cleavage of Macromolecule (Protein/Polysaccharide)-Phenolic Bond in Soybean Cell Wall through Lactobacillus Casei and Lactobacillus Helviticus Mixed Culture Solid-State Fermentation for Chlorogenic Acid Extraction. *Food Biosci.* **2023**, *55*, 102903. [CrossRef]
39. Pragasam, S.J.; Venkatesan, V.; Rasool, M. Immunomodulatory and Anti-Inflammatory Effect of p-Coumaric Acid, a Common Dietary Polyphenol on Experimental Inflammation in Rats. *Inflammation* **2012**, *36*, 169–176. [CrossRef]
40. Yeh, Y.-H.; Lee, Y.-T.; Hsieh, H.-S.; Hwang, D.-F. Dietary Caffeic Acid, Ferulic Acid and Coumaric Acid Supplements on Cholesterol Metabolism and Antioxidant Activity in Rats. *J. Food Drug Anal.* **2020**, *17*, 4. [CrossRef]
41. Aditya, N.P.; Aditya, S.; Yang, H.-J.; Kim, H.W.; Park, S.O.; Lee, J.; Ko, S. Curcumin and Catechin Co-Loaded Water-in-Oil-in-Water Emulsion and Its Beverage Application. *J. Funct. Foods* **2015**, *15*, 35–43. [CrossRef]
42. Yixuan, L.; Qaria, M.A.; Sivasamy, S.; Jianzhong, S.; Daochen, Z. Curcumin Production and Bioavailability: A Comprehensive Review of Curcumin Extraction, Synthesis, Biotransformation and Delivery Systems. *Ind. Crops Prod.* **2021**, *172*, 114050. [CrossRef]
43. Araiza-Calahorra, A.; Wang, Y.; Boesch, C.; Zhao, Y.; Sarkar, A. Pickering Emulsions Stabilized by Colloidal Gel Particles Complexed or Conjugated with Biopolymers to Enhance Bioaccessibility and Cellular Uptake of Curcumin. *Curr. Res. Food Sci.* **2020**, *3*, 178–188. [CrossRef] [PubMed]
44. Zhao, Y.; Jiang, C.; Lu, J.; Sun, Y.; Cui, Y. Research Progress of Proanthocyanidins and Anthocyanidins. *Phytother. Res.* **2023**, *37*, 2552–2577. [CrossRef]
45. Flores, G.; del Castillo, M.L.R.; Costabile, A.; Klee, A.; Guergoletto, K.B.; Gibson, G.R. In Vitro Fermentation of Anthocyanins Encapsulated with Cyclodextrins: Release, Metabolism and Influence on Gut Microbiota Growth. *J. Funct. Foods* **2015**, *16*, 50–57. [CrossRef]
46. Wang, H.; Li, Z.; Meng, Y.; Lv, G.; Wang, J.; Zhang, D.; Shi, J.; Zhai, X.; Meng, X.; Zou, X. Co-Delivery Mechanism of Curcumin/Catechin Complex by Modified Soy Protein Isolate: Emphasizing Structure, Functionality, and Intermolecular Interaction. *Food Hydrocoll.* **2024**, *152*, 109958. [CrossRef]
47. Ruengdech, A.; Mishra, D.K.; Siripatrawan, U. Multifaceted Roles of Foam-Mat Freeze-Dried Catechins Nanoencapsulation to Enhance Catechins Stability and Bioaccessibility, and Quality of Green Tea Catechins-Fortified Milk. *Food Chem. X* **2025**, *27*, 102391. [CrossRef]
48. Evans, D.F.; Pye, G.; Bramley, R.; Clark, A.G.; Dyson, T.J.; Hardcastle, J.D. Measurement of Gastrointestinal pH Profiles in Normal Ambulant Human Subjects. *Gut* **1988**, *29*, 1035–1041. [CrossRef]

49. Roy, B.C.; Das, C.; Hong, H.; Betti, M.; Bruce, H.L. Extraction and Characterization of Gelatin from Bovine Heart. *Food Biosci.* **2017**, *20*, 116–124. [CrossRef]
50. Do, U.T.; Kim, J.; Luu, Q.S.; Nguyen, Q.T.; Jang, T.; Park, Y.; Shin, H.; Whiting, N.; Kang, D.-K.; Kwon, J.-S.; et al. Accurate Detection of Enzymatic Degradation Processes of Gelatin–Alginate Microcapsule by 1H NMR Spectroscopy: Probing Biodegradation Mechanism and Kinetics. *Carbohydr. Polym.* **2023**, *304*, 120490. [CrossRef]
51. Gibson, G.R.; Roberfroid, M.B. Dietary Modulation of the Human Colonic Microbiota: Introducing the Concept of Prebiotics. *J. Nutr.* **1995**, *125*, 1401–1412. [CrossRef]
52. Santucci, N.R.; Velez, A. Physiology of Lower Gastrointestinal Tract. *Aliment. Pharmacol. Ther.* **2024**, *60*, S1–S19. [CrossRef]
53. Gromova, L.V.; Polozov, A.S.; Savochkina, E.V.; Alekseeva, A.S.; Dmitrieva, Y.V.; Kornyushin, O.V.; Gruzdkov, A.A. Effect of Type 2 Diabetes and Impaired Glucose Tolerance on Digestive Enzymes and Glucose Absorption in the Small Intestine of Young Rats. *Nutrients* **2022**, *14*, 385. [CrossRef]
54. Luan, Q.; Zhang, H.; Chen, C.; Jiang, F.; Yao, Y.; Deng, Q.; Zeng, K.; Tang, H.; Huang, F. Controlled Nutrient Delivery through a pH-Responsive Wood Vehicle. *ACS Nano* **2022**, *16*, 2198–2208. [CrossRef]
55. Serra, D.; Almeida, L.M.; Dinis, T.C.P. Dietary Polyphenols: A Novel Strategy to Modulate Microbiota-Gut-Brain Axis. *Trends Food Sci. Technol.* **2018**, *78*, 224–233. [CrossRef]
56. Amidon, S.; Brown, J.E.; Dave, V.S. Colon-Targeted Oral Drug Delivery Systems: Design Trends and Approaches. *AAPS PharmSciTech* **2015**, *16*, 731–741. [CrossRef] [PubMed]
57. Sousa, T.; Paterson, R.; Moore, V.; Carlsson, A.; Abrahamsson, B.; Basit, A.W. The Gastrointestinal Microbiota as a Site for the Biotransformation of Drugs. *Int. J. Pharm.* **2008**, *363*, 1–25. [CrossRef] [PubMed]
58. Rhee, S.H.; Pothoulakis, C.; Mayer, E.A. Principles and Clinical Implications of the Brain–Gut–Enteric Microbiota Axis. *Nat. Rev. Gastroenterol. Hepatol.* **2009**, *6*, 306–314. [CrossRef]
59. Backhed, F. Host-Bacterial Mutualism in the Human Intestine. *Science* **2005**, *307*, 1915–1920. [CrossRef]
60. Philip, A.; Philip, B. Colon Targeted Drug Delivery Systems: A Review on Primary and Novel Approaches. *Oman Med. J.* **2010**, *25*, 70–78. [CrossRef]
61. Lin, L.; Gu, Y.; Cui, H. Moringa Oil/Chitosan Nanoparticles Embedded Gelatin Nanofibers for Food Packaging against Listeria Monocytogenes and Staphylococcus Aureus on Cheese. *Food Packag. Shelf Life* **2019**, *19*, 86–93. [CrossRef]
62. Zhang, C.; Long, Y.; Li, J.; Li, M.; Xing, D.; An, H.; Wu, X.; Wu, Y. A Chitosan Composite Film Sprayed before Pathogen Infection Effectively Controls Postharvest Soft Rot in Kiwifruit. *Agronomy* **2020**, *10*, 265. [CrossRef]
63. Edo, G.I.; Yousif, E.; Al-Mashhadani, M.H. Chitosan: An Overview of Biological Activities, Derivatives, Properties, and Current Advancements in Biomedical Applications. *Carbohydr. Res.* **2024**, *542*, 109199. [CrossRef] [PubMed]
64. Cui, H.; Bai, M.; Rashed, M.M.A.; Lin, L. The Antibacterial Activity of Clove Oil/Chitosan Nanoparticles Embedded Gelatin Nanofibers against Escherichia Coli O157:H7 Biofilms on Cucumber. *Int. J. Food Microbiol.* **2018**, *266*, 69–78. [CrossRef] [PubMed]
65. Hassan, I.; Gani, A. Alginate-Based pH-Sensitive Hydrogels Encoated with Chitosan as a Bioactive Cargo Carrier with Caffeic Acid as a Model Biomolecule. *ACS Food Sci. Technol.* **2022**, *2*, 667–672. [CrossRef]
66. Yang, Z.; Li, M.; Li, Y.; Huang, X.; Li, Z.; Zhai, X.; Shi, J.; Zou, X.; Xiao, J.; Sun, Y.; et al. Sodium Alginate/Guar Gum Based Nanocomposite Film Incorporating β-Cyclodextrin/Persimmon Pectin-Stabilized Baobab Seed Oil Pickering Emulsion for Mushroom Preservation. *Food Chem.* **2024**, *437*, 137891. [CrossRef]
67. Surendhiran, D.; Cui, H.; Lin, L. Encapsulation of Phlorotannin in Alginate/PEO Blended Nanofibers to Preserve Chicken Meat from Salmonella Contaminations. *Food Packag. Shelf Life* **2019**, *21*, 100346. [CrossRef]
68. Jadach, B.; Świetlik, W.; Froelich, A. Sodium Alginate as a Pharmaceutical Excipient: Novel Applications of a Well-Known Polymer. *J. Pharm. Sci.* **2022**, *111*, 1250–1261. [CrossRef]
69. Sanchez-Ballester, N.M.; Bataille, B.; Soulairol, I. Sodium Alginate and Alginic Acid as Pharmaceutical Excipients for Tablet Formulation: Structure-Function Relationship. *Carbohydr. Polym.* **2021**, *270*, 118399. [CrossRef]
70. Zhao, B.; Alonso, N.F.; Miras, J.; Vílchez, S.; García-Celma, M.J.; Morral, G.; Esquena, J. Triggered Protein Release from Calcium Alginate/Chitosan Gastro-Resistant Capsules. *Colloids Surf. Physicochem. Eng. Asp.* **2024**, *693*, 133998. [CrossRef]
71. Zhang, L.; Tang, P.; Li, S.; Wang, X.; Zong, W. Sodium Alginate-Based Wall Materials Microencapsulated Lactobacillus Plantarum CICC 20022: Characteristics and Survivability Study. *Food Sci. Biotechnol.* **2022**, *31*, 1463–1472. [CrossRef]
72. González, E.; Gómez-Caravaca, A.M.; Giménez, B.; Cebrián, R.; Maqueda, M.; Martínez-Férez, A.; Segura-Carretero, A.; Robert, P. Evolution of the Phenolic Compounds Profile of Olive Leaf Extract Encapsulated by Spray-Drying during in Vitro Gastrointestinal Digestion. *Food Chem.* **2019**, *279*, 40–48. [CrossRef]
73. Wang, L.; Wu, P.; Hu, Z.; Chen, Y.; Jin, X.; Deng, R.; Kirk, T.V.; Chen, X.D. Curcumin-Loaded Microcapsules with Soy and Whey Protein as Wall Material: In Vitro Release, and Ex Vivo Absorption Based on the Rat Small Intestine. *J. Food Eng.* **2024**, *383*, 112254. [CrossRef]
74. Zhao, Y.; Jiang, Q. Roles of the Polyphenol–Gut Microbiota Interaction in Alleviating Colitis and Preventing Colitis-Associated Colorectal Cancer. *Adv. Nutr.* **2021**, *12*, 546–565. [CrossRef] [PubMed]

75. Zhao, Y.; Nakatsu, C.; Jones-Hall, Y.; Jiang, Q. Supplementation of Polyphenol-Rich Grapes Attenuates Colitis, Colitis-Associated Colon Cancer, and Disease-Associated Dysbiosis in Mice, but Fails to Mitigate Colitis in Antibiotic-Treated Mice. *J. Nutr. Biochem.* **2022**, *109*, 109124. [CrossRef] [PubMed]
76. Cheng, B.; Feng, H.; Li, C.; Jia, F.; Zhang, X. The Mutual Effect of Dietary Fiber and Polyphenol on Gut Microbiota: Implications for the Metabolic and Microbial Modulation and Associated Health Benefits. *Carbohydr. Polym.* **2025**, *358*, 123541. [CrossRef]
77. Wang, Y.; Li, J.; Li, B. Chitin Microspheres: A Fascinating Material with High Loading Capacity of Anthocyanins for Colon Specific Delivery. *Food Hydrocoll.* **2017**, *63*, 293–300. [CrossRef]
78. Hurtado, N.H.; Morales, A.L.; González-Miret, M.L.; Escudero-Gilete, M.L.; Heredia, F.J. Colour, pH Stability and Antioxidant Activity of Anthocyanin Rutinosides Isolated from Tamarillo Fruit (*Solanum betaceum* Cav.). *Food Chem.* **2009**, *117*, 88–93. [CrossRef]
79. Yan, J.-K.; Qiu, W.-Y.; Wang, Y.-Y.; Wu, J.-Y. Biocompatible Polyelectrolyte Complex Nanoparticles from Lactoferrin and Pectin as Potential Vehicles for Antioxidative Curcumin. *J. Agric. Food Chem.* **2017**, *65*, 5720–5730. [CrossRef]
80. Wu, L.-X.; Qiao, Z.-R.; Cai, W.-D.; Qiu, W.-Y.; Yan, J.-K. Quaternized Curdlan/Pectin Polyelectrolyte Complexes as Biocompatible Nanovehicles for Curcumin. *Food Chem.* **2019**, *291*, 180–186. [CrossRef]
81. Dongowski, G.; Lorenz, A.; Anger, H. Degradation of Pectins with Different Degrees of Esterification by Bacteroides Thetaiotaomicron Isolated from Human Gut Flora. *Appl. Environ. Microbiol.* **2000**, *66*, 1321–1327. [CrossRef] [PubMed]
82. Andishmand, H.; Tabibiazar, M.; Mohammadifar, M.A.; Hamishehkar, H. Pectin-Zinc-Chitosan-Polyethylene Glycol Colloidal Nano-Suspension as a Food Grade Carrier for Colon Targeted Delivery of Resveratrol. *Int. J. Biol. Macromol.* **2017**, *97*, 16–22. [CrossRef] [PubMed]
83. Yang, Z.; Li, M.; Li, Z.; Li, Y.; Shi, J.; Huang, X.; Sun, Y.; Zhai, X.; Zou, X.; Xiao, J. Incorporation of Hawthorn Pectin/β-Cyclodextrin-Stabilized Pickering Emulsion and Titanium Dioxide Nanoparticles for Improving the Physical, Biological, and Release Properties of Guar Gum/Agar/Sodium Alginate-Based Bilayer Films. *Ind. Crops Prod.* **2024**, *212*, 118302. [CrossRef]
84. Iftikhar, A.; Rehman, A.; Usman, M.; Ali, A.; Ahmad, M.M.; Shehzad, Q.; Fatim, H.; Mehmood, A.; Moiz, A.; Shabbir, M.A.; et al. Influence of Guar Gum and Chitosan Enriched with Lemon Peel Essential Oil Coatings on the Quality of Pears. *Food Sci. Nutr.* **2022**, *10*, 2443–2454. [CrossRef]
85. Singhal, A.; Jain, H.; Singhal, V.; Elias, E.J.; Showkat, A. Colon-Targeted Quercetin Delivery Using Natural Polymer to Enhance Its Bioavailability. *Pharmacogn. Res.* **2011**, *3*, 35. [CrossRef]
86. Ashames, A.; Ullah, K.; Al-Tabakha, M.; Khan, S.A.; Hassan, N.; Mannan, A.; Ikram, M.; Buabeid, M.; Murtaza, G. Development, Characterization and In-Vitro Evaluation of Guar Gum Based New Polymeric Matrices for Controlled Delivery Using Metformin HCl as Model Drug. *PLoS ONE* **2022**, *17*, e0271623. [CrossRef]
87. Chandel, D.; Uppal, S.; Mehta, S.K.; Shukla, G. Preparation and Characterization of Celecoxib Entrapped Guar Gum Nanoparticles Targeted for Oral Drug Delivery against Colon Cancer: An In-Vitro Study. *J. Drug Deliv. Ther.* **2020**, *10*, 14–21. [CrossRef]
88. Chourasia, M.K.; Jain, S.K. Design and Development of Multiparticulate System for Targeted Drug Delivery to Colon. *Drug Deliv.* **2004**, *11*, 201–207. [CrossRef]
89. Kumar, V.S.; Rijo, J.; Sabitha, M. Guargum and Eudragit ® Coated Curcumin Liquid Solid Tablets for Colon Specific Drug Delivery. *Int. J. Biol. Macromol.* **2018**, *110*, 318–327. [CrossRef]
90. Sun, R.; Lv, Z.; Wang, Y.; Li, M.; Qi, J.; Wang, K.; Yang, H.; Yue, T.; Yuan, Y. Different Polysaccharide-Enhanced Probiotic and Polyphenol Dual-Functional Factor Co-Encapsulated Microcapsules Demonstrate Acute Colitis Alleviation Efficacy and Food Fortification. *Carbohydr. Polym.* **2024**, *345*, 122572. [CrossRef]
91. Wen, P.; Hu, T.-G.; Li, L.; Zong, M.-H.; Wu, H. A Colon-Specific Delivery System for Quercetin with Enhanced Cancer Prevention Based on Co-Axial Electrospinning. *Food Funct.* **2018**, *9*, 5999–6009. [CrossRef]
92. Wang, T.; Xu, H.; Wu, S.; Guo, Y.; Zhao, G.; Wang, D. Mechanisms Underlying the Effects of the Green Tea Polyphenol EGCG in Sarcopenia Prevention and Management. *J. Agric. Food Chem.* **2023**, *71*, 9609–9627. [CrossRef] [PubMed]
93. Tian, X.-Y.; Aheto, J.H.; Bai, J.-W.; Dai, C.; Ren, Y.; Chang, X. Quantitative Analysis and Visualization of Moisture and Anthocyanins Content in Purple Sweet Potato by Vis–NIR Hyperspectral Imaging. *J. Food Process. Preserv.* **2020**, *45*, e15128. [CrossRef]
94. Ding, J.; Liang, T.; Min, Q.; Jiang, L.; Zhu, J.-J. "Stealth and Fully-Laden" Drug Carriers: Self-Assembled Nanogels Encapsulated with Epigallocatechin Gallate and siRNA for Drug-Resistant Breast Cancer Therapy. *ACS Appl. Mater. Interfaces* **2018**, *10*, 9938–9948. [CrossRef] [PubMed]
95. Harlen, W.C.; Prakash, S.; Yuliani, S.; Bhandari, B. Encapsulation of Gallic Acid in Alginate/Lactoferrin Composite Hydrogels: Physical Properties and Gallic Acid Diffusion. *Food Hydrocoll.* **2025**, *160*, 110784. [CrossRef]
96. Zhao, X.; Su, W.; Zhang, X.; Tan, M. Visual Foodborne Nanoparticles for Oral Site-Specific Delivery of Anthocyanins in the Treatment of Inflammatory Bowel Disease. *Mater. Today Nano* **2023**, *24*, 100431. [CrossRef]
97. Liu, L.; Zhang, J.; Zou, X.; Arslan, M.; Shi, J.; Zhai, X.; Xiao, J.; Wang, X.; Huang, X.; Li, Z.; et al. A High-Stable and Sensitive Colorimetric Nanofiber Sensor Based on PCL Incorporating Anthocyanins for Shrimp Freshness. *Food Chem.* **2022**, *377*, 131909. [CrossRef]

98. Gao, W.; Zhu, J.; Liu, P.; Cui, B.; El-Aty, A.M.A. Preparation and Characterization of Octenyl Succinylated Starch Microgels via a Water-in-Oil (W/O) Inverse Microemulsion Process for Loading and Releasing Epigallocatechin Gallate. *Food Chem.* **2021**, *355*, 129661. [CrossRef]
99. Liu, Y.; Liang, Q.; Liu, X.; Raza, H.; Ma, H.; Ren, X. Treatment with Ultrasound Improves the Encapsulation Efficiency of Resveratrol in Zein-Gum Arabic Complex Coacervates. *LWT—Food Sci. Technol.* **2022**, *153*, 112331. [CrossRef]
100. Baba, W.N.; Mudgil, P.; Regenstein, J.M.; Maqsood, S. Impact of Quercetin Conjugation Using Alkaline and Free Radical Methods with Tandem Ultrasonication on the Functional Properties of Camel Whey and Its Hydrolysates. *Food Res. Int.* **2024**, *190*, 114562. [CrossRef]
101. Wang, Y.; Zhao, L.; Wang, C.; Hu, J.; Guo, X.; Zhang, D.; Wu, W.; Zhou, F.; Ji, B. Protective Effect of Quercetin and Chlorogenic Acid, Two Polyphenols Widely Present in Edible Plant Varieties, on Visible Light-Induced Retinal Degeneration in Vivo. *J. Funct. Foods* **2017**, *33*, 103–111. [CrossRef]
102. Chen, C.; Zhong, Q.; Chen, Z. Improved Aqueous Solubility, Bioaccessibility and Cellular Uptake of Quercetin Following pH-driven Encapsulation in Whey Protein Isolate. *Int. J. Food Sci. Technol.* **2022**, *57*, 2747–2755. [CrossRef]
103. Chen, C.; Chen, Z.; Zhong, Q. Caseinate Nanoparticles Co-Loaded with Quercetin and Avenanthramide 2c Using a Novel Two-Step pH-Driven Method: Formation, Characterization, and Bioavailability. *Food Hydrocoll.* **2022**, *129*, 107669. [CrossRef]
104. Sabet, S.; Rashidinejad, A.; Qazi, H.J.; McGillivray, D.J. An Efficient Small Intestine-Targeted Curcumin Delivery System Based on the Positive-Negative-Negative Colloidal Interactions. *Food Hydrocoll.* **2021**, *111*, 106375. [CrossRef]
105. Chen, J.; Gu, Y.; Chen, Z.; Tan, Y. Stability and Digestibility of Quercetin Encapsulated in a Whey Protein Isolate-Inulin Complex Emulsion. *LWT—Food Sci. Technol.* **2025**, *216*, 117318. [CrossRef]
106. Wang, C.; Liu, Z.; Xu, G.; Yin, B.; Yao, P. BSA-Dextran Emulsion for Protection and Oral Delivery of Curcumin. *Food Hydrocoll.* **2016**, *61*, 11–19. [CrossRef]
107. Yu, Y.-B.; Wu, M.-Y.; Wang, C.; Wang, Z.-W.; Chen, T.-T.; Yan, J.-K. Constructing Biocompatible Carboxylic Curdlan-Coated Zein Nanoparticles for Curcumin Encapsulation. *Food Hydrocoll.* **2020**, *108*, 106028. [CrossRef]
108. Sebaaly, C.; Haydar, S.; Greige-Gerges, H. Eugenol Encapsulation into Conventional Liposomes and Chitosan-Coated Liposomes: A Comparative Study. *J. Drug Deliv. Sci. Technol.* **2022**, *67*, 102942. [CrossRef]
109. Hamadou, A.H.; Zhang, J.; Chao, C.; Xu, B. Stability of Rutin Using Pectin-Chitosan Dual Coating Nanoliposomes. *LWT—Food Sci. Technol.* **2022**, *170*, 114084. [CrossRef]
110. Shruthi, P.A.; Pushpadass, H.A.; Emerald, F.M.E.; Nath, B.S.; Naik, N.L. Resveratrol-Loaded Proniosomes: Formulation, Characterization and Fortification. *LWT—Food Sci. Technol.* **2020**, *134*, 110127. [CrossRef]
111. Zhou, J.; Cheng, W.; Liu, T.; Li, J.; Li, X. Preparation, Characterization, and in Vitro Antioxidant Activity of pH-Sensitive Resveratrol Microcapsule in Simulated Intestinal Fluids. *Int. J. Food Prop.* **2019**, *22*, 804–814. [CrossRef]
112. Xu, G.; Ren, G.; Xu, X.; Yuan, H.; Wang, Z.; Kang, L.; Yu, W.; Tian, K. Combination of Curcumin and Green Tea Catechins Prevents Dimethylhydrazine-Induced Colon Carcinogenesis. *Food Chem. Toxicol.* **2010**, *48*, 390–395. [CrossRef] [PubMed]
113. Eom, D.-W.; Lee, J.H.; Kim, Y.-J.; Hwang, G.S.; Kim, S.-N.; Kwak, J.H.; Cheon, G.J.; Kim, K.H.; Jang, H.-J.; Ham, J.; et al. Synergistic Effect of Curcumin on Epigallocatechin Gallate-Induced Anticancer Action in PC3 Prostate Cancer Cells. *BMB Rep.* **2015**, *48*, 461–466. [CrossRef] [PubMed]
114. Wu, X.; Li, M.; Xiao, Z.; Daglia, M.; Dragan, S.; Delmas, D.; Vong, C.T.; Wang, Y.; Zhao, Y.; Shen, J.; et al. Dietary Polyphenols for Managing Cancers: What Have We Ignored? *Trends Food Sci. Technol.* **2020**, *101*, 150–164. [CrossRef]
115. Liu, F.; Ma, D.; Luo, X.; Zhang, Z.; He, L.; Gao, Y.; McClements, D.J. Fabrication and Characterization of Protein-Phenolic Conjugate Nanoparticles for Co-Delivery of Curcumin and Resveratrol. *Food Hydrocoll.* **2018**, *79*, 450–461. [CrossRef]
116. Jing, H.; Nie, M.; Dai, Z.; Xiao, Y.; Song, J.; Zhang, Z.; Zhou, C.; Li, D. Identification of Carotenoids from Fruits and Vegetables with or without Saponification and Evaluation of Their Antioxidant Activities. *J. Food Sci.* **2023**, *88*, 2693–2703. [CrossRef]
117. Dai, Z.; Li, Z.; Shi, E.; Nie, M.; Feng, L.; Chen, G.; Gao, R.; Zeng, X.; Li, D. Study on the Interaction between Four Typical Carotenoids and Human Gut Microflora Using an in Vitro Fermentation Model. *J. Agric. Food Chem.* **2022**, *70*, 13592–13601. [CrossRef]
118. Wang, F.; Xu, H.; He, W.; Lu, Y.; Luo, H.; Guo, Q.; Li, D.; Bao, Y.; Zhang, Z. Exogenous Salicylic Acid Promotes Carotenoid Accumulation and Antioxidant Capacity in Germinated Maize Kernels by Regulating Carotenoid Biosynthetic Pathway. *Food Biosci.* **2024**, *59*, 103990. [CrossRef]
119. Sridhar, K.; Inbaraj, B.S.; Chen, B.-H. Recent Advances on Nanoparticle Based Strategies for Improving Carotenoid Stability and Biological Activity. *Antioxidants* **2021**, *10*, 713. [CrossRef]
120. Dai, L.; Zhou, L.; Zhou, H.; Zheng, B.; Ji, N.; Xu, X.; He, X.; Xiong, L.; McClements, D.J.; Sun, Q. Comparison of Lutein Bioaccessibility from Dietary Supplement-Excipient Nanoemulsions and Nanoemulsion-Based Delivery Systems. *J. Agric. Food Chem.* **2021**, *69*, 13925–13932. [CrossRef]
121. Tufail, T.; Bader Ul Ain, H.; Noreen, S.; Ikram, A.; Arshad, M.T.; Abdullahi, M.A. Nutritional Benefits of Lycopene and Beta-carotene: A Comprehensive Overview. *Food Sci. Nutr.* **2024**, *12*, 8715–8741. [CrossRef]

122. Shi, M.; Bai, J.; Zhao, L.; Yu, X.; Liang, J.; Liu, Y.; Nord, W.; Li, Y. Co-Loading and Intestine-Specific Delivery of Multiple Antioxidants in pH-Responsive Microspheres Based on TEMPO-Oxidized Polysaccharides. *Carbohydr. Polym.* **2017**, *157*, 858–865. [CrossRef] [PubMed]
123. Luo, S.; Yu, L.; Song, J.; Wu, C.; Li, Y.; Zhang, C. Hybridization of Glucosyl Stevioside and Hydroxypropyl Methylcellulose to Improve the Solubility of Lutein. *Food Chem.* **2022**, *394*, 133490. [CrossRef] [PubMed]
124. Jing, H.; Nie, M.; Wang, X.; Zhang, Z.; Xu, Y.; Zhang, G.; Li, D.; Dai, Z. Lutein Combined with EGCG Improved Retinitis Pigmentosa against *N*-Methyl-*N* Nitrosourea-Induced. *Food Funct.* **2023**, *14*, 9554–9566. [CrossRef] [PubMed]
125. Su, Y.; Sun, M.; Zhao, M.; Xu, B.; Li, J.; Zheng, T. Enhancement of the Physicochemical and in Vitro Release Properties of Lutein by Gelatin/Octenyl Succinic Anhydride (OSA)-modified Starch Composite as Vehicles. *Int. J. Food Sci. Technol.* **2022**, *57*, 738–750. [CrossRef]
126. Yan, Y.; Zhu, Q.; Diao, C.; Wang, J.; Wu, Z.; Wang, H. Enhanced Physicochemical Stability of Lutein-Enriched Emulsions by Polyphenol-Protein-Polysaccharide Conjugates and Fat-Soluble Antioxidant. *Food Hydrocoll.* **2020**, *101*, 105447. [CrossRef]
127. Wang, X.; Yang, Y.; Huycke, M.M. Risks Associated with Enterococci as Probiotics. *Food Res. Int.* **2020**, *129*, 108788. [CrossRef]
128. Virk, M.S.; Virk, M.A.; He, Y.; Tufail, T.; Gul, M.; Qayum, A.; Rehman, A.; Rashid, A.; Ekumah, J.-N.; Han, X.; et al. The Anti-Inflammatory and Curative Exponent of Probiotics: A Comprehensive and Authentic Ingredient for the Sustained Functioning of Major Human Organs. *Nutrients* **2024**, *16*, 546. [CrossRef]
129. Ji, H.; Yan, X.; Zhang, L.; Yang, L.; Xie, P.; Gu, F.; Bian, S.; Wan, H.; Nie, S. Prebiotics Empower Probiotics with Gastrointestinal Stress Resistance for Colon-Targeted Release to Synergistically Alleviate Colitis. *J. Control. Release* **2025**, *380*, 297–316. [CrossRef]
130. Sultana, K.; Godward, G.; Reynolds, N.; Arumugaswamy, R.; Peiris, P.; Kailasapathy, K. Encapsulation of Probiotic Bacteria with Alginate-Starch and Evaluation of Survival in Simulated Gastrointestinal Conditions and in Yoghurt. *Int. J. Food Microbiol.* **2000**, *62*, 47–55. [CrossRef]
131. Virk, M.S.; Virk, M.A.; Liang, Q.; Sun, Y.; Zhong, M.; Tufail, T.; Rashid, A.; Qayum, A.; Rehman, A.; Ekumah, J.-N.; et al. Enhancing Storage and Gastroprotective Viability of Lactiplantibacillus Plantarum Encapsulated by Sodium Caseinate-Inulin-Soy Protein Isolates Composites Carried within Carboxymethyl Cellulose Hydrogel. *Food Res. Int.* **2024**, *187*, 114432. [CrossRef]
132. Pešić, M.B.; Milinčić, D.D.; Kostić, A.Ž.; Stanisavljević, N.S.; Vukotić, G.N.; Kojić, M.O.; Gašić, U.M.; Barać, M.B.; Stanojević, S.P.; Popović, D.A.; et al. In Vitro Digestion of Meat- and Cereal-Based Food Matrix Enriched with Grape Extracts: How Are Polyphenol Composition, Bioaccessibility and Antioxidant Activity Affected? *Food Chem.* **2019**, *284*, 28–44. [CrossRef] [PubMed]
133. Chen, L.; Yang, T.; Song, Y.; Shu, G.; Chen, H. Effect of Xanthan-Chitosan-Xanthan Double Layer Encapsulation on Survival of Bifidobacterium BB01 in Simulated Gastrointestinal Conditions, Bile Salt Solution and Yogurt. *LWT—Food Sci. Technol.* **2017**, *81*, 274–280. [CrossRef]
134. Filannino, P.; Cavoski, I.; Thlien, N.; Vincentini, O.; Angelis, M.D.; Silano, M.; Gobbetti, M.; Cagno, R.D. Lactic Acid Fermentation of Cactus Cladodes (*Opuntia ficus-indica* L.) Generates Flavonoid Derivatives with Antioxidant and Anti-Inflammatory Properties. *PLoS ONE* **2016**, *11*, e0152575. [CrossRef]
135. Lee, K.W.; Han, N.S.; Kim, J.H. Purification and Characterization of Beta-Glucosidase from Weissella Cibaria 37. *J. Microbiol. Biotechnol.* **2012**, *22*, 1705–1713. [CrossRef]
136. Doo, H.; Kwak, J.; Keum, G.B.; Ryu, S.; Choi, Y.; Kang, J.; Kim, H.; Chae, Y.; Kim, S.; Kim, H.B.; et al. Lactic Acid Bacteria in Asian Fermented Foods and Their Beneficial Roles in Human Health. *Food Sci. Biotechnol.* **2024**, *33*, 2021–2033. [CrossRef]
137. Holkem, A.T.; Neto, E.J.S.; Nakayama, M.; Souza, C.J.F.; Thomazini, M.; Gallo, F.A.; da Silva, M.P.; de Queiroz Bomdespacho, L.; Luciano, C.G.; Moraes, I.C.F.; et al. Sugarcane Juice with Co-Encapsulated *Bifidobacterium animalis* subsp. lactis BLC1 and Proanthocyanidin-Rich Cinnamon Extract. *Probiotics Antimicrob. Proteins* **2019**, *12*, 1179–1192. [CrossRef]
138. Akpabli-Tsigbe, N.D.K.; Ma, Y.; Ekumah, J.-N.; Osabutey, J.; Hu, J.; Xu, M.; Johnson, N.A.N.; Quaisie, J. Two-Step Optimization of Solid-State Fermentation Conditions of Heilong48 Soybean Variety for Maximum Chlorogenic Acid Extraction Yield with Improved Antioxidant Activity. *Ind. Crops Prod.* **2021**, *168*, 113565. [CrossRef]
139. Tabasco, R.; Sánchez-Patán, F.; Monagas, M.; Bartolomé, B.; Moreno-Arribas, M.V.; Peláez, C.; Requena, T. Effect of Grape Polyphenols on Lactic Acid Bacteria and Bifidobacteria Growth: Resistance and Metabolism. *Food Microbiol.* **2011**, *28*, 1345–1352. [CrossRef]
140. Pereira-Caro, G.; Oliver, C.M.; Weerakkody, R.; Singh, T.; Conlon, M.; Borges, G.; Sanguansri, L.; Lockett, T.; Roberts, S.A.; Crozier, A.; et al. Chronic Administration of a Microencapsulated Probiotic Enhances the Bioavailability of Orange Juice Flavanones in Humans. *Free Radic. Biol. Med.* **2015**, *84*, 206–214. [CrossRef]
141. Sharma, P.; Nickerson, M.T.; Korber, D.R. Valorization of Berry Pomace for Extraction of Polyphenol Compounds and Its Co-Encapsulation with Probiotic Bacteria. *Food Biosci.* **2024**, *62*, 105124. [CrossRef]
142. Zhang, H.; Zhang, J.; Liu, B.; Xiao, J.; Stuart, M.A.C.; Hou, G.; Zhang, H.; Liang, S.; Li, Z.; Wang, Q.; et al. Natural Phenolic-Metal Framework Strengthened Mesona Chinensis Polysaccharides Microgels for Improved Viability of Probiotics to Alleviate the Liver Injury and Gut Microbiota Dysbiosis. *Adv. Funct. Mater.* **2024**, *34*, 2401064. [CrossRef]

143. Pimentel, T.C.; Brandão, L.R.; De Oliveira, M.P.; Da Costa, W.K.A.; Magnani, M. Health Benefits and Technological Effects of Lacticaseibacillus Casei-01: An Overview of the Scientific Literature. *Trends Food Sci. Technol.* **2021**, *114*, 722–737. [CrossRef]
144. Ma, L.; Su, C.; Li, X.; Wang, H.; Luo, M.; Chen, Z.; Zhang, B.; Zhu, J.; Yuan, Y. Preparation and Characterization of Bilayered Microencapsulation for Co-Delivery Lactobacillus Casei and Polyphenols via Zein-Chitosan Complex Coacervation. *Food Hydrocoll.* **2024**, *148*, 109410. [CrossRef]
145. Gaudreau, H.; Champagne, C.P.; Remondetto, G.E.; Gomaa, A.; Subirade, M. Co-Encapsulation of Lactobacillus Helveticus Cells and Green Tea Extract: Influence on Cell Survival in Simulated Gastrointestinal Conditions. *J. Funct. Foods* **2016**, *26*, 451–459. [CrossRef]
146. Colín-Cruz, M.A.; Pimentel-González, D.J.; Carrillo-Navas, H.; Alvarez-Ramírez, J.; Guadarrama-Lezama, A.Y. Co-Encapsulation of Bioactive Compounds from Blackberry Juice and Probiotic Bacteria in Biopolymeric Matrices. *LWT–Food Sci. Technol.* **2019**, *110*, 94–101. [CrossRef]
147. Hu, Q.; Li, J.; Wang, T.; Xu, X.; Duan, Y.; Jin, Y. Polyphenolic Nanoparticle-Modified Probiotics for Microenvironment Remodeling and Targeted Therapy of Inflammatory Bowel Disease. *ACS Nano* **2024**, *18*, 12917–12932. [CrossRef]
148. Benito, I.; Encío, I.J.; Milagro, F.I.; Alfaro, M.; Martínez-Peñuela, A.; Barajas, M.; Marzo, F. Microencapsulated *Bifidobacterium bifidum* and *Lactobacillus gasseri* in Combination with Quercetin Inhibit Colorectal Cancer Development in $Apc^{-/+}$ Mice. *Int. J. Mol. Sci.* **2021**, *22*, 4906. [CrossRef]
149. Xiao, M.; Zhang, C.; Duan, H.; Narbad, A.; Zhao, J.; Chen, W.; Zhai, Q.; Yu, L.; Tian, F. Cross-Feeding of Bifidobacteria Promotes Intestinal Homeostasis: A Lifelong Perspective on the Host Health. *Npj Biofilms Microbiomes* **2024**, *10*, 47. [CrossRef]
150. Xing, Z.; Han, W.; Dai, T.; Gong, D.; Zhang, G. Encapsulation of Ferulic Acid in Potato Protein-Pectin Nanocomplexes with Improved Stability and Controlled Release Properties. *Food Biosci.* **2024**, *62*, 105553. [CrossRef]
151. Liang, J.; Yan, H.; Wang, X.; Zhou, Y.; Gao, X.; Puligundla, P.; Wan, X. Encapsulation of Epigallocatechin Gallate in Zein/Chitosan Nanoparticles for Controlled Applications in Food Systems. *Food Chem.* **2017**, *231*, 19–24. [CrossRef]
152. Holkem, A.T.; Favaro-Trindade, C.S.; Lacroix, M. Study of Anticancer Properties of Proanthocyanidin-Rich Cinnamon Extract in Combination with Bifidobacterium Animalis Subsp. Lactis BLC1 and Resistance of These Free and Co-Encapsulated Materials under in Vitro Simulated Gastrointestinal Conditions. *Food Res. Int.* **2020**, *134*, 109274. [CrossRef]
153. Huang, H.; Belwal, T.; Liu, S.; Duan, Z.; Luo, Z. Novel Multi-Phase Nano-Emulsion Preparation for Co-Loading Hydrophilic Arbutin and Hydrophobic Coumaric Acid Using Hydrocolloids. *Food Hydrocoll.* **2019**, *93*, 92–101. [CrossRef]
154. Jang, Y.; Koh, E. Effect of Encapsulation on Stability of Anthocyanins and Chlorogenic Acid Isomers in Aronia during in Vitro Digestion and Their Transformation in a Model System. *Food Chem.* **2024**, *434*, 137443. [CrossRef]

Disclaimer/Publisher's Note: The statements, opinions and data contained in all publications are solely those of the individual author(s) and contributor(s) and not of MDPI and/or the editor(s). MDPI and/or the editor(s) disclaim responsibility for any injury to people or property resulting from any ideas, methods, instructions or products referred to in the content.

nutrients

MDPI

Article

Structural Characterization and Efficacy in Alleviating Lung Inflammation of Sialylated Glycopeptides from Edible Bird's Nest

Qiushi Li [1,2], Chenxi Zhang [1,2], Guandong Fang [1,2], Shuang Qiu [3], Man Yuan [3], Nan Qian [1,2], Dongliang Wang [1,3,*] and Xiangrong Cheng [1,2,*]

[1] School of Food Science and Technology, Jiangnan University, Wuxi 214122, China; liqiushi1023@163.com (Q.L.); chenxi.zhang@chinyou.com (C.Z.); fgd12232023@163.com (G.F.); qiannan202412@163.com (N.Q.)
[2] State Key Laboratory of Food Science and Resources, Jiangnan University, Wuxi 214122, China
[3] Hebei Edible Bird's Nest Fresh Stew Technology Innovation Center, Langfang 065700, China; qiushuang0614@163.com (S.Q.); codeyduck@163.com (M.Y.)
* Correspondence: wangdljp@126.com (D.W.); cheng-xiangrong@hotmail.com (X.C.)

Abstract: Objectives: This study aimed to characterize the basic structure of sialylated glycopeptide (SCP) from edible bird's nest, and to explore the intervention effect and mechanism of SCP based on a mouse lung inflammation model induced by lipopolysaccharide (LPS). **Methods:** C57BL/6 mice were randomly divided into the control group (CON), model group (LPS), EBN group, SCP group, and SA group. **Results:** The results showed that SCP had the typical structures of polypeptides and carbohydrates. SCP effectively intervened in the lung inflammation response. The number of neutrophils (Neu) in BALF decreased by 41.3%, the level of tumor necrosis factor-α (TNF-α) decreased by 36.4%, and the W/D ratio of lung tissues decreased by 27.2%, effectively preventing pathological changes in lung tissues. A total of 40 differential metabolites such as choline, linolenic acid, and xanthine were screened between the SCP group and the LPS group. These differential metabolites were mainly enriched in the metabolic pathways of glycerophospholipids, alpha-linolenic acid, and purines. **Conclusions:** The research results support that SCP, as the active substance of edible bird's nest, can effectively improve lung inflammation, providing theoretical guidance for the development of functional edible bird's nest products.

Keywords: edible bird's nest; sialylated glycopeptide; lung inflammation; metabolomics

1. Introduction

Edible bird's nest (EBN) is coagulated from the saliva secreted by several species of swiftlets in the genus *Aerodramus* of the *Apodidae* family mixed with other substances. As a traditional precious product with both medicinal and edible properties, it has a long history of consumption in Asian regions, especially in China [1]. The main component of EBN is primarily composed of macromolecular glycoproteins rich in sialic acid (SA), which typically exist as terminal residues at the non-reducing ends of glycan chains in these glycoproteins [2]. The SA content in EBN, a pivotal component of its bioactive glycopeptides, exhibits notable variability influenced by species origin, geographical provenance, and nesting environment [3]. For example, *Aerodramus fuciphagus* nests contain 1.9-fold higher conjugated SA (dry weight) than *A. maximus* nests, reflecting genetic differences in salivary glycoprotein biosynthesis. House-farmed EBN from Malaysia exhibits 63% higher SA levels than cave-nested counterparts, a disparity linked to environmental factors like dietary

composition and microhabitat [4]. Regionally, Vietnamese EBN harbors elevated sialoglycoprotein content (the primary molecular carriers of SA) compared to major producing regions such as Malaysia [5]. These variations in SA abundance and glycan architecture are critical determinants of glycopeptide structures, potentially influencing biological activities like inflammation modulation [6]. Compared with the untreated EBN, the enzymatically hydrolyzed EBN extract has higher biological activities such as anti-inflammatory, antioxidant, and immunological activities [7]. Glycopeptides prepared from the extraction of many natural foods, including *Lycium barbarum* and egg glycopeptides, have been demonstrated to play anti-inflammatory and immune-promoting roles [8,9]. Notably, EBN has the efficacy of moistening the lungs and nourishing yin in Chinese medicine. In existing studies, EBN can treat respiratory diseases by inhibiting inflammation, regulating the immune system, and maintaining oxidative balance [10,11]. Currently, research on the anti-inflammatory activities of EBN mainly focuses on peptides, but the role of glycopeptides has not been emphasized. Previous studies have proven that the sialylated glycopeptide (SCP) of the EBN is the main active component in edible bird's nest, and it can exert a neuroprotective effect through the gut–brain axis [12]. However, currently, the efficacy of SCP in alleviating lung inflammation remains unclear and requires further research.

Lung inflammation is an important pathological basis for many severe respiratory diseases, which can significantly affect the metabolic homeostasis of the body and weaken the body's functions. Its pathogenesis is extremely complex, involving multiple aspects including immune response, oxidative stress, cell apoptosis, and microbial infection [13]. When the lungs are invaded by pathogens or other harmful stimuli, the immune system is activated, triggering an inflammatory response, which subsequently leads to phenomena such as immune disorders, tissue damage, and metabolic abnormalities [14]. Currently, although traditional clinical intervention methods such as glucocorticoids and antibiotics can alleviate symptoms, long-term use is likely to trigger drug resistance and side effects. In recent years, extensive attention has been paid to searching for food-derived components with anti-inflammatory properties from the diet. A variety of food-derived glycoprotein complexes have been proven to possess anti-inflammatory effects [15]. Many natural foods, such as *Ganoderma lucidum*, contain abundant bioactive components and have been confirmed to be capable of intervening in lung inflammation [16]. Lipopolysaccharide (LPS), which serves as a key constituent of the cell wall in Gram-negative bacteria, can activate the immune system and trigger inflammatory reactions such as the massive release of pro-inflammatory cytokines and all kinds of tissue damage [17]. Thus, LPS is commonly used to induce lung injury [18,19].

Metabolomics has been extensively utilized to comprehensively investigate the patterns of metabolic dynamic responses in organisms when they are under exogenous stimuli or endogenous pathological changes [20]. It enables the precise identification and quantitative investigation of the metabolic components of small molecules in biological samples [21]. Subsequently, the matching of metabolic pathways and the elucidation of molecular mechanisms can be achieved. Existing studies have proven that when pulmonary inflammation exists in the organism, it will be accompanied by metabolic disorders. Therefore, investigating the metabolic changes in lung tissues helps understand the mechanism of lung inflammation induced by LPS and evaluate the regulatory effect of SCP.

In this study, the structure of SCP was characterized by combining the chemical composition and primary structure. A mouse model of lung inflammation was established using lipopolysaccharide. The intervention effect of SCP on lipopolysaccharide-induced lung inflammation in mice was evaluated from three aspects: the level of lung inflammation, the pathological structure of lung tissues, and the metabolic level of lung tissues.

2. Materials and Methods

2.1. Materials and Reagents

Edible bird's nests horn (from Malaysia) was purchased from a local supermarket in Wuxi. Sialic acid was purchased from Kesitan Biotechnology Co., Ltd. (Wuhan, China), and Alcalase 2.4L (2.4 AU/g), Papain (800 U/mg) were purchased from Novozymes (Bagsværd, Denmark). Beyoblue™ coomassie blue super fast staining solution, prestained color protein molecular weight marker (10–170 kDa), SDS-PAGE protein loading buffer (2×), periodic acid-Schiff staining kit, and BCA protein assay kit, protein precast gel (4–20%, 15 Wells) were purchased from Beyotime Biotechnology Co., Ltd. (Shanghai, China). Ethanol, $NaHSO_4$, o-phenylenediamine hydrochloride (OPA), glucose, phenol, sulfuric acid, etc., were all purchased from Sinopharm Chemical Reagent Co., Ltd. (Shanghai, China). Lipopolysaccharide (LPS) was purchased from Sigma-Aldrich (St. Louis, MO, USA). TNF-α, IL-1β, and IL-6 commercial kits were purchased from Xiamen Hui Jia Biotechnology Co., Ltd. (Xiamen, China). Acetone was procured from Zhejiang Hannuo Chemical Technology Co., Ltd. (Jinhua, China).

2.2. Experimental Animals

Forty 7-week-old male C57BL/6J mice (specific pathogen-free [SPF] grade) were obtained from Jiangsu GemPharmatech Co., Ltd. (Nanjing, China). The experimental procedures were approved by the Laboratory Animal Welfare and Ethics Committee of Jiangnan University (approval number: JN.No20230415c0800705[145]).

2.3. Preparation of Sialylated Glycopeptides (SCP) from EBN

The sequential enzymatic hydrolysis of EBN horn was performed using Alcalase 2.4 L followed by papain under optimized conditions. The first-step hydrolysis with Alcalase 2.4 L was conducted at 60 °C and pH 8.5 for 12 h with an enzyme–substrate ratio of 6000 U/g. Subsequently, papain hydrolysis was performed at 50 °C and pH 7.0 for 2 h using an increased enzyme-substrate ratio of 10,000 U/g. Enzyme inactivation was achieved through thermal denaturation (95 °C, 10 min). Finally, purification was achieved through our laboratory's established method [12]. After being frozen at −80 °C for 12 h, the extracted SCP powder was obtained by a lyophilizer (SCIENTZ-10N, SCIENTZ Biotech Co., Ltd. (Ningbo, China)).

2.4. Structural Characterization of SCP

2.4.1. Neutral Sugar and SA Content Quantification

The content of neutral sugars was measured via the phenol-sulfuric acid approach. To SCP samples, 1 mL of 5% phenol solution was added, followed by the rapid addition of 5 mL of concentrated sulfuric acid. After thorough mixing, the mixture was incubated in a water bath at 37 °C for 30 min. Subsequently, the absorbance was measured at 490 nm using a Microplate Reader 96 (EPOCH1, Bio Tek Instruments, Inc., Winooski, VT, USA). Glucose (anhydrous, dried to constant weight in an oven) was used as the standard reference [22].

SA content was determined by liquid chromatography (LC-20AT, Shimadzu, Kyoto, Japan). SCP sample (50 mg) was hydrolyzed with 5 mL 0.5 M $NaHSO_4$ at 80 °C for 30 min, after which, derivatization was performed with 5 mL 10 g/L OPA (in 0.25 M $NaHSO_4$) at 80 °C for 40 min. After filtration through the 0.22 μm filters, the solution was diluted to 25 mL and stored in the dark. In the HPLC analysis, the EF-C18Bio column (Galaksil, Rugao City, China) was applied at 30 °C. The mobile phase, acetonitrile–water (5:95, v/v), flowed at a 1.0 mL/min rate. Detection was performed at 230 nm with a 20 μL injection volume [12].

2.4.2. Amino Acid Composition Analysis

Approximately 100 mg of solid powder was hydrolyzed with 8 mL 6 M HCl under N_2 at 120 °C for 22–24 h. After neutralization with 10 M NaOH and dilution to 25 mL, the sample was filtered and centrifuged (10,000 rpm, 10 min). For tryptophan, 8 mL 5 M NaOH was used for initial hydrolysis, followed by neutralization with 6.7 mL 6 M NaOH. In the HPLC analysis (Agilent, Santa Clara, CA, USA), the ODS column (Agilent Hypersil, Santa Clara, CA, USA) was employed with gradient elution using mobile phases A (27.6 mmol/L sodium acetate-triethylamine-THF, 500:0.11:2.5, *v*/*v*/*v*, pH 7.2) and B (80.9 mmol/L sodium acetate-methanol-acetonitrile, 1:2:2, *v*/*v*/*v*, pH 7.2), 0–17 min (8–50% B), 17–20.1 min (50–100% B), 20.1–24 min (100–0% B). The flow rate was 1.0 mL/min at 40 °C, with UV detection at 338 nm. Quantification was via external calibration.

2.4.3. Molecular Weight Distribution Determination

SCP sample was vortexed with loading buffer (1:1, *v*/*v*), heat-denatured (100 °C, 3 min) and then centrifuged (8000 rpm, 3 min) to pellet aggregates. The molecular weight of SCP was determined through a discontinuous SDS-PAGE system (5% stacking/10% resolving gel) under reducing conditions, with a sample loading volume of 10 μL. Coomassie Brilliant Blue was used to stain protein, and Periodic acid-Schiff (PAS) reagent was used for glycan [23].

2.4.4. FTIR Spectral Analysis

ATR-FTIR spectroscopy (Thermo Fisher Scientific, Waltham, MA, USA) was employed to analyze secondary structures. Lyophilized SCP samples were directly placed on the ATR crystal and scanned over 4000–650 cm^{-1} with 32 scans at 4 cm^{-1} resolution [24].

2.5. Animal Grouping and Biological Sample Collection

Mice were kept at Jiangnan University's Laboratory Animal Centre (SYXK-(Su)-2021-0056) in a barrier environment. They experienced a 12 h light/dark cycle. The temperature ranged from 20 to 26 °C, and humidity was 40–70% under the artificial 12 h light/dark regime. Forty mice were first individually tagged with unique ear tags (numbered 1–40), and a random sequence was derived from a random number table. Mice were then assigned to five experimental groups (n = 8) based on this sequence. Mice were acclimated for 1 week in a standard environment with free access to food and water before the experiment. During the experiment, stress responses were monitored by observing behavioral status, such as activity level, food intake, and body weight changes. Procedures were performed gently to avoid unnecessary stress. The control group (CON) and LPS model group (LPS) were given 0.2 mL of saline by oral gavage daily, while the EBN group (EBN) was administered 200 mg/kg/d EBN homogenate (dry weight basis), the SCP group (SCP) received glycopeptides equivalent to EBN's sialic acid content, and the SA group was given an equimolar free sialic acid solution for 7 consecutive weeks. During the last week, all groups except CON were intraperitoneally injected with LPS (500 μg/kg/d) for 7 days. After the last LPS injection, the mice were fasted overnight. Following weighing, they were anesthetized by isoflurane inhalation. Subsequently, the mice were euthanized via cervical dislocation and immediately dissected. After sacrificing the mice, the bronchoalveolar lavage fluid (BALF) and lung tissue were collected (see Figure 1).

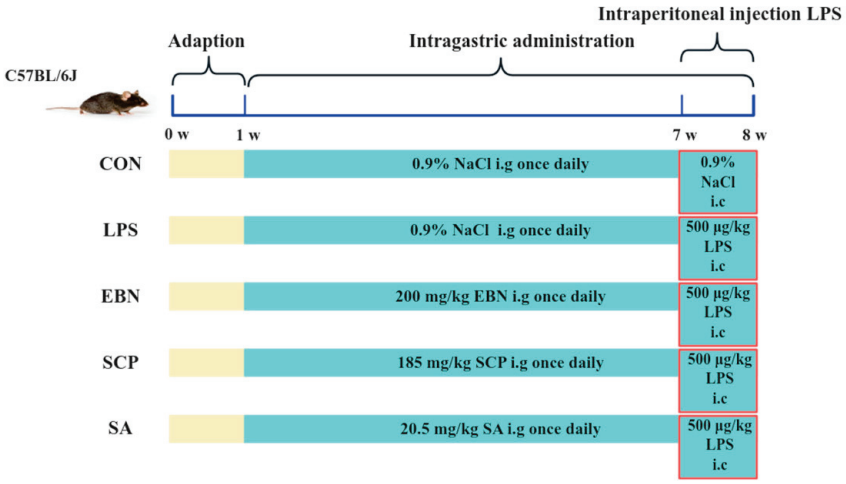


Figure 1. Animal grouping and intervention scheme.

BALF collection: Mice were euthanized, and limbs were secured with pins. The chest cavity and tracheal skin were incised, and the right lung was gently ligated with silk thread. After exposing the trachea, blunt forceps were used to puncture it, followed by the insertion of a tracheal cannula. Once stabilized, 0.5 mL of PBS buffer was injected via a syringe, held for 15–30 s, and then aspirated into a 1.5 mL microcentrifuge tube. This procedure was repeated three times.

Lung tissue homogenization: Frozen lung tissue was thawed and homogenized in PBS buffer (1:100, *m*/*v*). After mincing, 2–3 zirconia beads were added, and the tissue was disrupted using a tissue homogenizer (Jingxin Industrial, Dongguan City, China) at 70 Hz for 90 s (2–3 cycles). Then, it was centrifuged (4 °C, 4000 rpm, 20 min), and the supernatant was collected for biochemical assays.

2.6. Lung Inflammatory Markers

BALF was used to conduct cell count using an automatic hematology analyzer (BC-5000 Vet, Mindray Bio-Medical Electronics Co., Ltd., Dongguan City, China), including white blood cells (WBC), monocytes (Mon), neutrophils (Neu), eosinophils (Eos), basophils (Bas), and lymphocytes (Lym). Lung tissues were used to determine TNF-α, IL-1β, and IL-6 levels by ELISA kits (Xiamen Huijia Biotech, Xiamen, China, OD450 nm).

2.7. Lung Histopathology

Lung tissue was rinsed with PBS buffer, followed by blotting to remove surface moisture. The wet weight of the tissue was then measured. Subsequently, the tissue was dried at 80 °C for 48 h until a constant weight was achieved (dry weight). The wet/dry weight (W/D) ratio of the lung tissue was calculated accordingly [25].

Fresh lung tissues were fixed by immersion in 4% paraformaldehyde for 24 h. After fixation, the tissues underwent gradient ethanol dehydration, xylene clearing, paraffin embedding, and tissue sectioning. Subsequently, the sections were deparaffinized, rehydrated, and stained with hematoxylin solution for 10 min. Differentiation was performed using 1% hydrochloric acid-alcohol for 30 s, followed by rinsing with tap water and bluing with ammonia water. After rinsing again, the sections were stained with eosin for 3 min. Following dehydration, clearing, and mounting, the pathological changes in lung tissues from each group were observed under an optical microscope.

2.8. Lung Metabolomics

Lung tissue metabolomic profiling was performed according to the established LC-MS/MS protocol [26]. Chromatographic raw data were processed through Compound Discoverer 3.3 (Thermo Fisher Scientific) for baseline correction, peak alignment, and feature extraction. Subsequent analytical workflows included quantitative analysis of peak areas coupled with molecular formula prediction, with spectral matching conducted against the mzCloud, mzVault, and MassList databases, supplemented by a proprietary compound library (Shanghai Senschip Biotech, Shanghai, China).

2.9. Statistical Analysis

Data were presented as the mean ± standard deviation (SD). For data that conformed to a normal distribution, statistical analyses were performed as follows: For datasets with three or more groups, one-way analysis of variance (ANOVA) was conducted, followed by post-hoc pairwise comparisons using the Least Significant Difference (LSD) test and Duncan's multiple range test. For two-group comparisons, a *t*-test was applied. When the data did not meet the assumptions of parametric tests, the non-parametric Kruskal–Wallis (KW) rank sum test was utilized. A significance level of $p < 0.05$ was set to determine statistical differences among groups. Multivariate statistical analyses were carried out using MetaboAnalyst 6.0 and SIMCA 13.0 software.

3. Results

3.1. Chemical Composition Analysis of SCP

The sialic acid (SA) content in EBN was determined to be 10.25 ± 0.14%, with neutral sugars accounting for 11.84 ± 0.28%. In contrast, an increase in SA content (11.06 ± 0.22%) and a concomitant rise in neutral sugar levels (13.52 ± 0.35%) were observed in SCP (Figure 2). These results indicated an enriched glycan proportion in SCP compared to native EBN.

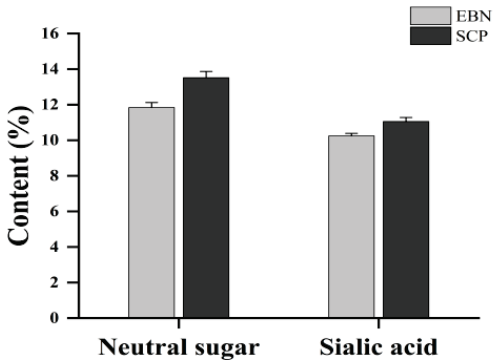


Figure 2. Neutral sugar contents and sialic acid contents of EBN and SCP.

An analysis of 18 amino acids in SCP was performed (Table 1). The top five amino acids by abundance in SCP were proline (Pro), aspartic acid (Asp) or asparagine (Asn), glutamic acid (Glu) or glutamine (Gln), valine (Val), and leucine (Leu). Additionally, SCP was rich in nine essential amino acids (with histidine (His) being essential for infants), which accounted for 42.22 ± 0.02% of the total amino acid content. The combined content of Asp or Asn, threonine (Thr), and serine (Ser) represented 23.34 ± 0.08% of the total amino acid content, suggesting the potential presence of glycosylation modifications in SCP.

Table 1. Amino acids distribution of SCP.

Amino Acids	Percentage Composition (%)	Amino Acids	Percentage Composition (%)
Asp	9.97 ± 0.04	Glu	8.25 ± 0.04
Cys	0.90 ± 0.02	Val *	8.03 ± 0.03
Ser	7.05 ± 0.02	Met *	1.07 ± 0.01
His *	3.56 ± 0.06	Phe *	6.89 ± 0.02
Gly	4.40 ± 0.00	Ile *	3.40 ± 0.01
Thr *	6.32 ± 0.02	Leu *	7.62 ± 0.01
Arg	7.14 ± 0.01	Lys *	4.13 ± 0.02
Ala	3.44 ± 0.01	Pro	10.39 ± 0.06
Tyr	6.23 ± 0.03	Trp *	1.22 ± 0.02

Aspartic acid (Asp), glutamic acid (Glu), cysteine (Cys), valine (Val), werine (Ser), methionine (Met), histidine (His), phenylalanine (Phe), glycine (Gly), isoleucine (Ile), threonine (Thr), leucine (Leu), arginine (Arg), lysine (Lys), alanine (Ala), proline (Pro), tyrosine (Tyr), tryptophan (Trp), * essential amino acids.

3.2. Primary Structure Analysis of SCP

FT-IR spectra of EBN and SCP revealed significant differences (Figure 3A). In EBN, a broad peak at 3600–3000 cm^{-1} was attributed to hydroxyl (−OH) stretching vibrations of polysaccharides [27]. Absorption bands at 1695–1630 cm^{-1} (amide I, C=O stretching) and 1560–1500 cm^{-1} (amide II, N-H bending) confirmed the presence of proteins/polypeptides [28,29]. For SCP, enhanced absorption bands at 1401 cm^{-1} (−COO− symmetric stretching), and 1066 cm^{-1} (C-O), coupled with a carbohydrate-specific peak at 1085–1050 cm^{-1}, demonstrated its glycopeptide nature [29]. Vibrations in the 1440–1395 cm^{-1} region likely corresponded to carboxyl groups from sialic acid (SA) and alduronic acids, consistent with characteristic glycopeptide spectral profiles. These results further supported the glycopeptide structure of SCP.

The molecular weight profiles were analyzed by SDS-PAGE (Figure 3B,C). EBN proteins' molecular weight was mainly between 70–170 kDa (69%). Following enzymatic hydrolysis, the proportion of this range was reduced to 13%, with a concurrent increase in the 25–70 kDa fraction to 48% and the emergence of low molecular weight fragments (10–25 kDa, 38%), confirming effective protein size reduction. PAS staining (Figure 3D,E) revealed that glycans uniformly occupied the 70–170 kDa range. Post-enzymatic treatment, this proportion decreased to 47%, while the 25–70 kDa fraction increased to 53%. Notably, glycans were not degraded below 25 kDa, suggesting covalent stabilization between glycan and protein backbones.

3.3. SCP Alleviated the Changes of LPS-Induced Lung Inflammation Levels

The counts of inflammatory cells in bronchoalveolar lavage fluid (BALF) among different experimental groups were determined (Figure 4A–D). LPS induction resulted in a statistically significant increase ($p < 0.01$) in the counts of neutrophils (Neu), white blood cells (WBC), eosinophils (Eos), and monocytes (Mon), suggesting that LPS successfully induced inflammatory cell disorder in BALF. Compared with the LPS group, intervention groups involving EBN, SCP, and SA were observed to significantly decrease the number of Mon in the BALF ($p < 0.01$). Furthermore, a significant reduction in the number of Neu within the BALF was also noted following interventions with EBN ($p < 0.05$), SCP ($p < 0.01$), and SA ($p < 0.01$). Specifically, under SCP intervention, the numbers of Neu in the BALF were reduced by 41.3%. It was indicated that EBN, SCP, and SA effectively modulated the aggregation of inflammatory cells within the BALF of mice induced by LPS. Among these interventions, SCP exhibited the most significant inhibitory effect on Neu recruitment.

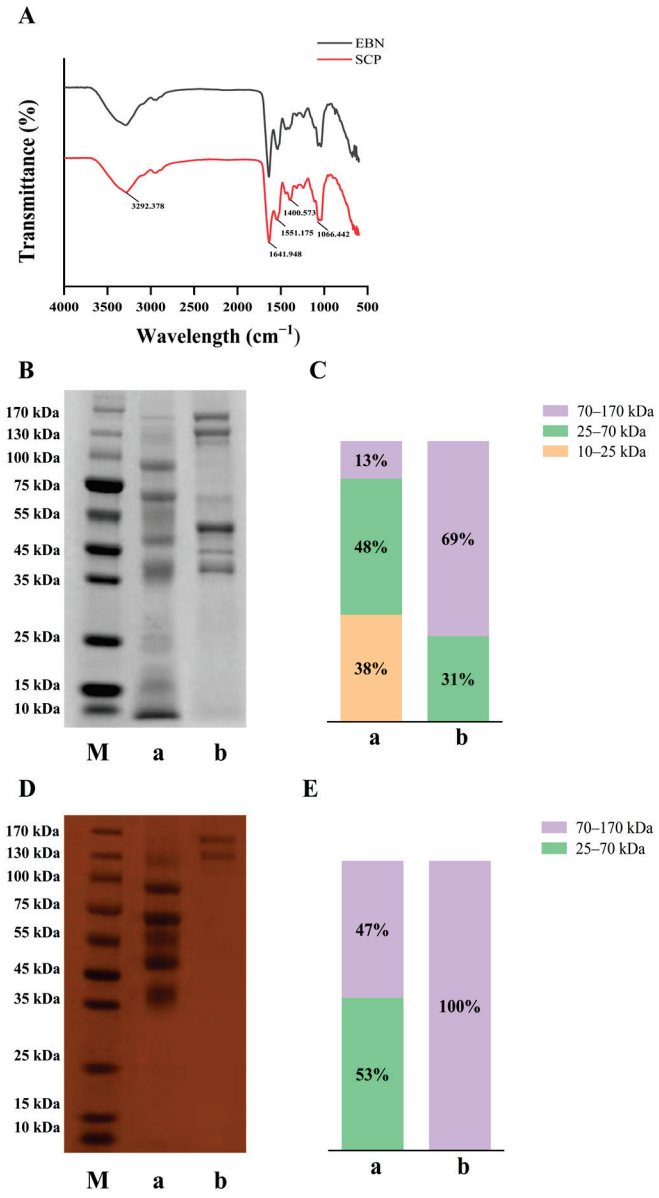


Figure 3. FT-IR spectral and molecular weight distribution of EBN and SCP. (**A**) The Fourier infrared spectra analysis of EBN and SCP. (**B**) Electrophoresis of EBN and SCP stained with carmine blue. (**C**) Relative molecular weight distribution of EBN and SCP under carmine blue staining. (**D**) Electrophoresis of EBN and SCP under PAS staining. (**E**) Relative molecular weight distribution of EBN and SCP under PAS staining. M: Marker, a: EBN, b: SCP.

Important pro-inflammatory cytokines in lung tissues of all groups, such as TNF-α, IL-1β, and IL-6, were determined (Figure 4E–G). Compared with the CON group, the levels of TNF-α ($p < 0.01$), IL-1β ($p < 0.01$), and IL-6 ($p < 0.05$) in the lung tissues of mice significantly increased after LPS induction. It was indicated that the intraperitoneal injection of LPS successfully induced inflammation in the lung tissues of mice. After the intervention of EBN, SCP, and SA, the levels of IL-1β and IL-6 in the lung tissues of mice were significantly decreased compared with those in the LPS group. Notably, compared with the LPS group, the level of TNF-α in the lung tissues decreased by 36.4% after the intervention of SCP, which was 3.6 times and 3.2 times the reduction ratios of EBN and SA intervention groups, respectively. It was suggested that the intervention groups of EBN, SCP, and SA all had a certain regulatory effect on the increase in the levels of pro-inflammatory cytokines. Among

them, the intervention of SCP had the most significant effect on improving the level of TNF-α in the lung tissues.

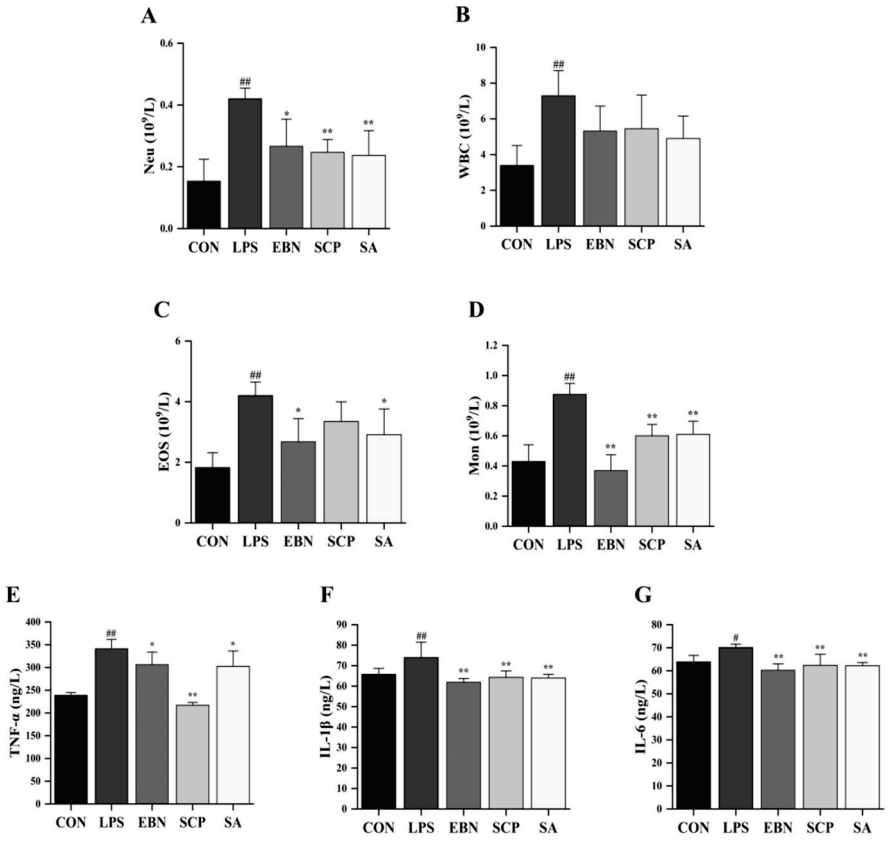


Figure 4. Changes in lung inflammation levels of mice in each group. (**A**–**D**) Counts of inflammatory cells (Neu, WBC, EOS, and Mon) in the BALF of mice in each group. (**E**–**G**) Levels of pro-inflammatory cytokines (TNF-α, IL-1β, and IL-6) in the lung tissue of mice in each group. $n = 8$; results are presented as mean ± SD. # $p < 0.05$, ## $p < 0.01$ vs. CON group, * $p < 0.05$, ** $p < 0.01$ vs. LPS group.

3.4. SCP Alleviated the Changes of LPS-Induced Lung Tissue Pathological Structures

To evaluate the protective effect of SCP against lung tissue injury induced by LPS, the wet-to-dry (W/D) weight ratio of lung tissues was measured (Figure 5A). Compared with the CON group, a significant increase in the W/D ratio was detected in the LPS group ($p < 0.01$), suggesting that an edema phenomenon might occur in the lung tissue. All intervention groups (EBN, SCP, and SA) mitigated this increase ($p < 0.05$). Notably, the SCP group showed the most remarkable improvement, with a 27.2% decrease in the W/D weight ratio.

Hematoxylin and Eosin (H&E) staining of lung tissues in each group further revealed structural alterations of the lung tissues (Figure 5B). The CON group exhibited intact alveolar architecture, orderly arranged epithelial cells, and no edema [30]. In contrast, the LPS group displayed collapsed alveoli, thickened alveolar walls, and increased interstitial exudation. Intervention groups (EBN, SCP, and SA) showed varying degrees of mitigation in tissue damage. Notably, the SCP group demonstrated near-normal alveolar structure with reduced inflammatory cell infiltration. All changes in the pathological structure of the lung tissues revealed that the intraperitoneal injection of LPS successfully led to pathological changes in the structure of the lung tissues. Compared with the LPS group, the lung tissue structures of the intervention groups of EBN, SCP, and SA all showed certain improvements. In addition, the lung tissue structure of the SCP intervention group was the closest to that of the CON group.

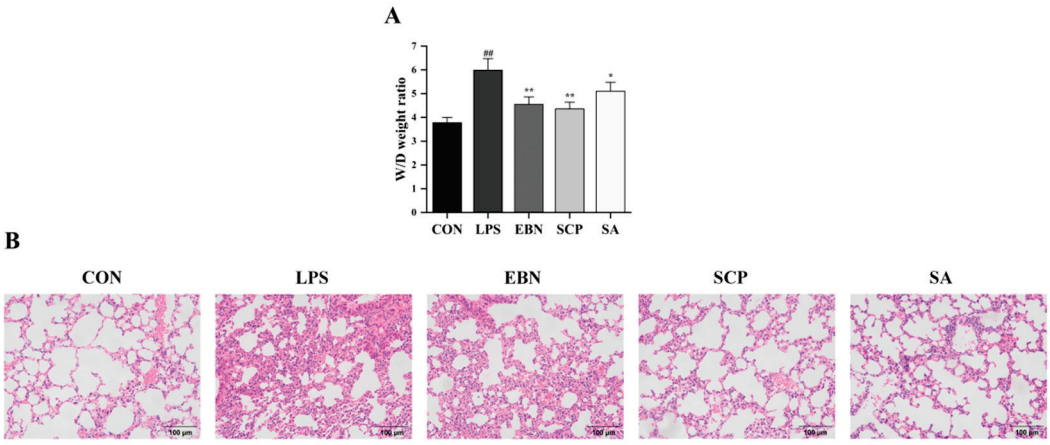


Figure 5. Changes in lung tissue pathological structures of mice in each group. (**A**) The ratio of W/D weight in the lung tissue of mice in each group. (**B**) H&E staining in the lung tissue of mice in each group (200×). n = 8; results are presented as mean ± SD. ## $p < 0.01$ vs. CON group, * $p < 0.05$, ** $p < 0.01$ vs. LPS group.

3.5. SCP Alleviated the Change of LPS-Induced Lung Tissue Metabolic Levels

3.5.1. Analysis of the Metabolic Profiles

After preprocessing the data and imputing the missing values, 417 chromatographic peaks were detected in the positive ion mode, and 358 were found in the negative ion mode. To assess the variations in the metabolic profiles, principal component analysis (PCA) and orthogonal partial least squares-discriminant analysis (OPLS-DA) models were built. In the PCA score plots (Figure 6A,C), the metabolic profile of the LPS group showed a significant divergence along the first principal component (PC1, x-axis), which verified the successful establishment of the inflammation model 30. Along the second principal component (PC2, y-axis), the groups treated with EBN, SCP, and SA presented distinct metabolic changes compared to the LPS group. Significantly, the SCP group was clustered nearest to the CON group, suggesting its excellent ability to restore metabolic homeostasis. The OPLS-DA model further effectively amplified the differences among the groups (Figure 6B,D).

3.5.2. Screening of Differential Metabolites

In the metabolomics analysis, the screening of differential metabolites is usually based on the variable importance in the projection (VIP) values obtained from the OPLS-DA model. VIP describes the overall contribution of each variable to the model, as well as the p values obtained from the t-test. A threshold of $p < 0.05$ and VIP > 1 was set to screen out the differential metabolites with statistical significance. The differential metabolites among groups under the positive and negative ion modes were screened respectively (Figure 7). A total of 35 differential metabolites were identified under the positive ion mode, and 45 differential metabolites were identified under the negative ion mode. Compared with the CON group, a total of 39 metabolites in the LPS group showed significant changes in their contents ($p < 0.05$). Among them, the contents of 25 metabolites such as L-glutamic acid, xanthine, uric acid, and PC (14:0/18:0) in the LPS group increased significantly, while the contents of 14 metabolites such as glycerophosphocholine, pyrophosphate, o-toluidine, and GPEtn (16:0/18:1) decreased significantly. This indicated that LPS may cause metabolic disorders in the lung tissues of mice by interfering with these 39 metabolites. Compared with the LPS group, a total of 40 metabolites in the SCP intervention group showed significant changes in their contents ($p < 0.05$). Among them, the contents of 28 metabolites such as linolenic acid, choline, LPC (18:1), and indoline in the SCP intervention group increased significantly, while the contents of 12 metabolites such as glycerophosphocholine,

xanthine, inosine, and LysoPC (18:1(11Z)/0:0) decreased significantly. This suggested that SCP may regulate the inflammation of the lung tissues in mice induced by LPS by interfering with these 40 metabolites.

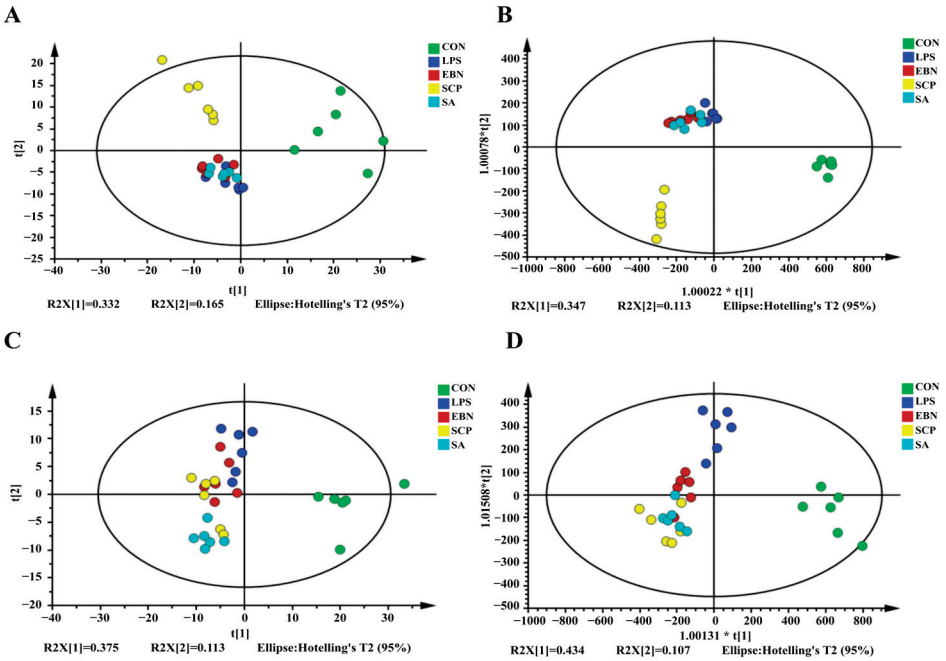


Figure 6. Pattern recognition analysis in positive and negative ion modes. (**A**,**C**) PCA diagram of positive ion mode and negative ion mode. (**B**,**D**) OPLS-DA diagram of positive ion mode and negative ion mode.

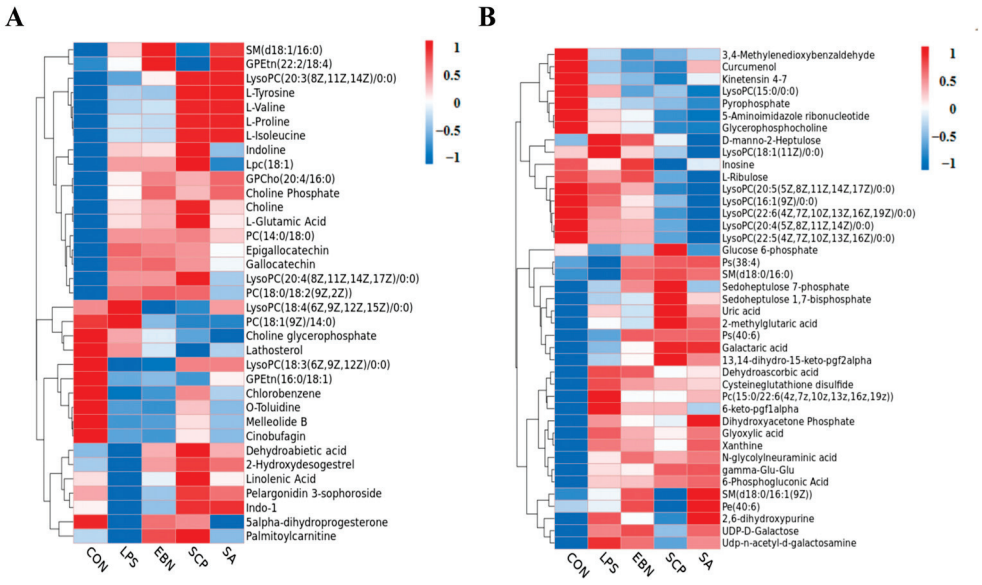


Figure 7. Clustering heat map of the expression of differential metabolites under positive and negative ion modes in the lung tissue of mice in each group. (**A**) Cluster heat map of differential metabolites in positive ion mode. (**B**) Cluster heat map of differential metabolites under negative ion mode.

3.5.3. Metabolic Pathway Analysis of Differential Metabolites

Differential metabolites were mapped to the KEGG database to identify metabolic pathways with $p < 0.05$ and Impact > 0 (Figure 8). Compared to the CON group, the LPS group showed significant enrichment in glycerophospholipid metabolism, purine

metabolism, glyoxylate, and dicarboxylate metabolism. Compared to the LPS group, the pathways enriched in EBN were glycerophospholipid metabolism and alpha-linolenic acid metabolism, the pathways enriched in SCP were glycerophospholipid metabolism, purine metabolism, and alpha-linolenic acid metabolism, and the pathways enriched in SA were glycerophospholipid metabolism, alpha-linolenic acid, and linoleic acid metabolism. Notably, the SCP group shared more overlapping pathways with the LPS group, suggesting its superior regulatory capacity at the metabolic pathway level.

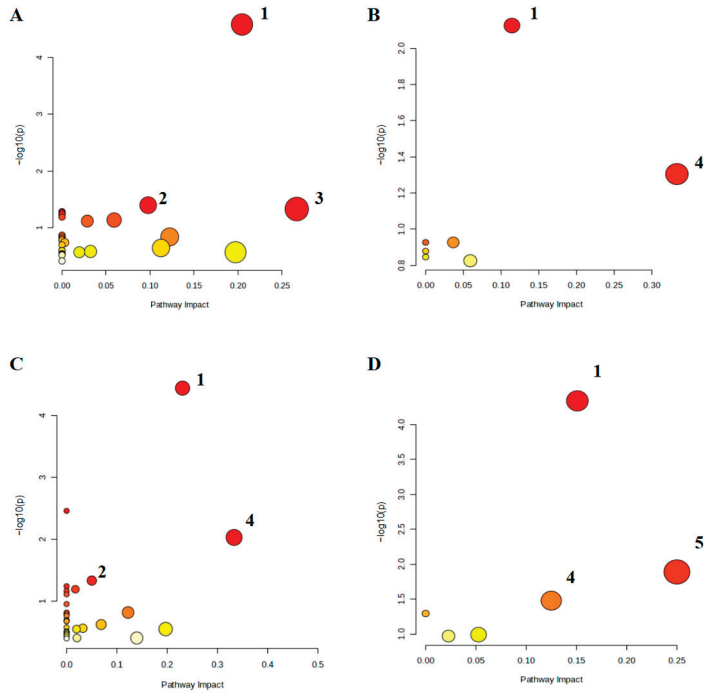


Figure 8. Heat map of differential metabolite expression in positive and negative ion modes in the lung tissue of mice in each group. (**A**–**D**) Differential metabolic pathways between the LPS and CON groups, the EBN and LPS groups, the SCP and LPS groups, and the SA and LPS groups. 1: glycerophospholipid metabolism, 2: purine metabolism, 3: glyoxylate and dicarboxylate metabolism, 4: alpha-linolenic acid metabolism, 5: linoleic acid metabolism.

4. Discussion

EBN proteins and carbohydrates are predominantly present as high-molecular-weight mucoproteins in the form of sialylated glycoproteins, which are characterized by low solubility and resistance to digestion [31]. In this study, EBN was digested using a two-step enzymatic hydrolysis protocol with Alcalase 2.4 L and papain. The contents of sialic acid (SA) and neutral sugars in SCP were both slightly higher than those in EBN, indicating that the optimization of the enzymatic hydrolysis process is conducive to the dissolution of neutral sugars and sialic acid [32]. Amino acids are the basic building blocks of proteins and polypeptides, and their composition and proportion are important factors influencing the physicochemical properties, biological activities, and other aspects of glycopeptides [33]. In this study, the contents of nine essential amino acids in SCP were abundant, according to the nutritional standards of essential amino acids recommended by the FAO/WHO. SCP has the potential to be an excellent choice for supplementing essential amino acids. Studies have shown that Asn is the main site where the sugar chain is linked to the protein during the *N*-glycosylation process, and Thr and Ser are the main sites where the sugar chain is linked to the protein during the O-glycosylation process [34]. The abundant

contents of these three amino acids in SCP indicated that there may be certain glycosylation modifications in SCP.

It was revealed by electrophoretic analysis that glycoproteins retained high molecular weights due to the tight conjugation of glycan and protein. After hydrolysis, the molecular weights of glycoproteins were reduced, and non-glycan-conjugated proteins were further degraded into smaller peptides [22]. This observation suggested that peptide bonds in glycoproteins were selectively targeted by enzymatic cleavage; low-molecular-weight peptides were released while glycan chains covalently bound to residual peptide fragments were preserved. The resistance of glycan-peptide conjugated to enzymatic degradation implies that the cleavage sites of Alcalase 2.4 L and papain are likely to be distant from glycosylation sites in EBN glycoproteins. Thus, the integrity of the glycan was maintained during hydrolysis. Furthermore, SCP displayed typical peptide and carbohydrate features, with spectral profiles resembling those of quinoa and *Stichopus japonicus* glycopeptides [35,36]. Compared to EBN, enhanced 1401 cm^{-1} ($-COO-$ symmetric stretching) and 1066 cm^{-1} (carbohydrate C-O) absorptions in SCP likely reflected increased SA and total carbohydrate content post-purification, confirming successful enrichment of glycan-rich moieties consistent with its sialylated glycopeptide identity.

The findings based on the C57BL/6 mouse model shared fundamental biological similarities with those based on human lung inflammation in LPS-induced mechanisms, and the experimental methods were universally used in the field, supporting the results' reference value for similar inflammatory mechanism studies. LPS induced significantly elevated lung pro-inflammatory cytokine levels (TNF-α, IL-1β, and IL-6) and inflammatory cell counts (Neu, WBC, Eos, and Mon) in BALF, confirming the induction of lung inflammation. Increased inflammatory cell infiltration can reflect the immune system's response to inflammatory stimuli, with cell counts as direct indicators of inflammatory severity [37,38]. In our study, all intervention groups significantly attenuated these inflammatory markers, with the SCP group demonstrating superior efficacy compared to EBN and SA groups, suggesting SCP as the primary bioactive component in EBN. In addition, the W/D ratio of lung issues, a key indicator of lung edema, was markedly increased in the LPS group, indicative of fluid accumulation in alveolar and interstitial spaces [39]. This observation was corroborated by histopathological analysis, which revealed alveolar structural damage, interstitial exudation, and neutrophil infiltration in the LPS group. Intervention groups alleviated lung tissue injury, with SCP exhibiting the most pronounced restorative effects. These findings align with prior studies showing that glycoprotein-bound SA exhibits enhanced anti-inflammatory activity compared to free SA [40].

Metabolomic profiling was conducted to elucidate SCP-mediated regulatory mechanisms on LPS-induced metabolic perturbations in the lung [41]. PCA and OPLS-DA demonstrated distinct metabolic profile alterations in the LPS group, with a clear separation between LPS and intervention groups, indicating metabolic homeostasis restoration. KEGG pathway enrichment analysis revealed that SCP primarily modulated glycerophospholipid, purine, and alpha-linolenic acid metabolism.

Glycerophospholipids, essential components of cellular membranes, are critically involved in membrane stability and functionality [42]. This study's glycerophospholipid-related metabolites accounted for the highest proportion of differential metabolites. Moreover, choline and lysophosphatidylcholines (LysoPCs) have been identified as biomarkers associated with lipid metabolism-related chronic lung diseases [43]. Choline, a key precursor for phosphatidylcholine synthesis, is integral to membrane integrity. Under LPS-induced lung inflammation, elevated choline levels in the LPS group may reflect compensatory mechanisms to enhance choline synthesis or uptake for membrane repair [44]. Notably, SCP intervention increased choline content, suggesting that SCP may indirectly

modulate choline metabolism by promoting synthesis or suppressing catabolism to support membrane homeostasis.

Purine metabolism dysregulation has been implicated in pulmonary injury and inflammation [45]. Xanthine, a key intermediate in purine metabolism, exacerbates oxidative stress and inflammatory responses when excessively accumulated. This study observed elevated xanthine levels in the LPS group, which may be attributable to the LPS-induced disruption of purine metabolic pathways, including enzymatic activation promoting xanthine synthesis [46]. Concurrently, LPS-mediated renal impairment increases uric acid production [47]. Following SCP intervention, xanthine levels were significantly reduced, suggesting the restoration of purine metabolism toward uric acid conversion. However, elevated uric acid levels persisted, potentially due to impaired renal clearance capacity. These findings indicate that SCP can alleviate LPS-induced lung inflammation partially through xanthine level modulation.

Alpha-linolenic acid, an essential fatty acid critical for maintaining physiological homeostasis, exhibits anti-inflammatory and antioxidant properties [48]. This study significantly reduced alpha-linolenic acid levels in the LPS group, likely due to its extensive consumption to counteract LPS-induced inflammatory responses [49]. Notably, alpha-linolenic acid levels were restored in the SCP intervention group. This restoration may be attributed to the SCP-mediated modulation of metabolic enzyme activity, which reduced inflammatory cell-driven alpha-linolenic acid depletion. These findings suggested that the anti-inflammatory effects of SCP against LPS-induced lung inflammation were mediated through the upregulation of endogenous alpha-linolenic acid levels.

5. Conclusions

In this study, SCP extracted from EBN exhibited typical structures of polypeptides and carbohydrates. EBN, SCP, and SA exerted effects on the level of pulmonary inflammation, the pathological structure of lung tissues, and the metabolic level of lung tissues, effectively improving the LPS-induced pulmonary inflammatory state in mice. Specifically, after SCP intervention, the number of Neu in BALF, the level of TNF-α in lung tissues, and the W/D ratio of lung tissues were significantly reduced. Moreover, the morphology of mouse lung tissues after SCP intervention was most similar to that of the CON group. SCP rectified the metabolic profiles of mice with pulmonary inflammation, regulated the expression of differential metabolites in lung tissues, such as choline, linolenic acid, and xanthine, and promoted the restoration of glycerophospholipid metabolism, alpha-linolenic acid metabolism, and purine metabolism pathways. However, the mechanism of action of SCP in vivo is complex and requires further investigation.

Author Contributions: Conceptualization, X.C. and D.W.; methodology, S.Q. and Q.L.; investigation, Q.L. and C.Z.; data curation, Q.L. and C.Z.; writing—original draft preparation, Q.L. and G.F.; writing—review and editing, N.Q., S.Q., M.Y., X.C. and D.W.; visualization, S.Q., M.Y. and D.W.; supervision, X.C. and D.W. All authors have read and agreed to the published version of the manuscript.

Funding: This research received no external funding.

Institutional Review Board Statement: The animal study protocol was approved by the Experimental Animal Welfare and Ethics Review Committee of Jiangnan University (JN.No20230415c0800705[145], approval date: 15 April 2023).

Informed Consent Statement: Not applicable.

Data Availability Statement: The original contributions presented in the study are included in the article, further inquiries can be directed to the corresponding author.

Conflicts of Interest: Hebei Edible Bird's Nest Fresh Stew Technology Innovation Center focuses on technological research and development in the field of instant bird's nest fresh stewing and is responsible for the transformation and application of related technologies in the Beijing Xiaoxiandun Biotechnology Co., Ltd. (Beijing, China). Jiangnan University has carried out collaborative research with the Hebei Edible Bird's Nest Instant Fresh Stew Technology Innovation Center, and the relevant work has been advanced based on the independent research plans of the cooperative laboratory and the technical service needs of the industry. The authors solemnly declare that there are no conflicts of interest involved. The research work described in this manuscript was carried out in strict accordance with scientific principles and ethical standards. All the authors have fulfilled their responsibilities in an unbiased manner, ensuring that the presented research findings are reliable and free from any undue influence.

References

1. Wang, M.; Qing, Y.; Fan, Q.; Li, S.; Yan, T.; Amakye, W.K.; Xu, Y.; Liu, X.; Ren, J. Identification of the Wound Healing Activity Peptidome of Edible Bird's Nest Protein Hydrolysate and the In Silico Evaluation of Its Transport and Absorption Potential in Skin. *J. Agric. Food Chem.* **2024**, *72*, 12529–12540. [CrossRef]
2. Dai, Y.; Cao, J.; Wang, Y.; Chen, Y.; Jiang, L. A comprehensive review of edible bird's nest. *Food Res. Int.* **2021**, *140*, 109875. [CrossRef]
3. Ling, J.W.A.; Chang, L.S.; Babji, A.S.; Latip, J.; Koketsu, M.; Lim, S.J. Review of sialic acid's biochemistry, sources, extraction and functions with special reference to edible bird's nest. *Food Chem.* **2022**, *367*, 130755. [CrossRef]
4. Quek, M.C.; Chin, N.L.; Yusof, Y.A.; Law, C.L.; Tan, S.W. Characterization of edible bird's nest of different production, species and geographical origins using nutritional composition, physicochemical properties and antioxidant activities. *Food Res. Int.* **2018**, *109*, 35–43. [CrossRef] [PubMed]
5. Careena, S.; Sani, D.; Tan, S.N.; Lim, C.W.; Hassan, S.; Norhafizah, M.; Kirby, B.P.; Ideris, A.; Stanslas, J.; Bin Basri, H.; et al. Effect of Edible Bird's Nest Extract on Lipopolysaccharide-Induced Impairment of Learning and Memory in Wistar Rats. *Evid.-Based Complement. Altern. Med.* **2018**, *2018*, 9318789. [CrossRef] [PubMed]
6. Rashed, A.A.; Ahmad, H.; Abdul Khalid, S.K.; Rathi, D.-N.G. The Potential Use of Sialic Acid from Edible Bird's Nest to Attenuate Mitochondria Dysfunction by In Vitro Study. *Front. Pharmacol.* **2021**, *12*, 633303. [CrossRef]
7. Ling, J.W.A.; Chang, L.S.; Babji, A.S.; Lim, S.J. Recovery of value-added glycopeptides from edible bird's nest (EBN) co-products: Enzymatic hydrolysis, physicochemical characteristics and bioactivity. *J. Sci. Food Agric.* **2020**, *100*, 4714–4722. [CrossRef] [PubMed]
8. Ou, Y.; Ma, J.H.; Tang, S.; Yu, Z.; Liu, S. Lycium barbarum Glycopeptide alleviated retinal inflammation via NF-κB/MAPK pathways in microglial cells. *Investig. Ophthalmol. Vis. Sci.* **2024**, *65*, 205.
9. He, H.; Wang, J.; Gong, P.; Xiao, Y.; Li, S.; Wang, J.; Geng, F. Structural identification and immunomodulatory effects of chicken egg white glycopeptides. *LWT* **2024**, *200*, 116195. [CrossRef]
10. Zeng, H.; Jian, Y.; Xie, Y.; Fan, Q.; Chang, Q.; Zheng, B.; Zhang, Y. Edible bird's nest inhibits the inflammation and regulates the immunological balance of lung injury mice by SO_2. *Food Front.* **2022**, *3*, 773–784. [CrossRef]
11. Ma, F.; Liu, D. Sketch of the edible bird's nest and its important bioactivities. *Food Res. Int.* **2012**, *48*, 559–567. [CrossRef]
12. Cheng, X.R.; Zhang, C.X.; Zhao, X.Y.; Li, Q.S.; Song, Y.; Zhang, L.; Ma, J.H.; Chen, Y.Y.; Yuan, M.; Wang, D.L. Prophylactic effects of sialylated glycopeptides from edible bird's nest on neuroinflammation in lipopolysaccharide-treated mice via the gut-brain axis. *Food Sci. Hum. Wellness* **2024**. [CrossRef]
13. Ahmad, S.; Zhang, X.L.; Ahmad, A. Epigenetic regulation of pulmonary inflammation. *Semin. Cell Dev. Biol.* **2024**, *154*, 346–354. [CrossRef] [PubMed]
14. Pervizaj-Oruqaj, L.; Ferrero, M.R.; Matt, U.; Herold, S. The guardians of pulmonary harmony: Alveolar macrophages orchestrating the symphony of lung inflammation and tissue homeostasis. *Eur. Respir. Rev.* **2024**, *33*, 230263. [CrossRef]
15. Zhong, Y.; Zhu, J.; Zhu, B.; Yin, H.; Wang, D.; Deng, Y.; Zhang, M.; Zhang, C. Recent advances in the structure and immunomodulatory activity of food-derived glycoprotein complex. *J. Future Foods* **2025**, *5*, 542–550. [CrossRef]
16. Xie, Y.K.; Pan, X.Y.; Liang, X.R.; Zhai, K.F.; Yu, Q. Research progress on structural characterization and bioactivities of Poria cocos and Ganoderma polysaccharides. *Food Med. Homol.* **2025**, *2*, 9420040. [CrossRef]
17. Fan, Y.; Wang, W.; Wang, X.; Yu, L.; Wei, Y.; Wei, L.; Xie, X.; Li, X. Ganoderma lucidum polysaccharide inhibits LPS-induced inflammatory injury to mammary epithelial cells. *J. Future Foods* **2023**, *3*, 49–54. [CrossRef]
18. Ye, J.; Guan, M.; Lu, Y.; Zhang, D.; Li, C.; Zhou, C. Arbutin attenuates LPS-induced lung injury via Sirt1/Nrf2/NF-κBp65 pathway. *Pulm. Pharmacol. Ther.* **2019**, *54*, 53–59. [CrossRef]

19. Gao, Z.; Liu, X.; Wang, W.; Yang, Q.; Dong, Y.; Xu, N.; Zhang, C.; Song, X.; Ren, Z.; Zhao, F.; et al. Characteristic anti-inflammatory and antioxidative effects of enzymatic- and acidic- hydrolysed mycelium polysaccharides by *Oudemansiella radicata* on LPS-induced lung injury. *Carbohydr. Polym.* **2019**, *204*, 142–151. [CrossRef]
20. Wang, S.; Tan, S.; Beng, H.; Liu, F.; Huang, J.; Kuai, Y.; Zhang, R.; Tan, W. Protective effect of isosteviol sodium against LPS-induced multiple organ injury by regulating of glycerophospholipid metabolism and reducing macrophage-driven inflammation. *Pharmacol. Res.* **2021**, *172*, 105781. [CrossRef]
21. Wang, X.; Zhang, K.; Zhang, J.; Xu, G.; Guo, Z.; Lu, X.; Liang, C.; Gu, X.; Huang, L.; Liu, S.; et al. Cordyceps militaris solid medium extract alleviates lipopolysaccharide-induced acute lung injury via regulating gut microbiota and metabolism. *Front. Immunol.* **2025**, *15*, 1528222. [CrossRef] [PubMed]
22. Hui Yan, T.; Mun, S.L.; Lee, J.L.; Lim, S.J.; Daud, N.A.; Babji, A.S.; Sarbini, S.R. Bioactive sialylated-mucin (SiaMuc) glycopeptide produced from enzymatic hydrolysis of edible swiftlet's nest (ESN): Degree of hydrolysis, nutritional bioavailability, and physicochemical characteristics. *Int. J. Food Prop.* **2022**, *25*, 252–277. [CrossRef]
23. Doerner, K.C.; White, B.A. Detection of glycoproteins separated by nondenaturing polyacrylamide gel electrophoresis using the periodic acid-Schiff stain. *Anal. Biochem.* **1990**, *187*, 147–150. [CrossRef]
24. Martins, M.S.; Nascimento, M.H.; Barbosa, L.L.; Campos, L.C.G.; Singh, M.N.; Martin, F.L.; Romão, W.; Filgueiras, P.R.; Barauna, V.G. Detection and quantification using ATR-FTIR spectroscopy of whey protein concentrate adulteration with wheat flour. *LWT* **2022**, *172*, 114161. [CrossRef]
25. Chen, X.; Yang, X.; Liu, T.; Guan, M.; Feng, X.; Dong, W.; Chu, X.; Liu, J.; Tian, X.; Ci, X.; et al. Kaempferol regulates MAPKs and NF-κB signaling pathways to attenuate LPS-induced acute lung injury in mice. *Int. Immunopharmacol.* **2012**, *14*, 209–216. [CrossRef]
26. Cheng, X.R.; Guan, L.J.; Muskat, M.N.; Cao, C.C.; Guan, B. Effects of Ejiao peptide–iron chelates on intestinal inflammation and gut microbiota in iron deficiency anemic mice. *Food Funct.* **2021**, *12*, 10887–10902. [CrossRef]
27. Hong, T.; Yin, J.Y.; Nie, S.P.; Xie, M.Y. Applications of infrared spectroscopy in polysaccharide structural analysis: Progress, challenge and perspective. *Food Chem: X* **2021**, *12*, 100168. [CrossRef] [PubMed]
28. Mistry, B. *A Handbook of Spectroscopic Data CHEMISTRY (UV, JR, PMR, JJCNMR and Mass Spectroscopy)*; Oxford Book Company Jaipur: Jaipur, India, 2009; pp. 39–42.
29. Mohamad Ibrahim, R.; Mohamad Nasir, N.N.; Abu Bakar, M.Z.; Mahmud, R.; Ab Razak, N.A. The Authentication and Grading of Edible Bird's Nest by Metabolite, Nutritional, and Mineral Profiling. *Foods* **2021**, *10*, 1574. [CrossRef]
30. Liu, H.; Wang, J.; Zhao, J.; Gu, S.; Chen, S.; Jia, W.; Huang, S.; Wu, J. *Potentilla anserina* L. polysaccharide ameliorates LPS-induced acute lung injury and relevant intestinal mucosal barrier impairment. *Int. J. Biol. Macromol.* **2025**, *305*, 140667. [CrossRef]
31. Zhang, S.; Lai, X.; Liu, X.; Li, Y.; Li, B.; Huang, X.; Zhang, Q.; Chen, W.; Lin, L.; Yang, G. Competitive Enzyme-Linked Immunoassay for Sialoglycoprotein of Edible Bird's Nest in Food and Cosmetics. *J. Agric. Food Chem.* **2012**, *60*, 3580–3585. [CrossRef]
32. Sriwilaijaroen, N.; Hanamatsu, H.; Yokota, I.; Nishikaze, T.; Ijichi, T.; Takahashi, T.; Sakoda, Y.; Furukawa, J.-I.; Suzuki, Y. Edible bird's nest: N- and O-glycan analysis and synergistic anti-avian influenza virus activity with neuraminidase inhibitors. *Antivir. Res.* **2024**, *232*, 106040. [CrossRef] [PubMed]
33. Bourgoin-Voillard, S.; Goron, A.; Seve, M.; Moinard, C. Regulation of the proteome by amino acids. *Proteomics* **2016**, *16*, 831–846. [CrossRef] [PubMed]
34. Shim, E.K.S.; Chandra, G.F.; Lee, S.-Y. Thermal analysis methods for the rapid identification and authentication of swiftlet (*Aerodramus fuciphagus*) edible bird's nest—A mucin glycoprotein. *Food Res. Int.* **2017**, *95*, 9–18. [CrossRef] [PubMed]
35. Yu, Y.; Shi, Y. Investigation the interaction between quinoa glycopeptides and polyphenol: Spectroscopic analyses and antioxidant activities. *J. Food Meas. Charact.* **2023**, *17*, 5594–5605. [CrossRef]
36. Sun, N.; Cui, P.; Lin, S.; Yu, C.; Tang, Y.; Wei, Y.; Xiong, Y.; Wu, H. Characterization of sea cucumber (*Stichopus japonicus*) ovum hydrolysates: Calcium chelation, solubility and absorption into intestinal epithelial cells. *J. Sci. Food Agric.* **2017**, *97*, 4604–4611. [CrossRef]
37. Medzhitov, R. The spectrum of inflammatory responses. *Science* **2021**, *374*, 1070–1075. [CrossRef]
38. Ning, E.-J.; Sun, C.-W.; Wang, X.-F.; Chen, L.; Li, F.-F.; Zhang, L.-X.; Wang, L.-P.; Ma, Y.-N.; Zhu, J.; Li, X.; et al. Artemisia argyi polysaccharide alleviates intestinal inflammation and intestinal flora dysbiosis in lipopolysaccharide-treated mice. *Food Med. Homol.* **2024**, *1*, 9420008. [CrossRef]
39. Bezerra, F.S.; Lanzetti, M.; Nesi, R.T.; Nagato, A.C.; Silva, C.P.E.; Kennedy-Feitosa, E.; Melo, A.C.; Cattani-Cavalieri, I.; Porto, L.C.; Valenca, S.S. Oxidative Stress and Inflammation in Acute and Chronic Lung Injuries. *Antioxidants* **2023**, *12*, 548. [CrossRef]
40. Qian, N.; Zhang, C.-X.; Fang, G.-D.; Qiu, S.; Song, Y.; Yuan, M.; Wang, D.-L.; Cheng, X.-R. Interventional Effects of Edible Bird's Nest and Free Sialic Acids on LPS-Induced Brain Inflammation in Mice. *Nutrients* **2025**, *17*, 531. [CrossRef]
41. Pang, H.; Hu, Z. Metabolomics in drug research and development: The recent advances in technologies and applications. *Acta Pharm. Sin. B* **2023**, *13*, 3238–3251. [CrossRef]

42. Sarkar, C.; Lipinski, M.M. Glycerophospholipid dysregulation after traumatic brain injury. *Neurochem. Int.* **2024**, *175*, 105701. [CrossRef] [PubMed]
43. Nambiar, S.; Bong How, S.; Gummer, J.; Trengove, R.; Moodley, Y. Metabolomics in chronic lung diseases. *Respirology* **2020**, *25*, 139–148. [CrossRef] [PubMed]
44. Gong, X.; Guo, C.; Huang, S.; Sun, B. Inhaled nitric oxide alleviates hyperoxia suppressed phosphatidylcholine synthesis in endotoxin-induced injury in mature rat lungs. *Respir. Res.* **2006**, *7*, 5. [CrossRef] [PubMed]
45. Li, J.; Hu, Y.; Liu, L.; Wang, Q.; Zeng, J.; Chen, C. PM2.5 exposure perturbs lung microbiome and its metabolic profile in mice. *Sci. Total Environ.* **2020**, *721*, 137432. [CrossRef]
46. Hassoun, P.M.; Yu, F.-S.; Cote, C.G.; Zulueta, J.J.; Sawhney, R.; Skinner, K.A.; Skinner, H.B.; Parks, D.A.; Lanzillo, J.J. Upregulation of Xanthine Oxidase by Lipopolysaccharide, Interleukin-1, and Hypoxia. *Am. J. Respir. Crit. Care Med.* **1998**, *158*, 299–305. [CrossRef] [PubMed]
47. Zhang, W.; Qi, R.; Li, T.; Zhang, X.; Shi, Y.; Xu, M.; Zhu, T. Kidney Organoids as a Novel Platform to Evaluate Lipopolysaccharide-Induced Oxidative Stress and Apoptosis in Acute Kidney Injury. *Front. Med.* **2021**, *8*, 766073. [CrossRef]
48. Yuan, Q.; Xie, F.; Huang, W.; Hu, M.; Yan, Q.; Chen, Z.; Zheng, Y.; Liu, L. The review of alpha-linolenic acid: Sources, metabolism, and pharmacology. *Phytother. Res.* **2022**, *36*, 164–188. [CrossRef]
49. Zhu, X.; Wang, B.; Zhang, X.; Chen, X.; Zhu, J.; Zou, Y.; Li, J. Alpha-linolenic acid protects against lipopolysaccharide-induced acute lung injury through anti-inflammatory and anti-oxidative pathways. *Microb. Pathog.* **2020**, *142*, 104077. [CrossRef]

Disclaimer/Publisher's Note: The statements, opinions and data contained in all publications are solely those of the individual author(s) and contributor(s) and not of MDPI and/or the editor(s). MDPI and/or the editor(s) disclaim responsibility for any injury to people or property resulting from any ideas, methods, instructions or products referred to in the content.

nutrients

MDPI

Article

Coix Seed Oil Alleviates Hyperuricemia in Mice by Ameliorating Oxidative Stress and Intestinal Microbial Composition

Guozhen Wu [1,2,†], Xinming Wang [3,†], Hongjing Dong [1], Jinqian Yu [1], Tao Li [1,*] and Xiao Wang [4,*]

[1] Shandong Engineering Research Center for Innovation and Application of General Technology for Separation of Natural Products, Shandong Analysis and Test Center, Qilu University of Technology (Shandong Academy of Sciences), Jinan 250014, China
[2] School of Pharmaceutical Sciences, Shandong University of Traditional Chinese Medicine, Jinan 250355, China
[3] Institute of Chinese Materia Medica Chemistry, Shandong Academy of Chinese Medicine, Jinan 250014, China
[4] Key Laboratory for Natural Active Pharmaceutical Constituents Research in Universities of Shandong Province, School of Pharmaceutical Sciences, Qilu University of Technology (Shandong Academy of Sciences), Jinan 250014, China
* Correspondence: litaosd@qlu.edu.cn (T.L.); wangx@sdas.org (X.W.); Tel.: +86-531-82964889 (X.W.)
† These authors contributed equally to this work.

Abstract: Background: Coix seed oil (YRO), rich in unsaturated fatty acids, has emerged as a promising intervention for hyperuricemia (HUA) due to its potential to alleviate oxidative damage and support organ health. **Methods**: The fatty acid composition of YRO was determined by gas chromatography–mass spectrometry (GC-MS). A HUA mouse model was established, and serum markers and hepatic enzymes were evaluated. Renal mitochondrial function was assessed using immunohistochemistry and immunofluorescence, and urate transporter expression, along with key signaling proteins, was quantified by Western blot analysis. Additionally, gut microbiota composition was analyzed, and non-targeted metabolomics was performed to observe alterations in serum lipid metabolites. **Results**: YRO significantly reduced serum uric acid (UA) levels and normalized hepatic enzyme activities. Histological evaluation revealed less tissue damage in both the kidney and the intestine. In the kidney, YRO improved mitochondrial function and supported antioxidant defenses via regulation of Keap1/Nrf2 signaling. In the intestine, YRO enhanced barrier integrity by increasing ZO-1, Occludin, and Claudin-1 expression. Moreover, YRO modulated gut microbiota by increasing beneficial bacteria (*Muribaculaceae*, *Prevotellaceae UCG-001*, *Lachnospiraceae_ NK4A136_group*, *Akkermansia*) while suppressing harmful species (*Bacteroides*, *Dubosiella*). Lipid metabolomics indicated a restoration of phospholipid balance through modulation of the PI3K/AKT/mTOR pathway. **Conclusions**: YRO supported metabolic health by promoting UA homeostasis, enhancing mitochondrial function, reinforcing antioxidant capacity, and maintaining gut integrity. These findings suggest that coix seed oil could serve as a nutritional supplement in managing HUA and related metabolic disturbances.

Keywords: coix seed oil; hyperuricemia; oxidative stress; gut microbiota; lipid metabolism

1. Introduction

Hyperuricemia (HUA) is a common metabolic disorder marked by elevated serum uric acid (UA) levels [1]. It results from excessive UA production or impaired renal and intestinal excretion [2]. Recent studies indicate that HUA is the second most prevalent metabolic disorder after diabetes, raising significant public health concerns [3]. Persistent

UA accumulation leads to oxidative stress, inflammation, and organ dysfunction, contributing to gout, renal dysfunction, and metabolic syndrome [4,5]. As diet plays a crucial role in UA metabolism, exploring food-based approaches for HUA management has gained increasing attention.

Coix seed (*Coix lacryma-jobi* L.), known as Yi Yiren in Chinese, has long been incorporated into daily diets in East Asia for its nutritional and functional properties [6]. It is rich in bioactive compounds and has been consumed for centuries as a traditional dietary supplement with potential health benefits. Emerging evidence indicated that coix seed might contribute to UA regulation, yet its key bioactive components and precise mechanisms remain unclear [7]. Coix seed oil, a major component of coix seed, is particularly rich in unsaturated fatty acids (UFAs), which are known to support oxidative balance and organ protection [8,9]. Furthermore, recent studies demonstrated that functional oils could significantly modulate gut microbiota composition and metabolic pathways, influencing immune responses and physiological homeostasis [10,11]. Given these properties, coix seed oil holds promise for the development of functional food products targeting HUA management.

The kidney is the primary organ responsible for UA excretion and exhibits high metabolic activity with a dense mitochondrial network [12]. Excessive UA accumulation disrupts mitochondrial homeostasis, leading to elevated reactive oxygen species production, which further exacerbates cellular damage [13]. The Keap1/Nrf2 pathway serves as a defense system by activating antioxidant enzymes such as HO-1 and NQO-1, protecting cells from UA-induced oxidative injury [14,15]. When renal UA excretion is impaired, compensatory mechanisms enhance the elimination of intestinal UA [16]. However, this process often disrupts gut microbiota composition and reduces short-chain fatty acids (SCFAs) production, further affecting UA metabolism [17,18]. Importantly, UA homeostasis is intricately intertwined with broader metabolic networks. Recent studies highlighted its close linkage to lipid metabolism [19]. For instance, abnormal glycerophospholipid levels not only impair renal tubular function but also interfere with UA transport mechanisms, potentially exacerbating systemic metabolic dysregulation [20].

This study investigates the mechanisms of YRO in HUA management by analyzing renal and intestinal tissues, gut microbiota, and lipid metabolites. It aims to establish a foundation for future research on YRO as a functional food ingredient with potential applications in metabolic health.

2. Materials and Methods

2.1. Materials and Reagents

Coix seeds were purchased from BWT Chinese Herbal Medicine Drinks Slice Co., Ltd. (Jinan, China). Potassium oxonate (PO) was obtained from Shanghai Macklin Biochemical Technology Co., Ltd. (Shanghai, China). Hypoxanthine (HX) and sodium carboxymethyl cellulose (CMC) were supplied by Shanghai Yuanye Bio-Technology Co., Ltd. (Shanghai, China). Detailed information on antibodies used in this study was provided in Table S1.

2.2. Extraction, Esterification, and GC-MS Analysis of Fatty Acids from YRO

YRO was extracted and esterified according to previously established methods with modifications [21,22]. Briefly, dried coix seeds were ground into powders and subjected to ultrasonic-assisted extraction using petroleum ether as the solvent. The extraction was performed twice at room temperature, with each cycle lasting 2 h. The combined extracts were filtered and concentrated under reduced pressure to obtain YRO. For methyl esterification, the YRO was treated with a sulfuric acid-methanol solution (2:98, v/v) and heated in a 70 °C water bath for 60 min. After cooling, the reaction mixture was extracted

with n-hexane to isolate the esterified compounds. The n-hexane layer was dried over anhydrous sodium sulfate, followed by filtration through a 0.45 μm membrane to yield the methyl-esterified YRO sample.

The composition of the fatty acid methyl esters was analyzed by gas chromatography-mass spectrometry (GC-MS) on a Shimadzu QP2020NX system (Kyoto, Japan) equipped with a quadrupole mass spectrometer and a DB5 column (30 m × 0.25 mm, 0.25 μm). The initial column temperature was set at 50 °C for 2 min, then increased at a rate of 6 °C/min to 250 °C, where it was held for 15 min. Helium was used as the carrier gas, with the injector temperature maintained at 250 °C and a split ratio of 1:30.

2.3. Animal Model and Experimental Design

All animal experiments were conducted following the ethical guidelines approved by the Animal Care and Ethics Committee at the Shandong Academy of Chinese Medicine (approval number: SDZYY20230621002, approval on 25 May 2023). Male Kunming mice (25–28 g) were procured from Vital River Laboratory Animal Technology Co., Ltd. (Beijing, China). The mice were housed under controlled environmental conditions (12 h light/dark cycle, temperature 23 ± 2 °C, relative humidity 50 ± 10%) with free access to standard chow and ultrapure water. According to previous reports [23], as shown in Figure 1A, thirty-six Kunming mice were randomly assigned to six groups (n = 6 per group) using a randomized complete block design: control group (CON), HUA model group (MOD), allopurinol-treated group (APL; 5 mg/kg), and three YRO-treated groups (100, 200, and 400 mg/kg) [24]. Except for the CON group, all mice received 300 mg/kg PO (oral) and 300 mg/kg HX (intraperitoneal injection) daily for 21 consecutive days to induce HUA. One hour after the model induction, treatment groups received the corresponding doses of YRO or allopurinol by oral gavage once daily. At the end of the 21-day experimental period, mice were fasted for 12 h before sample collection. Blood, liver, kidney, and intestinal samples were collected for subsequent analysis.

2.4. Biochemical and Oxidative Stress Measurements

The levels of serum UA, blood urea nitrogen (BUN), and creatinine (CR) were measured by commercial assay kits (Jiancheng Biotechnology Institute, Nanjing, China). Hepatic xanthine oxidase (XOD) and adenosine deaminase (ADA) activities were also analyzed. Serum lipid parameters, including triglycerides (TG), total cholesterol (TC), low-density lipoprotein cholesterol (LDL-C), and high-density lipoprotein cholesterol (HDL-C), were quantified. Furthermore, the concentrations of renal oxidative indicators, including superoxide dismutase (SOD), malondialdehyde (MDA), and glutathione (GSH), were detected using kits procured from Beyotime Biotechnology Co., Ltd. (Shanghai, China).

2.5. Western Blot Analysis

Western blot analysis was conducted according to the method described by Lin et al. [25]. Total proteins were extracted from the kidney and intestine tissues using RIPA lysis buffer (Beyotime Biotechnology Co., Ltd., Shanghai, China). After quantification and denaturation, proteins were separated by SDS-PAGE and transferred onto PVDF membranes. The membranes were blocked and incubated overnight at 4 °C with specific primary antibodies. This was followed by incubation with HRP-conjugated secondary antibodies. Protein bands were visualized using the ECL imaging system and quantified with ImageJ software (version 1.53q, National Institutes of Health, Bethesda, MD, USA). β-Actin or GAPDH was used as the internal loading control to normalize the target protein expression levels.

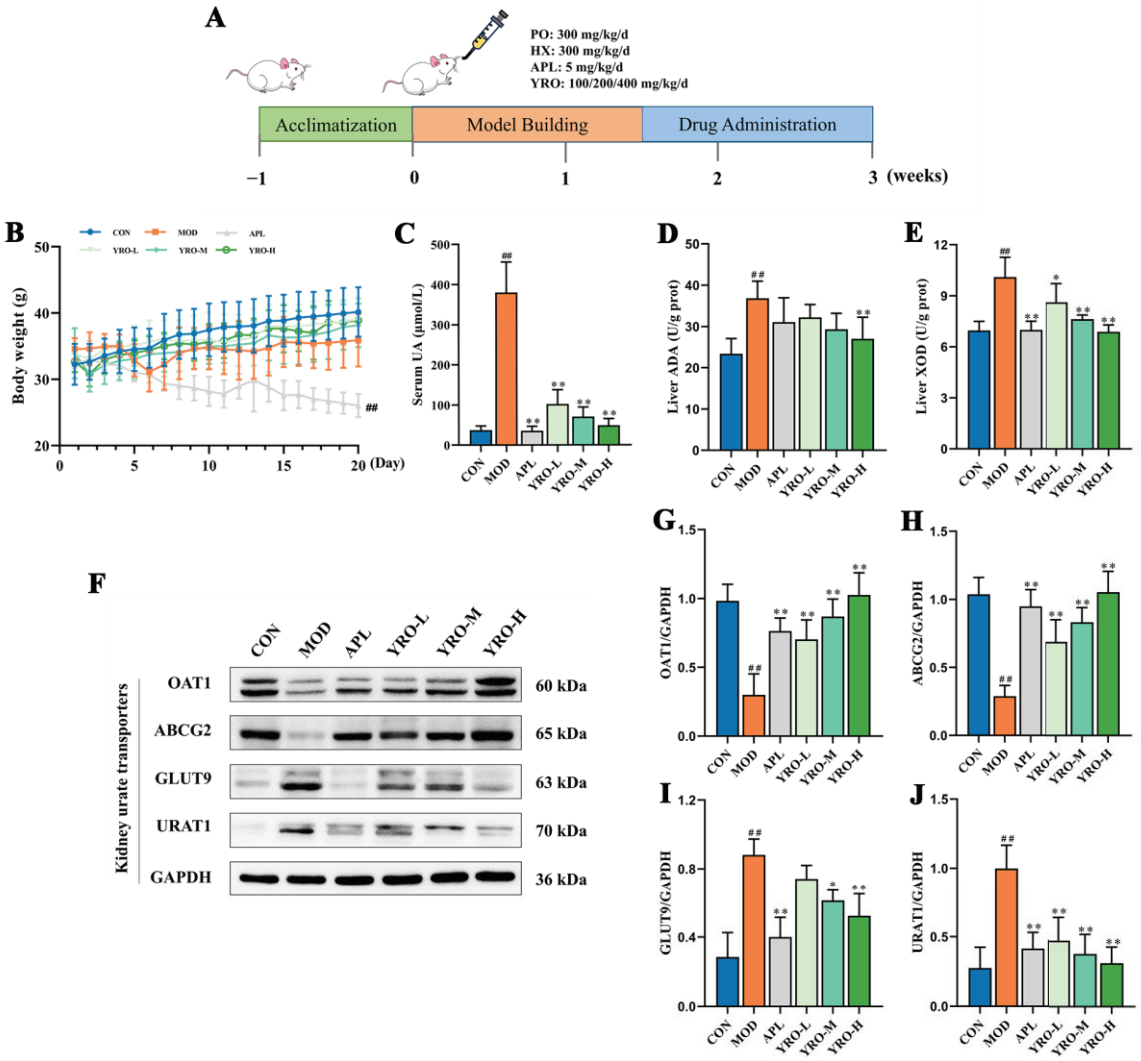


Figure 1. YRO alleviated HUA by improving UA metabolism. (**A**) Experimental scheme of animal procedures; (**B**) Changes in body weight during the experimental period; (**C**) Serum UA levels; (**D**) Hepatic ADA and (**E**) XOD activities; (**F**) Western blot analysis of renal urate transporters. Quantified protein expression levels of (**G**) OAT1, (**H**) ABCG2, (**I**) GLUT9, and (**J**) URAT1. Data are expressed as means ± SD (n = 6 mice/group). $^{\#\#}$ $p < 0.01$ vs. CON group; * $p < 0.05$, ** $p < 0.01$ vs. MOD group.

2.6. Histology, Immunohistochemistry (IHC), and Immunofluorescence (IF) Analysis

Kidney and intestinal tissues were fixed in 4% paraformaldehyde, embedded in paraffin, and sectioned into 4 μm slices. For morphological evaluation, hematoxylin and eosin (H&E) was performed. Masson's trichrome staining was used for fibrosis quantification.

IHC analysis was performed to detect the expression of 8-OHdG, PINK1, and Parkin. Following deparaffinization, rehydration, and antigen retrieval in citrate buffer (pH 6.0), sections were blocked with 3% bovine serum albumin (BSA) and incubated overnight at 4 °C with primary antibodies. After incubation with HRP-conjugated secondary antibodies, staining was visualized using 3,3′-diaminobenzidine (DAB) and counterstained with hematoxylin [26]. IF staining was used to assess the expression of Mfn2 and FIS1. After antigen retrieval and blocking with 5% BSA, sections were incubated overnight at 4 °C with primary antibodies. This was followed by incubation with fluorescently labeled secondary antibodies and counterstaining with DAPI [27]. All stained sections were scanned using a digital slide scanner (KF-PRO-020, Kfbio, Ningbo, China), and quantitative analysis was performed using ImageJ software.

2.7. Microbial Community Composition and SCFAs Analysis

Six fecal samples were collected from each of the CON, MOD, and YRO-H groups one day before sacrifice to assess bacterial community composition. Genomic DNA was extracted using the E.Z.N.A.® DNA LQ Kit (Omega Bio-tek, Norcross, GA, USA). The V3-V4 region of the 16S rRNA gene was amplified with primers 338 F and 806R. DNA libraries were constructed using the NEXTFLEX Rapid DNA-Seq Kit (PerkinElmer, Waltham, MA, USA). Sequencing was performed on the Illumina PE300 platform (Illumina Inc., San Diego, CA, USA). Alpha diversity indices, including Coverage, Chao1, ACE, Sobs, Shannon, and Simpson, were calculated to evaluate microbial richness and diversity. Beta diversity was assessed using principal coordinate analysis (PCoA).

For SCFA analysis, fecal samples were extracted with 80% methanol. Derivatization was performed by adding 200 mM 3-nitrophenylhydrazine hydrochloride (3NPH·HCl) and 120 mM 1-ethyl-3-(3-dimethylaminopropyl) carbodiimide hydrochloride (EDC·HCl). The supernatants were analyzed using LC-MS/MS on an ExionLC™ AD system coupled with a QTRAP® 6500+ mass spectrometer (Sciex, Framingham, MA, USA). The SCFAs, including acetic acid, propionic acid, butyric acid, isobutyric acid, valeric acid, and isovaleric acid, were quantified.

2.8. Lipid Metabolomics Analysis of Serum

Serum samples were centrifuged, and the supernatant was collected for lipid extraction. Lipids were extracted using methyl tert-butyl ether/methanol (3/1, *v*/*v*) solution containing an internal standard (1000 μL). The lipid extract was then reconstituted in acetonitrile/isopropanol (1/1, *v*/*v*) and centrifuged again. The final supernatant was collected for UPLC-MS/MS analysis, following a modified protocol [28]. Lipid profiling was performed using a SCIEX ExionLC™ AD UPLC-QTRAR system (SCIEX, Framingham, MA, USA) equipped with the Thermo Accucore™ C30 column (2.1 × 100 mm, 2.6 μm; Thermo Fisher Scientific, Waltham, MA, USA). The mobile phases consisted of 60% acetonitrile in water (A) and 10% acetonitrile in isopropanol (B), both supplemented with 0.1% formic acid and 10 mM ammonium formate. The gradient elution program was as follows: 0 min 20% B, 2 min 30% B, 4 min 60% B, 9 min 85% B, and 14 min 90% B with a flow rate of 0.35 mL/min. Mass spectrometry detection was conducted in high-resolution mode with an electrospray ionization (ESI) source. The source temperature was set at 500 °C, with ionization voltages of 5.5 kV in positive mode and 4.5 kV in negative mode.

2.9. Statistical Analysis

Statistical analysis and data visualization were performed using GraphPad Prism 8.0 (San Diego, CA, USA). Data are presented as mean ± standard deviation (SD). One-way ANOVA followed by Tukey's post hoc test was used for comparisons among multiple groups, while comparisons between two groups were performed using independent-sample *t*-tests. A *p*-value of less than 0.05 was considered statistically significant. Statistical significance indicators are specified in the figure legends.

3. Results

3.1. Fatty Acid Composition of YRO

The fatty acid composition of YRO after methyl esterification is shown in Table S2 and Figure S1. GC-MS analysis, using the area normalization method, identified the methyl esters of 9-octadecenoic acid, 9,12-octadecadienoic acid (Z,Z), and hexadecanoic acid as the primary components. These results indicated that YRO was predominantly composed of unsaturated long-chain fatty acids, which account for 77.11% of the total fatty acids. The most abundant components were oleic acid (42.63%) and linoleic acid (22.36%). Previous

studies suggested that diets rich in UFAs could improve lipid metabolism [29], reduce oxidative stress [30], and suppress inflammation [31]. These properties suggest that YRO might offer therapeutic benefits for managing HUA.

3.2. YRO Modulated UA Metabolism in HUA Mice

The levels of serum UA in the MOD group (380.31 μmol/L) were significantly higher than in the CON group (37.53 μmol/L) ($p < 0.01$), confirming the successful establishment of the HUA model [32]. YRO treatment at doses of 100, 200, and 300 mg/kg/d reduced serum UA levels in a dose-dependent manner to 102.12, 70.93, and 49.21 μmol/L, respectively (Figure 1C). HUA led to a 63.80% and 45.03% increase in ADA and XOD activities, respectively, compared with the CON group ($p < 0.01$). This significant upregulation demonstrated enhanced catalytic efficiency in UA metabolism within the model group [33]. YRO significantly reduced the activities of ADA and XOD ($p < 0.05$), with the YRO-H group showing decreases of 28.41% and 31.75%, respectively (Figure 1D,E). The expression of renal urate transporters was significantly altered in HUA mice (Figure 1F). The protein expression levels of GLUT9 and URAT1 (urate reabsorption transporters) were elevated, whereas the levels of OAT1 and ABCG2 (urate excretion transporters) were reduced ($p < 0.05$). YRO normalized these transporters levels, showing similar effects to the APL group. These findings indicated that YRO lowered the levels of serum UA partly by the suppression of ADA and XOD activities and modulation of urate transporter expression.

3.3. YRO Attenuated HUA-Induced Renal Injury in HUA Mice

As shown in Figure 1B, body weight gain was significantly slower in the MOD group ($p < 0.05$), while the YRO-treated groups showed no significant difference from the CON group. The kidney-to-body weight ratio was significantly higher in the MOD group, indicating renal impairment. YRO intervention significantly reduced this ratio ($p < 0.01$; Figure 2A), implying improved kidney health. YRO intervention also significantly decreased the levels of CR and BUN ($p < 0.05$; Figure 2B,C), demonstrating its protective effect on renal function. The histopathological analysis further confirmed these findings. H&E staining revealed distinct pathological changes in the MOD group, including renal tubular cavity dilation, glomerular atrophy, and inflammatory cell infiltration. YRO treatment significantly alleviated these pathological changes (Figure 2E). Similarly, Masson's trichrome staining showed significant renal fibrosis in the MOD group ($p < 0.05$), which was progressively reduced by YRO (Figure 2D,F). These results indicate that YRO mitigates renal damage and fibrosis in HUA mice.

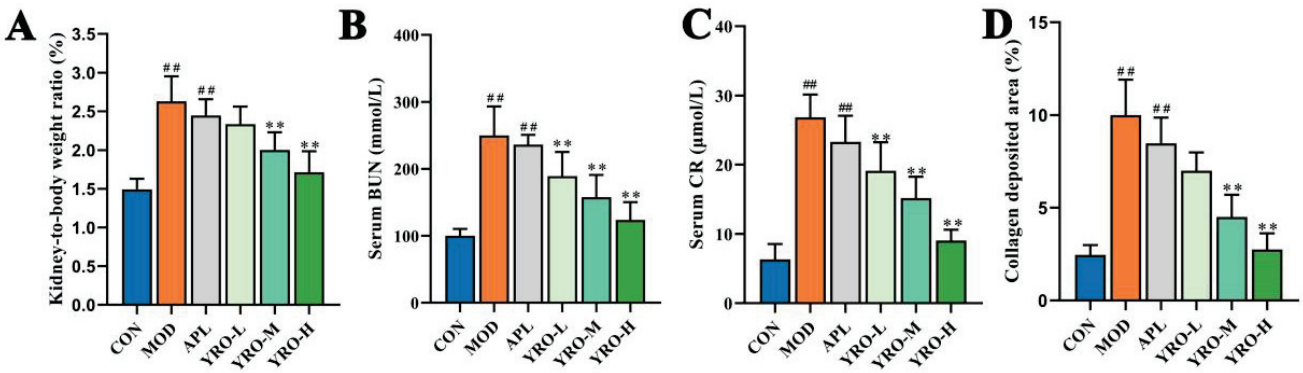


Figure 2. *Cont.*

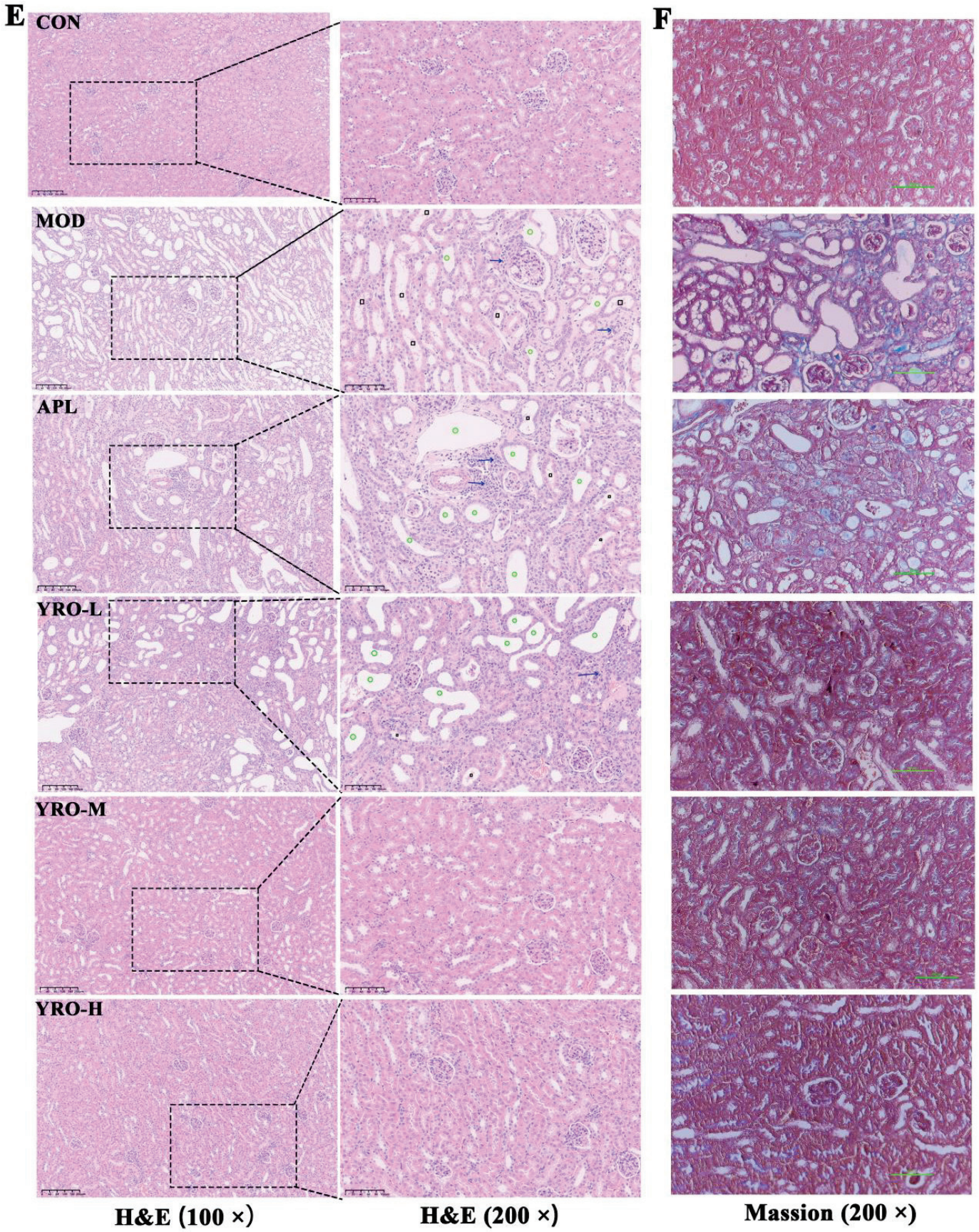


Figure 2. YRO mitigated renal injury in HUA mice. (**A**) Kidney organ coefficients; (**B**) BUN levels; (**C**) CR levels; (**D**) Quantification of the fibrotic area in Masson staining; Morphological assessment of kidney tissues by H&E (**E**) and Masson staining (**F**). Blue arrows, inflammatory cell infiltration; green circles, tubular ectasia; black squares, necrotic tubular epithelial cells. Data are expressed as means ± SD (n = 6 mice/group). $^{\#\#}$ $p < 0.01$ vs. CON group; ** $p < 0.01$ vs. MOD group.

3.4. YRO Mitigated Oxidative Stress and Mitochondrial Dysfunction in HUA Mice

Excessive UA induces oxidative stress, leading to cellular and mitochondrial damage [34]. In HUA mice, 8-OHdG levels were significantly elevated, indicating oxidative DNA damage, but YRO treatment markedly reduced its accumulation ($p < 0.05$, Figure 3A,B). Meanwhile, YRO supplementation reversed the elevation in MDA levels, and restored SOD activity and GSH levels (Figure 3C–E), indicating its antioxidant potential.

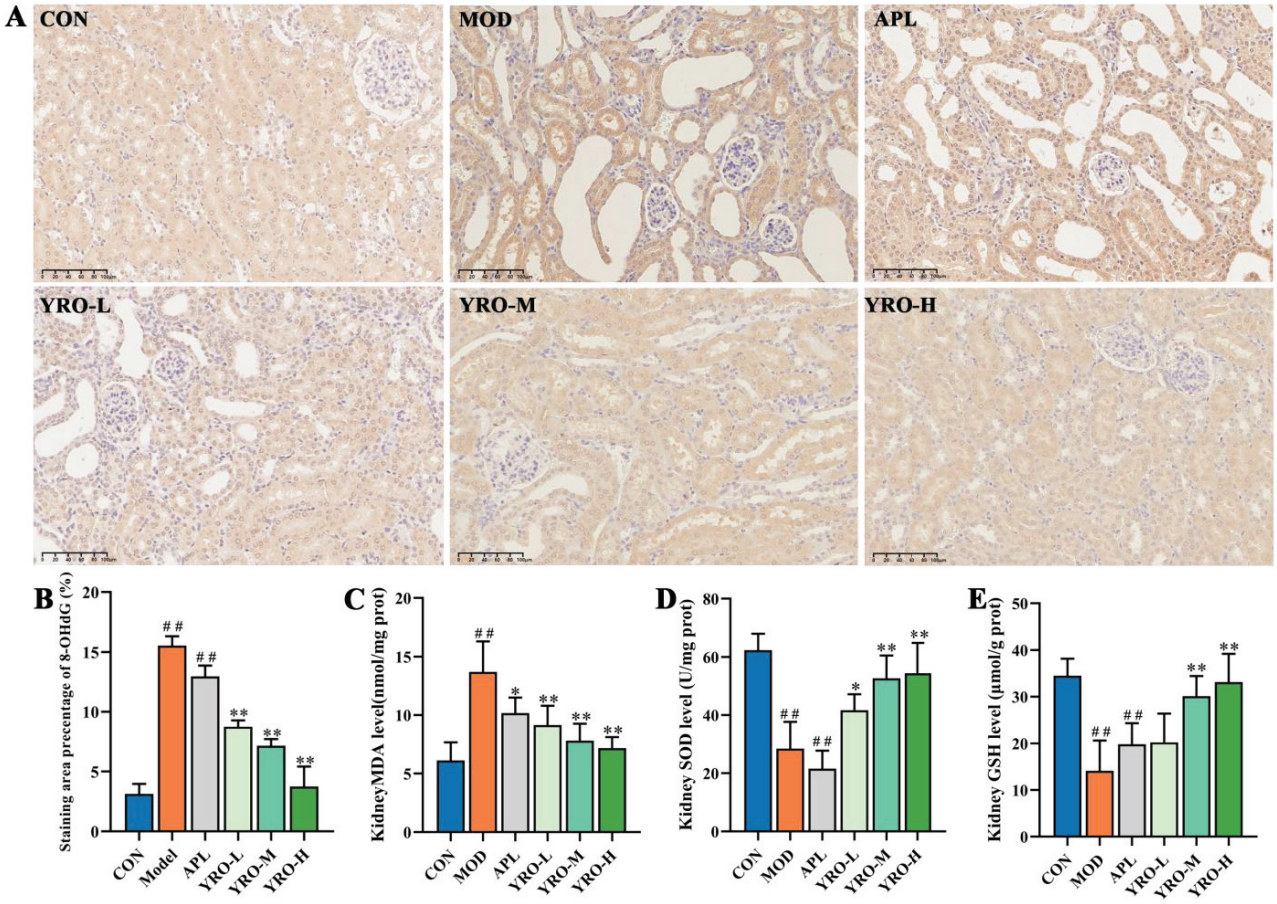


Figure 3. YRO reduced oxidative stress in HUA mice. (**A**) IHC staining of 8-OHdG in renal tubules (200×); (**B**) Quantitative analysis of 8-OHdG expression based on IHC results; (**C**–**E**) Levels of MDA, SOD, and GSH, representing oxidative damage and antioxidant capacity. Data are expressed as means ± SD (n = 6 mice/group). $^{\#\#}$ $p < 0.01$ vs. CON group; * $p < 0.05$, ** $p < 0.01$ vs. MOD group.

Given the mitochondrial-rich nature of renal tissues, we further investigated mitochondrial alterations in HUA mice [13]. IF analysis (Figure 4A,B) showed that the expression of Mfn2 was significantly decreased, whereas FIS1 expression was significantly increased in the MOD group ($p < 0.01$). YRO administration upregulated Mfn2 and downregulated FIS1 ($p < 0.05$), restoring mitochondrial fusion-fission balance. IHC analysis revealed that the levels of PINK1 and Parkin were significantly reduced in MOD kidneys ($p < 0.01$), indicating impaired mitophagy. YRO treatment upregulated PINK1 and Parkin, promoting mitochondrial quality control (Figure 4C,D).

To further elucidate the role of YRO in oxidative defense, the expression of key regulators in the Keap1/Nrf2 signaling pathway was examined, as it plays a critical role in maintaining redox balance [35]. Western blot analysis showed that Keap1 expression was significantly increased while Nrf2 levels were markedly suppressed in HUA mice ($p < 0.01$), impairing the antioxidant response. YRO intervention downregulated Keap1 and upregulated Nrf2, leading to the activation of NQO-1 and HO-1, two major antioxidant

enzymes (Figure 4E). These findings indicated that YRO enhanced mitochondrial function and antioxidant defenses by modulating the Keap1/Nrf2 pathway.

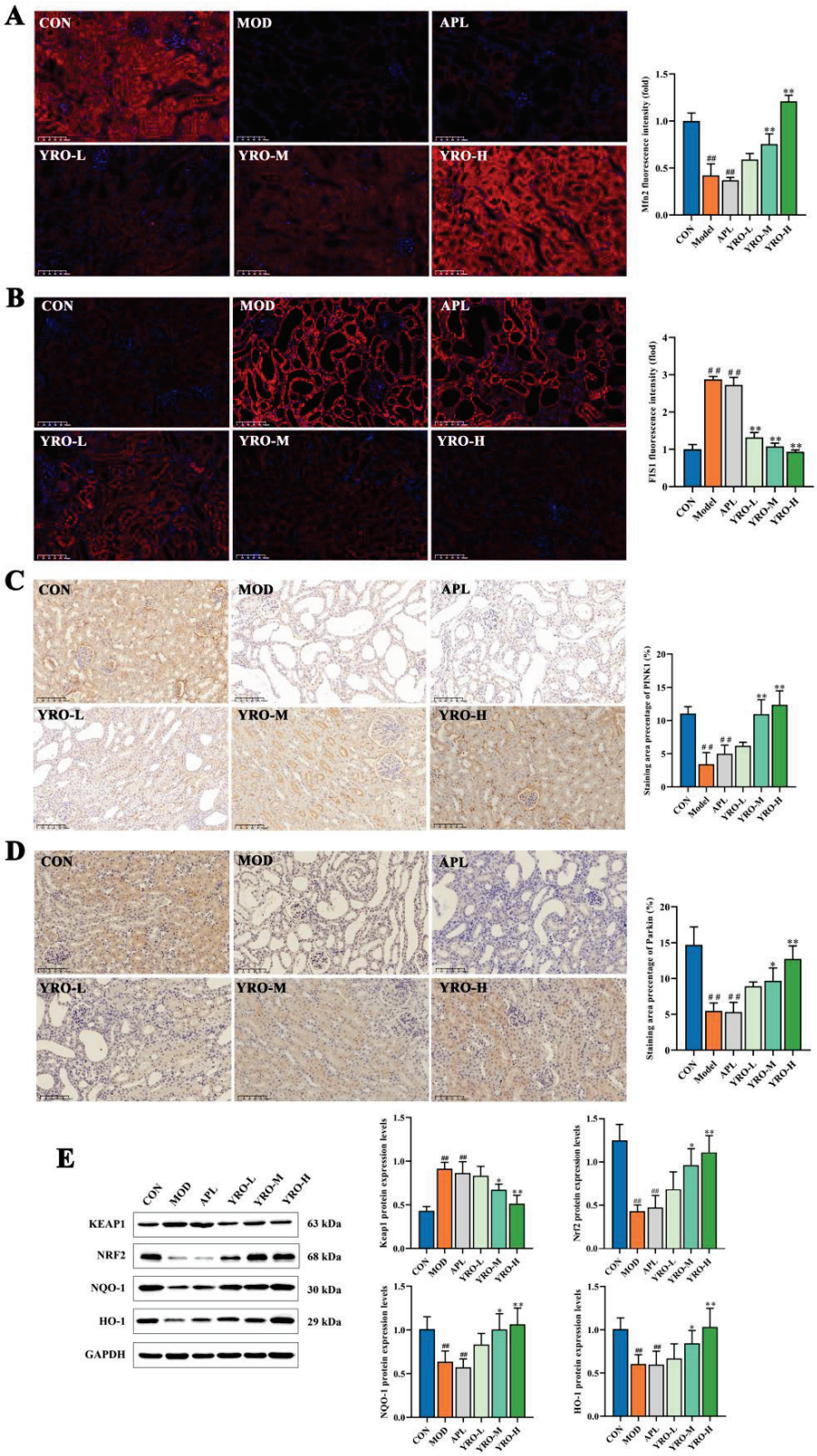


Figure 4. YRO improved mitochondrial function and modulated the oxidative stress pathway in HUA mice. IF staining and fluorescence intensity analysis of (**A**) Mfn2 and (**B**) FIS1; IHC staining and quantification analysis of (**C**) PINK1 and (**D**) Parkin; (**E**) Western blot analysis and protein expression of Keap1, Nrf2, NQO-1, and HO-1. Data are expressed as means ± SD (n = 6 mice/group). $^{\#\#}$ $p < 0.01$ vs. CON group; * $p < 0.05$, ** $p < 0.01$ vs. MOD group.

3.5. YRO Enhances Intestinal Barrier Integrity in HUA Mice

The intestinal barrier is critical for UA homeostasis by regulating UA excretion and gut permeability [36]. H&E staining showed significant structural changes in the MOD group (Figure 5A). These changes included reduced villus height, disorganized villus structure, and thinning of the muscle layer. Meanwhile, HUA induction led to tight junction proteins (ZO-1, Occludin, and Claudin-1) significant downregulation ($p < 0.05$; Figure 5C), suggesting compromised barrier integrity. The YRO intervention improved the intestinal structure and restored the expression of tight junction protein. Further analysis of intestinal UA transporters showed increased GLUT9 and ABCG2 expression in the YRO group compared with the MOD group (Figure 5B). These changes indicated that YRO promoted intestinal UA excretion, contributing to UA homeostasis.

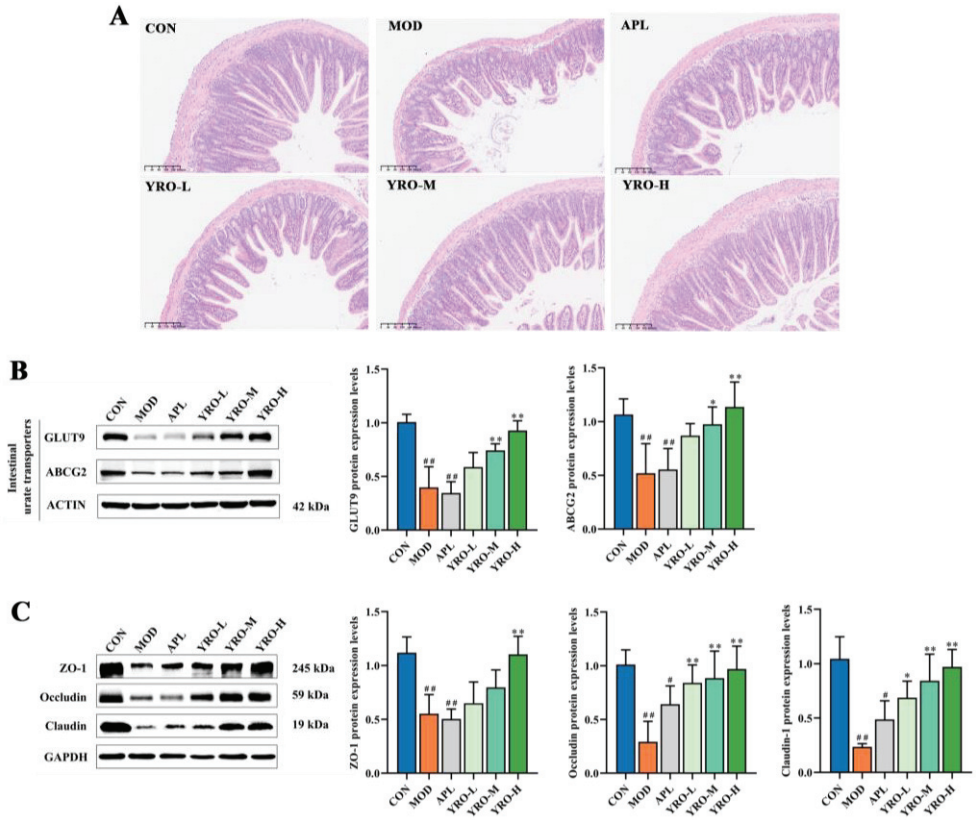


Figure 5. YRO relieved intestinal dysfunction and damage in HUA mice. (**A**) H&E staining of intestine (100×); (**B**) Western blot and quantification analysis of GLUT9 and ABCG2; (**C**) Western blot and quantification analysis of intestine tight protein, including ZO-1, Occludin, and Claudin-1. Data are expressed as means ± SD (n = 6 mice/group). $^{\#}$ $p < 0.05$, $^{\#\#}$ $p < 0.01$ vs. CON group; * $p < 0.05$, ** $p < 0.01$ vs. MOD group.

3.6. YRO Modulates Gut Microbiota Diversity and Composition in HUA Mice

To investigate the gut microbiota alterations, 16S rDNA sequencing was performed on fecal samples. The coverage index was close to 1, indicating sufficient sequencing depth. HUA mice exhibited significantly reduced microbial diversity and richness, as indicated by lower Chao1, ACE, Shannon, Simpson, and Sobs indices ($p < 0.05$). YRO-H treatment effectively reversed these declines, restoring gut microbiota diversity and richness (Figure 6A–F). The number of operational taxonomic units (OTUs) was higher in YRO-treated mice, with more overlapping OTUs between the YRO and CON groups (Figure 6G). PCoA based on unweighted UniFrac analysis further confirmed that YRO shifted microbial composition, with the YRO-H group clustering separately from the MOD group (Figure 6H).

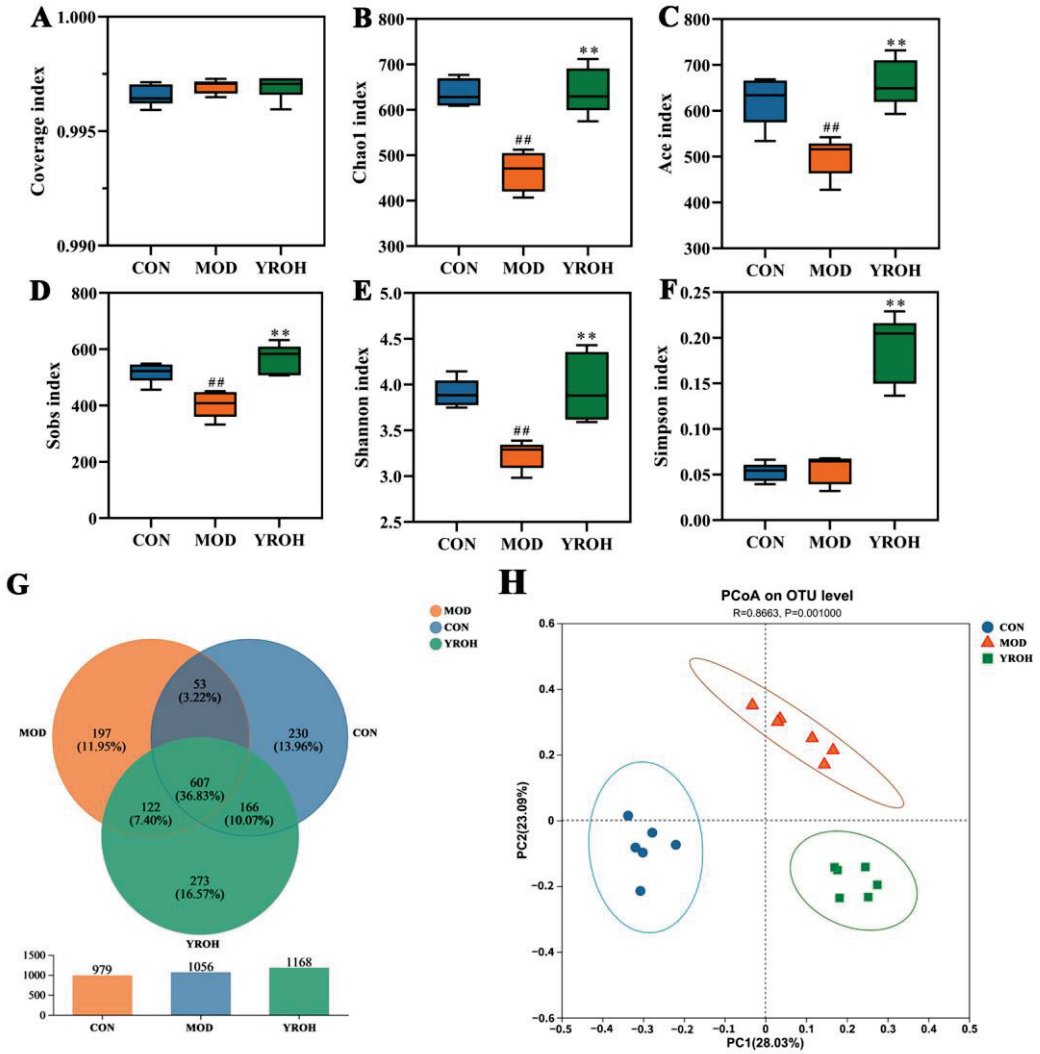


Figure 6. YRO altered gut microbiota structure in HUA mice. α-diversity indices, including (**A**) Coverage; (**B**) Choa1; (**C**) Ace; (**D**) Sobs; (**E**) Shannon; (**F**) Simpson; (**G**) Venn diagram of operational taxonomic units (OTUs); (**H**) PCoA analysis at the genus level. $^{\#\#}$ $p < 0.01$ vs. CON group; ** $p < 0.01$ vs. MOD group. Note: The total percentage of the pie chart is 100.01% due to rounding.

At the phylum level, *Firmicutes* and *Bacteroidetes* dominated all groups, followed by *Verrucomicrobia* and *Actinobacteria* (Figure 7A). The MOD group exhibited a significant decrease in the relative abundance of *Bacteroidetes* (40.57%) in comparison to the CON group (61.06%; $p < 0.05$). On the contrary, the relative abundance of *Firmicutes* was markedly increased in the MOD group (53.39%) compared with the CON group (29.44%). YRO-H treatment partially restored these imbalances, adjusting *Bacteroidetes* to 52.19% and *Firmicutes* to 42.78%. YRO-H also mitigated HUA-induced changes in *Verrucomicrobia* and *Actinobacteria*, bringing their abundances closer to those in the CON group.

At the genus level, YRO-H treatment displayed significant alterations in key bacterial genera (Figure 7B). Beneficial genera, including *norank_f__Muribaculaceae*, *Akkermansia*, *Lachnospiraceae_NK4A136_group*, and *Prevotellaceae_UCG-001* were significantly enriched ($p < 0.05$). These genera are associated with gut health, SCFAs production, and inflammation regulation. Furthermore, YRO-H reduced the abundance of *Lactobacillus*, *Bacteroides*, and *Dubosiella*, which were elevated in the MOD group ($p < 0.05$). These findings demonstrate that YRO-H effectively restored microbial diversity, rebalanced the dominant phylum, and promoted the enrichment of beneficial bacterial genera.

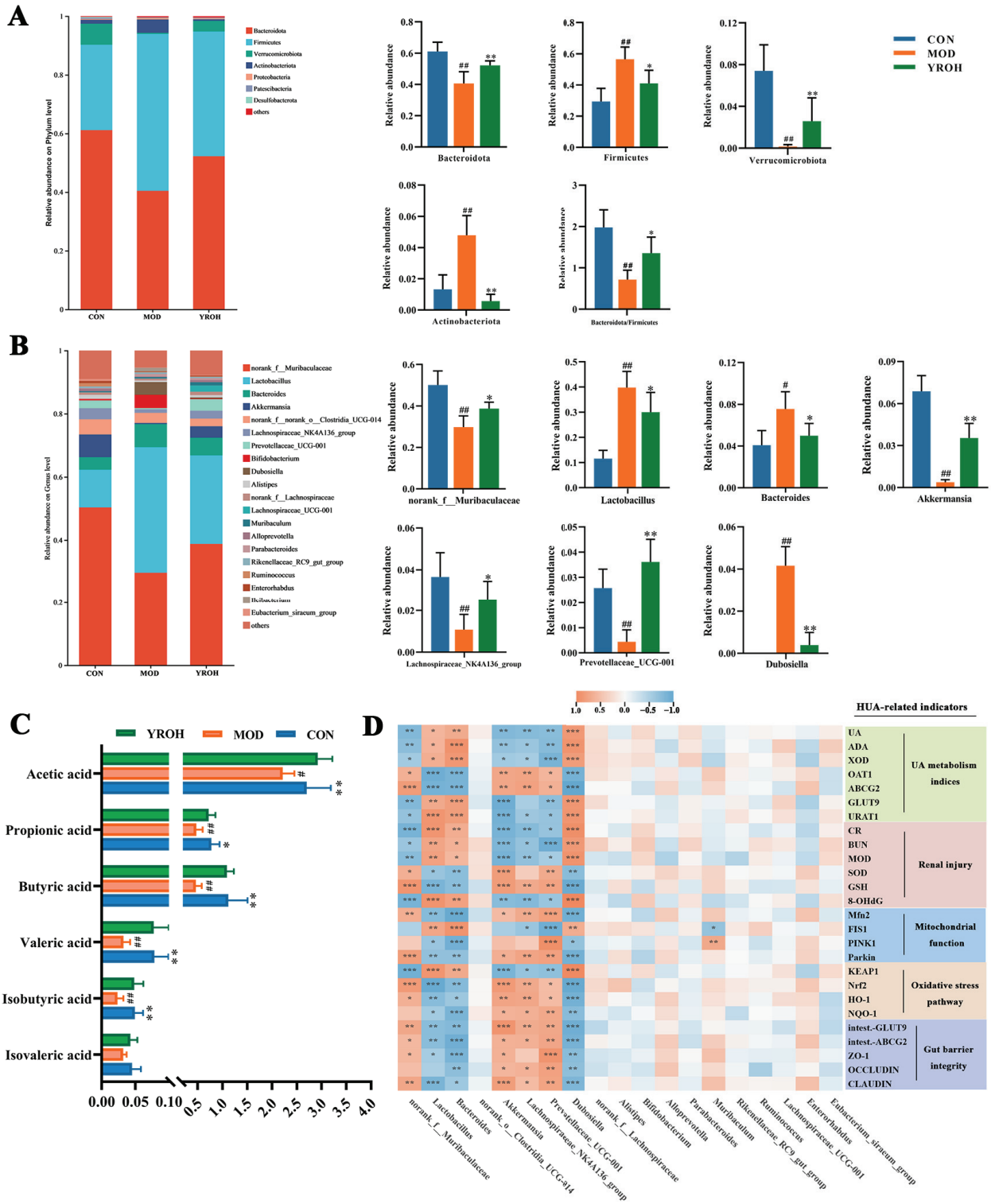


Figure 7. YRO modulated gut microbiota composition and SCFAs production in HUA mice. Microbial community composition and the relative abundance of major gut microbiota (**A**) at the phylum level and (**B**) at the genus level. (**C**) Concentrations of SCFAs. (**D**) Correlation analysis between gut bacteria genera and HUA-related indicators. Data are expressed as means ± SD (n = 6 mice/group). $^{\#}$ $p < 0.05$, $^{\#\#}$ $p < 0.01$ vs. CON group; * $p < 0.05$, ** $p < 0.01$ vs. MOD group. Correlation heatmap significance: * $p < 0.05$, ** $p < 0.01$, *** $p < 0.001$.

3.7. YRO Enhanced SCFAs Production in HUA Mice

As shown in Figure 7C, the MOD group exhibited significantly lower SCFA levels, including acetic acid, propionic acid, butyric acid, valeric acid, isobutyric acid, and isovaleric

acid, compared with the CON group ($p < 0.05$). YRO-H treatment significantly elevated the concentration of these SCFAs, bringing their levels closer to those observed in the CON group ($p < 0.05$). This restoration demonstrated that YRO-H enhanced SCFAs production, potentially improving gut microbial metabolism in HUA mice.

3.8. Correlation Between Intestinal Bacterial Abundances and HUA-Related Biomarkers

Spearman correlation analysis was conducted to explore associations between gut microbiota and physiological indicators (Figure 7D). Beneficial bacteria, including *norank_f__Muribaculaceae*, *Akkermansia*, *Lachnospiraceae_NK4A136_group*, and *Prevotellaceae_UCG-001*, positively correlated with urate excretion transporters, antioxidant capacity, and mitochondrial function markers. These genera were also associated with intestinal barrier integrity, reinforcing their role in gut health. In contrast, *Bacteroides*, *Dubosiella*, and *Lactobacillus* exhibited negative correlations with these physiological markers. Their abundance was linked to increased urate reabsorption, elevated oxidative stress, and compromised gut function. These results indicated the vital role of gut microbiota in mediating the protective effects of YRO against HUA.

3.9. YRO Attenuated Lipid Metabolism Disorders in HUA Mice

3.9.1. YRO Modulated Serum Lipid Profile in HUA Mice

Compared with the CON group, serum TC, TG, and LDL-C levels were significantly elevated in the MOD group ($p < 0.01$; Figure 8A), while HDL-C levels were reduced. YRO treatment significantly reversed these changes ($p < 0.05$), restoring lipid levels closer to normal. In the analysis of serum lipid metabolism, principal component analysis (PCA) demonstrated a clear separation between the MOD and YROH groups, with the YRO-H cluster closer to the CON group (Figure 8B). Orthogonal partial least squares discriminant analysis (OPLS-DA) further confirmed distinct metabolic profiles among the three groups (Figure 8C,D), indicating that YROH intervention modulated serum lipid metabolism in HUA mice.

Lipid metabolite alterations were identified using VIP > 1 and $p < 0.05$. The top 15 differentially abundant lipids were selected for both CON vs. MOD and YROH vs. MOD comparisons (Figure 8E,F). Phosphatidylethanolamine (PE) and phosphatidylinositol (PI) were the most significantly altered lipid classes in the MOD group, showing marked increases compared to the CON group (Table S3). YROH treatment reversed these changes, restoring PE and PI levels closer to normal (Figure 8G). Additionally, five specific lipid species were significantly altered in both comparisons, including PE (18:1_24:1), PI (15:1_21:1), PI (18:0_18:1), PI (18:1_18:1), and PI (18:1_20:3). Their levels were elevated in HUA mice but were restored by YRO treatment, suggesting a potential role in lipid homeostasis.

3.9.2. KEGG Pathway Enrichment Analysis

KEGG enrichment analysis identified the key metabolic pathways between the MOD and YROH groups (Figure 8H). YRO-H treatment significantly enriched pathways related to lipid metabolism, particularly glycerophospholipid metabolism and α-linolenic acid metabolism. Notably, choline metabolism in cancer exhibited the strongest enrichment trend, reflecting its involvement in choline utilization and cellular metabolic regulation.

3.9.3. YRO Modulated the PI3K/AKT/mTOR Signaling Pathway

As choline metabolism is closely linked to the PI3K/AKT/mTOR signaling pathway, western blot analysis was conducted to evaluate the regulatory effect of YRO on its activation (Figure 8I). In HUA mice, PI3K, phosphorylated AKT (P-AKT), and mTOR levels were significantly elevated, indicating activation of this pathway. Overactivation of this

pathway is associated with lipid metabolism dysfunction, oxidative stress, and cellular damage in HUA [37]. YRO intervention significantly downregulated PI3K, P-AKT, and mTOR expression, with the strongest inhibition observed in the YRO-H group. These findings suggested that YRO may mitigate oxidative stress in HUA mice by suppressing PI3K/AKT/mTOR activation.

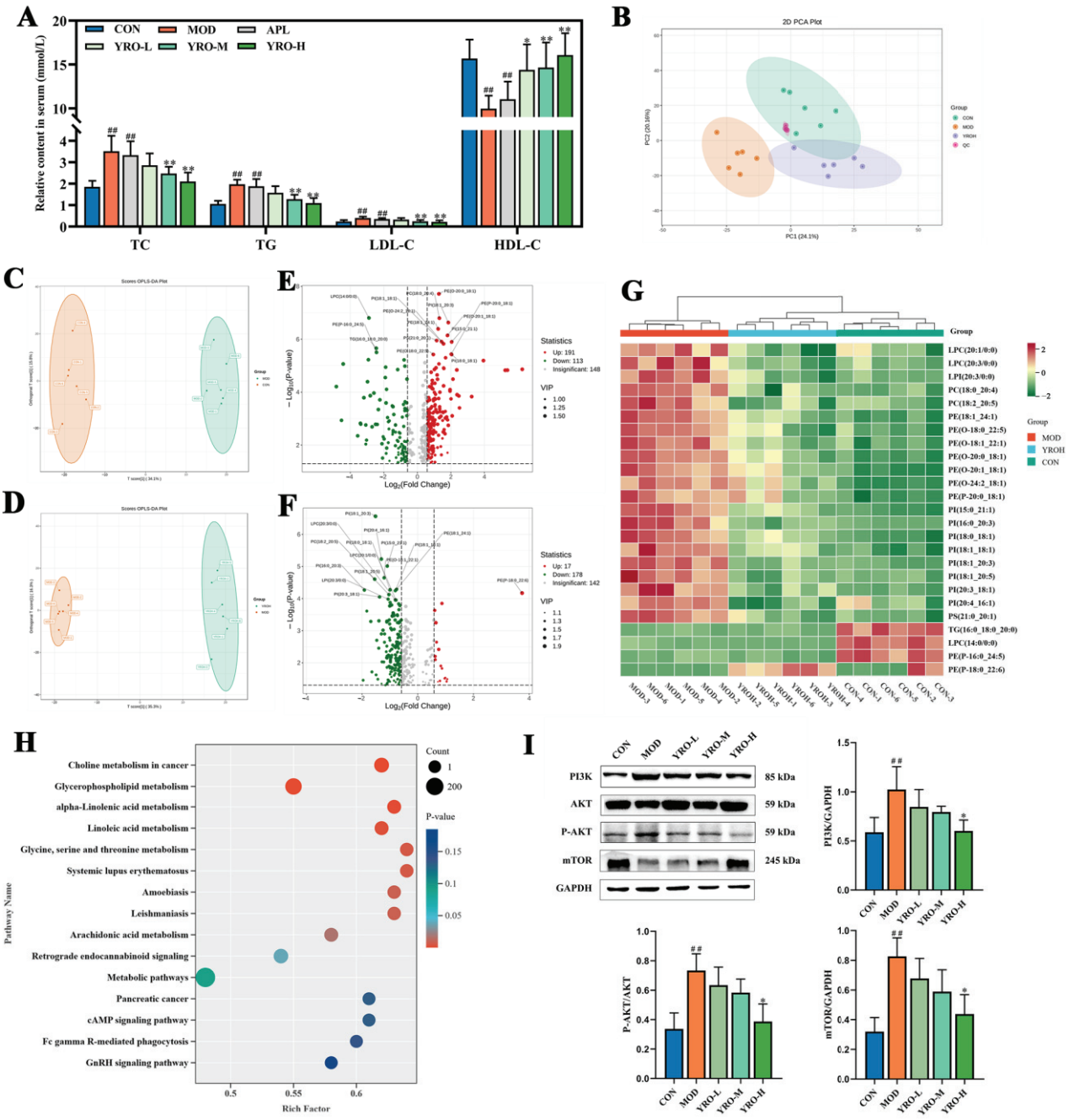


Figure 8. YRO attenuated serum lipid metabolism disorders in HUA mice. (**A**) Serum concentrations of TC, TG, LDL-C, and HDL-C; (**B**) PCA score plot of CON, MOD, YROH, and QC groups; OPLS-DA score plots of (**C**) CON vs. MOD and (**D**) YROH vs. MOD; Volcano maps and top 15 differential lipids of (**E**) CON vs. MOD and (**F**) YROH vs. MOD; (**G**) Heatmap of differential lipid metabolites in the CON, MOD, and YROH groups; (**H**) KEGG pathway annotation between the MOD and YROH groups; (**I**) Modulation of YRO on PI3K/AKT/m-TOR pathway protein expression in the kidney. $^{\#\#}$ $p < 0.01$ vs. CON group; * $p < 0.05$, ** $p < 0.01$ vs. MOD group.

4. Discussion

The increasing prevalence of HUA, driven by dietary and lifestyle changes, is a growing public health concern. HUA-related complications, including kidney dysfunction and intestinal barrier impairment, are closely linked to oxidative stress and metabolic disturbances. YRO is abundant in UFAs and has the potential to alleviate oxidative stress and support organ function. This study explored the mechanisms underlying the protective effects of YRO in HUA, focusing on UA metabolism, oxidative stress regulation, intestinal barrier integrity, and lipid homeostasis.

UA homeostasis depends on a dynamic balance between synthesis and excretion [38]. ADA and XOD are key enzymes involved in the purine degradation pathway, ultimately leading to UA formation [39]. In this study, YRO suppressed both ADA and XOD activity, reflecting a significant reduction in endogenous UA production. UA clearance is tightly regulated by renal and intestinal transport systems. In the kidney, reabsorption transporters GLUT9 and URAT1 were abnormally upregulated in HUA mice, leading to excessive UA retention and renal overload [40]. YRO intervention effectively downregulated these transporters while restoring the expression of the excretory transporters OAT1 and ABCG2. Notably, YRO also enhanced intestinal ABCG2 and GLUT9 expression, supporting an alternative route for UA elimination. By simultaneously reducing UA biosynthesis and enhancing renal and intestinal excretion, YRO comprehensively improved UA metabolism and alleviated systemic urate burden.

Excessive UA accumulation in the kidney disrupts renal function and exacerbates oxidative stress-related injury [41]. Histological analysis further confirmed that YRO preserved tubular integrity, reduced renal fibrosis, and improved kidney morphology. The decreases in CR and BUN levels provided additional evidence of improved renal function. Mitochondria, as the primary site of cellular energy metabolism, are highly vulnerable to UA-induced oxidative stress [42]. In HUA mice, disrupted mitochondrial dynamics, characterized by decreased Mfn2 and increased FIS1 expression, indicated excessive mitochondrial fragmentation [43]. Meanwhile, Keap1/Nrf2 signaling, a crucial antioxidant defense pathway, was suppressed, further exacerbating oxidative damage [44]. YRO administration restored mitochondrial fusion-fission balance, enhanced mitophagy via PINK1/Parkin activation, and promoted mitochondrial quality control.

Additionally, YRO alleviated Keap1-mediated inhibition of Nrf2, facilitating its nuclear translocation and upregulating antioxidant enzymes (NQO-1 and HO-1). Thereby reinforcing redox homeostasis and mitigating oxidative injury. Reactive oxygen species (ROS) contribute to UA-induced oxidative damage and are known activators of the NLRP3 inflammasome, a key driver of inflammation in HUA [45,46]. Notably, YRO reduced mitochondrial dysfunction and enhanced antioxidant defense, which may indirectly suppress NLRP3 activation. These observations align with emerging evidence linking redox balance to inflammasome regulation and a potential mechanism that warrants further investigation.

The kidneys and the intestine jointly regulated UA excretion, with intestinal excretion compensating for renal impairment [47]. In the HUA process, excessive UA accumulation damaged the intestinal barrier, increasing permeability and inflammation, which further disrupted UA elimination [48]. Tight junction proteins (ZO-1, Occludin, and Claudin-1) are essential for maintaining epithelial integrity, and their reduced expression in HUA mice indicated barrier dysfunction [49]. YRO effectively restored the expression of these tight junction proteins, strengthening the intestinal barrier and facilitating UA excretion.

The gut microbiota has always been proven to be a vital regulator in UA metabolism and gut functional homeostasis [27,50]. In this study, correlation analysis demonstrated that gut microbiota composition was closely associated with urate excretion transporters, antioxidant capacity, and mitochondrial function markers, reinforcing its role in HUA

progression and metabolic regulation. HUA mice exhibited significant microbial dysbiosis, characterized by a decreased Bacteroidetes-to-Firmicutes ratio (Figure 7A), an established marker of metabolic imbalance [51]. This dysbiosis was associated with an increase in pathogenic bacteria and a reduction in beneficial microbes, likely exacerbating intestinal barrier dysfunction and UA accumulation. Several studies have linked HUA-associated dysbiosis to an overabundance of *Bacteroides* and *Dubosiella*, which trigger gut-derived intestinal permeability disruption and oxidative stress [52,53]. In agreement with these findings, HUA mice in this study displayed significantly increased levels of *Bacteroides* and *Dubosiella*. This shift may contribute to enhanced UA reabsorption, further worsening HUA symptoms.

YRO intervention reduced the abundance of these pathogenic bacteria, suggesting that it may alleviate oxidative stress and gut metabolic dysfunction by modulating microbial composition. At the same time, YRO increased the abundance of beneficial bacteria, particularly *Lachnospiraceae_NK4A136_group* and *Akkermansia*, which have been reported to play a role in SCFAs production and metabolic stability [54,55]. SCFAs, including acetate, propionate, and butyrate, are essential for intestinal barrier integrity, immune modulation, and energy metabolism [56]. Previous studies reported that HUA mice often exhibit reduced SCFA levels, which may impair intestinal function and metabolic regulation. Our results confirmed this trend, as SCFA concentrations were significantly lower in HUA mice but were restored following YRO administration, reinforcing its role in *Lachnospiraceae_NK4A136 _group* and *Akkermansia* regulation. Another notable shift was observed in *Lactobacillus*, which was significantly elevated in HUA mice. This genus plays a key role in purine metabolism, and its increase may represent an adaptive response to excessive purine accumulation [57,58]. YRO supplementation normalized *Lactobacillus* levels, indicating a potential restoration of purine metabolism homeostasis and a reduction in UA synthesis.

Meanwhile, emerging human studies have consistently shown that HUA is associated with increased *Bacteroides* and *Dubosiella*, and other pathogenic bacteria, alongside reductions in SCFA-producing and barrier-supporting bacteria such as *Akkermansia* and *Lachnospiraceae* [59,60]. These microbial patterns are consistent with those reported in HUA patients, suggesting that YRO-induced microbiota remodeling may have translational relevance. Further studies incorporating fecal microbiota transplantation (FMT) from YRO-treated mice are needed to determine whether gut microbiota alterations directly mediate the observed benefits.

Lipid metabolism is fundamental to energy homeostasis, membrane stability, and cellular signaling, and its disruption is frequently associated with metabolic disorders, including HUA [61]. Glycerophospholipids, particularly PI and PE, are key regulatory lipids involved in these processes [62]. In this study, lipidomic analysis revealed significant alterations in PI and PE levels in HUA mice. YRO administration restored PI and PE levels and indicated its ability to stabilize lipid metabolism. Further pathway analysis using KEGG enrichment demonstrated that PI and PE metabolism were closely associated with the PI3K/AKT/mTOR signaling pathway. PI directly activates PI3K, modulating downstream metabolic and oxidative responses.

Previous studies have demonstrated that PI3K/AKT/mTOR signaling is abnormally activated in HUA, contributing to renal fibrosis [63]. The findings of this study are consistent with these reports, confirming that HUA-induced PI3K/AKT/mTOR hyperactivation is associated with kidney injury. However, in addition to its role in renal fibrosis, this pathway is also involved in mitophagy, apoptosis regulation, and antioxidant responses [64]. Further analysis revealed that PI3K/AKT/mTOR hyperactivation in HUA was accompanied by impaired Nrf2 signaling. The YRO intervention effectively reversed these

abnormalities. It not only restored Nrf2 activation, leading to enhanced antioxidant enzyme expression and reduced oxidative burden, but also suppressed PI3K/AKT/mTOR signaling, mitigating oxidative stress-related damage. These findings suggested that YRO regulated lipid metabolism and oxidative stress responses, thereby contributing to its protective effects in HUA.

Recent studies have identified several functional oils with hypouricemic potential, including *Sonneratia apetala* seed oil (SSO), cassia oil, and celery seed oil [24,65,66]. Among them, SSO primarily consists of linoleic acid (69.6%) and oleic acid (5.8%), exerting dual effects via XOD inhibition and modulation of urate transporter expression, while also attenuating renal oxidative damage through the Keap1–Nrf2 axis [24]. Similarly, YRO contains substantial amounts of oleic acid (42.63%) and linoleic acid (22.36%), which may synergistically contribute to its multi-target bioactivity. Future studies will investigate whether individual fatty acids, or their combinations, are responsible for the observed effects, supporting mechanistic dissection and targeted formulation development. In addition to restoring renal urate transporter balance and antioxidant, YRO reversed HUA-induced mitochondrial fragmentation and upregulation of antioxidant enzymes (HO-1 and NQO-1), indicating improved mitochondrial quality control and redox balance. These were essential aspects of renal resilience under urate stress. Meanwhile, YRO uniquely enhanced intestinal urate excretion and improved lipid disorder, further distinguishing its mode of action from previously studied oils. Although this study focused on the lipid composition of coix seed, the plant also contains other bioactive components, including flavonoids [67]. Notably, genistein has been shown to reduce risk markers of metabolic syndrome [68]. Given the increasing interest in plant-based dietary strategies for metabolic regulation, future studies may explore whether coix seed oil, in combination with other natural compounds, could provide added benefits for managing HUA and related diseases.

5. Conclusions

YRO effectively ameliorated HUA-related symptoms in mice and mitigated HUA-induced oxidative damage in the kidney. Importantly, YRO restored microbial homeostasis and improved lipid metabolism. This study revealed the UA-lowering role of YRO on hyperuricemia and its underlying mechanisms involving renal and intestinal regulation. While these findings are promising, further studies, including clinical trials, are warranted to validate their safety and efficacy in humans and to explore their potential as a nutraceutical intervention for hyperuricemia.

Supplementary Materials: The following supporting information can be downloaded at: https://www.mdpi.com/article/10.3390/nu17101679/s1, Figure S1: GC-MS total ions chromatogram of methyl esterification of YRO; Table S1: Antibody information for Western blotting, IHC, and IF; Table S2: Component and distribution of fatty acids on YRO; Table S3: Altered profiles of key lipid metabolites following YROH treatment in HUA.

Author Contributions: G.W.: conceptualization, data curation, and writing—original draft. X.W. (Xinming Wang): methodology, data curation, and writing—original draft. H.D.: methodology and project administration. J.Y.: software, formal analysis. T.L.: methodology, writing—review and editing, and supervision. X.W. (Xiao Wang): writing—review and editing, supervision, and funding acquisition. All authors have read and agreed to the published version of the manuscript.

Funding: This work was supported by the National Key Research and Development Project of China (2023YFC3503805), the Taishan Scholars Program of Shandong Province (NO. tsqnz20231230), the China Agriculture Research System of MOF and MARA (CARS-21), and the Traditional Chinese Medicine Science and Technology Project of Shandong (Q-2023021) are also acknowledged.

Institutional Review Board Statement: The animal study protocol was approved by the Animal Care and Ethics Committee at the Shandong Academy of Chinese Medicine (approval number: SDZYY20230621002; approval date: 25 May 2023).

Informed Consent Statement: Not applicable.

Data Availability Statement: The data sets generated and/or analyzed during the current study are either shown in the manuscript and Supplementary Materials or available from the corresponding author on reasonable request.

Conflicts of Interest: The authors declare no conflicts of interest.

References

1. Sato, Y.; Feig, D.I.; Stack, A.G.; Kang, D.H.; Lanaspa, M.A.; Ejaz, A.A.; Sánchez-Lozada, L.G.; Kuwabara, M.; Borghi, C.; Johnson, R.J. The case for uric acid-lowering treatment in patients with hyperuricaemia and CKD. *Nat. Rev. Nephrol.* **2019**, *15*, 767–775. [CrossRef]
2. Chen, Y.; Luo, L.Y.; Hu, S.S.; Gan, R.Y.; Zeng, L. The chemistry, processing, and preclinical anti-hyperuricemia potential of tea: A comprehensive review. *Crit. Rev. Food Sci. Nutr.* **2023**, *63*, 7065–7090. [CrossRef]
3. Dalbeth, N.; Phipps-Green, A.; Frampton, C.; Neogi, T.; Taylor, W.J.; Merriman, T.R. Relationship between serum urate concentration and clinically evident incident gout: An individual participant data analysis. *Ann. Rheum. Dis.* **2018**, *77*, 1048–1052. [CrossRef]
4. Kim, S.K.; Choe, J.Y.; Park, S.H.; Lee, H. SAT0542 oxidative stress by monosodium urate crystals promotes renal cell apoptosis through mitochondrial caspase-dependent pathway in human embryonic kidney 293 cells. *Ann. Rheum. Dis.* **2014**, *73*, 787. [CrossRef]
5. Sharaf El Din, U.A.A.; Salem, M.M.; Abdulazim, D.O. Uric acid in the pathogenesis of metabolic, renal, and cardiovascular diseases: A review. *J. Adv. Res.* **2017**, *8*, 537–548. [CrossRef]
6. Li, H.J.; Peng, L.X.; Yin, F.; Fang, J.H.; Cai, L.T.; Zhang, C.J.; Xiang, Z.; Zhao, Y.Y.; Zhang, S.F.; Sheng, H.D.; et al. Research on Coix seed as a food and medicinal resource, it's chemical components and their pharmacological activities: A review. *J. Ethnopharmacol.* **2024**, *319*, 117309. [CrossRef]
7. Sui, Y.L.; Xu, D.P.; Sun, X.L. Identification of anti-hyperuricemic components from Coix seed. *Food Biosci.* **2023**, *52*, 102461. [CrossRef]
8. Xu, Q.Q.; Kong, H.X.; Ren, S.; Meng, F.Y.; Liu, R.S.; Jin, H.X.; Zhang, J. Coix seed oil alleviates synovial angiogenesis through suppressing HIF-1α/VEGF-A signaling pathways via SIRT1 in collagen-induced arthritis rats. *Chin. Med.* **2023**, *18*, 119. [CrossRef]
9. Zeng, H.Y.; Zhu, A.R.; He, S.L.; Wu, M.J.; Mazhar, M.; Wen, A.Y.; Liu, N.; Qin, L.K.; Miao, S. Anti-lipid-oxidation effects and edible safety evaluation of the oil extracted by a supercritical CO_2 process from coix seed fermented by *Monascus purpureus*. *Food Sci. Hum. Wellness* **2023**, *12*, 1119–1127. [CrossRef]
10. He, W.S.; Li, L.L.; Rui, J.X.; Li, J.X.; Sun, Y.Y.; Cui, D.D.; Xu, B. Tomato seed oil attenuates hyperlipidemia and modulates gut microbiota in C57BL/6J mice. *Food Funct.* **2020**, *11*, 4275–4290. [CrossRef]
11. Huang, P.M.; Chen, Z.H.; Li, W.Z.; Su, A.H.; Cui, C. Inquiry of modulatory role of sea buckthorn fruit oil on dyslipidemia and gut microbiota in hyperlipidemia mice. *Food Sci. Hum. Wellnes* **2025**, *14*, 9250098. [CrossRef]
12. Zhan, M.; Brooks, C.; Liu, F.Y.; Sun, L.; Dong, Z. Mitochondrial dynamics: Regulatory mechanisms and emerging role in renal pathophysiology. *Kidney Int.* **2013**, *83*, 568–581. [CrossRef]
13. Ding, X.Q.; Jian, T.Y.; Gai, Y.N.; Niu, G.T.; Liu, Y.; Meng, X.H.; Li, J.; Lyu, H.; Ren, B.R.; Chen, J. Chicoric acid attenuated renal tubular injury in HFD-induced chronic kidney disease mice through the promotion of mitophagy via the Nrf2/PINK/Parkin pathway. *J. Agric. Food Chem.* **2022**, *70*, 2923–2935. [CrossRef]
14. Al-Mubarak, B.R.; Bell, K.F.S.; Chowdhry, S.; Meakin, P.J.; Baxter, P.S.; McKay, S.; Dando, O.; Ashford, M.L.J.; Gazaryan, I.; Hayes, J.D.; et al. Non-canonical Keap1-independent activation of Nrf2 in astrocytes by mild oxidative stress. *Redox Biol.* **2021**, *47*, 102158. [CrossRef]
15. Khan, A.U.H.; Rathore, M.G.; Allende-Vega, N.; Vo, D.N.; Belkhala, S.; Orecchioni, S.; Talarico, G.; Bertolini, F.; Cartron, G.; Lecellier, C.H.; et al. Human leukemic cells performing oxidative phosphorylation (OXPHOS) generate an antioxidant response independently of reactive oxygen species (ROS) production. *EBioMedicine* **2016**, *3*, 43–53. [CrossRef]
16. Mehmood, A.; Zhao, L.; Wang, C.T.; Hossen, I.; Raka, R.N.; Zhang, H.M. Stevia residue extract increases intestinal uric acid excretion via interactions with intestinal urate transporters in hyperuricemic mice. *Food Funct.* **2019**, *10*, 7900–7912. [CrossRef]
17. Li, X.Q.; Chen, Y.H.; Gao, X.X.; Wu, Y.J.; El-Seedi, H.R.; Cao, Y.; Zhao, C. Antihyperuricemic effect of green alga *Ulva lactuca* Ulvan through regulating urate transporters. *J. Agric. Food Chem.* **2021**, *69*, 11225–11235. [CrossRef]

18. Wang, Y.X.; Chen, X.L.; Zhou, K.; Wang, L.L.; Zhong, Y.Z.; Peng, J.; Ge, B.S.; Ho, C.T.; Lu, C.Y. Fucoidan dose-dependently alleviated hyperuricemia and modulated gut microbiota in mice. *Food Med. Homol.* **2025**. [CrossRef]
19. Shan, B.X.; Chen, T.; Huang, B.X.; Liu, Y.; Chen, J. Untargeted metabolomics reveal the therapeutic effects of Ermiao wan categorized formulas on rats with hyperuricemia. *J. Ethnopharmacol.* **2021**, *281*, 114545. [CrossRef]
20. Xu, M.; Xiao, H.Z.; Zou, X.; Pan, L.; Song, Q.Z.; Hou, L.Y.; Zeng, Y.H.; Han, Y.; Zhou, Z.J. Mechanisms of levan in ameliorating hyperuricemia: Insight into levan on serum metabolites, gut microbiota, and function in hyperuricemia rats. *Carbohydr. Polym.* **2025**, *347*, 122665. [CrossRef]
21. Manto, A.A.; Ramirez, I.F.T.; Arnado, L.M.; Damiotan, C.T.; Sumalpong, E.T.; Ido, A.L.; Arazo, R.O. Oil extraction from *Calophyllum inophyllum* L. seeds through ultrasonication with n-hexane and petroleum ether as solvents. *Biomass Conv. Bioref.* **2024**, *14*, 5423–5434. [CrossRef]
22. Cui, Y.; Wang, X.M.; Yang, Y.; Rong, R.; Gong, L.L.; Jiang, H.Q.; Han, B.B. Research on fusion-fingerprint of Coicis Semen oil. *Chin. Tradit. Herbal Drugs.* **2014**, *45*, 1698–1701.
23. Xu, L.Q.; Lin, G.S.; Yu, Q.X.; Li, Q.P.; Mai, L.T.; Cheng, J.J.; Xie, J.H.; Liu, Y.H.; Su, Z.R.; Li, Y.C. Anti-hyperuricemic and nephroprotective effects of dihydroberberine in potassium oxonate- and hypoxanthine-induced hyperuricemic mice. *Front. Pharmacol.* **2021**, *12*, 645879. [CrossRef]
24. Chen, J.F.; Xu, L.Q.; Jiang, L.Y.; Wu, Y.L.; Wei, L.; Wu, X.L.; Xiao, S.H.; Liu, Y.H.; Gao, C.J.; Cai, J.; et al. *Sonneratia apetala* seed oil attenuates potassium oxonate/hypoxanthine-induced hyperuricemia and renal injury in mice. *Food Funct.* **2021**, *12*, 9416–9431. [CrossRef]
25. Lin, X.; Zhou, Q.; Zhou, L.F.; Sun, Y.S.; Han, X.; Cheng, X.L.; Wu, M.Y.; Lv, W.; Wang, J.; Zhao, W. Quinoa (*Chenopodium quinoa Willd*) bran saponins alleviate hyperuricemia and inhibit renal injury by regulating the PI3K/AKT/NFκB signaling pathway and uric acid transport. *J. Agric. Food Chem.* **2023**, *71*, 6635–6649. [CrossRef]
26. Zhu, X.Y.; Si, F.; Hao, R.L.; Zheng, J.Q.; Zhang, C. Nuciferine protects against obesity-induced nephrotoxicity through its hypolipidemic, anti-inflammatory, and antioxidant effects. *J. Agric. Food Chem.* **2023**, *71*, 18769–18779. [CrossRef]
27. Wang, P.; Zhang, X.Q.; Zheng, X.; Gao, J.R.; Shang, M.F.; Xu, J.H.; Liang, H. Folic acid protects against hyperuricemia in C57BL/6J mice via ameliorating gut–kidney axis dysfunction. *J. Agric. Food Chem.* **2022**, *70*, 15787–15803. [CrossRef]
28. Wang, L.M.; Wang, P.; Teka, T.; Zhang, Y.C.; Yang, W.Z.; Zhang, Y.; Wang, T.; Liu, L.X.; Han, L.F.; Liu, C.X. ^{1}H NMR and UHPLC/Q-Orbitrap-MS-based metabolomics combined with 16S rRNA gut microbiota analysis revealed the potential regulation mechanism of Nuciferine in hyperuricemia rats. *J. Agric. Food Chem.* **2020**, *68*, 14059–14070. [CrossRef]
29. Abd El-Wahab, H.M.F.; Mohamed, M.A.; El Sayed, H.H.; Bauomy, A.E. Modulatory effects of rice bran and its oil on lipid metabolism in insulin resistance rats. *J. Food Biochem.* **2017**, *41*, e12318. [CrossRef]
30. El Kamouni, S.; El Kebbaj, R.; Andreoletti, P.; El Ktaibi, A.; Rharrassi, I.; Essamadi, A.; El Kebbaj, M.S.; Mandard, S.; Latruffe, N.; Vamecq, J.; et al. Protective effect of argan and olive oils against LPS-induced oxidative stress and inflammation in mice livers. *Int. J. Mol. Sci.* **2017**, *18*, 2181. [CrossRef]
31. Ait Eldjoudi, D.; Ruiz-Fernandez, C.; González-Rodriguez, M.; Ait Atmane, S.; Cordero-Barreal, A.; Farrag, Y.; Pino, J.; Sineiro, J.; Lago, F.; Conde-Aranda, J.; et al. Analgesic and antiinflammatory effects of *Nigella orientalis* L. seeds fixed oil: Pharmacological potentials and molecular mechanisms. *Phytother. Res.* **2022**, *36*, 1372–1385. [CrossRef]
32. Bao, R.X.; Chen, Q.; Li, Z.; Wang, D.; Wu, Y.Z.; Liu, M.Y.; Zhang, Y.; Wang, T. Eurycomanol alleviates hyperuricemia by promoting uric acid excretion and reducing purine synthesis. *Phytomedicine* **2022**, *96*, 153850. [CrossRef]
33. Lu, Y.; Fan, X.X.; Zhao, S.L.; Ishii, Y.; Yu, B.Y.; Li, R.S. Supplements extracted from *Lophatherum Gracile* Brongn. ameliorates hyperuricemia by regulating nucleotide metabolic enzymes and urate transporters. *Food Med. Homol.* **2025**. [CrossRef]
34. Spoto, B.; Politi, C.; Pizzini, P.; Parlongo, R.M.; Testa, A.; Mobrici, M.; Tripepi, G.L.; Mallamaci, F.; Zoccali, C. 8-hydroxy-2′-deoxyguanosine, a biomarker of oxidative DNA injury, in diabetic kidney disease. *Nutr. Metab. Cardiovasc. Dis.* **2024**, *35*, 103722. [CrossRef]
35. Ai, G.X.; Huang, R.L.; Xie, J.H.; Zhong, L.J.; Wu, X.Y.; Qin, Z.H.; Su, Z.R.; Chen, J.N.; Yang, X.B.; Dou, Y.X. Hypouricemic and nephroprotective effects of palmatine from Cortex Phellodendri Amurensis: A uric acid modulator targeting Keap1-Nrf2/NLRP3 axis. *J. Ethnopharmacol.* **2023**, *301*, 115775. [CrossRef]
36. Qi, X.F.; Ma, Y.F.; Guan, K.F.; Zhao, L.; Ma, Y.; Wang, R. Whey protein peptide Pro-Glu-Trp ameliorates hyperuricemia by enhancing intestinal uric acid excretion, modulating the gut microbiota, and protecting the intestinal barrier in rats. *J. Agric. Food Chem.* **2024**, *72*, 2573–2584. [CrossRef]
37. Yu, L.; Wei, J.; Liu, P.D. Attacking the PI3K/Akt/mTOR signaling pathway for targeted therapeutic treatment in human cancer. *Semin. Cancer Biol.* **2022**, *85*, 69–94. [CrossRef]
38. Zhou, Y.Q.; Zeng, Y.P.; Wang, R.J.; Pang, J.; Wang, X.; Pan, Z.J.; Jin, Y.F.; Chen, Y.; Yang, Y.; Ling, W.H. Resveratrol improves hyperuricemia and ameliorates renal injury by modulating the gut microbiota. *Nutrients* **2024**, *16*, 1086. [CrossRef]

39. Wei, L.Y.; Ji, H.W.; Song, W.K.; Peng, S.; Zhan, S.H.; Qu, Y.S.; Chen, M.; Zhang, D.; Liu, S.C. Hypouricemic, hepatoprotective and nephroprotective roles of oligopeptides derived from *Auxis thazard* protein in hyperuricemic mice. *Food Funct.* **2021**, *12*, 11838–11848. [CrossRef]
40. Balal, A.; Obeidat, A.M.; Fadul, K.Y.; Sati, W.; Ahmed, S.M.I.; Elgassim, M.; Nahid, S.; Balal, A.; Obeidat, A.M.; Fadul, K.Y.; et al. Sepsis-induced coagulopathy: From pathophysiology to patient care. In *Septic Shock—From Pathophysiology to Patient Care*; IntechOpen: London, UK, 2024; ISBN 978-0-85014-708-7.
41. Ponticelli, C.; Podestà, M.A.; Moroni, G. Hyperuricemia as a trigger of immune response in hypertension and chronic kidney disease. *Kidney Int.* **2020**, *98*, 1149–1159. [CrossRef]
42. Tang, C.; He, L.; Liu, J.; Dong, Z. Mitophagy: Mitophagy: Mitophagy: Basic mechanism and potential role in kidney diseases. *Kidney Dis.* **2015**, *1*, 71–79. [CrossRef]
43. Rovira-Llopis, S.; Bañuls, C.; Diaz-Morales, N.; Hernandez-Mijares, A.; Rocha, M.; Victor, V.M. Mitochondrial dynamics in type 2 diabetes: Pathophysiological implications. *Redox Biol.* **2017**, *11*, 637–645. [CrossRef]
44. Li, S.W.; Zheng, L.S.; Zhang, J.; Liu, X.J.; Wu, Z.M. Inhibition of ferroptosis by up-regulating Nrf2 delayed the progression of diabetic nephropathy. *Free Radic. Biol. Med.* **2021**, *162*, 435–449. [CrossRef]
45. Wang, M.; Lin, X.; Yang, X.M.; Yang, Y.L. Research progress on related mechanisms of uric acid activating NLRP3 inflammasome in chronic kidney disease. *Ren. Fail.* **2022**, *44*, 615–624. [CrossRef]
46. Ding, T.; Wang, S.F.; Zhang, X.Y.; Zai, W.J.; Fan, J.J.; Chen, W.; Bian, Q.; Luan, J.Y.; Shen, Y.L.; Zhang, Y.D.; et al. Kidney protection effects of dihydroquercetin on diabetic nephropathy through duppressing ROS and NLRP3 inflammasome. *Phytomedicine* **2018**, *41*, 45–53. [CrossRef]
47. Fan, S.Q.; Huang, Y.M.; Lu, G.D.; Sun, N.; Wang, R.; Lu, C.Y.; Ding, L.J.; Han, J.J.; Zhou, J.; Li, Y.; et al. Novel anti-hyperuricemic hexapeptides derived from Apostichopus japonicus hydrolysate and their modulation effects on the gut microbiota and host microRNA profile. *Food Funct.* **2022**, *13*, 3865–3878. [CrossRef]
48. Liu, C.Q.; Ruan, F.K.; Chen, Z.Y.; Han, J.R.; Ding, X.Y.; Han, C.S.; Ye, L.X.; Yang, C.; Yu, Y.; Zuo, Z.H.; et al. Phenanthrene-induced hyperuricemia with intestinal barrier damage and the protective role of theabrownin: Modulation by gut microbiota-mediated bile acid metabolism. *Sci. Total Environ.* **2024**, *949*, 174923. [CrossRef]
49. Mao, M.J.; Cao, X.Q.; Liang, Y.H.; Li, Q.Y.; Chen, S.M.; Zhou, L.P.; Zhang, Y.Y.; Guo, Y. Neuroprotection of rhubarb extract against cerebral ischaemia-reperfusion injury via the gut-brain axis pathway. *Phytomedicine* **2024**, *126*, 155254. [CrossRef]
50. Huang, S.N.; Li, F.F.; Quan, C.H.; Jin, D. Intestinal flora: A potential pathogenesis mechanism and treatment strategy for type 1 diabetes mellitus. *Gut Microbes.* **2024**, *16*, 2423024. [CrossRef]
51. Crovesy, L.; Masterson, D.; Rosado, E.L. Profile of the gut microbiota of adults with obesity: A systematic review. *Eur. J. Clin. Nutr.* **2020**, *74*, 1251–1262. [CrossRef]
52. Zhang, N.H.; Zhou, J.X.; Zhao, L.; Zhao, Z.; Wang, S.R.; Zhang, L.B.; Zhou, F. Ferulic acid supplementation alleviates hyperuricemia in high-fructose/fat diet-fed rats via promoting uric acid excretion and mediating the gut microbiota. *Food Funct.* **2023**, *14*, 1710–1725. [CrossRef]
53. Zhou, X.F.; Zhang, B.W.; Zhao, X.L.; Zhang, P.X.; Guo, J.T.; Zhuang, Y.; Wang, S. Coffee leaf tea extracts improve hyperuricemia nephropathy and its associated negative effect in gut microbiota and amino acid metabolism in rats. *J. Agric. Food Chem.* **2023**, *71*, 17775–17787. [CrossRef]
54. Fang, Q.; Lai, Y.; Zhang, D.; Lei, H.; Wang, F.; Guo, X.R.; Song, C. Gut microbiota regulation and prebiotic properties of polysaccharides from *Oudemansiella raphanipes* mushroom. *World J. Microbiol. Biotechnol.* **2023**, *39*, 167. [CrossRef]
55. Zhao, L.P.; Zhang, F.; Ding, X.Y.; Wu, G.J.; Lam, Y.Y.; Wang, X.J.; Fu, H.Q.; Xue, X.H.; Lu, C.H.; Ma, J.L.; et al. Gut bacteria selectively promoted by dietary fibers alleviate type 2 diabetes. *Science* **2018**, *359*, 1151–1156. [CrossRef]
56. Miao, C.; Dong, K.; Shen, Y.; Sun, Y.L.; Li, W.Y.; Man, C.X.; Zhang, Y.; Zhao, Q.Y.; Jiang, Y.J. Mechanism of *Lacticaseibacillus rhamnosus* JY027 alleviating hyperuricemia in mice through gut-kidney axis. *Food Biosci.* **2024**, *61*, 104757. [CrossRef]
57. Kilstrup, M.; Hammer, K.; Ruhdal Jensen, P.; Martinussen, J. Nucleotide metabolism and its control in lactic acid bacteria. *FEMS Microbiol. Rev.* **2005**, *29*, 555–590. [CrossRef]
58. Lee, Y.J.; Werlinger, P.; Suh, J.W.; Cheng, J.H. Potential probiotic *Lacticaseibacillus paracasei* MJM60396 prevents hyperuricemia in a multiple way by absorbing purine, suppressing xanthine oxidase and regulating urate excretion in mice. *Microorganisms* **2022**, *10*, 851. [CrossRef]
59. Yang, H.T.; Xiu, W.J.; Liu, J.K.; Yang, Y.; Hou, X.G.; Zheng, Y.Y.; Wu, T.T.; Wu, C.X.; Xie, X. Gut microbiota characterization in patients with asymptomatic hyperuricemia: Probiotics increased. *Bioengineered* **2021**, *121*, 7263–7275. [CrossRef]
60. Liu, P.; Yang, J.L.; Chen, Y.; Zhu, Y.F.; Tang, Y.Y.; Xu, X.D.; He, H.D. Alterations of gut microbiota and metabolome in early chronic kidney disease patients complicated with hyperuricemia. *Heliyon* **2023**, *9*, e20328. [CrossRef]
61. Pang, X.; Guo, Z.T.; Ao, L.; Yang, Y.L.; Liu, C.Y.; Gu, Z.H.; Xin, Y.; Li, M.Y.; Zhang, L. Integrated cell metabolomics and serum metabolomics to reveal the mechanism of hypouricemic effect of *Inonotus hispidus*. *J. Funct. Foods* **2023**, *105*, 105572. [CrossRef]

62. Wang, R.X.; Li, B.W.; Lam, S.M.; Shui, G.H. Integration of lipidomics and metabolomics for in-depth understanding of cellular mechanism and disease progression. *J. Genet. Genomics* **2020**, *47*, 69–83. [CrossRef] [PubMed]
63. Li, L.; Zhao, K.L.; Luo, J.; Tian, J.H.; Zheng, F.X.; Lin, X.M.; Xie, Z.J.; Jiang, H.Y.; Li, Y.M.; Zhao, Z.A.; et al. Piperine improves hyperuricemic nephropathy by inhibiting URAT1/GLUT9 and the AKT-mTOR pathway. *J. Agric. Food Chem.* **2024**, *72*, 6565–6574. [CrossRef] [PubMed]
64. Zhu, Y.Z.; Zhong, Y.; Zhou, Y.; Liu, Y.Y.; Huang, Q.L.; Huang, Z.; Wang, Y.C.; Ye, H.; Zeng, X.B.; Zheng, X.B. Acetylshikonin inhibits colorectal cancer growth via PI3K/Akt/mTOR signaling pathway. *Chin. Med.* **2018**, *9*, 126–143. [CrossRef]
65. Zhao, X.; Zhu, J.X.; Mo, S.F.; Pan, Y.; Kong, L.D. Effects of cassia oil on serum and hepatic uric acid levels in oxonate-induced mice and xanthine dehydrogenase and xanthine oxidase activities in mouse liver. *J. Ethnopharmacol.* **2006**, *103*, 357–365. [CrossRef] [PubMed]
66. Xu, W.H.; Liang, M.L.; Su, W.J.; Yang, J.L.; Pu, F.X.; Xie, Z.F.; Jin, K.L.; Polyakov, N.E.; Dushkin, A.V.; Su, W.K. Self-assembled nanocapsules of celery (*Apium graveolens* Linn) seed oil: Mechanochemical preparation, characterization and urate-lowering activity. *J. Drug Deliv. Sci. Tec.* **2021**, *66*, 102810. [CrossRef]
67. Zhu, F. Coix: Chemical composition and health effects. *Trends Food Sci. Tech.* **2017**, *61*, 160–175. [CrossRef]
68. Duan, Y.; Qi, Q.; Liu, Z.H.; Zhang, M.; Liu, H.Q. Soy consumption and serum uric acid levels: A systematic review and meta-analysis. *Front. Nutr.* **2022**, *9*, 975718. [CrossRef]

Disclaimer/Publisher's Note: The statements, opinions and data contained in all publications are solely those of the individual author(s) and contributor(s) and not of MDPI and/or the editor(s). MDPI and/or the editor(s) disclaim responsibility for any injury to people or property resulting from any ideas, methods, instructions or products referred to in the content.

nutrients

MDPI

Article

Effects of 12-Week Anti-Inflammatory Dietary Education on Depressive Symptoms Among Depressed Patients with Breast Cancer Undergoing Adjuvant Chemotherapy: A Randomized Controlled Trial

Lan Cheng †, Yue Chen †, Jianyun He, Xinxin Cheng, Yuting Wang, Xiaoxia Lin, Zhenzhen Huang, Xinyi Miao and Shufang Xia *

Wuxi School of Medicine, Jiangnan University, Wuxi 214122, China; chenglan@stu.jiangnan.edu.cn (L.C.); chenyue@stu.jiangnan.edu.cn (Y.C.); hejianyun@stu.jiangnan.edu.cn (J.H.); chengxinxin@stu.jiangnan.edu.cn (X.C.); wangyuting@stu.jiangnan.edu.cn (Y.W.); linxiaoxia@stu.jiangnan.edu.cn (X.L.); 6242807010@stu.jiangnan.edu.cn (Z.H.); 6242807017@stu.jiangnan.edu.cn (X.M.)

* Correspondence: xiashufang@jiangnan.edu.cn

† These authors contributed equally to this work.

Abstract: Background: Depressive symptoms (DepS) are prevalent among patients with breast cancer. Offering an anti-inflammatory diet is a promising strategy for DepS management, but it is costly and difficult to scale up. Instead, anti-inflammatory dietary education is cost-effective and may be more conducive to the promotion of an anti-inflammatory diet strategy. **Methods**: A prospective, assessor-blinded, two-arm randomized controlled trial was designed to determine the effects of 12-week anti-inflammatory dietary education on DepS in breast cancer patients with depression. Adult female patients with depression and receiving adjuvant chemotherapy were recruited. Participants in the intervention group received anti-inflammatory dietary education, while the control group received routine nursing care. Outcomes included the Center for Epidemiologic Studies Depression Scale (CES-D) score, energy-adjusted dietary inflammatory index (E-DII), plasma inflammatory biomarkers, and quality of life (QoL), which were all assessed at baseline and after a 12-week follow-up. The robustness of the estimates was investigated through sensitivity analyses. A post hoc power analysis was conducted to establish the observed effect sizes for the primary outcomes. **Results**: A total of 88.6% (62/70) of the participants completed the entire 12-week follow-up. No statistically significant between-group differences were found in the baseline characteristics, including sociodemographic factors, disease-related characteristics, and lifestyle factors. After the intervention, both the CES-D score ($p = 0.040$) and E-DII ($p < 0.001$) in the intervention group were significantly lower than in the control group, while the QoL was significantly increased ($p < 0.001$). Compared with the baseline, the tumor necrosis factor-α (TNF-α) ($p = 0.002$) and C-reactive protein (CRP) ($p = 0.045$) levels were significantly lower in the intervention group but not in the control group. **Conclusions**: Anti-inflammatory dietary education may improve DepS and QoL in breast cancer patients with depression and undergoing chemotherapy by regulating inflammation. Given its acceptability and practicality, this strategy may be incorporated into routine cancer care.

Keywords: breast cancer; depressive symptoms; anti-inflammatory diet; inflammation; education

1. Introduction

Breast cancer has become a global health concern due to its high mortality and morbidity, with 2.3 million new cases and 665,684 deaths in 2022 [1]. Due to the life-threatening and traumatic nature of cancer diagnosis and treatment, breast cancer patients are highly susceptible to mental disorders [2], and depressive symptoms (DepS) are common in breast cancer patients, with a global prevalence of 30.2% [3], usually peaking during adjuvant therapy and rebounding after the completion of treatment [4]. Cancer-related DepS not only exacerbates physical symptoms such as fatigue, pain, and insomnia, but also leads to decreased treatment adherence, severely impaired quality of life (QoL) [5], and even a higher risk of suicide [6]. In addition, depression has been proven to be an independent predictor of breast cancer recurrence and survival [7]. Studies have shown that early preventive interventions for cancer-related DepS during oncological treatment appear to improve their QoL, prognosis, and survival rates [8]. Medication, the most common antidepressant strategy, may decrease the effectiveness of anti-cancer treatments [4], and the high costs and side effects make it difficult to achieve satisfactory outcomes. Therefore, there is an urgent need for more cost-effective interventions for breast cancer-related DepS that have fewer side effects and do not interfere with oncology therapy.

A large number of studies have shown that the primary determinants of breast cancer-related DepS encompass sociodemographic factors (e.g., age, marital status, education level, and monthly income), disease-related characteristics (e.g., cancer stage, type of treatment, and surgery), and lifestyle factors (e.g., physical activity, smoking, and alcohol use) [9–13]. The diet, as a safe and modifiable lifestyle behavior, has also attracted extensive attention from researchers in recent years [14]. For instance, improving an individual's dietary behaviors, such as adopting a healthy dietary pattern that includes the consumption of vegetables, fish, olive oil, and grains, can enhance their overall mental health and reduce the risk of DepS [15,16]. A systematic review examined the association between dietary habits and depression and found that both following a healthy diet—in particular, incorporating vegetables and fruits—and avoiding a pro-inflammatory diet, consisting of junk foods, fast foods, and high meat intake, may lower the risk of developing DepS or clinical depression [17]. A meta-analysis that included 16 randomized controlled trials (RCTs) found that dietary interventions such as individualized dietary counseling, group dietary classes, and standardized dietary prescription were effective in improving DepS across the population [18]. The 'SMILES' RCT, which included 56 adults with major depressive disorder (MDD), showed significant improvements in depression in patients who received 12 weeks of personalized dietary advice and nutritional counseling support compared to a control group who received social support [19]. Similarly, another RCT including 152 adults with depression showed that a 6-month Mediterranean-style dietary intervention (including interactive nutrition education, cooking workshops, and fish oil supplements) improved depression to a greater extent than social support [20]. Therefore, dietary interventions are expected to be an effective way to prevent and treat DepS.

However, most breast cancer patients lack professional dietary guidance after the disease diagnosis [21] and exhibit unhealthy dietary patterns, poor dietary quality, and insufficient nutrient intake, which may be associated with an increased risk of DepS [22]. We previously found that the intake of dietary fiber, protein, some vitamins and minerals, and tryptophan was negatively correlated with DepS scores in breast cancer patients, and poor dietary quality was associated with an increased risk of DepS [23]. Accumulating evidence suggests that the diet has anti-inflammatory or pro-inflammatory potential and that its overall regulation of systemic inflammation may influence DepS [24]. Moreover, breast cancer patients are susceptible to chemotherapy side effects during adjuvant chemotherapy, and they prefer pro-inflammatory foods, leading to higher overall dietary inflammatory

potential [25]. Breast cancer patients with depression have been reported to consume a pro-inflammatory diet (as assessed by a higher energy-adjusted dietary inflammatory index (E-DII) score) [26]. It has been shown that a pro-inflammatory diet is independently associated with an increased risk of DepS, especially in women, suggesting that an anti-inflammatory diet might be a potential strategy for the management of DepS [27]. In the general population, an umbrella review of 28 meta-analyses of prospective studies revealed that healthy dietary patterns and the consumption of foods with anti-inflammatory properties alleviated the risk of depression, as well as reducing DepS [28]. However, to date, no clinical trials have been conducted to explore the effects of an anti-inflammatory dietary intervention on DepS among patients with breast cancer. In our previous investigation, we found that breast cancer patients lacked knowledge about anti-inflammatory/pro-inflammatory diets and had difficulty adjusting to a healthy diet on their own. Of note, offering an anti-inflammatory diet may be a promising strategy for DepS management, but it is costly and difficult to scale up. Instead, dietary education is an important and useful tool in influencing a patient's nutritional status [29]; it may be more cost-effective and achievable for the promotion of an anti-inflammatory diet strategy.

Therefore, the present study aimed to examine the effectiveness of 12-week anti-inflammatory dietary education in improving DepS among breast cancer patients with depression who underwent adjuvant chemotherapy. We hypothesized that, compared with the control group, patients in the intervention group would have (1) a greater improvement in DepS, (2) a greater reduction in inflammatory biomarkers, and (3) a greater improvement in QoL across the study period.

2. Materials and Methods

2.1. Study Design and Participants

This 12-week, prospective, assessor-blinded, and two-arm RCT (China Clinical Trials Registry, ChiCTR2200064967) was conducted in accordance with the Consolidated Standards of Reporting Trials (CONSORT) statement guidance [30]. Ethical approval was granted by the Medical Ethics Committee of Jiangnan University (JNU20220606IRB15) and implemented in compliance with the Declaration of Helsinki.

Female patients were recruited from October 2022 to June 2023 at the Department of Breast Surgery in the Affiliated Hospital of Jiangnan University. The inclusion criteria were (1) diagnosed with stage I~III breast cancer; (2) with a Center for Epidemiologic Studies Depression Scale (CES-D) score $\geq$ 16; (3) aged $\geq$ 18 years; (4) had undergone breast surgery and were scheduled to receive a minimum of four cycles of adjuvant chemotherapy; (5) had a smartphone to receive messages and communicate; (6) had normal cognitive function and reading abilities. The exclusion criteria included (1) recurrent or metastatic breast cancer; (2) previously diagnosed with other cancers; (3) comorbidities with serious somatic or organic brain diseases; (4) the presence of serious infectious diseases; (5) the use of antidepressant, anxiolytic, neurological, or psychiatric medication; (6) undergoing psychological treatments; (7) the recent use of antibiotics or immune-modulating medications; (8) being pregnant or lactating.

2.2. Recruitment and Randomization

The nursing staff identified potential participants from the medical records and then sent them invitations. Written informed consent was obtained from patients if they were eligible and interested in participating. A research assistant who did not participate in the recruitment process used the R software (version 4.3.2) to generate the randomization list with a 1:1 allocation ratio (block size of 4) and sealed the results in serially numbered opaque envelopes. Each envelope was opened only after baseline assessment completion.

Based on the order of enrollment and random codes in the envelopes, participants were randomly assigned to either the intervention or control group before chemotherapy. The randomization schedule and coding of group allocations were not, at any time, accessible to the outcome assessors. After randomization, three well-trained interveners provided hospital-based anti-inflammatory dietary education and invited the participants to join a WeChat group for online nutritional counseling support. Due to the behavioral nature of the dietary intervention, the blinding of the participants and interveners was not feasible. However, several strategies were employed to reduce the risk of bias: (1) upon admission to the hospital, we firstly assessed the patient's DepS and assigned the patients with depression to wards with patients without depression, ensuring that there would be at most one patient with depression in each ward; (2) the outcome assessors received separate training, emphasizing neutrality; (3) all assessments were conducted in dedicated rooms without intervention materials; (4) the laboratory technicians analyzing the inflammatory biomarkers were masked to the group allocations using anonymized sample IDs.

2.3. Sample Size

The sample size was calculated by using the following formula:

$$n = (Z_{\alpha} + Z_{\beta})^2 \times 2\sigma^2/\delta^2$$

The difference in the mean CES-D scores of patients in the intervention and control groups δ = 8.1, and the combined standard deviation of the two groups σ = 9.34. Therefore, a minimum of 28 participants for each group was required to provide the study with 80% power at a two-tailed 5% level of significance. Considering the 20% sample attrition rate, the required sample size was increased to 70 participants, with 35 in each group.

2.4. Intervention

The intervention included four sessions of hospital-based anti-inflammatory dietary education and 12 weeks of online nutritional counseling support. After the patients with breast cancer were admitted to receive chemotherapy, four sessions of dietary education were provided. The aim of these sessions was to teach the participants anti-inflammatory dietary knowledge and facilitate their home-based practice. After patients were admitted to the hospital, the trained interveners provided face-to-face teaching on how to consume an anti-inflammatory diet among the participants in the ward. They were encouraged to adhere to an anti-inflammatory dietary plan characterized by the reduced consumption of processed foods and increased consumption of "good" fats and whole foods [31]. The whole foods promoted for moderate consumption included lean meats, eggs, and dairy products, while those promoted for higher consumption were fish, fruits, vegetables, nuts, and seeds. "Good fats" included monounsaturated fats with a favorable ω-6–ω-3 ratio, such as fish, seeds, and olive oil. Meanwhile, the participants were asked to limit their consumption of highly processed and refined foods, such as refined carbohydrates (pasta, bread, rice), confectionary, and processed meats. Each session lasted about 20–30 min. Before the intervention began, we prepared a brochure on the anti-inflammatory diet, including the following topics: (1) the relationship between anti-inflammatory diets and disease; (2) anti-inflammatory dietary recipes and samples of common processed foods, "good" fats, and whole foods; (3) routine care during chemotherapy; and (4) tips for achieving dietary self-management. At the end of the first dietary education session, the participants were provided with the brochures to refer to when they went home to prepare their diets. During the home period, the participants were provided with online nutritional counseling support once a week via WeChat or by telephone, which included providing dietary knowledge or nutritional tips, answering participants' questions, reminding the

participants to keep dietary records, evaluating the reasonableness of the diets, and giving targeted recommendations for improvement.

Participants in the control group received 12-week routine care, including face-to-face counseling during hospitalization (4 sessions) and online support via WeChat or by telephone after discharge if necessary. The face-to-face counseling included topics such as general knowledge of breast cancer and frequently asked questions (e.g., the occurrence, risk factors, and treatment of breast cancer; care during chemotherapy; the prevention of lymphedema; and regular review after the completion of therapy). Each of the face-to-face sessions focused on one of the selected topics. The information used in the consultation sessions was developed based on the Guidelines for Breast Cancer Diagnosis and Treatment by the China Anti-Cancer Association (2024). The interveners never took the initiative to teach diet-related knowledge to the patients in the control group. If patients inquired about the diet, recommendations were provided based on the Dietary Guidelines for Chinese Residents (2022), a basic set of dietary guidelines without a specific anti-inflammatory focus. As for online support, the researchers provided the patients with friendly reminders of upcoming tests and treatment appointments and answered patients' questions.

To minimize the dropout rates, this study recruited breast cancer patients scheduled to receive at least four cycles (21 days per cycle) of adjuvant chemotherapy. This ensured that all patients were still at a stage requiring hospitalization for chemotherapy after the 12-week intervention. One or two days before each chemotherapy cycle, the interveners made a phone call to provide a friendly reminder of the upcoming appointment. Additionally, patients were offered prizes for completing each session of the intervention, encouraging their attendance at future follow-up visits.

2.5. Sociodemographic and Clinical Information

The participants' sociodemographic and clinical characteristics were collected at baseline. As both physical activity and drinking are critical factors affecting depression [32,33], they were also assessed at baseline. The physical activity level was assessed by the International Physical Activity Questionnaire Short Form (IPAQ-SF) to calculate the metabolic equivalent (MET) and then classified into three levels: low (<600 MET/min/week), moderate (600 to 1500 MET/min/week), and high (>1500 MET/min/week) [34]. Data were collected by trained phlebotomists, dieticians, nutritionists, and research assistants.

2.6. Primary Outcome

The CES-D scale, with good validity in breast cancer patients, was used to assess DepS. Participants with a CES-D score $\geq$ 16 were considered to have depression [35,36] and selected as research candidates. At the end of the 12 weeks of intervention, the participants were reassessed with the CES-D.

2.7. Secondary Outcomes

2.7.1. Dietary Intake Assessment and E-DII Calculation

For each intervention cycle, dietary intake was assessed using 3-day, 24 h dietary recalls [37], in which detailed types, amounts, and cooking methods of foods were recorded on one weekend day and two working days. In order to improve the accuracy of the dietary surveys, we collected the participants' dietary intake in the past 24 h after their admission to the hospital, and the remaining two dietary recalls were conducted via WeChat after the participants were discharged from the hospital and the chemotherapy-induced gastrointestinal symptoms had disappeared. After each dietary survey, daily nutrient intakes were then calculated using the Nutrition Calculator v2.7.8.8 (Chinese Center for Disease Control and Prevention, Beijing, China). Meanwhile, the dietitian evaluated the

participants' dietary and nutrient intake roughly, gave individualized recommendations for adjustments, and educated the participants via WeChat.

To control for the effect of total energy intake on the DII score, the E-DII score was calculated to assess the overall inflammatory potential of an individual's diet. The detailed calculation methods for the E-DII have been described in our previously published literature [26]. In this study, the E-DII scores were calculated using the following 25 food parameters: energy; total fat; protein; carbohydrates; dietary fiber; cholesterol; vitamins A, B1, B2, B6, C, D, and E; folate; niacin; β-carotene; magnesium; iron; zinc; selenium; saturated fatty acids; monounsaturated fatty acids; polyunsaturated fatty acids; and ω-3 and ω-6 fatty acids.

2.7.2. Plasma Inflammatory Biomarkers

After an overnight 12 h fast, blood samples were collected from 35 volunteer participants at baseline and week 12 by a trained phlebotomist. Plasma was prepared by centrifugation at 3500 rpm for 10 min, followed by inflammatory biomarker (interleukin (IL)-1β, IL-6, tumor necrosis factor-α (TNF-α), and C-reactive protein (CRP)) measurements using commercial ELISA kits (Meimian, Yancheng, China) for each time point according to the manufacturer's instructions.

2.7.3. Quality of Life

QoL was assessed using the Functional Assessment of Cancer Therapy—Breast (FACT-B) [38], which is a scale designed specifically for breast cancer patients. It consists of a general scale measuring the commonality of all cancer types (commonality module) and breast cancer-specific domains, covering physical, social/family, emotional, functional well-being, and additional breast cancer concerns. All items were scored on a 5-point Likert scale from 0 to 4 ("not at all" to "very much"), with a total score of 0 to 144. A higher total score represents better QoL. The Chinese version of the scale has been widely validated in breast cancer patients [39].

2.8. Statistical Analysis

Statistical analyses were performed on SPSS 27.0 (IBM Corp, Chicago, IL, USA). The normality of continuous variables was assessed using the Shapiro−Wilk test. Continuous variables were presented as the mean ± standard deviation (SD). Differences between groups were assessed by the 2-tailed independent-samples *t*-test for normally distributed variables or the Mann−Whitney U test for non-normally distributed variables. The paired-sample *t*-test and Wilcoxon test were used to assess the differences before and after the intervention for normally and non-normally distributed data, respectively. Categorical variables were presented as frequencies (n) and percentages (%). The chi-squared test, continuity-corrected chi-squared test, or Fisher's exact test was used to assess the differences in categorical variables between groups. The robustness of estimates was investigated through sensitivity analyses by comparing the baseline characteristics and outcomes of the subjects who consented to provide blood samples (summarized in Supplementary Materials). To aid in the interpretation of the primary outcomes, a post hoc power analysis was additionally conducted based on the observed effect sizes. A *p*-value of <0.05 was considered statistically significant.

3. Results

3.1. Overview

A total of 98 female breast cancer patients were assessed for eligibility, of whom 18 did not meet the inclusion criteria and 10 declined to participate (Figure 1). Finally, 70 eligible

participants were successfully recruited and randomly assigned to the intervention group (n = 35) or the control group (n = 35). At the endpoint, a total of 62 participants (31 in each group, with a retention rate of 88.6%) completed the entire 12-week follow-up, as eight dropped out (dropout rate 11.4%, n = 1 due to starting the use of antidepressants, n = 5 due to hospital changes, and n = 2 due to personal or family issues).

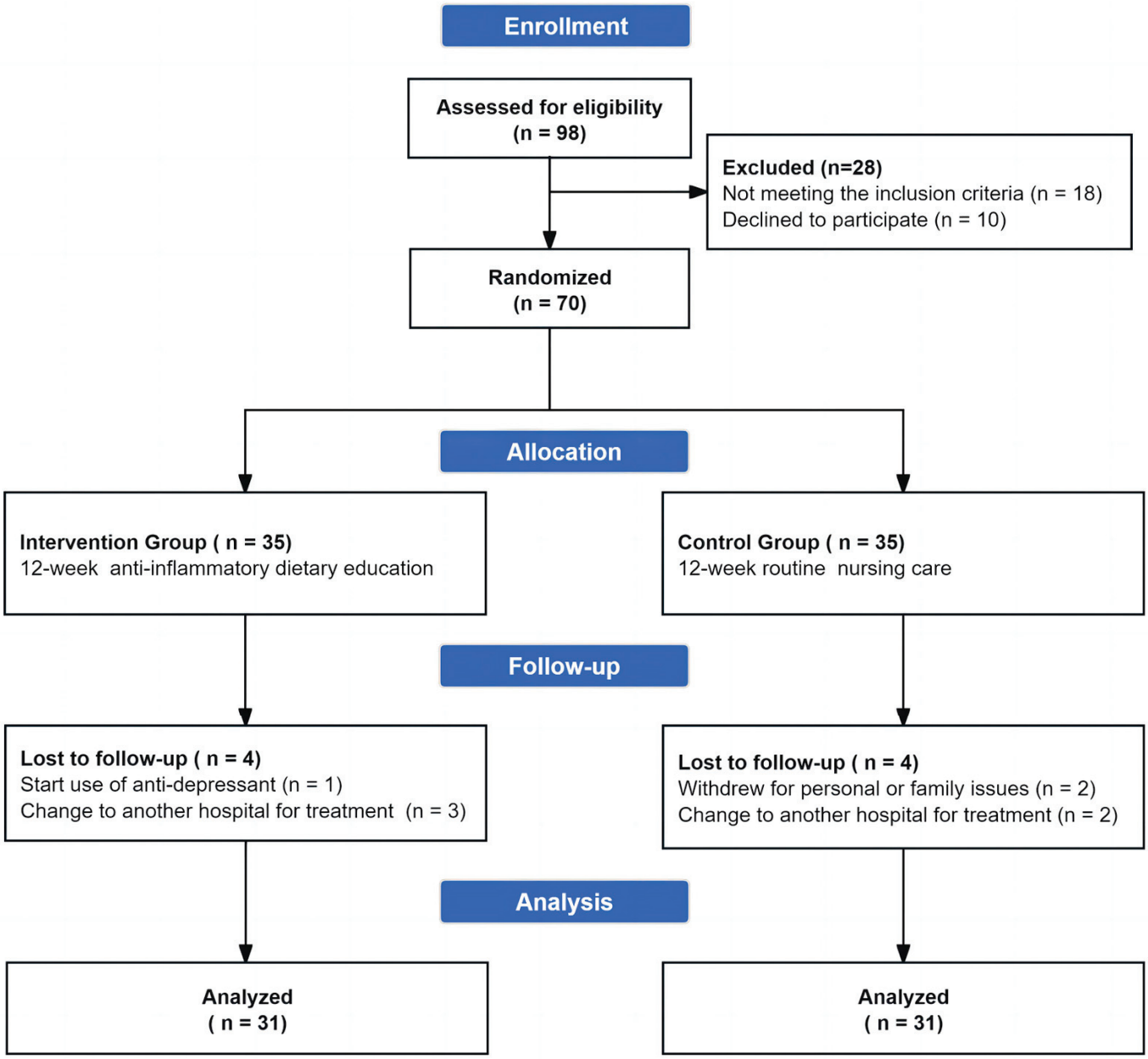


Figure 1. Flow diagram of participant recruitment during the trial according to CONSORT.

3.2. Participant Baseline Characteristics

The baseline characteristics of the participants are presented in Table 1. All female participants had a mean age of 52.90 ± 11.05 years, with a mean BMI of 24.18 ± 3.22 kg/m^2. The majority of the participants were post-menopausal (54.8%), diagnosed with stage II breast cancer (61.2%), and had undergone a mastectomy (67.7%). No statistically significant between-group differences were found in the baseline characteristics.

Table 1. Comparison of baseline characteristics between the intervention and control groups.

Variable	Total (n = 62)	Intervention (n = 31)	Control (n = 31)	p
Age (year) [a]	52.90 ± 11.05	52.61 ± 11.91	53.19 ± 10.32	0.838
BMI (kg/m^2) [b]	24.18 ± 3.22	24.17 ± 2.80	24.18 ± 3.63	0.800
Menopausal status [c]				
Pre-menopausal	28 (45.2)	14 (45.2)	14 (45.2)	1.000
Post-menopausal	34 (54.8)	17 (54.8)	17 (54.8)	
Marital status [d]				
Married	57 (91.9)	29 (93.5)	28 (90.3)	1.000
Widowed/divorced/single	5 (8.1)	2 (6.5)	3 (9.7)	
Education level [c]				
Primary school or lower	14 (22.6)	6 (19.4)	8 (25.8)	0.386
Middle school	27 (43.6)	15 (48.4)	12 (38.7)	
High school/secondary school	10 (16.1)	3 (9.7)	7 (22.6)	
Junior college or higher	11 (17.7)	7 (22.6)	4 (12.9)	
Employment [c]				
Employed	14 (22.6)	9 (29.0)	5 (16.1)	0.455
Unemployed	25 (40.3)	12 (38.7)	13 (41.9)	
Retired	23 (37.1)	10 (32.3)	13 (41.9)	
Residence [c]				
Rural areas	16 (25.8)	5 (16.1)	11 (35.5)	0.213
Towns	17 (27.4)	10 (32.3)	7 (22.6)	
Urban areas	29 (46.8)	16 (51.6)	13 (41.9)	
Family monthly income [e]				
<2000 CNY	5 (8.1)	3 (9.7)	2 (6.5)	0.617
2000~5000 CNY	20 (32.2)	8 (25.8)	12 (38.7)	
>5000 CNY	37 (59.7)	20 (64.5)	17 (54.8)	
Number of chemotherapy cycles completed [e]				
0	15 (24.2)	8 (22.6)	7 (25.8)	0.905
1	21 (33.9)	9 (38.7)	12 (29.0)	
2	19 (30.6)	10 (29.0)	9 (32.3)	
3	7 (11.3)	4 (9.7)	3 (12.9)	
Cancer stage [c]				
I	12 (19.4)	8 (25.8)	4 (12.9)	0.416
II	38 (61.2)	17 (54.8)	21 (67.7)	
III	12 (19.4)	6 (19.4)	6 (19.4)	
Surgery type [c]				
Mastectomy	42 (67.7)	20 (64.5)	22 (71.0)	0.587
Lumpectomy	20 (32.3)	11 (35.5)	9 (29.0)	
Presence of comorbidities [c]				
No	41 (66.1)	21 (67.7)	20 (64.5)	0.788
Yes	21 (33.9)	10 (32.3)	11 (35.5)	
Physical activity level [c]				
Low	26 (41.9)	12 (38.7)	14 (45.2)	0.607
Moderate	36 (58.1)	19 (61.3)	17 (54.8)	
Drinking status [d]				
Never	57 (91.9)	27 (87.1)	30 (96.8)	0.351
Former/current	5 (8.1)	4 (12.9)	1 (3.2)	

Data are shown as n (%) or mean ± SD. [a] Independent-samples t-test. [b] Mann−Whitney U test. [c] Chi-squared test. [d] Chi-squared test with continuity correction. [e] Fisher's exact test. BMI, body mass index; CNY, Chinese yuan.

3.3. Effects on Depressive Symptoms

At baseline, the CES-D score (20.81 ± 3.59 vs. 20.00 ± 3.17; p = 0.352) was not significantly different between the two groups (Figure 2A). However, after the 12-week follow-up, the CES-D score in the intervention group was significantly lower than in the control group (15.61 ± 3.55 vs. 17.61 ± 3.95; p = 0.040; Figure 2B). Compared to the baseline

data, a reduction in the CES-D scores was observed in both the intervention (Δ CES-D: −5.19 ± 3.94; $p < 0.001$; Figure 2C) and control (Δ CES-D: −2.39 ± 4.84; $p = 0.001$; Figure 2D) groups. In addition, a significant difference was also observed in the changes in the CES-D score between the two groups ($p = 0.015$).

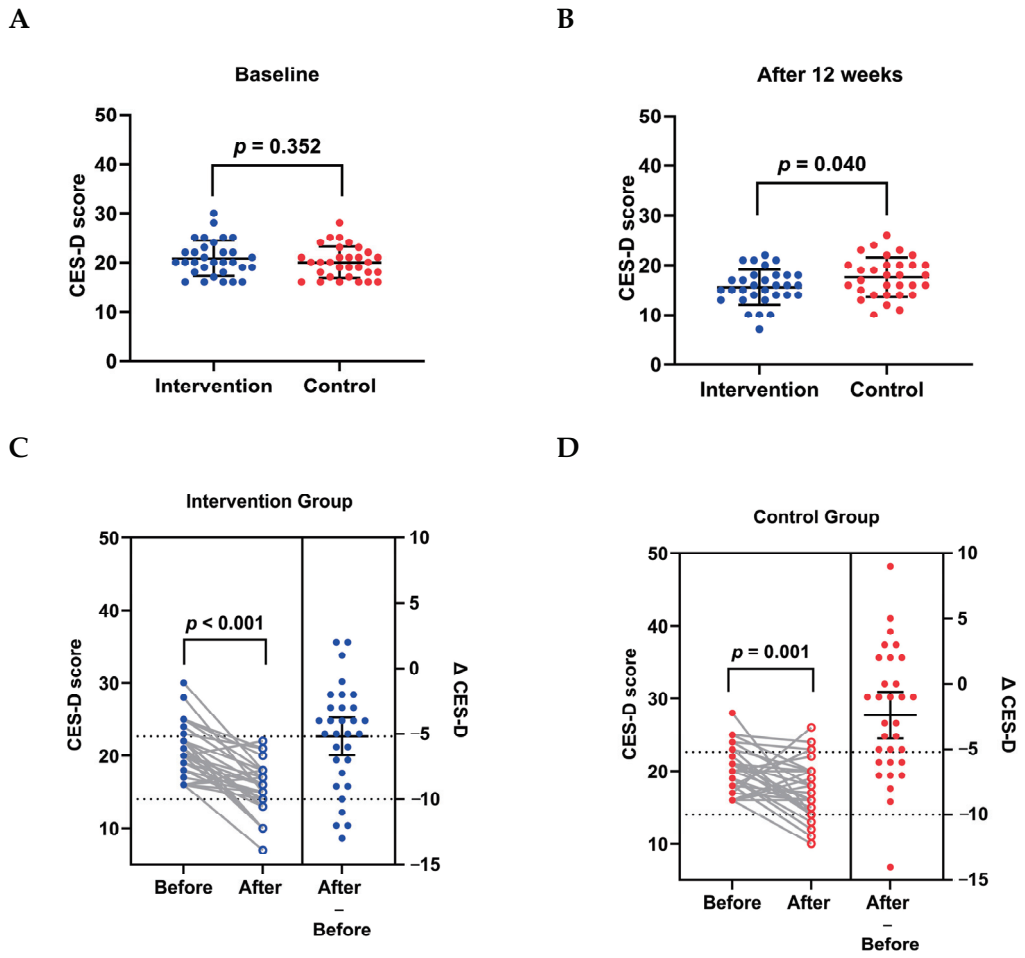


Figure 2. Effects on depressive symptoms in breast cancer patients with depression and receiving chemotherapy. (**A**,**B**): CES-D scores of intervention and control groups at baseline and after 12 weeks. Data are presented as mean ± SD. Independent-samples *t*-test was used. (**C**,**D**): CES-D scores of intervention and control groups from baseline to the end of follow-up. Paired *t*-test was used. CES-D, the Center for Epidemiologic Studies Depression Scale. The change (Δ) was defined as the value after the intervention minus the value at baseline for the same individual.

3.4. Effects on Dietary Inflammatory Potential

At baseline, no significant difference was found in the E-DII scores between the two groups ($p = 0.858$; Figure 3A). However, after the 12-week follow-up, the E-DII score in the intervention group was significantly lower than in the control group (−0.88 ± 1.65 vs. 0.65 ± 1.63; $p = 0.001$; Figure 3B). Compared to the baseline data, the E-DII score was significantly decreased in the intervention group (Δ E-DII: −0.76 ± 1.71; $p = 0.020$; Figure 3C), while it was significantly increased in the control group (Δ E-DII: 0.69 ± 1.21; $p = 0.003$; Figure 3D). A significant difference was also observed in the changes in the E-DII score between the two groups ($p < 0.001$).

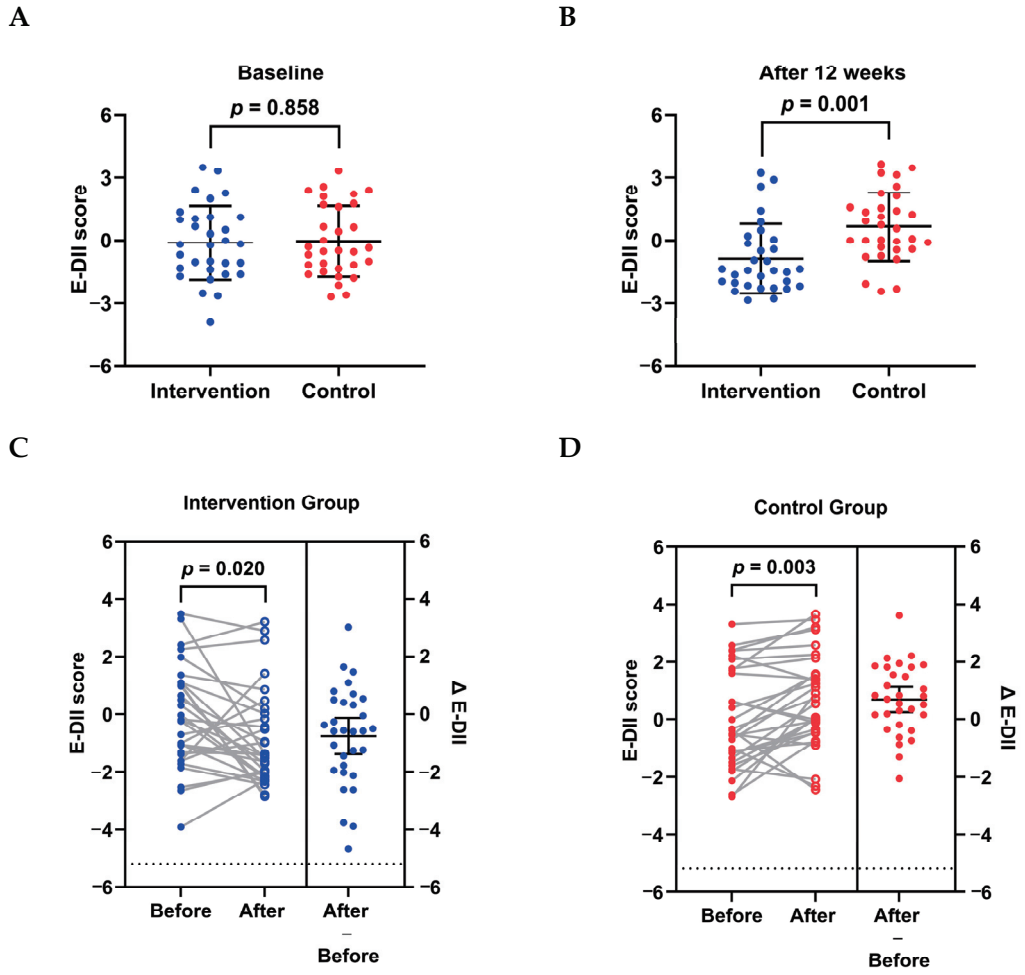


Figure 3. Effects on E-DII in breast cancer patients with depression and receiving chemotherapy. (**A**,**B**): E-DII scores of the intervention and control groups at baseline and after 12 weeks. Data are presented as mean ± SD. (**A**) Independent-samples *t*-test was used. (**B**) Mann−Whitney U test was used. (**C**,**D**): E-DII score changes of the intervention and control groups from baseline to the end of follow-up. Paired *t*-test was used. E-DII, energy-adjusted dietary inflammatory index. The change (Δ) was defined as the value after the intervention minus the value at baseline for the same individual.

3.5. Effects on Plasma Inflammatory Biomarkers

Since some patients had already received blood tests during their pre-admission outpatient visits, only 35 plasma samples were obtained from the patients for the determination of inflammatory biomarkers. Sensitivity analyses showed that the baseline characteristics of these 35 individuals were consistent with those of the 62 individuals and that the intervention had a similar effect on the study outcomes (summarized in Supplementary Materials). As shown in Table 2, there were no significant differences in all plasma inflammatory biomarkers between the two groups at baseline and at the end of the 12-week follow-up ($p > 0.05$). Compared with the baseline data, both the TNF-α (Δ TNF-α: −11.58 ± 15.27 pg/mL; $p = 0.002$) and CRP (Δ CRP: −0.98 ± 1.80 mg/L; $p = 0.045$) levels decreased significantly in the intervention group, but not in the control group. Additionally, there was a significant difference in Δ TNF-α between the two groups (Δ TNF-α: −11.58 ± 15.27 vs. −5.29 ± 21.02; $p = 0.041$).

Table 2. Changes in plasma inflammatory biomarkers.

Variable	Intervention (n = 18)	Control (n = 17)	p
IL-1β (pg/mL)			
Baseline	22.57 ± 13.01	18.40 ± 5.59	0.636 [b]
After 12 weeks	26.46 ± 11.16	21.46 ± 12.77	0.067 [b]
Δ IL-1β	3.89 ± 9.38	3.06 ± 12.85	0.287 [b]
p	0.096 [c]	0.795 [d]	
IL-6 (pg/mL)			
Baseline	15.30 ± 7.34	13.17 ± 5.73	0.318 [b]
After 12 weeks	15.02 ± 7.24	13.12 ± 4.64	0.351 [b]
Δ IL-6	−0.28 ± 4.67	−0.05 ± 6.88	0.568 [b]
p	0.744 [d]	0.463 [d]	
TNF-α (pg/mL)			
Baseline	59.74 ± 19.76	56.18 ± 37.52	0.110 [b]
After 12 weeks	48.17 ± 11.31	50.89 ± 21.07	0.636 [b]
Δ TNF-α	−11.58 ± 15.27	−5.29 ± 21.02	0.041 [b]
p	0.002 [d]	0.740 [d]	
CRP (mg/L)			
Baseline	9.43 ± 2.28	8.94 ± 3.49	0.184 [b]
After 12 weeks	8.45 ± 1.49	8.48 ± 1.68	0.961 [a]
Δ CRP	−0.98 ± 1.80	−0.46 ± 2.61	0.184 [b]
p	0.045 [d]	0.943 [d]	

Data are shown as mean ± SD. [a] Independent-samples t-test. [b] Mann−Whitney U test. [c] Paired t-test. [d] Wilcoxon test. CRP, C-reactive protein; IL-1β, interleukin 1β; IL-6, interleukin 6; TNF-α, tumor necrosis factor-α. The change (Δ) was defined as the value after the intervention minus the value at baseline for the same individual.

3.6. Effects on QoL

The changes in the QoL of the participants are shown in Table 3. There were no significant differences between the two groups at baseline in the FACT-B scores ($p > 0.05$). After the 12-week follow-up, the FACT-B score of the intervention group was significantly higher than that of the control group ($p < 0.001$). Although both groups experienced improved QoL following the 12-week follow-up, the intervention group showed a greater increase than the control group (Δ FACT-B: 16.77 ± 18.68 vs. 4.10 ± 17.17; $p = 0.007$). Moreover, at the end of the 12-week follow-up, the subscale scores of social/family (20.00 ± 4.82 vs. 17.10 ± 3.35; $p = 0.015$), emotional (18.39 ± 3.24 vs. 16.23 ± 3.68; $p = 0.016$), functional well-being (19.26 ± 4.41 vs. 15.39 ± 4.32; $p < 0.001$), and additional concerns (29.06 ± 3.26 vs. 26.84 ± 3.49; $p = 0.012$) were significantly higher in the intervention group than in the control group, but no significant difference was found in physical well-being.

Table 3. Changes in quality of life after the 12-week follow-up.

Variable	Intervention (n = 31)	Control (n = 31)	p
FACT-B score			
Baseline	91.74 ± 20.44	91.71 ± 17.45	0.995 a
After 12 weeks	108.52 ± 14.22	95.81 ± 13.09	<0.001 [a]
Δ FACT-B	16.77 ± 18.68	4.10 ± 17.17	0.007 [a]
p	<0.001 [c]	0.194 c	
Physical well-being			
Baseline	20.10 ± 4.08	20.32 ± 4.30	0.729 [b]
After 12 weeks	21.81 ± 3.69	20.26 ± 3.94	0.116 [a]
Δ Physical well-being	1.71 ± 5.62	−0.06 ± 5.03	0.195 [a]
p	0.101 [c]	0.944 [c]	

Table 3. *Cont.*

Variable	Intervention (n = 31)	Control (n = 31)	p
Social/family well-being			
Baseline	16.71 ± 5.22	16.13 ± 5.25	0.777 [b]
After 12 weeks	20.00 ± 4.82	17.10 ± 3.35	0.015 [b]
Δ Social/family well-being	3.29 ± 4.18	0.97 ± 4.65	0.025 [b]
p	<0.001 [c]	0.336 [d]	
Emotional well-being			
Baseline	13.74 ± 6.07	13.97 ± 5.38	0.877 [a]
After 12 weeks	18.39 ± 3.24	16.23 ± 3.68	0.016 [b]
Δ Emotional well-being	4.65 ± 5.14	2.26 ± 4.84	0.065 [a]
p	<0.001 [c]	0.014 [c]	
Functional well-being			
Baseline	15.55 ± 5.14	14.52 ± 4.73	0.414 [a]
After 12 weeks	19.26 ± 4.41	15.39 ± 4.32	<0.001 [a]
Δ Functional well-being	3.71 ± 5.29	0.87 ± 5.95	0.052 [a]
p	<0.001 [c]	0.422 [c]	
Additional concerns			
Baseline	25.65 ± 4.59	26.77 ± 4.00	0.299 [b]
After 12 weeks	29.06 ± 3.26	26.84 ± 3.49	0.012 [a]
Δ Additional concerns	3.42 ± 5.03	0.06 ± 3.99	0.005 [a]
p	<0.001 [c]	0.929 [c]	

Data are shown as mean ± SD. [a] Independent-samples t-test. [b] Mann−Whitney U test. [c] Paired t-test. [d] Wilcoxon test. FACT-B, the Functional Assessment of Cancer Therapy—Breast Scale. The change (Δ) was defined as the value after the intervention minus the value at baseline for the same individual.

4. Discussion

In this study, we examined the effectiveness of 12-week anti-inflammatory dietary education on DepS among breast cancer patients undergoing adjuvant chemotherapy. Patients who completed the dietary education showed significant improvements in DepS, dietary anti-inflammatory potential, and QoL compared to the control group. Moreover, we also found that this strategy played an important role in reducing the levels of inflammatory biomarkers (TNF-α and CRP) in breast cancer patients. Therefore, anti-inflammatory dietary education may be an effective strategy in managing DepS and improving QoL among breast cancer patients in clinical settings.

Numerous studies have indicated a positive impact of dietary interventions on the treatment of patients with depression [40]. We conducted this prospective study in breast cancer patients with depression and found that the 12-week anti-inflammatory dietary education was not only effective in enhancing the dietary anti-inflammatory potential but also exerted a beneficial effect on DepS, which was consistent with the findings of some previous studies. A systematic review and meta-analysis including seven longitudinal and four cross-sectional studies reported a significant association between a pro-inflammatory diet and an increased risk of DepS relative to an anti-inflammatory diet [41]. A randomized controlled trial including 67 adults with MDD found that, after 12 weeks of follow-up, the participants in the modified Mediterranean diet (a typical anti-inflammatory dietary pattern) group showed a better improvement in DepS than those in the control group [19]. A similar effect of this dietary pattern has also been observed in postmenopausal women, wherein long-term adherence to the Mediterranean diet not only improved mood and depression but also reduced the risk of breast cancer [42]. Of note, inconsistent results were found in overweight and obese breast cancer survivors, where anti-inflammatory dietary education had no beneficial effect on DepS in the aforementioned populations [43]. Several factors might be responsible for this discrepancy. First, the inclusion criteria for the

study participants were different. The baseline CES-D scores of the breast cancer survivors in the study conducted by Long et al. [43] were 3.07 ± 2.92 and 2.33 ± 2.40, indicating that nearly all breast cancer survivors in Long's study did not have depression, but, in the present study, all participants had depression. Second, the duration of the intervention was different. Long et al. [43] assessed the effect of the intervention at 6 and 12 months, both of which were longer than 12 weeks. Meanwhile, a two-year randomized trial designed to assess the effect of the Mediterranean diet in patients with previous depressive episodes showed no differences regarding the depression recurrence risk, but an improvement in DepS was seen at four and eight months [44]. Therefore, considering that a dietary nutrition intervention is a long-term lifestyle modification and the effects of the diet on DepS appear to undergo dynamic changes over time, future studies with more comprehensive designs, such as considering different disease stages, larger sample sizes, and longer follow-ups, are recommended to gain insights into the effects of an anti-inflammatory diet on DepS in breast cancer patients.

Inflammation is an important biological mechanism identified through which diet may plausibly affect DepS [45]. The present study revealed a notable decline in the levels of TNF-α and CRP among participants in the anti-inflammatory dietary education group, but only the change in TNF-α was significant between the intervention and control groups. This result was consistent with our previous findings that, among all determined inflammatory biomarkers (IL-1β, IL-6, TNF-α, and CRP), only TNF-α significantly mediated the relationship between the E-DII and DepS in breast cancer patients [26]. Similarly, Yao et al. [46] also found that patients with MDD had higher serum TNF-α levels, but, after 2 and 12 weeks of antidepressant treatment, there were significant decreases in their TNF-α levels. These findings indicate that depression is accompanied by the activation of TNF-α, which also has predictive value for the antidepressant treatment response in patients with depression. In breast cancer survivors, a high-quality diet that is typically rich in fruits, vegetables, whole grains, and polyunsaturated fatty acids has been reported to be associated with lower levels of pro-inflammatory biomarkers (e.g., CRP and TNF-α) [47]. Both of these inflammatory biomarkers have also been demonstrated to be strongly associated with DepS. A longitudinal study including 60 subjects with metabolic syndrome showed that, after six months of dietary treatment, DepS and the circulating CRP concentrations were decreased, and the decrease in DepS was significantly associated with declines in CRP [48]. A systematic review and meta-analysis of 63 studies indicated that circulating TNF and CRP were associated with DepS in cancer patients [49]. Thus, inflammation appears to be a key factor in the association between diet and DepS. However, considering the limited blood sample size and short-term follow-up, these observations are exploratory and require confirmation in future mechanistic studies.

Additionally, anti-inflammatory dietary education also resulted in a notable enhancement in overall QoL and its subscales of social/family, emotional and functional well-being, and additional concerns. Similar results were found in patients with relapsing–remitting multiple sclerosis and in overweight and obese women with knee osteoarthritis, where an anti-inflammatory dietary intervention significantly improved the participants' QoL compared with controls [50,51]. A randomized controlled trial with 106 lung cancer patients receiving chemotherapy also showed an improvement in QoL with an anti-inflammatory diet [52]. Meanwhile, Barchitta et al. [53] performed a systematic review of nine experimental studies (including seven RCTs and two single-arm trials) and found that breast cancer survivors showed significant improvements in overall QoL and/or its subscales after receiving dietary interventions that included measures such as diet provision, dietary education, and diet counseling. However, another study showed no significant effect of an anti-inflammatory diet on the QoL of breast cancer survivors [43]. A possible explanation

for this may be that the latter study had a longer intervention period, potentially masking a significant effect of the intervention on QoL in the short term [54]. Additionally, at the end of the intervention, there was no significant difference between the intervention and control groups in terms of the physical well-being domain. This finding is not surprising, as this subscale assesses patients' physical well-being by asking whether the patients have experienced symptoms such as weakness, nausea, pain, being bothered by the side effects of treatment, feeling ill, and being forced to lie down in the past 7 days. However, during the investigation, we found that the participants in both groups had these symptoms and most of them were related to chemotherapy. Therefore, the effect of anti-inflammatory dietary education on patients' physical well-being may be diminished by chemotherapy.

There are some limitations to this study. First, dietary intake was assessed using self-reported data collected through 3-day, 24 h dietary recalls, which may lead to recall bias. For most dietary components, unbiased reference instruments are lacking [55]. Although the food frequency questionnaire (FFQ) is commonly used to assess the long-term diets of individuals, we opted for the 3-day, 24 h dietary recall method instead. This change was necessitated by our observation that most patients' dietary habits had changed a lot after their breast cancer diagnosis. Additionally, the dietary information collected through the FFQ encompassed both intake before and after the diagnosis, making it impossible to accurately reflect the patients' diets during the disease stages. Second, anti-inflammatory dietary education is a lifestyle intervention that requires long-term adherence, whereas the present study was conducted for only 3 months and lacked long-term follow-up to assess the impact of the intervention on the patients. In the future, longer follow-up studies are needed to evaluate the long-term intervention effects. Third, only 35 plasma samples were obtained from the patients for the determination of inflammatory biomarkers. This was due to the fact that some patients had already received relevant blood tests during their pre-admission outpatient visits and were usually hospitalized a few days later to start chemotherapy immediately. Consequently, they were willing to complete the questionnaire but unwilling to have their blood drawn again specifically for inflammatory biomarker determination. Fourth, only IL-1β, IL-6, TNF-α, and CRP were assessed in this study. Several other important markers through which the diet affects DepS should be considered in future studies, including the anti-inflammatory cytokine IL-10, oxidative stress, the gut microbiome, and tryptophan [56]. Fifth, the absolute change in the CES-D scores and inflammatory biomarkers seemed minimal after the 12-week intervention. Considering the limited sample size, we conducted a post hoc power analysis for the primary outcome, achieving power of 54.1%, which is lower than the conventional threshold of 80%. However, it is much higher than the power values of 59 RCTs (median 0.16, IQR 0.08~0.32) in the surgical literature [57]. The conventional threshold is unattainable even for high-quality studies, particularly when considering studies with inherently small samples, such as many of those related to surgical science or rare diseases [58]. Finally, as a single-center study, the generalizability of the findings to other populations may be limited, and caution is needed when extrapolating these results. Whether similar benefits would extend to non-cancer populations or those with treatment-resistant depression remains unclear. Therefore, future prospective studies with more rigorous study designs, larger sample sizes, multi-center designs, and longer follow-up periods are still needed to determine the long-term effectiveness of anti-inflammatory dietary education on DepS in the breast cancer population.

The present study also has some implications. Although the observed effect sizes for the DepS scores and inflammatory biomarkers seemed minimal (potentially influenced by the limited sample size and short-term follow-up duration), the statistically significant changes suggest that anti-inflammatory dietary education may exert a measurable yet

modest therapeutic effect on both emotional regulation and inflammatory pathways in breast cancer patients with depression. This finding is consistent with existing evidence: a meta-analysis of 16 RCTs (n = 45,826) similarly demonstrated small but significant antidepressant effects of dietary interventions [18], suggesting that dietary improvement could be an ideal option for low-intensity treatment or for individuals to adopt as a self-management approach to reduce DepS. In addition, most breast cancer patients exhibited unhealthy dietary patterns due to a lack of professional dietary guidance after their disease diagnosis, which is associated with an increased risk of breast cancer recurrence and mortality [21,59]. In the present study, we also found that breast cancer patients without anti-inflammatory dietary education had a significant increase in their E-DII scores during chemotherapy, while patients who received anti-inflammatory dietary education had a significant decrease. A prospective cohort study included 1064 female breast cancer survivors and found that the post-diagnosis E-DII was significantly associated with the mortality risk among breast cancer survivors [60]. Breast cancer patients consuming the most pro-inflammatory diets had a 34% higher risk of death from all causes compared with patients consuming the most anti-inflammatory diets [60]. Therefore, the findings of the present study offer further support for the need to focus on addressing poor diets (especially higher dietary inflammatory potential) in oncology practice. For instance, healthcare providers could incorporate anti-inflammatory dietary education into standard care pathways during the treatment initiation and follow-up phases, implementing serial assessments using validated depression scales (e.g., CES-D) alongside dietary adherence tracking (e.g., the consumption of anti-inflammatory/pro-inflammatory food). Where feasible, behavioral measures should be supplemented with inflammatory biomarkers (e.g., IL-6, CRP, TNF-α) to quantify the biological impact objectively. This multimodal strategy (behavioral–biochemical synergy) may enhance patient engagement through visible progress indicators, thereby sustaining healthy dietary adherence. The resultant improvement could potentially amplify conventional cancer therapies while concurrently ameliorating depressive symptomatology and improving quality of life.

5. Conclusions

The present study provides evidence that anti-inflammatory dietary education could improve DepS, regulate inflammation, and improve QoL in breast cancer patients with depression undergoing chemotherapy. However, future prospective studies with more rigorous study designs, larger sample sizes, multi-center designs, and longer follow-up periods are still warranted to determine its long-term effects on DepS in the breast cancer population.

Supplementary Materials: The following supporting information can be downloaded at: https://www.mdpi.com/xxx/s1, Table S1. Comparison of characteristics of patients who consented to provide blood samples (n = 35); Table S2. Changes in CES-D score, E-DII score, and quality of life of patients who consented to provide blood samples (n = 35).

Author Contributions: Conceptualization, L.C. and Y.C.; methodology, L.C. and Y.C.; software, L.C., Y.C., J.H. and X.C.; validation, S.X.; formal analysis, L.C., Y.C., J.H. and X.C.; investigation, L.C., Y.C., J.H., Y.W. and X.L.; resources, S.X.; data curation, L.C., Y.C., Y.W., X.L., Z.H. and X.M.; writing—original draft preparation, L.C. and Y.C.; writing—review and editing, S.X.; visualization, S.X.; supervision, S.X.; project administration, S.X.; funding acquisition, S.X. All authors have read and agreed to the published version of the manuscript.

Funding: This research was funded by the National Natural Science Foundation of China (grant number: 81703222).

Institutional Review Board Statement: This study received approval from the Medical Ethics Committee of Jiangnan University (JNU20220606IRB15) on 27 June 2022 and was registered in the Chinese Clinical Trial Registry (ChiCTR2200064967) on 24 October 2022. The study was conducted in accordance with the Declaration of Helsinki.

Informed Consent Statement: Informed consent was obtained from all subjects involved in the study.

Data Availability Statement: The data presented in this study are available from the corresponding author upon request due to privacy.

Acknowledgments: The authors thank Yu-Qiu Ge from Wuxi School of Medicine, Jiangnan University, for the recommendations on the statistical analysis.

Conflicts of Interest: The authors declare no conflicts of interest.

Abbreviations

The following abbreviations are used in this manuscript:

BMI	Body mass index
CES-D	Center for Epidemiologic Studies Depression Scale
CNY	Chinese yuan
CRP	C-reactive protein
DepS	Depressive symptoms
E-DII	Energy-adjusted dietary inflammatory index
FACT-B	Functional Assessment of Cancer Therapy—Breast Scale
IL-1β	Interleukin-1β
IL-6	Interleukin-6
TNF-α	Tumor necrosis factor-α
MDD	Major depressive disorder
MET	Metabolic equivalent
QoL	Quality of life
RCT	Randomized controlled trial
SD	Standard deviation

References

1. Bray, F.; Laversanne, M.; Sung, H.; Ferlay, J.; Siegel, R.L.; Soerjomataram, I.; Jemal, A. Global cancer statistics 2022: GLOBOCAN estimates of incidence and mortality worldwide for 36 cancers in 185 countries. *CA Cancer J. Clin.* **2024**, *74*, 229–263. [CrossRef] [PubMed]
2. Carreira, H.; Williams, R.; Funston, G.; Stanway, S.; Bhaskaran, K. Associations between breast cancer survivorship and adverse mental health outcomes: A matched population-based cohort study in the United Kingdom. *PLoS Med.* **2021**, *18*, e1003504. [CrossRef]
3. Javan Biparva, A.; Raoofi, S.; Rafiei, S.; Masoumi, M.; Doustmehraban, M.; Bagheribayati, F.; Vaziri Shahrebabak, E.S.; Noorani Mejareh, Z.; Khani, S.; Abdollahi, B.; et al. Global depression in breast cancer patients: Systematic review and meta-analysis. *PLoS ONE* **2023**, *18*, e0287372. [CrossRef]
4. Zahid, J.A.; Grummedal, O.; Madsen, M.T.; Gögenur, I. Prevention of depression in patients with cancer: A systematic review and meta-analysis of randomized controlled trials. *J. Psychiatr. Res.* **2020**, *120*, 113–123. [CrossRef]
5. Wondimagegnehu, A.; Abebe, W.; Abraha, A.; Teferra, S. Depression and social support among breast cancer patients in Addis Ababa, Ethiopia. *BMC Cancer* **2019**, *19*, 836. [CrossRef] [PubMed]
6. Du, L.; Shi, H.Y.; Yu, H.R.; Liu, X.M.; Jin, X.H.; Yan, Q.; Fu, X.L.; Song, Y.P.; Cai, J.Y.; Chen, H.L. Incidence of suicide death in patients with cancer: A systematic review and meta-analysis. *J. Affect. Disord.* **2020**, *276*, 711–719. [CrossRef] [PubMed]
7. Wang, X.; Wang, N.; Zhong, L.; Wang, S.; Zheng, Y.; Yang, B.; Zhang, J.; Lin, Y.; Wang, Z. Prognostic value of depression and anxiety on breast cancer recurrence and mortality: A systematic review and meta-analysis of 282,203 patients. *Mol. Psychiatry* **2020**, *25*, 3186–3197. [CrossRef]
8. Khubchandani, J.; Banerjee, S.; Batra, K.; Beydoun, M.A. Depression Is Associated with a Higher Risk of Mortality among Breast Cancer Survivors: Results from the National Health and Nutrition Examination Survey-National Death Index Linked Study. *Brain Sci.* **2024**, *14*, 732. [CrossRef]

9. Sebro, E.; Biranu, E.; Nigussie, A.; Gebremedhin, T.; Sisay, M.M.; Shaweno, T. Depression and associated factors among adult breast cancer patients attending at selected public hospital in Addis Ababa, Ethiopia. *SAGE Open Med.* **2024**, *12*, 20503121241283727. [CrossRef]
10. Mao, Y.; Li, J.; Shi, R.; Gao, L.; Xu, A.; Wang, B. Construction of a nomogram risk prediction model for depressive symptoms in elderly breast cancer patients. *Sci. Rep.* **2024**, *14*, 26433. [CrossRef]
11. Zhang, Q.; Wu, G.; Chen, J.; Fang, K.; Liu, Q.; Zhang, P.; Zhu, H.; Zhang, C. Factors influencing depressive symptoms in Chinese female breast cancer patients: A meta-analysis. *Front. Psychol.* **2024**, *15*, 1332523. [CrossRef]
12. Li, A.; Zheng, X.; Liu, D.; Huang, R.; Ge, H.; Cheng, L.; Zhang, M.; Cheng, H. Physical Activity and Depression in Breast Cancer Patients: Mechanisms and Therapeutic Potential. *Curr. Oncol.* **2025**, *32*, 77. [CrossRef]
13. Nunes, E.V. Alcohol and the Etiology of Depression. *Am. J. Psychiatry* **2023**, *180*, 179–181. [CrossRef]
14. Tavakoly, R.; Moosburner, A.; Anheyer, D.; Cramer, H. Effect of Different Dietary Patterns on Patients with Depressive Disorders: A Systematic Review and Meta-Analysis of Randomized Controlled Trials. *Nutrients* **2025**, *17*, 563. [CrossRef]
15. Głąbska, D.; Guzek, D.; Groele, B.; Gutkowska, K. Fruit and Vegetable Intake and Mental Health in Adults: A Systematic Review. *Nutrients* **2020**, *12*, 115. [CrossRef]
16. Shafiei, F.; Salari-Moghaddam, A.; Larijani, B.; Esmaillzadeh, A. Mediterranean diet and depression: Reanalysis of a meta-analysis. *Nutr. Rev.* **2023**, *81*, 889–890. [CrossRef]
17. Selvaraj, R.; Selvamani, T.Y.; Zahra, A.; Malla, J.; Dhanoa, R.K.; Venugopal, S.; Shoukrie, S.I.; Hamouda, R.K.; Hamid, P. Association Between Dietary Habits and Depression: A Systematic Review. *Cureus* **2022**, *14*, e32359. [CrossRef]
18. Firth, J.; Marx, W.; Dash, S.; Carney, R.; Teasdale, S.B.; Solmi, M.; Stubbs, B.; Schuch, F.B.; Carvalho, A.F.; Jacka, F.; et al. The Effects of Dietary Improvement on Symptoms of Depression and Anxiety: A Meta-Analysis of Randomized Controlled Trials. *Psychosom. Med.* **2019**, *81*, 265–280. [CrossRef]
19. Jacka, F.N.; O'Neil, A.; Opie, R.; Itsiopoulos, C.; Cotton, S.; Mohebbi, M.; Castle, D.; Dash, S.; Mihalopoulos, C.; Chatterton, M.L.; et al. A randomised controlled trial of dietary improvement for adults with major depression (the 'SMILES' trial). *BMC Med.* **2017**, *15*, 23. [CrossRef] [PubMed]
20. Parletta, N.; Zarnowiecki, D.; Cho, J.; Wilson, A.; Bogomolova, S.; Villani, A.; Itsiopoulos, C.; Niyonsenga, T.; Blunden, S.; Meyer, B.; et al. A Mediterranean-style dietary intervention supplemented with fish oil improves diet quality and mental health in people with depression: A randomized controlled trial (HELFIMED). *Nutr. Neurosci.* **2019**, *22*, 474–487. [CrossRef] [PubMed]
21. Vuksanovic, D.; Sanmugarajah, J.; Lunn, D.; Sawhney, R.; Eu, K.; Liang, R. Unmet needs in breast cancer survivors are common, and multidisciplinary care is underutilised: The Survivorship Needs Assessment Project. *Breast Cancer* **2021**, *28*, 289–297. [CrossRef] [PubMed]
22. Tangney, C.C.; Young, J.A.; Murtaugh, M.A.; Cobleigh, M.A.; Oleske, D.M. Self-reported dietary habits, overall dietary quality and symptomatology of breast cancer survivors: A cross-sectional examination. *Breast Cancer Res. Treat.* **2002**, *71*, 113–123. [CrossRef]
23. Maitiniyazi, G.; Cao, X.; Chen, Y.; Zhang, R.; Liu, Y.; Li, Z.; Gu, D.; Li, T.; Xia, S. Impact of Gut Microbiota on the Association between Diet and Depressive Symptoms in Breast Cancer. *Nutrients* **2022**, *14*, 1186. [CrossRef] [PubMed]
24. Bizzozero-Peroni, B.; Ortolá, R.; Martínez-Vizcaíno, V.; Rodríguez-Artalejo, F.; Fernández-Rodríguez, R.; Banegas, J.R.; Lopez-Garcia, E.; Mesas, A.E. Proinflammatory dietary pattern and depression risk in older adults: Prospective analyses from the Seniors-ENRICA studies. *Clin. Nutr.* **2022**, *41*, 2614–2620. [CrossRef]
25. Custódio, I.D.D.; Franco, F.P.; Marinho, E.D.C.; Pereira, T.S.S.; Lima, M.T.M.; Molina, M.; Shivappa, N.; Hebert, J.R.; Paiva, C.E.; Maia, Y.C.P. Prospective Analysis of Food Consumption and Nutritional Status and the Impact on the Dietary Inflammatory Index in Women with Breast Cancer during Chemotherapy. *Nutrients* **2019**, *11*, 2610. [CrossRef]
26. Chen, Y.; Maitiniyazi, G.; Li, Z.; Li, T.; Liu, Y.; Zhang, R.; Cao, X.; Gu, D.; Xia, S. TNF-α Mediates the Association between Dietary Inflammatory Index and Depressive Symptoms in Breast Cancer. *Nutrients* **2022**, *15*, 84. [CrossRef]
27. Wang, J.; Zhou, Y.; Chen, K.; Jing, Y.; He, J.; Sun, H.; Hu, X. Dietary inflammatory index and depression: A meta-analysis. *Public Health Nutr.* **2019**, *22*, 654–660. [CrossRef]
28. Xu, Y.; Zeng, L.; Zou, K.; Shan, S.; Wang, X.; Xiong, J.; Zhao, L.; Zhang, L.; Cheng, G. Role of dietary factors in the prevention and treatment for depression: An umbrella review of meta-analyses of prospective studies. *Transl. Psychiatry* **2021**, *11*, 478. [CrossRef] [PubMed]
29. Ryu, K.W.; Bae, J.M.; Kim, E.M.; An, J.Y.; Choi, M.G.; Lee, J.H.; Sohn, T.S. Long-term effect of simplified dietary education on the nutritional status of patients after a gastrectomy. *PLoS ONE* **2021**, *16*, e0252168. [CrossRef]
30. Schulz, K.F.; Altman, D.G.; Moher, D. CONSORT 2010 statement: Updated guidelines for reporting parallel group randomised trials. *PLoS Med.* **2010**, *7*, e1000251. [CrossRef]
31. Cooper, I.; Brukner, P.; Devlin, B.L.; Reddy, A.J.; Fulton, M.; Kemp, J.L.; Culvenor, A.G. An anti-inflammatory diet intervention for knee osteoarthritis: A feasibility study. *BMC Musculoskelet. Disord.* **2022**, *23*, 47. [CrossRef] [PubMed]

32. Pearce, M.; Garcia, L.; Abbas, A.; Strain, T.; Schuch, F.B.; Golubic, R.; Kelly, P.; Khan, S.; Utukuri, M.; Laird, Y.; et al. Association Between Physical Activity and Risk of Depression: A Systematic Review and Meta-analysis. *JAMA Psychiatry* **2022**, *79*, 550–559. [CrossRef] [PubMed]
33. Visontay, R.; Mewton, L.; Slade, T.; Aris, I.M.; Sunderland, M. Moderate Alcohol Consumption and Depression: A Marginal Structural Model Approach Promoting Causal Inference. *Am. J. Psychiatry* **2023**, *180*, 209–217. [CrossRef]
34. Craig, C.L.; Marshall, A.L.; Sjöström, M.; Bauman, A.E.; Booth, M.L.; Ainsworth, B.E.; Pratt, M.; Ekelund, U.; Yngve, A.; Sallis, J.F.; et al. International physical activity questionnaire: 12-country reliability and validity. *Med. Sci. Sports Exerc.* **2003**, *35*, 1381–1395. [CrossRef] [PubMed]
35. Hann, D.; Winter, K.; Jacobsen, P. Measurement of depressive symptoms in cancer patients: Evaluation of the Center for Epidemiological Studies Depression Scale (CES-D). *J. Psychosom. Res.* **1999**, *46*, 437–443. [CrossRef]
36. Rankin, S.H.; Galbraith, M.E.; Johnson, S. Reliability and validity data for a Chinese translation of the Center for Epidemiological Studies-Depression. *Psychol. Rep.* **1993**, *73*, 1291–1298. [CrossRef]
37. Balogh, M.; Kahn, H.A.; Medalie, J.H. Random repeat 24-hour dietary recalls. *Am. J. Clin. Nutr.* **1971**, *24*, 304–310. [CrossRef]
38. Brady, M.J.; Cella, D.F.; Mo, F.; Bonomi, A.E.; Tulsky, D.S.; Lloyd, S.R.; Deasy, S.; Cobleigh, M.; Shiomoto, G. Reliability and validity of the Functional Assessment of Cancer Therapy-Breast quality-of-life instrument. *J. Clin. Oncol.* **1997**, *15*, 974–986. [CrossRef]
39. Ng, R.; Lee, C.F.; Wong, N.S.; Luo, N.; Yap, Y.S.; Lo, S.K.; Chia, W.K.; Yee, A.; Krishna, L.; Goh, C.; et al. Measurement properties of the English and Chinese versions of the Functional Assessment of Cancer Therapy-Breast (FACT-B) in Asian breast cancer patients. *Breast Cancer Res. Treat.* **2012**, *131*, 619–625. [CrossRef]
40. Swainson, J.; Reeson, M.; Malik, U.; Stefanuk, I.; Cummins, M.; Sivapalan, S. Diet and depression: A systematic review of whole dietary interventions as treatment in patients with depression. *J. Affect. Disord.* **2023**, *327*, 270–278. [CrossRef]
41. Tolkien, K.; Bradburn, S.; Murgatroyd, C. An anti-inflammatory diet as a potential intervention for depressive disorders: A systematic review and meta-analysis. *Clin. Nutr.* **2019**, *38*, 2045–2052. [CrossRef]
42. Cano, A.; Marshall, S.; Zolfaroli, I.; Bitzer, J.; Ceausu, I.; Chedraui, P.; Durmusoglu, F.; Erkkola, R.; Goulis, D.G.; Hirschberg, A.L.; et al. The Mediterranean diet and menopausal health: An EMAS position statement. *Maturitas* **2020**, *139*, 90–97. [CrossRef] [PubMed]
43. Long Parma, D.A.; Reynolds, G.L.; Muñoz, E.; Ramirez, A.G. Effect of an anti-inflammatory dietary intervention on quality of life among breast cancer survivors. *Support Care Cancer* **2022**, *30*, 5903–5910. [CrossRef]
44. Cabrera-Suárez, B.M.; Hernández-Fleta, J.L.; Molero, P.; González-Pinto, A.; Lahortiga, F.; Cabrera, C.; Chiclana-Actis, C.; Sánchez-Villegas, A. Mediterranean diet-based intervention to improve depressive symptoms: Analysis of the PREDIDEP randomized trial. *Nutr. Neurosci.* **2024**, *27*, 951–961. [CrossRef]
45. Marx, W.; Lane, M.; Hockey, M.; Aslam, H.; Berk, M.; Walder, K.; Borsini, A.; Firth, J.; Pariante, C.M.; Berding, K.; et al. Diet and depression: Exploring the biological mechanisms of action. *Mol. Psychiatry* **2021**, *26*, 134–150. [CrossRef] [PubMed]
46. Yao, L.; Pan, L.; Qian, M.; Sun, W.; Gu, C.; Chen, L.; Tang, X.; Hu, Y.; Xu, L.; Wei, Y.; et al. Tumor Necrosis Factor-α Variations in Patients with Major Depressive Disorder Before and After Antidepressant Treatment. *Front. Psychiatry* **2020**, *11*, 518837. [CrossRef] [PubMed]
47. George, M.A.; Lustberg, M.B.; Orchard, T.S. Psychoneurological symptom cluster in breast cancer: The role of inflammation and diet. *Breast Cancer Res. Treat.* **2020**, *184*, 1–9. [CrossRef]
48. Perez-Cornago, A.; de la Iglesia, R.; Lopez-Legarrea, P.; Abete, I.; Navas-Carretero, S.; Lacunza, C.I.; Lahortiga, F.; Martinez-Gonzalez, M.A.; Martinez, J.A.; Zulet, M.A. A decline in inflammation is associated with less depressive symptoms after a dietary intervention in metabolic syndrome patients: A longitudinal study. *Nutr. J.* **2014**, *13*, 36. [CrossRef]
49. McFarland, D.C.; Doherty, M.; Atkinson, T.M.; O'Hanlon, R.; Breitbart, W.; Nelson, C.J.; Miller, A.H. Cancer-related inflammation and depressive symptoms: Systematic review and meta-analysis. *Cancer* **2022**, *128*, 2504–2519. [CrossRef]
50. Mousavi-Shirazi-Fard, Z.; Mazloom, Z.; Izadi, S.; Fararouei, M. The effects of modified anti-inflammatory diet on fatigue, quality of life, and inflammatory biomarkers in relapsing-remitting multiple sclerosis patients: A randomized clinical trial. *Int. J. Neurosci.* **2021**, *131*, 657–665. [CrossRef]
51. Porciello, G.; Montagnese, C.; Crispo, A.; Grimaldi, M.; Libra, M.; Vitale, S.; Palumbo, E.; Pica, R.; Calabrese, I.; Cubisino, S.; et al. Mediterranean diet and quality of life in women treated for breast cancer: A baseline analysis of DEDiCa multicentre trial. *PLoS ONE* **2020**, *15*, e0239803. [CrossRef] [PubMed]
52. Zhang, Y.; Cui, G.; Xiu, Y.; Zhao, M. The Effect of Nutritional Support Based on the Dietary Anti-Inflammatory Index on Cancer-Related Fatigue in Lung Cancer Patients Undergoing Chemotherapy. *Cancer Nurs.* **2023**, *46*, 394–404. [CrossRef] [PubMed]
53. Barchitta, M.; Maugeri, A.; Magnano San Lio, R.; Quattrocchi, A.; Degrassi, F.; Catalano, F.; Basile, G.; Agodi, A. The Effects of Diet and Dietary Interventions on the Quality of Life among Breast Cancer Survivors: A Cross-Sectional Analysis and a Systematic Review of Experimental Studies. *Cancers* **2020**, *12*, 322. [CrossRef]

54. Anderson, N.; Ozakinci, G. Effectiveness of psychological interventions to improve quality of life in people with long-term conditions: Rapid systematic review of randomised controlled trials. *BMC Psychol.* **2018**, *6*, 11. [CrossRef]
55. Freedman, L.S.; Commins, J.M.; Willett, W.; Tinker, L.F.; Spiegelman, D.; Rhodes, D.; Potischman, N.; Neuhouser, M.L.; Moshfegh, A.J.; Kipnis, V.; et al. Evaluation of the 24-Hour Recall as a Reference Instrument for Calibrating Other Self-Report Instruments in Nutritional Cohort Studies: Evidence from the Validation Studies Pooling Project. *Am. J. Epidemiol.* **2017**, *186*, 73–82. [CrossRef]
56. Staudacher, H.M.; Teasdale, S.; Cowan, C.; Opie, R.; Jacka, F.N.; Rocks, T. Diet interventions for depression: Review and recommendations for practice. *Aust. N. Z. J. Psychiatry* **2025**, *59*, 115–127. [CrossRef] [PubMed]
57. Bababekov, Y.J.; Hung, Y.C.; Hsu, Y.T.; Udelsman, B.V.; Mueller, J.L.; Lin, H.Y.; Stapleton, S.M.; Chang, D.C. Is the Power Threshold of 0.8 Applicable to Surgical Science?-Empowering the Underpowered Study. *J. Surg. Res.* **2019**, *241*, 235–239. [CrossRef]
58. Madjarova, S.J.; Pareek, A.; Eckhardt, C.M.; Khorana, A.; Kunze, K.N.; Ollivier, M.; Karlsson, J.; Williams, R.J., 3rd; Nwachukwu, B.U. Fragility Part I: A guide to understanding statistical power. *Knee Surg. Sports Traumatol. Arthrosc.* **2022**, *30*, 3924–3928. [CrossRef]
59. Cava, E.; Marzullo, P.; Farinelli, D.; Gennari, A.; Saggia, C.; Riso, S.; Prodam, F. Breast Cancer Diet "BCD": A Review of Healthy Dietary Patterns to Prevent Breast Cancer Recurrence and Reduce Mortality. *Nutrients* **2022**, *14*, 476. [CrossRef]
60. Wang, K.; Sun, J.Z.; Wu, Q.X.; Li, Z.Y.; Li, D.X.; Xiong, Y.F.; Zhong, G.C.; Shi, Y.; Li, Q.; Zheng, J.; et al. Long-term anti-inflammatory diet in relation to improved breast cancer prognosis: A prospective cohort study. *NPJ Breast Cancer* **2020**, *6*, 36. [CrossRef]

Disclaimer/Publisher's Note: The statements, opinions and data contained in all publications are solely those of the individual author(s) and contributor(s) and not of MDPI and/or the editor(s). MDPI and/or the editor(s) disclaim responsibility for any injury to people or property resulting from any ideas, methods, instructions or products referred to in the content.

nutrients

MDPI

Article

Camel Milk Protein Ameliorates Ulcerative Colitis by Modulating Gut Microbiota and Amino Acid Metabolism

Ning Kang [1,2,3,†], Zhexin Fan [1,2,3,4,†], Li Yang [5], Jie Shen [1,2,3], Yuechenfei Shen [1,2,3], Zhifeng Fang [1,2,3,4], Baokun Li [1,2,3,4], Bo Yang [6,7] and Jiancheng Wang [1,2,3,4,*]

1 Key Laboratory of Agricultural Product Processing and Quality Control of Specialty (Co-Construction by Ministry and Province), School of Food Science and Technology, Shihezi University, Shihezi 832000, China; 20222111016@stu.shzu.edu.cn (N.K.); zhexin_fan@shzu.edu.cn (Z.F.); shenjie@stu.shzu.edu.cn (J.S.); shenyuechenfei@stu.shzu.edu.cn (Y.S.); zhifengf@jiangnan.edu.cn (Z.F.); libaokun@shzu.edu.cn (B.L.)
2 Key Laboratory for Food Nutrition and Safety Control of Xinjiang Production and Construction Corps, School of Food Science and Technology, Shihezi 832000, China
3 Engineering Research Center of Storage and Processing of Xinjiang Characteristic Fruits and Vegetables, Ministry of Education, School of Food Science and Technology, Shihezi University, Shihezi 832000, China
4 Functional Food Center, Key Laboratory of Xinjiang Medicinal Plant Resources Utilization, Ministry of Education, Shihezi University, Shihezi 832000, China
5 Alashankou Customs Technology Center, Alashankou 833418, China; 18997761304@163.com
6 State Key Laboratory of Food Science and Resources, School of Food Science and Technology, Jiangnan University, Wuxi 214122, China; bo.yang@jiangnan.edu.cn
7 International Joint Research Laboratory for Maternal-Infant Microbiota and Health, Jiangnan University, Wuxi 214122, China
* Correspondence: wjc202200036@shzu.edu.cn
† These authors contributed equally to this work.

Abstract: The protective effects of the milk fat globule membrane (MFGM) in alleviating inflammation have been reported. However, limited attention has been paid to the key fraction of milk fat globule membrane protein (MFGMP). This study investigated the protective effects of camel MFGMP against dextran sulfate sodium (DSS)-induced ulcerative colitis (UC) in mice. The results revealed that administering 50 mg/kg MFGMP significantly alleviated colonic inflammation, as evidenced by a marked decrease in IL-6, IL-1β, and TNF-α levels, along with pathological damage in DSS-induced mice with UC. MFGMP supplementation partially regulated gut microbiota dysbiosis in mice with UC by increasing α-diversity and the relative abundance of beneficial gut bacteria, such as *Lactobacillus*, while decreasing the abundance of *Akkermansia*. Additionally, MFGMP treatment exhibited significant regulatory effects on metabolites, particularly amino acid metabolism, in the feces. Specifically, this treatment restored L-valine to normal physiological levels and increased the concentrations of L-leucine, L-lysine, and L-tyrosine to nearly twice their baseline levels, whereas the concentration of L-tryptophan increased threefold. These upregulated amino acids were negatively correlated with pro-inflammatory cytokines and positively correlated with the anti-inflammatory cytokine IL-10, as indicated by Spearman's correlation analysis. Furthermore, the significant reduction in the mRNA expression levels of WNT-1, β-catenin, and Cyclin D1 suggests that MFGMP exerts a positive effect on UC via the Wnt/β-catenin pathway. These findings indicate that MFGMP exerts a protective effect against UC by modulating intestinal microbiota and amino acid metabolism in mice, with potential implications for treating intestinal inflammatory diseases.

Keywords: milk fat globule membrane protein; camel milk fat; ulcerative colitis; gut microbiota; amino acid metabolism

1. Introduction

Ulcerative colitis (UC) is a chronic inflammatory bowel disease (IBD) marked by symptoms such as weight loss, loose stools accompanied by hematochezia, diarrhea, and a dysregulated immune response [1]. Research indicates that the rising incidence of UC among children and adolescents points to the persistence of numerous environmental factors that contribute to increased susceptibility [2]. A family history of UC has been identified as the most significant risk factor for the disease [3]. Moreover, immune system dysfunction—characterized by T-cell abnormalities and an exaggerated immune response—has been linked to an elevated risk of developing UC [4]. These findings highlight the potential benefit of additional prophylactic measures for individuals at heightened risk, particularly those with a family history of UC or those chronically exposed to environmental and lifestyle factors. The medical community still lacks clarity regarding the pathological mechanisms of UC [5]. Although the exact mechanisms of UC are complex and remain unclear, it is mainly associated with intestinal disorders, including disrupted gut microbiota, gut inflammation, intestinal barrier dysfunction, and imbalanced immune responses. Promising strategies for the management of UC involve targeting the gut microbiota and its associated metabolites. There is widespread agreement that the gut microbiota plays a pivotal role in modulating UC. Recently, dietary and nutritional interventions, including proteins, probiotics, and polysaccharides, have been considered effective strategies to regulate UC. The relationship between UC and milk has gained increasing attention, with studies demonstrating that restricting milk production exacerbates UC disease.

Camel milk contains abundant nutrients, with higher lactoferrin and calcium levels, and is free of β-lactoglobulin (BLG) compared to bovine milk, making it a better mimic of breast milk in terms of nutrient composition [6]. Camel milk is generally used as a natural health supplement because of its superior antioxidant, immunomodulatory, anti-inflammatory, antidiabetic, and anti-apoptotic properties [7,8]. The milk fat globule membrane (MFGM) is a tri-layered protein–lipid structure that envelops fat globules. MFGM has gained increasing attention owing to its remarkable properties, including promotion of lipid uptake [9], restoration of intestinal barrier function [10], anti-inflammatory effects [11] and enhanced gut health [12]. Orally administering a combination of MFGM, fructo-oligosaccharides (FOSs), and galacto-oligosaccharides (GOSs) significantly improves UC in mice, primarily due to changes in the intestinal microbiota [13]. Studies have demonstrated that MFGM extracted from bovine milk can prevent and attenuate acute UC in mice. Moreover, several studies have suggested that MFGM modulates the immune response, strengthens intestinal barrier function, and promotes the diversity of the gut microbiota, thereby alleviating UC lesions [11].

Given that MFGM is a complex fraction containing 25–70% protein and a significant amount of lipids, it is difficult to determine which component is responsible for its biological functions. MFGMP, which includes epidermal growth factor 8 (EGF8), xanthine oxidoreductase (XOR), mucin 1 (MUC1), mucin 15, CD36, butyrophilin, and fatty acid-binding proteins, is highly regarded for its extensive biological functions despite being present in low amounts. Currently, studies on MFGMP have mainly focused on the variations in composition among different species and their protective effects on health. For example, XOR has been shown to contribute to mammary gland development and exert antimicrobial activity in the intestine, while proteins from the butyrophilin family are implicated in immunomodulation [14]. Moreover, MUC1, a member of the mucin family, plays a key role in protecting the mucosal barrier from pathogenic attack and is strongly associated with tumorigenesis, proliferation, and metastasis [15]. Recent studies have depicted that EGF8 from bovine milk MFGM can attenuate UC by increasing the production of butyric

acid and improving intestinal microbiota in the cecal content, suggesting that EGF8 may be a key functional constituent in regulating gut health. Despite the high abundance of EGF8 in camel milk, it is widely accepted that the composition of MFGMP varies among species, as evidenced by the different isoforms of EGF8 found in bovine and camel milk. However, to date, no studies have explored the potential protective role of MFGMP in UC. Consequently, the role of MFGMP in camel milk warrants further investigation.

To understand the role of MFGMP in UC treatment, we administered MFGMP via gavage to mice with UC induced by dextran sulfate sodium salt (DSS). The objectives of this study were to (1) investigate the effects of MFGMP on UC, (2) analyze changes in gut microbiota and metabolites, (3) determine the amount of short-chain fatty acids (SCFAs) in the cecum, and (4) determine the correlation between differential metabolites, gut microbiota, and inflammatory cytokines. By elucidating the underlying mechanisms, these findings lay the foundation for the future application of MFGMP as a functional food in the relief and management of ulcerative colitis.

2. Materials and Methods

2.1. Preparation of MFGM Proteins

Six mature camel milk samples were randomly collected from a local Bactrian camel farm in Shihezi City, Xinjiang Uygur Autonomous Region, China. All samples were pooled, placed in iceboxes, and immediately transported to the laboratory, where fresh raw camel milk was used for MFGMP preparation. MFGMP was prepared according to the method outlined by Dou et al. [16], with minor modifications. Raw milk samples were centrifuged at 8000 revolutions per minute (rpm) for 20 min at 4 °C. The upper layer, consisting of the cream, was carefully removed with a spatula and rinsed three times with phosphate-buffered saline (PBS) at pH 7.4. The milk fat globules were suspended in ultrapure water, incubated at 37 °C for 10 min to remove any residual PBS, and centrifuged at 10,000 rpm for 15 min, and the upper layer of milk fat was collected and crystallized at 4 °C overnight. Ultrapure water was added to the MFGM fraction, and the MFGM was homogenized by sonication in an ultrasonic cell disruption machine (sonication 3 s, interval 9 s, total 20 min). Homogenized MFGM was incubated in a shaker at 45 °C for 30 min to promote cream melting, followed by centrifugation at 12,000 rpm for 15 min at 4 °C. The resulting residue was identified as MFGMP.

2.2. Experimental Design and Animal Model

The animal protocol (A2023-087) was approved by the Ethics Committee of Laboratory Animals at the University of Shihezi, Xinjiang, China. Forty specific pathogen-free male C57BL/6 mice (six weeks old) were obtained from SCBS Biotechnology Co., Ltd. (Henan, China) and housed in cages at the Experimental Animal Center of Shihezi University, where the environment maintained 12:12 h light–dark cycles at 20–25 °C and 60 ± 5% humidity. After a week of acclimatization, the mice were randomly assigned to five groups (n = 8): control group (CON), DSS-induced colitis group (DSS), mesalazine treatment group (MES), low MGFMP treatment group (MP25, 25 mg/kg), and high MGFMP treatment group (MP50, 50 mg/kg). UC was induced using 3.0% (*w*/*v*) DSS in drinking water for 7 days according to previously described protocols [17]. The experimental design is illustrated in Figure 1A. After a 12 h fast, all mice were anesthetized with ether and euthanized by cervical dislocation at the end of the experiment.

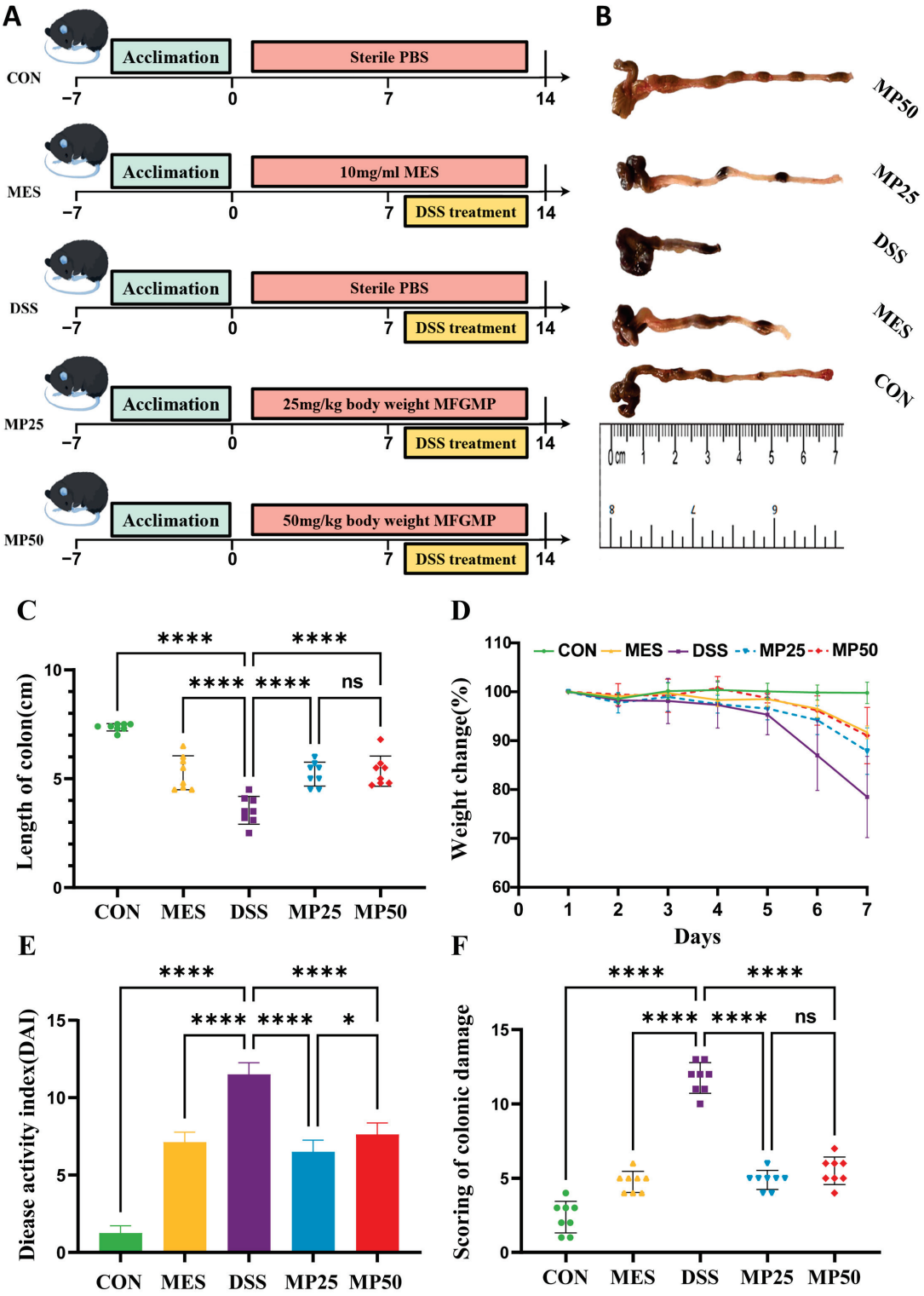


Figure 1. MFGMP alleviated DSS-induced UC in mice. (**A**) The diagram showcases this study's experimental design. For two weeks, mice received either oral PBS or MFGMP treatment prior to being provided with drinking water that contained 3% DSS. (**B**) Macroscopic images of the colon. (**C**) Colon length in each group (n = 6–8 per group). (**D**) Change in daily body weight during DSS treatment. (**E**) Kinetics of daily disease activity index (DAI) scores throughout DSS treatment. (**F**) Histological scores of the colon samples. Data are presented as mean ± standard deviation (SD) (n = 68 per group). Statistical significance was determined using a one-way analysis of variance (ANOVA), followed by Tukey's test. ns, non-significant, * $p \leq 0.05$ and **** $p \leq 0.001$ relative to the CON group.

2.3. Colitis Scores and Histological Analysis

The DAI was employed daily to evaluate the colitis scores in the mice, which encompassed factors such as weight loss, stool consistency, and rectal bleeding. These parameters were monitored as previously described. Colon length was measured after the mice were sacrificed. Samples from the distal colon were preserved in 4% paraformaldehyde (Xavier Biotechnology Co., Ltd., Wuhan, China), dehydrated using ethanol, and embedded in paraffin to create sections that were 5 μm thick. The sections underwent staining with hematoxylin and eosin (H&E) along with Alcian blue dye to facilitate histopathological analysis [18]. The tissue damage in each group of colon tissue sections was scored using Dieleman's scoring system, which evaluated four aspects: lesion extent, crypt destruction, lesion depth, and severity of inflammation [19].

2.4. Analysis of Inflammatory Cytokines

The serum levels of IL-6, IL-1β, TNF-α, and IL-10 were quantified using ELISA kits (Enzyme-linked Biotechnology Co., Ltd., Shanghai, China).

2.5. Analysis of Relative mRNA Expression in Colonic Tissues

Total RNA was extracted from colonic tissues using TRIzol (Invitrogen, Carlsbad, CA, USA) reagent following the manufacturer's protocol. Real-time PCR was conducted with SYBR Green PCR Master Mix (Thermo Fisher Scientific, Waltham, MA, USA) according to the manufacturer's instructions. β-Actin was used as the reference gene, and relative gene expression was calculated using the $2-\Delta\Delta Ct$ method. The primer sequences employed in this study are provided in Table S1.

2.6. Determination of Short-Chain Fatty Acids (SCFAs)

SCFAs were extracted using a method similar to that previously reported, with slight modifications [20]. Briefly, 30 mg of cecal content was transferred into a 2 mL tube, followed by the addition of 1.5 mL of ultrapure water. The mixture was vortexed for 30 s, then centrifuged at 5000 rpm for 4 min (room temperature). The supernatant was transferred to a new 2.0 mL tube and mixed with 100 μL of 25% metaphosphoric acid by vortexing for 30 s. After centrifugation at 15,000 rpm (room temperature), the supernatant was collected in an injection vial for gas-phase analysis. SCFAs in the cecal content were quantified by gas chromatography using a 30 m × 0.25 mm × 0.50 μm DB-WAX column (Agilent Technologies, PaloAlto, CA, USA).

2.7. Immunohistochemistry

Colonic tissue slides (4 μm) were deparaffinized and hydrated. Antigen retrieval from formalin-fixed tissues was performed by microwave heating (20 min) with 0.01 M citric acid. Tissue blocking was carried out using 5% bovine serum albumin for 1 h at 37 °C. Immunohistochemistry was performed using primary antibodies against WNT-1 (27935-1-AP), β-catenin (17565-1-AP), and Cyclin D1 (26969-1-AP) purchased from LifeScience Biological Experimental Equipment Co., Ltd (Wuxi, China). HRP-conjugated goat anti-rabbit IgG secondary antibody (G1213-100UL, Xavier Biotechnology Co., Ltd.) was used for detection. Antibodies were detected using a 3,3′-diaminobenzidine (DAB) staining kit (G1212-200T, Xavier Biotechnology Co., Ltd.). Hematoxylin served as a counterstain, and the slides were covered with neutral balsam and a coverslip.

2.8. Microbial Community Analysis

Total DNA from feces was extracted using the FastDNA® Spin kit (MP Biomedicals, Santa Ana, CA, USA) for soil following the manufacturer's instructions to ensure high-quality DNA and accuracy of analysis. Universal primers 338F (5′-ACTCCTACGGAGGCAGCAG-3′)

and 806R (5′-GGACTACHVGGGTWTCTAAT-3′) were used to amplify the V3–V4 region of the gene [21]. The samples were identified using barcodes and primers, and the sequences were dereplicated and discarded. The data were sequenced using the Miseq PE300 platform (Illumina, San Diego, CA, USA) and then searched for libraries. Raw FASTQ files were demultiplexed, quality-filtered using Trimmomatic (version 0.3.9), and merged using fast length adjustment of short reads to improve genome assembly. Bioinformatic analysis was performed using Tutu Cloud Platform (http://cloudtutu.com.cn/, accessed on 13 August 2024) and MICROKOM BioScience Cloud (https://www.bioincloud.tech, accessed on 13 August 2024) OECloud tools.

2.9. Metabolomics Analysis

Fecal samples from mice were combined with an extraction solution consisting of methanol and water in a 4:1 ratio (*v*:*v*) for the purpose of metabolite extraction. This mixture underwent low-temperature ultrasonic extraction for 30 min at 5 °C and 40 kHz, followed by centrifugation at 4 °C and 13,000× *g*. The resulting supernatant was transferred into injection vials equipped with internal cannulae for subsequent online analysis using LC-MS/MS (Thermo Fisher Scientific, USA). Analysis using LC-MS was conducted with a UHPLC-Q Exactive HF-X (Thermo Fisher Scientific, USA) system. This was succeeded by peak alignment, correction of retention times, and extraction of peak areas using Progenesis QI (Milford Waters, Milford, MA, USA) [22]. Data were matched to metabolic databases and uploaded to the Meggie BioCloud (https://cloud.majorbio.com, accessed on 17 August 2024) platform for analysis.

2.10. Statistical Analysis

Data are presented as mean ± SD. The analyses of all data were conducted using GraphPad Prism software (version 9.0.0). For statistical evaluation, a one-way ANOVA followed by Tukey's multiple comparison test was employed. A statistical significance threshold was established at * $p < 0.05$, ** $p < 0.01$, and *** $p < 0.001$. Values with ns indicate non-significance.

3. Results

3.1. MFGMP Mitigates the Symptoms of DSS-Induced UC in Mice

To assess the therapeutic potential of MP25 and MP50 for UC, key indicators of UC were characterized. The symptoms of DSS-induced UC were similar to those of human colitis. Mice in the DSS group exhibited a notable reduction in body weight and colon length. The symptoms of UC, including reduced colon length and weight loss, significantly improved in the MP25 and MP50 groups, with no notable differences between them (Figure 1B–D). However, MP25 significantly improved the DAI index compared to MP50 (Figure 1E).

3.2. MFGMP Attenuates Colon Pathology Symptoms of DSS-Induced UC in Mice

Damage to colonic tissue can be assessed by H&E staining. The colonic mucosa of the mice in the DSS group was nearly destroyed, with the crypts and goblet cells absent and marked inflammatory cell infiltration compared to the CON group. The colonic tissues of the mice in the MP25 and MP50 groups exhibited improvement, with tissues close to normal. Crypts in the MP25 group were not damaged and contained abundant goblet cells, resulting in better recovery than those in the MP50 group. Consequently, MFGMP alleviated DSS-induced colonic injury and protected the intestinal mucosa, especially in the MP25 group (Figure 2A). The colon histopathology score was based on the evaluation of key pathological features, including inflammatory cell infiltration, crypt disruption, and

epithelial damage. Colon histopathology scores revealed significantly higher scores in the DSS group compared to the CON group (Figure 1F). The MES, MP25, and MP50 groups exhibited significantly lower scores than the DSS group, with no significant difference between the MP25 and MP50 groups.

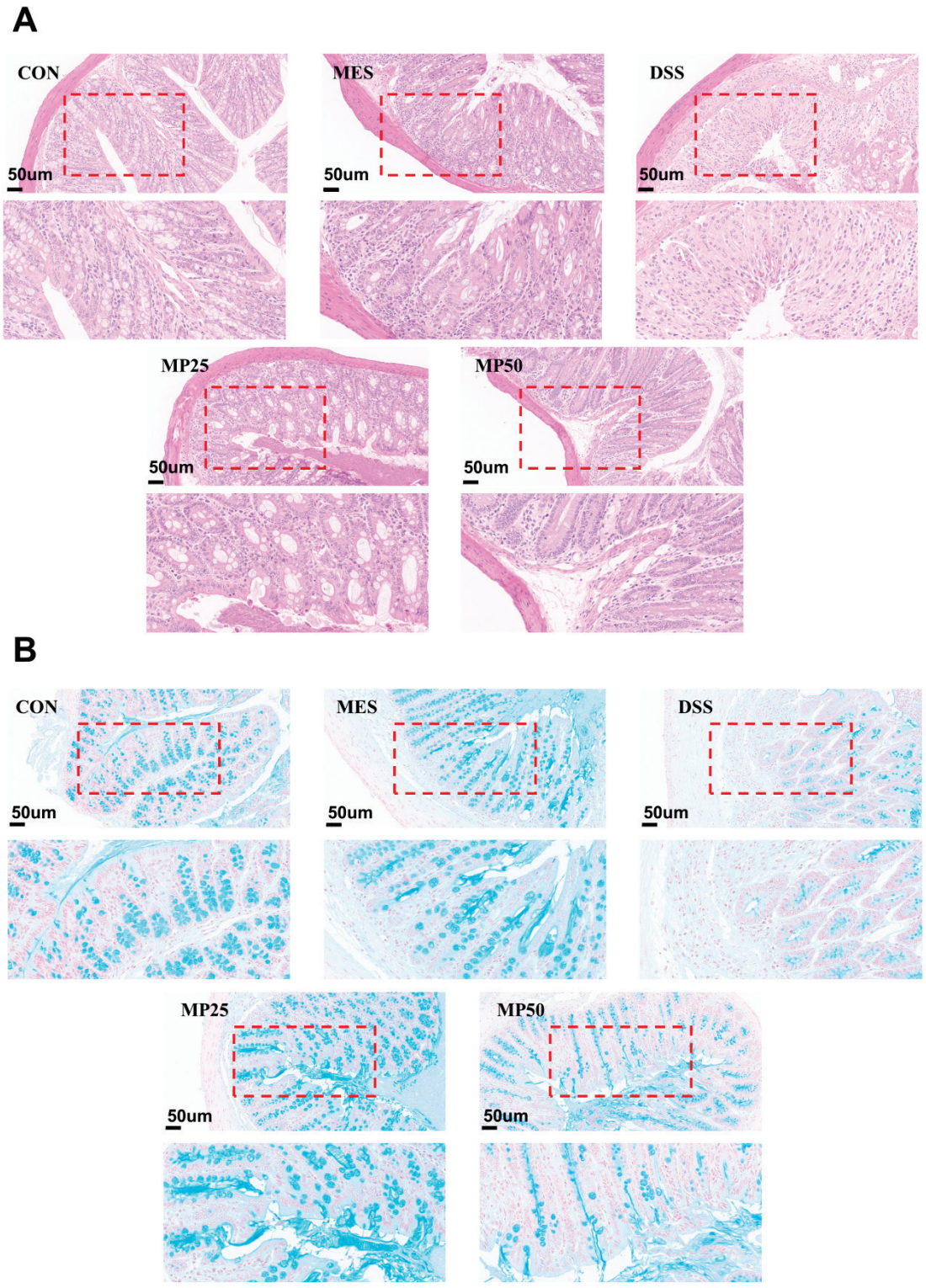


Figure 2. Colonic tissue staining sections. (**A**) H&E-stained colon sections (n = 6 per group) with scale bars representing 50 μm. (**B**) Alcian blue-stained colon sections (n = 6 per group), with scale bars representing 50 μm.

3.3. MFGMP Relieves the Amount and Distribution of Mucin in DSS-Induced UC in Mice

The mucus layer, the first barrier of the colon against harmful substances and microorganisms, consists of an inner layer of polymerized MUC2 and an outer layer of loosely packed MUC2. MUC2 is secreted by cup cells and forms a mesh-like structure that prevents microbial invasion and maintains intestinal homeostasis [23]. The distribution of mucin MUC2 was analyzed by Alcian blue staining, and the mucus layer was severely disrupted, with mucin significantly reduced in the DSS group. However, MES, MP25, and MP50 groups demonstrated improved mucin distribution and less damage to the intestinal mucus layer in the UC mice. Interventions with MGFMP significantly increased the mucin amount and restored mucus secretion. The mucin content in the MP25 group was significantly higher than in the MP50 group (Figure 2B). Tissue section staining demonstrated that MP25 was more effective than MP50 in alleviating localized inflammation and restoring intestinal injury.

3.4. MFGMP Modulates Systemic and Intestinal Local Inflammation in DSS-Induced UC in Mice

Since UC patients are often associated with immune dysregulation, the effect of MGFMP on both systemic and localized intestinal inflammation was further investigated. To evaluate the effect of MGFMP on systemic inflammation, the serum levels of IL-6, IL-1β, IL-10, and TNF-α were quantified using ELISA. The results showed that the MP25 group had significantly lower levels of pro-inflammatory cytokines, including IL-6, IL-1β, and TNF-α, compared to the DSS group. The MP50 group, meanwhile, exhibited significantly decreased levels of IL-6 and IL-1β (Figure 3A–C). Both MFGMP treatments resulted in a significant increase in the levels of the anti-inflammatory cytokine IL-10 (Figure 3D). Notably, the pro-inflammatory cytokine TNF-α levels in the MP25 group were significantly lower than those in the MP50 group.

RT-PCR was conducted to further examine the effect of MGFMP on localized intestinal inflammation. The mRNA expression levels of IL-6, IL-1β, and TNF-α in the DSS-induced UC group were significantly higher than those in the CON group. The MP25 and MP50 groups demonstrated significantly suppressed mRNA expression levels of IL-6 and IL-1β, which was consistent with the changes in cytokines observed in the serum. However, the mitigating effects on TNF-α and IL-10 were associated with the concentration of MFGMP, with significant effects observed only in the MP50 group (Figure 3E–H). The MP25 and MP50 groups demonstrated alleviated systemic inflammation, whereas only the MP50 group demonstrated a more pronounced effect on intestinal localization. Therefore, we explored the mechanism underlying the mitigation of DSS-induced UC through gavage administration of 50 mg/kg MFGMP.

3.5. Effect of MFGMP on the Intestinal Microbiota of DSS-Induced UC in Mice

UC is usually associated with changes in the composition and diversity of the gut microbiota [24]. Therefore, the effect of MFGMP on the intestinal flora of UC mice was investigated. DSS treatment decreased the α-diversity of the gut microbiota in mice, with Chao1, ACE, and Shannon indices significantly lower than those of the CON group. Orally administering MFGMP significantly restored the ACE index (Figure 4A–C). The β-diversity of intestinal bacteria depicted that mice in the DSS group were significantly different from mice in the CON group. After MFGMP treatment, intestinal bacteria tended to approach those in the CON group (Figure 4D).

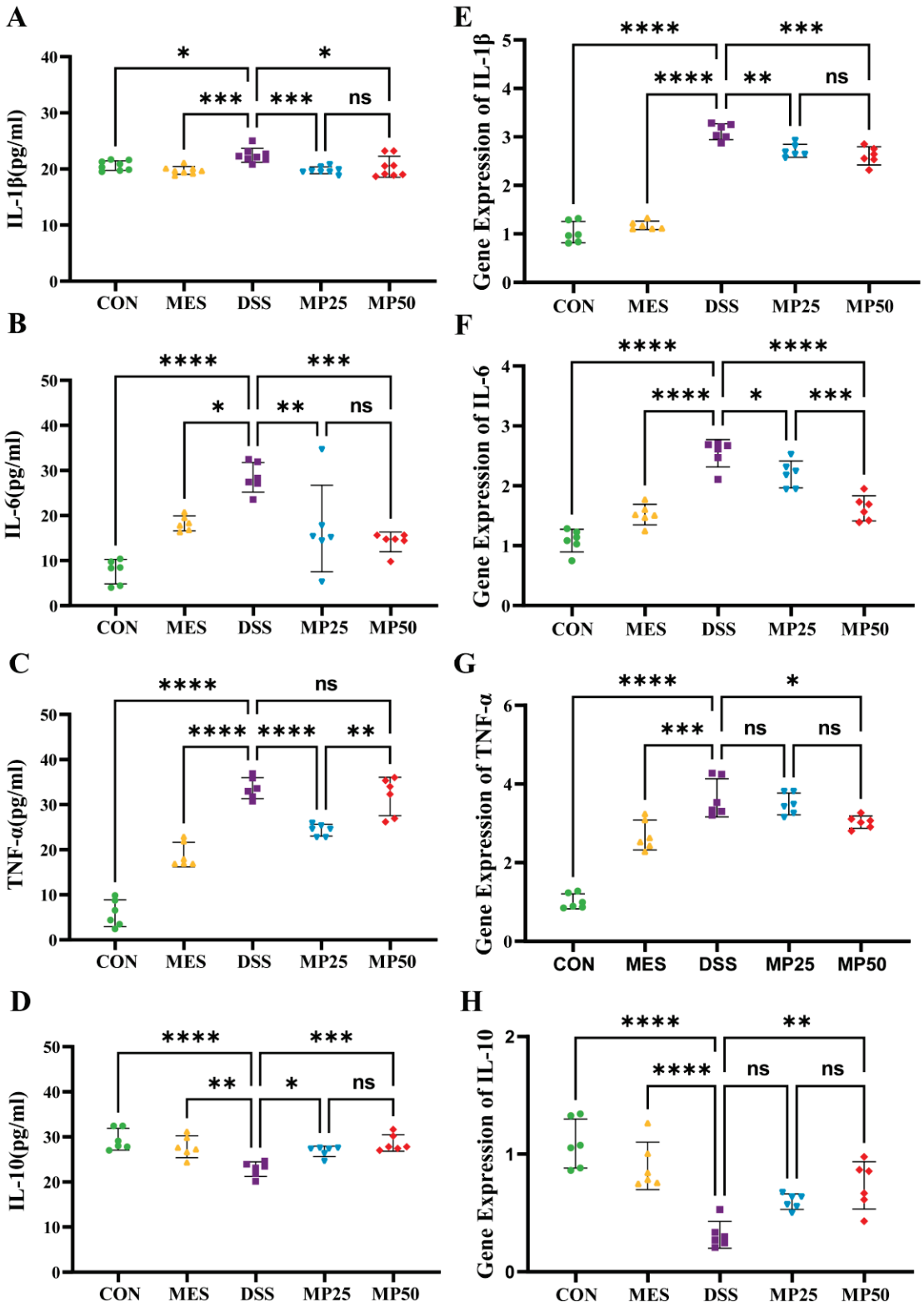


Figure 3. The concentrations of IL-6, IL-1β, TNF-α, and IL-10 and their mRNA expression levels were determined using ELISA kits and real-time PCR. Concentrations of four representative cytokines: IL-1β (**A**), IL-6 (**B**), TNF-α (**C**), and IL-10 (**D**) in the serum. The mRNA levels of four representative cytokines, IL-1β (**E**), IL-6 (**F**), TNF-α (**G**), and IL-10 (**H**), in colon tissues from the indicated groups were estimated by real-time quantitative PCR. Data are presented as mean ± SD (n = 6–8 per group). Statistical significance was determined using one-way ANOVA, followed by Tukey's test. ns, non-significant, * $p \leq 0.05$, ** $p \leq 0.01$, *** $p \leq 0.005$, and **** $p \leq 0.001$ relative to CON group.

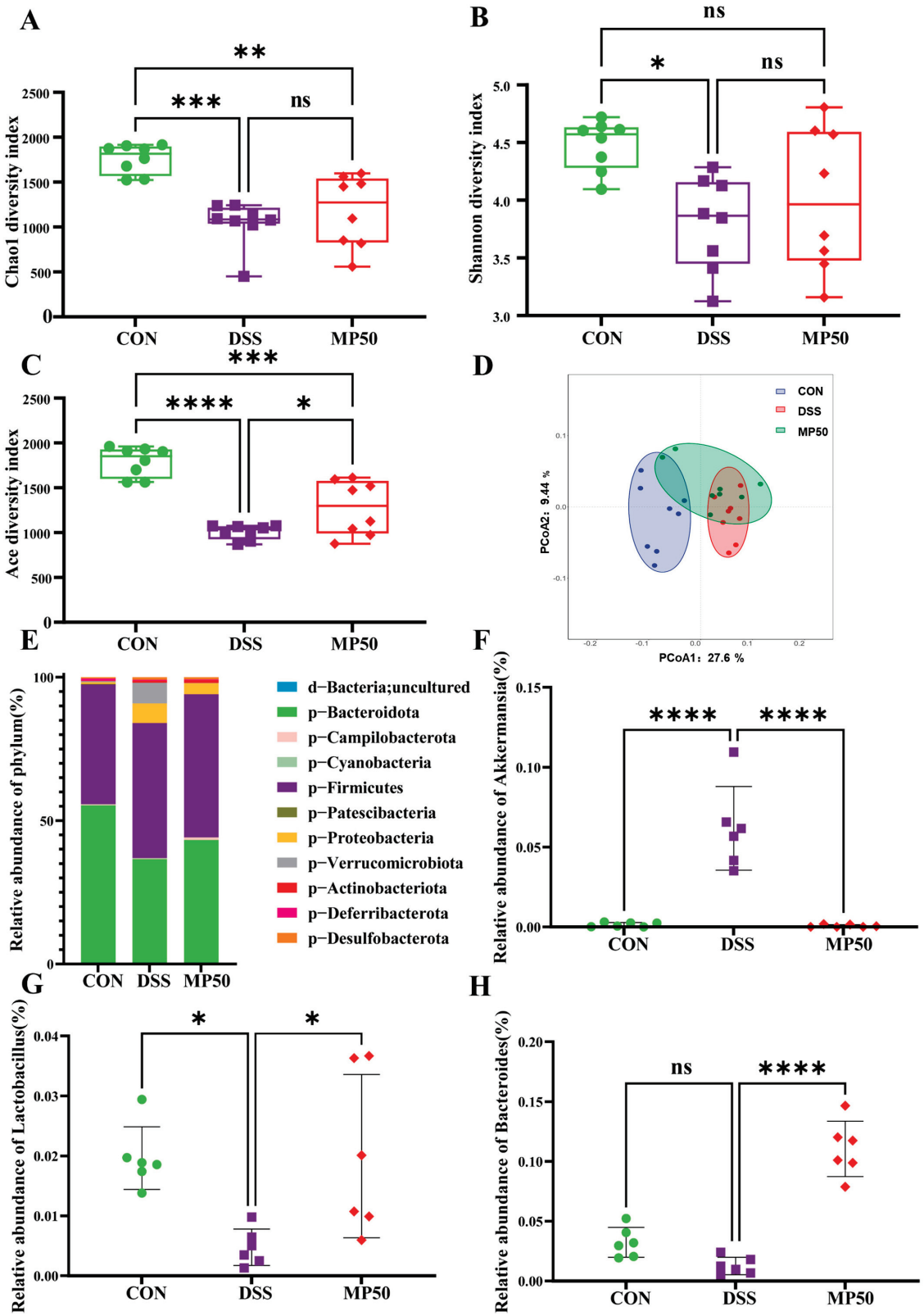


Figure 4. Effects of MFGMP on the composition of the gut microbiota. (**A**) Alpha diversity Chao1 index (n = 8). (**B**) Alpha diversity Shannon index (n = 8). (**C**) Alpha diversity ACE index (n = 8). (**D**) Principal coordinate analysis of weighted UniFrac distances. (**E**) Community structure analysis for each group at the phylum level. (**F**) Relative abundance of *Akkermansia* species (**G**) Relative abundance of *Lactobacillus* species. (**H**) Relative abundance of *Bacteroides* species. Statistical significance was determined using one-way ANOVA, followed by Tukey's test. ns, non-significant, * $p \leq 0.05$, ** $p \leq 0.01$, *** $p \leq 0.005$, and **** $p \leq 0.001$ relative to CON group.

At the phylum level, the relative abundance of Bacteroidota, Firmicutes, and Verrucomicrobiota was significantly different from that in CON group, with significant reversal of the change by MFGMP intervention (Figure 4E). At the genus level, MFGMP intervention significantly decreased the relative abundance of *Akkermansia* (Figure 4F) and *Clostridia_UCG-014* compared to the DSS group. In contrast, the relative abundance of *Lactobacillus* (Figure 4G), *Bacteroides* (Figure 4H), and *Alloprevotella* increased significantly.

The gene functions of known microorganisms were predicted using FAPROTAX (version 1.2.7) software, revealing that the gut microbiota in the DSS group was enriched in aerobic chemoheterotrophy. MFGMP interfered with the microbial function of chemoheterotrophy, as well as the functions of fermentation, the human gut, the mammalian gut, and automatic compound degradation (Figure 5A).

3.6. Effect of MFGMP on SCFAs of DSS-Induced UC in Mice

SCFAs are metabolic products of gut microbiota and play a crucial role in gut health and immune regulation. UC induced a decrease in SCFAs in the cecal content (Figure 5B). However, butyric acid and propionic acid significantly increased after MFGMP application compared to the DSS group, although the effect on total SCFAs was non-significant (Figure 5C,E). This suggested that the relief of inflammation by MFGMP may be related to butyric and propionic acids.

3.7. Effect of MFGMP on Intestinal Metabolites of DSS-Induced UC in Mice

Gut microbial metabolites are important molecular mediators between the host and gut microbes and have important and diverse effects on host physiology. A total of 12,991 metabolites in the cecal contents were analyzed using an untargeted metabolomics approach, and 181 major metabolites were identified as significantly different based on VIP > 1 ($p < 0.05$). Twenty-four key differential metabolites were identified by screening different metabolites in the DSS and CON groups, and metabolites that were significantly regulated by MFGMP gavage were further screened (Table S2). Principal component analysis (PCA) of the metabolites from the three groups of mice demonstrated that the model was highly interpretable and effective in differentiating between them (Figure 6A,B). PCA analyses of the CON, DSS, and MP50 groups depicted significant differences, with the MP50 group shifting from the DSS group to the CON group, which was located in between. This observation suggests that MFGMP may reduce the effects of DSS modeling (Figure 6C).

MetaboAnalyst (www.metaboanalyst.ca, accessed on 15 August 2024) was employed to perform KEGG pathway enrichment analysis on the list of differential metabolites [25]. The results depicted that MFGMP regulates 14 major metabolic pathways in a mouse model of UC (Figure 6D), particularly related to the metabolic pathways of amino acids, which encompass the biosynthesis of valine, leucine, and isoleucine; the degradation of lysine; the breakdown of valine, leucine, and isoleucine; as well as the metabolism of tryptophan and tyrosine.

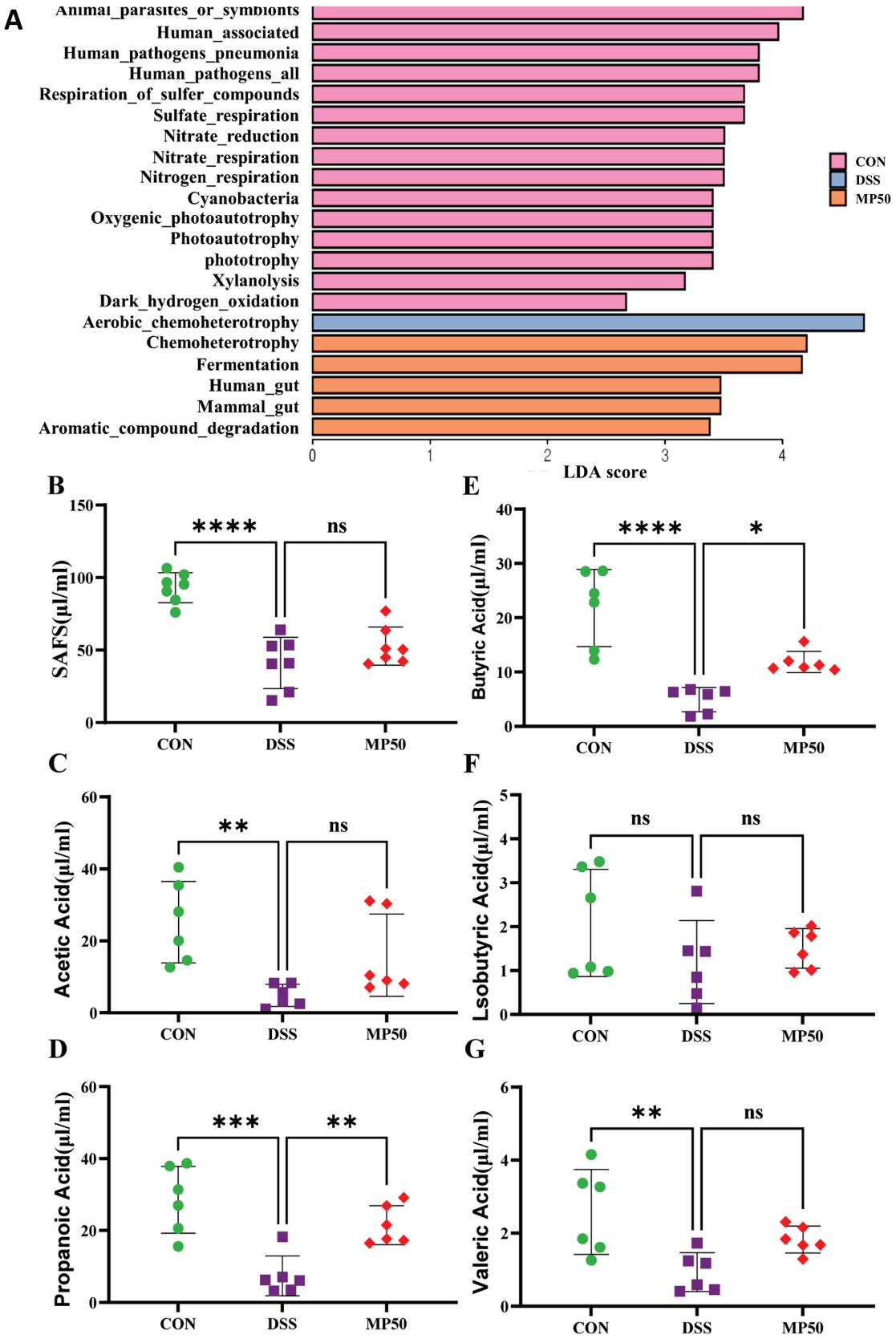


Figure 5. Determination of SCFAs in the cecum using gas chromatography–mass spectrometry. (**A**) Microbial gene functions predicted using FAPROTAX based on LDA scores. Total SCFAs (**B**), acetic acid (**C**), propanoic acid (**D**), butyric acid (**E**), isobutyric acid (**F**), and valeric acid (**G**) contents in mouse feces (n = 6). ns, non-significant, * $p \leq 0.05$, ** $p \leq 0.01$, *** $p \leq 0.005$, and **** $p \leq 0.001$ relative to CON group.

3.8. Impact of MFGMP on Amino Acid Metabolism in DSS-Induced UC in Mice

Some studies have found that the metabolism of specific amino acids may influence intestinal immune and inflammatory responses and that UC symptoms can be reduced by adjusting amino acid metabolism [26]. The levels of specific amino acids involved in the amino acid pathway were analyzed. The amino acid levels of L-valine, L-leucine, L-tryptophan, L-lysine, and L-tyrosine were lower in the DSS group compared to the CON group. After administering MFGMP through gavage, the level of L-valine returned to normal, while the concentrations of L-leucine, L-lysine, and L-tyrosine increased to nearly twice their normal levels, and the concentration of L-tryptophan increased to three times its original level (Figure 7A).

A correlation analysis was performed to investigate the relationship between amino acid content and inflammatory responses. L-valine, L-leucine, L-tryptophan, L-lysine, and L-tyrosine levels were negatively correlated with the mRNA expression levels of three pro-inflammatory cytokines (IL-6, IL-1β, and TNF-α). L-isoleucine was positively correlated with the mRNA expression levels of the four pro-inflammatory cytokines. L-valine, L-leucine, L-tryptophan, L-lysine, and L-tyrosine levels were positively correlated with the anti-inflammatory cytokine IL-10 and its mRNA expression levels. L-isoleucine was negatively correlated with IL-10 and its mRNA expression levels (Figure 7B). MFGMP inhibits inflammation primarily by regulating amino acid metabolic pathways.

3.9. Correlation Between Metabolites and Microbiota Composition

The top 20 differential microbial genera were filtered using fold change (FC) values (FC > 2 or FC < 0.5), and correlations with the previously identified 24 differential metabolites were assessed using Spearman's correlation analysis (Figure 7C). (R)-3-Hydroxybutyric acid, which is associated with butyric acid metabolism, was significantly positively correlated with *Lactobacillus* and *Clostridium_sensu_stricto*. There was a highly significant positive correlation between *Clostridia_UCG-014* and oxoadipic acid, fluvoxamine, ethylmorphine, and lomefloxacin, particularly oxoadipic acid, which is a product of tryptophan metabolism ($p < 0.01$). 4,4′-Dihydroxy-alpha-methylstilbene, coleonol, and Alloprevotella demonstrated a highly significant positive correlation ($p < 0.01$). MFGMP-derived metabolites, such as 3,4-dihydroxyphenylacetic acid, 3-methyl-2-oxovaleric acid, and oxoadipic acid, play important roles in tyrosine metabolism as well as valine, leucine, and isoleucine biosynthesis and tryptophan metabolism.

3.10. Effect of MFGMP on Wnt/β-Catenin Signaling Pathway in Mice Model

WNT-1 regulates cell proliferation and differentiation by activating β-catenin. In DSS-induced UC, β-catenin accumulates in the cytoplasm of cells and migrates to the nucleus due to inflammation, activating the expression of various genes such as Cyclin D1, which further promotes cell proliferation and inflammation [27,28]. DSS treatment significantly increased the expression of WNT-1, β-catenin, and Cyclin D1, as indicated by the immunohistochemical staining results (Figure 8A–C). RT-qPCR analysis revealed that the mRNA levels of WNT-1, β-catenin, and Cyclin D1 were significantly lower after MFGMP gavage compared to the DSS group (Figure 8D–F). MFGMP may alleviate DSS-induced UC through the Wnt/β-catenin signaling pathway.

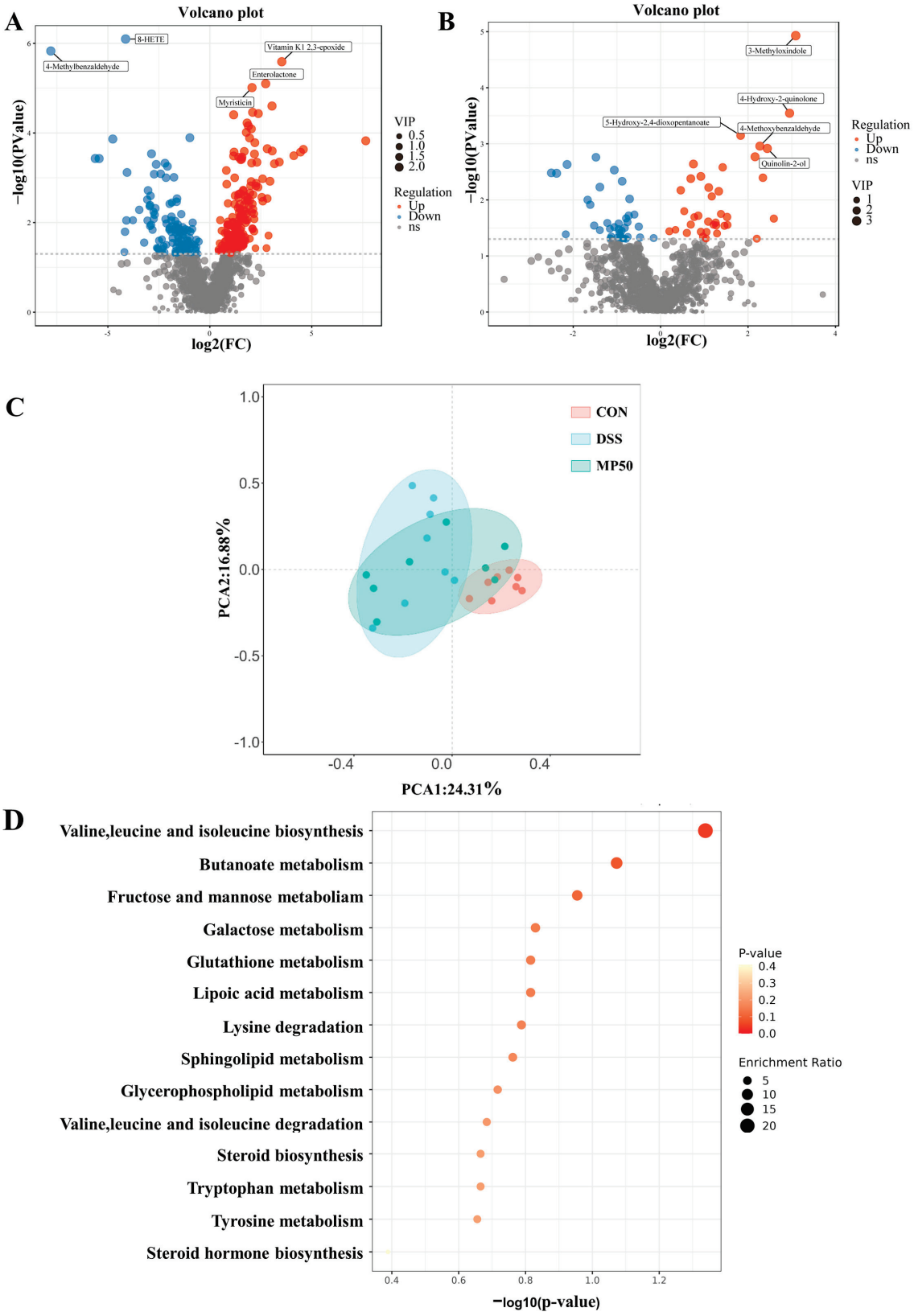


Figure 6. MFGMP altered metabolic profiles in DSS-induced UC. (**A**) Volcano map reflecting these variables between the CON and DSS groups. (**B**) Volcano map reflecting these variables between the DSS and MP50 groups. (**C**) Bubble diagram of KEGG enrichment analysis of 24 secondary differential metabolites. (**D**) PCA scores of the differential metabolites in the CON, DSS, and MP50 groups.

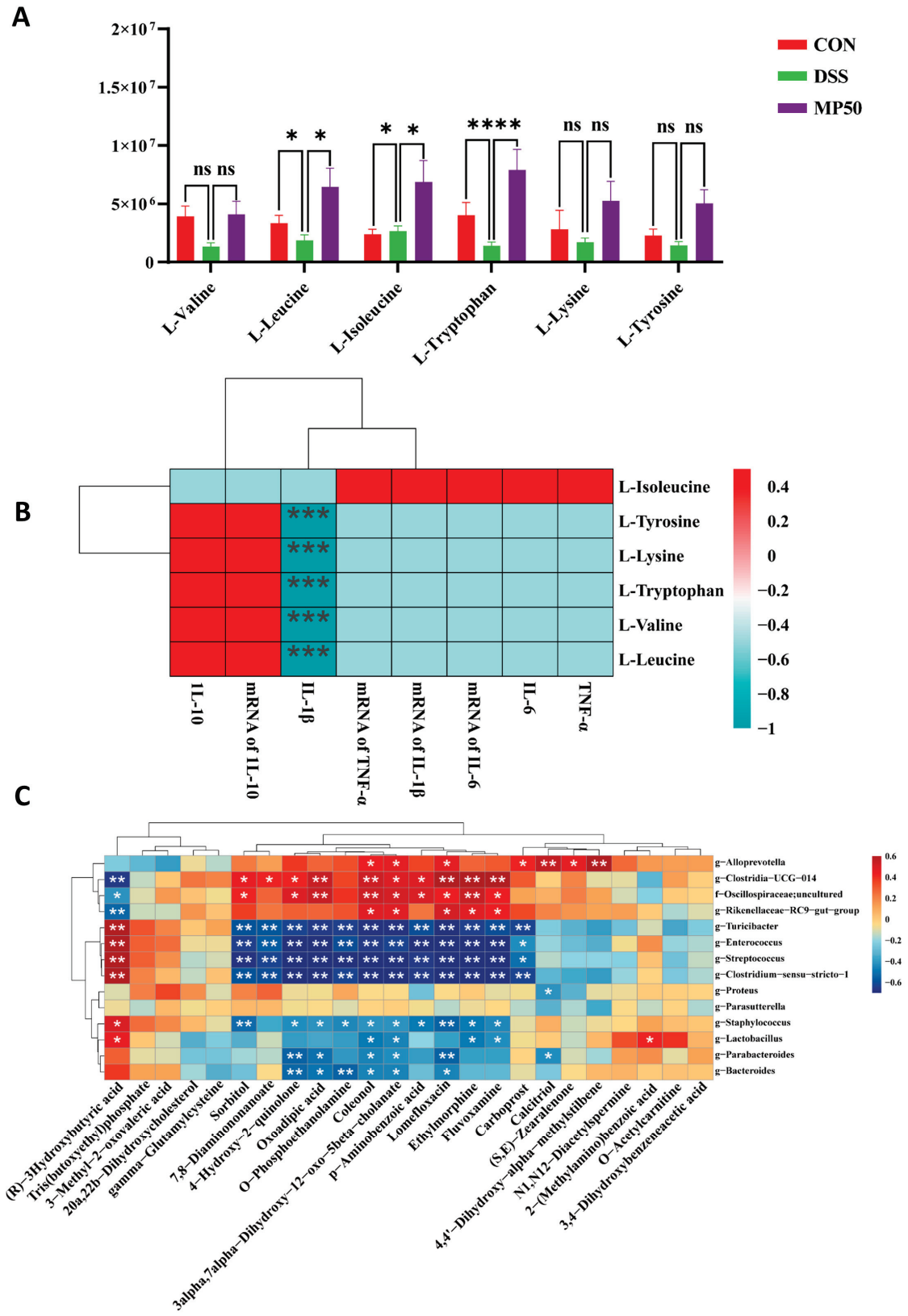


Figure 7. Effects of MFGMP on amino acid metabolism in mice with DSS-induced UC. (**A**) Specific amino acid content in mouse feces. (**B**) Heatmap of the correlation between the amino acid content in feces and cytokines. (**C**) Heatmap of the correlation between metabolites and microbiota composition in mice with DSS-induced UC. ns, non-significant, * $p < 0.05$, ** $p < 0.01$, and *** $p < 0.005$.

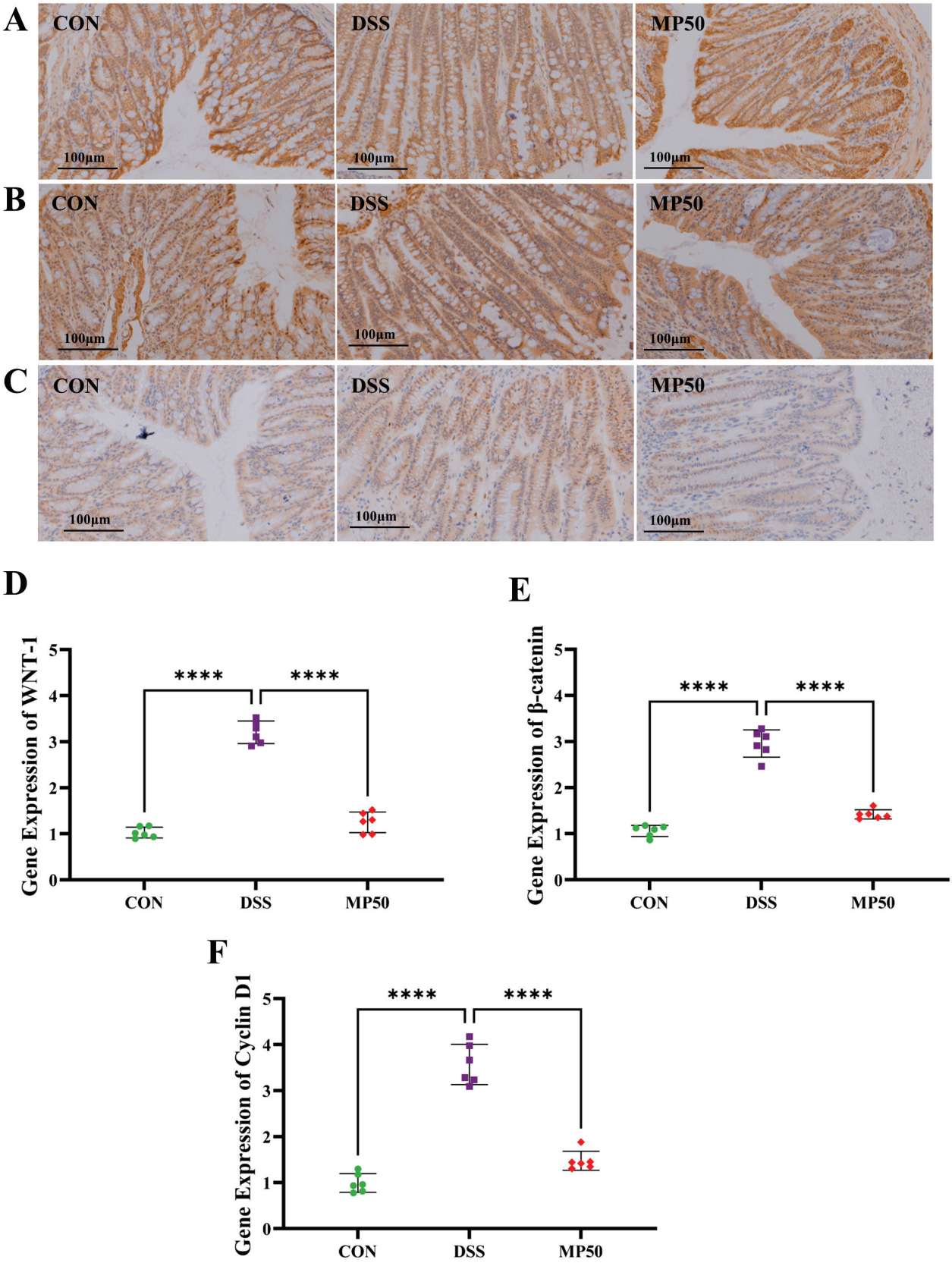


Figure 8. MFGMP downregulates the WNT-1-β-catenin-Cyclin D1 signaling pathway to alleviate inflammatory responses. Immunohistochemical staining for WNT-1 (**A**), β-catenin (**B**), and Cyclin D1 (**C**). Scale bars, 100 μm. The mRNA levels of three representative genes, WNT-1 (**D**), β-catenin (**E**), and Cyclin D1 (**F**), in colon tissues from the indicated groups were measured by real-time quantitative PCR. Statistical significance was determined using one-way ANOVA, followed by Tukey's test. **** $p \leq 0.001$ relative to the DSS group. The data are presented as mean ± SD (n = 6 per group).

4. Discussion

MFGM is commonly removed when milk fat is separated through centrifugation in the process of creating infant formula derived from bovine milk. However, the protective effects of MFGM in reducing inflammation, enhancing immunity, and improving cognitive function have been well documented. MFGM proteins have emerged as promising nutritional components that offer significant health benefits to mammals across all life stages [29]. Recently, substantial progress has been made in the clinical applications of MFGM peptides. Studies have demonstrated that MFGMP can regulate lipid metabolism, mimicking the structural advantages of breast milk in infant formulas and enhancing digestive efficiency [30]. Additionally, clinical trials have demonstrated that MFGMP can lower the incidence of hemorrhagic diarrhea and support intestinal maturation in infants [31]. Given these results, it can be inferred that MFGMP holds considerable promise for expanded use in dairy processing.

The mitigating effect of MGFMP on UC is related to its concentration. A 50 mg/kg dose was more effective in mitigating UC in mice, particularly in preventing weight loss and alleviating localized intestinal inflammation. However, it cannot be overlooked that 25 mg/kg MFGMP was more effective in lowering the DAI index and serum TNF-α levels. The DAI is an extensive evaluation system that takes into account alterations in weight, stool consistency, and instances of bleeding. Both 25 and 50 mg/kg MFGMP significantly decreased the DAI. However, loose stools in the MP50 group resulted in higher DAI. Protein degradation and absorption are disrupted in the intestinal tract, which is inflamed or infected by pathogens because of the inhibited secretion of digestive enzymes [32]. Concurrently, pro-inflammatory cytokines interfere with digestion, enhance smooth muscle contraction of the intestinal wall, accelerate the passage of contents, reduce water absorption, increase gas production, and aggravate diarrhea [33]. Therefore, high protein concentrations may impose an additional burden on the inflamed bowel, eventually leading to loose stools [34]. The elevated TNF-α levels in the MP50 group may have been due to the accumulation of leucine in feces in this study. Research conducted in the past has indicated that leucine stimulates the mammalian target of the rapamycin (mTOR) signaling pathway, which in turn enhances the synthesis of TNF-α [35,36].

Gut microbiota dysbiosis is widely considered a key factor contributing to UC. Many investigations have revealed that the makeup and by-products of the gut microbiome vary considerably between individuals suffering from intestinal disorders and those who are healthy [37,38]. MFGM, present in infant formulas, influences the gut microbiome in children and provides a protective effect against inflammation in the intestines. In normal mice, the dominant phyla include Firmicutes, Bacteroidetes, Desulfobacterota, Deferribacterota, and Proteobacteria [39]. Following DSS administration in mice, the relative abundances of Firmicutes, Verrucomicrobia, Actinobacteria, Desulfovibrio, and Proteobacteria were significantly elevated. Conversely, there was a simultaneous decline in the relative abundance of Deferribacterota and Bacteroidetes [40]. The research indicated that the administration of MGFMP at a dosage of 50 mg/kg led to a notable rise in the prevalence of Bacteroidetes in comparison to the DSS group. Within the phylum Bacteroidetes, species such as *B. fragilis*, *B. ovatus*, and *B. thetaiotaomicron* are capable of producing metabolites such as kynurenine, indole-3-acetic acid, and indole-3-lactic acid [41]. These substances are the critical products of tryptophan metabolism. The intricate interplay between gut microbes and their by-products profoundly influences immune homeostasis, substantially affecting immune development and responses. This pivotal role in modulating UC pathogenesis underscores the critical importance of comprehensively understanding the dynamic relationships within the disease process [42].

The Firmicutes-to-Bacteroidota (F/B) ratio is a well-established factor in maintaining normal intestinal homeostasis. Following DSS administration, an increased F/B ratio was observed in the mice, indicative of dysbiosis. In contrast, the administration of MFGMP reduced the F/B ratio in mice suffering from DSS-induced ulcerative colitis, thus emphasizing the regulatory role of MFGMP in maintaining intestinal balance. Enrichment of the phylum Proteobacteria, which includes many potentially harmful bacteria, has been observed in patients with UC. This study demonstrated that MFGMP supplementation counteracted this trend, exhibiting a tendency to restore the microbial composition to that of the CON group.

Verrucomicrobiota, especially *Akkermansia*, plays a crucial role in regulating intestinal inflammation. The results of this study indicated a significant increase in *Akkermansia* abundance in the DSS group compared to the CON group. Administering 50 mg/kg MFGMP restored the relative abundance of *Akkermansia*, in line with previous studies [43]. Phospholipids, an important component of MFGM, promote an increase in *Akkermansia* in the intestine, suggesting that individual MFGM components may influence *Akkermansia* differently [10]. Additionally, milk fat globules from different animal sources exert varying effects on *Akkermansia* [44]. Further studies are needed to demonstrate the intricate interactions between *Akkermansia* and the MFGM. Some studies have reported a reduction in *Akkermansia* in colitic mice [45]. These findings suggest that the role of *Akkermansia* in IBD pathogenesis is complex and multifaceted. Several studies have demonstrated that *Akkermansia* exerts a pro-inflammatory effect under specific conditions, particularly when harmful bacteria damage the intestinal mucosal barrier, thereby enabling pathogens to invade the intestinal wall. This phenomenon triggers an intense immune response [46]. Notably, the species and number of pathogenic microorganisms can influence the delicate role of *Akkermansia* in IBD [47]. Several studies have demonstrated the anti-inflammatory properties of *Akkermansia*. Specifically, *Akkermansia* strengthens the intestinal barrier to prevent inflammation, indirectly inhibits chronic low-grade inflammation by regulating metabolism, activates Toll-like receptor 2 (TLR2) on the surface of intestinal epithelial cells to increase the release of anti-inflammatory factors, and restores normal tryptophan metabolism in patients with UC [48–50]. Consequently, the role of *Akkermansia* in IBD pathogenesis is influenced by various factors, including host genetics, gut microbiota composition, environmental conditions, and microbial interactions [51,52].

Previous studies have identified a positive correlation between *Lactobacillus* and tryptophan metabolism in patients with UC. In the MP50 group, upregulation of *Lactobacillus* and *Bacteroides* was observed compared to the DSS group, further supporting their role in regulating tryptophan metabolism in DSS-induced colitis.

SCFAs produced by intestinal microorganisms play a crucial role in maintaining the morphology and function of intestinal epithelial cells and serve as key regulators of UC [53]. This study demonstrated that the SCFA content in the appendix significantly decreased, which was akin to the decrease in SCFA levels reported in patients with UC [54]. Butyric acid serves as a vital energy source for colon cells, supports the transformation of macrophages to the M2 phenotype, aids in the healing of injured colonic epithelial cells, and is important for sustaining colon health. Following MFGMP administration, butyric and propionic acid levels were markedly elevated. This aligns with an earlier study conducted by Gong, et al. [55], which found that the supplementation of MFGM led to an elevation in the fecal concentrations of propionic acid, butyric acid, isobutyric acid, valeric acid, and isovaleric acid in a mouse model with BLG-induced allergies. It has been found that butyric acid has significant anti-inflammatory properties and can reduce UC symptoms by inhibiting inflammatory pathway activation, modulating the energy metabolism of intestinal epithelial cells, and protecting intestinal barrier function [56,57].

Research has shown that *Akkermansia* is capable of inhibiting the inflammatory responses of macrophages, thereby helping to reduce symptoms associated with UC [58]. Additionally, butyric acid encourages the polarization of macrophages towards the M2 subtype [59].

Various investigations have investigated the function of metabolites in sustaining intestinal homeostasis. To determine the metabolic pathways that may be linked to the anti-colitis effects of MFGMP, we analyzed the connection between metabolic pathways and UC. Notable modifications in amino acid metabolism were observed, involving changes in processes like the metabolism of tyrosine, the breakdown of lysine, and the biosynthesis of valine, leucine, and isoleucine. Among these metabolic pathways, tryptophan metabolism has garnered particular attention because of its role in intestinal homeostasis. Microbial derivatives of tryptophan can activate the aryl hydrocarbon receptor, thereby contributing to gut homeostasis [60]. This study observed a significant increase in tryptophan levels in the MP50 group compared to those in the DSS group. Additionally, the levels of metabolites, such as indole, indole-3-acetaldoxime, indole-3-acetonitrile, indole-3-acetamide, and indoleacetate, were elevated, along with an increase in the content of 5-hydroxy-indole acetate and 6-hydroxymelatonin.

The current body of evidence indicates that early-stage therapeutic interventions, such as dietary modifications and microbiota modulation, may effectively decelerate disease progression and mitigate morbidity in UC through multifaceted mechanisms [61,62]. Therefore, as both an immunomodulator and a modulator of the gut microbiota, MFGMP may offer prophylactic protection in healthy individuals, potentially lowering their risk of developing UC. Further studies are required to fully demonstrate the mechanism by which MFGMP components exert their anti-colitis activity. MFGMP can be incorporated into food as a functional ingredient for the prophylactic effects of UC. Many challenges must be overcome to realize the transition from laboratory to clinical applications, including establishing standardized large-scale industrial production and legal policies for MFGMP, as well as determining the optimal dosage.

5. Conclusions

The present study found that 50 mg/kg of MFGMP alleviated DSS-induced weight loss, reduced DAI in mice with UC, and significantly inhibited both systemic and local inflammation. Moreover, MFGMP significantly improved the dysregulated gut microbiota induced by UC, restoring both α-diversity and β-diversity and increasing probiotic *Lactobacillus* while decreasing the mucolytic bacteria *Akkermansia*. Metabolomic analysis suggested that MFGMP intervention affected metabolites, particularly amino acid metabolism. Specifically, L-valine was normalized, whereas the concentrations of L-leucine, L-lysine, and L-tyrosine increased almost twofold, and the concentration of L-tryptophan increased threefold. Furthermore, based on Spearman's correlation analysis, increased amino acid levels were significantly negatively correlated with decreased pro-inflammatory cytokines in the colon, providing evidence that MFGMP alleviated intestinal inflammation by regulating amino acid metabolism. Lastly, the findings of this study revealed that MFGMP may regulate intestinal inflammatory processes through the Wnt/β-catenin signaling pathway. This finding further supports the potential of MFGMP as a functional food to prevent colonic inflammation.

Supplementary Materials: The following supporting information can be downloaded at: https://www.mdpi.com/article/10.3390/nu17050780/s1, Figure S1. SDS-PAGE profile of MFGMP. 1, 2, 3, and 4 are the MFGMP extracted at different times. Figure S2. (A) Weight change on day 7. (B) Length of the colon from each group. The MFGMP1 group was gavaged with only 25 mg/kg of MFGMP without DSS modeling, and the MFGMP2 group was gavaged with only 50 mg/kg of MFGMP without DSS modeling. Data were presented as means ± SD (n = 8). Statistical significance

was determined using one-way ANOVA, followed by Tukey's test. ns, non-significant. Table S1. Primer name. Table S2. Secondary difference metabolite.

Author Contributions: Conceptualization, Z.F. (Zhexin Fan); Software, B.L.; Formal analysis, J.W.; Investigation, L.Y.; Writing—original draft, N.K.; Visualization, J.S., Y.S. and Z.F. (Zhifeng Fang); Supervision, B.Y. All authors have read and agreed to the published version of the manuscript.

Funding: This work was supported by the Shihezi University High-level Talent Initiation Programme (2022ZK012), Tianchi Young Doctoral Programme of Excellence, the National Natural Science Foundation of China (32260594), and Corps Guiding Science and Technology Programme (2023ZD087).

Institutional Review Board Statement: This study was performed strictly per the Guidelines for the Care and Use of Laboratory Animals promulgated by the National Institutes of Health, and the Ethics Committee of Laboratory Animals of the University of Shihezi approved all experimental procedures (A2023-087, 12 August 2023).

Informed Consent Statement: Not applicable.

Data Availability Statement: Data that support the findings of this study are available from the corresponding author upon reasonable request.

Acknowledgments: The authors would also like to express their sincere thanks to the Figdraw online platform. Finally, the authors thank the Home for Researchers editorial team (www.home-for-researchers.com, accessed on 17 February 2025) for their language editing service.

Conflicts of Interest: The authors declare no conflicts of interest.

References

1. Kobayashi, T.; Siegmund, B.; Le Berre, C.; Wei, S.C.; Ferrante, M.; Shen, B.; Bernstein, C.N.; Danese, S.; Peyrin-Biroulet, L.; Hibi, T. Ulcerative colitis. *Nat. Rev. Dis. Primers* **2020**, *6*, 74. [CrossRef]
2. Sarter, H.; Crétin, T.; Savoye, G.; Fumery, M.; Leroyer, A.; Dauchet, L.; Paupard, T.; Coevoet, H.; Wils, P.; Richard, N.; et al. Incidence, prevalence and clinical presentation of inflammatory bowel diseases in Northern France: A 30-year population-based study. *Lancet Reg. Health Eur.* **2024**, *47*, 101097. [CrossRef] [PubMed]
3. Torres, J.; Gomes, C.; Jensen, C.B.; Agrawal, M.; Ribeiro-Mourão, F.; Jess, T.; Colombel, J.F.; Allin, K.H.; Burisch, J. Risk Factors for Developing Inflammatory Bowel Disease Within and Across Families with a Family History of IBD. *J. Crohns Colitis* **2023**, *17*, 30–36. [CrossRef] [PubMed]
4. Long, Y.; Zhao, X.; Xia, C.; Li, X.; Fan, C.; Liu, C.; Wang, C. Upregulated IL-17A secretion and CCR6 co-expression in Treg subsets are related to the imbalance of Treg/Th17 cells in active UC patients. *Scand. J. Immunol.* **2020**, *91*, e12842. [CrossRef] [PubMed]
5. Bennet, S.M.P.; Sundin, J.; Magnusson, M.K.; Strid, H.; Tap, J.; Derrien, M.; Le Nevé, B.; Doré, J.; Törnblom, H.; Simrén, M.; et al. Altered intestinal antibacterial gene expression response profile in irritable bowel syndrome is linked to bacterial composition and immune activation. *Neurogastroenterol. Motil.* **2018**, *30*, e13468. [CrossRef]
6. Nikkhah, A. Equidae, camel, and yak milks as functional foods: A review. *J. Nutr. Food Sci.* **2011**, *1*, 5. [CrossRef]
7. Ahamad, S.R.; Raish, M.; Ahmad, A.; Shakeel, F. Potential Health Benefits and Metabolomics of Camel Milk by GC-MS and ICP-MS. *Biol. Trace Elem. Res.* **2017**, *175*, 322–330. [CrossRef]
8. Aqib, A.I.; Kulyar, M.F.-E.; Ashfaq, K.; Bhutta, Z.A.; Shoaib, M.; Ahmed, R. Camel milk insuline: Pathophysiological and molecular repository. *Trends Food Sci. Technol.* **2019**, *88*, 497–504. [CrossRef]
9. Sun, Y.; Zhu, B.; Cong, P.; Li, X.; Liu, L.; Guo, C.; Zhao, K.; Qiu, J.; Ji, H.; Zhu, X.; et al. Regulating fat globule structure of infant formula based on MFGM to promote lipid uptake by improving lipolysis. *Food Hydrocoll.* **2024**, *155*, 110167. [CrossRef]
10. Gong, H.; Yuan, Q.; Du, M.; Mao, X. Polar lipid-enriched milk fat globule membrane supplementation in maternal high-fat diet promotes intestinal barrier function and modulates gut microbiota in male offspring. *Food Funct.* **2023**, *14*, 10204–10220. [CrossRef] [PubMed]
11. Wu, Z.; Liu, X.; Huang, S.; Li, T.; Zhang, X.; Pang, J.; Zhao, J.; Chen, L.; Zhang, B.; Wang, J.; et al. Milk Fat Globule Membrane Attenuates Acute Colitis and Secondary Liver Injury by Improving the Mucus Barrier and Regulating the Gut Microbiota. *Front. Immunol.* **2022**, *13*, 865273. [CrossRef]
12. Raza, G.S.; Herzig, K.-H.; Leppaluoto, J. Milk fat globule membrane-A possible panacea for neurodevelopment, infections, cardiometabolic diseases, and frailty. *J. Dairy Sci.* **2021**, *104*, 7345–7363. [CrossRef] [PubMed]

13. Liu, C.; Huang, S.; Wu, Z.; Li, T.; Li, N.; Zhang, B.; Han, D.; Wang, S.; Zhao, J.; Wang, J. Cohousing-mediated microbiota transfer from milk bioactive components-dosed mice ameliorate colitis by remodeling colonic mucus barrier and lamina propria macrophages. *Gut Microbes* **2021**, *13*, 1–23. [CrossRef] [PubMed]
14. Arnett, H.A.; Viney, J.L. Immune modulation by butyrophilins. *Nat. Rev. Immunol.* **2014**, *14*, 559–569. [CrossRef]
15. Chen, X.Y.; Sandrine, I.K.; Yang, M.; Tu, J.Y.; Yuan, X.L. MUC1 and MUC16: Critical for immune modulation in cancer therapeutics. *Front. Immunol.* **2024**, *15*, 1356913. [CrossRef] [PubMed]
16. Dou, Z.-H.; Yang, Y.-C.; Yang, J. Differential analysis of milk fat globule membrane proteins in bovine milk and bactrian camel milk. *Food Sci.* **2022**, *43*, 309–316. [CrossRef]
17. Ge, H.; Cai, Z.; Chai, J.; Liu, J.; Liu, B.; Yu, Y.; Liu, J.; Zhang, T. Egg white peptides ameliorate dextran sulfate sodium-induced acute colitis symptoms by inhibiting the production of pro-inflammatory cytokines and modulation of gut microbiota composition. *Food Chem.* **2021**, *360*, 129981. [CrossRef] [PubMed]
18. Luk, H.H.; Ko, J.K.S.; Fung, H.S.; Cho, C.H. Delineation of the protective action of zinc sulfate on ulcerative colitis in rats. *Eur. J. Pharmacol.* **2002**, *443*, 197–204. [CrossRef] [PubMed]
19. Dieleman, L.A.; Palmen, M.J.; Akol, H.; Bloemena, E.; Peña, A.S.; Meuwissen, S.G.; Van Rees, E.P. Chronic experimental colitis induced by dextran sulphate sodium (DSS) is characterized by Th1 and Th2 cytokines. *Clin. Exp. Immunol.* **1998**, *114*, 385–391. [CrossRef]
20. Kim, K.-S.; Lee, Y.; Chae, W.; Cho, J.-Y. An improved method to quantify short-chain fatty acids in biological samples using gas chromatography–mass spectrometry. *Metabolites* **2022**, *12*, 525. [CrossRef]
21. Chen, S.; Zhou, Y.; Chen, Y.; Gu, J. fastp: An ultra-fast all-in-one FASTQ preprocessor. *Bioinformatics* **2018**, *34*, 884–890. [CrossRef] [PubMed]
22. Ren, Y.; Yu, G.; Shi, C.; Liu, L.; Guo, Q.; Han, C.; Zhang, D.; Zhang, L.; Liu, B.; Gao, H.; et al. Majorbio Cloud: A one-stop, comprehensive bioinformatic platform for multiomics analyses. *iMeta* **2022**, *1*, e12. [CrossRef]
23. Peterson, L.W.; Artis, D. Intestinal epithelial cells: Regulators of barrier function and immune homeostasis. *Nat. Rev. Immunol.* **2014**, *14*, 141–153. [CrossRef] [PubMed]
24. Li, M.; Wu, Y.; Hu, Y.; Zhao, L.; Zhang, C. Initial gut microbiota structure affects sensitivity to DSS-induced colitis in a mouse model. *Sci. China Life Sci.* **2018**, *61*, 762–769. [CrossRef]
25. Xia, J.; Wishart, D.S. Web-based inference of biological patterns, functions and pathways from metabolomic data using MetaboAnalyst. *Nat. Protoc.* **2011**, *6*, 743–760. [CrossRef] [PubMed]
26. Yan, S.; Dong, R. Integrated Microbiome-Metabolomics Analysis Reveals the Potential Mechanism of Dandelion Root Polysaccharides to Ameliorate Ulcerative Colitis. *Metabolites* **2024**, *14*, 351. [CrossRef] [PubMed]
27. He, K.; Gan, W.-J. Wnt/β-catenin signaling pathway in the development and progression of colorectal cancer. *Cancer Manag. Res.* **2023**, *15*, 435–448. [CrossRef]
28. Doucas, H.; Garcea, G.; Neal, C.; Manson, M.; Berry, D. Changes in the Wnt signalling pathway in gastrointestinal cancers and their prognostic significance. *Eur. J. Cancer* **2005**, *41*, 365–379. [CrossRef]
29. Wang, Y.; Wu, J.; Zhang, H.; Yang, X.; Gu, R.; Liu, Y.; Wu, R. Comprehensive review of milk fat globule membrane proteins across mammals and lactation periods in health and disease. *Crit. Rev. Food Sci. Nutr.* **2024**, *2024*, 1–22. [CrossRef] [PubMed]
30. Li, Z.; Liu, A.; Cao, Y.; Zhou, H.; Shen, Q.; Wu, S.; Luo, J. Milk fat globule membrane proteins are crucial in regulating lipid digestion during simulated in vitro infant gastrointestinal digestion. *J. Dairy Sci.* **2024**, *107*, 7549–7563. [CrossRef]
31. Zavaleta, N.; Kvistgaard, A.S.; Graverholt, G.; Respicio, G.; Guija, H.; Valencia, N.; Lönnerdal, B. Efficacy of an MFGM-enriched complementary food in diarrhea, anemia, and micronutrient status in infants. *J. Pediatr. Gastroenterol. Nutr.* **2011**, *53*, 561–568. [CrossRef] [PubMed]
32. Peng, X.P.; Ding, W.; Ma, J.M.; Zhang, J.; Sun, J.; Cao, Y.; Lei, L.H.; Zhao, J.; Li, Y.F. Effect of Escherichia Coli Infection on Metabolism of Dietary Protein in Intestine. *Curr. Protein Pept. Sci.* **2020**, *21*, 772–776. [CrossRef]
33. Tang, Q.; Lan, T.; Zhou, C.; Gao, J.; Wu, L.; Wei, H.; Li, W.; Tang, Z.; Tang, W.; Diao, H.; et al. Nutrition strategies to control post-weaning diarrhea of piglets: From the perspective of feeds. *Anim. Nutr.* **2024**, *17*, 297–311. [CrossRef]
34. Pi, Y.; Mu, C.; Gao, K.; Liu, Z.; Peng, Y.; Zhu, W. Increasing the Hindgut Carbohydrate/Protein Ratio by Cecal Infusion of Corn Starch or Casein Hydrolysate Drives Gut Microbiota-Related Bile Acid Metabolism To Stimulate Colonic Barrier Function. *mSystems* **2020**, *5*, e00176-20. [CrossRef] [PubMed]
35. Iizumi, Y.; Masashi, S.; Yuki, I.; Handa, H.; Kishi, T.; Kanako, K.; Yamaguchi, Y. Role of N-end rule ubiquitin ligases UBR1 and UBR2 in regulating the leucine-mTOR signaling pathway. *Genes. Cells* **2010**, *15*, 339–349. [CrossRef]
36. Dong, L.; Du, H.; Zhang, M.; Xu, H.; Pu, X.; Chen, Q.; Luo, R.; Hu, Y.; Wang, Y.; Tu, H.; et al. Anti-inflammatory effect of Rhein on ulcerative colitis via inhibiting PI3K/Akt/mTOR signaling pathway and regulating gut microbiota. *Phytother. Res.* **2022**, *36*, 2081–2094. [CrossRef] [PubMed]

37. Lawal, S.A.; Voisin, A.; Olof, H.; Bording-Jorgensen, M.; Armstrong, H. Diversity of the microbiota communities found in the various regions of the intestinal tract in healthy individuals and inflammatory bowel diseases. *Front. Immunol.* **2023**, *14*, 1242242. [CrossRef]
38. Vila, A.V.; Imhann, F.; Collij, V.; Jankipersadsing, S.A.; Gurry, T.; Mujagic, Z.; Kurilshikov, A.; Bonder, M.J.; Jiang, X.; Tigchelaar, E.F. Gut microbiota composition and functional changes in inflammatory bowel disease and irritable bowel syndrome. *Sci. Transl. Med.* **2018**, *10*, 472. [CrossRef]
39. Do, K.-H.; Ko, S.-H.; Kim, K.B.; Seo, K.; Lee, W.-K. Comparative Study of Intestinal Microbiome in Patients with Ulcerative Colitis and Healthy Controls in Korea. *Microorganisms* **2023**, *11*, 2750. [CrossRef]
40. Yu, Z.; Li, D.; Sun, H. Herba Origani alleviated DSS-induced ulcerative colitis in mice through remolding gut microbiota to regulate bile acid and short-chain fatty acid metabolisms. *Biomed. Pharmacother.* **2023**, *161*, 114409. [CrossRef] [PubMed]
41. Nie, Q.; Sun, Y.; Li, M.; Zuo, S.; Chen, C.; Lin, Q.; Nie, S. Targeted modification of gut microbiota and related metabolites via dietary fiber. *Carbohydr. Polym.* **2023**, *316*, 120986. [CrossRef]
42. Schirmer, M.; Strazar, M.; Avila-Pacheco, J.; Rojas-Tapias, D.F.; Brown, E.M.; Temple, E.; Deik, A.; Bullock, K.; Jeanfavre, S.; Pierce, K.; et al. Linking microbial genes to plasma and stool metabolites uncovers host-microbial interactions underlying ulcerative colitis disease course. *Cell Host Microbe* **2024**, *32*, 209–226.e7. [CrossRef] [PubMed]
43. Xu, H.M.; Huang, H.L.; Liu, Y.D.; Zhu, J.Q.; Zhou, Y.L.; Chen, H.T.; Xu, J.; Zhao, H.L.; Guo, X.; Shi, W.; et al. Selection strategy of dextran sulfate sodium-induced acute or chronic colitis mouse models based on gut microbial profile. *BMC Microbiol.* **2021**, *21*, 279. [CrossRef] [PubMed]
44. Yao, Y.; Zhou, X.; Hadiatullah, H.; Li, C.; Wang, X.; Wang, S. Effects of Human, Caprine, and Bovine Milk Fat Globules on Microbiota Adhesion and Gut Microecology. *J. Agric. Food Chem.* **2021**, *69*, 9778–9787. [CrossRef] [PubMed]
45. Qu, S.; Fan, L.; Qi, Y.; Xu, C.; Hu, Y.; Chen, S.; Liu, W.; Liu, W.; Si, J. Akkermansia muciniphila Alleviates Dextran Sulfate Sodium (DSS)-Induced Acute Colitis by NLRP3 Activation. *Microbiol. Spectr.* **2021**, *9*, e00730-21. [CrossRef] [PubMed]
46. Shuang, Q.; Yinghui, Z.; Yichun, H.; Yicheng, F.; Kunyao, X.; Wei, Z.; Yawen, W.; Kaili, N.; Meng, Q. Excessive consumption of mucin by over-colonized Akkermansia muciniphila promotes intestinal barrier damage during malignant intestinal environment. *Front. Microbiol.* **2023**, *14*, 1111911. [CrossRef]
47. Zhao, Y.; Yang, H.; Wu, P.; Yang, S.; Xue, W.; Xu, B.; Zhang, S.; Tang, B.; Xu, D. Akkermansia muciniphila: A promising probiotic against inflammation and metabolic disorders. *Virulence* **2024**, *15*, 2375555. [CrossRef]
48. Shi, M.; Yue, Y.; Ma, C.; Dong, L.; Chen, F. Pasteurized Akkermansia muciniphila Ameliorate the LPS-Induced Intestinal Barrier Dysfunction via Modulating AMPK and NF-κB through TLR2 in Caco-2 Cells. *Nutrients* **2022**, *14*, 764. [CrossRef]
49. Xia, J.; Lv, L.; Liu, B.; Wang, S.; Zhang, S.; Wu, Z.; Yang, L.; Bian, X.; Wang, Q.; Wang, K.; et al. Akkermansia muciniphila Ameliorates Acetaminophen-Induced Liver Injury by Regulating Gut Microbial Composition and Metabolism. *Microbiol. Spectr.* **2022**, *10*, e0159621. [CrossRef]
50. Chen, S.; Qian, K.; Zhang, G.; Zhang, M. Akkermansia muciniphila and its outer membrane protein Amuc_1100 prophylactically attenuate 5-fluorouracil-induced intestinal mucositis. *Biochem. Biophys. Res. Commun.* **2022**, *614*, 34–40. [CrossRef] [PubMed]
51. Zheng, M.; Han, R.; Yuan, Y.; Xing, Y.; Zhang, W.; Sun, Z.; Liu, Y.; Li, J.; Mao, T. The role of Akkermansia muciniphila in inflammatory bowel disease: Current knowledge and perspectives. *Front. Immunol.* **2023**, *13*, 1089600. [CrossRef] [PubMed]
52. Massironi, S.; Viganò, C.; Palermo, A.; Pirola, L.; Mulinacci, G.; Allocca, M.; Peyrin-Biroulet, L.; Danese, S. Inflammation and malnutrition in inflammatory bowel disease. *Lancet Gastroenterol. Hepatol.* **2023**, *8*, 579–590. [CrossRef] [PubMed]
53. Yao, Y.; Liu, Y.; Xu, Q.; Mao, L. Short Chain Fatty Acids: Essential Weapons of Traditional Medicine in Treating Inflammatory Bowel Disease. *Molecules* **2024**, *29*, 379. [CrossRef]
54. Xu, H.-M.; Zhao, H.-L.; Guo, G.-J.; Xu, J.; Zhou, Y.-L.; Huang, H.-L.; Nie, Y.-Q. Characterization of short-chain fatty acids in patients with ulcerative colitis: A meta-analysis. *Bmc Gastroenterol.* **2022**, *22*, 117. [CrossRef] [PubMed]
55. Gong, H.; Li, T.; Liang, D.; Gao, J.; Liu, X.; Mao, X. Milk fat globule membrane supplementation protects against β-lactoglobulin-induced food allergy in mice via upregulation of regulatory T cells and enhancement of intestinal barrier in a microbiota-derived short-chain fatty acids manner. *Food Sci. Hum. Wellness* **2024**, *13*, 124–136. [CrossRef]
56. Tang, H.; Li, Q.; Zha, Z.; Jiao, Y.; Yang, B.; Cheng, Z.; Wang, T.; Yin, H. Xylan acetate ester ameliorates ulcerative colitis through intestinal barrier repair and inflammation inhibition via regulation of macrophage M1 polarization. *Int. J. Biol. Macromol.* **2024**, *280*, 135551. [CrossRef] [PubMed]
57. Firoozi, D.; Masoumi, S.J.; Mohammad-Kazem Hosseini Asl, S.; Labbe, A.; Razeghian-Jahromi, I.; Fararouei, M.; Lankarani, K.B.; Dara, M. Effects of short-chain fatty acid-butyrate supplementation on expression of circadian-clock genes, sleep quality, and inflammation in patients with active ulcerative colitis: A double-blind randomized controlled trial. *Lipids Health Dis.* **2024**, *23*, 216. [CrossRef] [PubMed]
58. Miao, Y.; Wang, M.; Sun, H.; Zhang, Y.; Zhou, W.; Yang, W.; Duan, L.; Niu, L.; Li, Z.; Chen, J. Akkermansia muciniphila ameliorates colonic injury in mice with DSS-induced acute colitis by blocking macrophage pro-inflammatory phenotype switching via the HDAC5/DAB2 axis. *Biochim. Biophys. Acta (BBA)-Mol. Cell Res.* **2024**, *1871*, 119751. [CrossRef]

59. Lee, S.Y.; Jhun, J.; Woo, J.S.; Lee, K.H.; Hwang, S.-H.; Moon, J.; Park, G.; Choi, S.S.; Kim, S.J.; Jung, Y.J. Gut microbiome-derived butyrate inhibits the immunosuppressive factors PD-L1 and IL-10 in tumor-associated macrophages in gastric cancer. *Gut Microbes* **2024**, *16*, 2300846. [CrossRef]
60. Scott, S.A.; Fu, J.; Chang, P.V. Microbial tryptophan metabolites regulate gut barrier function via the aryl hydrocarbon receptor. *Proc. Natl. Acad. Sci. USA* **2020**, *117*, 19376–19387. [CrossRef]
61. Barclay, A.R.; Russell, R.K.; Wilson, M.L.; Gilmour, W.H.; Satsangi, J.; Wilson, D.C. Systematic Review: The Role of Breastfeeding in the Development of Pediatric Inflammatory Bowel Disease. *J. Pediatr.* **2009**, *155*, 421–426. [CrossRef] [PubMed]
62. Ye, S.; Sun, Y.; Chen, X.; Fu, T.; Ruan, X.; Dan, L.; Chen, J.; Du, Z.; Wang, X. Greater adherence to the Mediterranean Dietary Approaches to Stop Hypertension Intervention for Neurodegenerative Delay (MIND) diet is associated with lower risk of inflammatory bowel disease: A prospective cohort study. *Food Funct.* **2024**, *15*, 7631–7640. [CrossRef] [PubMed]

Disclaimer/Publisher's Note: The statements, opinions and data contained in all publications are solely those of the individual author(s) and contributor(s) and not of MDPI and/or the editor(s). MDPI and/or the editor(s) disclaim responsibility for any injury to people or property resulting from any ideas, methods, instructions or products referred to in the content.

nutrients

MDPI

Article

Interventional Effects of Edible Bird's Nest and Free Sialic Acids on LPS-Induced Brain Inflammation in Mice

Nan Qian [1,2], Chen-Xi Zhang [1,2], Guan-Dong Fang [1,2], Shuang Qiu [3], Yu Song [1,4], Man Yuan [3], Dong-Liang Wang [3,*] and Xiang-Rong Cheng [1,2,*]

[1] School of Food Science and Technology, Jiangnan University, Wuxi 214122, China; qiannan202412@163.com (N.Q.); chenxi.zhang@chinyou.com (C.-X.Z.); fgd12232023@163.com (G.-D.F.); ssongyuu@163.com (Y.S.)
[2] State Key Laboratory of Food Science and Resources, Jiangnan University, Wuxi 214122, China
[3] Hebei Edible Bird's Nest Fresh Stew Technology Innovation Center, Langfang 065700, China; shuang.qiu@xxdun.com (S.Q.); man.yuan@xxdun.com (M.Y.)
[4] Central Nervous System Drug Key Laboratory of Sichuan Province, Luzhou 646000, China
* Correspondence: dongliang.wang@xxdun.com (D.-L.W.); cheng-xiangrong@hotmail.com (X.-R.C.)

Abstract: Objectives: Our study investigated the effects and mechanisms of edible bird's nest (EBN) and free sialic acids (SA) on LPS-induced brain inflammation in mice. **Methods**: The experiment divided the mice into four groups: control group (CON), lipopolysaccharide group (LPS), EBN intervention group (EBN, 200 mg/kg/d in dry EBN), and sialic acid intervention group (SA, dosage was calibrated based on the concentration of sialic acid in EBN). **Results**: The results showed that LPS caused a decrease followed by upregulation in body weight in female mice, and EBN exhibited renal protective effects. In the Morris water maze, the learning and memory abilities of mice in the LPS group first declined and then recovered. At the same time, the escape latency improved in the EBN and SA groups. In the Open field test, both the EBN and SA groups exhibited anti-anxiety and anti-depressive effects. Immunohistochemistry in the hippocampus showed significant cell damage in the LPS group, while the damage was alleviated in the EBN and SA groups. LPS promoted the expression of TICAM1 and MYD88 in the NF-κB pathway, while both the EBN and SA groups could inhibit the expression of TICAM1. **Conclusions**: The study has found that both EBN and SA exhibited noteworthy anti-inflammatory effects, indicating that the main active component in EBN that provides neuroprotective effects is SA. The bound SA in EBN confers additional effects, supporting the development of prevention and treatment strategies for brain inflammation.

Keywords: sialic acid; edible bird's nest; lipopolysaccharides; neuroinflammation

1. Introduction

Brain inflammation, as a key link in the pathogenesis of many neurological diseases, has become one of the research hotspots in neuroscience today. Among the many factors that induce brain inflammation, lipopolysaccharide (LPS), as a major component of the cell wall of Gram-negative bacteria, can effectively mimic the state of bacterial infection [1]. LPS can cause dysbiosis of the mouse gut microbiota, disrupt the gut barrier, and trigger gut inflammation [2]. And then activate the body's immune response, triggering a complex and intense inflammatory response in the brain [3]. This inflammatory response involves over-activation of microglia, massive release of pro-inflammatory cytokines, alteration of blood-brain barrier permeability, and neuronal dysfunction [4,5], which often causes severe

damage to the central nervous system, significantly affecting the normal physiological functions of the body, such as cognition and behaviour, and posing a heavy burden on the well-being of patients and a serious challenge to public health.

Sialic acid (SA), a class of acidic aminoglycans widely present in living organisms, has recently attracted much attention in medical and biological research [6]. There are many members in the SA family, commonly including N-acetylneuraminic acid (Neu5Ac) and its derivatives [7]. The basic structure of SA is a nine-carbon glycoside derivative formed by the condensation reaction of a pyruvic acid molecule with a mannosamine molecule. From a morphological point of view, SA exists in different structural forms, and the SA derived from edible bird's nest (EBN) primarily exists in a bound state [8], which is usually connected with sugar chains in biological macromolecules such as glycoproteins and glycolipids through specific glycosidic bonds. For example, in EBN, SA is often combined with proteins to form glycoprotein complexes, which show complex glycan chain branching in their structure, and the SA group is at the end of the glycan chain [9]. This structural feature endows it with unique biological properties, enabling it to recognize and bind organisms, and also influences the metabolization, transition, and interaction with other biomolecules [10]. EBN positively affects intestinal health [11,12] and regulates the body's brain and liver through metabolites produced by intestinal flora [13–15]. EBN is beneficial to women's health and can prevent and treat neurological disorders in menopausal women [16].

On the other hand, free SA is not covalently bound to other macromolecules and exists as a monomer in the organism. Compared to glycoprotein-bound SA, free SA molecular structure is relatively simple and independent. It has an intact basic structure of acidic aminosugars and free carboxyl and amino functional groups that exhibit unique chemical activities in solutions. It is more likely to interact with small molecules or ions. Its diffusion and transport mechanism through the cell may vary from that of glycoprotein-bound sialic acid.

SA has been shown to play important roles in various biological processes, including immune regulation, cell signalling and neural development, and some studies have suggested that they have potential anti-inflammatory properties [17]. EBN is associated with the improvement of cognitive functions. Studies indicate that it has neuroprotective effects on Alzheimer's disease, with the ability to inhibit neuroinflammation [18] and neuronal cell death [19]. Therefore, EBN benefits cognitive functions, which may be attributed to its antioxidant and anti-inflammatory activities [20]. Studies have shown that SA is the main neuroprotective active ingredient in EBN, and both free and bound SAs have been found to be present in EBN in comparable amounts. However, systematic and in-depth studies have yet to be conducted on different forms of SA, especially glycoprotein-bound SA and free SA from EBN, in addressing LPS-induced brain inflammation in mice and the specific mechanisms that affect brain inflammation development.

Given this, the present study was designed to construct an LPS-induced brain inflammation model in mice. By using free SA and EBN in mice, this work attempted to compare if free or bound SA confer greater bioactivity in EBN, namely from neurobehavioural, inflammation-related indexes, and inflammation pathways standpoint. It is expected to reveal further the mechanism of different forms of SA on brain inflammation and to provide a valuable theoretical and experimental basis for developing sialic acid-based preventive and therapeutic strategies for brain inflammation-related diseases.

2. Materials and Methods

2.1. Materials and Reagents

Edible bird's horn (from Malaysia, provided by Beijing Yungshutang Biotechnology Co., Ltd., Beijing, China); sialic acid (Neu5Ac, prepared by immobilised enzyme method, Wuhan Kostan Biotechnology Co., Ltd., Wuhan, China); lipopolysaccharides (LPS, L2280, Sigma, Saint Louis, MI, USA); PBS buffer tablets (Solebo, Beijing, China); physiological saline (Shuanghe Pharmaceuticals Co. Ltd., Anhui, China); GFAP primary antibody (A14673, ABclonal, Wuhan, China); IBA-1 primary antibody (Ab178846, Abcam, Shanghai, China); secondary FITC goat anti-rabbit (111-095-003, Jackson, Wuhan, China); anhydrous ethanol, $NaHSO_4$, o-phenylenediamine hydrochloride, glucose, phenol, concentrated sulfuric acid, methanol, etc. were purchased from Sinopharm Chemical Reagent Co. Ltd., Shanghai, China; tumor necrosis factor alpha (TNF-α), interleukin-1β (IL-1β), interleukin-6 (IL-6) commercial kits were purchased from Xiamen Huijia Co. Ltd., Xiamen, China; acetonitrile for liquid chromatography was all LC grade and purchased from Sinopharm Chemical Reagent Co. Ltd., Shanghai, China.

2.2. Experimental Animals

A total of 32 7-week-old female C57BL/6J mice (SPF grade) were purchased from Jiangsu Jicui Pharmachem Biotechnology Co., Nanjing, China. The experiment was approved by the Experimental Animal Welfare and Ethics Committee of Jiangnan University, with the approval number JN. No. 20230415c0800705.

2.3. Instruments and Equipment

The following equipment was used: a constant temperature oscillation incubator (TXA-120, Taicang Qiangle Experimental Equipment Co., Ltd., Taicang, China); a liquid chromatograph (LC-20AT, SHIMADZU, Kyoto, Japan); EF-C18 Bio column (Galaksil, Wuxi, China); a 96-well plate enzyme labeller (EPOCH1, Bio Tek Instruments Inc, Winooski, VT, USA); a panoramic section scanner (PANNORAMIC DESK/MIDI/250/1000, 3DHISTECH, Budapest, Hungary); an optical microscope (NIKON ECLIPSE E100, Nikon, Tokyo, Japan); and a decolourisation shaker (SK-0180-E, SCILOGEX, LLC, Los Angeles, CA, USA).

2.4. Determination of Sialic Acid Content

Referring to Wang Hui [21], the O-phenylenediamine (OPD) pre-column derivatisation method was used for the determination with appropriate modifications. Free SA was determined in a water bath at 50 °C protected from light for 2.5 h, and the temperature was changed to 4 °C to continue derivatisation for 48 h. HPLC working conditions: EF-C18-Bio column, SPD detector, column temperature and detector cell temperature of 30 °C, mobile phase acetonitrile: water = 5: 95, flow rate: 1.0 mL/min, detection wavelength: 230 nm, injection volume: 20 μL, isocratic elution: 45 min.

2.5. Animal Grouping and Biological Sample Collection

Mice were housed in the barrier facility of Jiangnan University Laboratory Animal Centre (SYXK-(Su)-2021-0056) and were subjected to a cycle of light and darkness every 12 h. Temperature: 20~26 °C, humidity: 40~70%, under an artificial light/dark cycle for 12 h. All mice were randomly divided into four groups, which were set as blank control group (CON), lipopolysaccharide group (LPS), EBN intervention group (EBN), and sialic acid intervention group (SA), with eight mice in each group. The CON and LPS groups were given 0.2 mL of 0.9% saline by gavage daily from week 2. The intervention groups were given equal volumes of EBN homogenate (200 mg/kg/d in dry EBN) and SA solution (dosage was calibrated based on the concentration of sialic acid in EBN) [18,19,22] for

7 weeks, respectively. From the last week onwards, 0.2 mL of 0.9% saline was injected intraperitoneally daily in the CON group, and an equal volume of LPS solution (500 μg/kg) was injected intraperitoneally in the other groups for 7 day (d) [23]. As shown in Figure 1, behavioural tests were carried out six hours after daily intraperitoneal injection for 7 d. After the end of all behavioural tests, the mice were fasted overnight and anesthetized with isoflurane inhalation after weighing. They were euthanized using the cervical dislocation method, and then immediately dissected. Organ samples were collected on ice and weighed, and plasma, serum, and organ tissues were frozen at −80 °C.

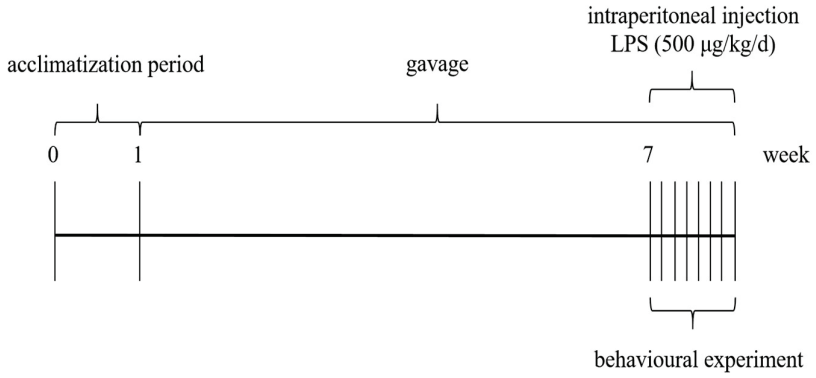


Figure 1. Timeline of animal experiments.

2.6. Behavioural Experiment

2.6.1. Morris Water Maze (MWM)

The Morris water maze apparatus consisted of a circular white water tank (120 cm in diameter and 50 cm in height) placed in the center, surrounded by an opaque cloth. A stationary platform (10 cm in diameter) was submerged 1 cm below the water surface, which was dyed white to obscure the platform. The water temperature was maintained at 25 °C.

On the 1st–5th day of the MWM, mice underwent spatial localization training. Each day, mice were introduced into the maze from four different quadrants facing the pool wall and were given 60 seconds (s) to spontaneously search for the hidden platform. The latency and path taken by the mice to reach the platform were recorded. If a mouse failed to find the platform within 60 s, it was guided to the platform and allowed to stay there for 15 s. In such cases, the escape latency was recorded as 60 s. To prevent the mice from locating the platform through inertia, the entry points were varied each day.

On the 6th day, a spatial exploration test was conducted to assess memory consolidation. The platform was removed from the maze, and the diagonal of the platform's original position was used as the new entry point (180° from the original platform location). Mice were allowed to swim freely for 60 s. Their trajectories were monitored, and the number of times each mouse crossed the former platform position, as well as the time spent in the target quadrant, were recorded [24].

2.6.2. Open Field Test (OFT)

The open field test was conducted in a white, rectangular box with dimensions of 50 cm × 50 cm × 40 cm (length × width × height). A camera was mounted on the top of the box to record the trajectories of the mice. The test was performed in a quiet, gray environment to minimize external disturbances. Mice were gently placed on the edge of the box facing the wall and allowed to move freely for a period of 5 min. Their trajectories were recorded throughout this time. After each mouse's behavioral data were collected, the box was sprayed with 75% alcohol to eliminate any residual odors, ensuring that the behavior of subsequent mice would not be influenced by the scent of previous animals. The

mice's behavior was analyzed based on several parameters, including central area dwell time, total distance, freezing time, and standing number [25].

2.7. Measurement of Inflammatory Factor Levels

Levels of cytokines TNF-α, IL-1β, and IL-6 in mouse brain (hippocampus, cortex) homogenates were determined using commercially available Elisa kits (Xiamen Huijia Co. Ltd., Xiamen, China), following the instruction guide. Enzyme-labeled reagents were added to a 96-well plate according to the instructions, followed by incubation and washing steps. After the color reaction, 1.0 M H_2SO_4 solution was added to stop the reaction. Immediately thereafter, the absorbance values of each well were measured at a wavelength of 450 nm, and the cytokine concentration was calculated based on the obtained standard curve equation.

2.8. Nissl Staining and Immunofluorescence Staining of Hippocampus

Fresh mouse brains were preserved in paraformaldehyde fixative, paraffin-embedded, and made into tissue sections, which were later deparaffinized to water and stained by adding toluidine blue for 2–5 min. After washing in water, 0.1% glacial acetic acid was added to differentiate the reaction, and the reaction was terminated by washing with tap water, and dried in the oven. Xylene was added for 10 min and the sections were sealed with neutral gum. The slices were examined microscopically under a light microscope and images were collected after Nissl staining.

After dewaxing paraffin-embedded brain sections to water, they were subjected to antigen retrieval in a microwave oven. Following cooling, the sections were decolorized with PBS (pH 7.4). The sections were then air-dried and blocked with 3% BSA for 30 min at room temperature. Next, primary antibodies against GFAP and IBA-1 (diluted 200-fold and 1000-fold, respectively, in PBS) were added dropwise to the sections, followed by overnight incubation at 4 °C in the dark. After decolorization and drying, secondary antibodies specific to the primary antibodies (diluted 400-fold in PBS) were applied and incubated at room temperature in the dark. Subsequently, DAPI was added dropwise and incubated for 10 min at room temperature. Finally, the sections were mounted with a fluorescence quenching sealer, and panoramic images of the hippocampus were captured using a tissue section scanner. The mean optical density (MOD) values of green fluorescence in the images were analysed using Image-Pro Plus 6.0 software. Calibration standards are converted to optical density values. Measurements selection "Area" and "IOD". Colors selection "Histogram Based", and threshold setting "0–250". The mean optical density was calculated according to Formula (1), as follows:

$$\mathrm{MOD} = \frac{\mathrm{IOD}}{\mathrm{Area}} \tag{1}$$

2.9. Quantitative Real-Time PCR (qPCR) Analysis

RNA was extracted from hippocampus tissue using a column extraction method according to the instructions. Total RNA was then reverse-transcribed into cDNA using the HiScript® III RT Super Mix reverse transcription kit (Vazyme Biotechnology Co., Ltd., Nanjing, China). Quantitative real-time reverse transcription polymerase chain reaction (RT-qPCR) amplification was performed using the 2× Taq Pro Universal SYBR qPCR Master Mix (Vazyme Biotechnology Co., Ltd., Nanjing, China). The β-actin was used as an endogenous control for normalizing tar-get gene mRNA expression. The relative expression levels of target genes were calculated using the $2^{-\triangle\triangle CT}$ method. The primer sequences (designed by NCBI GenBank) are listed in Table 1.

Table 1. Gene primer sequence for qPCR.

Gene	Forward Primer (5′-3′)	Reverse Primer (5′-3′)
β-actin	GGCTGTATTCCCCTCCATCG	CCAGTTGGTAACAATGCCAT
TICAM1	CAAGCTATGTAACACACCGCT	TGGTAACCCTAAGGAGACACTG
NF-κB p65	ACTGCCGGGATGGCTACTAT	TCTGGATTCGCTGGCTAATGG
MYD88	CAGGAGATGATCCGGCAACT	CATGCGGCGACACCTTTTC
Iκκβ	GGCACCCAATGATTTGCCAC	TCTAAGAGCCGATGCGATGT
COX-2	TTCCAATCCATGTCAAAACCGT	AGTCCGGGTACAGTCACACTT
CHUK	AAGGCCATTCACTATTCTGAGGT	GTCGTCCATAGGGGCTCTT

2.10. Data Processing and Analysis

The data results conforming to normal distribution were expressed as mean ± standard deviation of the mean (Mean ± SEM). GraphPad Prim 8 software was used to carry out statistical analysis of the data and to draw pictures. Data conforming to normal distribution were analysed using non-parametric tests, one-way ANOVA with post hoc two-by-two comparisons using Tukey's model for data in 3 or more groups; a *t*-test was used for data in 2 groups. The KW rank sum test was chosen for parametric tests, and a threshold of $p < 0.05$ was set to distinguish whether the groups were statistically different from each other.

3. Results

3.1. Characterisation of Different Forms of Salivary Acids

The treatment was performed using the OPD pre-column derivatisation method and quantified by HPLC. The free SA content of edible bird's horn was 7.35 ± 0.16%, and the total SA content was 14.07 ± 0.03%, consistent with the literature reports [26].

3.2. Analysis of Body Weight Organ Index

The changes in body weight of female mice in each group during the modelling time are shown in Figure 2A. Compared with the control group, it was clear that the body weight of female mice under continuous LPS invasion continued to decrease on days 2–3. It was significantly lower than that of the CON group, with a gradual increase in body weight from day 4 onwards. There was no significant difference between the LPS and the CON groups on day 5, which is consistent with the transient nature of LPS-induced mold formation reported by previous research [3,27], and suggests that the body can promote the restoration of homeostasis, but the recovery of body weight does not indicate fully repaired metabolic disorders. Notably, the EBN and SA groups showed similar changes in body weight as the LPS group, with no significant difference, indicating that they did not have any significant restorative ability on the body weight of female mice invaded by LPS.

The protective effects of structurally different SAs of EBN on the organs are shown in Figure 2B–D. The liver, kidney, and spleen indexes became significantly more prominent in the LPS group compared with the control group ($p < 0.001$). These indexes were reduced to different degrees in the EBN and SA groups compared with the LPS group. Among them, the EBN group showed a significant kidney index difference compared to the LPS group ($p < 0.05$), and the kidney index recovered by 5.05%. It can be shown that both EBN and free SA have partial protective effects on the organs, especially EBN, which exhibited more obvious protective effects on the kidneys.

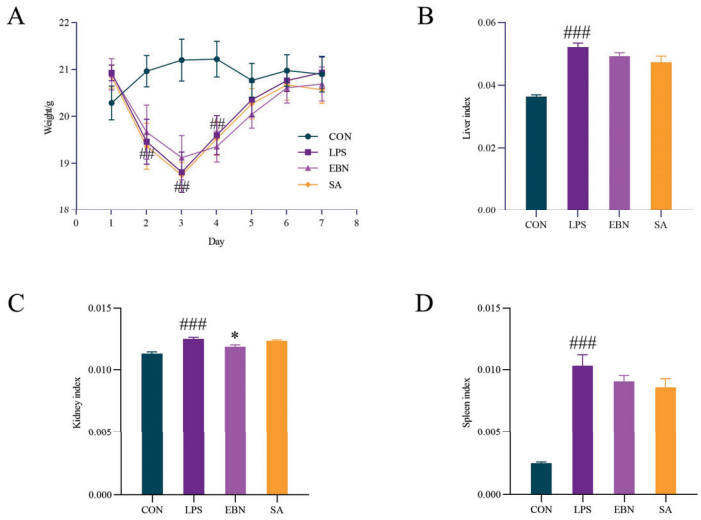


Figure 2. Comparison of body weight changes and organ indices of female mice in each group. (**A**) Body weight changes of female mice in each group during 1–7 days of modelling time. (**B**) Liver index of female mice in each group. (**C**) Kidney index of female mice in each group. (**D**) Spleen index of female mice in each group. Data are expressed as mean ± SEM. ## $p < 0.01$ and ### $p < 0.001$ vs. control group; * $p < 0.05$ vs. LPS group.

3.3. Behavioural Analysis

3.3.1. MWM Analysis

Excessive inflammatory responses in the brain can adversely affect learning and memory abilities [28]. Therefore, the MWM is used to examine mice's learning and memory capabilities through the cognitive assessment of mammalian rodents. As shown in Figure 3A, the Morris water maze experiment can reveal a significant difference in latency between the 1–4 d LPS group and the CON group ($p < 0.05$), indicating a significant decrease in spatial learning and memory ability. As shown in Figure 3B–D, the Escape period of EBN and SA groups on day 2–3 was significantly lower than that of LPS group ($p < 0.05$), and the Escape period on day 2 was decreased by 25.85% and 21.51%, suggesting their ameliorative effect. On day 4, SA group increased to the same level as LPS group, but the latency of EBN group was still significantly lower than LPS group ($p < 0.05$).

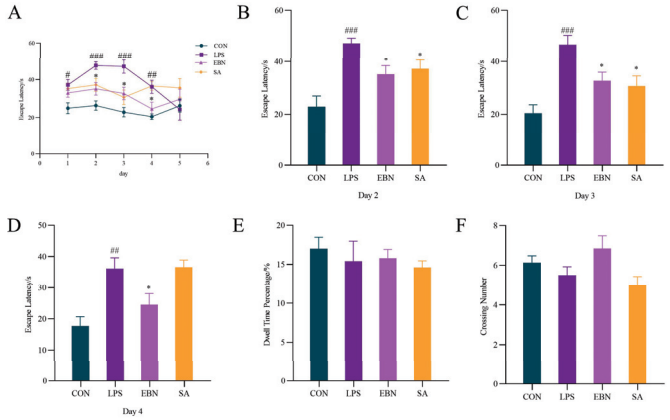


Figure 3. Comparison of behavioural indices in the Morris water maze of female mice in each group. (**A**) Changes in escape latency in female mice of each group during days 1–5 of training. (**B**) Escape latency of female mice in each group on day 2 of training. (**C**) Escape latency of female mice in each group on day 3 of training. (**D**) Escape latency of female mice in each group on day 4 of training. (**E**) Ratio of time spent in the target quadrant by each group of female mice. (**F**) Frequency of female mice passing the target quadrant in each group. Data are expressed as mean ± SEM. # $p < 0.05$, ## $p < 0.01$ and ### $p < 0.001$ vs. control group; * $p < 0.05$ vs. LPS group.

Figure 3E–F reveals no significant difference between the groups on the test metrics in the MWM in the probe experiment on day 6, indicating little difference in spatial memory ability between the groups. For the LPS group, this indicated that their spatial memory capacity was restored from day 5. Seven consecutive days of intraperitoneal injection of model-ling in the LPS group resulted in a significant decrease in the learning memory capacity of the female mice on days 1–4, while the capacity was restored from day 5 onwards. This was similar to the trend of body weight.

3.3.2. OFT Analysis

The OFT can reflect the degree of tension, anxiety, or depression of female mice in an unfamiliar environment. Excessive inflammatory responses in the brain are associated with depression [29]. The proportion of time spent in the central area by female mice in each group during the total time is shown in Figure 4A, which measures of anxiety-like behaviour. There was no significant difference between the LPS group and the CON group, whereas SA group showed a significant increase in the proportion of time spent in the central area, suggesting that SA has an anxiolytic effect. The total distance moved in each group within the open field experiment is shown in Figure 4B, and the LPS group showed a significant decrease in the distance compared to the control group ($p < 0.05$), suggesting that LPS induced depression-like behaviour in female mice. In the SA group, the distance moved by the female mice was significantly increased ($p < 0.05$) compared to the LPS group, indicating that SA can better exert antidepressant effects.

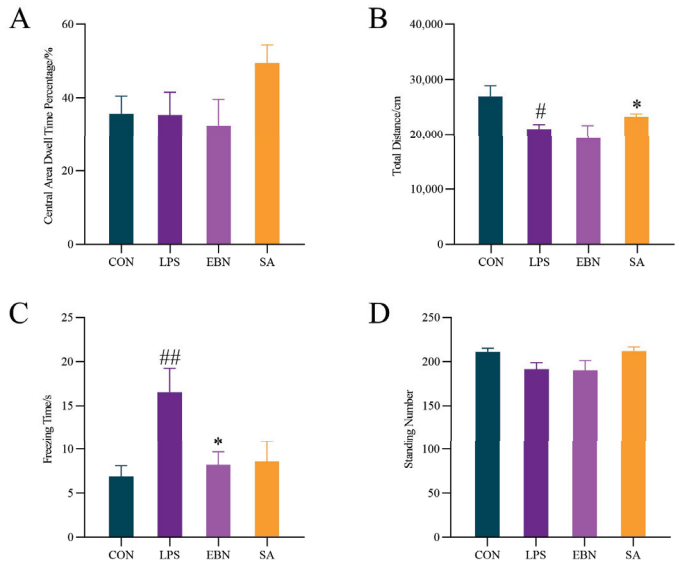


Figure 4. Comparison of behavioral indices of Open field test in female mice in each group. (**A**) Percentage of time spent in the central area by female mice in each group. (**B**) Distance moved within the experiment by each group of female mice. (**C**) Resting time of female mice in each group in the experiment. (**D**) Number of times female mice in each group stood upright in the experiment. Data are expressed as mean ± SEM. # $p < 0.05$, ## $p < 0.01$ vs. control group; * $p < 0.05$ vs. LPS group.

As shown in Figure 4C, the resting time of female mice in each group reflects the anxiety level and locomotor ability of female mice. Compared with the CON group, LPS significantly increased the resting time ($p < 0.01$), suggesting that LPS made female mice more anxious, depressed, and less capable of exercise. Compared with LPS group, the rest time of female mice in EBN group and SA group was reduced by 50.42% and 48.23%, respectively. It indicated that both structurally different SAs in EBN alleviated the depression-like behaviour. The number of erections of female mice in each group is shown in Figure 4D, reflecting the exploratory behaviour of the mice and the degree of curiosity

about the new environment. It was found that there was no significant difference between the groups in the number of erections compared with the CON group. Taken together, at day 7, LPS-induced female mice still showed some degree of depression-like behaviour. Moreover, both EBN and SA could alleviate the depression-like behaviour of female mice.

3.4. Analysis of Brain Inflammatory Factors

Intraperitoneal injection of LPS promotes transient and strong expression of inflammatory cytokines in various brain regions of mice, such as IL-1β, TNF-α, and IL-6 [30]. As shown in Figure 5, the LPS group had different effects on the expression of inflammatory factors: IL-1β is a pro-inflammatory factor, and the LPS group increased the expression of IL-1β compared with the control group, which can be seen that LPS induced inflammation in female rats. The expression of IL-1β in the EBN and SA groups was reduced to different degrees compared with that of the LPS group. The expression of TNF-α is a pro-inflammatory factor. Compared with CON group, LPS had no significant effect on the expression of TNF-α in mice brain.

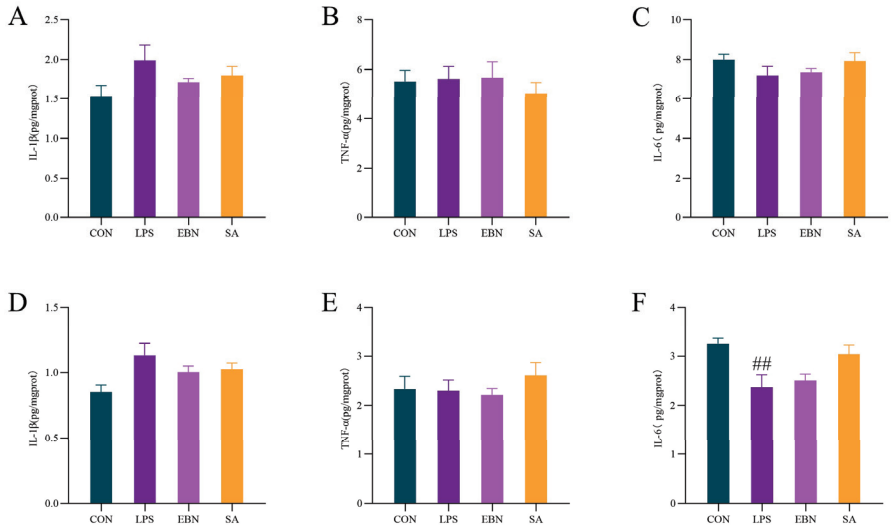


Figure 5. Comparison of inflammatory factors in the brain of female mice in each group. (**A**–**C**) Inflammatory factors (IL-1β, TNF-α, IL-6) in the hippocampus of the brain of female mice in each group. (**D**–**F**) Inflammatory factors (IL-1β, TNF-α, IL-6) content in the cortex of the brain of female mice in each group. Data are expressed as mean ± SEM. ## $p < 0.01$ compared to control.

Meanwhile, no significant difference was observed between the EBN and SA groups compared with the LPS group. IL-6 is a pro-inflammatory and anti-inflammatory factor, and IL-1β and TNF-α inflammatory factors mainly activate its expression. Compared with the CON group, the LPS group reduced the expression of IL-6 inflammatory factors in the brain, especially in the cortical area ($p < 0.01$). The EBN and SA groups were alleviated compared with the LPS group, and the expression of IL-6 inflammatory factor was recovered by 15.95% and 75.57%.

3.5. Immunohistochemistry of the Hippocampus

The results of Nissl staining revealed the morphological changes of neurons in hippocampal CA1, CA2, and DG regions. CA1 plays a key role in memory consolidation and is considered an important link in converting short-term memory into long-term memory. Damage to the CA1 region can seriously impact spatial memory [31]. Damage to the CA2 region reduces social memory ability, affects subsequent memories' storage and retrieval, and is involved in a certain degree of emotional memory [32]. The DG region helps the brain distinguish similar but different inputs to avoid memory confusion. This region

is closely related to the plasticity of the brain and its ability to learn and adapt to new environments and things [33].

As shown in Figure 6, in the CA1, CA2, and DG regions, the single-cell structure in the CON group had a complete outline, clear nuclei, and a high number of intact nerve cells. In contrast, the number of intact neurons was significantly reduced in the LPS group, with cell lysis in the marginal layer, diffuse cellular debris, and thick nucleoli. There may be cellular morphology alterations in the LPS group due to inflammatory response [34]. Unlike the LPS group, neurons increased in the EBN and SA groups, with some apoptotic cells but reduced fragmentation. The morphology and arrangement of cells in both groups were more ordered and tightly packed than in the LPS-treated group, with less cellular debris in the hollow space, and the cellular structure appeared more intact. The EBN and SA groups may have some cytoprotective effects, which could alleviate the cellular damage induced by the LPS group to a certain extent. In response to LPS, EBN, and SA, the CA1, CA2, and DG regions did not show noticeable specific differences, which may indicate that these treatments' effects on different hippocampus regions are somewhat consistent. This experiment found that SAs in EBN alleviated the release of inflammatory factors induced by LPS and reduced neuronal structural damage in the hippocampus by combining the levels of inflammatory factors in the brain.

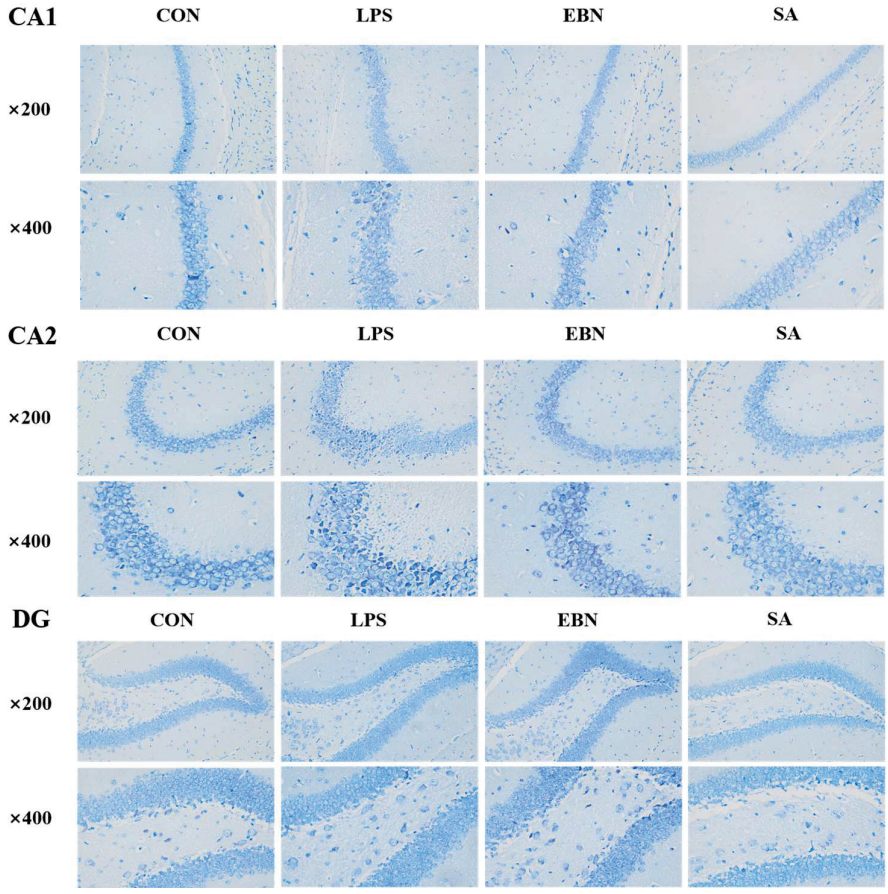


Figure 6. Morphological structure of neurons in CA1, CA2 and DG regions of the hippocampus of female mice in each group (×200, ×400).

Ionized calcium binding adapter molecule 1 (IBA-1) is a microglia-specific intracellular protein and is therefore commonly used as a marker to determine microglia specificity. Glial fibrillary acidic protein (GFAP) can be used as a biomarker for astrocyte proliferation during CNS injury. As illustrated in Figure 7, the immunofluorescence staining and quantitative analysis of fluorescence intensity revealed that hippocampal IBA-1 staining was enhanced

in LPS-treated mice, indicating increased microglial activation. Additionally, the number of GFAP-positive cells, indicative of astrocyte activation, was also elevated in these mice. Both EBN and SA interventions attenuated the increase in IBA-1-positive and GFAP-positive cells within the hippocampus. Among them, the intervention with EBN demonstrated a better efficacy compared to SA in reducing the activation of these glial cells.

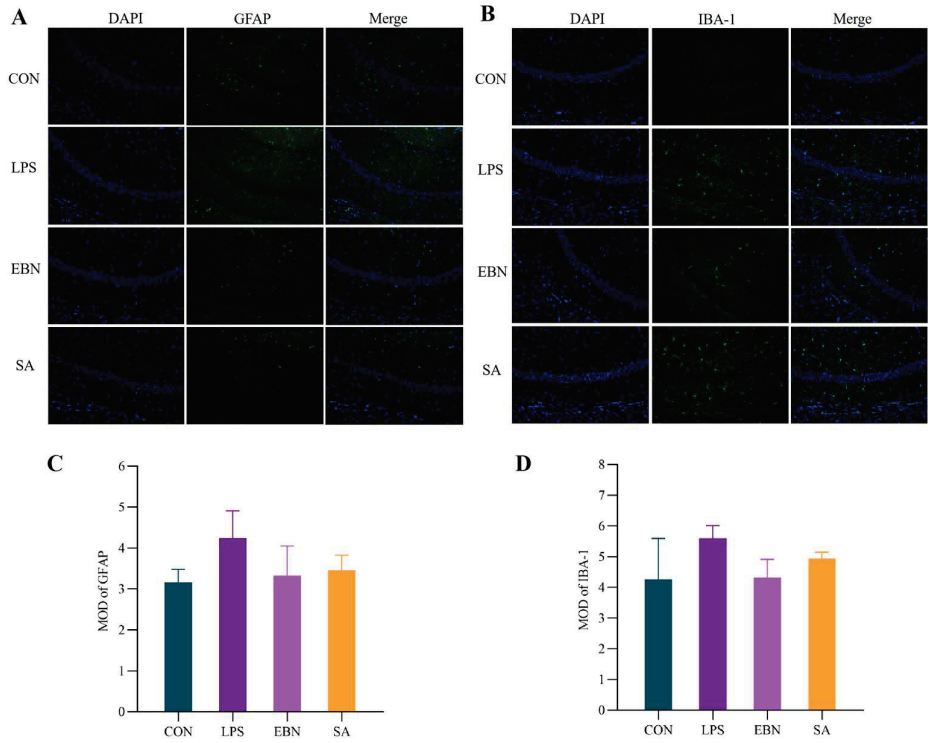


Figure 7. Immunofluorescence staining images and quantitative analysis in the CA1 region of the hippocampus of female mice in each group. (**A**,**B**) Immunofluorescence staining of the CA1 region of the hippocampus with specific antibody labelled GFAP and IBA-1 proteins (×200). (**C**,**D**) Mean optical density in the CA1 region of the hippocampus for specific antibody-tagged IBA-1 and GFAP proteins. Data are expressed as mean ± SEM.

3.6. NF-κB Inflammatory Signalling Pathway

NF-κB is a nuclear transcription factor with pleiotropic regulatory effects widely present in various cells. In inflammatory responses, the NF-κB signaling pathway plays a key regulatory role. Researchers have found that inhibiting the activation of key NF-κB signaling targets can reduce the expression of inflammatory factors and alleviate inflammation [35]. Under normal conditions, NF-κB is bound to its inhibitory protein IκB in the cytoplasm, remaining inactive [36–39]. As can be seen in Figure 8A, the expression of the TICAM1 gene was significantly elevated under LPS treatment conditions ($p < 0.05$). It was suggested that LPS could trigger inflammatory responses by activating the Toll-like receptor 4 (TLR4) signalling pathway. The TICAM1 gene may play an important role in this inflammatory response, and its high expression may be related to the immune defense mechanism. Compared with the LPS group, the TIC AMI gene expression was lower under treatment in the EBN and SA groups ($p < 0.05$), which implied that EBN and SA inhibited the expression of the TICAM1 gene and might have an anti-inflammatory effect.

In Figure 8B, compared with the control group, NF-κB p65 gene expression in LPS group was significantly increased ($p < 0.05$). NF-κB is an important transcription factor in inflammatory responses, immune responses, and cell survival. LPS stimulation resulted in the degradation of IκκB by phosphorylation and NF-κB release, which enabled the NF-κB p65 subunit to enter the nucleus and initiate the transcription of a series of genes

related to inflammatory response, immune response, and cell survival. The relatively low expression of NF-κB p65 gene in EBN and SA treatments compared to LPS may indicate that they inhibit the NF-κB signaling pathway activation, and thus have potential anti-inflammatory properties.

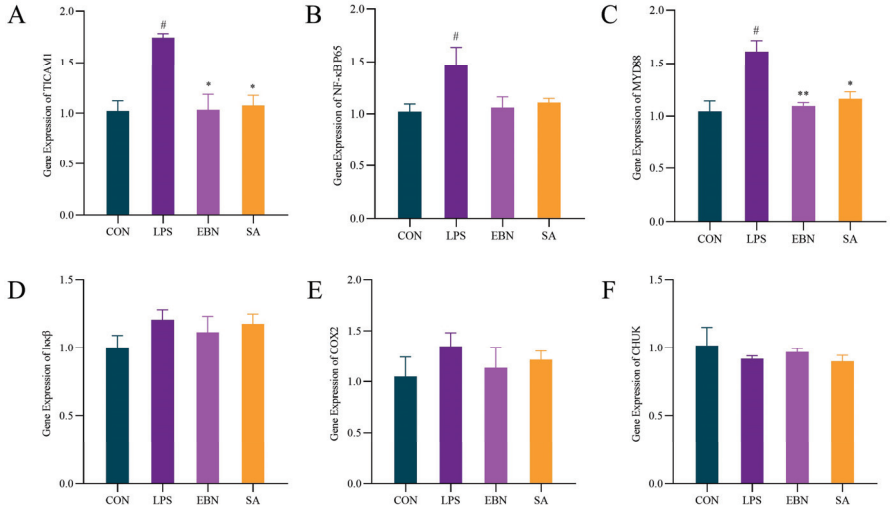


Figure 8. Expression of inflammation-related genes on the NF-κB pathway in each group. (**A**) TICAM1 gene expression in each group. (**B**) NF-κB p65 gene expression in each group. (**C**) MYD88 gene expression in each group. (**D**) IκκB gene expression in each group. (**E**) COX-2 gene expression in each group. (**F**) CHUK gene expression in each group. Data are expressed as mean ± SEM. # $p < 0.05$ vs. control group; * $p < 0.05$, ** $p < 0.01$ vs. LPS group.

Figure 8C showed significantly increased expression of the MYD88 gene under LPS treatment ($p < 0.05$). MYD88 is a key junction protein in the TLR4 signalling pathway in LPS-induced inflammatory response. It can activate downstream NF-κB and other inflammation-related signalling pathways. MYD88 gene expression was significantly decreased in EBN ($p < 0.01$) and SA ($p < 0.05$) groups, which indicated that EBN and SA can reduce the LPS-induced inflammatory response by inhibiting the expression of MYD88.

The expression levels of Iκκβ gene in each group were shown in Figure 8D. Normally, NF-κB binds to the IκB protein in an inactivated state in the cytoplasm. When the cell is stimulated, the Iκκβ is activated and phosphorylates the IκB protein, resulting in the degradation of the IκB protein, NF-κB release, and allows it to enter the nucleus to initiate transcription. Compared with CON group, the expression of Iκκβ gene was increased in LPS group, but there was no significant change, which may indicate that LPS activate the NF-κB pathway with little effect on Iκκβ gene transcription level. This may be because regulation of Iκκβ occur more at the post-translational level, such as its own phosphorylation and activation, rather than at gene transcription.

In Figure 8E, LPS treatment led to the elevation of the expression of the COX-2 gene, an inducible enzyme mainly in the nucleus of cells. COX-2 is an inducible enzyme that mainly impacts inflammation and tumour development. LPS can induce the expression of COX-2 by activating NF-κB and other signalling pathways to produce inflammatory mediators such as prostaglandins. The expression of the COX-2 gene was reduced to a certain extent under EBN and SA treatment, which indicated that EBN and SA has the anti-inflammatory effect of inhibiting COX-2 expression.

CHUK gene expression was shown in Figure 8F. CHUK is part of the Iκκ complex and is involved in the activation of NF-κB. There was no significant change in CHUK gene expression under each treatment, which may indicate that these treatments had little effect on CHUK gene transcription.

4. Discussion

LPS caused a significant increase in organ indices, while EBN and SA groups reduced these indices. This may be due to LPS disrupting the body's metabolism and physiological functions. SA is the main active component in EBN that suggests neuroprotection in mice [14]. Studies suggest that various plant polysaccharides (mycelia selenium polysaccharides, Hericium Erinaceus polysaccharide, etc.) have a positive impact on inflammation-related diseases in mice [40–42], indicating that polysaccharides could serve as a novel anti-inflammatory agent. In contrast, EBN can alleviate the damage to organs caused by inflammation, reducing the organ stress response and pathological changes caused by inflammation, although not affecting weight recovery. This may be related to its high SA content which can regulate immune responses, inhibit inflammatory mediator release, and reduce oxidative stress damage that created a relatively stable internal environment for the organs. Among them, EBN is particularly prominent in protecting the kidneys. The bound SA from EBN may confer additional effects on it, which is consistent with previous studies. Researchers have found that bound SA is beneficial for regulating the intestinal probiotics of pregnant women [8], and protein-bound Neu5Ac exhibits higher prebiotic activity than its free monomeric form [43].

MWM reveal that the LPS group experienced a significant decline in learning and memory in the early stages. Although there is a tendency for recovery in the later stages, it is due mainly to limited compensatory mechanisms of the body. This experiment revealed that supplementation with different forms of SA could alleviate the decline in learning and memory ability induced by LPS, playing a role in cognitive protection. The EBN and SA groups significantly improved anti-inflammatory, anti-oxidative, and neuroprotective properties, inhibiting inflammatory factors, enhancing neurotrophic factors, repairing neurotransmitter metabolism, and regulating the endocrine system. On day 4 of MWM, EBN still had good spatial cognitive abilities. However, the SA group had declined to the same level as the LPS group, which further confirms that bound SA in EBN exhibits higher anti-inflammatory activity than SA groups (free SA). The impact of different forms of SA on learning and memory functions has been studied to some extent, and it is believed that SA is closely related to the function and stability of the nervous system. SA is a major component of gangliosides and glycoproteins in the brain, such as neural adhesion molecules, which play a key role in forming neural synapses and the process of neural central conduction [44]. Memory is closely related to stable synaptic connections and neural conduction. The experimental results from infant rats [45] and piglet [46] models suggest that SA is likely a conditional nutrient during the rapid growth phase of the brain. The chemical structure of polysaccharides is the basis of their biological activity. The proteins that bind to polysaccharides are different, making it difficult to characterize them to obtain an accurate structure [47]. Neural adhesion molecule (NCAM) is a glycoprotein on the surface of cells, which can be modulated by the addition of SA chains, namely salivation. Sialylated NCAM (PSA-NCAM) can affect the nature of cell adhesion, which in turn affects neuronal growth, migration, and synapse formation. The SA in EBN may theoretically be able to exert a salivating effect on NCAM, but this effect depends on some factors, including bioavailability, dose, and metabolic pathway. Overall, the SA in EBN may have potential salivating effects on neural adhesion molecules.

OFT reveal that LPS group exhibited depression-like behavior. However, there is no clear evidence that SA directly causes significant changes in GABA, serotonin or dopamine levels. SA's anxiolytic effects may be achieved through mechanisms such as modulation of the function of neurotransmitter systems, enhancement of GABA neuron activity, or activation of AMP-activated protein kinase (AMPK). Other research also found that the total distance traveled, average speed, and frequency of rearing behavior were signifi-

cantly reduced in the LPS group of mice ($p < 0.0001$). At the same time, the intervention with dihydrolipoic acid improved these indicators ($p < 0.01$) and significantly alleviated the depressive state [48]. A new compound, QTC-4-MeOBnE, significantly increased the grooming frequency in LPS mice during the sucrose splash test ($p < 0.001$) and reduced the immobility time in the forced swim test ($p < 0.001$) [25]. It is speculated that the improvement in depressive behavior is related to restoring BBB permeability and reducing inflammation mediated by NF-κB in the hippocampus and cortex. Given the immunomodulatory and anti-inflammatory activities of structurally different SAs, it is speculated that EBN and its potential active component, namely SA may alleviate depression in LPS mice through anti-inflammatory pathways. However, whether the additional effects of bound SA in EBN are caused by the change in the form of SA or by the synergistic effect of the proteins [49,50] bound to it is currently unclear. We require further investigation to specific mechanism of action of SA at the neurochemical level in future studies, which can guide interventions for cognitive disorders, provide targets for mood disorder research, and lead to the development of functional foods or adjunctive medications, promoting the prevention and treatment of brain diseases.

LPS has varying effects on different inflammatory factors, and the EBN and SA groups can generally reduce the expression of inflammatory factors. The results showed that individual inflammatory factor indexes in LPS female mice did not differ significantly from the CON group. At the same time, EBN and SA had different levels of interventional effects on alleviating inflammation in mice, which indicates that SAs in EBN can alleviate the increase of inflammatory factors in the brain induced by LPS, exerting regulatory activity on neuroinflammation [51]. Research has found that EBN affects changes in gut microbiota, often accompanied by changes in immune cells and inflammatory factors [52], such as the increase of Bacteroides and Akkermansiaceae and the decrease of Firmicutes in the intestinal flora caused an increase in the levels of TNF-alpha and improved immunity [53,54]. In addition, EBN and SA may act on blocking the activation of surface receptors on immune cells (microglia, astrocytes) [39]. Studies indicate that the modeling method of intraperitoneal injection of 500 μg/kg or 700 μg/kg LPS for seven consecutive days results in significant loss of hippocampal neurons in mice [23]. Researchers have pointed out that natural small-molecule substances in food and medicine have neuroprotective effects, and prevention and treatment strategies may improve neurodegenerative diseases [55]. In experiments, SA has shown good anti-inflammatory activity, providing a specific reference value for treating neurological diseases. The EBN and SA groups exert protective effects through anti-inflammatory and antioxidative actions, regulating intracellular signaling pathways and promoting cell repair and regeneration. However, studies on the combination of EBN with other neuroprotective drugs are still in the preliminary stage. The combined application of EBN with antioxidant drugs, anti-inflammatory drugs and brain-derived neurotrophins is a future research direction.

LPS activates genes related to the pathways, while EBN and SA inhibit the expression of some genes, showing an anti-inflammatory trend. In summary, LPS showed significant induction of expression on TICAM1, MYD88 and NF-κB p65 genes, which is consistent with previous studies on the mechanism of LPS-induced inflammatory response [56]. TICAM1, an adaptor molecule with Toll-interleukin-1 receptor domains, is activated after Toll-like receptors (TLRs) recognize pathogen-associated molecular patterns, which in turn activates transcription factors such as NF-κB, initiating the expression of genes related to inflammatory responses [57,58]. LPS triggers the inflammatory response by activating the TLR4- MYD88-NF-κB signalling pathway and up-regulating inflammation-related genes. EBN and SA exhibited inhibitory potential in several inflammatory genes. This may imply that EBN and SA have anti-inflammatory effects, which may be related to inhibition of LPS-activated inflammatory signaling pathways, such as TLR4-MYD88-NF-κB. The NF-κB

pathway is at the core of inflammation, and LPS activates the TICAM1-dependent pathway through TLR4. By screening key targets in the pathway, small molecule inhibitors can be designed, and functional peptides that mimic the effects of EBN and bound SA can be developed, combined with gene editing technology to reveal the function and regulatory network of pathway genes, leading to the development of precise anti-inflammatory therapies and nutritional health products.

5. Conclusions

LPS significantly elevated the organ index, disrupted the metabolic and physiological functions of the organism, and led to the decline in learning and memory abilities and the emergence of depression-like behaviours. However, the organ index was significantly reduced under EBN and SA treatments, which attenuated the damage of inflammation to the organs and ameliorated the LPS-induced decline in learning and memory ability. The EBN group performed better than the SA group in spatial cognitive ability, implying that the bound SA in EBN may have higher anti-inflammatory activity. In addition, LPS significantly induced the expression of inflammatory genes (TICAM1, MYD88, and NF-κB p65), which activated the TLR4-MYD88-NF-κB signalling pathway and triggered an inflammatory response. EBN and SA exerted their anti-inflammatory effects by inhibiting the inflammatory signalling pathway. Although EBN and SA showed significant potential in anti-inflammation and neuroprotection, their specific mechanisms of action require further study. Future studies should focus on the mechanism of action of SA at the neurochemical level, as well as the differences in biological activity between bound and free SAs. In addition, studies on the combined application of EBN with other neuroprotective drugs will provide an important reference for the development of novel anti-inflammatory therapies and nutraceuticals.

Author Contributions: Conceptualization, X.-R.C. and C.-X.Z.; methodology, N.Q.; investigation, N.Q. and C.-X.Z.; data curation, C.-X.Z. and G.-D.F.; writing—original draft preparation, N.Q.; writing—review and editing, N.Q. and G.-D.F.; visualization, S.Q. and Y.S.; supervision, X.-R.C.; project administration, S.Q., M.Y. and D.-L.W. All authors have read and agreed to the published version of the manuscript.

Funding: This work was supported by Central Nervous System Drug Key Laboratory of Sichuan Province (Grant No. 230048-01SZ).

Institutional Review Board Statement: The animal study protocol was approved by the Experimental Animal Welfare and Ethics Review Committee of Jiangnan University (JN. No. 20230415c0800705, approval date: 15 April 2023).

Informed Consent Statement: Not applicable.

Data Availability Statement: The original contributions presented in the study are included in the article, further inquiries can be directed to the corresponding author.

Conflicts of Interest: The authors declare no conflicts of interest.

References

1. Zhou, S.; Chen, G.; Qi, M.; El-Assaad, F.; Wang, Y.; Dong, S.; Chen, L.; Yu, D.; Weaver, J.C.; Beretov, J.; et al. Gram Negative Bacterial Inflammation Ameliorated by the Plasma Protein Beta 2-Glycoprotein I. *Sci. Rep.* **2016**, *6*, 33656. [CrossRef] [PubMed]
2. Ning, E.-J.; Sun, C.-W.; Wang, X.-F.; Chen, L.; Li, F.-F.; Zhang, L.-X.; Wang, L.-P.; Ma, Y.-N.; Zhu, J.; Li, X.; et al. Artemisia argyi polysaccharide alleviates intestinal inflammation and intestinal flora dysbiosis in lipopolysaccharide-treated mice. *Food Med. Homol.* **2024**, *1*, 9420008. [CrossRef]
3. Catorce, M.N.; Gevorkian, G. LPS-induced Murine Neuroinflammation Model: Main Features and Suitability for Pre-clinical Assessment of Nutraceuticals. *Curr. Neuropharmacol.* **2016**, *14*, 155–164. [CrossRef] [PubMed]

4. Yu, H.; Kan, J.; Tang, M.; Zhu, Y.; Hu, B. Lipopolysaccharide Preconditioning Restricts Microglial Overactivation and Alleviates Inflammation-Induced Depressive-like Behavior in Mice. *Brain Sci.* **2023**, *13*, 549. [CrossRef]
5. Meng, F.; Yu, W.; Duan, W.; Wang, T.; Liu, Y. Dexmedetomidine attenuates LPS-mediated BV2 microglia cells inflammation via inhibition of glycolysis. *Fundam. Clin. Pharmacol.* **2019**, *34*, 313–320. [CrossRef]
6. Cao, Y.; Song, W.; Chen, X. Multivalent sialic acid materials for biomedical applications. *Biomater. Sci.* **2023**, *11*, 2620–2638. [CrossRef]
7. Ling, A.J.W.; Chang, L.S.; Babji, A.S.; Latip, J.; Koketsu, M.; Lim, S.J. Review of sialic acid's biochemistry, sources, extraction and functions with special reference to edible bird's nest. *Food Chem.* **2022**, *367*, 130755. [CrossRef]
8. Lu, P.; Wu, J.; Liu, X.; Hua, Y.; Zhan, X.; Gao, M.; Zhang, H. Regulation of bacteria growth of five probiotics and intestinal flora of pregnant women by bound sialic acid of edible bird's nest. *Food Ferment. Ind.* **2023**, *49*, 53–61. [CrossRef]
9. Unal, K.I.; Chang, L.S.; Wan Mustapha, W.A.; Mohd Razali, N.S.; Babji, A.S.; Lim, S.J. Extraction, structural analysis and biological activities of edible bird's nest sialylated mucin (SiaMuc) glycoproteins: A review. *Food Biosci.* **2024**, *61*, 104791. [CrossRef]
10. Young, W.; Egert, M.; Bassett, S.; Bibiloni, R. Detection of Sialic Acid-Utilising Bacteria in a Caecal Community Batch Culture Using RNA-Based Stable Isotope Probing. *Nutrients* **2015**, *7*, 2109–2124. [CrossRef]
11. Zhang, W.; Zhao, G.P.; Lin, X.X.; Li, C.G.; Zhu, H.Q.; Bi, R.; Fang, B.; Xiong, W.; Yuan, M.; Wang, D.L.; et al. Maternal supplementation with edible birds' nest during gestation and lactation enhances intestinal barrier function by upregulating Claudin-1 in rat offspring. *J. Funct. Foods* **2024**, *116*, 11. [CrossRef]
12. Liu, Z.; Liu, M.; Meng, J.; Wang, L.; Chen, M. A review of the interaction between diet composition and gut microbiota and its impact on associated disease. *J. Future Foods* **2024**, *4*, 221–232. [CrossRef]
13. Zhang, W.; Zhu, M.Z.; Liu, X.C.; Que, M.Y.; Dekyi, K.; Zheng, L.X.; Zhang, Y.C.; Lv, Y.P.; Fan, Q.Y.; Wang, X.Y.; et al. Edible bird's nest regulates glucose and lipid metabolic disorders via the gut–liver axis in obese mice. *Food Funct.* **2024**, *15*, 7577–7591. [CrossRef] [PubMed]
14. Cheng, X.-R.; Zhang, C.-X.; Zhao, X.-Y.; Li, Q.-S.; Song, Y.; Zhang, L.; Ma, J.-H.; Chen, Y.-Y.; Yuan, M.; Wang, D.-L. Prophylactic effects of sialylated glycopeptides from edible bird's nest on neuroinflammation in lipopolysaccharide-treated mice via the gut-brain axis. *Food Sci. Hum. Wellness* 2024. [CrossRef]
15. Xiaoyi, Z.; Jiahao, F.; Yijun, G.; Qiushi, L.; Man, Y.; Chenxi, Z.; Xiaoxian, L.; Dongliang, W.; Xiangrong, C. Research progress on neuroprotective effects of edible bird's nests. *Food Ferment. Ind.* **2024**, *50*, 367–374. [CrossRef]
16. Chenxi, Z.; Xiaoxian, L.; Weiyue, Z.; Dongliang, W.; Xiangrong, C. Research progress of the potentially regulatory effect of edible bird's nest on females in different lifecycles. *Food Ferment. Ind.* **2023**, *49*, 328–336. [CrossRef]
17. Payazdan, M.; Khatami, S.; Galehdari, H.; Delfan, N.; Shafiei, M.; Heydaran, S. The anti-inflammatory effects of sialic acid on the human glia cells by the upregulation of IL-4 and IL-10 genes' expressions. *Gene Rep.* **2021**, *24*, 101218. [CrossRef]
18. Careena, S.; Sani, D.; Tan, S.N.; Lim, C.W.; Hassan, S.; Norhafizah, M.; Kirby, B.P.; Ideris, A.; Stanslas, J.; Bin Basri, H.; et al. Effect of Edible Bird's Nest Extract on Lipopolysaccharide-Induced Impairment of Learning and Memory in Wistar Rats. *Evid. -Based Complement. Altern. Med.* **2018**, *2018*, 9318789. [CrossRef]
19. Yew, M.Y.; Koh, R.Y.; Chye, S.M.; Othman, I.; Soga, T.; Parhar, I.; Ng, K.Y. Edible bird's nest improves motor behavior and protects dopaminergic neuron against oxidative and nitrosative stress in Parkinson's disease mouse model. *J. Funct. Foods* **2018**, *48*, 576–585. [CrossRef]
20. Loh, S.P.; Cheng, S.H.; Mohamed, W. Edible Bird's Nest as a Potential Cognitive Enhancer. *Front. Neurol.* **2022**, *13*, 12. [CrossRef]
21. Wang, H.; Ni, K.; Wang, Y. Determination of sialic acid in Edible bird's nest. *Chin. J. Pharm. Anal.* **2006**, *9*, 1251–1253. [CrossRef]
22. Fan, Y.; Fan, Y.; Liu, K.; Lonan, P.; Liao, F.; Huo, Y.; Zhong, X.; Liang, Y.; Wang, Y.; Hou, S.; et al. Edible Bird's Nest Ameliorates Dextran Sulfate Sodium-Induced Ulcerative Colitis in C57BL/6J Mice by Restoring the Th17/Treg Cell Balance. *Front. Pharmacol.* **2021**, *12*, 632602. [CrossRef] [PubMed]
23. Zhao, J.Y.; Bi, W.; Xiao, S.; Lan, X.; Cheng, X.F.; Zhang, J.W.; Lu, D.X.; Wei, W.; Wang, Y.P.; Li, H.M.; et al. Neuroinflammation induced by lipopolysaccharide causes cognitive impairment in mice. *Sci. Rep.* **2019**, *9*, 12. [CrossRef] [PubMed]
24. Luo, H.; Hu, J.; Wang, Y.; Chen, Y.; Zhu, D.; Jiang, R.; Qiu, Z. In vivo and in vitro neuroprotective effects of Panax ginseng glycoproteins. *Int. J. Biol. Macromol.* **2018**, *113*, 607–615. [CrossRef] [PubMed]
25. Fronza, M.G.; Baldinotti, R.; Fetter, J.; Rosa, S.G.; Sacramento, M.; Nogueira, C.W.; Alves, D.; Praticò, D.; Savegnago, L. Beneficial effects of QTC-4-MeOBnE in an LPS-induced mouse model of depression and cognitive impairments: The role of blood-brain barrier permeability, NF-κB signaling, and microglial activation. *Brain Behav. Immun.* **2022**, *99*, 177–191. [CrossRef]
26. Song, Y.; Lin, Y.; Zhang, N. Detection Status and Composition Difference of Nutritional Components in Different Types of Edible Bird's Nests. *Food Nutr. China* **2024**, *30*, 42–51. [CrossRef]
27. Ormerod, B.K.; Hanft, S.J.; Asokan, A.; Haditsch, U.; Lee, S.W.; Palmer, T.D. PPARγ activation prevents impairments in spatial memory and neurogenesis following transient illness. *Brain Behav. Immun.* **2013**, *29*, 28–38. [CrossRef]
28. Janelidze, S.; Mattsson, N.; Stomrud, E.; Lindberg, O.; Palmqvist, S.; Zetterberg, H.; Blennow, K.; Hansson, O. CSF biomarkers of neuroinflammation and cerebrovascular dysfunction in early Alzheimer disease. *Neurology* **2018**, *91*, E867–E877. [CrossRef]

29. Setiawan, E.; Wilson, A.A.; Mizrahi, R.; Rusjan, P.M.; Miler, L.; Rajkowska, G.; Suridjan, I.; Kennedy, J.L.; Rekkas, P.V.; Houle, S. Role of Translocator Protein Density, a Marker of Neuroinflammation, in the Brain During Major Depressive Episodes. *JAMA Psychiatry* **2015**, *72*, 268–275. [CrossRef]
30. Dou, X.; Zhang, Y.; Chen, Q.; Li, W.; Li, Y.; Yu, C.; Su, X. Down-regulation of TSPO expression doesn't affect the productions of TNF-alpha, IL-1beta and IL-6 in LPS-stimulated BV-2 microglia. *Chin. J. Cell. Mol. Immunol.* **2014**, *30*, 897–900.
31. Shao, S.; Zheng, Y.W.; Fu, Z.B.; Wang, J.X.; Zhang, Y.; Wang, C.; Qi, X.T.; Gong, T.T.; Ma, L.Y.; Lin, X.; et al. Ventral hippocampal CA1 modulates pain behaviors in mice with peripheral inflammation. *Cell Rep.* **2023**, *42*, 19. [CrossRef] [PubMed]
32. Shishmanova-Doseva, M.; Atanasova, D.; Ioanidu, L.; Uzunova, Y.; Atanasova, M.; Peychev, L.; Tchekalarova, J. The anticonvulsant effect of chronic treatment with topiramate after pilocarpine-induced status epilepticus is accompanied by a suppression of comorbid behavioral impairments and robust neuroprotection in limbic regions in rats. *Epilepsy Behav.* **2022**, *134*, 14. [CrossRef] [PubMed]
33. Gao, Z.W.; Li, Z.F.; Deng, R.; Liu, Q.; Xiao, Q.X.; Han, J.; Pu, C.X.; Zhang, Y. Dexmedetomidine improves postoperative neurocognitive disorder after cardiopulmonary bypass in rats. *Neurol. Res.* **2021**, *43*, 164–172. [CrossRef] [PubMed]
34. Okuyama, S.; Makihata, N.; Yoshimura, M.; Amakura, Y.; Yoshida, T.; Nakajima, M.; Furukawa, Y. Oenothein B Suppresses Lipopolysaccharide (LPS)-Induced Inflammation in the Mouse Brain. *Int. J. Mol. Sci.* **2013**, *14*, 9767–9778. [CrossRef]
35. Zhang, S.-S.; Feng, D.; An, J.-z.; Zhao, J.; Zhao, J.-y.; Guo, Y.; Jiang, Y.-j.; Yan, W.-j. Total Glycosides of Cistanche deserticola attenuates DSS-induced inflammatory bowel disease by regulating intestinal environmental homeostasis. *Food Med. Homol.* **2025**, *2*, 9420048. [CrossRef]
36. Huang, Y.; Lu, Y.; Zhang, L.; Yan, J.; Jiang, J.; Jiang, H. Perineural Dexmedetomidine Attenuates Inflammation in Rat Sciatic Nerve via the NF-κB Pathway. *Int. J. Mol. Sci.* **2014**, *15*, 4049–4059. [CrossRef]
37. Tang, Y.L.; Dong, X.Y.; Chen, G.F.; Ye, W.; Kang, J.W.; Tang, Y.; Feng, Z. Vagus Nerve Stimulation Attenuates Early Traumatic Brain Injury by Regulating the NF-κB/NLRP3 Signaling Pathway. *Neurorehabil. Neural Repair.* **2020**, *34*, 831–843. [CrossRef]
38. Meunier, A.; Latrémolière, A.; Dominguez, E.; Mauborgne, A.; Philippe, S.; Hamon, M.; Mallet, J.; Benoliel, J.J.; Pohl, M. Lentiviral-mediated targeted NF-κB blockade in dorsal spinal cord glia attenuates sciatic nerve injury-induced neuropathic pain in the rat. *Mol. Ther.* **2007**, *15*, 687–697. [CrossRef]
39. Ran, B.; Dan, Z.; Rui, Q.; Lin, X.; Wen, Z.; Li, C.; Man, Y.; Bing, F.; Wang, D.; Li, Y. Edible bird's nest alleviates pneumonia caused by tobacco smoke inhalation through the TNFR1/NF-kappaB/NLRP3 pathway. *Food Sci. Nutr.* **2024**, *12*, 4196–4210. [CrossRef]
40. Ren, M.; Ahmed, A.F.; Li, M.; Li, M.; Yan, Z.; Wang, J. A review: The mechanism of plant-derived polysaccharides on osteoblasts and osteoclasts. *J. Future Foods* **2024**, *4*, 183–192. [CrossRef]
41. Sun, J.; Gou, Y.R.; Liu, J.; Chen, H.; Kan, J.; Qian, C.L.; Zhang, N.F.; Niu, F.X.; Jin, C.H. Anti-inflammatory activity of a water-soluble polysaccharide from the roots of purple sweet potato. *RSC Adv.* **2020**, *10*, 39673–39686. [CrossRef] [PubMed]
42. Jianhui, L.; Weiwei, W.; Qiuhui, H.; Xuyang, W.; Hui, X.; Anxiang, S.; Minhao, X.; Wenjian, Y. Bioactivities and molecular mechanisms of polysaccharides from Hericium erinaceus. *J. Future Foods* **2022**, *2*, 103–111. [CrossRef]
43. Wu, J.R.; Lu, P.H.; Zhang, H.T.; Fan, Q.Y.; Liu, X.C. Comparison of prebiotic activity of dietary sialoglycoprotein and N-acetylneuraminic acid: Sialylation is a key factor. *Food Biosci.* **2023**, *56*, 11. [CrossRef]
44. Wielgat, P.; Braszko, J.J. Significance of the cell adhesion molecules and sialic acid in neurodegeneration. *Adv. Med. Sci.* **2012**, *57*, 23–30. [CrossRef]
45. Yuan, L. Extraction and Purification of Sialic Acid from Edible Bird's Nest Fragment and Its Effect on Learning and Memory Abilities of Young Rats. Master's Thesis, Jiangnan University, Wuxi, China, 2016.
46. Bing, W.; Bing, Y.; Karim, M.; Honghua, H.; Yun, S.; McGreevy, P.; Petocz, P.; Held, S.; Brand-Miller, J. Dietary sialic acid supplementation improves learning and memory in piglets. *Am. J. Clin. Nutr.* **2007**, *85*, 561–569.
47. Shi, R.Y.; Dan, B.; Lü, L.J. Bioactive effects advances of natural polysaccharides. *J. Future Foods* **2023**, *3*, 234–239. [CrossRef]
48. Bian, H.T.; Wang, G.H.; Huang, J.J.; Liang, L.; Zheng, Y.G.; Wei, Y.Y.; Wang, H.; Xiao, L.; Wang, H.L. Dihydrolipoic acid protects against lipopolysaccharide-induced behavioral deficits and neuroinflammation via regulation of Nrf2/HO-1/NLRP3 signaling in rat. *J. Neuroinflamm.* **2020**, *17*, 13. [CrossRef]
49. Lee, C.H.; Hamdan, N.; Nyakuma, B.B.; Wong, S.L.; Wong, K.Y.; Tan, H.Y.; Jamaluddin, H.; Lee, T.H. Purification, identification and molecular docking studies of antioxidant and anti-inflammatory peptides from Edible Bird's Nest. *Food Chem.* **2024**, *454*, 15. [CrossRef]
50. Lee, C.H.; Hamdan, N.; Nyakuma, B.B.; Wong, S.L.; Wong, K.Y.; Jamaluddin, H.; Lee, T.H. Functional and biological activities of Edible Bird's Nest (EBN) protein by proteomic and bioinformatic analyses. *J. Food Meas. Charact.* **2024**, *18*, 3018–3031. [CrossRef]
51. Chu, W.Y.; Phan, C.W.; Lim, S.J.; Babji, A.S. Insights on the molecular mechanism of neuroprotection exerted by edible bird?s nest and its bioactive constituents. *Food Sci. Hum. Wellness* **2023**, *12*, 1008–1019. [CrossRef]
52. Li, C.; Xu, X.H.; Lin, X.X.; Yuan, M.; Wang, D.L.; Zhang, X.K. Edible bird's nest plays an immune regulation by influencing intestinal flora changes in mice. *J. Funct. Foods* **2024**, *118*, 13. [CrossRef]

53. Clemente, J.C.; Manasson, J.; Scher, J.U. The role of the gut microbiome in systemic inflammatory disease. *BMJ-Br. Med. J.* **2018**, *360*, 16. [CrossRef] [PubMed]
54. Zheng, J.Y.; Lou, L.H.; Fan, J.J.; Huang, C.L.; Mei, Q.X.; Wu, J.H.; Guo, Y.C.; Lu, Y.Y.; Wang, X.P.; Zeng, Y. Commensal Escherichia coli Aggravates Acute Necrotizing Pancreatitis through Targeting of Intestinal Epithelial Cells. *Appl. Environ. Microbiol.* **2019**, *85*, 15. [CrossRef] [PubMed]
55. Ye, X.-S.; Tian, W.-J.; Wang, G.-H.; Lin, K.; Zhu, S.-X.; Xia, Y.-Y.; Sun, B.-L.; Shu, X.-J.; Liu, W.; Chen, H.-F. The food and medicine homologous Chinese Medicine from Leguminosae species: A comprehensive review on bioactive constituents with neuroprotective effects on nervous system. *Food Med. Homol.* **2025**, *2*, 9420033. [CrossRef]
56. Ono, J.; Shime, H.; Takaki, H.; Takashima, K.; Funami, K.; Yoshida, S.; Takeda, Y.; Matsumoto, M.; Kasahara, M.; Seya, T. The TLR3/TICAM-1 signal constitutively controls spontaneous polyposis through suppression of c-Myc in Apc Min/+ mice. *J. Biomed. Sci.* **2017**, *24*, 9. [CrossRef]
57. Tao, S.S.; Zhu, L.X.; Lee, P.K.; Lee, W.M.; Knox, K.; Chen, J.; Di, Y.P.; Chen, Y. Negative Control of TLR3 Signaling by TICAM1 Down-Regulation. *Am. J. Respir. Cell Mol. Biol.* **2012**, *46*, 660–667. [CrossRef]
58. Li, Z.L.; Gao, W.K.; Yuan, H.; Pan, X.L.; Yuan, R.Q.; Wang, W.J.; Guan, L.; Hu, L.L.; Chen, Y.; Cheng, Z.L.; et al. Suppression of intestinal Ticam1 ameliorated MASH via Akkermansia muciniphila QAA37749.1 mediated betaine transformation. *Biochim. Biophys. Acta-Mol. Basis Dis.* **2025**, *1871*, 16. [CrossRef]

Disclaimer/Publisher's Note: The statements, opinions and data contained in all publications are solely those of the individual author(s) and contributor(s) and not of MDPI and/or the editor(s). MDPI and/or the editor(s) disclaim responsibility for any injury to people or property resulting from any ideas, methods, instructions or products referred to in the content.

MDPI AG
Grosspeteranlage 5
4052 Basel
Switzerland
Tel.: +41 61 683 77 34

Nutrients Editorial Office
E-mail: nutrients@mdpi.com
www.mdpi.com/journal/nutrients



Disclaimer/Publisher's Note: The title and front matter of this reprint are at the discretion of the Guest Editors. The publisher is not responsible for their content or any associated concerns. The statements, opinions and data contained in all individual articles are solely those of the individual Editors and contributors and not of MDPI. MDPI disclaims responsibility for any injury to people or property resulting from any ideas, methods, instructions or products referred to in the content.





Academic Open
Access Publishing

mdpi.com

ISBN 978-3-7258-9164-1